Molecular Dynamics Simulations for the Study of Biophysical Processes on Biological Membranes

Sukit Leekumjorn

Dissertation submitted to the Faculty of the

Virginia Polytechnic Institute and State University

in partial fulfillment of the requirements for the degree of

Doctor of Philosophy

in

Chemical Engineering

Amadeu K. Sum, Chair

David F. Cox

Aaron S. Goldstein

Diego Troya

September 19, 2008

Blacksburg, Virginia

Keywords: molecular dynamics, stabilization, phase transition, membrane toxicity,

phospholipids, saccharides

Molecular Dynamics Simulations for the Study of Biophysical Processes on Biological Membranes

Sukit Leekumjorn

(ABSTRACT)

Phospholipid bilayers constitute the primary structural element of biological membranes, and as such, they play a central role in biochemical and biophysical processes at the cellular level, including cell protection, intercellular interactions, trans-membrane transport, cell morphology, and protein function, to name a few. The properties of phospholipid bilayers are thus of great interest from both experimental and theoretical standpoints. Although experiments have provided much of the macroscopic functions and properties of biological membranes, insight into specific mechanisms at the molecular level are seldom accessible by conventional methods. To obtain a better understanding of biochemical and biophysical processes at the molecular level involving phospholipid bilayers, we apply molecular simulation methods to investigate the complexity of the membrane matrix using atomistic models. Here, we discuss three specific biological processes that are associated with biological membranes: 1) membrane stabilization, 2) membrane phase behavior, and 3) fatty acid-induced toxicity in cell membranes.

For membrane stabilization, molecular dynamics studies were performed for mixed phospholipid bilayers containing two of the most prevalent phospholipids (phosphatidylcholine and phosphatidylethanolamime) in biological membranes. We presented structural and dynamics properties of these systems, as well as the effect of stabilizing agents, such as trehalose, on their properties. Furthermore, we performed a comprehensive analysis of the phase transition of lipid bilayers and investigated the interactions of stabilizing agents (glucose or trehalose) with lipid bilayers under dehydrated conditions to understand the mechanisms for preservation of cellular systems.

For membrane phase behavior, a comprehensive study of the structural properties of

saturated and monounsaturated lipid bilayers near the main phase transition were investigated using molecular dynamics simulations. In this study, we demonstrated that atomistic simulations are capable of capturing the phase transformation process of lipid bilayers, providing a valuable set of molecular and structural information at and near its transition state.

Lastly, the third study investigated the mechanism for fatty acid-induced toxicity by integrating *in vitro* and *in silico* experiments to reveal the biophysical interactions of saturated fatty acid (palmitate) with the cellular membranes and the role of trehalose and unsaturated fatty acids (oleate and linoleate) in preventing changes to the membrane structure. Knowledge gained from this study is essential in the prevention and treatment of obesity-associated cirrhosis diseases.

Dedication

To Ling, without your constant love and support, none of this would have been possible.

Acknowledgments

I would like to acknowledge many people for helping me during my doctoral work. I would especially like to thank my advisor, Professor Amadeu K. Sum, for his generous time and commitment. Throughout my doctoral work he encouraged me to develop independent thinking and research skills. He continually stimulated my analytical thinking and greatly assisted me with scientific writing.

I am also very grateful for having an exceptional doctoral committee and wish to thank Professors David F. Cox, Aaron S. Goldstein, and Diego Troya for their continual support and encouragement.

Special thanks to Yifei Wu and Professor Christina Chan in the Department of Chemical Engineering & Material Sciences at Michigan State University for a fruitful collaboration as a part of my research at Virginia Tech. I am also particularly grateful to Professor Chan for providing the financial resources for my participation at a Biophysical Society and an AIChE meetings.

I owe a special note of gratitude to the Department of Chemical Engineering Head, Professor John Y. Walz, and his supportive staffs for helping me in many ways throughout my Ph.D. career.

I am very grateful to Dr. Bradley Feuston for giving me the opportunity to intern at Merck Research Laboratories, West Point, PA. It was a memorable and enriching experience working with him and his research team (Molsys). I learned many new ideas and teamwork

skills during my time at Merck. Most importantly, I was able to expand my Ph.D. training to address very challenging problems in the pharmaceutical industry. I will treasure this invaluable experience with me in my future endeavors.

Thanks also to all my colleagues in the Thai Student Association (TSA) for providing a memorable living experiences in Blacksburg and work-life balance.

My deepest gratitude goes to my aunt whom I have been raised with and been supporting me for the past 16 years in the United States. I owe much of my success to her.

Finally, I would also like to acknowledge the computational resources provided by Virginia Tech Advanced Research Computing Facility (System X). As one of the first users of this system, unlimited time was granted for usage, without which, none of this dissertation would be possible.

Lipid Abbreviations

DLPC	1,2-Dilauroyl-*sn*-Glycero-3-Phosphocholine
DLPE	1,2-Dilauroyl-*sn*-Glycero-3-Phosphoethanolamine
DMPC	1,2-Dimyristoyl-*sn*-Glycero-3-Phosphocholine
DMPE	1,2-Dimyristoyl-*sn*-Glycero-3-Phosphoethanolamine
DMTAP	Dimyristoyltrimethylammonium Propane
DOPC	1,2-Dioleoyl-*sn*-Glycero-3-Phosphocholine
DOPE	1,2-Dioleoyl-*sn*-Glycero-3-Phosphoethanolamine
DPPC	1,2-Dipalmitoyl-*sn*-Glycero-3-Phosphocholine
DPPE	1,2-Dipalmitoyl-*sn*-Glycero-3-Phosphoethanolamine
DSPCd-70	1,2-Distearoyl-d70-*sn*-Glycero-3-Phosphocholine
EPC	Egg Phosphatidylcholine
Lyso PC	Lysophosphatidylcholine
PC	Phosphatidylcholine
PE	Phosphatidylethanoamine
PLPC	1-Palmitoyl-2-Lauroyl-*sn*-Glycero-3-Phosphocholine
POPC	1-Palmitoyl-2-Oleoyl-*sn*-Glycero-3-Phosphocholine
POPG	1-Palmitoyl-2-Oleoyl-*sn*-Glycero-3-[Phospho-rac-(1-glycerol)]
POPE	1-Palmitoyl-2-Oleoyl-*sn*-Glycero-3-Phosphoethanolamine
SOPE	1-Stearoyl-2-Oleoyl-*sn*-Glycero-3-Phophoethanolamine
SOPC	1-Stearoyl-2-Oleoyl-*sn*-Glycero-3-Phophocholine

Abbreviations

BSA	Bovine Serium Albumin
CG	Coarse-Grained
DPD	Dissipative Particle Dynamics
DPH	1,6-diphenyl-1,3,5-hexatriene
DSC	Differential Scanning Calorimetry
DTA	Differential Thermal Analysis
EDM	Electron Density Map
FABP	Fatty Acid Binding Protein
FA	Fatty Acid
FFA	Free Fatty Acid
FTIR	Fourier Transform Infrared Spectroscopy
FWHH	Full-Width Half-Height
GL	Glycerolipids
GP	Glycerophospholipids
HepG2	Human Hepatocellular Liver Carcinoma Cell Line
LDL	Low-Density Lipoproteins
LDH	Lactate Dehydrogenase
LINC	Linear Constraint Solver
MC	Monte Carlo
MD	Molecular Dynamics
MSD	Mean-Squared Displacement

Abbreviations (Continued)

NMR	Nuclear Magnetic Resonance
OPLS-AA	Optimized Potential for Liquid Simulations-All Atoms
PBC	Periodic Boundary Conditions
PK	Polyketides
PME	Particle-Mesh Ewald
PpIX	Photoporphyrin IX
PR	Prenol Lipids
QENS	Quasielastic Neutron Scattering
RDF	Radial Distribution Function
ROS	Reactive Oxygen Specie
SCD1	Stearoyl-CoA Desaturase 1
SL	Saccharolipids
SPC	Single Point Charge
SP	Sphingolipids
TG	Triglyceride

List of Symbols

H_{II}	Inverted Hexagonal Phase
L_α	Liquid-Crystalline Phase
L_β	Gel Phase
L_c	Crystal Phase
$L_{c'}$	Sub-Gel Phase
NPT	Constant Pressure and Temperature Simulation
NP_zAT	Constant Surface Area and Temperature Simulation
NVT	Constant Volume and Temperature Simulation
$P_{\beta'}$	Ripple Gel Phase
$T^{\text{simul.}}$	Simulation Temperature
T_m	Experiment Phase Transition Temperature
$T_\text{m}^{\text{simul.}}$	Simulation Phase Transition Temperature

Contents

List of Figures

List of Tables

Chapter 1

Introduction

Computer simulations have proven to be a valuable tool for investigating and understanding the behavior of bio-molecular systems [1]. In many cases, computer simulations serve as a complement to conventional laboratory experiments. In other cases, they serve as an enabling tool to study and understand complex systems and natural phenomena that would otherwise be too expensive, difficult, or even impossible to study by direct measurements. By implementing this tool, insight into biochemical and biophysical processes is made possible.

As a tool for scientists and engineers, computer simulation has been central in evaluating and optimizing the design and production of means for enhancing the quality of life [2, 3]. The ever-increasing power of computational resources allows us to explore further-reaching complex systems, as those in biological systems [4], the most complex of all. That is, by harnessing the power of computers, we are able to gain insight into molecular interactions to obtain a better understanding of biological functions. Due to the complexity and vast number of processes simultaneously occurring in living organisms, one must be selective and approximate specific processes by isolating their behavior and function. Therefore, our focus is on biological membranes, a vital structural component of all living matter [5].

Biological membranes are mainly composed of lipids. A pictorial representation of
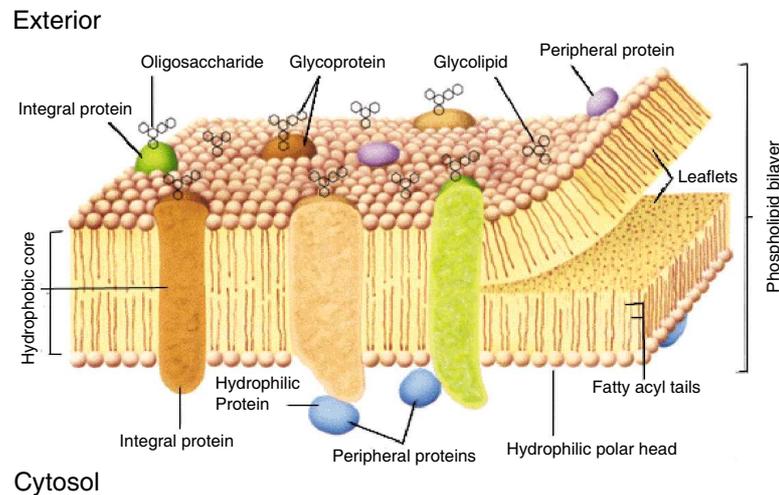
Figure 1.1: Pictorial representation for a segment of a biological membrane. Reproduced from Lodish *et al.* [5]

a biological membrane is shown in Figure 1.1. In general, lipids are molecules that exhibit either hydrophobic or amphiphilic (molecules containing both hydrophilic and hydrophobic moieties) properties [6]. The typical functions of lipids in membranes include cell protection, intercellular interactions, trans-membrane transport, cell morphology, cell recognition, selective receptivity, signal transductions, protein functionalities, and cell motility [5]. To help distinguish various types of lipids based on their chemical structures, Lipid Metabolites And Pathways Strategy (Lipid MAPS) have categorized lipids into eight major classifications [6]. They are glycerolipids (GL), fatty acids (FA), glycerophospholipids (GP), sterol lipids (ST), sphingolipids (SP), prenol lipids (PR), saccharolipids (SL), and polyketides (PK). The abundance of each lipid and an example of each are shown in Figures 1.2 and 1.3, respectively. Because there are a large number of lipid species (∼9,000 lipids in total) with various compositions found in biological membranes [6], for the purpose of this study, two of the most abundant lipids (glycerophospholipids): phosphatidylcholine (PC) and phosphatidylethanolamine (PE) are consider.

PC and PE lipids are a subclass of glycerophospholipids, commonly referred as phospholipids. The headgroup in this subclass often contains at least one negatively charged
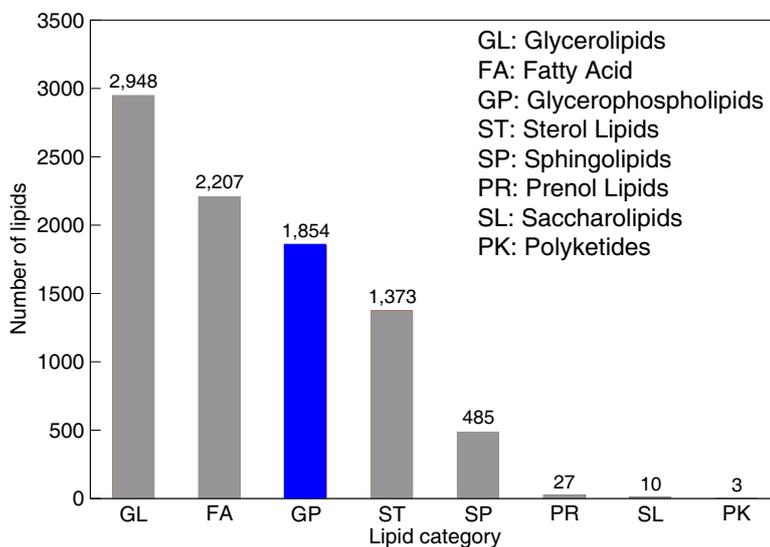
Figure 1.2: Classification of lipids. Adapted from Lipid MAPS [7].

phosphate group (PO_4^-) and fatty acids tails (see Figure 1.3g). The amphiphilic nature of these molecules at hydrated conditions induces spontaneous formation of bilayer structures by a self-assembly process in which the non-polar parts of a lipid molecule aggregate to exclude water molecules. This is an entropic effect because water molecules surrounding the lipid tails decrease the entropy of the water shell structure, resulting in an unfavorable condition. Therefore, self-aggregation of the lipid tails into a bilayer structure is favorable.

In this dissertation, several types of phospholipid molecules are selected to model biological membrane: 1,2-dipalmitoyl-*sn*-glycero-3-phosphocholine (DPPC), 1,2-dipalmitoyl-*sn*-glycero-3-phosphoethanolamine (DPPE), 1-palmitoyl-2-oleoyl-*sn*-glycero-3-phosphocholine (POPC), 1-palmitoyl-2-oleoyl-*sn*-glycero-3-phosphoethanolamine (POPE), and 1,2-dioleoyl-*sn*-glycero-3-phosphocholine (DOPC). In general, PC and PE are two of the most important neutral lipid components found in all living organisms. The abundance of PE is highly variable among organisms and cell types. PE is found in high concentration in bacteria (70-80% in *E. Coli*), moderate-low concentration in blood cells (6%), and extremely low concentration in animal cells [8]. On the other hand, PC lipids are predominantly found in animal cells [9]. The difference between PE and PC lipids is in the chemical composition
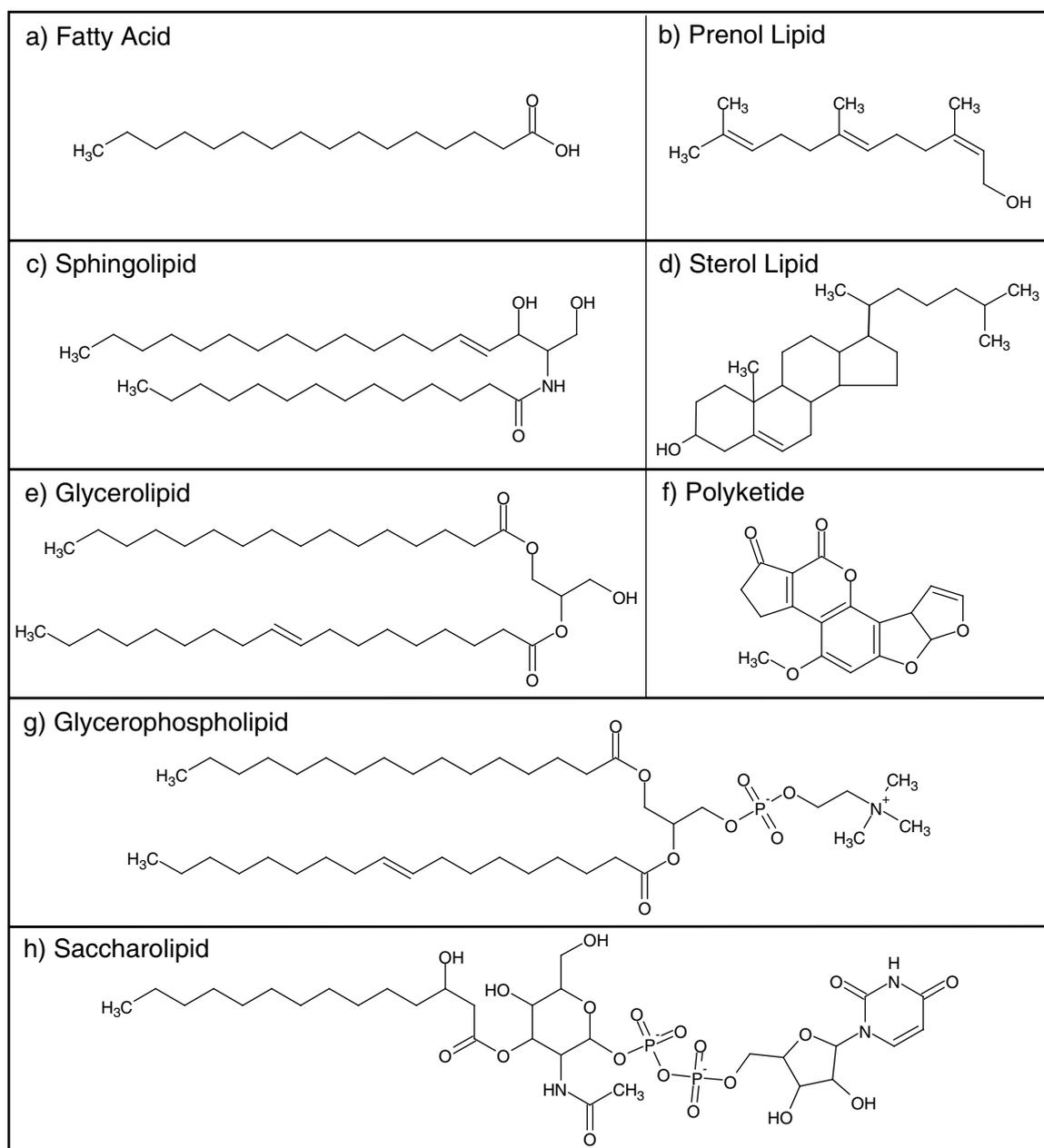
Figure 1.3: Example of lipid molecules for each classification: a) palmitic acid, b) 2*E*,6*E*-farnesol, c) *N*-(tetradecanoyl)-sphing-4-enine, d) cholest-5-*en*-3*β*-ol, e) 1-hyxadecanoyl-2-(9*Z*-octadecenoyl)-*sn*-glycerol, f) aflatoxin *B*1, g) 1-hexadecanoyl-2-(9*Z*-octadecenoyl)-*sn*-glycero-3-phosphocholine, and h) UDP-3-*O*-(3*R*-hydroxy-tetradecanoyl)-*αD*-*N*-acetyl-glucosamine. Chemical symbols correspond to hydrogen (H), carbon (C), nitrogen (N), oxygen (O), and phosphorus (P).
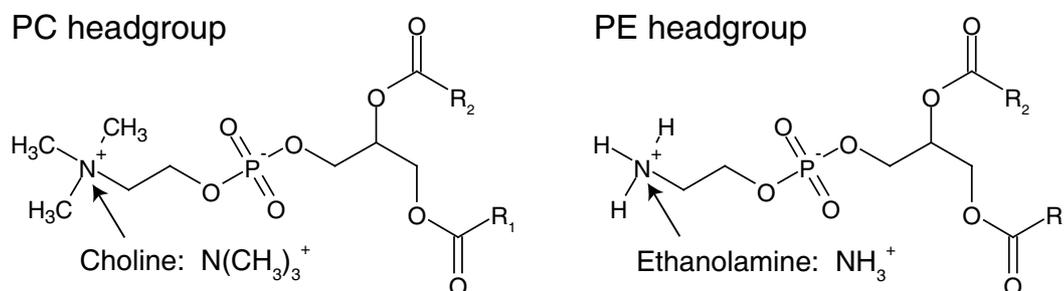
Figure 1.4: Chemical structure of PC and PE lipid headgroups. R_1 and R_2 are the fatty acid chains that are commonly referred to as *Sn*-1 and *Sn*-2, respectively. Chemical symbols correspond to hydrogen (H), carbon (C), nitrogen (N), oxygen (O), and phosphorus (P).

of the headgroups, namely the primary amine group for PE and the choline group for PC (see Figure 1.4). With the amine headgroup, PE is associated with a wide variety of biological functions including cell division, growth, reproduction, and motility [10–13]. Most often found concentrated in the inner leaflet of membranes, PE plays an important role in membrane fusion and vesicle formation [14, 15]. Although phospholipid bilayers containing choline headgroup express less functionalities, it is essential for maintaining membrane integrity [16]. The smaller headgroup in PE results in significantly lower area per lipid [17] and highly ordered hydrocarbon lipid tails [18, 19] compared to other lipids. Comparative studies of PE and PC show that PE molecules can form intermolecular and intramolecular hydrogen bonds, including association with other types of lipids [20], in which the amine group (hydrogen-donor) can interact strongly with the phosphate/carbonyl groups or water (hydrogen-acceptor). These strong intermolecular interactions cause an increase in the liquid-crystalline phase transition temperature [21], thus affecting membrane permeability, stability, and other biological properties normally associated with the functional activity of internal cell organelles.

Despite the various functionalities of lipid bilayers based on the phospholipid headgroups, lipid tails, which are composed of fatty acids, are equally important structural components in biological membranes. That is, the structural properties of the phospholipid

tails play a central role in determining hydrophobicity, reactivity, and stability of the membrane [22]. In general, fatty acids are classified according to their chain structures and functional groups. There are three main classes of fatty acids: straight, branched, and ring containing chains (see Figures 1.5a-c). In this study, phospholipid molecules with straight chains fatty acid are used in the modeled bilayers, thus a brief description of this type of fatty acid is discussed. The straight chain fatty acid can be classified as: saturated, monounsaturated, and polyunsaturated [23–26] (see Figures 1.5d-f). The degree of unsaturation is based on the number of double bonds present within a given lipid chain. Because of these differences, polyunsaturated lipids are more fluid-like, as opposed to gel-like, at normal or below-normal temperatures [27–31]. The most pronounced change in lipid physical properties occurs when comparing saturated to monounsaturated lipids (assuming the same lipid headgroup) [32, 33]. One of the most distinguishable properties is the main phase transition temperature from a gel to a liquid-crystalline phase. In general, the phase transition temperature is defined as the temperature required to induce a change in the lipid physical state from an ordered gel phase (hydrocarbon chains are fully extended and closely packed) to a disordered liquid-crystalline phase (hydrocarbon chains are randomly oriented and fluid) [34]. These changes in the physical state of the lipid are related to the changes in molar volume and heat capacity of a system when transforming from a gel to a liquid-crystalline phase. This is demonstrated in Figure 1.6 where the heating scan of a DPPC bilayer shows significant changes in these properties near the main thermal phase transition from gel (L_β) to liquid-crystalline (L_α).

There are several factors which directly affect the phase transition temperature; however, the length and the degree of unsaturation of the hydrocarbon chain are major contributions to the overall transition temperature. Table 1.1 summarizes reported experimental values of the phase transition temperature for various PC lipids with different acyl composition and degree of unsaturation. As shown in Table 1.1, unsaturated lipids have significantly lower melting temperature and behave more fluid-like below normal physiological temperature (below 37°C). For this reason, unsaturated lipids are a major component of biological
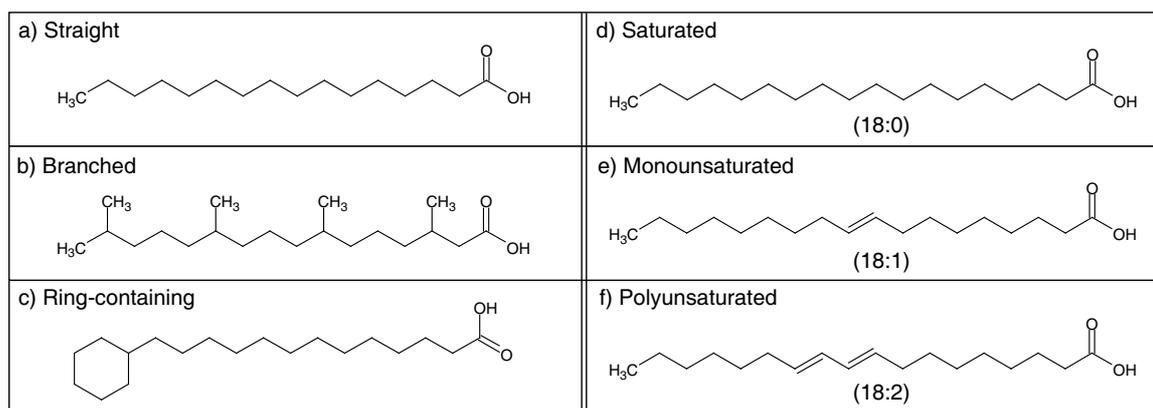
Figure 1.5: Classification of fatty acids: a) straight chain (palmitic acid), b) branched chain (phytanic acid), and c) ring-containing chain (13-cyclohexyltridecanoic acid). Subclassification of straight chain fatty acid: d) saturated (stearic acid), e) monounsaturated (*trans*-oleic acid), and f) polyunsaturated (*trans*-linoleic acid). Chemical symbols correspond to hydrogen (H), carbon (C), and oxygen (O).
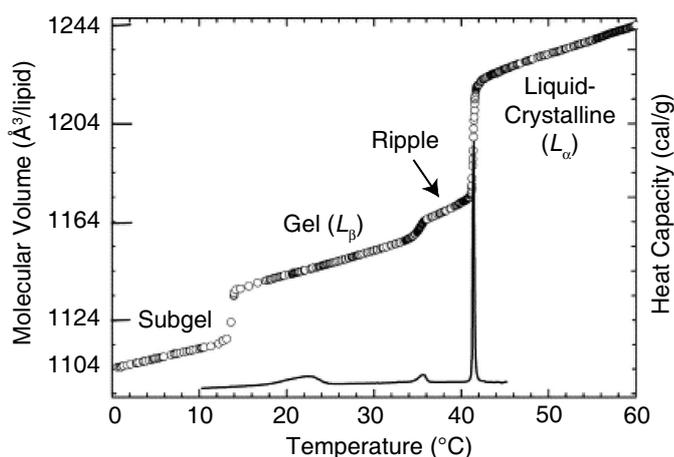
Figure 1.6: Differential scanning calorimetry heating scan of fully hydrated DPPC bilayer. Opened circles and solid line are changes in the lipid molecular volume and heat capacity, respectively, with increasing temperature. Reproduced from Tristram-Nagle and Nagle [35].

Table 1.1: Selected phase transition temperature (T_m) for PC lipids categorized according to acyl composition and degree of unsaturation. Lipid tail refers to the length of each acyl chain in glycerophospholipids (only 16 or 18 carbon lipids are shown). The number following the colon indicates the degree of unsaturation of each lipid tail: 0 (no double-bond), 1 (one double-bond), 2 (two double-bonds).

Saturated		Monounsaturated		Polyunsaturated	
Lipid tail	$T_m(°C)$	Lipid tail	$T_m(°C)$	Lipid tail	$T_m(°C)$
16:0-18:0	49[a]	16:0-18:1	0[b]	16:0-18:2	-19.5[c]
18:0-18:0	55[a]	18:0-18:1	6[a]	18:0-18:2	-13.7[c]
		18:1-18:0	9[a]	18:1-18:1	-20[a]

[a] Avanti Polar Lipid, Inc. [44]; [b] Litman *et al.* [45]; [c] Keough *et al.* [46]

membranes and provide a stable cellular structure at physiological conditions [27, 28, 31]. From experimental studies, these factors greatly affect the phase behavior of lipid bilayers such that both ordered and disordered phases co-exist within cell membranes [36]. This is important from a biological standpoint because the ordered domains formed (lipid raft formation) are closely associated with their functions, including signal transduction [37, 38], protein transport [37, 39, 40], and membrane sorting [37, 39]. Other studies of these ordered domains have also suggested that they serve as a possible binding site for various pathogens and toxins [41–43]. With a variety of lipid headgroups and lipid tails present in cell membranes, the complexity of these systems is of great interest from both experimental and theoretical standpoints.

To obtain a better understanding of biochemical and biophysical processes at the molecular level involving phospholipid bilayers, molecular simulations are used to investigate the properties of the membrane matrix. Molecular simulation is a computational tool capable of providing detailed molecular interactions at the microscopic scale. Moreover, it has the power to predict structural and dynamic properties by considering a microscopic representation of macroscopic systems. Among the simulation methods, classical molecular dynamics (MD), is the most suitable to study biological systems because it has the ability to provide both dynamic and equilibrium properties.

1.1   Motivation and Goals

In general, biological processes that are associated with biological membranes are complex and difficult or even impossible to study by direct laboratory measurements. With the establishment of lipid bilayers models and the advancement in computational simulations, it is now possible to combine these two aspects and utilize computational tools to study, understand, and predict complex systems and natural phenomena at a molecular level.

In this dissertation, molecular dynamics (MD) simulations are chosen because they are capable of mimicking actual laboratory experiments while detailed analyses are performed at the atomistic/molecular level. Although several biological processes are studied in this dissertation, the common premise is the use of MD simulations to gain insight into biophysical processes associated with biological membranes.

1.2   Organization of the Dissertation

Chapter 2 begins with a literature review of the topics presented in this dissertation. This includes a brief introduction on mixed lipid bilayers, lipid bilayers with disaccharides, dehydrated lipid bilayers, structural properties of lipid bilayers near the main phase transition, and fatty acid induced toxicity in cell membranes.

Chapter 3 describes MD simulations. The theory of the methods and the development of computational algorithms employed in this study are discussed.

Chapter 4 exposes a comprehensive study of lipid bilayers containing DPPC, DPPE, and their mixtures, including their interactions with disaccharides.

Chapter 5 details the interactions of stabilizing agents (glucose or trehalose) with lipid bilayers under dehydrated conditions to understand the mechanisms for preservation of cellular systems.

Chapter 6 discusses structural and dynamic properties of saturated and unsaturated lipid bilayers pertaining to the main phase transition.

Chapter 7 investigates the mechanism for fatty acid-induced toxicity by integrating *in vitro* and *in silico* experiments to reveal the biophysical interactions of saturated fatty acid (palmitate) and trehalose with cellular membranes.

Chapter 8 describes the effect of unsaturated fatty acids (oleate and linoleate) in reducing the toxicity of cell membranes. These studies are the first step toward broadening our knowledge to prevent and treat obesity-associated cirrhosis diseases.

Chapter 9 summarizes the major conclusions presented in Chapters 4 through 8. In addition, suggested future studies are outlined.

Lastly, the Bibliography section contains a comprehensive list of all citations used in this dissertation.

All of the molecular force-fields used in this study are listed in appendix A. The analysis codes used are listed in appendix B. An additional publication not discussed in the main body of the dissertation is included in appendix C.

1.3   Publications

The results presented in Chapters 4-8 were published or are in preparation for publication. The citation for the publications are:

- S. Leekumjorn and A. K. Sum, "Molecular Simulation Study of Structural and Dynamic Properties of Mixed DPPC/DPPE Bilayers" *Biophysical Journal*, 90 (11), 3951-3965 (2006).

- S. Leekumjorn and A. K. Sum, "Molecular Investigation of the Interactions of Trehalose

with Lipid Bilayers of DPPC, DPPE, and their Mixture" *Molecular Simulation*, 32 (3-4), 219-230 (2006).

- S. Leekumjorn and A. K. Sum, "Molecular Studies of the Gel to Liquid-Crystalline Phase Transition for Fully Hydrated DPPC and DPPE bilayers" *Biochimica et Biophysica Acta-Biomembranes*, 1768 (2), 354-365 (2007).

- S. Leekumjorn and A. K. Sum, "Molecular Studies of the Gel to Liquid-Crystalline Phase Transition for Fully Hydrated POPC and POPE Bilayers" *Journal of Physical Chemistry B*, 111 (21), 6026-6033 (2007).

- S. Leekumjorn, Y. Wu, A. K. Sum, and C. Chan, "Experimental and Computational Investigation of Trehalose Protection from Palmitate Induced Toxicity of HepG2 Cells" *Biophysical Journal*, 97 (7), 2869-2883 (2008).

- S. Leekumjorn and A. K. Sum, "Molecular Dynamics Study on the Stabilization of Dehydrated Lipid Bilayers with Glucose and Trehalose" *Journal of Physical Chemistry B*, 112 (34), 10732-10740 (2008).

- S. Leekumjorn, H. J. Cho, Y. Wu, N. T. Wright, A. K. Sum, and C. Chan, "Fatty Acid Induced Toxicity: The Role of Saturation in Degrading and Benefiting Cell Survival" in preparation (2008).

Appendix C contains a re-print of an additional publication not discussed in the main body of the dissertation.

- S. Leekumjorn and A. K. Sum, "Molecular Study of the Diffusional Process of DMSO in Double Lipid Bilayers" *Biochimica et Biophysica Acta-Biomembranes*, 1758 (11), 1751-1758 (2006).

Chapter 2

Literature Review

This chapter provides the relevant literature review for the topics discussed in this dissertation. The first section provides a broad overview of pure and mixed lipid bilayer systems (PC and PE phospholipids). The second and third sections discuss the role of stabilizing agent (trehalose) in biological preservation processes and their interactions with model hydrated and dehydrated lipid bilayers. Here, several preservation hypotheses are introduced. The fourth section gives a comprehensive review on the phase behavior of model lipid bilayers (DPPC, DPPE, POPC, and POPE phospholipids) with emphasis on structural and dynamic properties of lipid bilayers near the main phase transition. The fifth and sixth sections discuss the role of saturated fatty acids (palmitate), a stabilizing agent (trehalose), and unsaturated fatty acids (oleate and linoleate) in hepatocyte-induced toxicity. Each section presents a brief background to the research topic along with several significant contributions from experimental and computational studies.

2.1 Mixed Lipid Bilayers

2.1.1 Background

In-depth analysis of lipid bilayers began when the first crystal structure of PC and PE lipids were identified by X-ray diffraction in an attempt to provide structural data and quantitative interpretation of phospholipid arrangement/interaction in artificial and natural membranes [47, 48]. Since then, a number of experimental studies have been conducted to identify, verify, and predict biological membrane properties normally associated with the functional activity of cells and model cell membranes. Lipid rafts [49–54], preservation of cells [55–57], protein/peptide interactions with membrane [58–62], drug delivery vehicles [63–68], and validation of model drug molecules [69–73] are among the applications that are of current interest. In complement to these studies, investigations using computational methods have been employed to provide insight into the molecular interactions and mechanism, and to better understand these important biological processes.

For many years, experimental and computational studies of model lipid bilayers containing one type of lipid have shown valuable results of the features and functions of biological membranes. Recently, it has become apparent that a bilayer with more than one type of lipid is necessary to obtain a better representation of complex biological membranes and their functions. The following sections briefly describe some of the major findings from both experimental and computational studies of pure and mixed PC/PE bilayer systems.

2.1.2 Experimental Studies

Several experimental studies have investigated the structure of model cell membranes (phospholipid bilayers), including pure and mixed PC/PE lipids. For pure PC systems, the most commonly used lipid in model bilayers is DPPC. Inexpensive and relatively easy to make,

DPPC liposome provides a useful model for understanding lipid-lipid and lipid-water interactions that mimic interactions between membranes and intra/extracellular matter. Using DPPC as a model membranes, structural and dynamic properties have been analyzed using a range of analytical tools including X-ray diffraction [74–77], neutron scattering [78], and nuclear magnetic resonance (NMR) [17, 79–81]. Typical properties of interest are 1) the area per lipid, 2) volume per lipid, 3) lamellar repeated spacing, 4) bilayer thickness, 5) order parameter, and 6) diffusion coefficient. Depending on the biological process or function, other types of PC lipids such as DMPC (1,2-dimyristoyl-*sn*-glycero-3-phosphocholine) [82–84], POPC [45], and DOPC (1,2-dioleoyl-*sn*-glycero-3-phosphocholine) [85, 86] have been used as model lipid bilayer systems as well.

For PE and mixed PC/PE systems, most studies focused on the mechanism of intermolecular and intramolecular hydrogen bonds and the consequences of these interactions on the structure and phase behavior of PE lipid bilayers. This is because PE lipids have an amine headgroup (hydrogen-donor) which can form multiple hydrogen bonds with various hydrogen acceptors. Several analytical tools have been used to investigate these phenomena, including X-ray diffraction [48], NMR [20], differential scanning calorimetry (DSC) [87], Fourier transform infrared spectroscopy (FTIR) [88], and X-ray scattering [89]. Hitchcock *et al.* used X-ray diffraction to observe the structure and quantitatively measure the arrangement of artificial and natural membranes of DMPE molecules that were specifically labeled to characterize vibrational isotope effects [48]. They showed that the arrangement of the two lipid tails are asymmetric, where the first tail (*Sn*-1) extends perpendicular to the bilayer plane, and the second tail (*Sn*-2) extends in the bilayer plane and then bends and becomes parallel to the first tail (see Figure 1.4 for more information on the location of the *Sn*-1 and *Sn*-2 tails for a typical PC or PE lipid). This resulted in a different conformation of the ester carbonyl groups in which preferential hydrogen bonding between PE lipids or lipid-water can occur. Blume *et al.* used solid state ^{13}C and ^{2}H NMR to examine the phase equilibria and dynamic structure of binary mixtures of DPPC and DPPE [20]. They found a correlation

that relates the phase transition of the bilayer to the PE concentration. They further described lipid mixtures as non-ideal systems, where the existence of intermolecular hydrogen bonds in PE plays an important role in determining membrane properties. Boggs *et al.* used DSC to study the effect of hydrogen bonding and non-hydrogen bonding compound on the phase transition temperature [87]. They found that DPPE, as a hydrogen bond-donor, has the greatest effect on increasing the phase transition temperature. Hübner and Blume used FTIR to study intermolecular interactions of isotopically labeled lipids and water at the interface [88]. Their findings showed that the molecular vibrational modes of the phosphate and ester carbonyl groups are greatly altered as a result of hydrogen bonding between DMPE lipids or DMPE mixtures. Using this method, they were able to distinguish different hydration sites that exist in PE lipids. Recently, Dyck *et al.* used surface-sensitive X-ray scattering to study the surface of PE and their mono-, di-, trimethylated (DPPC) derivatives in monolayer conformations [89]. They determined that pure PE monolayers have the smallest headgroup and the orientation of the lipid nitrogen and phosphorus atoms aligned closer to the lipid/water interface as the headgroup size increased.

2.1.3 Computational Studies

Several computational studies have been performed on pure or mixed PC/PE bilayers. For pure PC systems, comprehensive summaries of the structural and dynamics properties of model membranes have been reported by several researchers using MD simulations [90–95]. In good agreement with experimental results, MD simulations of DMPC [96–101], DPPC [102–110], POPC [100, 101, 111], and DOPC [112, 113] have served as a benchmark for bilayer simulations. Typical structural and dynamic properties calculated from the simulations are: area per lipid, lipid components density profiles, membrane thickness, radial distribution functions (RDFs) of water around lipid headgroups, mean squared displacement of lipid headgroups (short-time diffusion coefficient), lipid tail deuterium order parameter, and headgroup hydration.

Recently, simulations of PE and mixed PE bilayers have received much attention as several biological functions have shown direct connection to PE lipids (see Chapter 1 for more details). Several studies have been carried out to identify the changes in membrane properties and investigate the mechanism of hydrogen bonding as PE is present in the bilayer. Damodaran and Merz used MD simulations to examine the water structure around DMPC and DLPE headgroups [114]. They were able to observe various structural properties, such as the hydrogen bonding interactions between the amine group of DLPE and neighboring phosphate oxygens, the tight alignment of lipid tails, and the ordering of the lipid tails compared to experimental deuterium order parameters. de Vries *et al.* also used MD simulations to examine DOPC and DOPE lipid mixtures at various concentrations [115]. They were able to observe a significant reduction in the cross-sectional area of the bilayer by having a small amount of DOPE in model lipid bilayers, which was attributed to the hydrogen bonding formed by DOPE. They also noted that by increasing the concentration of DOPC in lipid mixtures, the reverse effect was not observed because DOPC cannot disrupt the hydrogen bond network. Recently, Murzyn *et al.* used MD to examine POPG and POPE mixtures to mimic the interior of bacteria membrane [116]. They were able to predict the number of hydrogen bonded pairs that exist in the model membrane systems. This included intermolecular and intramolecular hydrogen bonds between lipids, lipid-water hydrogen bonds, water bridges, and lipid-water bridges. Their observations included structural properties, such as the atomic packing between POPG/POPE, average area per lipid molecule, and alkyl chain alignment, which has large effect in the membrane permeability and stability. In another recent study, Pitman *et al.* performed MD simulations of mixed SOPE and SOPC bilayers in the presence of cholesterol and rhodopsin to mimic the biological function of the photoreceptor protein [117]. Their findings included various structural properties, such as lipid-protein density profiles and Voronoi area, which provided evidence for the mechanism for cholesterol and rhodopsin stabilization of the lipid bilayers. In separate studies, detailed structural and dynamic properties of SOPE bilayer has been reported by Suits *et al.* [118] and Pitman *et al.* [119], respectively; the properties analyzed included

electron density distribution, lipid order parameter, amine-phosphate hydrogen bonding network, compressibility modulus, lateral organization, and diffusion. Marrink and Mark used a coarse-grained model with MD to study the fusion and budding mechanism using DOPC and DOPE mixtures [120]. To mimic this phenomenon, they specifically enhanced the hydrogen bonding capability of DOPE, so these strong interactions allowed a membrane fusion process to occur. Shi and Voth also used a coarse-grained model with MD to investigate the phase separation of mixed DPPC/DPPE lipids [121]. Using this model, they were able to simulate a large lipid mixture system containing a 1:1 ratio of DPPC/DPPE (2,048 lipid molecules in total). Their observations included various structural properties, such as the atomic packing, average surface area per lipid molecule, alkyl chain alignment, and lateral diffusion coefficient in both liquid-like and solid-like phases.

2.2 Lipid Bilayers with Disaccharides

2.2.1 Background

For several decades, the widespread usage of cryoprotectant agents in biological preservation has attracted multidisciplinary research to further understand these phenomena. There have been numerous studies and hypotheses on the effectiveness of these agents based on their chemical properties and their interactions with biological organisms. Naturally occurring stabilizing agents such as monosaccharides (e.g., glucose) and disaccharides (e.g., trehalose, and sucrose) have been experimentally found to be effective cryo- and lyo-protectants (protect against freezing-ice and freezing-dry, respectively) for animal and plant cells [122, 123]. Molecular structure of these molecules are shown in Figure 2.2.1. With trehalose acting as a stabilizing agent, cryo- and lyo-protection have allowed the preservation of animal cells at conditions above and below normal physiological conditions. The focus of these studies showed the direct interaction of trehalose with the cell membrane, consisted primarily of a phospholipid bilayer. For example, addition of a disaccharide into a liposome suspension
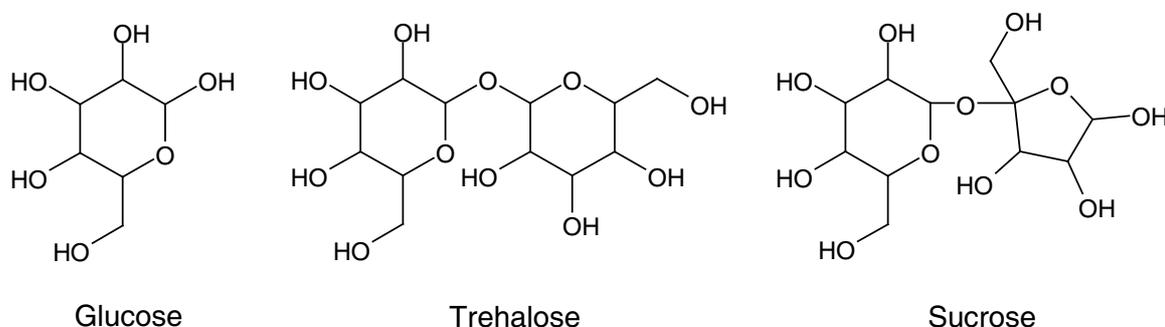
Figure 2.2.1: Molecular structure of monosaccharide (glucose) and disaccharides (trehalose and sucrose). Chemical symbols are hydrogen (H) and oxygen (O).
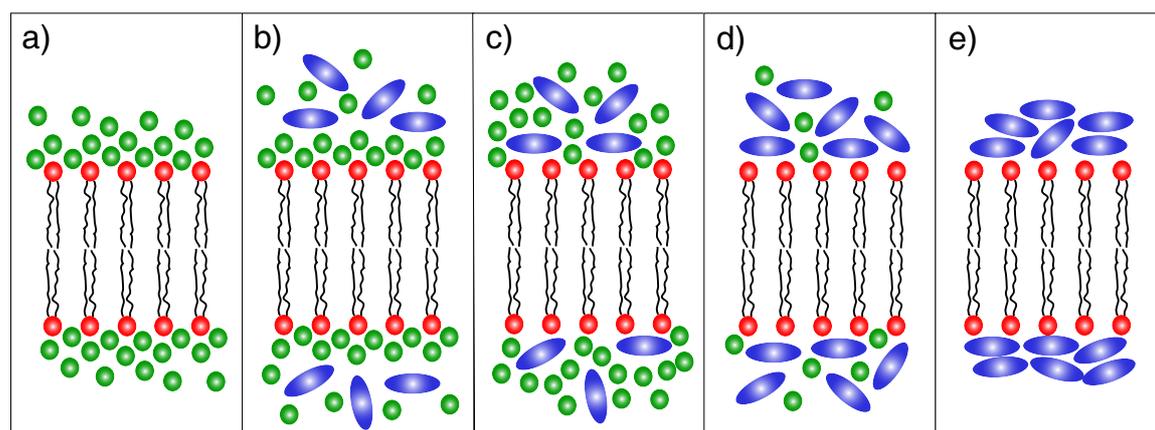
Figure 2.2.2: Schematic representation of the cell stabilization hypotheses: a) fully hydrated bilayer; b) "preferential exclusion principle"; c) water entrapment; d) water replacement; and e) vitrification. Lipids are represented in red, trehalose in blue, and water in green.

significantly prevented encapsulated solution leakage during freezing and freeze-drying [124, 125]. Inhibition of cell fusion, phase separation, and formation of non-bilayer phases were also observed in membrane experiments in the presence of trehalose [122, 126, 127]. Theoretical models and hypotheses have been proposed to explain the mechanism by which trehalose interacts with the phospholipid bilayer to stabilize the cell structure and biological function. A schematic representation of the stabilization hypotheses is shown in Figure 2.2.2.

In the preferential exclusion model (Figure 2.2.2b), it is suggested that disaccharide molecules are excluded from the vicinity of the biological structure, thus stabilizing the

hydration shell and maintaining the needed hydration of the lipids in the bulk under water deficit conditions [128]. In this case, disaccharide molecules directly interact with water within the solvation shell and act as an additional protective layer, excluding water from the surrounding. In the preferential interaction model (from hydrated to dehydrated to dry states shown in Figures 2.2.2c-e), several hypotheses have been proposed to explain the direct interaction of disaccharide molecules with the hydrophilic domain of biological structures under harsh condition, exhibiting protective and stabilizing effects [129].

Three of these hypotheses are 1) water-entrapment [130], 2) water-replacement [126], and 3) vitrification [131] (see Figure 2.2.2). In the water-entrapment hypothesis (Figure 2.2.2c), it is suggested that, during the drying process, trehalose strongly interacts with both water and phospholipid headgroups causing a slight increase in the hydration near the membrane interface [130, 132, 133]. Trehalose molecules that come in contact with the phospholipids provide additional and favorable exposure for water to bind to the hydroxyl groups in trehalose. This is a result of the hydrogen bonding between phospholipid-trehalose and trehalose-water, which helps to stabilize the membrane structure by maintaining a certain hydration level. In the water-replacement hypothesis (Figure 2.2.2d), it is suggested that trehalose serves as a substitute for water nearby the phospholipid polar headgroups in the drying process [122, 134]. In this case, trehalose forms hydrogen bonds with the phospholipid headgroups, resulting in the stabilization of the membrane structure in the dehydrated state.

Finally, in the vitrification hypothesis (Figure 2.2.2e), trehalose acts as a vitrified structure, protecting the membrane structure through the formation of an amorphous solid matrix in the drying process [131, 135–138]. This maintains the membrane structure in its fully hydrated state and prevents mechanical stress to the membrane under harsh conditions. Within the last decade, a number of experimental studies have linked these hypotheses, indicating that the water-replacement, the water-entrapment, and the vitrification processes are not mutually exclusive processes, but altogether they play a part in the preservation of biological structures [134, 135, 139, 140].

2.2.2   Experimental Studies

For a better understanding of the stabilization mechanisms, several investigations of model cell membranes (phospholipid bilayers) in the presence of disaccharides have been reported [55, 126, 141–144]. These studies included a number of analytical methods to probe the interactions between trehalose and the bilayer structure. Crowe *et al.* used DSC to measure the phase transition temperature of phospholipid bilayers containing DPPC with and without trehalose [126]. It was found that trehalose caused a significant drop of 30 K in the phase transition temperature from a gel to a liquid-crystalline state. This change was suggested to be caused by the replacement of water molecules surrounding phospholipids by trehalose. To verify this phenomenon, infrared spectroscopy was used to demonstrate the hydrogen bonding between the polar headgroups in DPPC and the hydroxyl groups in trehalose. Lee *et al.* used solid-state NMR to monitor the ^{31}P spectra of phospholipid bilayers; their studies indicated less mobility of the phospholipid headgroups upon binding of trehalose [141]. Luzardo *et al.* used FTIR to describe the hydration state of bilayers composing of DMPC and trehalose [142]. They determined that three trehalose molecules were able to bind to one DMPC by replacing 11 of 14 water molecules per phospholipid. It was concluded that water replacement occurs at the carbonyl and phosphate groups where the hydroxyl groups of trehalose change the water activity within the phospholipid solvation shell. Lambruschini *et al.* investigated the interaction of trehalose and phospholipid headgroups using Langmuir monolayers [143]. They showed that the critical area corresponding to the surface potential increased in phospholipid-trehalose systems, indicating that trehalose bound to the phospholipid polar headgroups. At high surface pressure, they also demonstrated a strong binding interaction, as trehalose remained intact on the phospholipid headgroups without being expelled from the surface. Ricker *et al.* used FTIR to study the phase behavior of 1,2-dilauroyl-*sn*-glycero-3-phosphocholine (DLPC) and 1,2-distearoyl-d70-*sn*-glycero-3-phosphocholine (DSPCd-70) bilayer mixtures in the presence of trehalose [55]. They observed that the DLPC component of the mixture is strongly fluidized by trehalose, while the DSPCd-70 component is unaffected when undergoing the drying process. After

a heating process, they observed that the phase separation between phospholipids is maintained, suggesting that trehalose preserves the structure and composition of the phases in microdomains. Recently, Ohtake *et al.* used DSC to investigate the melting temperature of DPPC, DPPE, and 1:1 DPPC/DPPE mixtures in the presence and absence of trehalose [144]. They found that trehalose caused the largest decrease in the melting temperature in DPPC, and the smallest decrease in DPPE, suggesting that DPPE exhibits strong interactions with the phospholipids, thus limiting the ability of trehalose to hydrogen bond with the polar headgroups in DPPE.

2.2.3   Computational Studies

Several computational studies have also been recently performed on model cell membranes in the presence of disaccharides to investigate the mechanism of interaction between phospholipids and disaccharides. Chandrasekhar and Gaber performed energy minimization on a phospholipid-trehalose system (without water) and found a slight increase in the area per phospholipid headgroup in the presence of trehalose [145]. They also showed that trehalose has favorable conformation to bridge several phospholipids by means of hydrogen bonds. In a similar study, Rudolph *et al.* found the phospholipid-saccharide interaction energy in the order of most to least stable (trehalose < glucose < sucrose) [146]. A more detailed study with molecular simulation was performed by Sum *et al.* [147], Pereira *et al.* [148], and Villarreal *et al.* [149] to investigate the interaction of trehalose with a model cell membrane (DPPC bilayer). These three independent studies reached similar conclusions in that trehalose interacts favorably with the DPPC polar headgroups at the phospholipid-water interface without altering the bilayer structure. At the concentrations studied, no significant changes in the area per headgroup and in the order parameter of lipid tails were observed from the simulations. The water replacement hypothesis was highlighted as a potential mechanism of interaction, where direct hydrogen bonding was observed between trehalose and DPPC; and these interactions were enhanced when the bilayer was subjected to dehydrated conditions.

Recently, Doxastakis *et al.* performed detailed MD simulations of model lipid bilayers embedded with cholesterol in the presence of trehalose [150]. That study investigated the stabilization mechanism of trehalose on a more realistic composition of a cell membrane, in which a wide range of cholesterol concentrations were used in the models. At high concentrations of cholesterol, they found that trehalose is able to stabilize the bilayer structure by preventing a phase separation between lipid and cholesterol. The stabilization mechanism of trehalose was confirmed by the interactions between lipids and trehalose, which resulted in the slow movements of lipid molecules and consequently inhibited the changes in lateral organization of the bilayer. In another study, Pereira and Hünenberger performed detailed MD simulations of model bilayer in the presence of glucose, maltose, and trehalose [151]. At high solute concentrations, they observed that glucose, maltose, and trehalose interact directly with the lipid headgroup and replace 20-25% of the total number of hydrogen bonds between lipid and water molecules. For disaccharides, they observed an increase in the number of hydrogen bonds that bridge three or more lipids. Unlike disaccharides, glucose replaced water around the lipid headgroup by increasing the number of interactions rather than forming multiple hydrogen bonds.

2.3 Dehydrated Lipid Bilayers with Saccharides

2.3.1 Background

In general, cells cannot survive under dehydrated conditions mainly because cell membranes are unable to maintain their normal functionalities of protecting and preserving the cellular content [137, 152], and controlling the transport and permeability activities through the cell membrane [153–156]. A number of organisms have been found to survive under anhydrobiotic conditions over extended periods of time. A common characteristic of these organisms is their abundant production of saccharides in the cellular environment, which has been identified to be essential to their survival [140, 157]. It was concluded that the ability of living organisms

to survive in such conditions is determined from the functional state of the cell membrane, that is, the membrane fluidity. These findings have led to the successful use of saccharide compounds (e.g., glucose, maltose, sucrose, and trehalose) as additives to protect animal and plant cells at low temperature and/or dehydrated conditions [122, 123].

2.3.2 Experimental Studies

A number of experimental studies have investigated the properties of low hydration or dehydrated lipid bilayers in the presence of saccharide compounds [158–162]. Crowe *et al.* investigated the effect of saccharides (glucose, inositol, sucrose, trehalose, and raffinose) on DMPC and DPPC monolayer films under dehydrated conditions using a Langmuir film balance [158]. Their results showed that the area per lipid increased with increasing saccharide concentrations, with trehalose providing the largest monolayer lateral expansion. Furthermore, Crowe *et al.* used DSC to investigate the phase behavior of dry DPPC liposomes and found that the phase transition temperature of liposomes is significantly lowered with increasing saccharide molecular size from $T_{\mathrm{m}} = 110°C$ (no saccharide) to $T_{\mathrm{m}} = 40°C$ with glucose (MW = 180.16 g/mol), to $T_{\mathrm{m}} = 24°C$ with trehalose (MW = 342.40 g/mol), and to $T_{\mathrm{m}} = 17°C$ with raffinose (MW = 504.44 g/mol) [159]. Based on these results, it was proposed that saccharide molecules preferentially interact with the lipid headgroups through hydrogen bonding, thus increasing the membrane fluidity by spacing the lipids in the bilayer. Similarly, Koster *et al.* investigated the phase behavior of liposomes/saccharides during the vitrification process and the effect of saccharide molecular size on the phase transition temperature [160–162]. They concluded that the presence of saccharides with MW≤1000 prevents membrane fusion by keeping membranes partially in their original hydrated state, preventing close interactions between neighboring membrane surfaces, and reducing the mechanical stresses between membranes, which was induced by structural reorientation prior to fusion. This was explained in details by Bryant and Wolfe [163], who attributed osmotic (keeping water on the membrane surface) and volumetric (keeping lipid components in the membrane apart) effects as

important factors in lowering the phase transition temperature of model bilayers containing saccharide compounds.

2.3.3 Computational Studies

From a computational/modeling approach, only a few studies have addressed the impact of saccharides on the properties of low hydration or dehydrated lipid bilayers [164–166]. Skibinsky *et al.* used molecular dynamics (MD) simulations to investigate changes to lipid bilayer and monolayer structures exposed to a high trehalose concentration (1:2 trehalose/lipid ratio) [164]. Their studies considered constant surface area and constant surface tension simulations for the lipid monolayers and bilayers, respectively. Note that these monolayers were constructed by inverting a lipid bilayer system, such that the aqueous phase was in the middle of the simulation box and the lipid tails exposed to a vacuum (this results in two monolayers). At hydration levels of 20-29 water per lipid for the monolayers and bilayers, they observed that trehalose displaced a significant amount of water from the lipid interface while slightly increasing the bilayer lateral pressure, which consequently decreased the overall bilayer surface tension. Their results suggested that the penetration of trehalose is only superficial (along the lipid surface) and the mechanism of stabilization occurs in the lipid headgroup region. Recently, Doxastakis *et al.* studied the phase transition of anhydrous DPPC liposomes, representative of lipid bilayers at dehydrated conditions [165]. Both elastic and quasielastic neutron scattering (QENS) were utilized to evaluate the dynamics of the lipid headgroups and lipid tails, above and below the phase transition temperature. The scattering measurements showed that the movement of the lipid tails was significantly greater than the lipid headgroups and highly sensitive to temperature changes. Upon reducing the water content, it was observed that the mobility of the lipid tails was closely coupled to that of the headgroups. This was confirmed by their MD simulation studies of the identical bilayer systems using dehydrated multi-lamellar DPPC bilayers. Another study

investigated lipid bilayers at different hydration states by considering the interactions between DPPC liposomes and saccharide compounds (glucose and sucrose) [166]. Their results from DSC measurements and thermodynamic modeling showed a significant increase in the phase transition temperature upon decreasing the hydration of the bilayer in the absence of glucose or sucrose. On the other hand, the presence of glucose or sucrose reduced the phase transition temperature. From this data, an optimal amount of saccharide was experimentally measured (1.5 sugar-rings per lipid) and predicted from the thermodynamic model (0.5 sugar-rings per lipid). They attributed this discrepancy to the exclusion effect of saccharides near the bilayer interface.

2.4 Phase Transition of Phospholipid Bilayers

2.4.1 Background

The ordered (gel) and disordered (liquid-crystalline) lipid phases have been a major focus of studies on the phase behavior of biological membranes, which relates structural characteristics and dynamics of membranes to individual lipid components. From recent studies, it has become apparent that both ordered and disordered lipid phases co-exist within eukaryotic cell membranes [36]. Structurally, ordered domains are enriched with phospholipids, sphingolipids, and cholesterol. From a biological standpoint, several studies have suggested that ordered domains in cell membranes are partly associated with their function, including signal transduction [37, 38], protein transport [37, 39, 40], and membrane sorting [37, 39]. Other studies of these ordered domains have also suggested that they serve as a possible binding site for various pathogens and toxins [41–43]. In related studies, a prominent role of cholesterol in membranes has been shown to create ordered lipid domains and lipid rafts [167–169].

2.4.2 Experimental Studies

Several experimental investigations for the lipid bilayers phase behavior have characterized the structural and dynamic properties of saturated lipid bilayers in gel, liquid-crystalline, and transition states. Suurkuusk *et al.* provided quantitative analysis based on calorimetric and fluorescent studies of uni- and multi-lamellar DPPC vesicles [170]. Their heating scan of multi-lamellar vesicles showed a transition process that closely resembled a first-order phase transition, which was confirmed by fluorescent measurements. For uni-lamellar vesicles, the heating scan showed significantly different phase behavior, as two distinct endotherm peaks with subtle changes in the fluorescence measurement during the phase transition were observed. Although these differences were identified between uni- and multi-lamellar vesicles, no clear explanation was provided to justify their findings. Davis used deuterium magnetic resonance to study the liquid-crystalline, gel phase, and phase transition of multi-lamellar labeled DPPC vesicles [171]. His work provided quantitative measurements based on the deuterium spectra, which showed a sharp drop in the order parameter values upon heating the vesicle, a clear indication of a first-order transition. Huang and Li reported an extensive summary of studies of the main phase transition (gel to liquid-crystalline) of phospholipid bilayers using high-resolution differential scanning calorimetry (DSC) [21]. The lipids used in their investigation were saturated and unsaturated PC, PE, and PG (phosphatidylglycerol) with different acyl chain lengths. Based on their DSC measurements, a clear identification of a first-order phase transition was found from the sharp endotherm peak in their heating scans of the bilayers. Nagle and Tristram-Nagle compiled studies of lipids at the liquid-crystalline state for DPPC, DMPC, DOPC, and DLPE containing structural data based on X-ray diffraction, NMR, and neutron scattering [172]. Their discussion also included a brief review of structural properties of DPPC at the gel, sub-gel, and ripple phases. Metso *et al.* provided an extensive DSC analysis and timed-resolved fluorescence spectroscopy to determine the nature of the phase transition of uni-lamellar DPPC liposomes [173], obtaining similar results to those by Suurkuusk *et al.* [170]. From their analysis, however, they attributed the subtle

changes in fluorescence intensity at the phase transition for uni-lamellar bilayers to a second-order rather than a first-order phase transition.

Currently, there is less molecular evidence for the mechanism of structural changes of the phase transition for unsaturated lipids than for saturated ones. A number of analytical tools, such as differential thermal analysis (DTA), differential scanning calorimetry (DSC), Raman spectroscopy, nuclear magnetic resonance (^{2}H NMR), and electron density map (EDM), have been employed to study the phase transition for various type of unsaturated lipids [45, 163, 174–178]. Barton and Bunstone were the first to investigate the phase transition of PC derivatives with varying chain length and degree of unsaturation using DTA and DSC [174]. With experiments on DPPC, POPC, and DOPC, they determined that a single unsaturation (a double bond) near the center of the *Sn*-2 tail of POPC is the most effective in lowering the melting temperature. They also concluded that changes in the chain packing are indicative of a phase change. Litman *et al.* used Raman spectroscopy to measure the intensity of the carbon-carbon and carbon-hydrogen bond stretching modes for monounsaturated and polyunsaturated lipids at several temperatures [45]. Based on the temperature profile derived from the carbon-hydrogen stretching intensity, they determined a phase transition temperature for POPC at approximately 270 K. They also observed that an increase in the degree of unsaturation results in an increase in lattice defects in the gel-phase, which were expressed as a lowering of chain melting temperature.

Bryant *et al.* used ^{2}H NMR to investigate the reduction in spectral splitting of the deuterium spectra of D$_2$O/phospholipid systems for POPC and POPE near the main phase transition [163]. For POPC the splitting intensities were stable above and below the phase transition, but dropped to zero at or near the phase transition. For POPE, similar splitting intensities were observed, however, the intensities became unstable near the main phase transition, corresponding to a temperature range of 20 degrees. From these findings, they concluded that the phase transition for POPE occurs at a much broader range of temperatures compared to POPC. Huang and co-workers used DSC to measure the phase transition of PC and PE derivatives with different carbon number in the saturated

and unsaturated tails [175, 176]. Their studies determined structural features of the lipid systems that included the bilayer thickness, the length of the hydrocarbon tail segment before and after a double bond, and the level of interdigitation. With this collection of results, a correlation was derived for the phase transition temperature. However, the authors presented no clear explanation for the mechanism of phase changes. Recently, Shalaev and Steponkus performed a combination of DSC and NMR experiments to investigate the phase transition of POPE liposomes at different hydration levels [177]. Measured parameters included the lateral diffusion, axial rotation of the molecule, *tran-gauche* isomerization, and rotational moment of the phosphorus headgroup. A phase diagram for the POPE/water system was constructed as a function of water content and temperature. Their analysis determined a main phase transition temperature (L_β to L_α) at approximately 313 K for 7.3 wt% water content. In another study using EDM, Sengupta *et al.* reported a stable phase between a gel and a liquid-crystalline which was identified as a ripple phase (a combination of lipids in the gel and liquid-crystalline phase which resulted in the unevenness of bilayer strucutres) for several types of PC lipids, including POPC [178]. Results from their experiments showed that POPC exhibits less ripple formation than other PC lipids mainly due to the asymmetric unsaturated chain lengths.

2.4.3   Computational Studies

A number of computational studies investigating the phase behavior of saturated phospholipids have been reported using various modeling techniques, such as Monte Carlo (MC) simulations [179–182], mean field theory [183], dissipative particle dynamics (DPD) simulations [184], atomistic [185–187] and coarse-grained (CG) [188, 189] molecular dynamics simulations. Mouritsen *et al.* used MC simulations to study the first-order gel-fluid phase transition of lipids [179]. Since at that time thermodynamic properties at the transition state were scarce, they were the first to report the average lipid chain cross-sectional area, internal and free energies, coherence length, lateral compressibility, and specific heat. Nielson *et*

al. also applied MC methods to investigate the phase behavior of single and multi-component membranes containing cholesterol [180]. However, their model was developed based on an off-lattice model with lipid and cholesterol molecules represented by hard-spheres. Their simulations provided consistent interpretation of a first-order phase behavior for pure lipid and lipid-cholesterol bilayer systems. Using a similar approach, Polson *et al.* determined the lateral diffusion coefficient of lipids across the main phase transition temperature [181]. Their results suggested a significant change in the lateral diffusion of the lipids, which was found to be comparable to available experimental results. Later, Brannigan *et al.* investigated the phase behavior of a spherocylinder lipid model with MC simulations [182]. Their simulations showed distinct differences in the area per lipid and lateral diffusion coefficient for the solid and liquid phases. They also observed a third regime corresponding to a hexatic phase, a transition state between gel and liquid-crystalline phases, exhibiting intermediate values for the area per lipid and lateral diffusion coefficient. Chen *et al.* applied a macroscopic model based on the Gibbs potential to describe the transition state of lipids [183]. They reported the estimated values for phase transition temperature, enthalpy, van der Waals energy, number of *gauche* bonds, and chain orientational order parameter. The prediction using their model provided excellent agreement with experiment and thermodynamic properties such as internal energy and entropy of the system. Kranenburg *et al.* used DPD to study the phase behavior of lipid bilayers using model surfactants [184]. This technique allowed them to monitor the area per lipid and the bilayer thickness, both of which drastically changed at the phase transition from a gel to a liquid-crystalline phase.

Atomistic simulations of the phase transition for saturated lipid bilayers are scarce. Heller *et al.* [185] and Venable *et al.* [186] performed MD simulations of lipid bilayers in both gel and liquid-crystalline states. Despite the short duration of their simulations, their results provided insight into several lipid properties, such as, internal pressure, lipid self-diffusion coefficient, order parameter, D-spacing (repeated spacing normal to bilayer), chain tilt, and *%gauche*. Recently, de Vries *et al.* performed a detailed MD study of the phase behavior of lecithin (DPPC) using atomistic models [187]. Their simulation showed a spontaneous

formation of a ripple phase upon cooling of a fully hydrated DPPC bilayer below the main phase transition temperature. More recently, there have been a number of studies based on CGMD models to investigate the phase behavior of lipids. Stevens showed that DPPC bilayers have tilted lipid chains at low temperatures [188]. Moreover, the simulations indicated a large hysteresis in the area per lipid and bilayer thickness in heating and cooling cycles of the lipid bilayer, resulting in conditions that are difficult to identify the phase transition. In another CG study, Marrink *et al.* investigated a gel phase formation for DPPC membranes [189]. They suggested a four-stage reversible process from a gel to a liquid-crystalline phase: nucleation, growth, limited growth, and optimization. Their simulations yielded a main phase transition at about 295 ± 5 K and a lateral diffusion coefficient in the order of 1×10^{-9} cm^2/s.

While simulation studies of unsaturated lipids are abundant, there are only a few that address the structural properties in relation to the phase transition [111, 175, 190]. Wang *et al.* performed molecular mechanics on several monounsaturated PE lipids to examine the influence of the position of the unsaturation in the Sn-2 tail on the phase transition temperature [175]. As an approximation, the lipids were replaced by the corresponding diglyceride components. The energy-minimized structures and steric energies for the diglyceride moieties were related to the main phase transition temperature for the different positions of the unsaturation along the Sn-2 tail, which were confirmed by DSC experiments. It was proposed that a major component for the phase transition was an entropy-driven process. For POPE, their experimental and calculated phase transition temperature was about 306 K. In another study, Ceccarelli and Marchi performed atomistic MD simulations of a POPC bilayer at low hydration, by varying the temperature from 260 to 420 K, in increments of 40 K every 50 ps [111]. From snapshots of the bilayer structure at 260 K, a bent configuration at the *cis* double bond in the Sn-2 tail and a tilted configuration in the Sn-1 tail was observed. From the volumetric analysis of the bilayer at different temperatures, a discontinuity around 340 K was identified, which was assumed to correspond to the main phase transition temperature for POPC bilayer. The phase transition mechanism was not discussed from

their results mainly because their simulations were unable to achieve equilibrium at each time interval. Based on another approximate method, Marsh employed a thermodynamic model to relate the phase transition temperature of monounsaturated lipids to structural and entropic/enthalpic data [190]. Comparison of his results to Huang and co-workers [176] showed good agreement with previous experimental and computational results. This mathematical model provided a thermodynamic basis for understanding the dependence of the phase transition on structural parameters.

2.5 Cellular Toxicity and Protective Role of Trehalose

2.5.1 Background

Nonesterified long-chain free fatty acids (FFAs) are major sources of cellular energy [191] and essential components in triglycerides (TGs), cholesteryl esters, prostaglandins, and phospholipid syntheses [192, 193]. There have been numerous reports on the toxic effects of fatty acids on model cells *in vitro*. Andrade *et al.* showed that both saturated and unsaturated fatty acids exert toxic effects on melanoma cells through the loss of membrane integrity or DNA fragmentation [194]. Lima *et al.* evaluated the toxicity of various fatty acids on Jurkat (T-lymphocytes) and Raji (B-lymphocytes) cells [195] and found a positive correlation between the toxicity and the chain length and number of double bonds in the fatty acids. Their experiments identified palmitate among the most toxic of the fatty acids. FFAs, especially saturated fatty acids, can cause cell death in many types of cells, including pancreatic beta-cell [196, 197], cardiomyocytes [198, 199] and hepatocytes [200–202].

2.5.2 Experimental Studies

Most of the research up until now on the mechanism of cell death focused on the production of potential or toxic intermediates, such as stearoyl-CoA desaturase 1 (SCD1) [203–205],

acids from omega oxidation [206, 207], reactive oxygen species (ROS), ceramide [208, 209], reduced mitochondrial potential [198], and reduction of mitochondrial Bcl-2/Bax ratio [201]. Recent studies by Srivastava and Chan suggested that palmitate can cause lipotoxicity in liver cells through increased production of hydrogen peroxide (H_2O_2) and hydroxyl ($^*OH$) radicals [202]. Their measurements indicated that the cytotoxicity was not completely prevented upon treatment with mitochondrial complex inhibitors or free radical scavengers. This suggests that mechanisms other than ROS production in the mitochondria may be contributing to the toxicity of palmitate. Therefore, it is necessary to investigate the possibility that palmitate-induced toxicity may be due to hydrophobic effects on the cellular membrane. Fatty acids are known to have toxic and fusogenic effects on cells [210, 211]. Furthermore, the mechanism by which fatty acids exert cytotoxicity has been identified as the "detergent effect" [212]. According to this hypothesis, ionized fatty acid micelles solubilize membrane lipids or proteins and disrupt the physical and functional integrity of cell membranes [210, 211].

Identifying chemical agents to prevent or reverse the effect of fatty acid induced cellular toxicity has been a major focus of research in the past decades. Studies have suggested that saturated and unsaturated fatty acids have different effects on toxicity. For example, there is evidence indicating that dietary oleic acid can protect endothelial cells against hydrogen peroxide-induced oxidative stress and reduce the susceptibility of low-density lipoproteins (LDLs) to oxidative modifications [213–215]. Similarly, Srivastava and Chan found that oleic acid does not induce the same level of cytotoxicity as palmitic acid in HepG2 cells (human hepatocellular liver carcinoma cell line) at similar concentrations [202] and the addition of oleic acid reduces the cytotoxicity induced by palmitate [216]. In another related study, Kinter *et al.* investigated the protective role of unsaturated FFA in oxygen-induced toxicity of hamster fibroblasts and found that monounsaturated FFA increased cell survival as compared to saturated and polyunsaturated FFAs [217]. Furthermore, it has been shown that unsaturated FFAs rescued palmitated-induced apoptosis by converting palmitate into triglycerides [203]. Recently, Natali *et al.* investigated the effects of various types of FFAs

in glial cells and found that oleic acid was a potent inhibitor of fatty acid and cholesterol synthesis [218].

In recent years, it has been established experimentally that trehalose has a stabilizing effect on biological membranes [219] by protecting cells from dehydration, heat, and cold [126, 220, 221]. Moreover, evidence is mounting suggesting that trehalose acts as an antioxidant, possibly serves as a free radical scavenger [222–224], and inhibits the peroxidation of unsaturated fatty acids by heat or oxygen radicals [224, 225]. In addition, trehalose has been found to protect yeast cells and cellular proteins from damage by oxygen radicals during oxidative stress [226].

2.5.3   Computational Studies

There have been MD simulations to investigate separately the biological functions of trehalose [148–151, 227, 228] and saturated fatty acid molecules [229–231] and their interaction with the lipid bilayer. Extensive reviews for bilayers with saccharides are described in Sections 2.3-2.4. For bilayers with saturated fatty acids, Choi *et al.* investigated the effect of long chain transmembrane dicarboxylic acid (32 carbon chain with terminal carboxylic acids) on palmitic or oleate bilayers [229]. Their simulations results indicated that the movement of fatty acids adjacent to the dicarboxylic acid (measured from the mean-squared displacement) were significantly reduced and the lipid tail order parameters increased. They concluded that the presence of dicarboxylic compounds regulates the mechanical and transport properties of biological membranes by controlling membrane fluidity. In another study, Ulander and Hayman used MD simulations to study the diffusion and permeation of valproate/valproic acid (a branched saturated fatty acid) through the model DPPC bilayers [230]. Based on their simulation results, they estimated the free energy profiles (5-8 kcal/mol), permeation coefficient (2.0×10^{-3} cm/s), and diffusion coefficient ($\sim 10^{-6}$ to $\sim 10^{-5}$ cm^2/s) of valproic acid translocation along the bilayer normal. Furthermore, Knecht *et al.* investigated the mechanism of membrane fusion of model bilayers containing palmitate by monitoring the

change in phase behavior of the bilayers using MD simulations [231]. With a ratio of 1:2 for DPPC/palmitate, they observed a direct phase transformation from a gel to an inverted hexagonal phase. During the transformation process, a metastable bilayer was observed with interlamellar connections or stalks formed and elongated prior to the formation of an inverted hexagonal phase.

2.6 Effect of Fatty Acids on Biological Membranes

2.6.1 Background

Unbound free fatty acids (FFAs), derived from dietary triglycerides (TGs) and phospholipids, are aliphatic monocarboxylic acids, which are among the most important energy sources for cells and tissues [192, 193]. Typically containing a lipid chain between 4 and 28 carbons, FFAs are classified according to the degree of unsaturation: saturated, monounsaturated, and polyunsaturated [23–26]. The FFA concentration in the plasma is regulated by plasma protein albumin, that leaves about 0.01 mmol/l unbounded [211, 232]. Recently, *in vitro* studies confirmed that saturated FFAs induced significant toxic effects on various cells types, however, unsaturated FFAs have been shown to reduce and/or prevent toxic effects by saturated FFAs [194, 197, 201, 202]. Note that both saturated and unsaturated FFAs can be transported through the membrane into cells through passive and active transport. Once inside the cells, FAs can modify the lipid membrane properties by altering the membrane fluidity and in turn affecting cellular function [233, 234]. Based on this fact, it is speculated that, unlike saturated FAs, the presence of unsaturated FAs may help maintain or restore membrane fluidity to its normal state.

2.6.2 Experimental Studies

There have been numerous studies that examined the effects of unsaturated FAs on lipid bilayers or liposomes. For example, Sunamoto *et al.* investigated the autoxidation of egg phosphatidylcholine (EPC), arachidonic and linoleic acids in homogeneous solution and liposomal membrane systems [235]. Using 1,1-diphenyl-2-picrylhydrazyl as radical, they found that the oxidation rate of unsaturated FAs or lipids was faster with the membrane systems as compared to the reaction in solution. Using fluorescence polarization technique, their results suggested that the reaction mechanism is controlled by membrane fluidity. In another related studies, Lee *et al.* exposed liposomes containing different amounts of oleic, linoleic, and arachidonic acid to oxidizing medium and found that liposomes containing linoleic and arachidonic acid were less susceptible to oxidation than oleic acid [236]. After exposing the fragments of lipid peroxidation to endothelial cells, it was found that the amount of monocyte chemotaxis and monocyte adhesion were significantly increased, thus concluding that oxidation products of linoleic and arachidonic acids can trigger cellular immune response. Furthermore, Samuni *et al.* investigated the oxidative damage of EPC liposomes containing arachidonic acid (C20:4), *cis*-7,10,13,16,19-docosapentaenoic acid (C22:5), and *cis*-4,7,10,13,16,19-docosahexaenoic acid (C22:6) in the presences of vitamin E, antioxidant (Tempo), and cholesterol [237]. Their results showed that all polyunsaturated FFAs are highly sensitive to oxidation and hydrolytic degradation. Based on the residual fragment of FFAs collected over time, cholesterol demonstrated selective protective effect, while Tempo was better antioxidant than vitamin E. Recently, Watabe *et al.* examined the decomposition rate of unsaturated FAs in DPPC liposomes, containing photoporphyrin IX (PpIX), from light irradiations and determined the oxidation rate, from fast to slow: arachidonic acid < oleic acid < α-linoleic acid < linoleic acid [238]. Although oleic acid contains fewer double-bonds than linoleic derivatives, it has a greater oxidation rate because the location of the double-bond is in close proximity to the PpIX molecules embedded within the bilayer. In summary, experimental studies mentioned above are based on the resulting products of lipid oxidation, however, none have addressed the interactions between the lipid constituents and

the FAs at the initial stage of this process.

2.6.3   Computational Studies

To gain insight and understanding of the effect of unsaturated FAs on cell membranes, several studies using molecular dynamics (MD) simulations have been reported investigating, separately, the biological functions of fatty acid molecules and their interactions with the lipid bilayers [231, 239, 240]. Hyvönen *et al.* investigated the phospholipid component of membranes that are hydrolyzed into fatty acids by phospholipases A2 enzyme [239]. Using PLPC, lyso-PC molecules (a PC headgroup with glycerol backbone and palmitic acid chain), and linoleate/linoleic acid in the model, they found that the bilayers became unstable, as a result of the penetration of water into the core region of the bilayer. Furthermore, Knecht *et al.* investigated the mechanism of membrane fusion of model bilayers containing fatty acids by monitoring the change in phase behavior of the bilayers using MD simulations [231]. With a lipid/fatty acid (DPPC/palmitic acid) ratio of 1:2, they observed a phase transformation from a gel to an inverted hexagonal phase. During the transformation process, a metastable bilayer was observed where interlamellar connections or stalks were formed and elongated prior to the formation of an inverted hexagonal phase. Recently, Wong-ekkubut *et al.* investigated the structural properties of PLPC bilayers in the presence of oxidized lipids and fatty acid derivatives, at different concentrations [240]. The fatty acids considered were 9-*trans*, *cis*-hydroperoxide linoleic acid, 13-*trans*, *cis*-hydroperoxide linoleic acid, 9-oxo-nonanoic acid, and 12-oxo-9-dodecenoic acid. Their results showed an inverse correlation between the degree of oxidation and membrane thickness. By increasing the fatty acid content in the bilayers, they found an increase in the bilayer surface area while the bilayer thickness was significantly reduced. Their permeation analysis showed that water molecules were able to penetrate more easily through the bilayer, thus destabilizing the bilayer structure. They attributed the toxicity effect of the oxidized lipids to an increase in the membrane permeability.

2.7 Conclusions

The relevant literature review for the topics of this study is divided into six sections: mixed lipid bilayers, lipid bilayers with disaccharides, dehydrated lipid bilayers with saccharides, phase transition of lipid bilayers, and protective role of trehalose and unsaturated fatty acids in cellular toxicity. Each section is presented with a detailed background to the research topic along with several significant contributions from experimental and computational studies.

For the mixed lipid bilayers, MD simulations are shown to be an essential tool in understanding the complexity of the membrane matrix. Two MD simulations methods have been proposed: atomistic and coarse-grained models. The main advantage of atomistic over the coarse-grained models is the ability to investigate fine structural details, however, at the cost of computational time and smaller bilayer size. As a result, the lipid bilayer size is an important factor when considering a basic building block for membrane studies using atomistic models. Another important factor in modeling the membrane structure is the bilayer composition. Due to the many types of PC and PE lipids that exist in biological membranes (PC and PE derivatives), the use of mixed PC and PE bilayers have been limited in modeling complex membrane structures. As such, mixture of lipids is considered in Chapter 4. The results discussed in Chapter 4 provide a detailed analysis of structural and dynamic properties of DPPC/DPPE mixtures commonly encountered in biological systems.

For lipid bilayers with disaccharides, only one kind of lipid bilayer (DPPC) has been used to model the interactions with trehalose using atomistic model. However, cell membranes are composed of a range of lipids that vary both in the headgroup and fatty acid composition. In order to obtain a better assessment of the interactions of trehalose with a more realistic bilayer structure, the studies reported in Chapter 4 also present the simulations of mixed lipid bilayers containing DPPC and DPPE in the presence of trehalose. The simulations provide a detailed analysis of the structural and dynamic properties of DPPC/DPPE-trehalose systems commonly encountered in biological systems.

Even though the process of preserving liposomes in the dehydrated state is well-known, there is still limited knowledge at the molecular level on the properties of dehydrated bilayers and the role of saccharides in their stabilization. Since few attempts have been made to study uni-lamellar bilayers under dehydrated conditions in the presence of saccharides, Chapter 5 reports the interactions of lipid bilayers with glucose or trehalose under dehydrated conditions using MD simulations. The simulations presented also provide insight into how mono- and disaccharides stabilize the bilayer structure.

For the phase transition of lipid bilayers, lipid bilayers composed of DPPC have been used extensively to model the phase behavior from a gel to a liquid crystalline phase. It has been shown that the mechanism of phase transition for lipid bilayers is directly related to structural changes in the bilayer. This is important because, from a biological standpoint, studies have suggested that the co-existence of two lipid phases in cell membranes is closely associated with their functions, including signal transduction, protein transport, membrane sorting, and presentation of putative binding sites for pathogens and toxins. Despite a number of studies in this field, coarse-grained models are better suited to obtain insight into the phase behavior of lipids, as large bilayers and long simulations are required to obtain multi-scale properties of membranes. However, coarse-grained models are unable to capture detailed molecular features and characteristics of the lipid molecules and more subtle structural properties of the bilayers. As such, the phase transition studies of complex lipids cannot be modeled by coarse-grained methods, as important molecular features are not explicitly shown. The study in Chapter 6 investigates the structural changes of various lipid bilayers near the main phase transition using atomistic models. In this case, lipid bilayers composed of DPPC, DPPE, POPC, and POPE are considered. The simulations provide insightful information of saturated and monounsaturated lipid bilayers at and near the main transition state and valuable structural data to understand the mechanism underlying phase transitions.

For fatty acid-induced cellular toxicity, a series of experimental and computational

measurements are collected to gain insight into how trehalose interacts with liver cells (human hepatocellular carcinoma cell line, HepG2 cells) in the presence of palmitate. As shown in Chapter 7, the experimental measurements focused on determining the influence of palmitate and trehalose on the fate of HepG2 cells (performed by collaborators at Michigan State University), and the computational part aims at interpreting and understanding the experimental results, shedding light into the role of palmitate and trehalose in the toxicity of HepG2 cells. In addition to Chapter 7, Chapter 8 adds computational investigations using DOPC lipid bilayers exposed to saturated and unsaturated fatty acids (palmitate, oleate, and linoleate). These are modeled to determine the role of unsaturated fatty acids in reducing cellular toxicity. This study aims at predicting and understanding the interactions of fatty acids embedded inside the lipid bilayers and identifying the role of unsaturated fatty acids in preventing changes in membrane fluidity. Insight into these mechanism will add to our understanding of processes (i.e., metabolic, signaling, and biophysical) that are induced by free-fatty acids. This study represents the first attempt to obtain a comprehensive understanding of the biochemical and biophysical processes leading to and resulting from the toxicity of palmitate on cells.

Chapter 3

Molecular Dynamics Simulations

The vast majority of experimental measurements report average molecular properties, either as time average and/or ensemble average. For biological membranes, molecular properties measured from experiments are limited to those obtained from X-ray diffraction/scattering, NMR, differential scanning calorimetry (DSC), and Fourier transform infrared spectroscopy (FTIR), to name a few (see previous experimental studies in Chapter 2). The ability to predict the structure and dynamics of membranes at the atomic level using these analytical tools is a rather difficult task. This is partly due to the complexity of biological membranes, the fluid state of membranes at physiological conditions, and the lack of experimental data that correlate the position and motion of atoms/molecules. Within the past two decades, the increasing power of computational resources has created many new approaches to study lipid bilayers and has enhanced the experimentalist with the ability to provide detailed structural and dynamic properties of model lipid bilayers.

Since the main tool for this study is molecular dynamics (MD), other theoretical approaches such as stochastic dynamics [241, 242], continuum electrostatic methods [243], Monte Carlo [241], mean-field [244], and phenomenological [245, 246] methods will not be discussed (see previous computational studies in Chapter 2 for more details). MD was originally developed to study the dynamics of liquids, which were represented by solid spheres

and Lennard-Jone particles [247, 248]. Today, MD simulations have become an indispensible tool in the molecular understanding of biochemical and biophysical processes, made possible by accessible and efficient simulation programs, such as AMBER [249], CHARMM [250], GROMOS [251], GROMACS [252], and NAMD [253], to name a few. Among the many applications of MD simulations is the study of lipid bilayer systems [254–257]. It was evident from early studies that atomistic models of lipid bilayers were able to provide insight into the molecular properties of lipids and their interactions and role in biological environments.

Most MD codes are suitable to model lipid bilayers, however, GROMACS has gained considerable acceptance as one of the best simulation platform. In additional to being an open-source code, GROMACS is capable of performing large-scale simulations with good scalability in parallel architectures [258, 259]. MD simulations most often describe systems with empirical force-fields, so that interactions at the atomistic level can be related to predict microscopic and macroscopic properties of the system. A brief overview of molecular dynamics, in the context of the methods implemented in GROMACS, is discussed in this chapter.

3.1　Simulation Methods

Molecular dynamics simulations are based on Newton's Second Law of Motion [260], given by,

$$\mathbf{F}(\mathbf{r}_i) = \nabla_i E_p(\mathbf{r}_1, \mathbf{r}_2, ..., \mathbf{r}_N) = m_i \mathbf{a}_i = m_i \frac{d\mathbf{v}_i}{dt} = m_i \frac{d^2 \mathbf{r}_i}{dt^2}, \ i = 1, 2, ..., N \qquad (3.1.1)$$

where $\mathbf{F}$ is the force; E_p is the potential energy; m_i, $\mathbf{a}_i$, $\mathbf{v}_i$, and $\mathbf{r}_i$ are the mass, acceleration, velocity, and position of particle i, respectively; t is time; and N is the number of particles in the system.

The basis of MD simulations is the solution of the differential equation shown in Equation 3.1.1 by numerically integrating it to determine positions and velocities over time.

The most common numerical schemes are based on the Verlet algorithm [261] and its modifications [262]. The Verlet algorithm is a combination of two Taylor expansions for particle positions $\mathbf{r}(t)$ moving forward $(t+\delta t)$ and backward $(t-\delta t)$ in time. Equations 3.1.2 and 3.1.3 show the first four terms of the expansion series,

$$\mathbf{r}(t + \delta t) = \mathbf{r}(t) + \frac{\partial \mathbf{r}(t)}{\partial t}\delta t + \frac{1}{2}\frac{\partial^2 \mathbf{r}(t)}{\partial t^2}\delta t^2 + \frac{1}{3!}\frac{\partial^3 \mathbf{r}(t)}{\partial t^3}\delta t^3 + ... \tag{3.1.2}$$

$$\mathbf{r}(t - \delta t) = \mathbf{r}(t) - \frac{\partial \mathbf{r}(t)}{\partial t}\delta t + \frac{1}{2}\frac{\partial^2 \mathbf{r}(t)}{\partial t^2}\delta t^2 - \frac{1}{3!}\frac{\partial^3 \mathbf{r}(t)}{\partial t^3}\delta t^3 + ... \tag{3.1.3}$$

The new positions $\mathbf{r}(t + \delta t)$ are obtained by adding the two series expansions, as shown by Equation 3.1.4.

$$\mathbf{r}(t + \delta t) \approx 2\mathbf{r}(t) - \mathbf{r}(t - \delta t) + \mathbf{a}(t)\delta t^2 \tag{3.1.4}$$

where, $\mathbf{a}(t)$ is the acceleration (second derivative). Note that $\mathbf{a}(t)$ is determined by dividing the force $\mathbf{F}(\mathbf{r})$ by the mass m, which is obtained from the gradient of the potential energy $E_p(\mathbf{r})$ (see the next section for more details on the potential energy),

$$\mathbf{a}(t) = -\frac{1}{m}\mathbf{F}(\mathbf{r}) = -\frac{1}{m}\nabla E_p(\mathbf{r}) \tag{3.1.5}$$

The velocity is then determined from the trajectories of the forward and backward position,

$$\mathbf{v}(t) = \frac{\mathbf{r}(t + \delta t) - \mathbf{r}(t - \delta t)}{2\delta t} \tag{3.1.6}$$

Another equivalent numerical integration scheme implemented in GROMACS is the half-step Leap-Frog algorithm. In this algorithm, the stored quantities are the current positions $\mathbf{r}(t)$, the half-step velocities $\mathbf{v}(t - \frac{1}{2}\delta t)$, and the accelerations $\mathbf{a}(t)$. The velocities at $\mathbf{v}(t + \frac{1}{2}\delta t)$ and future positions $\mathbf{r}(t + \delta t)$ are calculated from,

$$\mathbf{v}\left(t + \frac{1}{2}\delta t\right) = \mathbf{v}\left(t - \frac{1}{2}\delta t\right) + \mathbf{a}(t)\delta t \tag{3.1.7}$$

Figure 3.1.1: General procedure for the Leap-Frog algorithm. a) Forces are calculated from the known particle positions at time t. b) With the known forces at step t and velocities at step $t - \frac{1}{2}\delta t$, the velocities for the next half-step $t + \frac{1}{2}\delta t$ are calculated using Equation 3.1.7. c) The particle positions at step $t + \delta t$ is calculated using Equation 3.1.8 and the forces at step $t + \delta t$ are calculated as described in a). d) The procedure is repeated.

$$\mathbf{r}(t + \delta t) = \mathbf{r}(t) + \mathbf{v}\left(t + \frac{1}{2}\delta t\right)\delta t \tag{3.1.8}$$

Since the velocity terms are evaluated at half-step, the current velocity is calculated by,

$$\mathbf{v}(t) = \frac{\mathbf{v}\left(t + \frac{1}{2}\delta t\right) + \mathbf{v}\left(t - \frac{1}{2}\delta t\right)}{2} \tag{3.1.9}$$

The term Leap-Frog reflects the fact that the positions are evaluated at t and the velocities at $t \pm \frac{1}{2}\delta t$. The general procedure for the Leap-Frog algorithm is shown in Figure 3.1.1.

3.2   Potential Energy

In a typical simulation, a force-field (collection of interaction parameters) is used to describe the interactions between the particles in the system. A force-field is comprised of pair-additive potentials representing inter molecular and intramolecular interactions. In general, the functional form and parameters in a force-field are empirically derived from experimental

properties or are obtained from quantum mechanics calculations. The following sections describe the pertinent functional forms of the force-field employed herein (parameters for the corresponding systems are listed in Appendix A).

3.2.1 Intermolecular Potentials

Intermolecular potentials are generally described by Coulombic and Lennard-Jones (LJ) potentials, used to express electrostatic and van der Waals interactions, respectively, between particles. Their mathematical representations are,

$$V_{\text{Coulomb}} = \sum_{i,j>i}^{N} \frac{q_i q_j}{4\pi\epsilon_o r_{i,j}} = \sum_{i,j>i}^{N} f \frac{q_i q_j}{r_{i,j}} \tag{3.2.1}$$

$$V_{\text{LJ}} = \sum_{i,j>i}^{N} 4\varepsilon_{i,j} \left[\left(\frac{\sigma_{i,j}}{r_{i,j}}\right)^{12} - \left(\frac{\sigma_{i,j}}{r_{i,j}}\right)^{6} \right] \tag{3.2.2}$$

where V_{Coulomb} and V_{LJ} are the Coulombic and Lennard-Jones potentials, respectively; ϵ_o is the permittivity constant; $f = \frac{1}{4\pi\epsilon_o} = 138.935485$ kJ mol^{-1} nm e^{-2} [263]; ε and σ are LJ parameters for particle i and j; q is the charge; and r is the distance between i and j. A schematic representation of the intermolecular potential is shown in Figure 3.2.1.

       Calculation of the Coulombic and Lennard-Jones potentials are the most demanding part of simulations, as they account for pair interactions between all particles in the system. These interactions decay with increasing distances (see Figure 3.2.1), therefore, they are usually truncated outside a primary cutoff radius r_c. For this reason, all simulations performed here apply the cutoff method. To improve the accuracy of the simulations, the truncation of the potentials are corrected to account for long-range interactions by the Particle Mesh Ewald (PME) method [108, 263] for electrostatic interactions and dispersion correction for the van der Waals interactions.
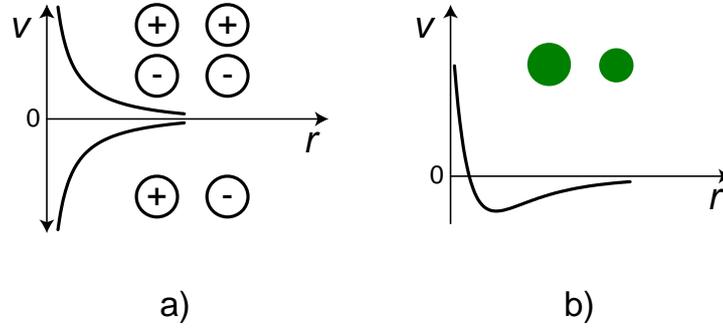
Figure 3.2.1: Schematic representation of a) Coulombic and b) Lennard-Jones potentials. Note that both repulsive and attractive charges are shown for the Coulombic potential.

3.2.2 Intramolecular Potentials

Intramolecular potentials are used to describe the interactions between covalently bonded atoms within a molecule. Generally, the potentials are represented by harmonic and periodic functions giving by Equations 3.2.3 to 3.2.7. These equations describe the energy contributions for bond, angle, improper dihedral, torsion, and Ryckaert-Bellemans (RB) torsion potentials, respectively. A schematic representation of the intramolecular potentials is illustrated in Figure 3.2.2.

$$V_{\text{bond}} = \sum_{i,j}^{N} \frac{k_{i,j}^{b}}{2}(l_{i,j} - l_{i,j}^{o})^2 \tag{3.2.3}$$

$$V_{\text{angle}} = \sum_{i,j,k}^{N} \frac{k_{i,j,k}^{\theta}}{2}(\theta_{i,j,k} - \theta_{i,j,k}^{o})^2 \tag{3.2.4}$$

$$V_{\text{improper}} = \sum_{i,j,k,l}^{N} k_{i,j,k,l}^{\xi}(\xi_{i,j,k,l} - \xi_{i,j,k,l}^{o})^2 \tag{3.2.5}$$

$$V_{\text{torsion}} = \sum_{i,j,k,l}^{N} k_{i,j,k,l}^{\phi}[1 + cos(n\phi_{i,j,k,l} - \phi_{i,j,k,l}^{o})] \tag{3.2.6}$$

$$V_{\text{RB}} = \sum_{i,j,k,l}^{N}\sum_{m=0}^{5} C_m[cos(1 - \phi_{i,j,k,l})]^m \tag{3.2.7}$$
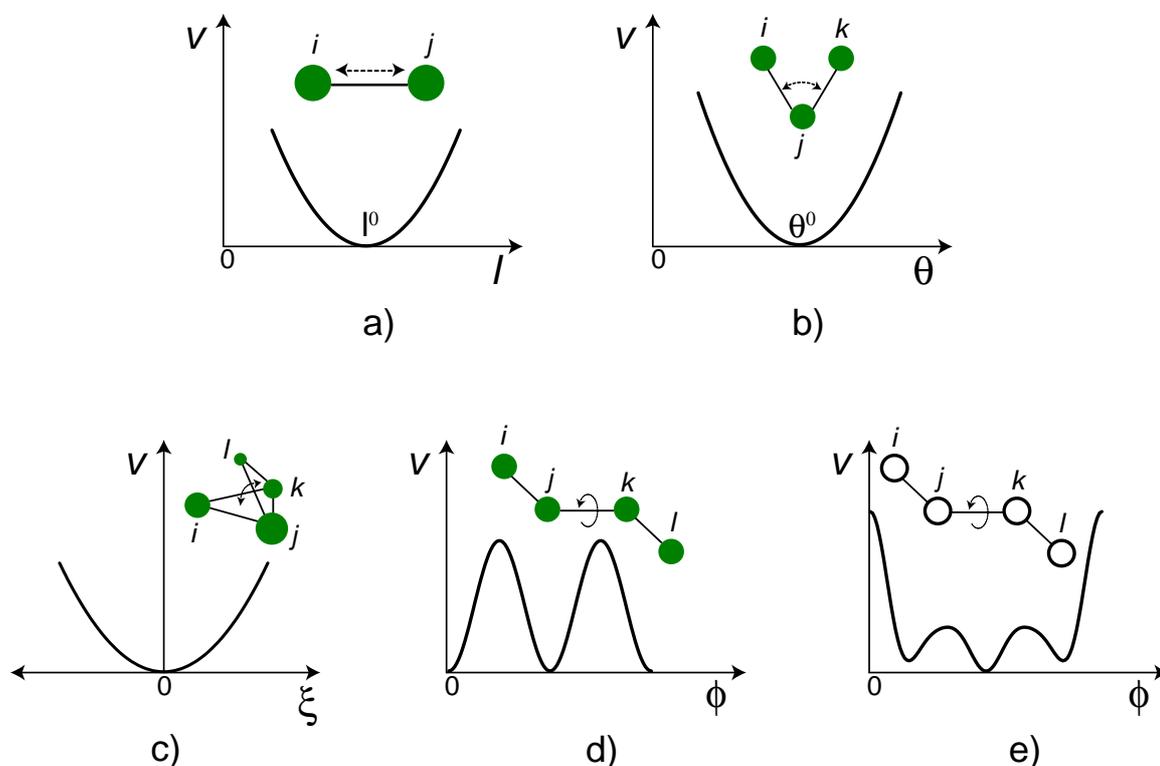
Figure 3.2.2: Schematic representation for a) bond, b) angle, c) improper dihedral, d) torsion, and e) Ryckaert-Bellemans potentials. Note that improper dihedral potential is used to keep planar atoms from flipping to its isomers and Ryckaert-Bellemans potential is used specifically for hydrocarbon atoms.

For V_{bond}, V_{angle}, and V_{improper}, the potentials are represented by harmonic functions where the force constants (k^b, k^θ, k^ξ) are listed as the parameter sets along with the equilibrium bond length l^o, bond angle θ^o, and plane angle ξ^o, respectively. For V_{torsion}, the potential is governed by a periodic function with three parameters sets: periodic constants (k^ϕ), equilibrium torsion angle (ϕ^o), and periodicity (n). Lastly, for V_{RB}, the potential is described by five periodic functions with constant coefficients C_m.

3.3 Kinetic Energy, Temperature, and Pressure

The kinetic energy of a system is calculated from the velocity of each particle by,

$$E_k = \sum_i^N \frac{1}{2} m_i \mathbf{v}_i^2 \tag{3.3.1}$$

where E_k is the kinetic energy; N is number of particles in a system; and m and $\mathbf{v}$ are the mass and velocity of particle i, respectively.

From the kinetic energy, the temperature T of a system is calculated from the Boltzmann relation,

$$E_k = \frac{3}{2} N k_B T \tag{3.3.2}$$

where k_B is the Boltzmann's constant.

To compute the system pressure, the kinetic energy is first expressed as a tensor,

$$\mathbf{E}_k = \sum_i^N \frac{1}{2} m_i \mathbf{v}_i \otimes \mathbf{v}_i \tag{3.3.3}$$

where m and $\mathbf{v}$ are mass and velocity of particle i, respectively.

The pressure tensor $\mathbf{P}$ is then calculated from the difference between the kinetic energy $\mathbf{E}_k$ and the virial $\boldsymbol{\Xi}$ term,

$$\mathbf{P} = \frac{2}{V} (\mathbf{E}_k - \boldsymbol{\Xi}) \tag{3.3.4}$$

where V is the volume of the simulation box.

The virial $\boldsymbol{\Xi}$ tensor is definded as,

$$\boldsymbol{\Xi} = -\frac{1}{2} \sum_{i<j}^N \mathbf{r}_{ij} \otimes \mathbf{F}_{ij} \tag{3.3.5}$$

where $\mathbf{r}$ is the position vector ($\mathbf{r}_{ij} = \mathbf{r}_j - \mathbf{r}_i$) and $\mathbf{F}$ is the force on particle i exerted by j.

Finally, the scalar pressure P is computed as,

$$P = \frac{\text{trace}(\mathbf{P})}{3} \tag{3.3.6}$$

3.4   Ensembles

An ensemble is a collection of all possible systems which have different microscopic states but have an identical macroscopic or thermodynamic state [264]. Depending on the nature of systems considered, one can consider different ensembles. For example, the canonical ensemble specifies the number of particles N, volume V, and temperature T; the isobaric-isothermal ensemble has constant number of particles N, pressure P, and temperature T. In this study, NPT ensembles are largely employed as they are the most suitable for the desired conditions, and provide a direct comparison to laboratory environments. In the NPT ensemble, the number of particles N is fixed, and the temperature T and pressure P are controlled by a thermostat and barostat, respectively, to ensure the average system temperature and pressure are maintained at the set points. The following two sections briefly describe the implementation of the thermostat and barostat controls in MD simulations.

3.5   Thermostat

As implemented in GROMACS, the system temperature, calculated from the particle velocities, is controlled by the Berendsen weak coupling technique [265], which assumes an isolated system coupled to an external heat bath. In practical terms, this corresponds to the addition of a temperature coupling term to the equation of motion as,

$$m_i \frac{d\mathbf{v}_i}{dt} = \mathbf{F}_i + \frac{m_i}{2\tau_T} \left(\frac{T_0}{T} - 1 \right) \mathbf{v}_i \qquad (3.5.1)$$

where τ_T is the coupling time-constant (strength of the coupling); T_0 is the set temperature; and T is the instantaneous temperature.

The heat flow into or out of the system is adjusted by scaling the particle velocities with a time-dependent factor, λ. The temperature scaling factor for each half-step in the Leap-Frog integration is given by,

$$\lambda = \left[1 + \frac{\delta t}{\tau_T} \left(\frac{T_0}{T(t - \delta t/2)} - 1 \right) \right]^{1/2} \qquad (3.5.2)$$

3.6   Barostat

Similarly to the thermostat, the pressure on a system is controlled by the Berendsen weak coupling technique [265]. Since the pressure is a direct measure of the forces normal to a surface, controlling the pressure implies scaling the particles coordinates and box vectors along the x-, y-, and z-directions [266]. The change in the equation of motion follows,

$$\frac{d}{dt} \mathbf{r}_N(t) = \mathbf{v}_N(t) - \frac{\beta (P_o - P)}{3\tau_P} \mathbf{r}_N(t) \qquad (3.6.1)$$

where $\mathbf{r}$ and $\mathbf{v}$ are the position and velocity of particle N, respectively; β is the isothermal compressibility of the system; P_o is the set pressure; P is the instantaneous pressure; and τ_P is the coupling time-constant [265, 266].

In general, the Berendsen algorithm rescales the coordinates and box vector with a scaling matrix, μ, given by,

$$\mu_{ij} = \delta_{ij} - \frac{\Delta t}{3\tau_p}\beta\left[P_{0ij} - P_{ij}(t)\right] \tag{3.6.2}$$

where i and j are the components of the pressure tensor; and δ is a delta function. In all simulations presented in this study, all off-diagonal elements of the scaling matrix are zero.

There are three pressure coupling schemes available in GROMACS: isotropic, semi-isotropic, and anisotropic. In isotropic coupling, all three components of the box vector are equally scaled, ensuring that the simulation box remains proportional. In semi-isotropic pressure coupling, two dimensions are coupled isotropically and the third scales independently. And in anisotropic coupling, all components of the box vector are uncoupled, and as such, it imposes the least amount of constraint on the system.

3.7   Properties Measurement

Basic equilibrium properties can be calculated from MD simulations as time average $\langle A \rangle_{\text{time}}$ after the system is equilibrated. That is, the average value of property A over the simulation period can be obtained from,

$$\langle A \rangle_{\text{time}} = \lim_{x \to \infty} \frac{1}{\tau} \int_{t_0}^{t_0+x} A\left[\mathbf{p}^N(t), \mathbf{r}^N(t)\right] dt \approx \frac{1}{M}\sum_{i=1}^{M} A_i\left[\mathbf{p}^N(t_i), \mathbf{r}^N(t_i)\right] \tag{3.7.1}$$

where τ is the simulation time; M is the number of time steps in the simulation; A_i is the instantaneous value of A, expressed as a function of the momentum $\mathbf{p}$ and positions $\mathbf{r}$ of the atoms N in the system. The ergodic hypothesis assumes that $\langle A \rangle_{\text{time}}$ is independent of the choice of time t_0, and it is equivalent to the ensemble average $\langle A \rangle$ [267].

3.8   Summary

All the MD simulations presented in this dissertation are performed with GROMACS, a parallel molecular simulation suite originally developed in the Department of Biophysical Chemistry at the University of Gröningen [252]. GROMACS has the capability of performing large scale simulations which is necessary for the model lipid bilayers. With suitable force-field parameters (see appendix A), simulations are performed by integrating the equation of motion using the Verlet scheme with the half-step Leap-frog algorithm. Berendsen thermostat and barostat are implemented in typical simulations to control the temperature and pressure of the model bilayers, thus simulating NPT ensembles. A complete description on how to set up MD simulations for a particular system using GROMACS can be found in the user's manual [252].

Chapter 4

Molecular Investigation of Trehalose with Mixed Lipid Bilayers

Cell membranes are composed of a wide range of phospholipids, differing in headgroup and fatty acid composition (see Chapter 1). From both experimental and theoretical standpoints, structural and dynamic properties of model lipid bilayers composed of one or more types of lipids are of great interest in many applications involving biological membranes (see Chapter 2.1 for details on mixed lipid systems). In particular, in the field of biological stabilization, model lipid bilayers containing DPPC have provided insight into the mechanism by which disaccharide molecules interact with the lipid bilayer to preserve the membrane structure and biological functions (see Chapter 2.2 for more details on biological preservation). In order to obtain a better assessment of the interactions of trehalose with a more realistic bilayer structure, this chapter presents MD simulations of mixed lipid bilayers containing DPPC and DPPE, two of the most abundant lipids found in biological membranes. The aim is to characterize mixed DPPC and DPPE bilayers at different membrane compositions and the interactions of trehalose therewith. The simulations presented here also resolve issues related to the distribution of hydrogen bonds between DPPE, DPPC, trehalose, and water molecules. This work provides detailed analysis of structural and dynamic properties of

DPPC/DPPE bilayers and trehalose.

4.1   Simulation Details

Molecular dynamics simulations were performed on systems containing a total of 256 lipid molecules (128 per leaflet) arranged in a bilayer structure. Fully hydrated systems (30 waters/lipid) containing DPPC and DPPE were studied for the compositions shown in Table 4.1.1. Figure 4.1.1 shows the structure and the assigned numbering considered for the atoms in DPPC and DPPE. The initial configuration for Lipid-A (pure DPPC) was constructed from the replication of a previous equilibrated bilayer containing 64 lipids [268]. The configurations for the mixed systems (Lipid-B, C, D) were created by randomly replacing DPPC molecules with DPPE molecules, namely the $N(CH_3)_3^+$ (choline) moiety of DPPC by the NH_3^+ (amine) group of DPPE (in the united-atom representation used, the CH_3 group is a single site, thus these were replaced by hydrogen atoms and the bond length with nitrogen adjusted to 1.0 Å). Note that a force-field for DPPE is currently unavailable but it is proposed to be composed of the combination of the lipid hydrocarbon tails from DPPC and the lipid headgroup from POPE [269]. Figure 4.1.2a shows a snapshot of Lipid-C system containing 128 DPPC and 128 DPPE molecules (note that a uniform distribution of DPPC/DPPE molecules was set for both leaflets). For the pure DPPE system (Lipid-E), all DPPC molecules from Lipid-A were converted to DPPE using the same approach described above. Lipid-F, G, and H were constructed by randomly inserting trehalose molecules into the aqueous region of previously equilibrated Lipid-A, C, and E, respectively. During the insertion process, overlapping water molecules with trehalose were deleted and additional water molecules were subsequently removed to obtain a 5 wt% trehalose concentration. Figure 4.1.3 shows the structure and assigned atomic numbering for trehalose. A low trehalose concentration was chosen since it is in the range of values reported in cryopreservation, lyophilization, and other modeled membrane-trehalose studies [124–127]. Figure 4.1.2b shows a snapshot of 1:1 DPPC/DPPE-trehalose system (Lipid-G system).

Table 4.1.1: Composition for mixed DPPC/DPPE bilayers with and without trehalose. A total of 256 lipids were used for all systems. Numbers for lipids are per leaflet and each leaflet contains the same number of DPPC and DPPE molecules.

System	DPPC/leaflet	DPPE/leaflet	Water	Trehalose
Lipid-A	128	0	7,680	–
Lipid-B	96	32	7,680	–
Lipid-C	64	64	7,680	–
Lipid-D	32	96	7,680	–
Lipid-E	0	128	7,680	–
Lipid-F	128	0	7,225	20
Lipid-G	64	64	7,225	20
Lipid-H	0	128	7,225	20

Figure 4.1.1: Molecular structure and assigned numbering of atoms for DPPC (above) and DPPE (below). Chemical symbols are hydrogen (H), nitrogen (N), oxygen (O), and phosphorus (P).

Figure 4.1.2: Snapshot of a) Lipid-C and b) Lipid-G at 350 K. Colored molecules are the DPPC headgroup (blue), DPPE headgroup (green), lipid tails (gray), water (red), and trehalose (brown). See Table 4.1.1 for additional information.
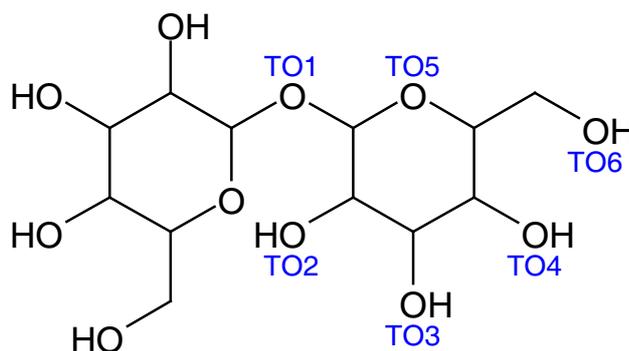
Figure 4.1.3: Molecular structure and naming of oxygen atoms in trehalose. Chemical symbols are hydrogen (H) and oxygen (O). Hydrogen atoms bound to carbon atoms are not shown. The assigned numbering and naming of all atoms for trehalose is listed in Appendix A.2.11.

The force-fields for DPPC and DPPE were consistent with those employed in the previous studies which included intramolecular parameters for bonds, angles, proper dihedral, and improper dihedral [103, 270]. The Ryckaert-Bellemans potential was used for the torsion potential of the hydrocarbon chains [271]. Non-bonded interactions were described by the parameters from Berger *et al.* [104, 110, 272] and partial atomic charges were obtained from Chiu *et al.* [96]. The single point charge (SPC) model was adopted for water [273]. To improve computational efficiency, the united-atom representation was used for the methyl/methylene groups in the alkyl chains of both DPPC and DPPE.

Steepest-decent energy minimization was performed on each system before starting the simulations. Each lipid system was allowed to equilibrate for at least 1 ns, followed by 50 ns runs for all systems. Simulations were performed in the NPT ensemble. Temperature and pressure of the simulation box were kept constant using the weak coupling technique [265], with correlation times $\tau_T = 0.1$ ps and $\tau_P = 2.0$ ps for the temperature and pressure, respectively. Temperature for all systems was set at 350 K, which is above the liquid-crystalline phase transition temperature of the fully hydrated pure and mixed DPPC/DPPE bilayers [18]. Constant pressure was attained by semi-isotropic pressure coupling to a pressure of $P = 1$ bar (compressibility $\kappa = 0.46 \times 10^{-5}$ bar^{-1}), thereby allowing the xy- and z- dimensions of the simulation box containing the bilayer to fluctuate independently. Periodic boundary conditions were imposed in all three directions.

The linear constraint solver (LINCS) algorithm was used to constrain all bonds of the lipid molecules [274], and the SETTLE algorithm for water molecules [275]. These constraint algorithms allowed simulations to be carried out with a 2 fs time-step using the Leap-Frog integration method [248]. Non-bonded interactions were cut off beyond 9 Å. Due to the shortcomings of electrostatic interaction truncations resulting from a simple large cutoff and reaction-field dielectric [276], along with well documented simulations of biological systems [277–280], particle-mesh Ewald (PME) [108, 263] was implemented in all simulations to account for the long-range electrostatic correction (0.12 nm for the grid size, 4$^{\text{th}}$ order spline interpolation, and real-space cutoff at 9 Å). Trajectories were collected every 2 ps.

All simulations were performed with the GROMACS 3.3 software package [258, 259] (single-precision mode) in parallel (about 5 ns/day in 12 nodes) using Virginia Tech's SystemX [281].

4.2   Analysis of Mixed DPPC/DPPE Bilayers

Equilibrium properties, structure, and dynamics for pure and mixed lipid bilayers were calculated over the 50 ns simulation runs. To maintain the stability of the lipid systems, all simulations were performed above the experimental liquid-crystalline phase transition temperature ($\sim$315 K for pure DPPC [282], $\sim$324 K for 25 mol% DPPE, $\sim$329 K for 50 mol% DPPE, $\sim$333 K for 75 mol% DPPE, and $\sim$337 K for pure DPPE, as reported by Petrov *et al.* [18]). Since the abundance of PE across organisms and cell types is highly variable, it is necessary to examine compositions spanning the concentration spectrum (see Table 4.1.1). An evenly distributed bilayer of DPPC and DPPE molecules on each leaflet was necessary to create a stable system in which the average area per lipid in each leaflet was not significantly different and distortion of the simulation box could be neglected. The stability of fully equilibrated lipid systems was verified by monitoring the average area per lipid over the simulation runs.

4.2.1   Area per Lipid

The average area per lipid was calculated from the cross sectional area of the simulation boxes (plane of the bilayer, in this case, along the xy-plane) divided by the number of lipids per leaflet (128 lipids). Figure 4.2.1a shows the time average area per lipid for Lipid-A to E. The average values for pure DPPC and DPPE systems are 0.69±0.01 nm^2 and 0.58±0.01 nm^2, respectively. For the pure DPPC system, the value obtained agrees well with previous MD simulation results at 350 K of 0.668±0.007 nm^2 [147]. For the pure DPPE system, the value agrees well with previous simulation results at 343 K of $\sim$0.58 nm^2 [115] and the experimental result of $\sim$0.60 nm^2 at 342 K [283]. Coarse-grained MD simulation has
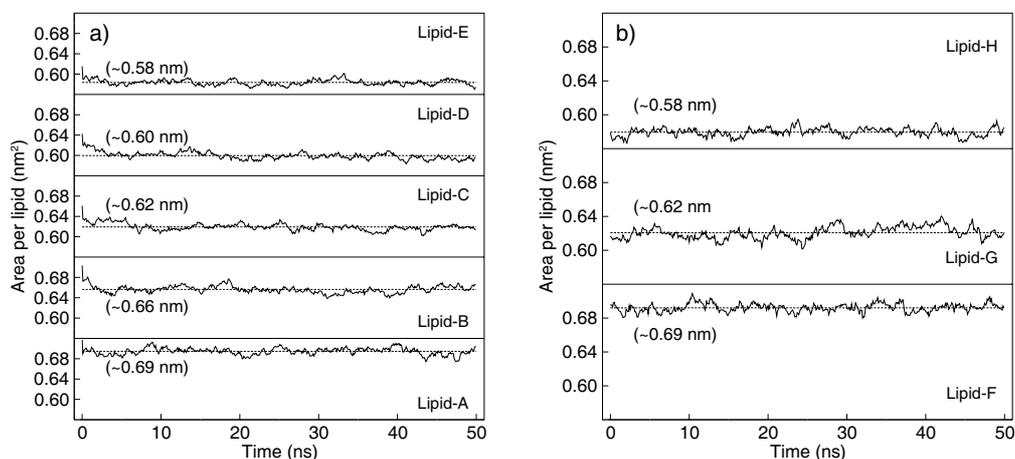
Figure 4.2.1: Area per lipid for the lipid bilayers over the course of the simulations: without trehalose and with trehalose. Straight dash lines show the average area per lipid (number in parentheses).

reported an area per lipid of ∼0.58 nm^2 in the liquid-crystalline phase of an 1:1 DPPC/DPPE bilayer [121], a value smaller than that obtained here for the same bilayer mixture (∼0.62 nm^2).

4.2.2 Lipid Tail Deuterium Order Parameter

The lipid tail deuterium order parameter S_{CD} [92] is a measure of the orientation and ordering of the phospholipid tails in the bilayer with respect to the bilayer normal. Note that a S_{CD} value of −0.5 corresponds to the perfect alignment of the lipid tails to the bilayer normal. Figure 4.2.2a shows the average S_{CD} as a function of the carbon atom along the lipid tails for Lipid-A to E. The carbon atoms are numbered as follow: Sn-1 tail consists of carbon atoms C34, C36-C50 and Sn-2 of C15, C17-C31 (see Figure 4.1.1). For the mixed systems, the combined values obtained for the two lipid tails of DPPC and DPPE are reported as a single set of values. Previous experimental results are also shown in Figure 4.2.2a for comparison, which includes NMR measurements of pure DPPC at 353 K [283] and pure DPPE at 342 K [17]. Large differences are seen between the experimental and simulation results in the
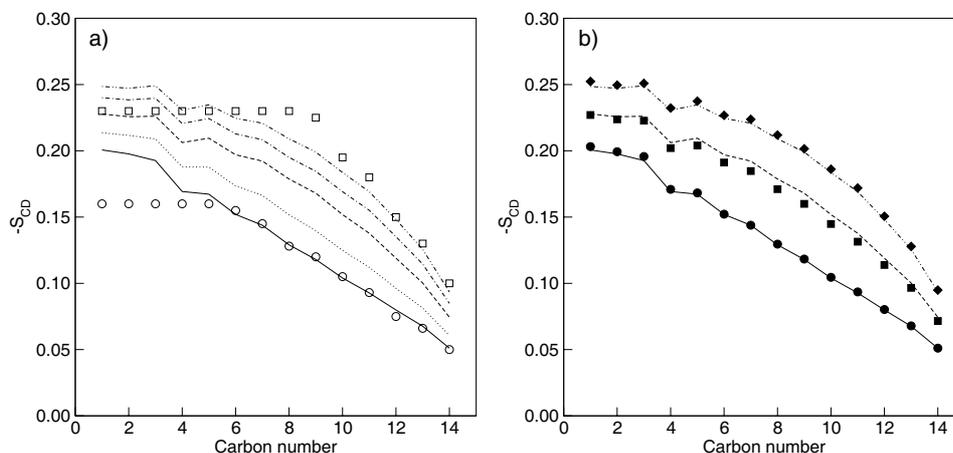
Figure 4.2.2: Deuterium order parameter (S_{CD}) of the phospholipid tails at 350 K for a) Lipid-A to E and b) Lipid-F to H. Lines correspond to Lipid-A (solid), Lipid-B (dot), Lipid-C (dash), Lipid-D (dot-dash), and Lipid-E (dot-dot-dash). Closed circles, squares, and diamonds correspond to Lipid-F, Lipid-G, Lipid-H, respectively. Open circles and squares are experimental NMR measurement of pure DPPC at 353 K [283] and pure DPPE at 342 K [17]. For clarity, the average value for the two lipid tails is shown.

lower carbon number because lipid force-fields need further development. However, the results obtained lie within an acceptable range with a similar trend in the order parameter of the lipid tails. Even though there are no data available for the mixed lipid systems, the values obtained lie within the two limits of the pure systems.

4.2.3 Mean-Squared Displacement for the Lipids

Figure 4.2.3 shows the mean-squared displacement for the lipid molecules for all systems considered. The solid and dashed lines show the results for DPPC and DPPE, respectively. The calculated 2D diffusion coefficients using the Einstein relation range from $0.32 \pm 0.20 \times 10^{-6}$ cm^2/s to $0.79 \pm 0.10 \times 10^{-6}$ cm^2/s. These results are comparable to those obtained from previous MD simulations of pure DPPC of $0.127 \pm 0.005 \times 10^{-6}$ cm^2/s at 323 K [284], of $0.33 \pm 0.1 \times 10^{-6}$ cm^2/s at 350 K [147], and coarse-grained MD simulations in the liquid-crystalline phase of $\sim 0.32 \times 10^{-6}$ cm^2/s [121]. The values of diffusion coefficient for the

Table 4.2.1: Calculated equilibrium properties for the lipid bilayers. D_{DPPC} and D_{DPPE} represent the 2D (lateral) diffusion coefficient. D_{TRE} represents the 3D diffusion coefficient. Distance P-P is the estimated bilayer thickness. All results are for simulations at 350 K.

System	$D_{\mathrm{DPPC}}{}^{a}$	$D_{\mathrm{DPPE}}{}^{a}$	$D_{\mathrm{TRE}}{}^{a}$	Distance P-P^{b}
Lipid-A	0.79 ± 0.1	$-$	$-$	3.43 ± 0.01
Lipid-B	0.59 ± 0.1	0.59 ± 0.1	$-$	3.66 ± 0.01
Lipid-C	0.51 ± 0.1	0.48 ± 0.1	$-$	3.79 ± 0.01
Lipid-D	0.57 ± 0.2	0.53 ± 0.2	$-$	3.86 ± 0.01
Lipid-E	$-$	0.32 ± 0.2	$-$	4.00 ± 0.01
Lipid-F	0.56 ± 0.1	$-$	3.62 ± 0.1	3.56 ± 0.01
Lipid-G	0.41 ± 0.1	0.35 ± 0.1	4.48 ± 0.1	3.78 ± 0.01
Lipid-H	$-$	0.30 ± 0.2	4.93 ± 0.1	3.95 ± 0.01

^{a} values reported as $D \times 10^{6}$ cm^{2}/s
^{b} values reported in nm

various lipid systems are also listed in Table 4.2.1. Due to a large uncertainty in determining the diffusion coefficients by fitting a line of unity slope in Figure 4.2.3, larger error estimates were imposed for Lipid-D and Lipid-E systems due to the high fluctuations in the mean-squared displacement at the diffusive region (see values in Table 4.2.1). It is clear that the lipid molecules in Lipid-D and Lipid-E require a longer time to reach the diffusive regime.

4.2.4   Component Density Profiles for Lipid Bilayers

Figures 4.2.4a-c show the component density profiles for pure DPPC, DPPE, and mixed 1:1 DPPC/DPPE bilayers along the normal direction to the bilayer interface. The interface is the region with the highest molecular density ($|1.5 - 2.5|$ nm), corresponding to the lipid headgroups. This location of the interface is confirmed by the phosphorus and nitrogen density profiles for DPPC bilayers (see Figure 4.2.4a). Similar features are also observed for the mixed and pure DPPE bilayers (see Figures 4.2.4b-c). The region ($|2.5 - 4.0|$ nm) of approximately 950 kg/m^{3} corresponds to the aqueous phase, and the section with the lowest density is at the center of the bilayer structure corresponding to the terminal lipid tails.

Figure 4.2.3: Mean-squared displacement for pure and mixed DPPC and DPPE bilayers: a) without trehalose and b) with trehalose. Solid and dash lines represent the displacement of PC and PE lipids, respectively. Circles and squares are the corresponding results without trehalose. Short solid line has unity slope. Numbers indicate the displacement of the lines, shifted for clarity.

Another useful property to describe the structure of the bilayers is the nitrogen and phosphorus density profiles, as shown in Figures 4.2.4a-c (the height of the distributions corresponds well with the lipid compositions). For the pure DPPC system (Figure 4.2.4a), it is clear that the nitrogen density profile is aligned at about the same position as the phosphorus density profile. A closer inspection shows that the distribution of nitrogen extends slightly further to the aqueous phase, that is, the $N(CH_3)_3^+$ (choline) group is fully hydrated. In contrast, the density profile of nitrogen for the pure DPPE system (Figure 4.2.4c) extends toward the bilayer core beyond the phosphorus density profile. This indicates that the NH_3^+ (amine) group in DPPE favors interactions with the phosphate and/or carbonyl groups. One explanation for this behavior is the preferential hydrogen bonding with the lipid oxygens located around the headgroups (experimentally observed by Hübner and Blume [88] and predicted computationally by Damodaran and Merz [114], de Vries *et al.* [115], and Murzyn *et al.* [116]). This observation is more pronounced in the mixed lipids (Figure 4.2.4b) where the profile for the DPPC choline group extends into the aqueous phase and the DPPE amine group toward the bilayer core. Note that the profiles of the phosphorus atoms for the mixed
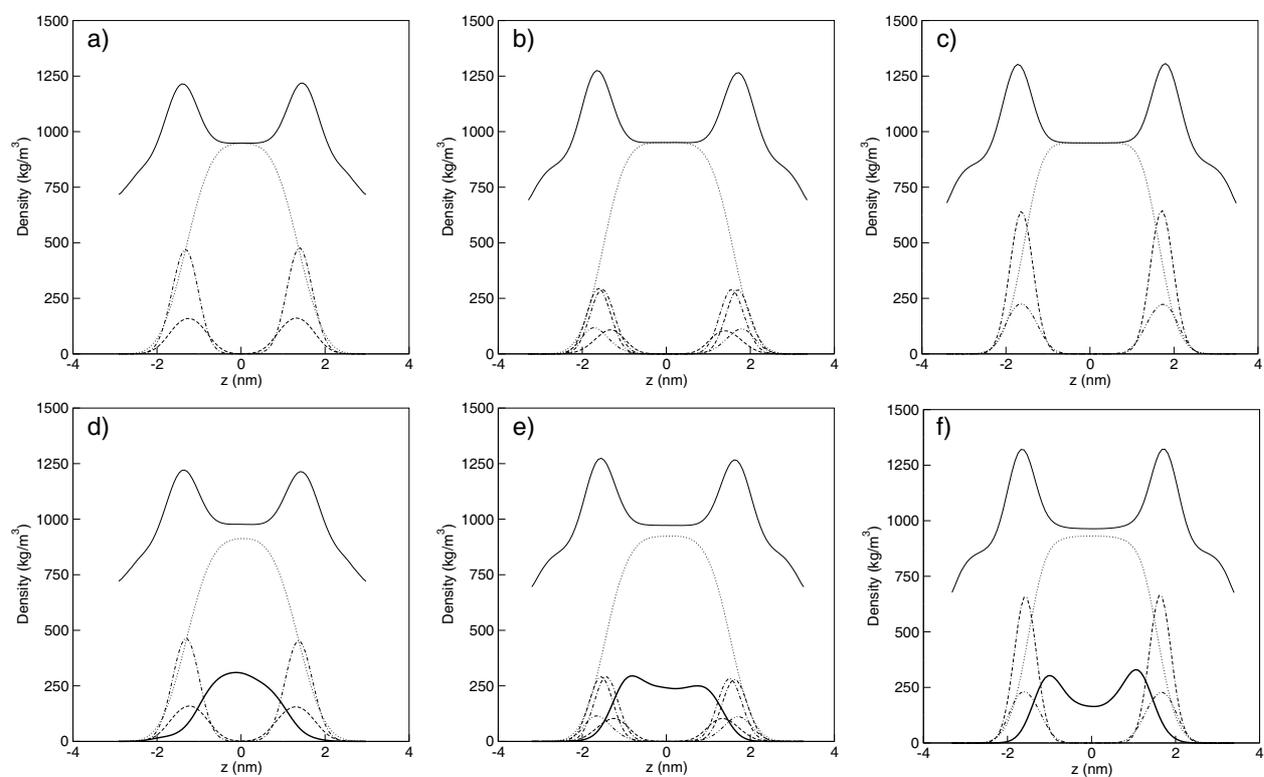
Figure 4.2.4: Component density profiles for lipid bilayers at 350 K: a) Lipid-A, b) Lipid-C, c) Lipid-E, d) Lipid-F, e) Lipid-G, and f) Lipid-H. Line representation corresponds to: total density (solid), water (dot), PC-nitrogen (dash), PC-phosphorus (dot-dash), PE-nitrogen (dot-dot-dash), PE-phosphorus (dot-dash-dash), and trehalose (bold-solid). The density profiles for nitrogen, phosphorus, and trehalose are magnified 5×.

1:1 DPPC/DPPE system are almost overlapping, and the profiles of the nitrogen atoms are either closer to the water interface (DPPC nitrogen) or closer to the bilayer core (DPPE nitrogen). This preferential interaction of the headgroups results from the type of interactions, which in the case for choline is the hydrophobic hydration around the CH_3 groups, and for amine is the competition of hydrogen bonds with water and oxygen atoms in the headgroups. Figure 4.1.2a clearly demonstrates these phenomena for the mixed 1:1 bilayer system where most of the DPPC headgroups (represented in blue) point toward the aqueous phase and the majority of DPPE headgroups (represented in green) point toward the bilayer core (gray color region).

4.2.5   Bilayer Thickness

From Figures 4.2.4a-c, the distance between the two maximum peaks, which is directly related to the bilayer thickness, is estimated to increase with increasing DPPE concentration, from about 3.43 nm in pure DPPC to about 4.00 nm in pure DPPE (this thickness is referred as the distance P-P in Table 4.2.1). The decrease in the area per lipid (see Figure 4.2.1) accompanied with an increase in the bilayer thickness has been previously observed in both experiments and simulations, which is attributed to the smaller DPPE headgroups and results in a closer packing of the lipids according to the number of DPPE molecules in the system. From this simple quantitative analysis, the smaller area per lipid reduces the mobility of lipid tails by partially constraining the lipid orientation in the plane of the bilayer surface, therefore causing the lipid tails to extend in the direction normal to the bilayer. This reasoning is consistent with the observations of increased bilayer thickness with increasing DPPE concentration. However, other factors, such as hydrogen bonding, also play an important role in the structure and dynamics of the bilayer, and these will be considered in detail as well.

4.2.6   Phosphorus-Nitrogen Angle Distribution

To further confirm and quantify the preferential positioning of the choline and amine groups, the average intramolecular angle was calculated for the phosphorus (P) to nitrogen (N) vector for both DPPC and DPPE. The intramolecular angle was computed from the angle formed between the P-N vector (phosphorus and nitrogen in the same lipid) and the axis normal to the bilayer surface (z-axis). Figure 4.2.5a illustrates the vector and angles considered, as well as the normalized angle distribution for the P-N vector for the lipid systems. An angle of zero degree corresponds to a vector aligned with the axis of reference pointing toward the aqueous phase, and an angle of 180 degrees corresponds to a vector pointing toward the bilayer core. The angle distributions for DPPC and DPPE are shown in Figures 4.2.5b and c, respectively. For DPPC, the angle distributions of Lipid-A to D are broad with a distinct maximum. For Lipid-A, the wide distribution peaks at about 100 degrees, indicating that the choline groups are exposed to the aqueous phase and are unhindered to take any orientation. As the concentration of DPPC decreases, the angle distribution for the DPPC groups shifts to lower values (maxima at approximately 40 degrees in Lipid-D), suggesting that most of the choline groups are more exposed to the aqueous phase. This is caused by the closer packing of the lipids in the presence of DPPE, as observed in the reduction of the area per lipid. For DPPE in Lipid-B to E, the majority of the angles for the P-N vector are greater than 90 degrees, indicating that most of the amine groups in DPPE are favorably interacting with lipid oxygen atoms (Figures 4.2.5c). A bimodal distribution for the angle of the P-N vector is observed and becomes more pronounced with increasing DPPE concentration. This suggests that there are two preferential hydrogen bonding sites: one near the interface (distribution less than 90 degrees) and one near the lipid oxygen atoms (distribution greater than 90 degrees). In general, it is expected that additional DPPE molecules should induce more hydrogen bonds of DPPE with lipid oxygen atoms and, consequently, increase the angle in the distribution curves in the limit to pure DPPE. However, the results indicate otherwise, and they can be reasoned as follows: the fact that there are more H-donors from NH_3^+ groups in DPPE than available H-acceptors from lipid oxygens means that there is a competition
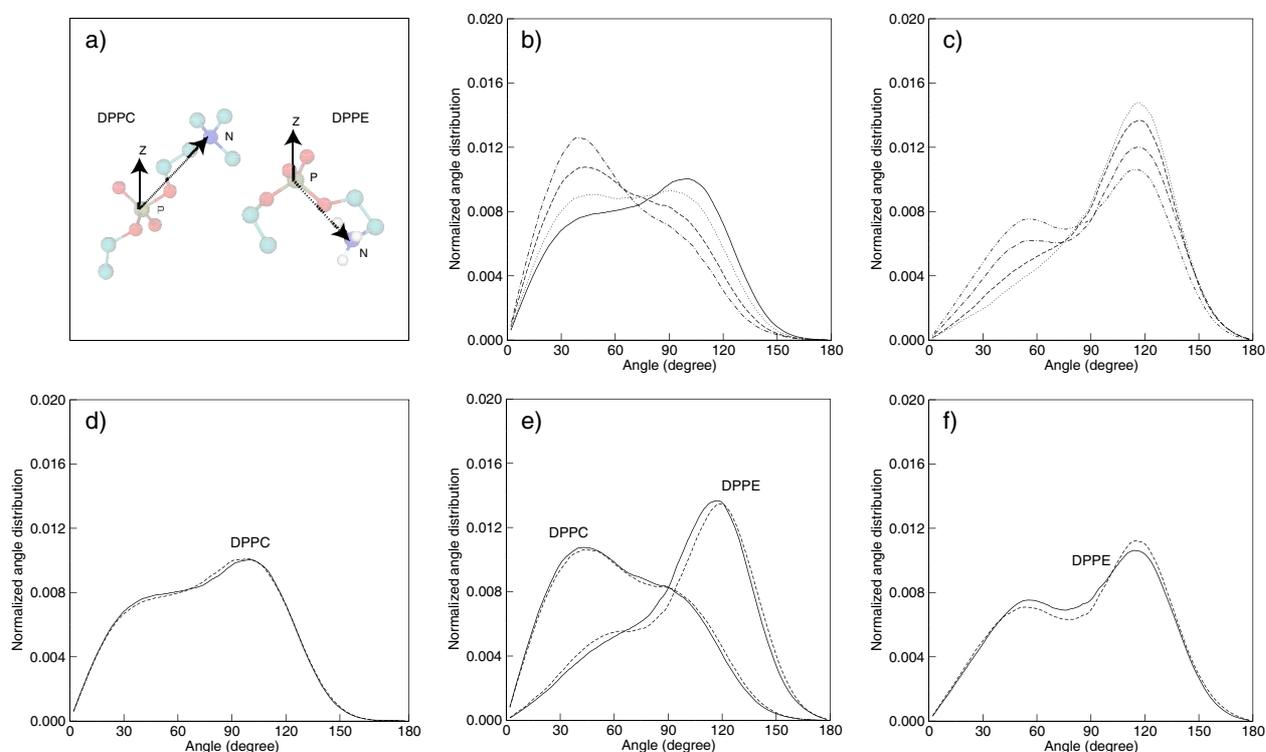
Figure 4.2.5: Top row: a) Pictorial representation for P-N vector for DPPC and DPPE. b) Normalized angle distribution for P-N vector for DPPC in Lipid-A to D and c) DPPE in Lipid-B to E. Lipid systems are represented by: solid (Lipid-A), dot (Lipid-B), dash (Lipid-C), dot-dash (Lipid-D), and dot-dot-dash (Lipid E). Bottom row: Normalized angle distribution for the P-N vector for d) DPPC between Lipid-A and F, e) DPPC and DPPE between Lipid-C and G, and f) DPPE between Lipid-E and H. Systems with and without trehalose are represented by solid and dash lines, respectively. All angles are measured with respect to the normal of the bilayer surface (z-axis).

for hydrogen bonds between lipid oxygens and water. Since H-donors are in excess, hydrogen bonds with water near the lipid-water interface becomes more favorable, thus decreasing the average tilt angle of the P-N vector as seen in the bimodal distribution curves.

4.2.7   Hydrogen Bonding Analysis: DPPE as H-Donor

An extensive analysis of the hydrogen bonding with the NH_3^+ group was performed to provide greater insight into the structure of the bilayer. Here, a hydrogen bond is defined according

Table 4.2.2: Average number of hydrogen bonds between the NH_3^+ group in DPPE and H-acceptors in water, lipid (lipid oxygen atoms), and trehalose (trehalose oxygen atoms). Average number of inter and intramolecular H-bonds are calculated separately for the lipids. Note that all values are reported per NH_3^+.

	Lipid-B	Lipid-C	Lipid-D	Lipid-E	Lipid-G	Lipid-H
Inter H-bond/NH_3^+	1.13	1.11	0.98	0.90	1.05	0.93
Intra H-bond/NH_3^+	1.04	0.98	0.97	0.98	0.98	0.97
H-bond H_2O/NH_3^+	0.75	0.75	0.85	0.93	0.77	0.89
H-bond trehalose/NH_3^+	–	–	–	–	0.01	0.04
Total H-bond/NH_3^+	2.92	2.85	2.80	2.81	2.82	2.81

to the criteria suggested by Brady and Schmidt [285], with the distance between the donor and acceptor (in this case, nitrogen-oxygen) to be within 0.35 nm and the angle donor-hydrogen-acceptor between 120 and 180 degrees. Table 4.2.2 shows the average number of hydrogen bonds between NH_3^+ in DPPE and all other oxygen atoms, including lipids and water, for each system with DPPE (Lipid-B to E). The oxygen sites available as H-acceptor are located at the phosphate group (O7, O9, O10 and O11), at the two carbonyl groups (O14, O16, O33, O35), and water (OW). Figure 4.1.2 shows the pertinent oxygen sites on the lipids. Separate calculations were performed for DPPC and DPPE to differentiate the hydrogen bond contributions from each lipid. Hydrogen bond contributions resulting from intermolecular and intramolecular hydrogen bonds for DPPE are separately reported for each system. From the results shown in Table 4.2.2, the total average number of hydrogen bonds per NH_3^+ group is independent of the DPPE concentration at about 2.80-2.92 (last row in Table 4.2.2). This is expected because NH_3^+ has three H-donors, thus able to form a total of three hydrogen bonds. To maintain a number of hydrogen bonds per NH_3^+, both intermolecular and intramolecular hydrogen bonds are reduced with increasing DPPE concentrations while intermolecular hydrogen bonds with water significantly increase. This is related to a shifting between intermolecular and intramolecular hydrogen bonds with water due to an excess of H-donors (competitive hydrogen bonding effects).

Evidently, the total number of hydrogen bonds between NH_3^+ and lipid oxygens or water plays an important role in determining the average area per lipid. The total number of DPPE increases from 25 mole% (Lipid-B) to 100 mole% (Lipid-E) while the average area per lipid decreases from 0.66 to 0.58 nm^2. If assuming that the area per lipid for the mixed systems is simply a linear average of the pure lipids, the dash line shown in Figure 4.2.6 is obtained. However, as shown in the figure, the area per lipid significantly deviates from the ideal case. For example, there is approximately a 9.5% reduction in area per lipid from Lipid-A (pure DPPC) to Lipid-B (25% DPPE), whereas the ideal case predicts a 5.2% reduction. The percentage reduction in the area per lipid from Lipid-B to C, Lipid-C to D, and Lipid-D to E are 6.1%, 4.5%, and 3.0%, respectively. The fact that the area per lipid decreases non-linearly and the percentage reduction becomes smaller with increasing DPPE concentration can be explained by the presence of more H-donors than available H-acceptors as the DPPE concentration increases, resulting in a competition between the lipid oxygens and water for hydrogen bonds with the NH_3^+ group. The presence of more water molecules near the NH_3^+ groups in DPPE increases the hydration of the lipids, thus causing a smaller decrease in the area per lipid than would otherwise occur. This is seen from the data in Table 4.2.2 that shows the increase in the number of hydrogen bonds between NH_3^+ and water per DPPE, while the number of inter and intramolecular hydrogen bonds per NH_3^+ decreases with increasing DPPE concentration. A similar behavior has been observed by de Vries et al. in DOPC/DOPE mixtures in which the area per lipid decreased non-linearly with increasing PE content [115]. The study by Gurtovenko *et al.* on DMPC and dimyristoyltrimethylammonium propane (DMTAP) mixtures, a neutral and cationic lipid, respectively, also showed a non-linear dependence of the area per lipid, with a minimum at about 0.5 mole fraction [286]. For the systems considered, DPPC and DPPE are both neutral lipids and their mixtures do not expand due to the increased charge concentration and electrostatic repulsion, unlike the results observed by Gurtovenko *et al.* for mixed DMPC/DMTAP lipid systems [286].

Figure 4.2.6: Average area per lipid for DPPC/DPPE bilayers at 350 K. Actual values are reported in Table 4.2.2. Dash line is the ideal case if the area per lipid linearly decreased with increasing DPPE concentration. Error bars are estimated standard deviation of the trajectories collected over the last 30 ns.

4.2.8   Radial Distribution Functions for Lipid Oxygen Atoms

Additional analysis of the hydrogen bonds was performed to investigate the effect of lipid hydration with increasing DPPE concentration. Various radial distribution functions (RDF) between lipid oxygen atoms and water were calculated, as those shown in Figure 4.2.7 for the Lipid-C system (RDFs were calculated separately for DPPC and DPPE). RDFs for the other compositions are not shown for the sake of brevity, but they are all similar to those in Figure 4.2.7. The hydration radius for each lipid oxygen was found by determining the distance of the first minimum in the RDFs. Most RDFs showed a well-defined peak below 0.35 nm, confirming possible hydrogen bonds within the hydration radius based on the criteria suggested by Brady and Schmidt [285]. Table 4.2.3 summarizes the hydration radius for the various lipid oxygens obtained from the RDF curves. As seen in Figure 4.2.7, hydration radii for the O7 from DPPE and O33/O35 from both DPPC and DPPE are unavailable because no minima were found in the RDFs. Once the number of water molecules within the hydration radius are determined, the number of hydrogen bonds between lipid oxygen atoms (H-acceptor) and water (H-donor) can be calculated using the prior criteria

Figure 4.2.7: Radial distribution functions for lipid oxygen atoms and water for a mixed 1:1 DPPC/DPPE bilayer. The plots correspond to water interacting with a) DPPC phosphate group, b) DPPE phosphate group, c) DPPC ester group, and d) DPPE ester group. Phosphate oxygen atoms are represented as follow: O7 (solid line), O9 (dot line), O10 (dash line), and O11 (dot-dash line). Ester oxygen atoms are represented as follow: O14 (solid line), O16 (dot line), O33 (dash line), and O35 (dot-dash line)

defining a hydrogen bond [285].

4.2.9   Hydrogen Bonding Analysis: Water as H-Donor

Table 4.2.4 shows the average number of hydrogen bonds between lipid oxygen atoms and water for DPPC/DPPE bilayers (Lipid-A to E). Note that the small number of hydrogen bonds in DPPE between water and O7 or O16 results from the preferred association of these sites with the amine group, which in turn expels most of the water around O7 (closest to the amine group). This also explains why a hydration shell around O7 was absent (see Table 4.2.3). On the other hand, the low number of hydrogen bonds between water and O33 was somewhat unexpected because the formation of hydrogen bonds with the amine group (Table 4.2.2) and the hydration shell were not observed (Figure 4.2.7). In this case, it may be

Table 4.2.3: Hydration radius for lipid oxygen atoms. All values reported in nm.

	PC headgroup				PE headgroup			
	Lipid-A	Lipid-B	Lipid-C	Lipid-D	Lipid-B	Lipid-C	Lipid-D	Lipid-E
O7	0.320	0.320	0.320	0.320	—	—	—	—
O9	0.326	0.324	0.326	0.326	0.326	0.326	0.324	0.324
O10	0.326	0.324	0.324	0.322	0.324	0.322	0.322	0.322
O11	0.316	0.312	0.312	0.312	0.312	0.312	0.314	0.314
O14	0.352	0.352	0.350	0.350	0.356	0.354	0.350	0.352
O16	0.386	0.388	0.392	0.398	0.390	0.390	0.392	0.394
O33	—	—	—	—	—	—	—	—
O36	—	—	—	—	—	—	—	—

simply caused by the alignment of the lipids that prevents favorable hydrogen bond interactions with O33 (discussed by Hitchcock *et al.* [48]). Note that there are a significant number of hydrogen bonds occurring at O35 (located below O33) which eliminates the possibility that O33 is too deep into the bilayer. The total number of hydrogen bonds between water and lipid oxygen atoms is found to decrease with increasing DPPE concentration, as shown in Table 4.2.4 from 1,615 (pure DPPC) to 1,241 (pure DPPE). The average number of hydrogen bonds per DPPC molecule, between water and lipid oxygen atoms, still decreases with increasing DPPE concentration (approximately 6.31 to 5.91 in Table 4.2.4). However, for DPPE, the number of water/lipid oxygen hydrogen bonds per DPPE decreases with DPPE concentration (approximately 5.27 to 4.85 in Table 4.2.4). These results are expected and are a confirmation of earlier discussions: the number of hydrogen bonds between NH_3^+ and water per DPPE increases while the average number of inter and intramolecular hydrogen bonds between lipid molecules decreases with increasing DPPE concentration, thus making lipid oxygen atoms in DPPE and water available to form hydrogen bonds.

Table 4.2.4: Intermolecular hydrogen bonds with water. Tabulated values are the ensemble average of hydrogen bonds. Average number of hydrogen bonds per lipid are also shown below. Averages for pure DPPC and DPPE bilayers are shown in Lipid-A and Lipid-E, respectively.

Acceptor	Lipid-A^a	Lipid-B^a	Lipid-B^b	Lipid-C^a	Lipid-C^b	Lipid-D^a	Lipid-D^b	Lipid-E^b
O7	151.4	115.4	6.4	78.5	13.2	39.5	21.3	29.1
O9	447.5	319.2	112.2	202.7	209.1	98.4	291.7	377.7
O10	403.1	273.5	90.9	168.1	162.0	81.0	234.4	297.9
O11	75.8	57.6	16.3	39.1	36.1	20.1	51.7	72.0
O14	108.7	88.6	18.1	52.2	38.0	26.8	58.9	82.5
O16	280.2	208.9	54.1	134.6	124.8	72.7	172.0	229.1
O33	27.5	19.9	8.6	13.7	15.1	6.5	23.5	27.9
O35	121.1	90.0	30.8	62.7	60.8	33.2	92.7	124.8
Total	1,615	1,173	337	752	659	378	946	1,241
H-bond/lipid	6.31	6.11	5.27	5.87	5.15	5.91	4.93	4.85

^{a} Hydrogen bonds in DPPC molecules
^{b} Hydrogen bonds in DPPE molecules

4.2.10   Lateral Movement of DPPE Molecules

To verify the dynamic properties of DPPE in the mixed systems (Lipid-B to E), in particular the mixing of the lipids, the lateral movement of the DPPE molecules in the bilayer was investigated based on the trajectories accumulated over the length of the simulations. Figures 4.2.8a-c show the lateral movement (along the xy-plane) of the phosphorus atoms on one of the leaflets of Lipid-B, Lipid-C, and Lipid-D, respectively. Each color represents a different phosphorus atom in the system. Figures 4.2.8d-f show only the initial (open circles) and final (closed circles) positions of the phosphorus atoms after 50 ns. Periodic boundaries were removed from the coordinates for clarity. It is clear that the movement of DPPE is random and the molecules have no tendency to move in any particular direction along the bilayer. Note that the majority of the DPPE molecules move rapidly around the membrane surface (approximately 1.73 nm from the initial position in Lipid-B), but they become more restricted with increasing DPPE concentration (approximately 1.62 nm in Lipid-C and 1.23

nm in Lipid-D). The displacements are estimated from the distances the DPPE molecules travel laterally during the simulation (see Figures 4.2.8d-f for the initial and final positions). The high mobility of DPPE from their original position in Lipid-B suggests that there are strong interactions causing the molecules to diffuse laterally through the bilayer. It is probable that intermolecular hydrogen bonds between the lipids facilitate their diffusion. At a higher DPPE concentration (Lipid-D), DPPE seems to show less mobility as the displacement of the molecules is relatively small. This may be a direct result of hydrogen bond competition between NH_3^+ in DPPE and water at the interface, which reduces the interactions between lipids, and thus make the movement of DPPE to be more localized. It is also seen from the plots in Figure 4.2.8 that there is no aggregation between lipids, as their diffusion along the membrane leaflet seems random.

4.3   Analysis of Mixed Lipid Bilayers with Trehalose

A number of quantities were analyzed to characterize the effect of trehalose on the properties of pure and mixed bilayers, including: area per lipid, lipid tail order parameter, mean-squared displacement, density profiles, lipid binding and configuration, hydrogen bonding, and binding and diffusion of trehalose. To accomplish this task, trehalose is introduced to selected systems in order to investigate and characterize its effect on the properties of pure and mixed bilayers (see Table 4.1.1). Results for the lipid systems without trehalose have been reported in the previous sections and, where appropriate, are shown side by side for comparison. All simulations were performed at 350 K to keep lipid bilayers in a stable liquid-crystalline state. Experimentally, the phase transition for the compositions considered are: 315 K for pure DPPC [282], 329 K for 1:1 DPPC/DPPE, and 337 K for pure DPPE, as reported by Petrov *et al.* [18]. As noted in previous sections, the mixed 1:1 DPPC/DPPE bilayer contained an even number of DPPC and DPPE molecules on each leaflet which is a condition necessary in order to obtain a stable system.
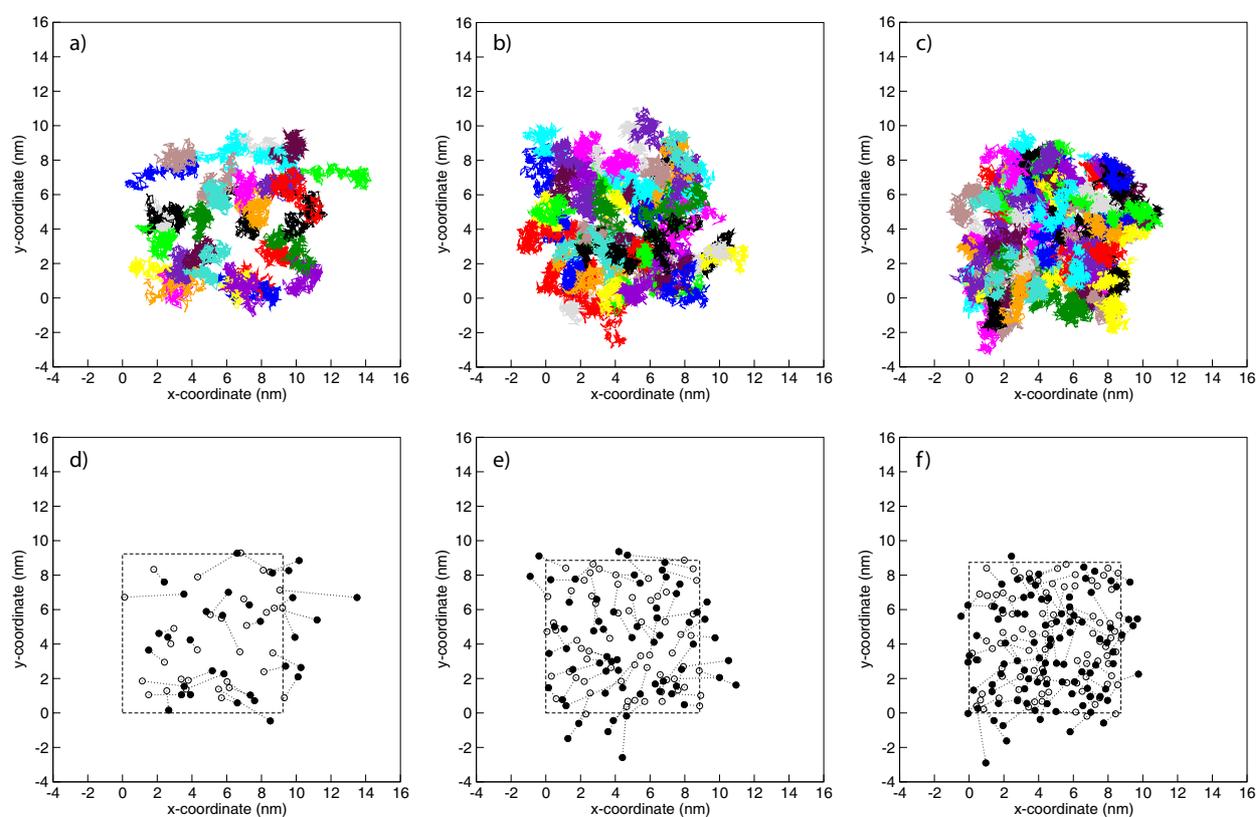
Figure 4.2.8: Lateral movement of phosphorus atoms in DPPE along the xy-plane on one of the leaflets in a) Lipid-B, b) Lipid-C, and c) Lipid-D systems. Each color represents one DPPE molecule. For clarity, the corresponding initial (open circles) and final (closed circles) positions of the phosphorus atoms are shown in d), e), and f). Outline of the final simulation box dimension is shown as dash line. Coordinates are plotted without periodic boundary conditions. Trajectories are collected from the last 30 ns of the simulations.

4.3.1   Area per Lipid

The area per lipid, calculated from the cross-sectional area of the simulation boxes (plane along the bilayer interface), for the systems containing trehalose are shown in Figure 4.2.1b. The average area per lipid for pure and mixed DPPC/DPPE bilayers are 0.69 ± 0.01 nm^2, 0.62 ± 0.01 nm^2, and 0.58 ± 0.01 nm^2 for Lipid-F to H, respectively. For the DPPC-trehalose system, previous simulations results reported the average area per lipid of $\sim$0.666 nm^2 at 350 K for 3.4-18.1 wt% trehalose [228], 0.56-0.58 nm^2 at 325 K for 25.5-51.0 wt% trehalose [148], and $\sim$0.629 nm^2 at 323 K for 13.5 wt% trehalose [149]. For the DPPE-trehalose and mixed 1:1 DPPC/DPPE-trehalose systems, experimental or simulation data are currently unavailable. As seen from the results, the area per lipid is unchanged by the presence of trehalose, whether the bilayer is composed of DPPC, DPPE or a mixture thereof. In a similar manner as explained previously for DPPC [228], the interactions of trehalose with DPPE and DPPC/DPPE bilayers are only superficial, along the interface through occasional binding to the headgroups, and for this reason, trehalose is unable to deform the bilayer at low concentrations. Further reasoning is given in the following sections.

4.3.2   Lipid Tail Deuterium Order Parameter

The effect of trehalose on the bilayer structure was also measured from the lipid tail deuterium order parameter (S_{CD}) [92]. Figure 4.2.2b shows S_{CD} as a function of the carbon atom along the lipid tails for lipid systems with and without trehalose. The average order parameter of the two lipid tails (Sn-1 and Sn-2) are independently reported for DPPC and DPPE. From the properties analyzed, the presence of trehalose at the concentrations studied is seen as minimal and because trehalose is unable to penetrate into the bilayer core, the lipid tail should be minimally affected or unaffected at all. This is indeed what is observed, with the order parameter for the systems with and without trehalose being very similar.

4.3.3   Mean-Squared Displacement of Lipids and Trehalose

Figure 4.2.3b shows the mean-squared displacement (MSD) of the lipid molecules for all lipid-trehalose systems. Previous MSD of DPPC, DPPE, 1:1 DPPC/DPPE bilayers without trehalose (see Figure 4.2.3a) are also shown for comparison. From the plot, it is evident that the displacement of the lipids is slightly reduced in the systems containing trehalose. This suggests that trehalose interacts with the lipid molecules and their dynamics change due to this binding. For Lipid-H, in comparison to Lipid-E, it is observed that trehalose reduces the movement of the lipid molecules. Minor differences in the MSD for Lipid-G and C suggest weaker interactions between trehalose and lipid molecules. The calculated 2D diffusion coefficients for the lipids (shown in Table 4.2.1) range from $0.30\pm0.2\times10^{-6}$ cm^2/s to $0.56\pm0.1\times10^{-6}$ cm^2/s. For the DPPC-trehalose system, the estimated values for the lateral diffusion coefficient of lipids are $0.31-0.37\times10^{-6}$ cm^2/s at 325 K [148] and $\sim0.33\times10^{-6}$ cm^2/s at 350 K [228], which are also in good agreement with the current results. Due to the large uncertainty in determining the diffusion coefficients by fitting a line of unity slope to the curves in Figure 4.2.3, a larger error estimate was imposed in the value for Lipid-H. This reflects the long time required for the lipid molecules to reach a diffusive regime. The diffusion coefficients of trehalose, also shown in Table 4.2.1, range from $3.62\pm0.1\times10^{-6}$ cm^2/s in DPPC-trehalose to $4.93\pm0.1\times10^{-6}$ cm^2/s in DPPE-trehalose at 350 K. These values are comparable to those obtained from previous DPPC-trehalose simulations of $0.8-3.5\times10^{-6}$ cm^2/s for $3.40-18.1$ wt% trehalose at 350 K [228], $\sim2.5\times10^{-6}$ cm^2/s for $25.5-51.0$ wt% trehalose at 325 K [148], and from NMR measurements of trehalose in aqueous solutions of $10.1-15.6\times10^{-6}$ cm^2/s for $3.40-18.1$ wt% trehalose at 358 K [287].

4.3.4   Component Density Profiles for Lipid Bilayers with Trehalose

From the individual component density profile of Lipid-A, C, and E, shown in Figures 4.2.4a-c, respectively, in comparison to Lipid-F, G, and H, shown in Figures 4.2.4d-f, trehalose is observed to remain in the aqueous phase without penetrating into the bilayer core region. Note that the density profiles are shifted so that the center of the plot is in the aqueous phase. In the Lipid-F system (Figure 4.2.4d), the trehalose density profile is uniform along the aqueous phase, whereas in Lipid-G (Figure 4.2.4b) and Lipid-H (Figure 4.2.4c), the density distributions for trehalose are uneven with a slight concentration of trehalose near one interface of the membrane, indicating a preferential binding of trehalose with the lipids. As observed in Figures 4.2.5b-c, the amine group of DPPE is exposed to the aqueous phase at the interface where it can interact strongly with trehalose through hydrogen bonding. For all of the systems considered, trehalose molecules are able to superficially interact with the bilayer interface and hydrogen bond favorably to the phosphate and ester headgroups in the lipid molecules. This is seen from the density profiles extending into the headgroup region as far as the phosphorus density profile. As it will be shown, the ester oxygen atoms in the lipids are the binding sites for the hydroxyl groups in trehalose.

4.3.5   Phosphorus-Nitrogen Angle Distribution

In order to further quantify the structure of the lipid bilayers and the effect of trehalose on their structure, the orientation of the vector formed from the phosphorus to nitrogen atoms (P-N) was analyzed for both DPPC and DPPE. The intramolecular angle was computed from the angle formed between the P-N vector (see Figure 4.2.5a for an illustration of the angle). Figures 4.2.5d-f show the normalized distribution for the P-N vector angle for the Lipid-F to H systems. The angle distributions for DPPC in Lipid-F and G are both broad but with distinct maximum values for the angles. In Lipid-F (Figure 4.2.5d), the wide

distribution peaks at about 100 degrees, indicating that the choline groups are exposed to the aqueous phase and unhindered to any preferred orientation. In Lipid-G (Figure 4.2.5e), the distribution for the PC groups shifts to lower values, suggesting most of the choline groups are more exposed toward the aqueous phase. This is caused by closer packing of the lipids in the presence of DPPE (lower area per lipid). For DPPE in Lipid-G, the majority of the P-N angles is larger than 90 degrees, indicating that all the amine groups of DPPE in the mixed lipid-trehalose system favorably interact with the lipid oxygen atoms (Figure 4.2.5e). A bimodal distribution for the P-N angle is observed for DPPE in Lipid-H (Figure 4.2.5f) showing two preferential sites near the interface (distribution less than 90 degrees) and those near the lipid oxygen atoms (distribution greater than 90 degrees). This demonstrates that there are more H-donors from NH_3^+ groups in DPPE than available H-acceptors from lipid oxygen atoms, causing the excess H-donors to interact with water at the interface. Comparison of the angle distribution between lipid systems with and without trehalose shows a slight shift in the distributions, thus supporting the idea that trehalose interacts with the membrane but does not alter its structure (see Figures 4.2.5d-f).

4.3.6   Hydrogen Bonding Analysis: DPPE as H-Donor

The hydrogen bonding of the NH_3^+ (amine) group in DPPE provides great insight into the structure of the bilayer and the interactions with trehalose. Table 4.2.2 shows the ensemble average number of hydrogen bonds between NH_3^+ in DPPE and all oxygen atoms (H-acceptor) in the lipid, trehalose and water, for Lipid-G and Lipid-H. The oxygen sites available as H-acceptor are located at the phosphate group (O7, O9, O10, O11), at the two ester groups (O14, O16, O33, O35), trehalose oxygens (O1, O2, O3, O4, O5, O6 shown in Figure 4.1.3), and water. Separated contributions resulting from intra and intermolecular hydrogen bonds for DPPE are also reported for inter and intramolecular H-bond between DPPE. From this analysis, a summary of the average number of hydrogen bonds between the NH_3^+ group of DPPE and various hydrogen acceptors from water, lipid, and trehalose

is shown in Table 4.2.2. The total average number of hydrogen bonds per NH_3^+ is about $2.81-2.82$ (see last row of Table 4.2.2), independent of the DPPE concentration (this value is expected since there are three H-donors per NH_3^+). Moreover, it is interesting to see that the total number of hydrogen bonds from the amine group in DPPE is also unaffected by trehalose. In the presence of trehalose, the amine group is able to hydrogen bond with trehalose, which results in a decrease of intermolecular hydrogen bonds between lipids and, consequently, an increase in the number of hydrogen bonds with water. This is shown in Lipid-G where the number of hydrogen bonds between NH_3^+ and water per DPPE increases from 0.75 (Lipid-G) to 0.77 (Lipid-C) while intermolecular hydrogen bonds decreased from 1.11 (Lipid-G) to 1.05 (Lipid-C). The same behavior is not observed in Lipid-H mainly because the NH_3^+ groups are more exposed to water due to the competition for hydrogen bonds, which creates preferential hydrogen bonding sites for trehalose oxygen atoms to bind. As a result, the interaction between trehalose and the NH_3^+ group occurs by replacing the interactions between water and the NH_3^+ group.

From Table 4.2.2, the total number of hydrogen bonds per NH_3^+ (ensemble average) between NH_3^+ and all trehalose oxygen atoms is significantly increased from Lipid-G to H (approximately 0.01 to 0.04). The large difference in value demonstrates a preferential binding of trehalose to the amine group in DPPE in Lipid-H. This is expected because the amine group is more exposed in the interface in Lipid-H than in Lipid-G, as observed from the normalized P-N angle distribution previously calculated (see Figure 4.2.5). This is explained by the fact that there are more H-donors than available H-acceptors as the DPPE concentration increases, resulting in a competition between lipid oxygen atoms and water for hydrogen bonds with the NH_3^+ groups. From these results, it is concluded that hydrogen bonds are formed between NH_3^+ and trehalose oxygen atoms near the interface in Lipid-H. However, due to the preferential binding of NH_3^+ to lipid oxygen atoms in Lipid-G, interactions with trehalose are less than expected.

4.3.7   Hydrogen Bonding Analysis: Trehalose as H-Donor

A hydrogen bond analysis was also performed to investigate the binding of trehalose as H-donor to other H-acceptors (lipid oxygen atoms). For this analysis, the H-donors are the hydroxyl (OH) groups in trehalose denoted by TO2, TO3, TO4, and TO6 (see Figure 4.1.3). Note that trehalose has two glucose rings with the same hydroxyl groups on each ring. Instead of calculating the ensemble average of hydrogen bonds between the OH groups and lipid oxygen atoms, which is relatively small in number, the actual number of hydrogen bond contacts between these two groups over the course of the simulations are determined, as shown in Table 4.3.1. Lipid-H shows the largest number of contacts ($\sim$5.8$\times$10^5). This is expected because Lipid-H has the largest number of amine groups which can preferentially hydrogen bond with trehalose. Lipid-F has the least number of contacts ($\sim$4.9$\times$10^5) because this system does not contain strong H-donors (NH_3^+). Using the same analysis, it is expected that Lipid-G would have the average number of contacts in between Lipid-H and F, however, only a slight increase in the number of contacts is observed ($\sim$5.0$\times$10^5). This can be explained by two factors. First, the trehalose density profile (as shown in Figure 4.2.4) and the P-N angle distribution (as shown in Figure 4.2.5) suggest that a significant amount of amine groups in DPPE are more exposed to the aqueous phase in Lipid-H compared to Lipid-G. These amine groups are at the interface and they can easily hydrogen bond to the hydroxyl groups in trehalose. Consequently, at the interface, the hydroxyl groups are then in the range to form hydrogen bonds with lipid oxygen atoms. Note that for every trehalose molecule that comes in contact with an amine group, there are a total of eight hydroxyl groups that can potentially form hydrogen bonds with lipid oxygen atoms. Second, due to the competition between excess H-donors and H-acceptors in lipid oxygen atoms or water, a significant increase in the hydration of the amine group of DPPE in Lipid-H is observed, resulting in a reduction of inter and intramolecular hydrogen bond between lipids. This results in a greater increase in the number of hydrogen bond contacts of trehalose with lipid oxygen atoms in Lipid-H than in Lipid-G.

Table 4.3.1: Approximate number of hydrogen bond contacts between trehalose hydroxyl groups and lipid oxygen atoms over the course of 50 ns simulations. Individual contact points are independently reported for DPPC and DPPE in the mixed lipid systems. Contacts are counted only for trajectories saved every 2 ps. All values reported as # of `contact` $\times 10^{-3}$.

Lipid	Lipid-F^a	Lipid-G^a	Lipid-G^b	Lipid-H^b
O7	65.8	45.5	5.5	12.8
O9	175.0	96.9	124.5	244.1
O10	133.2	70.5	65.2	189.9
O11	32.5	20.5	15.9	35.2
O14	29.8	7.1	1.0	14.7
O16	39.6	16.1	10.0	56.7
O33	4.2	2.0	1.4	2.3
O35	14.8	8.3	5.3	26.8
Total	494.9	266.9	228.7	582.6

Trehalose	Lipid-F^a	Lipid-G^a	Lipid-G^b	Lipid-H^b
TO2	121.4	65.1	61.1	148.1
TO3	143.2	73.2	68.6	165.8
TO4	139.1	82.2	65.0	158.6
TO6	91.3	46.5	34.0	110.1
Total	494.9	266.9	228.7	582.6

[a] Interaction between DPPC and trehalose
[b] Interaction between DPPE and trehalose

4.3.8   Dynamics of Trehalose in Pure and Mixed Lipid Bilayers

To summarize the properties of trehalose in the pure and mixed DPPC/DPPE bilayers, the dynamics of trehalose from the trajectories were monitored over the length of the simulations. Here, one trehalose molecule was selected (represented by the position of TO1 atom-see Figure 4.1.3) from each of Lipid-F, G and H, and investigated its interaction with the lipid oxygen atoms, as shown in Figures 4.3.1a-c, respectively (trajectories shown are with respect to the z-direction only). From the figures, it is clear that trehalose is randomly interacting with the membrane interface. Figures 4.3.1a-c show close contact of trehalose with the bilayer as the trajectories of trehalose overlap the phosphorus layer at certain times. Furthermore, Figures 4.3.1d-f illustrate the hydrogen bond pairs which are responsible for each contact between trehalose and lipid molecules. The hydroxyl groups in trehalose are assumed as H-donors and lipid oxygen atoms as H-acceptors. The plots show the interaction of H-donors with lipid oxygen atoms, denoted by O7, O9, O10, O11, O14, O16, O33, and O35 for DPPC, and O7E, O9E, O10E, O11E, O14E, O16E, O33E, and O35E for DPPE. Comparison of the trajectories plots in the top and bottom rows indicates the times when trehalose binds to the headgroups. For example, Figures 4.3.1a and d correspond to the trajectory of a trehalose molecule and its binding to the lipids. In this case, trehalose predominantly binds to the phosphate oxygen atoms, while fewer interactions occur with the ester groups. On the other hand, the interactions of trehalose with pure DPPE (Figures 4.3.1f) show that the ester groups are more exposed and more accessible to bind with trehalose, as previously reported [228]. Even though the binding of trehalose with DPPE is more than with DPPC, the interactions are superficial along the interface, that is, there are fewer interactions of trehalose with the ester headgroups.
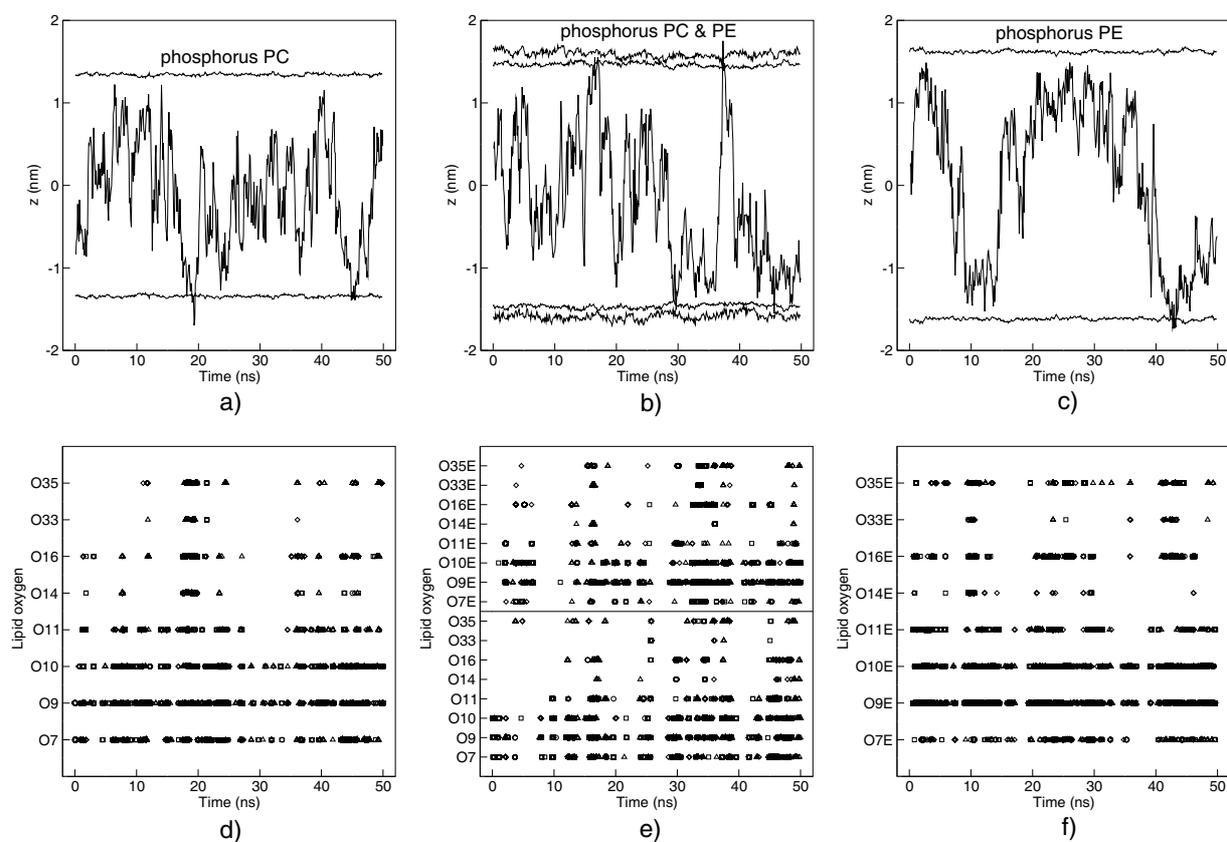
Figure 4.3.1: Dynamics of one selected trehalose molecule represented by the position of the oxygen atom (TO1) from a) Lipid-F, b) Lipid-G, and c) Lipid-H. Corresponding hydrogen bond interaction between the hydroxyl groups of the selected trehalose molecule and lipid oxygen atoms are shown for d) Lipid-F, e) Lipid-G, and f) Lipid-H. The hydroxyl groups are TO2 (circles), TO3 (squares), TO4 (diamonds) and TO6 (triangles). The average position of phosphorus atoms illustrates the location of the bilayer interface. The position $z = 0$ corresponds to middle of the aqueous phase. The average position of the phosphorus atoms in DPPC and DPPE are independently reported in b) for clarity.

4.4   Summary

4.4.1   Pure and Mixed DPPC/DPPE bilayers

Molecular dynamics simulations have been used to study structural and dynamic properties of fully hydrated mixed DPPC and DPPE bilayers at 0, 25, 50, 75, and 100 mol% DPPE. Simulations were performed for 50 ns at 350 K and 1 bar for the liquid-crystalline state of the mixtures. Results show that the average area per lipid reduces from 0.69 ± 0.01 nm^2 in pure DPPC to 0.58 ± 0.01 nm^2 in pure DPPE systems. The lipid tails become more ordered with increasing DPPE concentration, resulting in a slight increase in membrane thickness (3.43 ± 0.01 nm in pure DPPC to 4.00 ± 0.01 nm in pure DPPE). In-depth analysis of the hydrogen bond distribution in DPPE molecules shows that the amine groups strongly interact with the phosphate and carbonyl groups through inter/intramolecular hydrogen bonds. This yields a bilayer structure with DPPE headgroups preferentially located near the lipid phosphate and ester oxygens. It is observed that increasing DPPE concentrations causes competitive hydrogen bonding between the amine groups (H-donor) and the phosphate/carbonyl groups or water (H-acceptor). Due to the increasing number of H-donors from DPPE molecules with increasing concentration, DPPE becomes more hydrated. Trajectory analysis shows that DPPE molecules in the lipid mixtures move laterally and randomly around the membrane surface and the movement becomes more localized with increasing DPPE concentration. For the conditions and simulation time considered, no aggregation or phase separation was observed between DPPC and DPPE.

4.4.2   Pure and Mixed 1:1 DPPC/DPPE bilayers with Trehalose

Molecular dynamics simulations were performed to study structural and dynamic properties of fully hydrated pure and mixed bilayers of DPPC and DPPE in the presence of trehalose (5 wt%). Simulations were performed for 50 ns at 350 K and 1 bar in the liquid-crystalline

state of the lipid bilayers. At the concentration considered, the effect of trehalose on the structure of pure and mixed DPPC/DPPE is minimal, with the area per lipid and lipid tail order parameter unchanged compared to systems without trehalose. Density profiles indicate a larger concentration of trehalose near the interface, suggesting preferential binding of trehalose with the bilayer. Hydrogen bond analysis between trehalose and the bilayers shows that the largest number of interactions occurs with pure DPPE lipids, whereas the fewest interactions occur in a pure DPPC bilayer. The latter is a result of the intermolecular and intramolecular binding of the amine group in DPPE, thus attracting trehalose to hydrogen bond to the bilayer. For the mixed 1:1 DPPC/DPPE bilayer, the effect of H-donors (amine groups) is due to the decrease in bindings with neighboring lipids. In this case, trehalose is concentrated near the interface; however, the binding of trehalose with the bilayer is significantly reduced compared to pure DPPE bilayers.

Chapter 5

Stabilization of Dehydrated Lipid Bilayers with Glucose and Trehalose

In addition to Chapter 4, the focus of this chapter is to obtain a better understanding on how saccharides (glucose and trehalose) protect and preserve the structure of DPPC bilayers at dehydrated conditions and lower the phase transition temperature. A key concept on the preservation mechanism by saccharides was proposed by Crowe *et al.* [159], suggesting that the stabilization of the bilayer results from the saccharide molecules that fit in spaces between lipids at the bilayer interface. In principle, this is unattainable in typical bilayer simulations, because the relaxation time of the lipids is very long. In addition, the exerted pressure in the lateral directions prevents an expansion of the bilayer to allow the saccharide molecules from intercalating between the lipid molecules. Previous DPPC-trehalose simulations in the fully-hydrated state have shown that hydrogen bonds between trehalose and lipid molecules are random, temporary, and seldom form with multiple lipids at the interface [148–151, 227, 228]. At low hydration and high trehalose concentration, previous MD simulations predicted that the interactions become more prominent, as trehalose displace interfacial water and preserve the bilayer structure by increasing the bilayer lateral pressure [164]. Therefore, to further gain insight into the interactions of saccharides with the bilayer as suggested by Crowe *et*

al. [159], constant surface area (NP_zAT) simulations of lipid bilayers were performed with and without saccharides. This computational study aims to determine whether saccharides can stabilize dehydrated bilayers as in a manner similar to predictions for the fully-hydrated state.

5.1   Difficulties and Challenges

Three difficulties arise when performing MD simulations to model uni-lamellar bilayers at dehydrated conditions. First, phospholipid force-fields developed for fully-hydrated conditions may be unsuitable for simulations under dehydrated conditions. Using the current lipid force-fields, a recent study by Doxastakis *et al.* obtained reasonable structural properties of dehydrated lipid bilayers (0.78 water/lipid) from MD simulations, which were in agreement with elastic and quasielastic neutron scattering results [165]. Second, periodic boundary conditions (PBC) implemented in typical MD simulations with long-range electrostatic corrections essentially create a multi-lamellar bilayer structure (see Figure 5.1.1a). Therefore, an alternative setup is required for uni-lamellar bilayers. Third, due to the low water content at dehydrated conditions, the lipid bilayer lateral compressibility is no longer the same as the typical compressibility derived from a fully-hydrated state; as such the bilayer structure can be overly compressed with the parameters from the fully-hydrated state. To overcome the PBC and compressibility problems, the two lipid bilayer setups used in this study are described in the following paragraphs.

In typical fully-hydrated lipid bilayer simulations without long-range electrostatic corrections (cutoff method), even though a multi-lamellar structure is represented using PBC, each bilayer is effectively shielded from interactions with its periodic image because a large continuous water layer separates the bilayer images (see Figure 5.1.1a and c), thus making the bilayer essentially uni-lamellar. Inclusion of long-range electrostatic corrections (e.g., Ewald summation) results in a more accurate account of the interactions in the simulations,
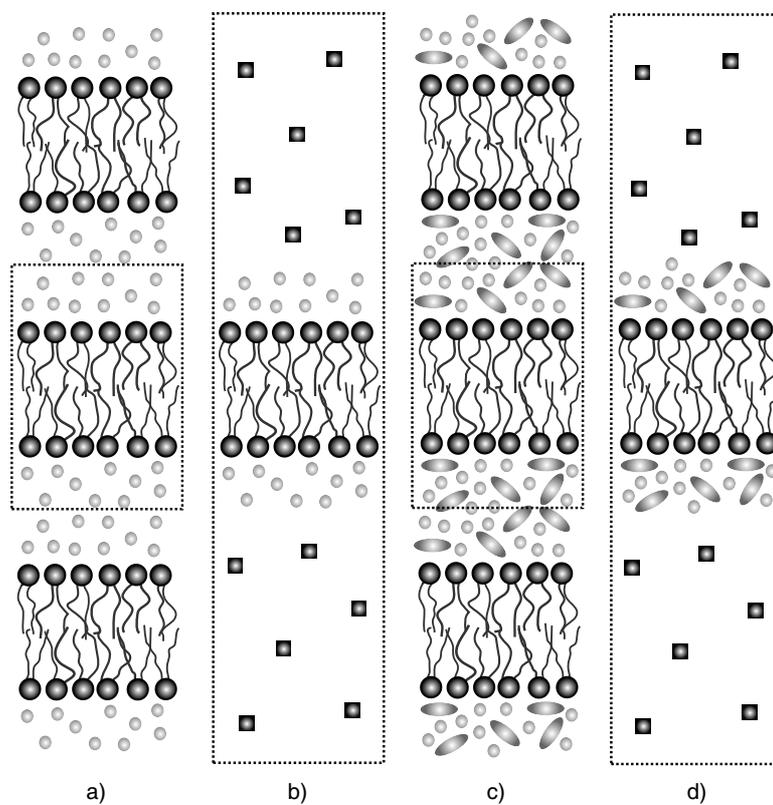
Figure 5.1.1: Schematic representation of lipid bilayers without (a and b) and with (c and d) glucose and trehalose. a) and c) are conventional lipid bilayer setups. b) and d) are gas-containing lipid bilayer setups. A lipid molecule is represented with a black circle and two lipid tails. Gray circle, oval, and square are water, saccharide, and gas molecules, respectively. Two periodic images of the bilayers are shown in a) and c) to differentiate the two types of bilayer settings (dotted rectangular lines are the bounds of the simulation boxes).

however, in doing so, each bilayer is no longer shielded from the periodic images, resulting again in a multi-lamellar structure. Under dehydrated conditions, the water layer is significantly reduced, causing the bilayer images to self-interact. Note that the influence of periodic images becomes more apparent in dehydrated lipid bilayer simulations regardless of the method for the long-range interactions. This was the approach used by Doxastakis *et al.* for their dehydrated multi-lamellar bilayers [165]. To model a uni-lamellar bilayer at dehydrated conditions, enough water has to be present so that the bilayer images do not self-interact due to the PBC. To accomplish this, the number of water per lipid was reduced to 20 (lower limit also used by Skibinsky *et al.* [164]) in the first setup. It was determined that 12 and 30 water/lipid are typical values for dehydrated and fully-hydrated bilayers, respectively [288, 289]. At this ratio, a water layer of about 1 nm separates the bilayer images. Note that saccharide molecules present in this water layer may experience interactions with both leaflets at the same time, due to PBC.

In a typical bilayer simulation with PBC, the bilayer is still considered as a multi-lamellar structure because of its periodic images. To overcome this problem, a continuous inert gas layer was introduced to separate the water layers from each side of the bilayer in the second bilayer setup (schematic representation of this bilayer is shown in Figure 5.1.1b). Note that this structural representation is significantly different from the previous work on monolayers by Skibinsky *et al.* [164]. The gas layer was composed of 44 argon atoms, filling the vapor space of the simulation box with lateral dimensions equal to the bilayer surface ($A_{xy} \sim 0.645$ nm^2) [276, 284] and height ($L_z \sim 19.6$ nm), such that the normal pressure (P_N) exerted on the bilayer was 1 bar. Although this is an unconventional method for lipid bilayer simulations, the benefits from this setup are that the bilayer is truly uni-lamellar and dehydrated conditions can be considered without self-interaction of the bilayers. For these bilayer structures, a ratio of 10 water/lipid was used in all cases.

Table 5.2.1: Composition and simulation time for the bilayer systems considered.

DPPC[a]	Water	Glucose	Trehalose	Argon	Time (ns)
144	5,760	–	–	–	240, 240, 180
144	5,760	120	–	–	240, 240, 180
144	5,760	–	60	–	240, 240, 180
144	1,440[a]	–	–	44	30, 30, 30
144	1,440[a]	60[a]	–	44	30, 30, 30
144	1,440[a]	–	30[a]	44	30, 30, 30

[a]per leaflet

5.2 Simulation Details

All bilayers considered here contained a total of 288 DPPC molecules (144 per leaflet). For each bilayer setup, three sets of bilayer simulations were considered: without saccharides, with 32.8 wt% glucose, and with 16.5 wt% trehalose (see Table 5.2.1 for more details); these are considered high concentrations of saccharides. The concentration of glucose to trehalose of 2:1 was chosen to preserve the number of glucose-rings in each system. Glucose and trehalose molecules were randomly inserted in the aqueous phase of a fully-hydrated bilayer and the excess water removed to obtain a ratio of 20 water/lipid (details of this procedure can be found in Chapter 4.1. After the insertion of saccharides, the bilayers were equilibrated for at least 5 ns. For uni-lamellar bilayers (Figure 5.1.1b), a large vapor space with an inert gas was superimposed in the system. Short annealing simulations of 5 ns were performed on these systems (heated to 325 K and then cooled to the set temperature). For uni-lamellar bilayers with saccharides (Figure 5.1.1d), 60 glucose or 30 trehalose molecules were placed on each side of the bilayer. These systems were annealed for 5 ns (heated to 380 K, temperature above the glass transition temperature for glucose and trehalose [290, 291], and then cooled to the set temperature). All systems were simulated at 290, 300, and 310 K.

The force-fields for DPPC and water were consistent with those employed in the studies reported in Chapter 4.1, which included intramolecular parameters for bonds, angles, proper dihedral, and improper dihedral [103, 270]. The Ryckaert-Bellemans potential was

used for the torsion potential of the lipid hydrocarbon chains [271]. Non-bonded interactions were described by the parameters from Berger *et al.* [104, 110, 272] and partial atomic charges were obtained from Chiu *et al.* [96]. The united-atom representation was used for the methyl/methylene groups in the alkyl chains of DPPC. Although the lipid force-field was optimized for fully-hydrated conditions in the temperature range of 320-330 K, recent studies demonstrated that it can also be applied to study lipid bilayer phase transition, including the gel state [94, 95] and dehydrated conditions [165]. The optimized potential for liquid simulations (OPLS-AA) force-field was used for glucose and trehalose [292]. Argon parameters were obtained from the Gromos force-field [293]. The single point charge (SPC) model was adopted for water [273].

Another unknown parameter in the simulation of lipid bilayers at dehydrated conditions is the lateral compressibility factor. Since the amount of water is low at dehydrated conditions, the typical compressibility of 4.5×10^{-5} bar^{-1} (water compressibility at $\sim 45°$C) is inappropriate. To eliminate this unknown, constant surface area simulations (NP_zAT) were performed, where the lateral (xy-directions) and normal (z-direction) compressibilities were set to zero and 4.5×10^{-5} bar^{-1}, respectively. Similar conditions were previously applied in a study by de Vries *et al.* that found that lipid bilayers undergo a ripple phase transition (a combination of ordered and disordered lipid tails with interdigitation) [187]. For all bilayers considered here, the surface area ($A_{xy} \sim 0.645$ nm^2) was constrained to that at 325 K and 1 bar [276, 284]. In comparison to the previous study by Skibinsky *et al.*, in which trehalose was shown to slightly increase the bilayer lateral pressure [164], the first part of this study investigated the bilayer stabilization below the main phase transition temperature caused by an increase in the bilayer lateral pressure in the presence of saccharide molecules. For the uni-lamellar systems with a vapor phase, the surface area was also constrained, and because the gas exerted a constant pressure of 1 bar normal to the bilayer, the box height was also fixed (NVT simulations). This setup allowed us to study the bilayer stabilization at dehydrated conditions in the presence of saccharide molecules.

A timestep of 2 and 3 fs was used for the simulations (see Table 5.2.1 for the total

simulation times). Note that the results obtained using a 3 fs timestep provided stable bilayer structures comparable to those simulated with a 2 fs timestep (the total energy for both cases was statistically identical – e.g., -5310.1$\pm$3.5$\times10^2$ kJ/mol and -5312.2$\pm$3.9$\times10^2$ kJ/mol for the 2 and 3 fs simulations, respectively, for the DPPC bilayer at 290 K). Other studies in the literature have reported simulations of lipid bilayers with timesteps as large as 5 fs [294]. Short-range Coulombic and van der Waal interactions were cutoff at 1.0 nm. Long-range electrostatic interactions were corrected with the particle-mesh Ewald (PME) method [108, 263] (0.12 nm for the grid size, fourth-order spline interpolation, and real-space cutoff at 1.0 nm). Trajectories were collected every 3 ps. All simulations were performed with GROMACS 3.3.3 [258, 259, 295] (single-precision) in parallel using Virginia Tech's System X [281].

5.3   Analysis of Multi-lamellar Bilayers with Sugars

The following sections describe the structural properties of lipid bilayer (20 water/lipid) with and without glucose and trehalose at 290, 300, and 310 K. The properties that were analyzed are lipid tail density profiles, average bilayer thickness, and surface plots of bilayer thickness.

5.3.1   Snapshots of the Lipid Bilayers

Figure 5.3.1 shows snapshots of the lipid bilayers (20 water/lipid) with and without glucose or trehalose at 300 and 310 K (snapshots of bilayers at 290 K are almost identical to those at 300 K). It is visually evident from the snapshots that the bilayer structures (side-view) are almost identical with and without glucose or trehalose. At 290 and 300 K, the lipid tails are predominantly aligned with the bilayer normal showing significant lipid tail inter-digitation (Figures 5.3.1a-c). At 310 K, the lipid tails are random and disordered with little interdigitation between the leaflets (Figures 5.3.1d-f). To confirm this observation, the over-lap between lipid tails from opposite leaflets was measured from the density profile of the
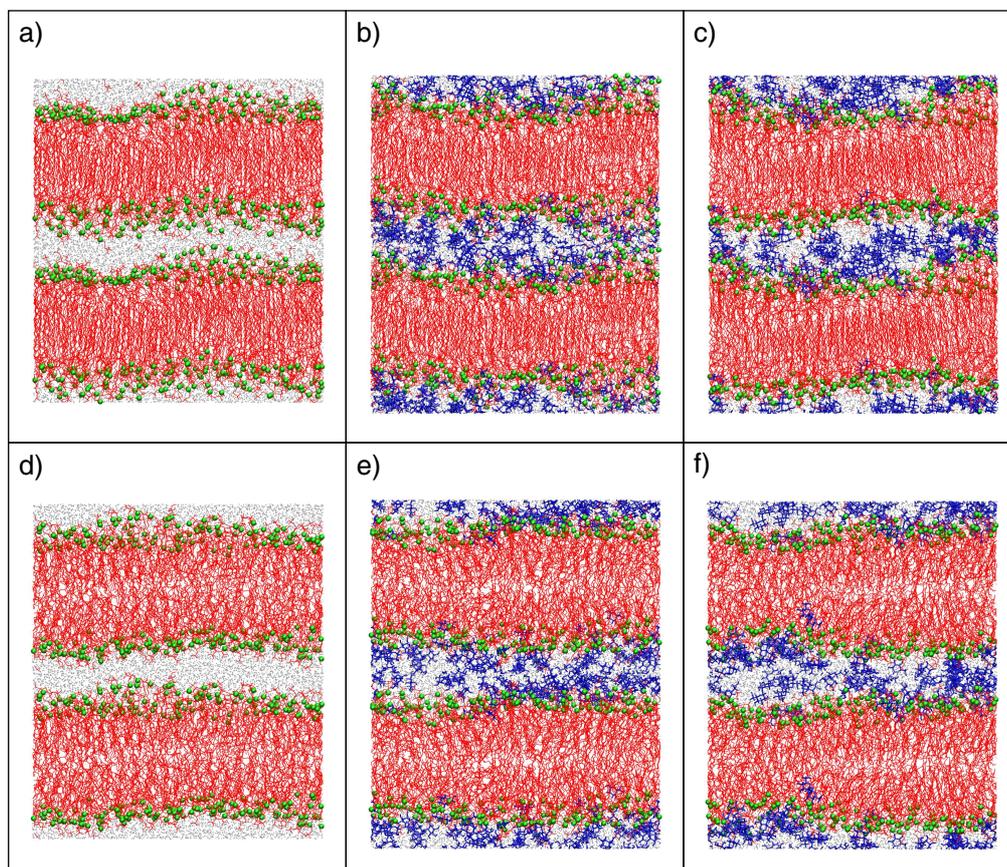
Figure 5.3.1: Snapshot of DPPC bilayers at 300 K: a) without saccharides, b) with glucose, and c) with trehalose. For comparison, snapshots of the same bilayers at 310 K are shown in d-f, respectively. Two periodic images are shown to explicitly indicate the aqueous phase separating the bilayers.

individual carbon atoms in the acyl chains, as described by Flack *et al.* [168]. As observed from the density profiles shown in Figure 5.3.2, there was significant overlap among the lipid tails from opposing leaflets at 290 and 300 K, indicating interdigitation of the lipid tails. At 310 K, the interdigitation was less pronounced. However, the snapshots and the level of interdigitation are insufficient to distinguish the stabilization effect of glucose and trehalose.
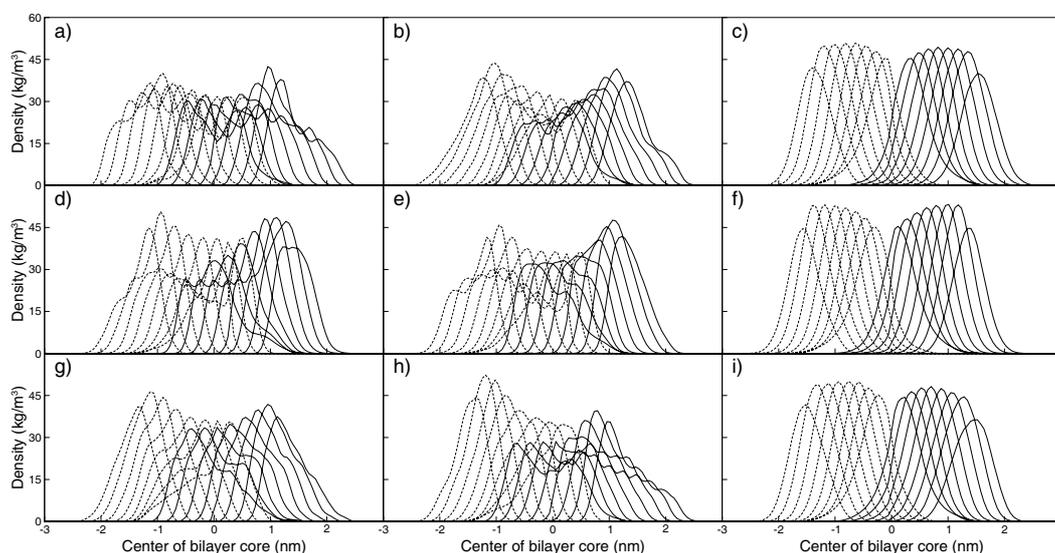
Figure 5.3.2: Density profile for the alternating carbon atoms in the Sn-2 tail for the lipid bilayers with: no saccharide (a-c), glucose (d-f), and trehalose (g-i). Temperatures considered are 290, 300, and 310 K (1st to 3rd column, respectively). Profiles are centered with respect to the middle of the bilayer core. Solid and dash lines represent density profiles for each leaflet. For clarity, only the Sn-2 tail is considered (those for the Sn-1 tail are nearly identical - data not shown here).

5.3.2 Bilayer Thickness

To differentiate the properties of glucose and trehalose and their interactions with the dehydrated lipid bilayers, the degree of lipid tail interdigitation was measured from the average bilayer thickness. The average bilayer thickness is the distance between the average positions of the phosphorus atoms in each leaflet. The results are shown in Figure 5.3.3 for bilayers with and without glucose or trehalose at 290, 300, and 310 K. All the bilayer structures without saccharide remained stable at 310 K. However, at 290 and 300 K, the bilayer thickness is significantly reduced along with the lipid molecular volume and lipid tail interdigitation, indicating the bilayer underwent a phase transition. This shows that a phase transition occurred with significant reduction in the lipid molecular volume, leading to lipid tail interdigitation. As shown in Figures 5.3.3b and c, a similar bilayer thickness reduction for bilayers containing glucose and trehalose was observed, suggesting that glucose and trehalose are unable to prevent lipid tail interdigitation. One explanation for this behavior is the competitive hydrogen bond between water and saccharides in the aqueous phase, which prevents saccharides from binding to the lipid headgroups. This interaction has been discussed by Lenne *et al.*, where the mismatch of their model with experimental results was attribute to exclusion effects [166]. Furthermore, because the aqueous layer is very thin (low hydration and PBC), saccharide molecules are essentially interacting with lipids in both leaflets at any given time, thus potentially reducing their effectiveness as stabilizing agents. Lastly, the setup of the simulations simply induces lipid tail interdigitation, because of the pressure exerted in the *z*-direction. Based on the model predictions, it was postulated that glucose and trehalose are unable to stabilize the bilayer structure in preventing interdigitation.

5.3.3 Bilayer Surface Analysis

As a consequence of lipid tail interdigitation shown in Figure 5.3.1, the average bilayer thickness is inadequate to measure the changes in the bilayer structure. To address this problem, the bilayer surface was segmented into 144 grids (12×12) and the average bilayer
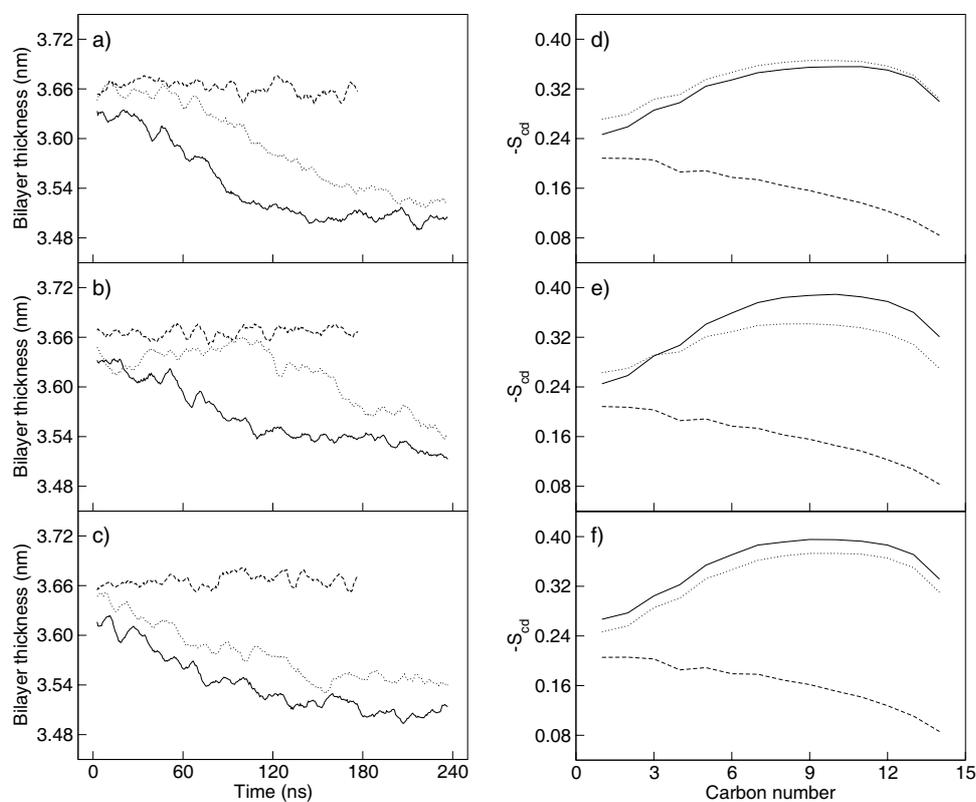
Figure 5.3.3: Average bilayer thickness for bilayers a) without saccharide, b) with glucose, and c) with trehalose. The corresponding lipid tail order parameters are shown in the adjacent plots (d-f). Lines correspond to 290 (solid), 300 (dot), and 310 K (dash).

thickness estimated at each grid. Since the bilayers considered here contain 144 lipid/leaflet, each grid approximately contains one lipid. An added benefit of using this approach is the ability to monitor the structural evolution of the bilayer (see Figure 5.3.4 for surface plots of the bilayer thickness without saccharide over the course of the simulation). This method was implemented to quantify the changes in the bilayer structure and differentiate the properties of glucose and trehalose on the bilayer structures. Figure 5.3.5 shows surface plots of the bilayer thickness based on the segmentation of the bilayers. As shown in the plots, the bilayers have well-defined single or multiple domain regions at 290 and 300 K (indicated by the red-colored regions), whereas at 310 K the domains are less prominent. The latter is in good agreement with the results obtained from the average bilayer thickness (Figures 5.3.3a-c), in which all bilayers remained in the fluid state at 310 K (ordered domains were absent). To verify the formation of order domains, the lipid tail order parameters were calculated for the bilayers with and without saccharides, as shown in Figures 5.3.3d-f. It is clear from the order parameter that the lipid bilayers are in a gel-like (ordered) state at 290 and 300 K and a fluid-like (disordered) state at 310 K. These results are in agreement with the bilayer snapshots shown in Figure 5.3.1. For the bilayers without saccharides at 290 and 300 K, relatively thick domains are long and narrow. This is related to the ripple formation in bilayers previously identified by de Vries *et al.* [187]. Unlike the bilayers without saccharides, multiple small thick and isolated large thick domains are observed for the bilayers containing glucose and trehalose, respectively. If the periodic images along the surface were shown on the bilayers containing trehalose in Figure 5.3.5 at 290 and 300 K, the surface plots would contain multiple domains as well, however, the size and distance between the domains would be greater than those containing glucose. Based on these findings, it is evident that the saccharides altered the formation of ordered domains and their size is important in determining the domain morphology. These results do not demonstrate the stabilizing effect of saccharides on the bilayers, but they provide a comparison of the effects of mono- and di-saccharides on the bilayer structure.
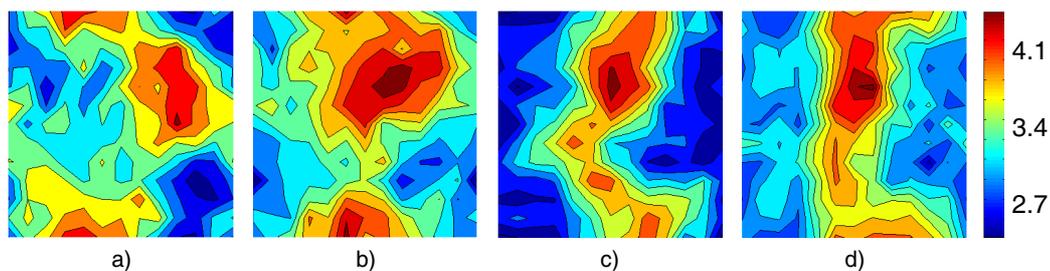
Figure 5.3.4: Surface plots of bilayer thickness at a) 0 ns, b) 90 ns, c) 180 ns, and d) 240 ns for bilayer without saccharide at 300 K. Red and blue coloring corresponds to the thickest and thinnest bilayer domains, respectively.
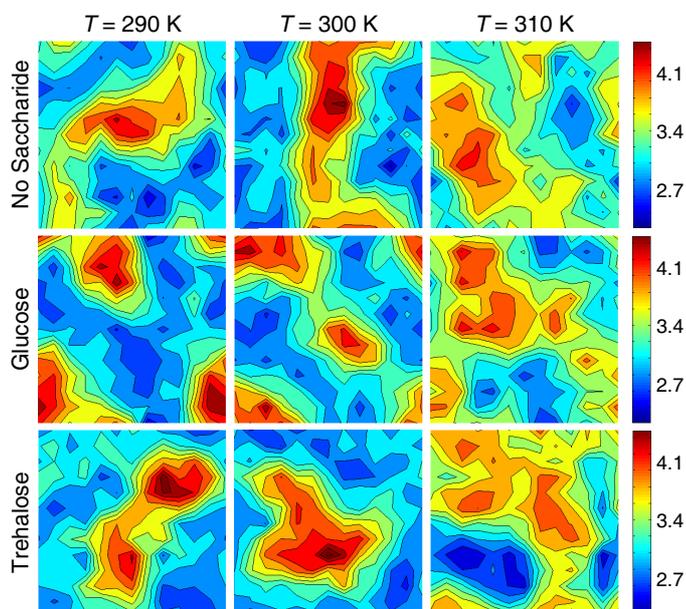
Figure 5.3.5: Surface plots of bilayer thickness (in nm) for bilayers without saccharide, with glucose, and with trehalose at 290, 300, and 310 K at the end of the simulations.

5.4   Analysis of Bilayers Containing a Gas phase

To overcome some of the deficiencies in the simulations of bilayers at dehydrated conditions, the two aqueous phases were exposed to a vapor phase containing inert gas molecules (see Figure 5.1.1 and Section 5.1 for more details). This configuration prevented lipid self-interaction and allowed a lower water/lipid ratio (true uni-lamellar dehydrated bilayer). Furthermore, the pressure exerted along the bilayer normal is controlled by the inert gas molecules, thus eliminating the force induced on the bilayers due to the pressure coupling in the simulations, which accentuated lipid tail interdigitation. Because the pressure exerted in the lateral directions of the lipid bilayer can easily compress the bilayer under dehydrated condition, the bilayer surface area was fixed.

5.4.1   Snapshots of the Lipid Bilayers

Figure 5.4.1 shows snapshots of the dehydrated bilayers without saccharide at 290, 300, and 310 K initially and after 30 ns, respectively. Here, the original bilayer structure (Figures 5.4.1a) quickly becomes unstable and disintegrates to a non-bilayer structure (Figures 5.4.1d, g, and j). The cause for this breakdown of the bilayer is due to the low water/lipid ratio, which affects the hydrophobic/hydrophilic interactions between water and lipid for a stable bilayer structure. In contrast, the bilayers containing glucose and trehalose (Figures 5.4.1b and c) remained stable for more than 30 ns of simulation time. It is seen from the snapshots that the saccharide molecules are able to penetrate deep into the bilayer, stabilize the lipid headgroups, and potentially maintain the hydration layer.

5.4.2   Depth of Saccharide Penetration

To determine the penetration depth of the saccharides into the bilayer, the component density profiles were calculated, as shown in Figure 5.4.2. For clarity and brevity, only the density
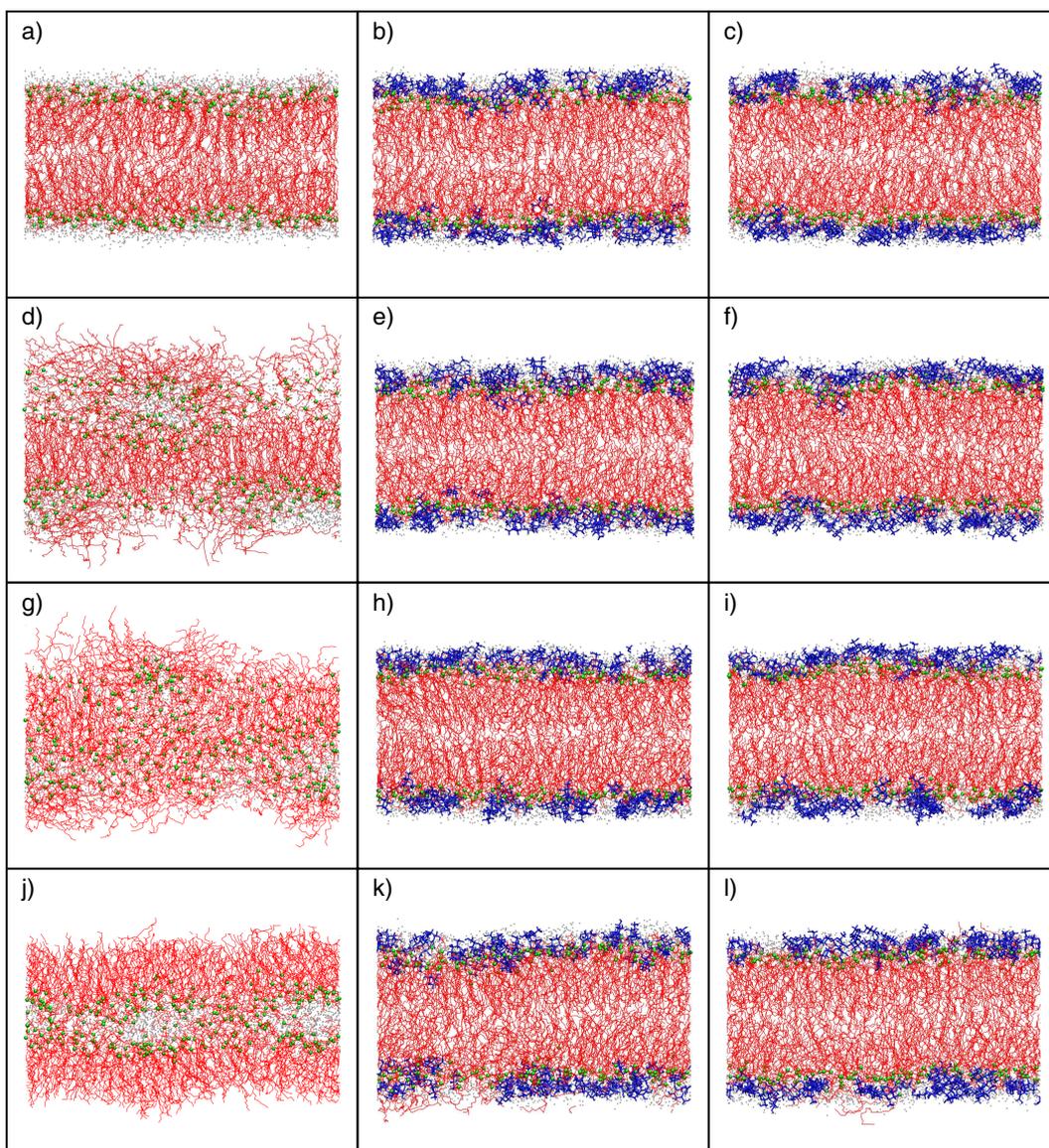
Figure 5.4.1: Snapshot of DPPC bilayers containing an inert gas layer: without saccharides (1st column), with glucose (2nd column), and with trehalose (3rd column). For comparison, the starting configuration are shown on the 1st row and final configurations at 290, 300, and 310 K of the bilayers are shown on the consecutive rows, respectively. Inert gas molecules are not shown.

profiles for water, trehalose and phosphorus atoms at 300 K are shown. As the density profiles show, most saccharide molecules remain in the aqueous phase (see Figures 5.4.2a and b), as also predicted in previous simulations of lipid bilayers with trehalose in the fully-hydrated state [148–151, 227, 228]. However, unlike previous simulations of bilayers with trehalose at 350 K (density profiles shown in Figure 5.4.2c) [227], this study shows that a fraction of the saccharide molecules penetrate deeper into the bilayer. Figures 5.4.2d-f show the magnification of the density profiles shown in Figures 5.4.2a-c at the interfacial regions, which indicate the presence of glucose or trehalose below the mean position of the phosphorus atoms.

5.4.3   Bilayer Surface Analysis

To verify that the bilayers containing a vapor phase were stable with saccharides, the bilayer surface uniformity with the bilayer thickness surface plots were measured (see Figure 5.4.3 for the surface plots for the bilayers shown in Figures 5.4.1e, f, h, i, k, and l). As seen from the figure, the bilayer surfaces are largely uniform (even color distribution) compared to the surface plots for the bilayers shown in Figure 5.3.5. To confirm this, the bilayer thickness distribution was calculated (see Figure 5.4.4) for the systems shown in Figures 5.3.5 and 5.4.3 by considering the ensemble average over the last 30 and 20 ns for multi-lamellar and uni-lamellar bilayers, respectively. The bilayer thickness distributions clearly demonstrate a more uniform bilayer (narrow and sharp distribution) for the uni-lamellar bilayers, suggesting that for these systems, there is little interdigitation, order domains are absent, and the lipid molecules are evenly distributed in the bilayer.
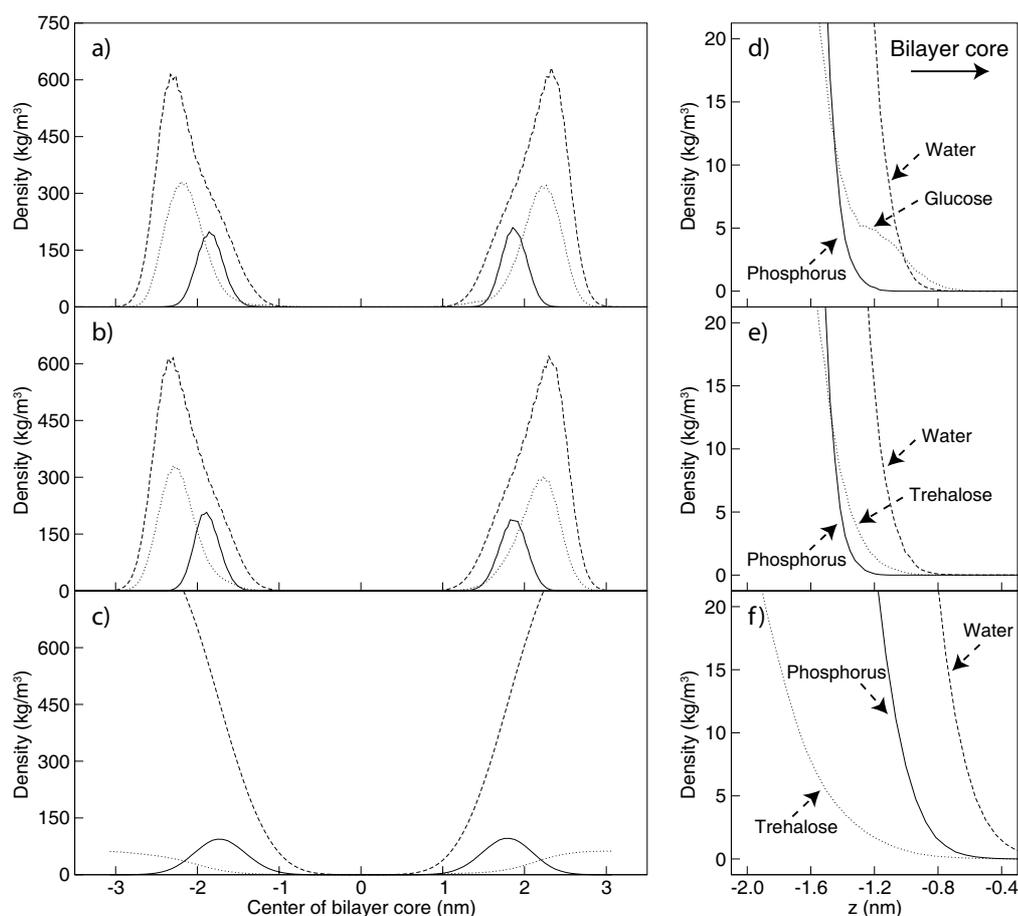
Figure 5.4.2: Component density profiles for lipid bilayers exposed to a vapor phase at 300 K: a) with glucose and b) with trehalose. For comparison, the density profiles for the fully-hydrated bilayer containing trehalose obtained from previous simulations at 350 K with PBC are shown in c) [227]. Line representation corresponds to: phosphorus atoms (solid), saccharide (dot), and water (dash). Center of the plot is the bilayer core region. For clarity, the magnification of the density profiles at one of the water-lipid interfaces is shown on the right (d-f).
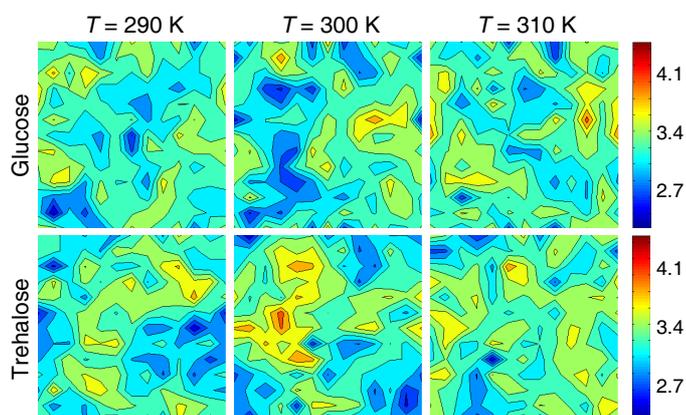
Figure 5.4.3: Surface plots of bilayer thickness (in nm) for the uni-lamellar bilayers exposed to an inert gas layer with glucose and trehalose at 290, 300, and 310 K. Thickness calculated from bilayer structure obtained at the end of the simulations. See Figure 5.3.5 for more details.
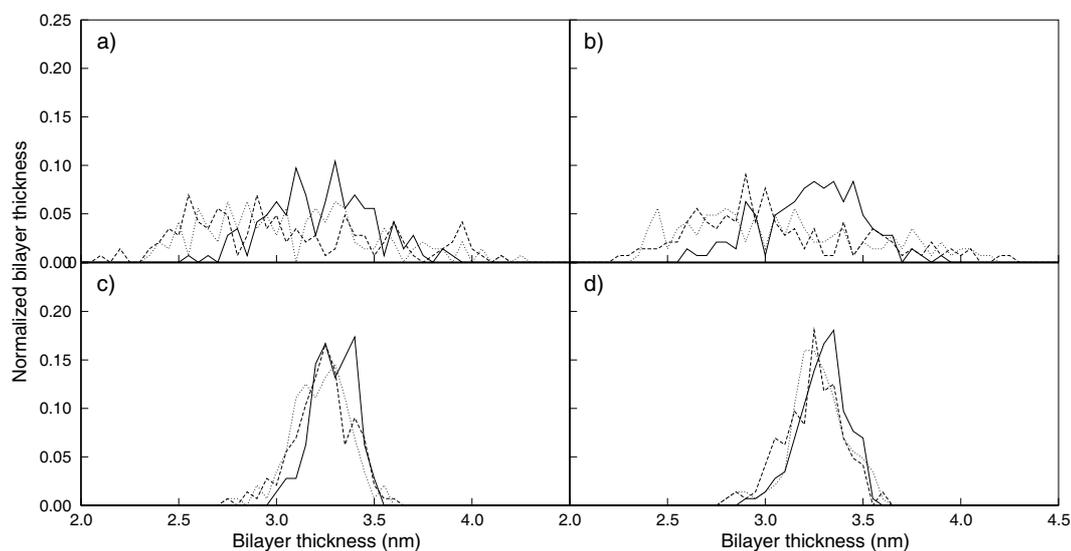
Figure 5.4.4: Normalized bilayer thickness distribution obtained from the bilayer surface plot analysis. Distributions were calculated from ensemble average of the thickness for the bilayers containing glucose (a and c) and trehalose (b and d). Averages were taken over the last 20 and 30 ns for bilayers with (c and d) and without (a and b) a gas layer, respectively. Lines correspond to 290 (dash), 300 (dot), and 310 K (solid).

5.4.4   Hydrogen Bond Analysis: Water as H-donor

To gain insight into how the saccharide molecules stabilize the bilayer structure, an extensive hydrogen bonding analysis was performed on the dehydrated bilayers. The number of hydrogen bonds between water (H-donor) and lipid/saccharide (H-acceptor) was calculated. For this analysis, a hydrogen bond was defined according to the criteria suggested by Brady and Schmidt [285], with the distance between the donor and acceptor $(O-O)$ within 0.35 nm and the donor-hydrogen-acceptor $(O-H-O)$ angle between 120 and 180 degrees. Figure 5.4.5 shows the average number of hydrogen bonds (collected in the last 20 ns) for the systems with and without glucose or trehalose at 290, 300, and 310 K. From the figure, the presence of saccharides decreased the number of hydrogen bonds of water with the lipids from $\sim$1,690 for systems without saccharides to $\sim$1,520 and $\sim$1,550 for bilayers with glucose and trehalose, respectively. This decrease in hydrogen bonds results from the preferential binding of saccharides to the lipids, which in turn prevents water from forming hydrogen bonds with the lipids. One reason for similar numbers of hydrogen bonds for bilayers containing saccharides is because glucose and trehalose form about the same number of hydrogen bond to the lipids, thus displacing the same amount of water molecules that are bounded on the bilayer interface. This finding was verified by considering the saccharide molecules as H-donors.

Analysis of the hydrogen bonding between water (H-donor) and saccharides (H-acceptor) also provided support for the bilayer stabilization. Based on the fact that most of the saccharide molecules were bounded at the bilayer interface, the number of hydrogen bonds between water and saccharide molecules was estimated ($\sim$470 for glucose and $\sim$410 for trehalose systems as shown in Figure 5.4.5). The reason there were slightly less hydrogen bonds for trehalose than glucose is because the total amount of H-acceptors is lower for trehalose. Altogether, glucose and trehalose have 720 (6 per glucose) and 660 (11 per trehalose) H-acceptors, respectively. Note that the sum of the number of hydrogen bonds between water-lipid and water-saccharide surpasses that for the bilayer without saccharide. This implies that the binding of saccharides with the lipids increases the exposed bilayer
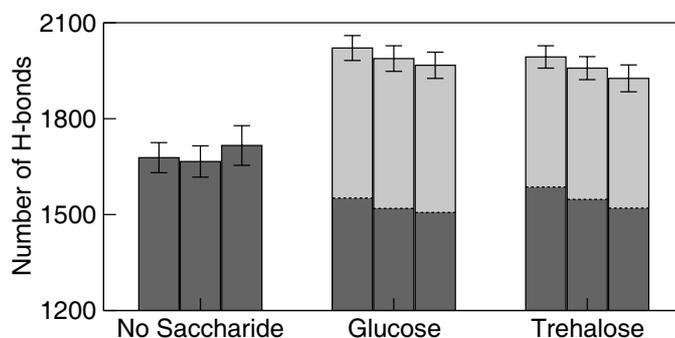
Figure 5.4.5: Average number of hydrogen bonds for bilayers without saccharide, with glucose, and with trehalose and water as H-donors. Adjacent bar plots are for bilayers at 290, 300, and 310 K, respectively. Dark-gray are the average number of hydrogen bonds between water and lipid-oxygen atoms. Light-gray are the average number of hydrogen bonds between water and saccharide-oxygen atoms. Error bars represent standard deviations.

surface, thus allowing water to bind with the lipids and consequently hydrating the bilayer.

5.4.5   Hydrogen Bond Analysis: Saccharide as H-donor

To differentiate the properties of glucose and trehalose, an extensive hydrogen bond analysis was performed with the saccharides as H-donors. Here, the H-acceptors are the lipid-oxygen, the water-oxygen, and the saccharide-oxygen atoms. Since the total number of H-donors differs for bilayers containing glucose (120 glucose × 5 H-donors) and trehalose (60 trehalose × 8 H-donors), the results were reported based on the hydrogen bond distribution per H-donor. Table 5.4.1 shows the average H-bond distribution for the bilayers containing glucose and trehalose at 290, 300, and 310 K (data collected from the last 20 ns). To improve the statistics of the results, the sampling from six independent simulations containing the saccharides for a total of 36 simulations with timestep of both 2 and 3 fs (consistent results were obtained with both timesteps) were considered. The data show that approximately 95% of the H-donors are hydrogen bonded to an H-acceptor. Among this distribution, trehalose seems to form slightly more hydrogen bonds with lipids than glucose (36% vs 32%). While this difference is small, it suggests that trehalose may preferentially bind to the lipids in

Table 5.4.1: Intermolecular hydrogen bond with saccharides (H-donor) for uni-lamellar bilayers exposed to an inert gas layer. Values are fraction of H-bond/donor. Average and total H-bond/donor are also shown below. Deviations are estimated standard error of the mean.

Temperature	Glucose			Trehalose		
290 K	0.32 ± 0.01^a	0.50 ± 0.02^b	0.13 ± 0.01^c	0.35 ± 0.02^a	0.52 ± 0.02^b	0.08 ± 0.01^c
300 K	0.32 ± 0.01^a	0.49 ± 0.02^b	0.14 ± 0.01^c	0.36 ± 0.02^a	0.52 ± 0.02^b	0.08 ± 0.01^c
310 K	0.32 ± 0.02^a	0.49 ± 0.02^b	0.13 ± 0.01^c	0.37 ± 0.02^a	0.49 ± 0.02^b	0.07 ± 0.01^c
Average	$\sim0.32^a$	$\sim0.50^b$	$\sim0.13^c$	$\sim0.36^a$	$\sim0.51^b$	$\sim0.08^c$
Total	~0.95			~0.95		

H-acceptors: ^{a}lipid-oxygen atoms, ^{b}water-oxygen atoms, ^{c}saccharide-oxygen atoms

the bilayer more than glucose. Hydrogen bonds of glucose and trehalose with water (H-acceptor) are equally formed, accounting for $\sim50\%$ of the total. The remaining hydrogen bonds (glucose-glucose and trehalose-trehalose) show glucose having almost twice as many H-bonds with other glucose ($\sim13\%$) than those between trehalose molecules ($\sim8\%$). This difference can be explained by the fact that glucose, which is smaller than trehalose, has greater mobility to bind with the other glucose molecules. Because trehalose preferentially bind to lipids and it has less mobility (bulkier molecule), it can serve as a better stabilizing agent than glucose.

5.5   Summary

In this study, molecular dynamics simulations were used to investigate and compare the properties of DPPC bilayers with and without saccharides (glucose or trehalose) under dehydrated conditions. Results from the simulations indicate that uni-lamellar bilayers lose their structural integrity under dehydrated conditions in the absence of saccharides, however, in the presence of either glucose or trehalose, the bilayers maintain their stability. Hydrogen bond analysis shows that the saccharide molecules displace a significant amount of water surrounding the lipid headgroups. At the same time, the additional hydrogen bonds formed

between water and saccharide molecules help to maintain a hydration layer on the lipid bilayer interface. Based on the hydrogen bond distributions, trehalose forms more hydrogen bonds with the lipids than glucose and it is less likely to interact with neighboring saccharide molecules. These results suggest that the preferential interaction between the saccharide and lipid molecules through hydrogen bonds is an essential component of the mechanism for stabilization and protective effect of lipid bilayers.

Chapter 6

Molecular Studies of Lipid Bilayers Near the Main Phase Transition

From recent studies, it has become apparent that both ordered and disordered lipid phases within eukaryotic cell membranes are essential for various cellular functionalities [37–43]. The ordered (gel) and disordered (liquid-crystalline) lipid phases have been central in studies of the phase behavior of biological membranes, which relates the overall structural characteristics and dynamics of membranes to individual lipid components. Several experimental and computational phase behavior investigations have been reported to characterize structural and dynamic properties of lipid bilayers in a gel, liquid-crystalline, and transition states (see Section 2.3 for more details). Of all the modeling techniques presently available, coarse-grained (CG) models are better suited to obtain insight into the properties of order domains, as large bilayers and long simulation times can be achieved to model large-scale properties of membranes. Using this approach, Marrink *et al.*, clearly showed the transformation process associated with a phase transition [189]. However, CG models are unable to capture the molecular features and characteristics of the lipid molecules and the more subtle structural properties of the bilayers. As such, atomistic simulations for the transition state may establish additional understanding of properties on lipid domains. In this chapter, a series of MD

simulations for four types of lipids bilayers (DPPC, DPPE, POPC, and POPE) is presented to determine the possible mechanisms underlying the phase transition process.

6.1 Simulation Details

Two sets of simulations were considered in this study. First, annealing simulations were performed for DPPC, DPPE, POPC, and POPE bilayers containing a total of 128 lipids (64 per leaflet with 40 water/lipid). Second, separate simulations of DPPC, DPPE, POPC, and POPE bilayers were performed at fixed temperatures ranging from 250 K to 350 K, above and below the experimental phase transition temperature. The set temperatures and the approximate main phase transition temperature for each lipid bilayer system are summarized in Table 6.1.1. Although the size of the bilayers considered remains relatively small compared to previous CG simulations, they are about the same size or larger than previous atomistic simulations on phase transitions [94, 185, 186, 190]. Also, the bilayer systems presented in this study are too small to form a ripple phase, as observed by Sengupta *et al.* [178]; therefore, bilayers that exhibit characteristics of a ripple phase (co-existence of "ordered" and "disordered" domains) will be referred as "mixed" domains (see Chapter 2.3 for more information).

In the annealing simulations, previously equilibrated lipid bilayers underwent a series of annealing steps from 250 to 350 K for both DPPC and DPPE bilayers, and from 250 to 330 K for both POPC and POPE bilayers, as part of the heating scan. These were then followed by the reverse path (cooling scan), thus tracing the hysteresis curves. These temperature ranges were chosen to include the main phase transition from a gel to a liquid-crystalline phase, as indicate in Table 6.1.1. The heating and cooling rates for the saturated lipid bilayers (DPPC and DPPE) were set at 2.5 K per nanosecond and at 2.0 K per nanosecond for the monounsaturated bilayers (POPC and POPE). As it will be shown, the selected rate is adequate to obtain a number of structural properties that allow identification of the

Table 6.1.1: Experimental values for the main phase transition temperature for the lipid bilayers and the set temperatures considered in the fixed temperature simulations.

Lipid	Experimental T_m(K)	Set Temperatures (K)
DPPC	315[a]	250, 280, 290, 300, 310, 320, 330, 340, 350
DPPE	337[b]	290, 300, 310, 320, 330, 340, 350
POPC	270[c]	260, 270, 280, 290, 300, 310, 320
POPE	306[d]	260, 270, 280, 290, 300, 310, 320

[a] Differential scanning calorimetry [282]
[b] Optical detection and differential scanning calorimetry [18]
[c] Raman spectroscopy [45]
[d] Differential scanning calorimetry [175]

transitional process from ordered to disordered states and vice-versa.

In the fixed temperature simulations, separate simulations were performed on lipid bilayers at the set temperatures above and below the main phase transition, as indicated in Table 6.1.1. Each configuration was processed through a series of heating and cooling steps from the desired temperature to 450 K and back to erase any hysteresis of the system prior to the start of each simulation. Beyond the equilibration, a total simulation time of 50-60 ns was collected for each system, of which the last 30 ns were used in the evaluation of the equilibrium properties.

Because periodic boundary conditions were imposed on the systems in the simulations, the bilayer configuration is essentially that of a multi-lamellar system. It is known that uni- and multi-lamellar bilayers exhibit different phase behavior [170]. To minimize the periodicity of a multi-lamellar systems, the systems considered contained 40 water/lipid, which is above the swelling limit proposed by Nagle and Tristran-Nagle [172], thus making the systems behave in a manner that is similar to a uni-lamellar configuration.

The force-field for DPPC and DPPE were previously described in Chapter 4. The force-fields for POPC and POPE are consistent with those employed in a previous study of Tieleman *et al.* [296, 297], which include intramolecular parameters for bonds, angles,
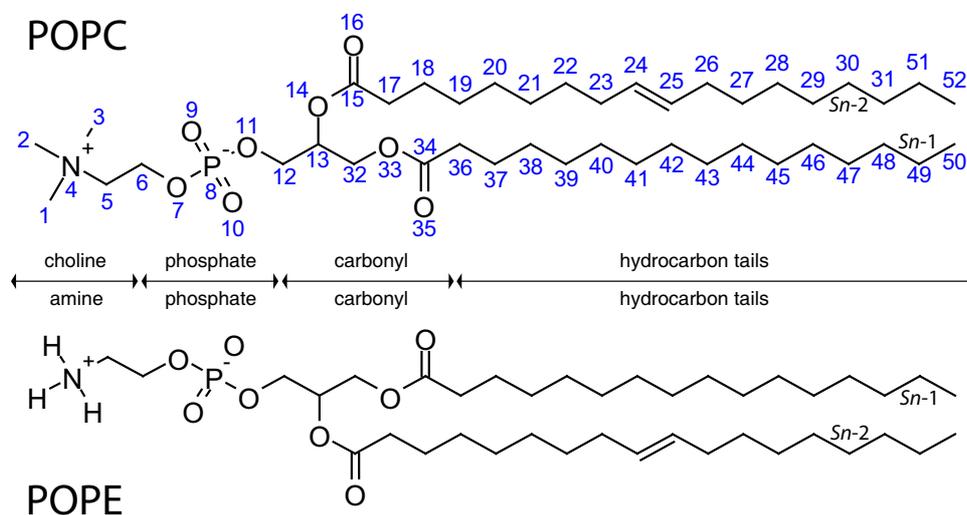
Figure 6.1.1: Molecular structure and assigned numbering of atoms for POPC (above) and POPE (below). Chemical symbols are hydrogen (H), nitrogen (N), oxygen (O), and phosphorus (P).

proper dihedral, and improper dihedral [269]. The structure and assigned atomic numbering considered for POPC and POPE are shown in Figure 6.1.1. The Ryckaert-Bellemans potential was used for the torsion potential of the lipid hydrocarbon chains [271]. Non-bonded interactions were described by the parameters from Berger *et al.* [104, 110, 272] and partial atomic charges were obtained from Chiu *et al.* [96] The single point charge (SPC) model was adopted for water [273]. The united-atom representation was used for the methyl/methylene groups in the acyl chains of both POPC and POPE. For POPE, explicit hydrogen atoms in the ethanolamine headgroup are considered.

Since the available force-fields employed here were originally developed for the liquid-crystalline phase, it was unclear whether they are suitable to represent bilayer properties at and near the main phase transition. Nevertheless, results from this study are intended to demonstrate that one can use atomistic simulations to obtain important information of lipid bilayers at and near the transition state (gel to liquid-crystalline) and to provide insight into the structural changes of the lipid bilayers at and near the main phase transition.

All simulations were performed in the NPT ensemble, at a pressure of 1 bar and at temperatures between 250 and 350 K (see Chapter 4 for more details on the parameters used in the simulations). A time-step of 2 fs was used for all simulations. Coulombic and van der Waals interactions were cutoff at 9 Å. Long-range electrostatic interactions were corrected with the particle-mesh Ewald method (PME) (0.12 nm for the grid size, fourth-order spline interpolation, and real-space cutoff at 9 Å) [108, 263]. Periodic boundary conditions were applied in all directions. Trajectories were collected every 2 ps. All simulations were performed with the GROMACS 3.3 software package [258, 259] (single-precision mode) in parallel using Virginia Tech's System X [281].

6.2   Annealing Simulations

The focus of this study is to obtain a better understanding of the phase transition of typical saturated (DPPC and DPPE) and monounsaturated (POPC and POPE) lipid bilayers. To verify the properties of the lipid bilayers near the main phase transition, a series of heating and cooling annealing scans were performed on each lipid bilayer system starting from previously equilibrated structures at the two ends of the annealing temperatures (250/350 K for DPPC and DPPE bilayers and 250/330 K for POPC and POPE bilayers). Several annealing simulations were conducted with different starting configurations and initial velocities to improve the statistical analysis of the results (three simulations for each lipid system). The structural properties considered for this analysis were the area per lipid and the bilayer thickness, both of which are sensitive to the phase state of the bilayer [298]. The average area per lipid was calculated from the cross-sectional area of the simulation box (plane along the bilayer interface, xy-plane) divided by the number of lipids per leaflet (64 lipids). The bilayer thickness is quantified from the distance of the mean position of the phosphorus atoms in each leaflet. Figures 6.2.1a-d show the approximate area per lipid resulting from the heating and cooling scans for the DPPC, DPPE, POPC, and POPE bilayers, respectively. The approximate bilayer thickness resulting from the heating and cooling scans of

DPPC, DPPE, POPC, and POPE bilayers are shown in Figures 6.2.1e-h, respectively.

From Figures 6.2.1a-b, the heating scans of each lipid system show a transition point around 295 K for DPPC and 320 K for DPPE, which corresponds to the temperature at which there is a change in the slope of the heating curves. However, for the cooling scans, the identification of a phase transition is not as clear, as the area per lipid and bilayer thickness decreases more gradually with decreasing temperature. Similar results are observed in Figures 6.2.1e-f for the bilayer thickness: the phase transition can be easily identified in the heating scans, but less clearly in the cooling scans. The heating and cooling scans shown in Figures 6.2.1a-b represent hysteresis loops, a prominent characteristic of systems undergoing a first-order phase transition. This type of behavior for lipid bilayers is also observed in experimental [21, 170, 171] and other computational [180, 184, 188] studies, supporting a first-order phase transition mechanism. One of the reasons the heating and cooling do not form a closed-loop is that the same annealing rate for heating and cooling was used, and the process from a disordered to ordered state is much more susceptible to metastability than the reverse path. Note that the structural properties of the simulated bilayers seem insensitive to doubling the bilayer size to 256 lipids for DPPC and DPPE bilayers, as the tracing in the average area per lipid for both small and large systems follows the same trend (see Figs 6.2.1a-b). As such, lipid bilayers containing 128 lipids were used for all others simulations.

From Figures 6.2.1c-d and g-h, the heating scans for both POPC and POPE indicate a transition point around 270 K and 280 K, respectively, which corresponds to the temperature at which there is a break in the slope of the heating curves. For the cooling scans, the identification of the phase transition is similar to that of the heating scan, although not as clear. Compared to the heating and cooling scans for DPPC and DPPE in which a mismatch of the hysteresis loop upon heating and cooling are observed, POPC and POPE lipid bilayers are more susceptible to a phase change as heating and cooling scans show similar trends. From this analysis, it is evidence that a kinked configuration due to the double bond in the *Sn*-2 tail of monounsaturated lipids (see Figure 6.1.1) is an important structural
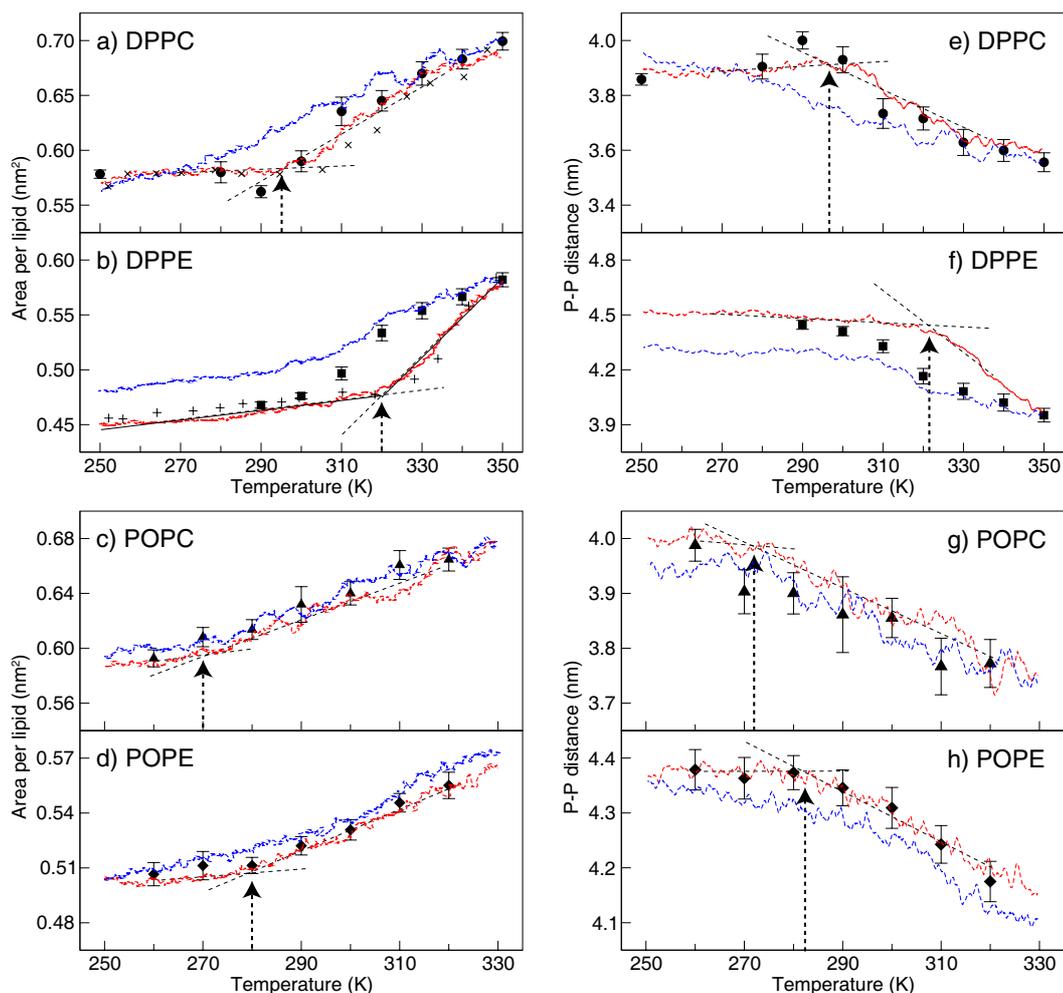
Figure 6.2.1: Area per lipid (a-d) and bilayer thickness (e-h) obtained from annealing and fixed temperature simulations. Red and blue lines correspond to the heating and cooling scans, respectively. Heating and cooling rates of 2.5 K/ns (DPPC and DPPC) and 2.0 K/ns (POPC and POPE) were used to obtain the hysteresis loops. The intersection of the dashed lines corresponds to the phase transition point. "×" and "+" symbols shown in a) and b) correspond to the area per lipid obtained from annealing simulations of larger DPPC and DPPE bilayers containing a total of 256 lipids. Circles, squares, triangles, and diamonds are results from the fixed temperature simulations. Error bars are estimated standard deviation.

feature that creates a loose packing between the lipid tails, thus allowing the bilayer to be more susceptible to a phase change. As a result, narrow hysteresis loops are observed from the simulations, a characteristic of lipid bilayers undergoing a first-order phase transition. Although the phase transition temperatures obtained for DPPC and POPC ($T_\mathrm{m}^\mathrm{simul.}$ vs. T_m) are similar to experimental values, and slightly off for DPPE and POPE ($T_\mathrm{m}^\mathrm{simul.}$ vs. T_m), the current results are an affirmation of the phase behavior of lipid bilayers and the molecular changes associated with phase transformations. Based on these results, a closer look at the equilibrium properties of the lipid bilayers at selected temperatures above and below the phase transition is discussed in the following sections.

6.3   Simulations at Fixed Temperatures

Clear structural changes in the lipid bilayers above and below the main phase transition can be observed from the packing of the lipid tails in the bilayers, as shown in Figure 6.3.1 for pairs of snapshots from the MD trajectories for DPPC, DPPE, POPC, and POPE bilayers at selected temperatures. For DPPC, two distinct domains are observed at 250 K, as shown in Figure 6.3.1a. The first domain consists of lipids that are fully stretched with no overlap between lipid tails from the adjacent leaflet, to be referred as "ordered" domain. The second domain is identified as the overlapping section of lipid tails from each leaflet, and to be referred as the "disordered" domain. From the snapshot, the lipid tails are tilted in the "ordered" domain and partially overlapped in the "disordered" domain. This type of lipid alignment has been previously reported as a ripple phase in lecithin by de Vries *et al.* [187]. Since the bilayer systems presented here are too small to form a ripple phase, this packing of the lipid tails is referred as a "mixed" domain. To verify the stability of these structures, instantaneous heating and cooling was performed on each system in an annealing process to ensure that the resulting structures were not in a metastable state. This was accomplished by heating the system to 450 K and then cooling it to the respective temperature in the *NVT* ensemble. At the desired temperature, systems were equilibrated for at least 10 ns

a) DPPC $T_m^{\text{simul.}} \approx$ 290-300 K $T_m \approx$ 315 K

b) DPPE $T_m^{\text{simul.}} \approx$ 320-330 K $T_m \approx$ 337 K
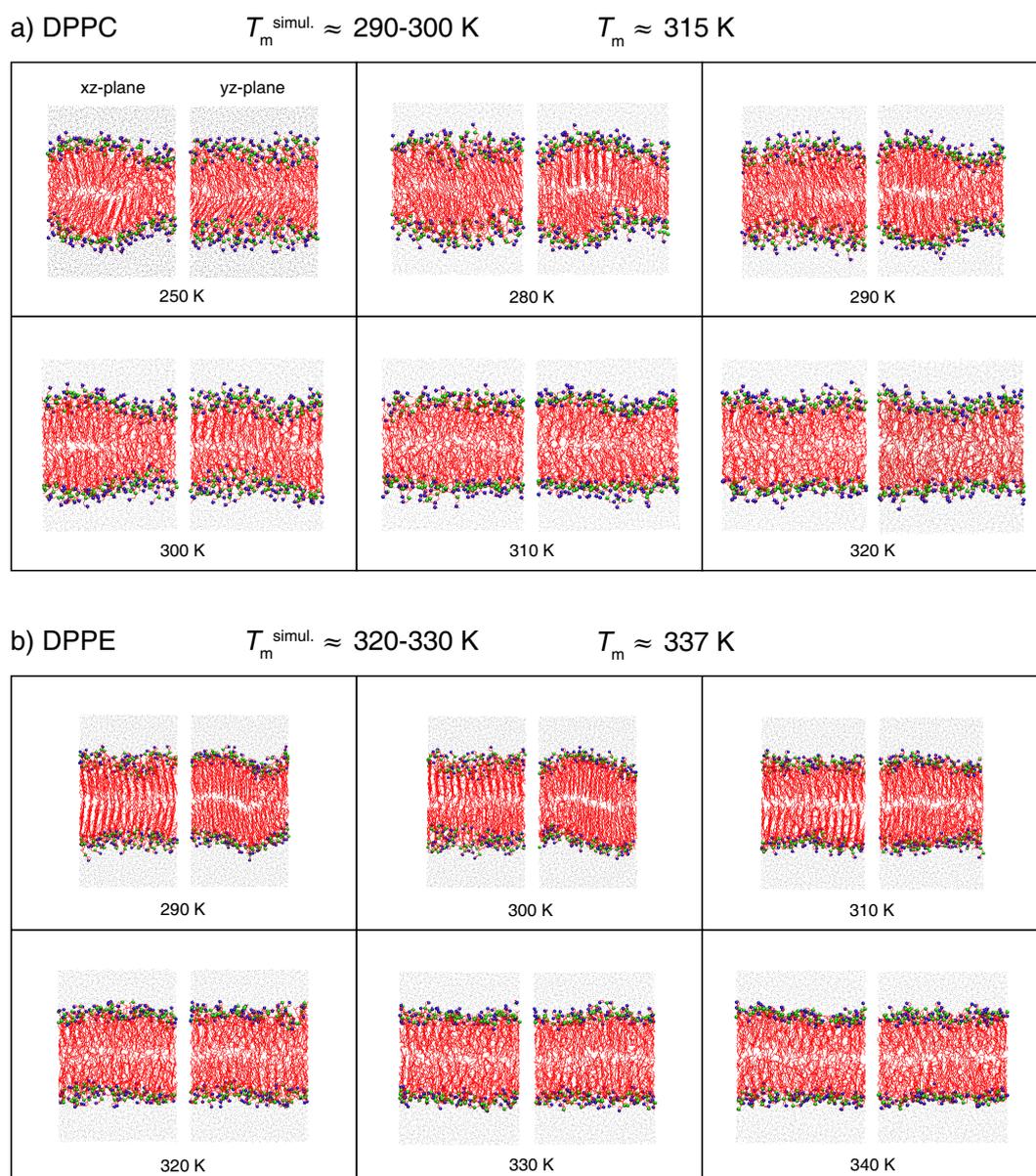
Figure 6.3.1: Snapshots of a) DPPC and b) DPPE bilayers at selected temperatures demonstrating a change in the bilayer structure below and above the phase transition point. Views of the simulation box are shown for the xz-planes and yz-planes. The z-axis is normal to the bilayer interface. The bilayer core region is centered in the middle of the snapshots. T_m and $T_m^{\text{simul.}}$ are the experimental and estimated phase transition temperatures, respectively.

before production runs. At the higher temperatures (Figure 6.3.1a), the lipid tails of DPPC are fully random, which is characteristic of a liquid-crystalline phase.

A similar procedure was applied to DPPE. For DPPE, only the "ordered" domain with tilted lipid tails was observed at low temperature, as shown in Figure 6.3.1b. In this case, all lipid tails are tightly packed, with less interdigitation between them. Compared to DPPC, the "mixed" domain in DPPE is not observed from the simulations as the "ordered/disordered" patterns seem absent. This is consistent with the experimental study by Yao *et al.* [299], in which they were unable to distinguish a stable phase from a gel to a liquid-crystalline phase for DPPE using X-ray scattering, unlike the case for DPPC. Even though the experiments by Yao *et al.* were insufficient to provide insight into the phase transition mechanism of DPPE, current simulation results suggest that DPPE undergoes a phase transition without existing as a "mixed" domain. At higher temperatures, the DPPE lipid tails are fully random, as shown in Figure 6.3.1b.

Unlike saturated lipids, typical monounsaturated lipids, such as POPC and POPE, contain asymmetric lipid tails, one with 16 carbons in the Sn-1 tail and another with 18 carbons and a *cis* double bond in the middle of the Sn-2 tail. Previous simulations studies of POPC and POPE have shown that the lipid tails are predominantly tilted with kinks at the double bond at low temperatures [111, 175]. Based on these previous findings, it is expected that POPC and POPE bilayers would have a complex packing in a gel state. From the snapshot of POPC in Figure 6.3.2a, there is evidence of a tilted/untilted lipid arrangements at 260 K. This may be caused by the kinked configuration of the Sn-2 tails that disrupt the tilted configuration of the Sn-1 tails when the lipids are tightly packed at low temperatures. Slight interdigitation of the lipids between each leaflet is also observed in some parts of the bilayer, which possibly relates to a "mixed" domain formation. At higher temperatures, the POPC lipid tails are fully random, which represents a characteristic of lipid bilayers in a liquid-crystalline state, as shown in Figure 6.3.2a. For POPE, a tilted lipid arrangement is observed at 260 K with little or no interdigitation between each leaflet (Figure 6.3.2b). The tilted arrangement is more pronounced in POPE than in the POPC bilayers mainly because
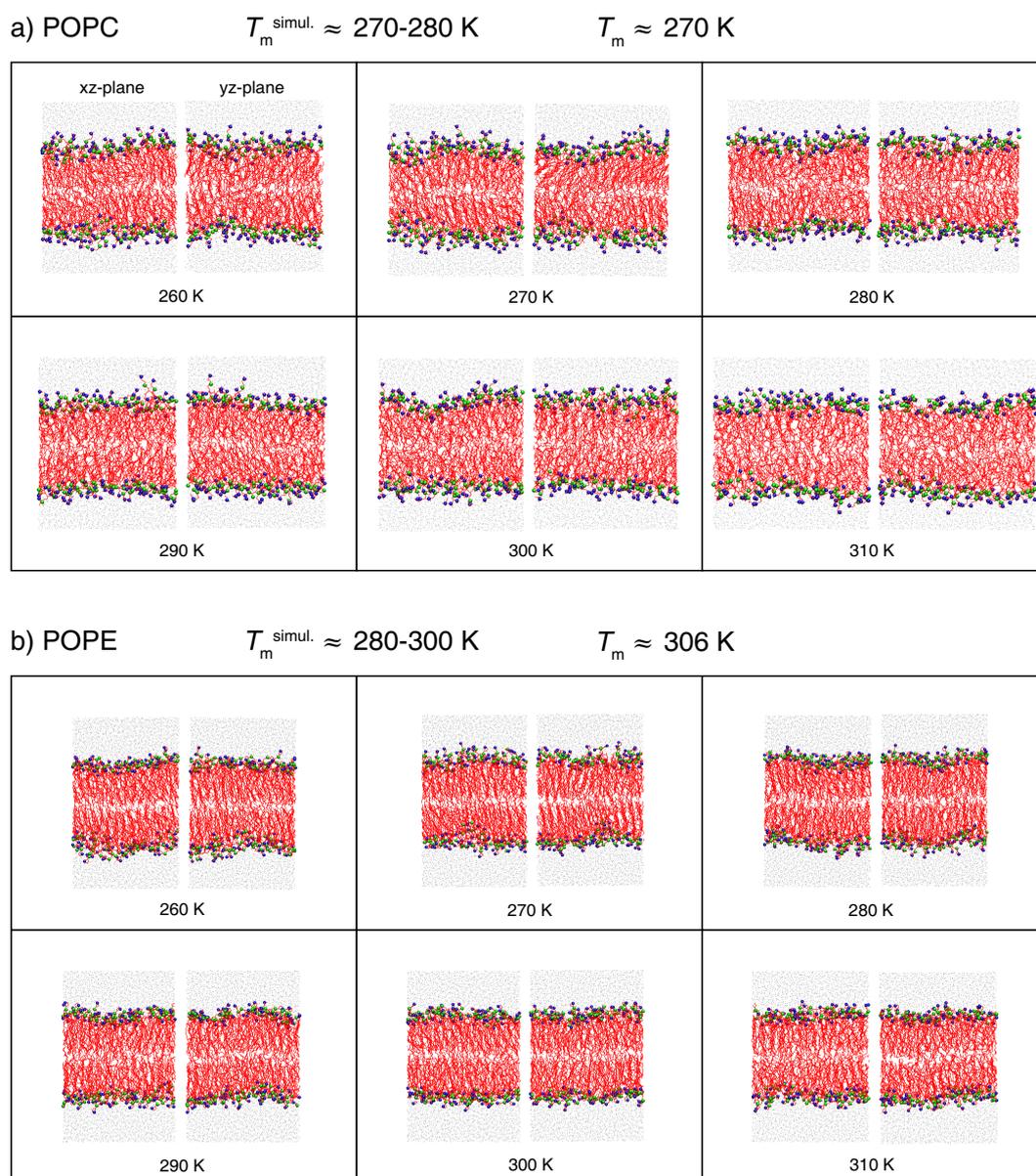
Figure 6.3.2: Snapshots of a) POPC and b) POPE bilayers at selected temperatures demonstrating a change in the bilayer structure below and above the phase transition point. Views of the simulation box are shown for the xz-planes and yz-planes. The z-axis is normal to the bilayer interface. The bilayer core region is centered in the middle of the snapshots. T_{m} and $T_{\mathrm{m}}^{\mathrm{simul.}}$ are the experimental and estimated phase transition temperatures, respectively.

of the tighter packing with the smaller PE headgroup. Fewer defects are noticed along the tilted lipid arrangement which is most likely caused by the tight packing of the *Sn*-1 tails and kinks in the *Sn*-2 tails. At a higher temperature, the lipid tails are fully random, as shown in Figure 6.3.2b (right). From a visual inspection of all bilayer structures above and below the phase transition, distinguishable structural changes associated with each phase are observed.

From the full series of snapshots for the lipid bilayers at the various temperatures, the phase transition temperature for the bilayer systems can be reasonably estimated at ∼295 K for DPPC, ∼315 K for DPPE, ∼270 K for POPC, and in the range of 280-300 K for POPE, which compare to the experimental values of ∼315 K for DPPC [282], ∼337 K for DPPE [18], ∼270 K for POPC [45], and ∼306 K for POPE [175]. Further quantitative analysis of the structural properties is discussed in the following sections to support these observations.

6.4   Results and Discussion

A number of properties were analyzed to characterize and quantify the changes in the bilayer structure with respect to the phase transition temperature for all lipid bilayer systems, including: area per lipid, bilayer thickness, lipid tail tilt-angle, lipid tail order parameter, hydrocarbon *trans-gauche* isomerization, and level of interdigitation. These properties were obtained from the ensemble average of the trajectories over the last 30 ns of the simulations for each system listed in Table 6.1.1. The stability of each system was monitored by the average area per lipid.

6.4.1   Area per Lipid

For DPPC bilayers at the lower temperatures, it is observed that the bilayer surface showed abnormal defects resulting from the rigidity and packing of the phospholipids (see Figure 6.3.1a). As such, it was unclear that the area per lipid for those systems can be adequately quantified. Note that these defects were less obvious at higher temperatures (see Figure 6.3.1a). As shown in Figure 6.2.1a, the area per lipid of the bilayers at the different temperatures (discrete data points) showed consistent agreement with the annealing simulations, with exception of the data at 290 K that deviated from the expected value. The average area per lipid for DPPC increases almost linearly with temperature above 310 K. A similar linear relationship was reported by Sum *et al.* for DPPC in the liquid-crystalline state [228]. At the lower temperatures, the average area per lipid for DPPC is more scattered due to the "mixed" domains, exhibited by the many stable configurations of the systems. That is, the average area per lipid significantly increases when the lipid tails are predominantly tilted with large tilt-angles and decreases when they are tightly packed with the lipid tails and aligned along the bilayer normal. This finding agrees well with previous X-ray diffraction experiments on fully hydrated DPPC by Ruocco *et al.* that observed a tilted lipid arrangement in the gel phase and a more parallel alignment to the bilayer normal near the transition point [300]. For DPPE, because the "mixed" domains seem absent from the structures at low temperature (see Figure 6.3.1b), the average area per lipid obtained from the individual simulations is between the values obtained from the annealing simulations.

For POPC and POPE, since the kinked and straight lipid tail configurations are observed in Figures 6.3.2a-b, the spacing between lipids in one leaflet is expected to be loosely packed along the bilayer surface. This is related to the way monounsaturated lipids are packed within the bilayer (straight Sn-1 and kinked Sn-2) which prevents lipids from overlapping each other at low temperatures. As shown in Figures 6.2.1c-d (discrete data points), the average area per lipid for both POPC and POPE increases gradually with temperature. Although the discrete values obtained are within the range of the heating and cooling scans,

no direct correlation between these data points identifies a phase transition point (a clearer identification is observed from the annealing simulations). Several experiments suggest a stable ripple phase between a gel and a liquid-crystalline phase for POPC bilayers [178], however, this phase is not observed from the current simulations as the bilayer size is relatively small. Despite this fact, this POPC bilayer model provides a tilted lipid arrangement that is common in a gel and ripple state. For POPE, no ripple phase formation has been reported in the literature. As such, the transition from a gel to a liquid-crystalline state for POPE is rather an entropy-driven process with subtle changes in the bilayer structure [175]. Unlike the phase transformation of saturated lipids, the phase transition of monounsaturated lipid bilayers seems less sensitive to changes in the area per lipid, mainly caused by the kinked configurations of the Sn-2 tails. This fact was briefly discussed by Chen *et al.* in their mathematical model relating the changes in the area per lipid to the phase transition of saturated lipids [183]. The results from this analysis demonstrate a complex phase transition process for monounsaturated lipid bilayers; the area per lipid alone is insufficient to describe the mechanism of phase transition.

6.4.2   Bilayer Thickness

As shown in Figures 6.2.1e-h, the bilayer thickness was also compared between the annealing and fixed temperature simulations. The results for both DPPC and DPPE yield similar trends with a decrease in the bilayer thickness accompanying the phase transition from an ordered to a disordered state. This also verifies that the system size and the heating rate chosen are sufficient to describe the phase behavior near the main transition state. A closer inspection of the results for DPPC in Figure 6.2.1e indicates a slight increase in the bilayer thickness prior (at 290 K) to the phase transition temperature. This increase in the bilayer thickness is related to a change in the alignment of the lipid tails from a "mixed" to an "ordered" phase, causing the bilayer to expand. A similar behavior is not observed for DPPE (see Figure 6.2.1f) because a "mixed" phase seems absent.
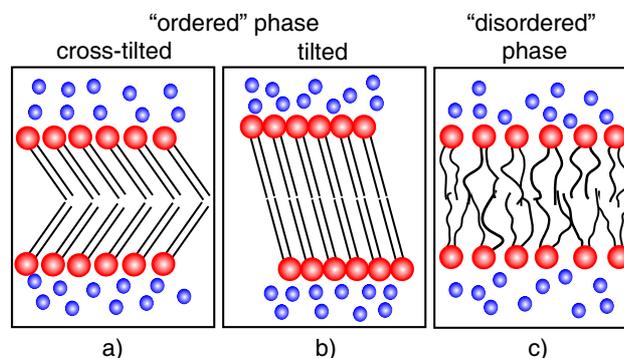
Figure 6.4.1: Schematic representation of the alignment of the lipids in the "ordered" and "disordered" phases: a) cross-tilted, b) tilted, and c) random. Both tilted and cross-tilted alignments are observed in the gel phase (see Figures 6.3.1a for comparison). Red and blue spheres represent the lipid headgroup and water, respectively.

In Figure 6.3.1a, a "mixed" domain configuration is observed below the melting temperature (T_m), which in turn resulted in a bilayer with uneven thickness. As discussed in the previous section, the DPPC structure experienced a noticeable increase in the bilayer thickness below T_m, which corresponded to a transformation from a cross-tilted (Figure 6.4.1a) to a tilted lipid arrangement (Figure 6.4.1b). This rearrangement causes a slight increase in the area per lipid near T_m (see Figure 6.2.1e), as the lipid molecules align perpendicular to the bilayer surface at temperatures near the phase transition, which in turn causes a slight increase in the bilayer thickness upon heating the bilayer. Once T_m has been reached, the lipid tails become interdigitated, resulting in a decrease of the bilayer thickness and an increase in the area per lipid (see Figure 6.4.1c). Although this cooperative phenomenon is observed, the analysis suggests that an increase in the area per lipid is an essential step to induce a rearrangement of lipid molecules before transforming to a liquid-crystalline phase. Unlike DPPC, DPPE bilayers are predominantly in the "ordered" phase with little tilt of the lipid tails below T_m. Therefore, the rearrangement of DPPE is minimal and the bilayer thickness slightly reduces until it reaches the phase transition temperature (see Figure 6.2.1f).

In contrast to DPPC and DPPE, the results for both POPC and POPE shown in Figures 6.2.1g-h yield a subtle decrease in the bilayer thickness, accompanied by a subtle
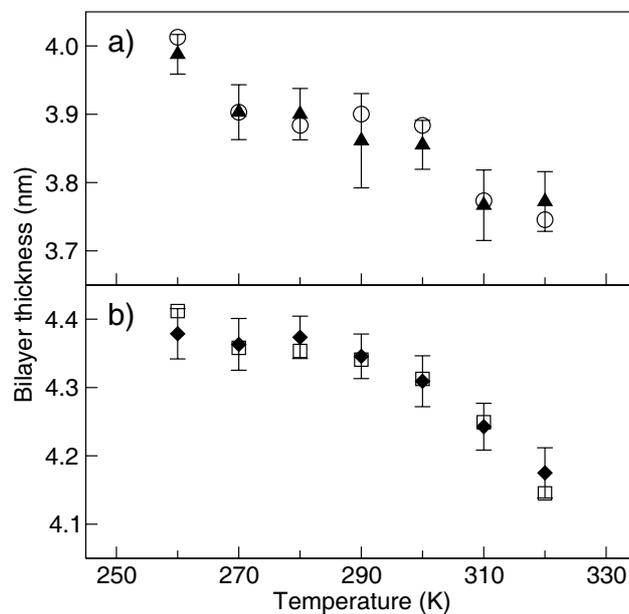
Figure 6.4.2: Two methods for determining the bilayer thickness for a) POPC and b) POPE. Circles and squares are results obtained from the average distance between the two peaks of the phosphorus density profile in the bilayers. Triangles and diamonds are results obtained from the average position of the phosphorus atoms in each leaflet. Error bars are estimated standard deviation.

increase in area per lipid as the phase transition progresses from an ordered to a disordered state. The data points in Figures 6.2.1g-h are within the range of the annealing simulations, however, the phase transition cannot be clearly identified (a clearer identification is observed from the annealing simulations). The average position of the phosphorus atoms is equivalent to the thickness calculated from the phosphorus density profiles. Figure 6.4.2 shows a comparison for the thickness of the bilayer based on the two approaches. Based on the bilayer thickness, it remains uncertain how structural changes of monounsaturated lipids are related to the phase transition.

6.4.3 Lipid Tail Tilt-Angle

To further verify the structural transformation during the phase transition, the lipid tail tilt-angle of all lipid systems was measured with respect to the bilayer normal. One measure of a lipid bilayer in a liquid-crystalline state is that the lipid tails are fully random and unhindered to take any orientation within the bilayer. If the bilayer exhibits a preferred orientation (ordered domain), as the low temperature structures shown in Figure 6.3.1, it is considered to be in a gel state. The angle distribution of each carbon segment in the lipid tails is calculated with respect to the bilayer normal to determine the orientation of the lipids in the bilayer. The carbon segment, in this case, refers to a vector between alternating carbon units along the lipid tail, as demonstrated in Figure 6.4.3. Note that the angle can be either positive or negative depending on the alignment of the lipid tails (a zero degree corresponds to a vector aligned along the bilayer normal).

Figures 6.4.3a-d show the normalized tilt-angle distribution for DPPC, DPPE, POPC, and POPE with respect to the xz-plane of the simulation box (results obtained along the yz-plane are very similar but are not shown for brevity). There are three distinct structural alignments of the lipids that can be used to determine the phase transition point. In the gel phase, two of these structures were observed: one produces the double peak in the distribution and the other shows a narrow angle distribution. In the liquid-crystalline phase, a wide distribution centered around zero degree is observed. The analysis indicates that the double peak refers to the cross-tilted lipid arrangement shown in Figure 6.4.1a. The narrow distribution implies that the lipid tails are predominantly tilted to some degree, as illustrated in Figure 6.4.1b. A wide distribution centered at around zero degree indicates that the lipid tails are fully random (Figure 6.4.1c). To quantify the phase change from the distribution curves, the full-width at half-height (FWHH) of the distribution of the peak maximum was calculated and placed as inset in each plot shown in Figure 6.4.3. The systems with the double peaks were not considered in this calculation as they introduced biased results. For DPPC, there is a significant jump in the FWHH value from 300 to 310 K (see inset in
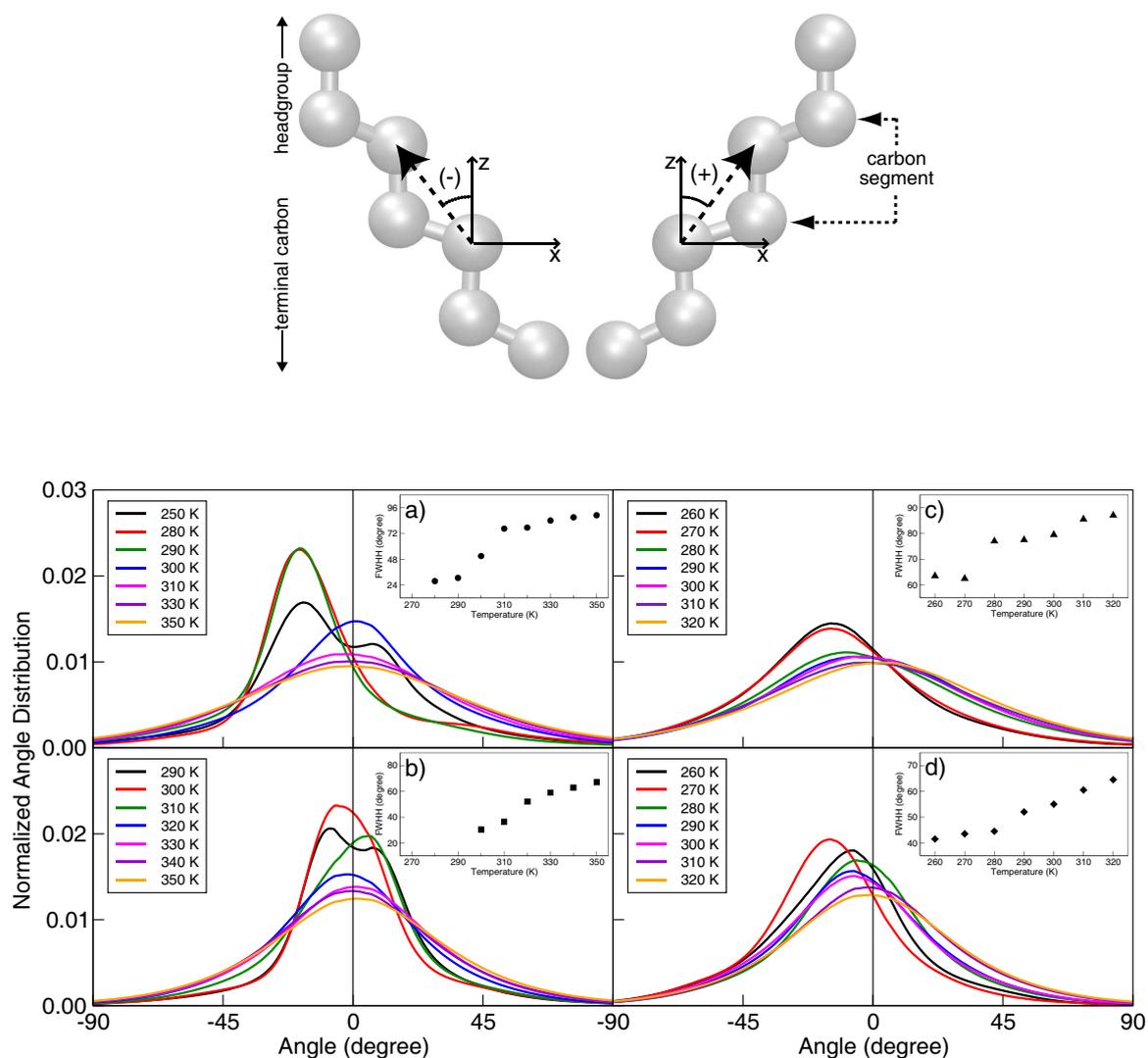
Figure 6.4.3: Top: pictorial representation of the vector formed by alternating carbon units along the lipid tails. The positive (+) and negative (−) tilt-angles are measured with respected to the z-axis (zero degree). Note that only the xz-plane is shown in the figure for clarity. A similar tilt-angle can be defined in the yz-plane. Bottom: normalized angle distribution for all carbon segments in the lipid tails of a) DPPC, b) DPPE, c) POPC, and d) POPE. Calculations were performed with respect to the xz-plane of the simulation box. Each line color corresponds to systems at a fixed temperature. Insets are the calculated full-width at half-height (FWHH) of the distribution curves.

Figure 6.4.3a). This shows that the tilted alignment of the lipids significantly reduces in this temperature range. Again, this is consistent with previous analysis and it was concluded that the phase transition temperature for DPPC occurs between 300 and 310 K. For DPPE, a significant jump in the FWHH value at any temperature interval was not observed, thus it was concluded that the phase transition for DPPE is related to lesser changes in the lipid configuration in the vicinity of T_m (see the inset in Figure 6.4.3b). For POPC, there is a significant increase in the FWHH value from 270 K to 280 K (see inset in Figure 6.4.3c). This shows that the tilted alignment of the lipid tails is significantly reduced in this temperature range. Again, this is consistent with the other properties previously analyzed and it was concluded that the phase transition temperature for POPC occurs between 270 and 280 K. Similarly, there is a large increase in the FWHH value for POPE from 280 to 290 K, a temperature range in which the phase transition is speculated (see inset in Figure 6.4.3d).

Aside from the lipid tail tilt-angle, the average intramolecular angle for the phosphorus (P) to nitrogen (N) vector relative to the bilayer normal for both POPC and POPE was calculated. Distribution plots for the P-N vector angle are summarized in Figure 6.4.4. For POPC, the P-N vector angle distributions are broad, from 30 to 110 degrees. At low temperatures, the distributions peak around 40 degrees, indicating that most choline groups are pointing toward the aqueous phase, which is caused by the tight packing of the lipids in the gel phase. At high temperatures, the distributions shift to higher values ($\sim$100 degrees), representing bending of the choline groups and unhindered motion in the fluid phase. Similar characteristics are observed for POPE, with broad distributions at low temperatures and bimodal distributions at high temperatures. For both POPC and POPE, the P-N vector angle distributions at high temperatures are consistent with results reported for DPPC and DPPE. As seen from Figure 6.4.4, the P-N vector angle distributions do not show any systematic changes from the low (gel phase) to high (liquid-crystalline phase) temperatures, and as such, it was difficult to identify the phase transition temperature from the distributions plots. However, comparison of the distributions at the lowest and highest temperatures shows distinct features. At the lowest temperature corresponding to a gel phase structure,
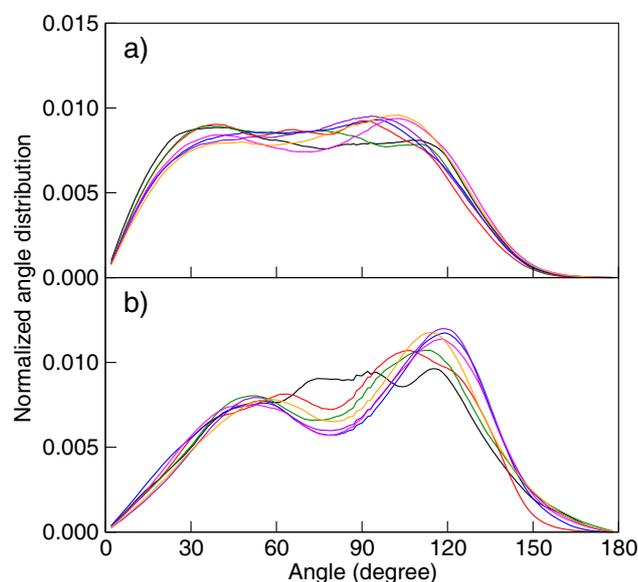
Figure 6.4.4: Normalized angle distribution for P-N vector for a) POPC and b) POPE. Angle is measured with respect to the bilayer normal (z-axis). Line colors are described in the legend of Figure 6.4.3.

the distributions for both POPC and POPE are about uniform over the range of all angles (30 to 110 degrees for POPC and 40 to 120 degrees for POPE). At the highest temperature corresponding to a liquid-crystalline phase, the distributions are more defined showing bimodal configurations. Therefore, while the P-N vector angle distribution cannot be used to identify the phase transition temperature, it does provide a qualitative measure of the fluid state for POPC and POPE bilayers.

6.4.4 Lipid Tail Deuterium Order Parameter

The deuterium order parameter, a measurement of the orientation and ordering of the lipid tails in the bilayer, was calculated for bilayers in the fixed temperature simulations to help identify the mechanism for phase transition. The ordering of the tails is expected to change significantly at the phase transition, that is, the alignment of the lipid tails in a gel state is more ordered (higher $|S_{CD}|$ value) than those in a liquid-crystalline state. Figures 6.4.5a-b

show the calculated order parameter for DPPC and DPPE along with previous experimental results for DPPC at 353 K [283] and DPPE at 342 K [17]. For DPPC (Figure 6.4.5a), a large decrease in the order parameter is observed from 300 to 310 K. This suggests that the change is associated with a phase transition for DPPC. For DPPE (Figure 6.4.5b), the order parameter decreases significantly from 310 to 320 K. Again, this change is associated with a phase transition for DPPE.

Since the lipid tails are asymmetric for POPC and POPE, the order parameter is calculated separately for the Sn-1 and Sn-2 tails. Figures 6.4.5c-f show the calculated order parameters for POPC and POPE along with previous experimental results for POPC at 300 K [185] and POPE at 303 K [301]. For both systems, the order parameter seems to decrease with increasing temperature. For POPC in Figures 6.4.5c-d, the order parameter for both lipid tails shows significantly lower absolute values from 270 to 280 K. The jump in the order parameter over this temperature range suggests that this change is associated with a phase transition for POPC. Unlike POPC, POPE has a two-step transformation when monitoring the changes in the order parameter (see Figures 6.4.5e-f), one at 280-290 K for the Sn-1 tail and another at 290-300 K for the Sn-2 tail. This finding implies that the mechanism of phase transition for POPE is more complex, as the lipid tails may experience several structural changes before transforming into a liquid-crystalline state, thus giving evidence for a broad transitional temperature range. A possible reason for this may result from the lipid reorientation after the Sn-2 tails are less constrained from the tight packing in the gel state. The same behavior is not observed for POPC because POPC bilayers are not as tightly packed as POPE bilayers in the gel state ("mixed" domains are observed in this case).

6.4.5   Hydrocarbon *Trans-Gauche* Isomerization

The hydrocarbon *trans-gauche* isomerization has also been used to determine the phase transition of lipids [302]. In general, the lipid tails in the gel state are predominantly present
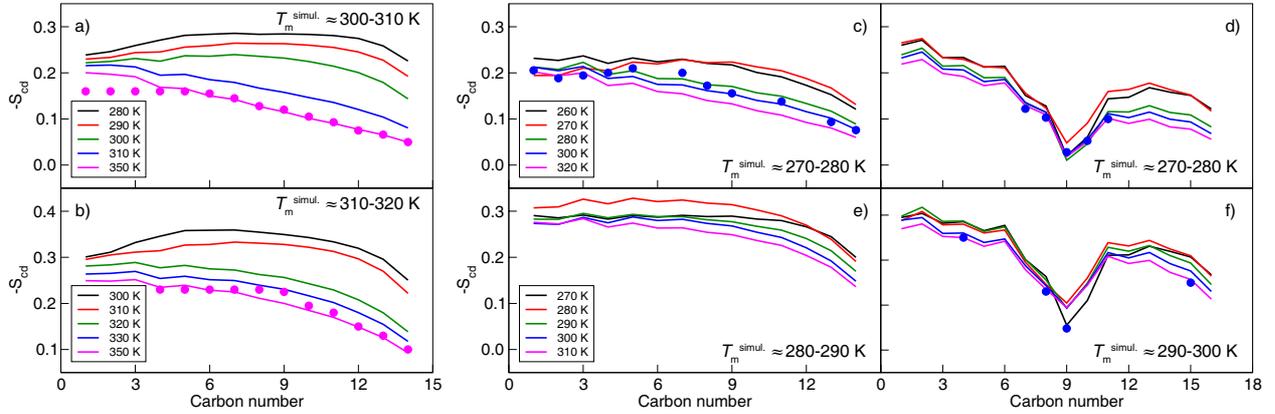
Figure 6.4.5: Deuterium order parameter of the lipid tails for DPPC, DPPE, POPC, and POPE. Average deuterium order parameter for a) DPPC and b) DPPE. Deuterium order parameter for c) *Sn*-1 and d) *Sn*-2 of POPC, and e) *Sn*-1 and f) *Sn*-2 of POPE. Line colors are described in the legend. Circles are experimental NMR measurements of pure DPPC at 353 K [283], DPPE at 342 K [17], POPC at 300 K [185], and POPE at 303 K [301], respectively. $T_m^{\text{simul.}}$ is the estimated phase transition temperature.

as *trans* conformers, whereas both *trans* and *gauche* conformers are present in a liquid-crystalline state. At low temperatures, the *trans* conformations are preferred because they are energetically more favorable for the lipids in the bilayer arrangement. As the temperature increases above the phase transition point, the carbon atoms in the lipid tails are less restricted to move, thus creating defects in the hydrocarbon tails (*gauche* formation). As the bilayer transitions from a gel to a liquid-crystalline phase, one expects a significant change in the number of *trans* and *gauche* conformations, reported as %*gauche*. The %*gauche* was analyzed according to the criteria suggested by Tu *et al.* [90]. The criteria set a limit from 0 to 360 degrees in the axial rotation of the second bond of a dihedral, starting from a *cis* conformer at 0 degree to a *trans* conformer at 180 degrees. Based on these criteria, a *gauche* conformation would consist of angles ranging from 0 to 120 and 240 to 360 degrees. Figure 6.4.6 shows the average %*gauche* formed along the lipid tails for all lipid bilayer systems at selected temperatures. As seen in the figure, the %*gauche* increases with increasing temperature for all systems. For DPPC, the temperature range of 300-310K was identified to correspond to a phase transition as a large increase in %*gauche* is observed

(see Figure 6.4.6a). This is consistent with previous analysis. For DPPE, a large increase in %*gauche* occurs between 310 and 320 K, which is a reasonable estimate for the phase transition temperature, consistent with previous results and discussion (see Figure 6.4.6b).

For POPC and POPE, both saturated and unsaturated lipid tails are analyzed as part of the interdigitation analysis. Since a *cis* double bond is present in the *Sn*-2 tail, it was difficult to correlate the change in phase transition to the calculated %*gauche*. A clearer identification is obtained from the *Sn*-1 tail, as shown in Figures 6.4.6c-d. For both lipids, the most pronounced change in the %*gauche* was identified in the range 270-280 K. For POPC, the changes in the %*gauche* in this temperature range agree well with the phase transition point identified with the other structural properties analyzed. However, the changes for POPE are most likely associated with a pre-transition state. In this case, a transformation from *trans* to *gauche* conformation can occur prior to the main transition temperature, which is related to the reorientation of the dihedrals formed along the lipid tails of POPE. This is possible considering the tight packing of the POPE molecules at low temperatures, as kinked *Sn*-2 tails can disrupt the *trans* conformation of neighboring *Sn*-1 tails. In the case of POPC, the pre-transition state is absent because POPC bilayers are loosely packed with "mixed" domains. Therefore, alignment and conformational changes can occur simultaneously. The %*gauche* provides further evidence for the phase transition of POPC at about 270 K. However, for POPE, the results suggest a pre-transition state in which structural reorientations from *trans* to *gauche* drastically change prior to the main phase transition.

6.4.6   Level of Interdigitation

The last quantity considered is the transformation from partial (gel phase) to mixed (liquid-crystalline phase) interdigitation near the phase transition, as described by Chen *et al.* [183]. Partial interdigitation refers to the chain mismatch of the two leaflets that is, at most, three
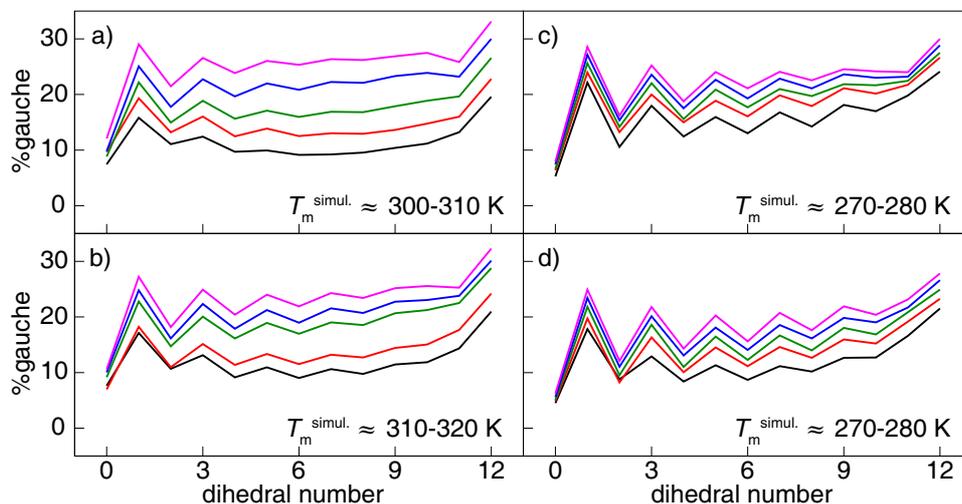
Figure 6.4.6: Average %*gauche* formed along the *Sn*-1 tails of a) DPPC, b) DPPE, c) POPC, and d) POPE. Line colors are described in the Figure 6.4.5. $T_m^{\text{simul.}}$ is the estimated phase transition temperature.

methylene units from the terminal carbon of the lipid tail (the bilayer thickness is approximately the sum of the acyl chain length of each leaflet [303, 304]). Pictorial representations of partial and mixed interdigitation are shown in Figure 6.4.7. This is seen from DPPE at 290 K in Figure 6.3.1b , where the terminal carbon of the lipid tails of each leaflet do not overlap one another. Note that the bilayer thickness in this configuration is about the sum of the fully stretched lipid molecules in the two leaflets. On the other hand, mixed interdigitation refers to greater overlap, which is commonly seen in lipid bilayers in a liquid-crystalline state.

To verify this, overlap between lipid tails from opposite leaflets was measured by computing the density profile of the individual carbon atoms in the acyl chains, as described by Flack *et al.* [168]. Figures 6.4.8a-d shows the acyl chain density profiles of DPPC from 300 to 310 K and DPPE from 310 to 320 K. These temperature ranges were chosen because it was identified to cover the phase transition region for DPPC and DPPE. For clarity, only the alternating carbon atoms of the *Sn*-2 tail are considered (the density profile for the *Sn*-1 tails are nearly identical - data not shown here). As seen in the plots, the density
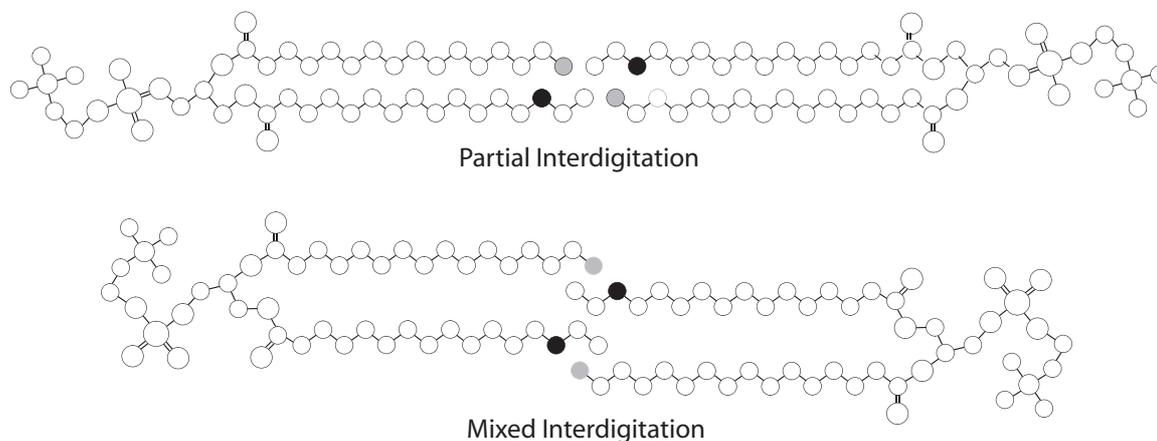
Figure 6.4.7: Pictorial representation of partial and mixed interdigitation. The third methylene groups from the lipid tail terminal carbon are shown in black for the *Sn*-2 tail and in gray for the *Sn*-1 tail.

profiles are very distinct above and below the phase transition temperature. For DPPC below T_m (Figure 6.4.8a), the density profiles are broader away from the center of bilayer and become narrower near the center. A broad density profile suggests that DPPC has a "mixed" phase with partial and mixed interdigitation co-existing. A narrow density profile of the terminal carbon atoms indicates that lipid tails are not predominantly overlapping. Above T_m (Figure 6.4.8b), the density profiles for all carbon atoms are uniform, suggesting that the lipid tails are fully random and the lipid molecules are evenly distributed in the bilayer. Note that the density profile for the terminal carbon atoms does not show a narrow distribution, unlike the structure below T_m, indicating overlap between the lipid tails of opposite leaflets. Similar results were observed for DPPE above and below T_m. For the density profiles below T_m, the distributions are relatively narrow (Figure 6.4.8c), suggesting an absence of a "mixed" phase. Above T_m, the density profiles show limited overlap of the lipid tails, as indicated by the distribution of the terminal carbon atom (Figure 6.4.8d).

For POPC and POPE, the same analysis shows the most significant changes in the density profiles between 270-280 K and 290-300 K, respectively. As seen in Figures 6.4.8e-h, the density profiles are very similar above and below the phase transition temperature. The
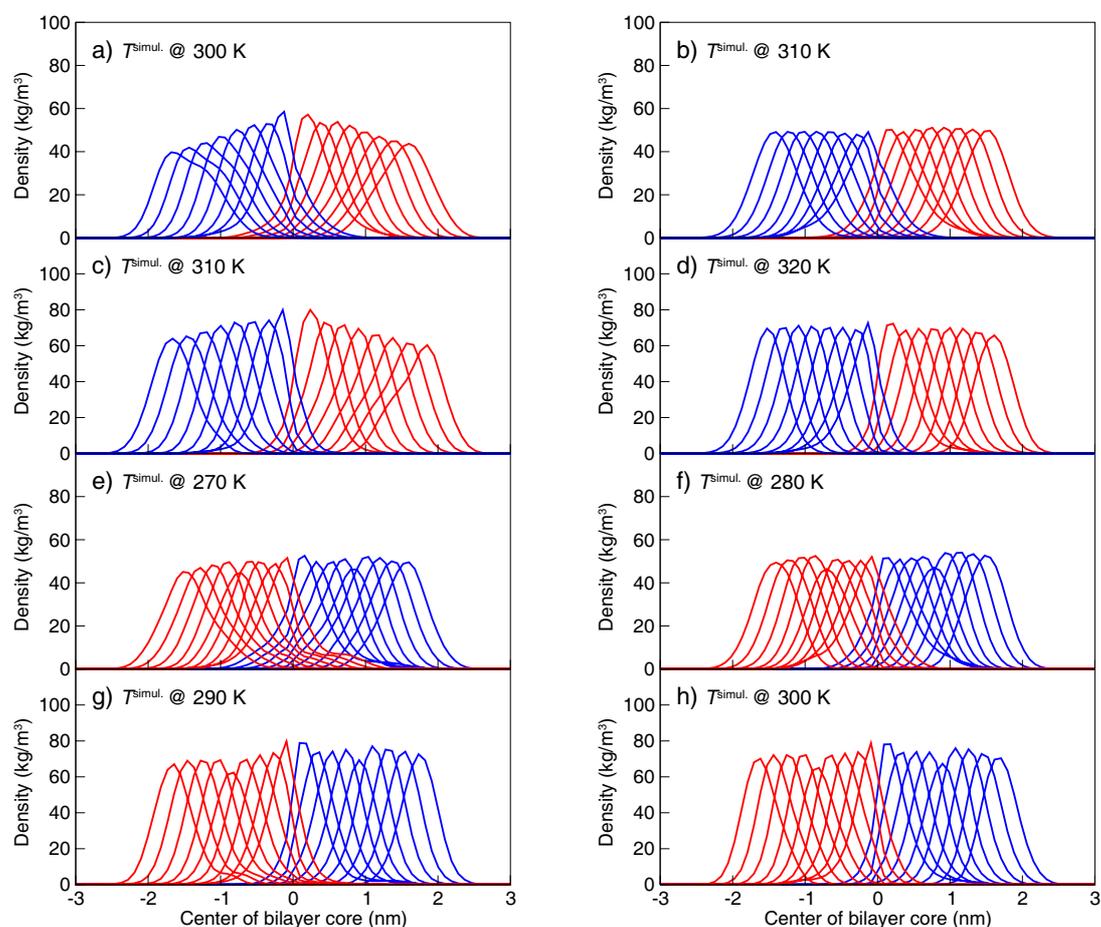
Figure 6.4.8: Density profile for each carbon segments in the *Sn*-2 tail for DPPC, DPPE, POPC, and POPE above and below the estimated transition temperature. $T^{\text{simul.}}$ is the system temperature. Profiles are centered with respect to the middle of the bilayer core. Red and blue lines represent density profiles for each leaflet.

only difference between these plots is the shape of the distributions, which are asymmetric at 270 K for POPC and 290 K for POPE. This demonstrates that the packing of the lipids hinders the full random motion of the *Sn*-2 tails, a characteristic of lipids in a gel state. Upon increasing the temperature by 10 K, all density profiles become symmetric, which characterizes lipids in a liquid-crystalline state. Therefore, the phase transition for POPC and POPE occurs at the temperature range of 270-280 K and 290-300 K, respectively, as the constrained displacement of the carbon atoms along the lipid tails seem to disappear in these temperature ranges.

6.5   Summary

Molecular dynamics simulations were used for a comprehensive study of the structural properties of saturated and monounsaturated lipid bilayers near the main phase transition. Though the chemical structure of DPPC and DPPE or POPC and POPE are largely similar (choline versus ethanolamine headgroup), their transformation processes from a gel to a liquid-crystalline state are contrasting. From this study, the main phase transition temperature was identified at about 300 K, 320 K, 275 K, and 285 K for DPPC, DPPE, POPC, and POPE bilayers, respectively, compared to the experimental values of 315 for DPPC [282], 337 K for DPPE [18], 270 K for POPC [45], and 306 K for POPE [175]. Based on the structural properties analyzed, Table 6.4.1 summarizes the temperature ranges identified as the main phase transition for all lipid bilayers considered.

For DPPC, three distinct structures can be identified relative to the melting temperature (T_m): below T_m with "mixed" domains consisting of lipids that are tilted with partial overlap of the lipid tails between leaflets; near T_m with a slight increase in the average area per lipid, resulting in a rearrangement of the lipid tails and an increase in the bilayer thickness; and above T_m with unhindered lipid tails in random motion resulting in an increase in *%gauche* formed and increase in the level of interdigitation between lipid leaflets. For DPPE,

Table 6.4.1: Summary of the phase transition temperature ranges identified for DPPC, DPPE, POPC, and POPE bilayers. The structural properties analyzed are shown separately for the annealing simulations and simulations at fixed temperature. The experimental phase transition temperatures (T_m) are shown in the last row.

Properties/$T_m^{simul.}$ (K)	DPPC	DPPE	POPC	POPE
Area per lipid^a	290-300	320-330	270-280	280-290
Bilayer thickness^a	290-300	320-330	270-280	280-290
Bilayer structure^b	290-300	320-330	270-280	280-300
Area per lipid^b	300-310	310-320	-	-
Bilayer thickness^b	300-310	310-320	-	-
Lipid tail tilt-angle^b	300-310	310-320	270-280	280-290
Order parameter^b	300-310	310-320	270-280	280-300
Trans-Gauche isomerization^b	300-310	310-320	270-280	270-280
Interdigitation^b	300-310	310-320	270-280	290-300
T_m	$\sim$315	$\sim$337	$\sim$270	$\sim$306

^{a} Annealing simulations
^{b} Simulations at fixed temperature

the structures identified were: below T_m with "ordered" domains consisting of slightly tilted lipid tails and non-overlapping lipid tails between leaflets; near T_m with minimal rearrangement of the lipids as the bilayer thickness reduces slightly with increasing temperature; and above T_m with unhindered lipid tails as that for DPPC. For DPPE, most of the lipid tails do not overlap as observed to DPPC, which is due to the tight packing of the DPPE molecules. The non-overlapping behavior of DPPE above T_m is confirmed from the density profile of the terminal carbon atoms in each leaflet, which shows a narrow distribution near the center of the bilayer core.

For POPC and POPE, the lipid tails for both systems are tilted below the phase transition and become more random above the phase transition temperature. The average area per lipid and bilayer thickness were found less sensitive to phase transition changes as the unsaturated tails are able to buffer reordering of the bilayer structure, as observed from hysteresis loops in annealing simulations. For POPC, changes in the structural properties

such as the lipid tail order parameter, hydrocarbon *trans-gauche* isomerization, lipid tail tilt-angle, and level of interdigitation identified a phase transition at about 270 K. For POPE, three temperature ranges were identified, in which the lower one (270-280K) was associated with a pre-transition state and the higher one (290-300 K) with the post-transition state. In the pre-transition state, there was a significant increase in the number of *gauche* formed along the lipid tails. Near the main transition (280-290 K), there was a lowering of the lipid order parameter and a disappearance of the tilted lipid arrangement. In the post-transition state, the carbon atoms along the lipid tails became less hindered as their density profiles showed uniform distributions. This study also demonstrates that atomistic simulations of current lipid force-fields are capable of capturing the phase transition behavior of lipid bilayers, providing a rich set of molecular and structural information at and near the transition state.

Chapter 7

Investigation of Trehalose Protection from Palmitate Induced Toxicity

This chapter investigated the mechanism for fatty acid induced toxicity on HepG2 cells by integrating experimental and computational modeling components to reveal the biophysical interactions of fatty acids with the cellular membrane and the role of trehalose in preventing changes to the membrane structure. This study resulted from a collaborative effort with Professor Christina Chan in the Department of Chemical Engineering and Material Sciences at Michigan State University. All experiments related to this study were conducted by Yifei Wu, a graduate student in Professor Chan's group at Michigan State University. All modeling studies were performed and analyzed by myself. The computational modeling is a vital part of the project to interpret and understand the concurrent experimental results, providing knowledge at the molecular level and a link from the molecular interactions to the role of palmitate and trehalose in the toxicity of HepG2 cells. Knowledge gained from this study is essential in the prevention and treatment of diseases such as obesity-associated cirrhosis.

7.1   Experimental Materials and Methods

7.1.1   Cell Culture

Human hepatocellular carcinoma cell line, HepG2 (American Type Culture Collection, Manassas, VA), was cultured in Dulbecco's modified Eagle's medium (DMEM, Invitrogen, Carlsbad, CA) containing 10% fetal bovine serum (FBS, American Type Culture Collection) and 2% penicillin-streptomycin (Invitrogen). They were seeded in 6-well plates and incubated at 37 °C in humidified atmosphere containing 10% CO_2. After cells reached confluence, the media were replaced with 2 ml control medium (4% fatty-acid free BSA - bovine serum albumin) or palmitate (0.7 mM with 4% BSA) and changed every 24 hrs. The BSA level used was close to physiological conditions [305]. 0.7 mM FFAs was employed in this study because the plasma FFA levels in the obese and type 2 diabetic patients have been reported to be approximately this level [306–309]. Experiments were conducted after 48 hrs of treatment. To determine the optimal amount of trehalose to add, a dose-response of HepG2 cells with trehalose ranging from 0 to 0.2 mM was performed.

7.1.2   Cytotoxicity Assay

Cell viability was assessed by lactate dehydrogenase (LDH) leakage through the membrane into the medium. The cell culture supernatant from control and palmitate-treated cultures were tested after 48 hrs of incubation for the presence of LDH (LDH_{medium}) using an LDH assay kit (Roche Applied Science, Indianapolis, IN). Cells were washed with phosphate buffered saline (PBS) and lyzed with 1% triton-X 100 for 12 hrs at 37 °C. The cell lysate was then centrifuged at 5000 G for 10 minutes and tested for LDH activity (LDH_{triton}). The LDH released was normalized to the total LDH, given by:

$$\%LDH_{\mathrm{release}} = \frac{LDH_{\mathrm{medium}}}{LDH_{\mathrm{medium}} + LDH_{\mathrm{triton}}} \times 100 \qquad (7.1.1)$$

7.1.3   Membrane Fluidity

Two different stearic acid derivatives were used to detect changes in the membrane fluidity, 5-*n*-doxylstearic acid (5-*n*-SASL) and 16-*n*-doxylstearic acid (16-*n*-SASL) (Invitrogen, Carlsbad, CA). The 5-*n*-SASL probe monitors the portion of the membrane closest to the lipid headgroups, while the 16-*n*-SASL reflects changes in the middle/end of the lipid hydrocarbon chains [310].

A stock solution of the spin labeled stearic acids at 10^{-3} M was prepared in DMSO and the aliquots stored at $-20\,^{\circ}$C. Immediately before use, the stock solution was thawed and diluted 50 times with PBS. Preliminary experiments were conducted to confirm that the spin label solution did not affect the cell viability. Cell suspensions collected after Trypsin-EDTA (GIBCO) exposure were centrifuged and the pellets were re-suspended in spin label solution and kept on ice. The labeled cell suspensions were then transferred to a flat cell and placed in the cavity of the electron paramagnetic resonance (EPR) spectrometer (Bruker model ESP-300E X-band). The microwave power was set at 15.8 mW, the modulation frequency at 100 kHz, and the modulation amplitude at 2.53 G. For indexes of membrane fluidity, the values of the outer and inner hyperfine splitting ($2T_{\perp}$ and $2T_{\parallel}$ in Gauss, respectively) in the EPR spectra for 5-*n*-SASL were evaluated . The order parameter was calculated from $2T_{\perp}$ and $2T_{\parallel}$ by:

$$S = \frac{T_{\parallel} - (T_{\perp} + C)}{T_{\parallel} + (2T_{\perp} + C)} \times 1.66 \tag{7.1.2}$$

where $C = 1.4 - 0.053(T_{\parallel} - T_{\perp})$. In the EPR spectra for 16-*n*-SASL, the peak height ratio ($h_o/h-1$) for an index of the membrane fluidity was used [311, 312], where h_o and $h-1$ are the heights of the central and high-field peaks, respectively. The greater the values of the order parameter and peak height ratio, the lower is the freedom of motion of the spin labels in the membrane bilayers, indicating lower membrane fluidity [310].

7.1.4   Liposome Preparation and DSC Measurement

To correlate the fluidity measurements to the computational studies, a simpler model cell membrane also was used. Liposomes (multi-lamellar vesicles or MLVs) were prepared by the thin film method according to the protocol from Avanti Polar Lipids. The lipid 1,2-dioleoyl-*sn*-glycero-3-phosphocholine (DOPC, Avanti Polar Lipids, Alabaster, Al) and palmitic acid (Sigma-Aldrich, St. Louis, MO), obtained in chloroform stock solutions, were mixed in appropriate amounts in a glass tube. After vortexing, the solvent was dried under nitrogen. This formed a thin lipid film on the inside wall of the glass tube. The film was dried in a freeze-dryer to ensure complete evaporation of chloroform. Deionized water was added into the tube before it was placed in a bath sonicator for 10 minutes. Differential scanning calorimetry (DSC) analysis were performed on the liposomes samples at a scan rate of 1°C /min. Samples containing 20 mg/ml of lipid and 10 μL of liposome suspensions were used. DOPC was used in these experiments because its phase transition temperature ($\sim$19°C) allowed us to obtain clean and clear DSC scans, whereas POPC (one of the lipids used in the simulations studies) has a phase transition temperature near the normal melting point of water ($-$2°C for POPC), which causes severe interference in obtaining reliable data.

7.2   Simulation Details

To gain insight into how palmitate induces cytotoxicity, MD simulations were used to investigate the role palmitate and trehalose play in the structure and integrity of lipid bilayers (model biological membranes). The lipid bilayers used here were equimolar POPC/POPE bilayers with a total of 288 lipid molecules evenly distributed in each leaflet (System 1 in Table 7.2.1). This mixed bilayer was chosen for these studies because it represents the main phospholipid constituents of HepG2 cells [27]. Note that other major lipid constituents (e.g., cholesterol) were not included in these simplified model bilayers. Combinations of palmitate and trehalose were introduced into the lipid bilayer systems. The structure of the molecules

Table 7.2.1: Composition for lipid bilayers. All systems contain 144 lipids per leaflet with 40 waters per lipid. Each leaflet contains an equal number of POPC and POPE.

System	Trehalose	Palmitate	Ensemble
1	-	-	NPT
2	30^a	-	NPT
3	-	1^a	NPT
4	30^a	1^a	NPT
5	-	16^b	NPT
6	-	32^b	NPT
7	-	48^b	NPT
8	-	64^b	NPT
9	-	16^b	NP_zAT^*
10	-	32^b	NP_zAT^*
11	-	48^b	NP_zAT^*
12	-	64^b	NP_zAT^*

[a] Molecules inserted in the aqueous phase
[b] Molecules embedded in the bilayer
* Compressibility set to zero in the x- and y-directions

considered are shown in Figure 7.2.1.

To mimic the exposure of palmitate to cells with and without trehalose, a palmitate molecule was inserted into the middle of the aqueous phase of previously equilibrated lipid bilayers (System 3 in Table 7.2.1). For the systems with trehalose, a concentration of ∼5 wt% trehalose was used in the aqueous phase (Systems 4 in Table 7.2.1). A low trehalose concentration was chosen because it represents the range of concentrations reported in cryopreservation, lyophilization, and other modeled membrane-trehalose studies [124–127]. To obtain a statistical analysis of the diffusion process, ten sets of simulations were performed on each bilayer with and without trehalose. These simulations were setup with a single palmitate molecule in the aqueous phase because of aggregation at higher concentrations (see Figure 7.2.2) and experimental evidence that shows the free unbound palmitate in solution (about ∼10 nM) is largely responsible for the biophysical changes to the membrane [313]. Note that BSA, used in the experiments to prevent palmitate aggregation, is not considered
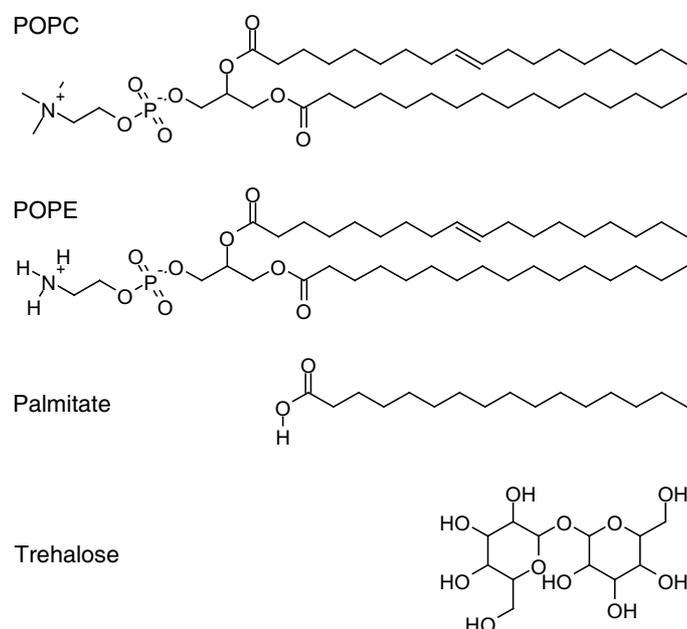
Figure 7.2.1: Molecular structure of POPC, POPE, trehalose, and palmitate. Note that all the double bonds have the *cis* configuration. Chemical symbols are hydrogen (H), nitrogen (N), oxygen (O), and phosphorus (P).

in the simulations. Because palmitate is a relatively long molecule (in its fully stretched conformation – sixteen carbon long), it was necessary to consider systems with a large aqueous phase (40 water per lipid), so that the palmitate molecule would interact with only one of the bilayer interfaces at any given time.

Experimental studies have shown that moderate to high concentrations of palmitate induce significant structural changes to the bilayer, including membrane swelling [314], membrane fusion [315, 316], and degradation of membrane integrity [315, 317]. To understand the effect of these phenomena, two sets of simulations were proposed to explain the global and local effect of palmitate on the membranes (see Figure 7.2.3 for pictorial representation). For the global effect, NPT simulations were performed. Here the simulations captured the effect of large membrane structures, as the bilayer surface was allowed to adjust as palmitate molecules were embedded into the bilayer. To avoid aggregation of palmitate in the aqueous phase, the bilayer structures were constructed to have various concentrations of palmitate
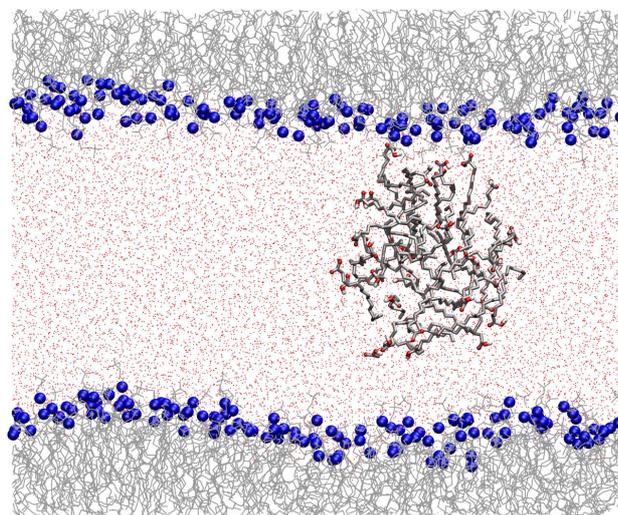
Figure 7.2.2: Snapshot of palmitate aggregation in the aqueous phase. The colored groups correspond to the DPPC headgroups (blue), lipid tails (light gray), palmitate (red/dark gray), and water (pink).

embedded into the bilayer prior to equilibration (Systems 5-8 in Table 7.2.1). Simulations of these systems were used to address the overall changes of the membrane structure in the presence of palmitate. For the local effect, the changes in bilayer structure are limited to a specific portion of the membrane that is concentrated with palmitate. Here, NP_zAT (constant surface area) simulations were performed (surface area of the bilayer constrained to that without palmitate). Similarly, palmitate molecules were embedded in the bilayers prior to the start of the simulations (Systems 9-12 in Table 7.2.1). The goal of these latter studies was to investigate the membrane swelling induced by palmitate, which may eventually lead to membrane deformation or formation of ordered domains that alter the membrane fluidity.

The force-fields for POPC, POPE, and water are consistent with those employed in previous studies [95, 296, 297], which include intramolecular parameters for bonds, angles, proper dihedral, and improper dihedral. The Ryckaert-Bellemans potential was used for the torsion potential of the lipid hydrocarbon chains [271]. Non-bonded interactions were described by the parameters from Berger *et al.* [104, 110, 272] and partial atomic charges were obtained from Chiu *et al.* [96]. The united-atom representation was used for
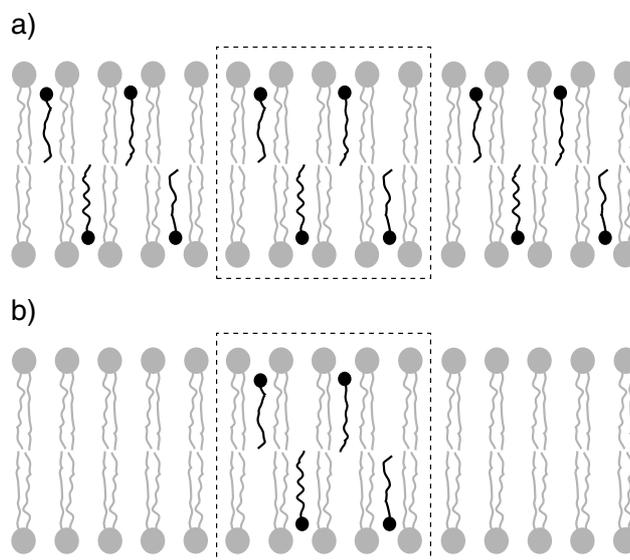
Figure 7.2.3: Pictorial representation of a) global and b) local effect of palmitate in membranes. Phospholipid and fatty acid molecules are represented in gray and black, respectively. Only the portion of the membrane in the square box is considered in the simulations.

the methyl/methylene groups in the acyl chains of both POPC and POPE. For POPE, the hydrogen atoms in the amine group are explicitly listed in the topology. The optimized potential for liquid simulations (OPLS-AA) force field was used for trehalose [292]. Palmitate was modeled in the protonated state and described using parameters derived from the lipid force-field. The carboxylic acid group was based on the parameters of glutamic acid, which were available from the Gromos force-field [293]. The single point charge (SPC) model was adopted for water [273].

Temperature of the simulation box was kept constant at 310 K using the weak coupling technique [265], with correlation times $\tau_T = 0.1$ ps. The linear constraint solver (LINCS) algorithm was used to constrain all bonds of the lipid molecules [274], and the SETTLE algorithm for water molecules [275]. These constraint algorithms allowed simulations to be carried out with a 2 fs time-step using the Leap-Frog integration method [248]. Coulombic and van der Waal interactions were cutoff at 1.0 nm. Long-range electrostatic interactions were corrected with the particle-mesh Ewald method (PME) [108, 263] (0.12 nm for

the grid size, fourth-order spline interpolation, and real-space cutoff at 1.0 nm). Periodic boundary conditions were applied in all directions. Trajectories were collected every 2 ps. All simulations were performed with the GROMACS 3.3.1 software package [258, 259, 295] (single-precision mode) in parallel using Virginia Tech's System X [281].

7.3   Experimental Results

7.3.1   Palmitate Cytotoxicity and Trehalose Protective Role

Previous studies by Srivastava and Chan found that palmitate induced toxicity led to ROS production in HepG2 cells [202], but its effect was not prevented upon treating with ROS scavengers. During oxidative stress, yeast cells produce trehalose to protect themselves from damage by oxygen radicals [226]. Therefore, the effect of trehalose on palmitate-induced toxicity in HepG2 cells was evaluated. The level of cytotoxicity was measured by the relative amount of LDH released in the medium. The control consisted of HepG2 cells exposed to DMEM with 4% BSA. From Figure 7.3.1, the measurements indicate that palmitate significantly increased the amount of LDH released, relative to the control. As the concentration of trehalose increased, the LDH released reduced significantly. This protective effect reached a maximum at a trehalose concentration of 0.13 mM, whereupon further increase in the trehalose concentration was detrimental to the HepG2 cells. Although the mechanism of trehalose-induced toxicity is not a focus of this study, previous studies have shown that trehalose preferentially bound to the membrane and possibly caused surface modifications that may affect cellular activity [148–151, 227, 228]. As it will be demonstrated in this Chapter, trehalose can induce local hydrophobic/hydrophilic domains along the bilayer interface, a membrane reorganization process which may have potentially detrimental effects. Based on these findings, a trehalose concentration of 0.13 mM was optimum for alleviating the palmitate-induced toxicity in HepG2 cells and it was used in all subsequent experiments.
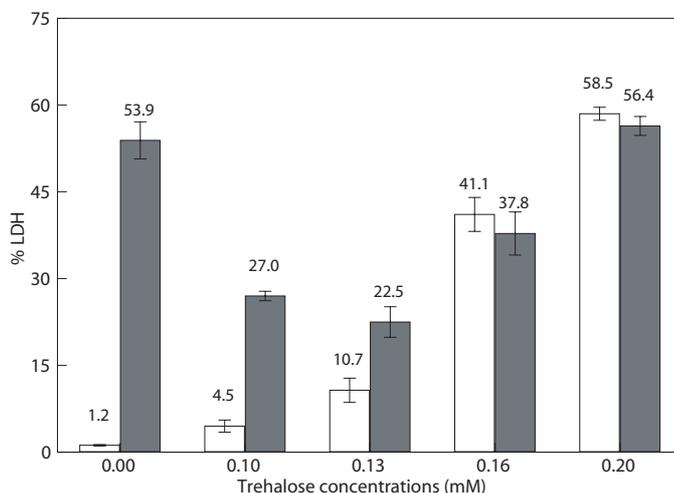
Figure 7.3.1: Effect of trehalose on the HepG2 cells cytotoxicity in response to palmitate. Confluent HepG2 cells in Bovine serum albumin (BSA) medium were exposed to 0.7 mM palmitate in the presence of different concentrations of trehalose. The LDH released was measured after 48 hrs. White and gray bars represented the effect of trehalose alone or the mixtures of trehalose/palmitate, respectively. Note that the first gray bar shows the effect of palmitate alone. Error bars are standard deviation of three independent experiments.

7.3.2   Trehalose on H_2O_2 Release

Hydrogen peroxide (H_2O_2) has been previously identified as one of the ROS species involved in the palmitate-induced toxicity of hepatoma cells [202]. To determine whether trehalose protected HepG2 cells by scavenging H_2O_2, the measured H_2O_2 released into the medium was normalized to total cellular protein. As shown in Figure 7.3.2, 48 hrs of palmitate exposure enhanced H_2O_2 release into the medium, while trehalose significantly reduced the H_2O_2 release in the presence of palmitate. The results suggest that trehalose protects the cells in part by reducing H_2O_2 release.

7.3.3   Membrane Fluidity for HepG2 Cells

Since palmitate is amphiphilic, there may be non-specific cytotoxic effects due to its hydrophobicity. It has been established experimentally that trehalose has a stabilizing effect
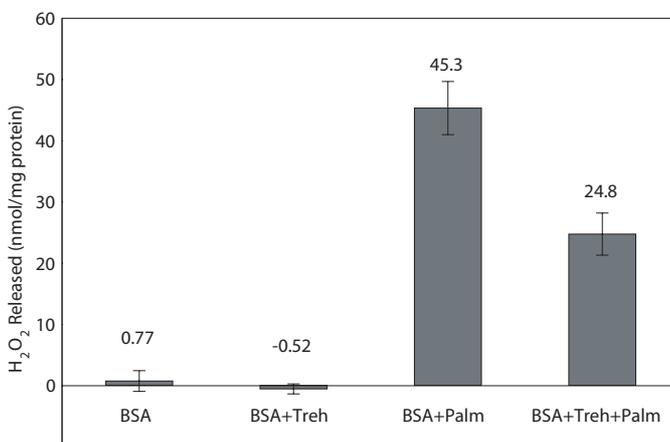
Figure 7.3.2: Effects of trehalose and palmitate on H_2O_2 release. Confluent HepG2 cells in Bovine serum albumin (BSA) medium were treated with 0.7 mM palmitate (Palm) with or without 0.13 mM trehalose (Treh) for 48 hrs. The H_2O_2 released into the medium was measured and normalized to total cellular protein. Error bars are standard deviation of three independent experiments.

on biological membranes [318], therefore the changes in cellular membrane structure upon exposure to palmitate in the presence and absence of trehalose were investigated. The cellular membrane fluidity of HepG2 cells in the presence of palmitate or trehalose was measured by EPR. The EPR spectra of the spin-label agents were used to detect changes in the freedom of motion of the lipids in the cell membrane, thus providing a measure of the membrane fluidity. The membrane fluidity of HepG2 cells was measured after 48 hrs of exposure to palmitate, trehalose, and combinations thereof. The control was HepG2 cells exposed to DMEM with 4% BSA. Using 16-n-SASL as a probe to monitor the ordering of the lipid tails near the center of the bilayer core, a greater peak height ratio was observed for the palmitate treated cells as compared to the control, which correlated with reduced freedom of motion of the spin labels in the membrane. This indicates a decrease in membrane fluidity of the cells treated with palmitate for 48 hrs, as shown in Figure 7.3.3a. The exposure of HepG2 cells to trehalose had an insignificant effect on the bilayer core region since trehalose is excluded from the bilayer. The interaction of trehalose with the membrane is only at the surface of the bilayer. Treating HepG2 cells with trehalose and palmitate increased the peak

height ratio. This suggests that a complex interaction exists between the cellular membrane, palmitate, and trehalose. Similarly, using 5-n-SASL as a probe to monitor the lipid carbons near the lipid headgroups, the presence of trehalose in the palmitate treated cells increased the fluidity near the surface of the membrane (see Figure 7.3.3b).

To corroborate the membrane fluidity results, the phase transition temperature of DOPC liposomes was measured by DSC measurements. The DSC thermographs for DOPC liposomes with varying mole fractions of palmitate (see Figure 7.3.4) showed that the phase transition temperature of the DOPC liposomes increased with increasing concentration of palmitate. This suggests that palmitate increases the ordering of the phospholipids in the liposomes, which correlates with the decrease in membrane fluidity measured by EPR.

7.4   Computational Results

Based on the experimental results, exposure of healthy cells to palmitate resulted in cytotoxicity, while the presence of trehalose partially alleviated the negative effect by palmitate. As such, there must be a complex interaction between palmitate, trehalose, and the cell membrane to enable this process to occur. Based on the large number of hydroxyl groups present in trehalose, it was hypothesized that the distribution of hydrogen bonds between trehalose, phospholipid and palmitate is the key in determining the protective mechanism. Therefore, MD simulations were performed on lipid bilayers to elucidate the possible mechanisms of palmitate induced toxicity and the mechanism by which trehalose protects cells from palmitate induced toxicity. It should be noted that while MD simulations to investigate the biological function of trehalose [148–151, 227, 228] and palmitate [231, 239], separately, are present in the literature, their combined role is scarce.
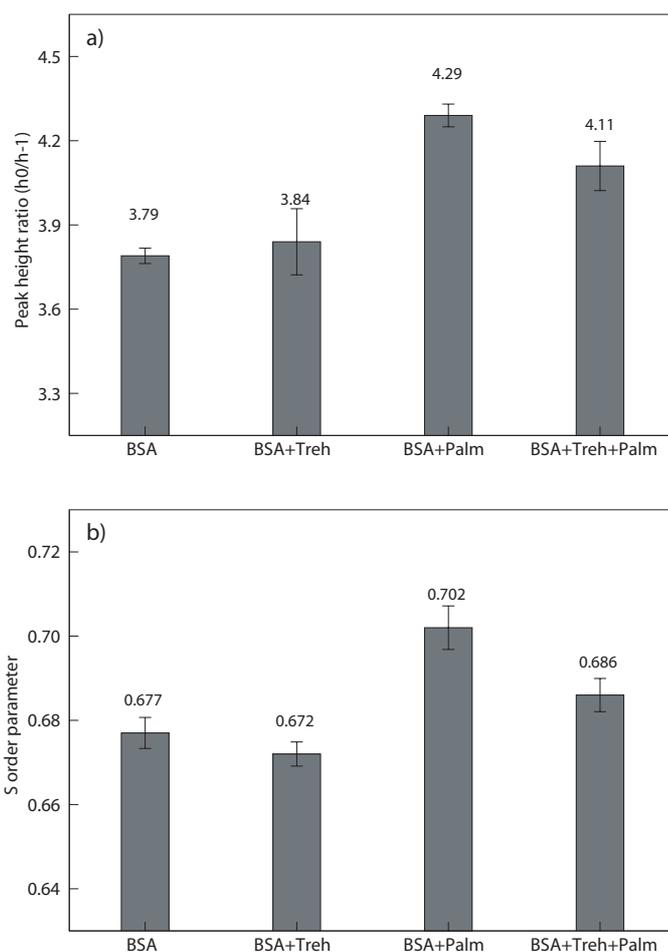
Figure 7.3.3: Effect of palmitate exposure on cellular membrane fluidity. Cells in Bovine serum albumin (BSA) medium were treated with 0.7 mM palmitate (Palm) in the presence or absence of 0.13 mM trehalose (Treh) for 48 hrs. The cellular membrane fluidity was measured using EPR. a) Values are peak height ratio for 16-n-SASL labeled HepG2 cells. b) Values are order parameter for 5-n-SASL labeled HepG2 cells. Error bars are standard deviation of three independent experiments.
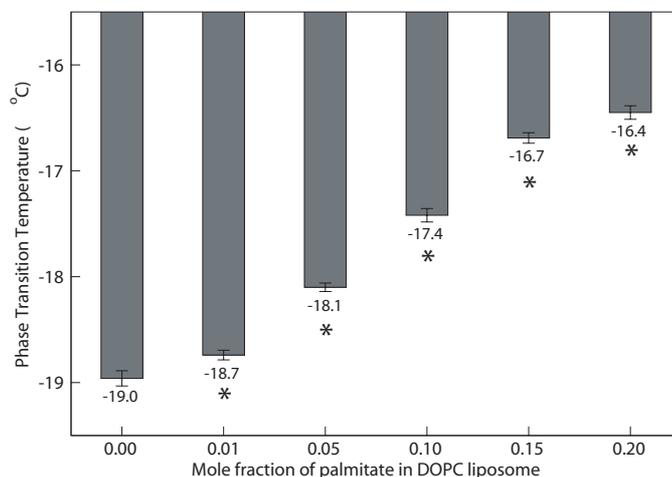
Figure 7.3.4: Phase transition temperature of DOPC liposomes containing palmitate. The phase transition was measured with DSC. Error bars are standard deviation of three independent experiments. "*" indicates statistical difference from control, 0% palmitate ($p < 0.01$).

7.4.1   Palmitate Dynamics

The initial stage of cell exposure to palmitate is modeled by introducing a single palmitate molecule in the aqueous phase of previously equilibrated bilayers with and without trehalose. Snapshots of the two systems at the start of the simulation are shown in Figure 7.4.1. To obtain a statistical sampling of the palmitate penetration into the bilayer, ten sets of simulations were performed for each system with different starting configurations and initial velocities. All simulations lasted 40 ns regardless of the time when palmitate penetrated the bilayer. Figures 7.4.1b and d show representative trajectories of palmitate along the simulation (trajectory is traced by the position of the central carbon atom in the palmitate tail). As seen in the figure, palmitate can penetrate the bilayer within the simulation time considered. Eight of the ten simulations resulted with palmitate in the bilayer and two palmitates remained in the aqueous phase for the duration of the simulations. For the simulations with trehalose, similar results were obtained. The observed penetration of palmitate in the bilayer is consistent with experimental studies that demonstrated that palmitate can be readily incorporate into the hydrophobic region of the bilayer [319, 320].
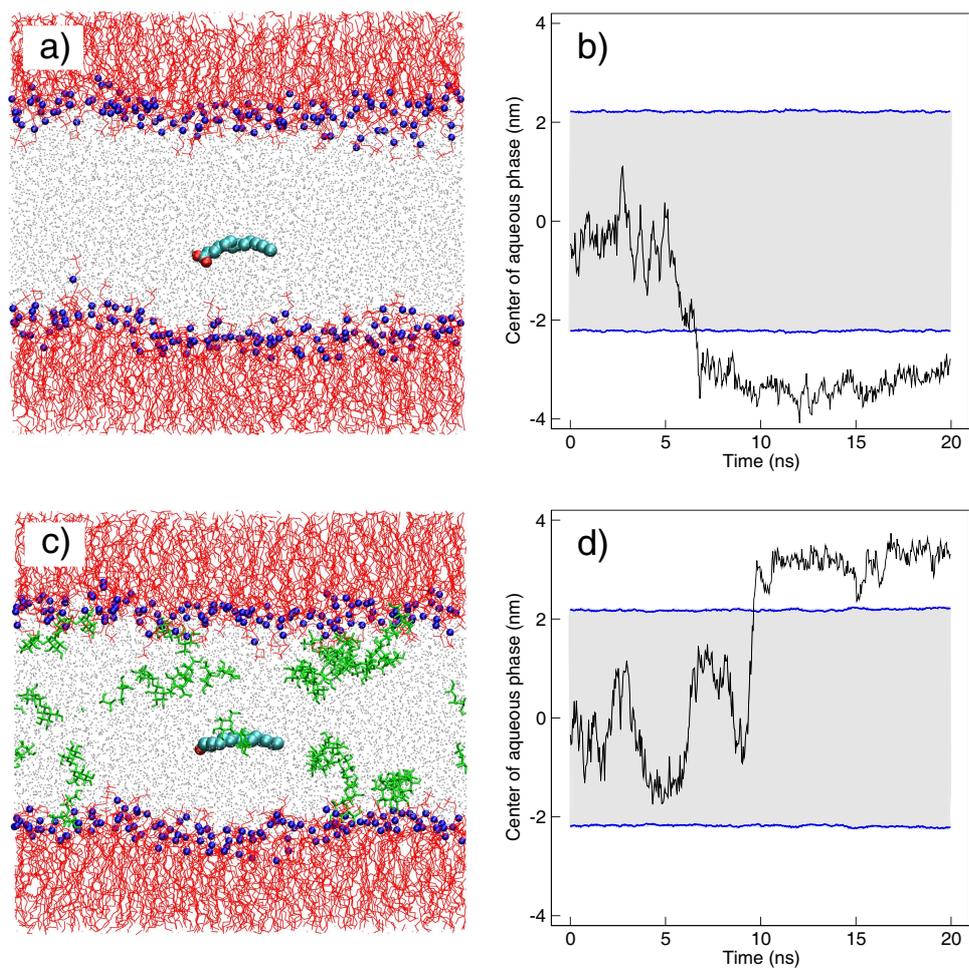
Figure 7.4.1: Starting structure of POPC/POPE bilayer with one palmitate inserted into the aqueous phase. Bilayers are modeled a) without and c) with trehalose. Colored molecules are POPC/POPE headgroup (blue), lipid tails (red), water (gray), trehalose (green), and palmitate (cyan). See Table 7.2.1 for composition. The dynamics of palmitate, represented by the position of central carbon atom in its tail, are shown in b) and d). Blue horizontal lines correspond to the average position of the phosphorus atoms of POPC and POPE along the interface and are used to identify the interface. Gray area denote the aqueous regions. The position $z = 0$ corresponds to middle of the aqueous phase.

The following observations were made from the simulations containing palmitate in the absence of trehalose. Initially in the aqueous phase, palmitate freely diffuses through the water molecules. Due to the hydrophobic nature of palmitate, entropic forces drive palmitate to migrate toward the bilayer core region (hydrophobic environment). As palmitate approaches the bilayer interface, numerous interactions must occur before the hydroxyl group of palmitate (H-donor) can favorably interact with the lipid oxygen atoms (H-acceptor) through hydrogen bonding. Note that the lipid oxygen atoms are those in the phosphate and carbonyl groups. First, at least two hydrogen bond pairs, one between water (H-donor) and lipid oxygen atoms (H-acceptor) and another between the palmitate hydroxyl group (H-donor) and water (H-acceptor) must be broken for the palmitate to interact with the lipids, a process that requires substantial amount of energy. Second, since the bilayer contains both POPC and POPE, an additional hydrogen bond between the amine groups of POPE (H-donor) and neighboring lipid oxygen atoms (H-acceptor) must be broken as well, if palmitate penetrates to the bilayer near POPE. Finally, the hydrophobic nature of palmitate is the driving force bringing palmitate closer to the bilayer interface and eventually into the bilayer core, nevertheless the bilayer interface is hydrophilic and poses a barrier for palmitate to penetrate into the bilayer core. For these reasons, palmitate is often not readily incorporated into the bilayer core as it approaches the interface. This is illustrated in the trajectory shown in Figure 7.4.1b, where palmitate frequently interacts with the lipid interface before penetrating the bilayer. Once the alignment and interactions of palmitate at the interface are favorable, palmitate penetrates the bilayer with the hydrocarbon tail first. This is also seen from Figure 7.4.1b, where the palmitate trajectory remains almost stationary prior to crossing the interface and then quickly moving into the bilayer core. For lipid bilayers containing trehalose, the interactions of palmitate appeared to be much more complex, as the exchange of hydrogen bonds between lipids, trehalose, and palmitate have significant effects on the dynamics of the system.

7.4.2   Hydrogen Bond Analysis

To investigate the protective role of trehalose on palmitate induced toxicity, the number of hydrogen bonds was correlated between the bilayer lipids and palmitate up to the penetration time. The H-donors consisted of the palmitate hydroxyl group and the POPE amine group. The lipid and palmitate oxygen atoms were the H-acceptors. A hydrogen bond is defined according to the criteria suggested by Brady and Schmidt, with the distance between the donor and acceptor within 0.35 nm and the angle donor-hydrogen-acceptor between 120 and 180 degrees [285]. The penetration time is the time at which palmitate crosses the interface from the aqueous phase into the bilayer. In the absence of trehalose, palmitate penetrates the bilayer faster and forms more hydrogen bonds with the lipids than in the presence of trehalose. In the latter case, trehalose competes with palmitate for hydrogen bonds with the lipids, and thus trehalose can interfere with the interactions between the lipids and palmitate. Therefore, longer penetration time and less hydrogen bond between the lipids and palmitate are expected. From the 20 simulations considered (10 with and 10 without trehalose), 16 showed palmitate penetrating into the bilayer within 40 ns of simulation. As shown in Figure 7.4.2a, the data do not seem correlated with the number of hydrogen bonds (lipid-palmitate) and the penetration time. This suggests that the probability of palmitate penetrating the bilayer and interacting with the lipids and trehalose are more complex than initially proposed.

Following a similar approach, the number of hydrogen bonds was correlated between trehalose and palmitate up to the penetration time to provide insight into how trehalose may prevent palmitate induced toxicity. Here, the H-donors and H-acceptors consisted of trehalose and palmitate hydrogens and oxygen atoms in the hydroxyl group, respectively. The results, shown in Figure 7.4.2b, demonstrate a direct correlation between the number of hydrogen bonds and the penetration time, suggesting that trehalose may be directly interacting with palmitate. Therefore, it is possible that by interfering with the interaction of palmitate with the bilayer lipids, trehalose reduces the probability of palmitate inducing
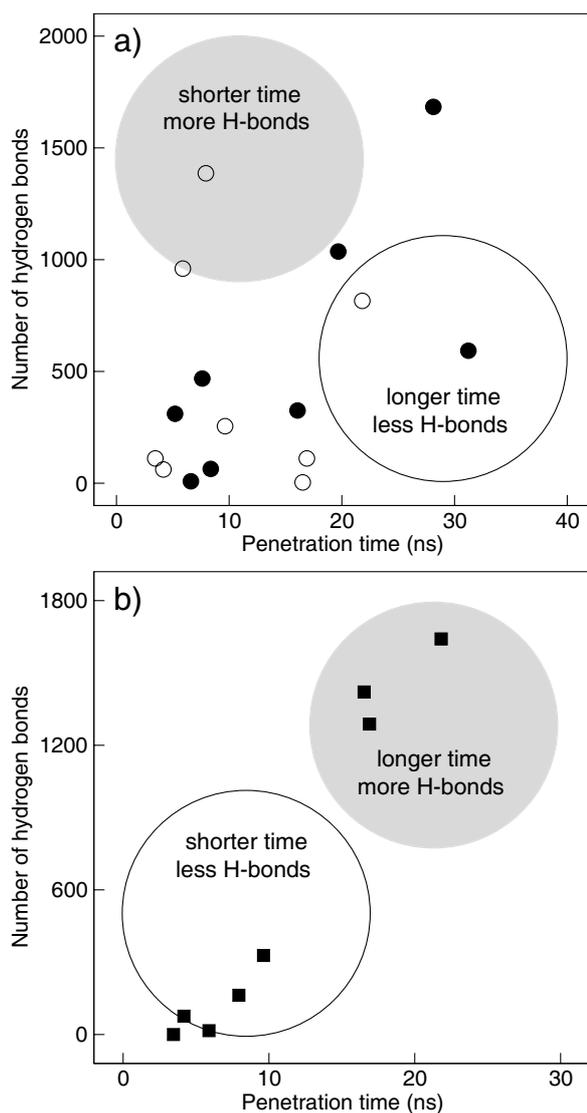
Figure 7.4.2: Correlation between the number of hydrogen bonds and palmitate penetration time. Closed and opened circles shown in a) are the number of hydrogen bonds between lipid headgroups and palmitate for bilayers without and with trehalose, respectively. Squares shown in b) are the number of hydrogen bonds between palmitate and trehalose. Highlighted circular areas are the speculated regions for the results to lie within.

toxicity.

An extensive hydrogen bond analysis was carried out to investigate the interactions between lipids, trehalose, and palmitate. Here, a correlation was made between the penetration time and the number of hydrogen bonds present in the system. From Figure 7.4.2b, shorter penetration time was observed for systems with fewer hydrogen bond interactions between palmitate and trehalose. This suggests that, without trehalose, palmitate should penetrate more quickly into the bilayer. However, the results indicated that the penetration times are about the same for the systems with and without trehalose. Since the penetration of palmitate is dependent upon the lipid molecules exposed to the aqueous phase, the bilayer interface was investigated to explain these results. Since the bilayers consisted of two types of lipids, with POPE acting as an H-donor, the intermolecular H-bond distribution between lipids (the amine groups as H-donors and the lipid oxygen atoms as H-acceptors) may provide insight into this inconsistency. To accomplish this task, the H-bond distribution was calculated in the bilayer interface at the time of penetration. Note that the interface is one to which palmitate penetrates through. For clarity and discussion purposes, four bilayers without trehalose and four bilayers with trehalose were selected. Figure 7.4.3 shows the intermolecular hydrogen bond distribution between lipids at the time of palmitate penetration. The penetration time and location are indicated in the figure. The first observation from the plots is that palmitate penetrates the bilayer in regions with fewer H-bonds between lipids. The void regions in the plots generally represent the choline headgroup in POPC molecules exposed to the aqueous phase. Note that the choline groups have three methyl groups, which are hydrophobic in nature. These facts and observations led us to conclude that palmitate, a hydrophobic molecule, prefers to penetrate the bilayer through hydrophobic regions. Secondly, the H-bond distributions are more random in systems without trehalose and become more localized in systems with trehalose. As a result, there are fewer but large hydrophobic regions exposed to the aqueous phase for systems containing trehalose, implying that trehalose has the ability to modify the bilayer surface [164, 321]. Furthermore, the penetration time varies depending on the palmitate location and distribution of H-bonds on the surface.

As seen in Figure 7.4.3d for a system without trehalose, the H-bond distributions are very similar to those systems containing trehalose (Figures 7.4.3e-g); as a result, palmitate penetrates the bilayer with the shortest amount of time. On the other hand, palmitate does not penetrate the bilayer surface with large hydrophobic regions, as shown in Figure 7.4.3h, mainly because palmitate interacts with trehalose in the aqueous phase, thus preventing palmitating from approaching the bilayer surface.

To verify that trehalose has the ability to modify the bilayer surface, the intermolecular H-bond distribution between lipids over the course of the simulation was monitored. The time considered for this analysis was between 5-15 ns. Selected snapshots are shown in Figures 7.4.3i-p for bilayers with and without trehalose. It is evident from Figures 7.4.3i-l (system without trehalose) that the H-bond distributions are random throughout the bilayer surface, even at the time when palmitate penetrates the bilayer. A different behavior is observed for systems with trehalose, where significant changes in the H-bond distribution are observed before and after the penetration time, as shown in Figures 7.4.3m-p. A shift in H-bond distribution may have resulted from the multiple hydrogen bonds between trehalose and lipid oxygen atoms, thus facilitating the local accumulation of polar regions on the bilayer interface (see Figure 7.4.4). This demonstrates the dual role of trehalose: on the bilayer surface trehalose can alter the H-bond distribution, thus inducing hydrophobic regions for palmitate to penetrate the bilayer, while in the aqueous phase trehalose can interact with palmitate and prevent it from approaching the bilayer surface. These two competing processes help us to understand why the experimental measurements have shown that trehalose at high concentrations (> 0.13 mM) is detrimental to HepG2 cells. At high trehalose concentrations, the bilayer surface is significantly modified by trehalose such that hydrophobic regions are more accessible for palmitate to penetrate the bilayer.
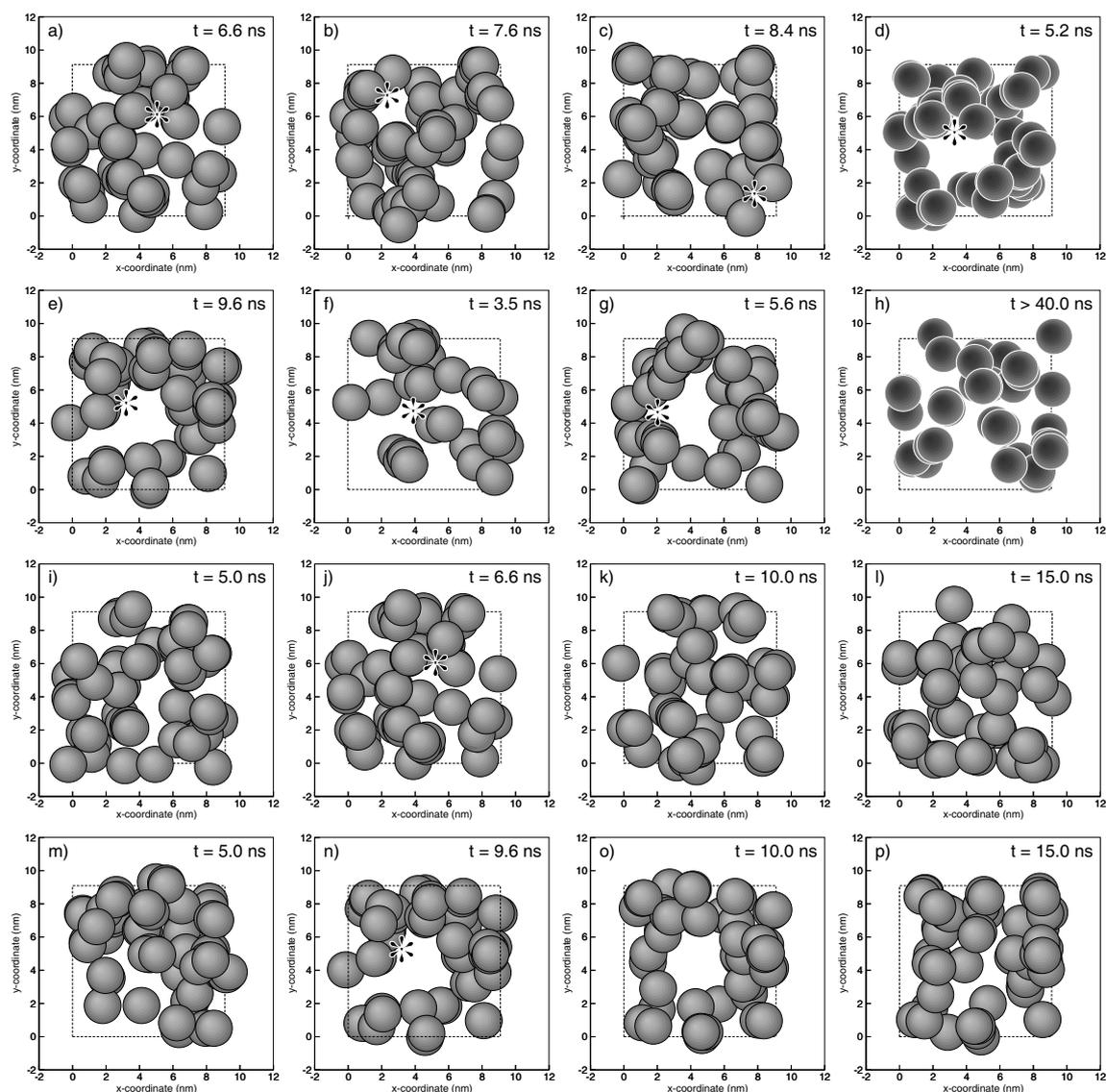
Figure 7.4.3: Snapshots of the hydrogen bond distribution on a bilayer leaflet during the time of palmitate penetration for bilayers without (a-d) and with trehalose (e-h) and over the course of simulations for bilayers without (i-l) and with trehalose (m-p). Circles represent the location of intermolecular hydrogen bonds between the amine groups of POPE and neighboring lipid oxygen atoms. For bilayers considered with and without trehalose, the majority shows uniform hydrogen bond distributions (gray circles in a-c and e-g). Inconsistent hydrogen bond distributions are shown in dark-gray (d and h). Over the course of the simulation, the snapshots show uniform hydrogen bond distributions for a bilayer without trehalose (i-l). Significant changes in the distribution are observed for bilayers with trehalose (m-p). Outlined square boxes are the approximate bilayer surface. The penetration time and location ("∗") are shown in each figure.
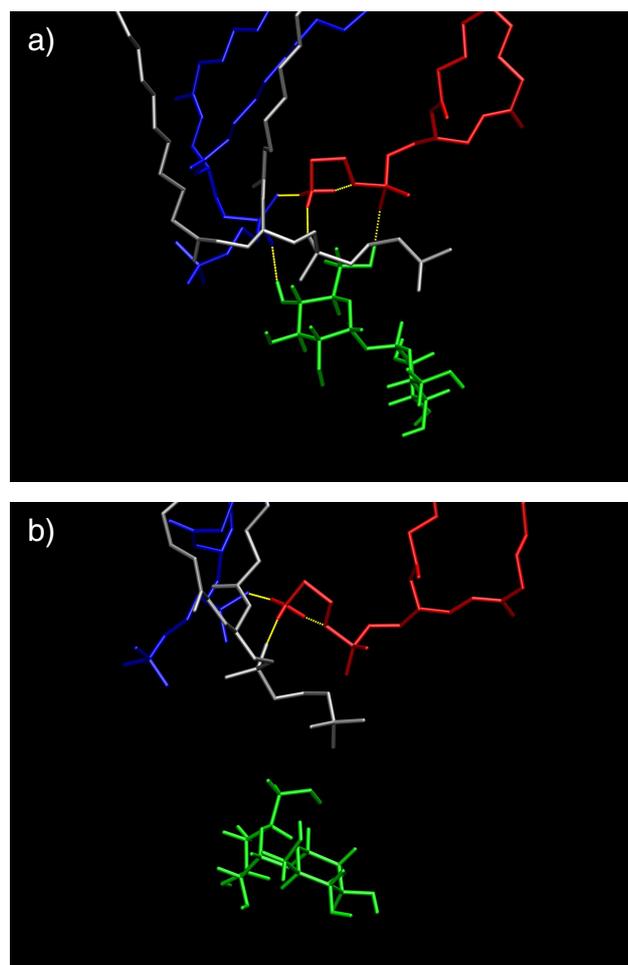
Figure 7.4.4: Snapshots of a trehalose (green) interacting with POPE (red) and POPC (blue and gray) at the bilayer interface, demonstrating a formation of triple hydrogen bonds between lipids. a) Hydrogen bonds formed by the hydroxyl groups of trehalose and the lipid oxygen atoms act as a bridge for intermolecular hydrogen bonds between the amine group of POPE and the neighboring lipid oxygen atoms. b) Hydrogen bonds between lipids remain after trehalose leaves the interface.

7.4.3   Embedded Palmitate in Bilayers

Thus far, the computational analysis indicated that a palmitate molecule can penetrate into the bilayer core within a short time ($<$ 40 ns). Although systems with more than one palmitate were also considered, their dynamics and properties contrast. This is because hydrophobic/hydrophilic interactions between palmitate molecules induce aggregation with characteristics similar to micelles. The aggregation of palmitate molecules in the aqueous phase partially shields the hydrophobic tails, which in turn lessen the driving force for palmitate to penetrate the bilayer. Moreover, the time for a sufficient number of palmitate molecules to penetrate the bilayer would likely require simulations into the microsecond domain. Therefore, to overcome this limitation, several model bilayers were created with palmitate molecules embedded in the bilayer structure (see Section 7.2). Since the amount of palmitate varies depending on the cell type and the level of toxicity, a range of palmitate concentrations was considered (11-44 mole% – see Table 7.2.1 for more details). To be consistent with previous analysis, the total number of lipids remained the same.

The following sections describe the global effect of palmitate embedded in the lipid bilayers (Systems 5-8 in Table 7.2.1). Since the bilayer surface was allowed to expand or contract as palmitate molecules were added into the bilayer, a correlation was established between the palmitate concentration and the bilayer surface area. As shown in Figure 7.4.5, the total area per leaflet increases almost linearly with increasing palmitate concentration. This is seen because palmitate occupies an additional volume within the bilayer and, due to its alignment with the lipid tails, the bilayer expands in the lateral dimensions. An approximate area per lipid and palmitate can be determined using the criteria suggested by Edholm and Nagle, which deals specifically with heterogeneous systems [322]. Although the bilayers considered here are multi-component systems (POPC, POPE, and palmitate), for simplification, the lipids are grouped as one component and palmitate as the other. The area per molecule can be obtained from:
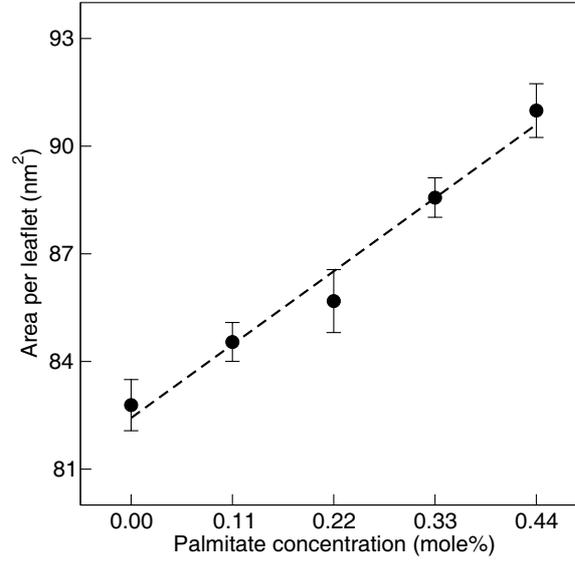
Figure 7.4.5: Average area per leaflet at 310 K. Dashed line is the ideal case (area increases linearly with increasing concentration), $R^2 = 0.989$. Error bars are estimated standard deviation.

$$\frac{A_{\text{total}}(x_{\text{palmitate}})}{N_{\text{lipid}}} = a_{\text{lipid}}(x_{\text{palmitate}}) + \frac{x_{\text{palmitate}}}{(1 - x_{\text{palmitate}})} a_{\text{palmitate}}(x_{\text{palmitate}}) \qquad (7.4.1)$$

where A_{total} is the total area per leaflet; $x_{\text{palmitate}}$ is the mole fraction of palmitate in the bilayer; N_{lipid} is the total number of lipids per leaflet; and a_{lipid} and $a_{\text{palmitate}}$ are the area per lipid and area per palmitate, respectively. By plotting $A_{\text{total}}(x_{\text{palmitate}})/N_{\text{lipid}}$ versus $x_{\text{palmitate}}/(1 - x_{\text{palmitate}})$, as shown in Figure 7.4.7a, a_{lipid} and $a_{\text{palmitate}}$ can be determined from the y-intercept and slope, respectively. This analysis resulted in an average area per lipid and area per palmitate of approximately 0.576 and 0.071 nm^2, respectively. Result for mixed 1:1 POPC/POPE systems is in the range of the experimental area per lipid for pure POPC ($\sim$0.64 nm^2) and POPE ($\sim$0.56 nm^2) bilayers at 300 K [76, 323].

To further investigate the global effect of palmitate inside the membrane, a 2-D Voronoi tessellation analysis [324] was conducted on the equilibrium bilayer structure for

systems containing palmitate (Systems 1, 5-8 in Table 7.2.1). For the analysis considered, the Voronoi plane was defined by the position of carbonyl carbon atoms of the lipid and palmitate molecules, as these were located at about the same depth in the bilayer. The result of a Voronoi tessellation analysis is a plot representing the spatial distribution of the molecules in the bilayer (see Figure 7.4.6 for the actual plots). In particular, the Voronoi plots show a random and disordered arrangement of the lipids and palmitate in the bilayer. Another useful property obtained from Voronoi plots is the area occupied by the lipid and palmitate molecules (calculated from the area of the polygons), as shown in Figures 7.4.7b and c, respectively. As shown in the figure, the area per lipid decreases with increasing palmitate concentration, whereas the area per palmitate remains constant, within statistical uncertainty. This demonstrates that palmitate, a fatty acid molecule with a long hydrocarbon tail, is laterally incompressible within the bilayer and its presence in the bilayer decreases the void space between the lipid molecules, and consequently decreases the average area per lipid. These observations are consistent with the reduced membrane fluidity (see Figure 7.3.4) caused by the ordering induced by palmitate in the bilayer. Note that the average areas obtained from the Voronoi analysis differ from those based on the Edholm and Nagle method (Figure 7.4.7a), with exception of the pure bilayer where the estimate area per lipid are $\sim$0.576 and $\sim$0.572 nm^2, respectively. Based on this analysis, it is believed that the Voronoi tessellation analysis provides a more reliable estimate of the areas because it accounts for structural changes of the molecules in the bilayer and it links the structure from the simulations to the DSC measurements.

To investigate the local effect of palmitate embedded in the membranes, the lateral expansion of the bilayers is constrained (see Section 7.2). This is intended to mimic the local accumulation of palmitate in the bilayer. Figure 7.4.8 demonstrates a significant change in bilayer structure after 44 mole% of palmitate is embedded into the bilayer. Unlike the global effect of palmitate embedded into the bilayer shown in Figure 7.4.8b, straight lipid tails with tilted arrangements are observed at higher palmitate concentrations (Figure 7.4.8c). This is related to the ordered lipid phase, which has been shown to be detrimental to cells by limiting
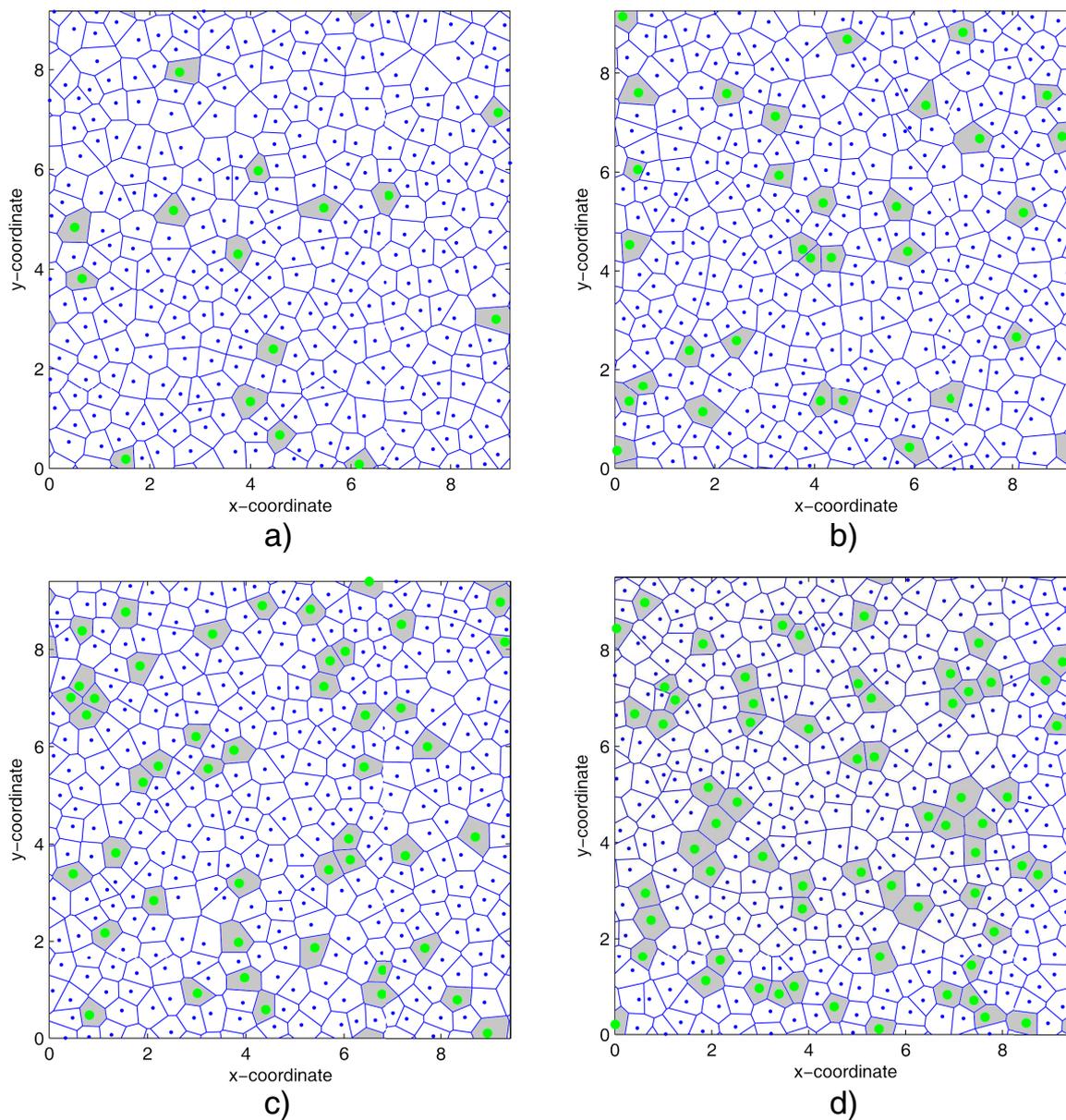
Figure 7.4.6: 2-D Voronoi tessellation for bilayers embedded with various concentrations of palmitate. Shaded (gray) and un-shaded polygons correspond to the area occupied by palmitate and the lipid tails, respectively.
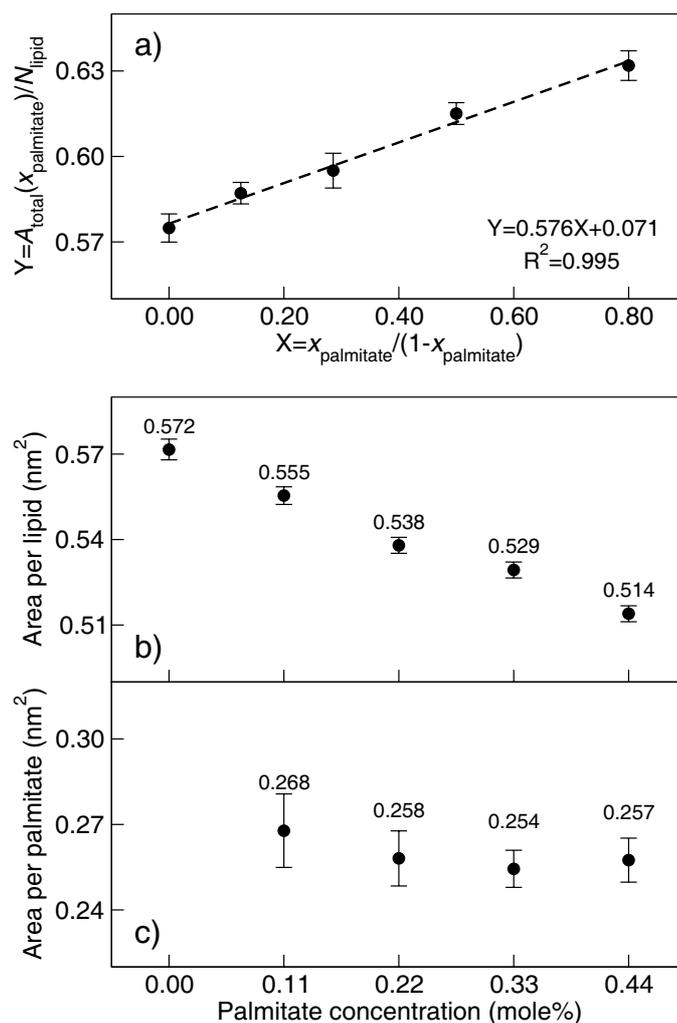
Figure 7.4.7: a) Average area per leaflet and palmitate concentration. Dashed line is a linear regression of the data (fitted equation and correlation coefficient are shown). Error bars are estimated standard deviation of the trajectories collected over 50 ns. Plots b) and c) show the average area per lipid and palmitate obtained from Voronoi tessellation analysis for the corresponding lipid bilayers containing palmitate. Error bars are estimated standard error of the mean area of Voronoi polygons.

a) Normal bilayer   b) Membrane swelling   c) Lipid order phase
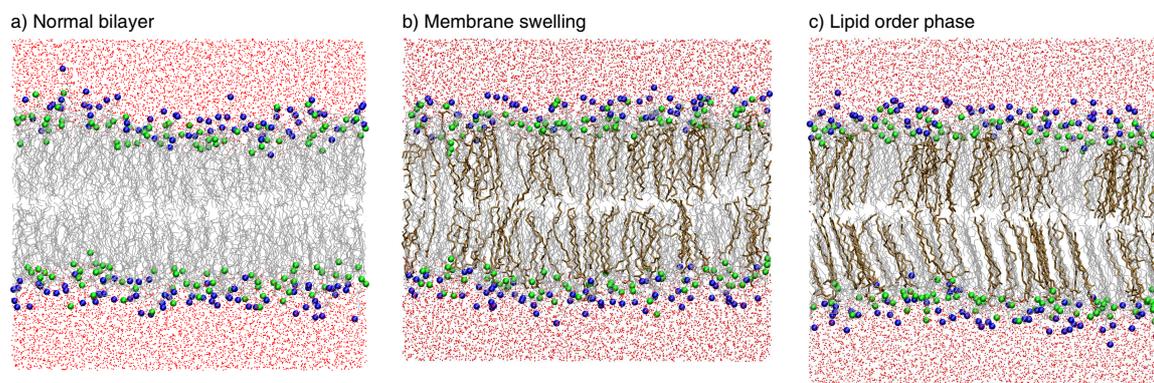
Figure 7.4.8: Snapshots of bilayer structures with (44 mole%) and without palmitate. a) No palmitate is embedded in the bilayer. b) The bilayer is allowed to expand as more palmitate molecules are embedded in the bilayer. c) The bilayer is constrained in the lateral directions as more palmitate molecules are embedded in the bilayer. Colored molecules are POPC headgroup (blue), POPE headgroup (green), lipid tails (silver), water (red), and palmitate (brown). Compositions are described in Table 7.2.1.

their transport activities [153, 154], binding sites for pathogens and toxins [41–43], and possibly the cause of palmitate induced toxicity. As the palmitate concentration decreases, the arrangement of the lipid tails becomes more random as observed in Figure 7.4.8a, thus restoring the bilayer to its normal structure.

According to results shown in Figure 7.4.7, it is implied that each palmitate molecule occupies a specific volume within the bilayer. This suggests that the structure of the lipid tails in the vicinity of the palmitate molecules can be significantly altered. Figure 7.4.9 shows the lipid tail order parameter for Systems 5-8. As seen in the figure, there is an increase in the order parameter of the lipid tails as the palmitate concentration increases. One reason for this behavior is the additional volume occupied by the palmitate molecules, forcing the surrounding lipid molecules to become highly packed, resulting in a more ordered structure. Mechanistically, the area per headgroup remains relatively the same despite the palmitate concentration, however, the area per lipid chain reduces significantly because palmitate occupies the void spaces that exist between the lipid chains. Since the lipid chains become more ordered (gel state) at the current state, it would require a higher temperature to transform
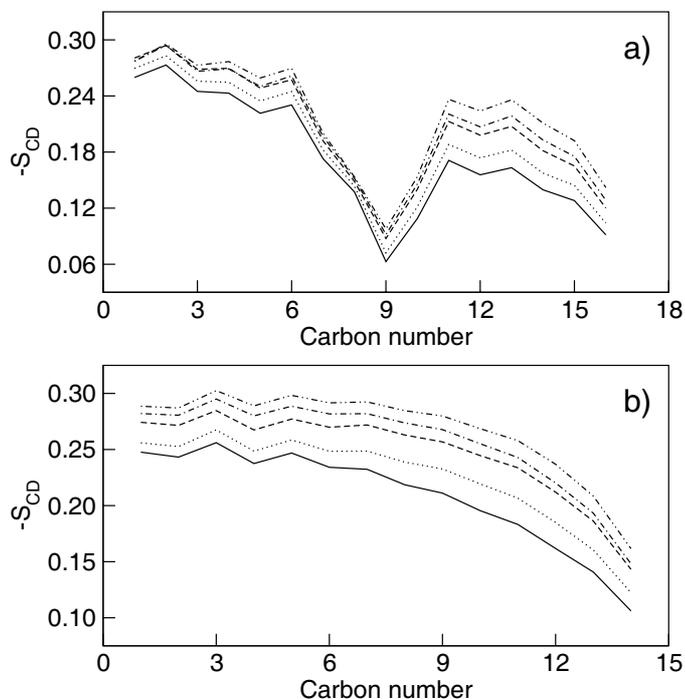
Figure 7.4.9: Deuterium order parameter for a) monounsaturated and b) saturated tails of POPC and POPE at 310 K. Lines correspond to: System 1 (solid), System 5 (dot), System 6 (dash), System 7 (dot-dash), and System 8 (dot-dot-dash) – see Table 7.2.1.

them into a more disorder state (liquid-crystalline state). Therefore, these results demonstrated that the presence of palmitate increases the phase transition temperature of mixed 1:1 POPC/POPE bilayers.

Because the palmitate molecules are embedded in the bilayer at random, it was difficult to quantify the local order parameter near each palmitate molecule, and as such, an average order parameter for the entire leaflet is reported. Note that the aggregation of palmitate within the bilayer cannot be captured within the time scale considered. However, the results do demonstrate swelling of the bilayers (see Figure 7.4.8b), which may eventually cause the bilayer structure to rupture or fuse with other cells, as reported by several experimental studies [314–316]. Figure 7.4.8 shows the changes to the bilayer structure caused by the addition of palmitate for the cases where the bilayer freely expands and remains constrained as palmitate is embedded in the bilayer (all bilayers contain the same number

of palmitate in each leaflet – condition needed to prevent distortion of the simulation box). As seen from the structures, the increase in the ordering of the lipid tails is related to the mixing of lipid and fatty acid components, where the straight chain fatty acid exhibits higher order parameters. Since the ordering of the lipid tails is directly related to the phase transition, the simulation results agree well with the DSC measurements for DOPC liposomes containing palmitate, EPR measurements of HepG2 cells exposed to palmitate (see previous section), and other related experiments [319, 320], all of which showed an increase in the phase transition temperature with increasing palmitate concentration. In comparison to the effect of cholesterol on membranes, another predominant component in animal cells, simulation results from the local and global effects of palmitate embedded within the membranes agree well with previous simulations of fully hydrated bilayers containing cholesterol, where increasing ordering of the lipids in the membrane is observed [325–328].

7.5   Discussion

FFAs are known to play important roles in the development of many hepatic disorders. A number of studies have shown that elevated levels of fatty acids are important mediators of lipotoxicity and can impair cellular functions and/or cause cell death [329]. Others have found that the negative effect of FFA induced toxicity may be reduced or alleviated by the addition of unsaturated fatty acids, antioxidants, or, as of more recently, disaccharides. To evaluate whether palmitate-induced toxicity can be reduced by adding trehalose, HepG2 cells were exposed to palmitate alone or a combination of trehalose and palmitate. As demonstrated from the experiment (Figures 7.3.1 and 7.3.2), cells exposed to palmitate resulted in a significant amount of LDH and H_2O_2 released into the medium, indicating cell death or compromised cellular membrane. With increasing trehalose concentration, reduced amount of LDH released is observed in the presence of palmitate, up to about 13 mM, an optimal concentration for HepG2 cells. Furthermore, a significant reduction in H_2O_2 released is observed for these cells. To provide insight into the biochemical and biophysical

processes altered by the presence of palmitate in HepG2 cells and to interpret these results from a molecular level, the effect of palmitate and trehalose on model cell membranes (lipid bilayers) was studied using molecular dynamic simulations.

Based on the results obtained from the simulations, a potential mechanism by which palmitate incorporates into the bilayer and the binding of trehalose to palmitate through hydrogen bonding may prevent palmitate from reaching the cell membrane and being taken up. The incorporation process of palmitate into the bilayer may be similar to that in the detergent effect, where FFAs solubilize membrane components and create holes in the membrane. However, because the simulations are limited to nanosecond time scale and the solubilization of the membrane in the detergent effect process may occur in microseconds to seconds, it is difficult to determine at present time whether the detergent effect is actually the mechanism governing the toxicity by palmitate. Based on the results obtained from previous studies, trehalose has been shown to bind preferentially to the bilayer surface [148, 149, 227, 228]. This suggests that the hydrogen bonding between trehalose (up to a certain concentration) and the phospholipid components may prevent the formation of pores, thus preserving the normal membrane function and structure.

Modification of the membrane lipid composition may alter the membrane fluidity and in turn affect cellular function [233, 234]. As palmitate molecules are embedded within the membrane, it is observed from the EPR measurements that the membrane fluidity is significantly decreased, especially in the bilayer core region (see Figure 7.3.3a). This phenomenon can be explained by many factors. First, palmitate is hydrophobic in nature and by exposing it to cell membranes, palmitate is most likely dissolving into the membrane, thus reducing the membrane fluidity. Second, as palmitate can be metabolized into phospholipid components of cell membranes, these additional components can cause an increase in the packing between the lipids, consequently decreasing the membrane fluidity [233, 234]. Last, since H_2O_2 and $^*OH$ are present in cultured cells exposed to palmitate, it has been reported that unsaturated phospholipids are oxidized into fragment of saturated hydrocarbons with various headgroup functionalities, some of which are highly toxic to cells [330–333]. Although,

the oxidation of unsaturated lipids generally results in an increase in fluidity and permeability of the membrane [334–337], the remaining fragments inside the membrane, which are hydrophobic in nature, can reduce the membrane fluidity. In this study, it was found that palmitate decreased the cellular membrane fluidity of HepG2 cells. In support, a previous study found that palmitate enrichment in HepG2 cells results in decreased membrane fluidity, as demonstrated by higher fluorescence polarization of 1,6-diphenyl-1,3,5-hexatriene (DPH) [27]. This was expected, since others have shown that fatty acids incorporated into the membrane disrupted the bilayer structure and changed the lipid phase transition temperature [319, 320]. Similar results were observed: increasing the concentration of palmitate increases the phase transition temperature of DOPC.

7.6   Summary

Understanding the mechanism of saturated fatty acid-induced hepatocyte toxicity may provide insight into cures for diseases such as obesity-associated cirrhosis. Trehalose, a nonreducing disaccharide shown to protect proteins and cellular membranes from inactivation or denaturation caused by different stress conditions, also protects hepatocytes from palmitate induced toxicity. Results suggest that trehalose serves as a free radical scavenger and alleviates damage from hydrogen peroxide secreted by the compromised cells. Also, trehalose was observed to protect HepG2 cells by interacting with the plasma membrane to counteract the changes in membrane fluidity induced by palmitate. The experimental results are supported by molecular dynamics simulations of model cell membranes that closely reflect the experimental conditions. Simulations were performed to understand the specific interactions between lipid bilayers, palmitate, and trehalose. The simulations results reveal the early stages of how palmitate induces biophysical changes to the cellular membrane and the role of trehalose in protecting the membrane structure.

Chapter 8

Understanding the Effect of Fatty Acids on Biological Membranes

In addition to Chapter 7, this chapter provides another set of experimental and computational studies investigating the influence of unsaturated fatty acids on HepG2 cells. This study also resulted from a collaborative effort with Professor Christina Chan in the Department of Chemical Engineering and Material Sciences at Michigan State University. All experimental materials, methods, and results presented in this chapter were provided by Professor Chan and her graduate student, Yifei Wu. All the modeling studies were conducted and analyzed myself. The computational modeling is a vital part of the project to interpret and understand the concurrent experimental results, providing knowledge at the molecular level and a link from the molecular interactions to the role of oleate and linoleate in reducing the toxicity of HepG2 cells. Knowledge gained from comparative study among different types of fatty acids is essential for better understanding the mechanism for fatty acid induced toxicity on HepG2 cells.

8.1 Experimental Materials and Methods

8.1.1 Cell Culture

Human hepatocellular carcinoma cell line, HepG2 (American Type Culture Collection, Manassas, VA), was cultured in Dulbecco's modified Eagle's medium (DMEM, Invitrogen, Carlsbad, CA) containing 10% fetal bovine serum (FBS, American Type Culture Collection) and 2% penicillin-streptomycin (Invitrogen). They were seeded in 6-well plates and incubated at 37 °C in humidified atmosphere containing 10% CO_2. After cells reached confluence, the media were replaced with 2 mL control medium (4% fatty-acid free BSA - bovine serum albumin) or FFAs (0.7 mM palmitate, oleate, or linoleate with 4% BSA) and changed every 24 hrs. The BSA level used was close to physiological conditions [305]. 0.7 mM FFAs was employed in this study because the plasma FFA levels in the obese and type 2 diabetic patients have been reported to be approximately this level [306–309]. Experiments were conducted after 48 hrs of treatment.

8.1.2 Cytotoxicity Assay and Membrane Fluidity

Experimental protocols for cytotoxicity assay and membrane fluidity measurements are described in details in Sections 7.1.2-7.1.3. In short, cell viability was assessed by lactate dehydrogenase (LDH) leakage through the membrane into the medium and the changes in membrane fluidity were measured using two different stearic acid derivatives, 5-*n*-doxylstearic acid (5-*n*-SASL) and 16-*n*-doxylstearic acid (16-*n*-SASL) (Invitrogen). The 5-*n*-SASL probe monitors the portion of the membrane closest to the lipid headgroups, while the 16-*n*-SASL reflects changes in the middle/end of the lipid hydrocarbon chains.

8.1.3   Liposome Preparation and DSC Measurement

To correlate the fluidity measurements to computational studies, a simpler model cell membrane also was used. Liposomes (multi-lamellar vesicles or MLVs) made of DOPC (Avanti Polar Lipids, Alabaster, Al) and palmitic (palmitate), oleic (oleate), or linoleic (linoleate) acid (Sigma-Aldrich, St. Louis, MO) were prepared by the thin film method according to the protocol from Avanti Polar Lipids (see Section 7.1.4 for more details). Differential scanning calorimetry (DSC) analysis were performed on the liposome samples at a scan rate of 1°C /min to determine the phase transition temperature.

8.2   Simulation Details

MD simulations were performed to investigate the role of unsaturated FAs (oleate and linoleate) in the structure and integrity of lipid bilayers in comparison to pure lipid bilayer and bilayers containing saturated FAs (palmitate). The lipid bilayers used in this study were composed of DOPC with a total of 200 lipid molecules (100 per leaflet). This model bilayer was chosen for these studies because it gives an approximate representation of the phospholipid constituents in HepG2 cells [27]. Note that other major lipid constituents (e.g., cholesterol) were not included in these simplified model bilayers. Several concentrations of palmitate, oleate, and linoleate were introduced into the lipid bilayer systems (see Table 8.2.1 for the actual compositions). The structure of molecules considered in this study are shown in Figure 8.2.1.

To avoid aggregation of FFAs in the aqueous phase, the bilayer structures were initially constructed to have various concentrations of FAs embedded into the bilayer prior to equilibration (Systems 2-13 in Table 8.2.1). Simulations of these systems were used to address the overall changes in the membrane structure in the presence of FAs.

The force-fields for DOPC and water are consistent with those employed in previous

Table 8.2.1: Compositions of fatty acids in the lipid bilayers. All bilayers contain 200 DOPC (100 per leaflet) at a hydration of 40 waters per lipid. Each bilayer was constructed to have equal number of fatty acids per leaflet. Number of fatty acids per system: e.g., 10 palmitate in System 2, 10 oleate in System 3, etc. FA concentrations (mole%) are shown in the last column.

System	Palmitate	Oleate	Linoleate	Concentration
1	0	0	0	0
2-4	10	10	10	5
5-7	22	22	22	11
8-10	36	36	36	18
11-13	50	50	50	25
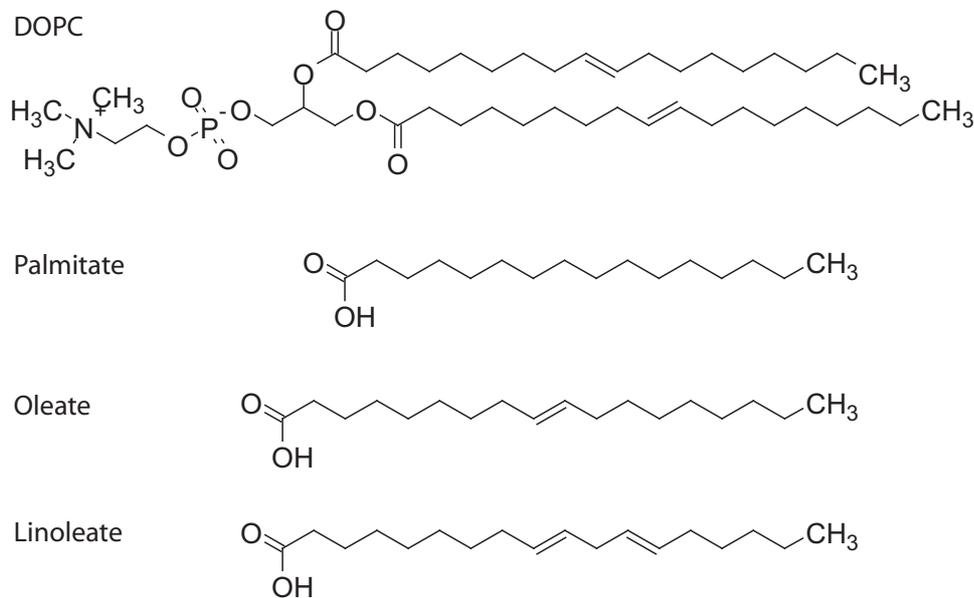
Figure 8.2.1: Molecular structure of DOPC, palmitate, oleate, and linoleate. Note that, although not shown in the drawings, all the double bonds have *cis* configuration. Chemical symbols are carbon (C), hydrogen (H), nitrogen (N), oxygen (O), and phosphorus (P).

studies, which include intramolecular parameters for bonds, angles, proper dihedral, and improper dihedral [268, 296]. The Ryckaert-Bellemans potential was used for the torsion potential of the lipid hydrocarbon chains [271] with modification of lipid tail force-field for the double-bonds [338, 339]. Non-bonded interactions were described by the parameters from Berger *et al.* [104, 110, 272] and partial atomic charges were obtained from Chiu *et al.* [96]. All FAs were modeled in the protonated state and described using parameters derived from the lipid force-field. The carboxylic acid group was based on the parameters of glutamic acid, which were available from the Gromos force-field [293]. The single point charge (SPC) model was adopted for water [273]. The united-atom representation was used for the methyl/methylene groups in the acyl chains of DOPC, palmitate, oleate, and linoleate.

All simulations were performed in the NPT ensemble, at a pressure of 1 bar and at a temperature of 310 K (see Section 7.2 for more details on the parameters used in the simulations). A time-step of 3 fs was used for all simulations with the total simulation times of 105 ns. Note that the results obtained using a 3 fs timestep provided stable bilayer structures comparable to those simulated with a 2 fs timestep (the total energy for both cases were statistically identical). Simulations of DPPC bilayers with timesteps up to 5 fs have been reported [294]. Coulombic and van der Waals cutoff interactions were at 1.0 nm. Long-range electrostatic interactions were corrected with the particle-mesh Ewald method (PME) [108, 263] (0.12 nm for the grid size, fourth-order spline interpolation, and real-space cutoff at 1.0 nm). Periodic boundary conditions were applied in all directions. Trajectories were collected every 3 ps. All simulations were performed with the GROMACS 3.3.3 software package [258, 259, 295] (single-precision mode) in parallel using Virginia Tech's System X [281].

8.3   Experimental Results

The experimental results are divided into four sections: cytotoxicity, peroxide (H_2O_2) release, membrane fluidity, and DSC measurements. Cytotoxicity and peroxide measurements were used to determine HepG2 cell viability after exposure to palmitate, oleate, or linoleate. Membrane fluidity was measured by EPR using stearic acid probes, 5-*n*-SASL and 16-*n*-SASL embedded inside HepG2 cells. Lastly, phase transition study of DOPC liposomes containing various concentrations of palmitate, oleate, and linoleate were measured by DSC.

8.3.1   Cytotoxicity Measurements

The level of cytotoxicity was measured by the relative amount of LDH released in the medium after exposure of HepG2 cells with palmitate, oleate, or linoleate. The control consisted of HepG2 cells exposed to DMEM with 4% BSA alone. From Figure 8.3.1a, the measurements indicate that palmitate significantly increased the amount of LDH released, relative to the control. Oleate and linoleate did not induce sizable toxic effects on HepG2 cells.

8.3.2   Peroxide Measurements

Relative to the amount of LDH released, a direct correlation was found in the amount of LDH and H_2O_2 released into the medium. The amount H_2O_2 released after 24 hrs of exposure of HepG2 cells to palmitate, oleate, or linoleate are shown in Figure 8.3.1b. The results suggest that palmitate induced cell death.

8.3.3   Membrane Fluidity Measurements

Since typical FFAs are amphiphilic in nature, the non-specific cytotoxic effect due to their hydrophobicity was investigated. For this study, the changes in cellular membrane structure
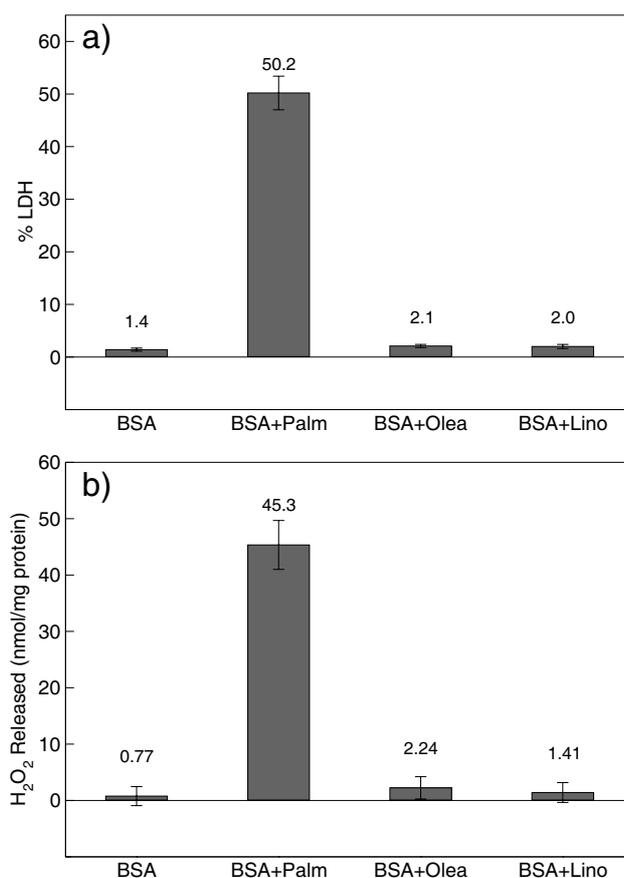
Figure 8.3.1: a) HepG2 cells cytotoxicity in response to FFAs. Confluent HepG2 cells in BSA medium were exposed to 0.7 mM palmitate (Palm), oleate (Olea), or linoleate (Lino). LDH released was measured after 48 hrs. b) Effects of FFAs on H_2O_2 release. Confluent HepG2 cells in BSA medium were treated with 0.7 mM palmitate (Palm), oleate (Olea), or linoleate (Lino) for 48 hrs. The H_2O_2 released into the medium was measured and normalized to total cellular protein. Error bars are standard deviation of three independent experiments.
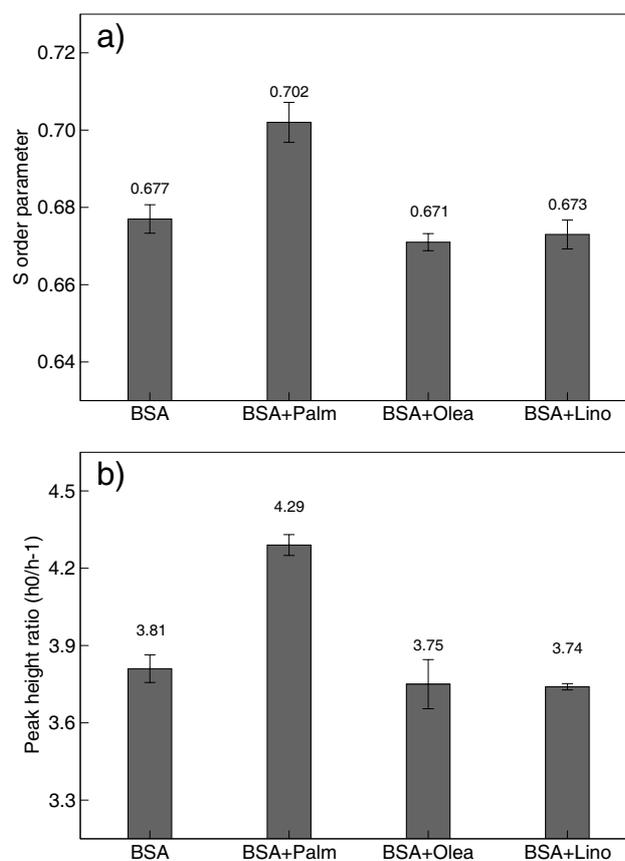
Figure 8.3.2: Effect of FFAs exposure on cellular membrane fluidity. Cells were treated with 0.7 mM palmitate (Palm), oleate (Olea), or linoleate (Lino) for 48 hrs. Cellular membrane fluidity was measured using EPR. a) Values are order parameter for 5-n-SASL labeled HepG2 cells. b) Values are peak height ratio for 16-n-SASL labeled HepG2 cells. Error bars are standard deviation of three independent experiments.

upon exposure to saturated and unsaturated FAs using EPR were investigated (see Section 7.1.3). The membrane fluidity of HepG2 cells were measured after 48 hrs of exposure to palmitate, oleate, or linoleate. The control was HepG2 cells exposed to DMEM with 4% BSA. Using both 5-n-SASL and 16-n-SASL as probes to monitor the ordering of the lipid tails near the lipid headgroups and the center of the bilayer core, an increase in the S order parameter and peak height ratio for HepG2 cells exposed to palmitate was observed, as shown in Figure 8.3.2. No significant changes are observed for HepG2 cells exposed to either oleate or linoleate, in comparison to the control. The results suggest a greater reduction of membrane fluidity due to the hydrophobic effect of saturated than unsaturated FAs.

8.3.4   DSC Measurements

To corroborate the membrane fluidity results, the phase transition temperature of DOPC liposomes was measured by DSC measurements. The phase transition temperature obtained from the DSC thermographs for DOPC liposomes with increasing mole fractions of palmitate, oleate, or linoleate are shown in Figure 8.3.3. The results demonstrate a significant increase in the phase transition temperature of the DOPC liposomes with increasing concentration of palmitate, however, slight changes are observed for DOPC liposome containing the same concentration of oleate and linoleate. This suggests that only palmitate increases the ordering of the phospholipids in the liposomes, which correlates well with the decrease in membrane fluidity measured by EPR (lower fluidity, higher phase transition temperature).
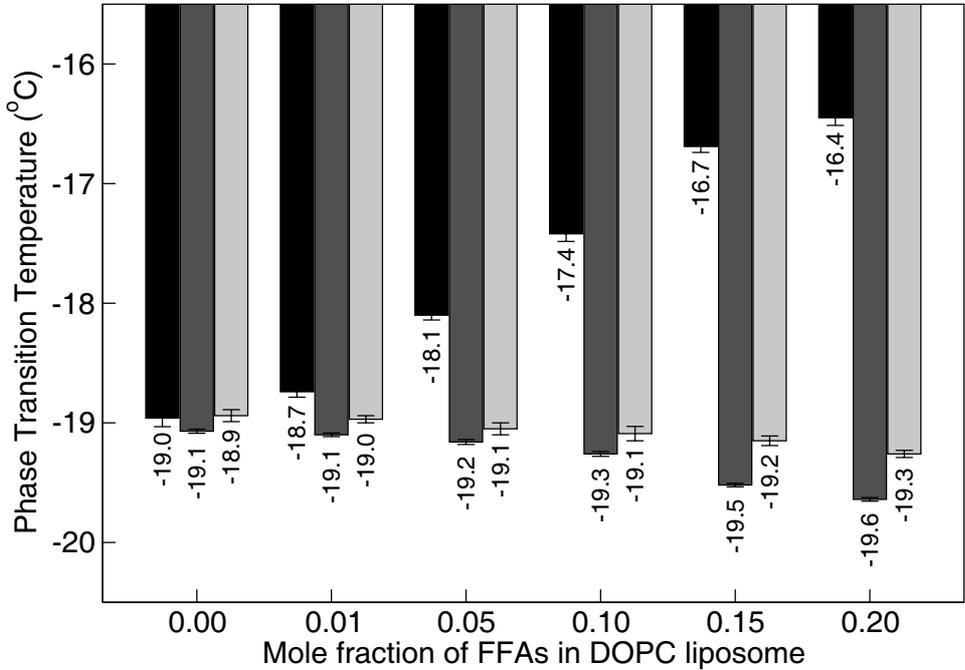
Figure 8.3.3: Phase transition temperature of DOPC liposomes with increasing concentrations of palmitate (black), oleate (grey), and linoleate (light grey). Phase transition was measured with DSC. Error bars are standard deviation of three independent experiments.

8.4 Computational Results

The focus for this part of the study was to obtain a molecular level understanding on how unsaturated FAs interact with the lipid bilayers in comparison to the effects induced by saturated FAs. Therefore, a number of quantities were analyzed to characterize the effect of unsaturated FAs (oleate and linoleate) on the properties of DOPC bilayers, including: bilayer surface area, bilayer thickness, lipid tail order parameters, area per lipid/FA, and hydrogen bonding. All results were calculated from the ensemble average over the last 60 ns of the simulations. Results for the bilayer systems without FA are also shown for comparison. Interactions of other types of lipid bilayers containing POPC and palmitate have been reported in Chapter 7 and, where appropriate, are mentioned here for comparison. The actual FA content in the bilayers is shown in Table 8.2.1. Note that the bilayers were constructed by having equal number of fatty acids on each leaflet, a condition necessary to
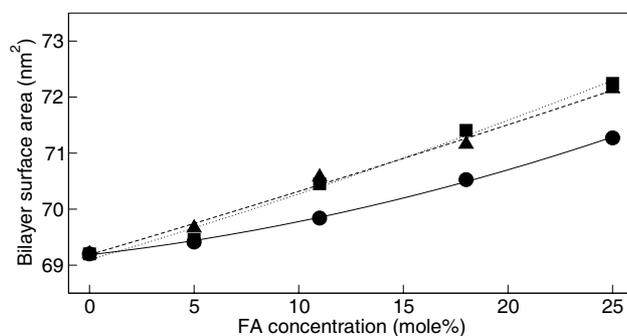
Figure 8.4.1: Surface area of the lipid bilayers containing various concentrations of palmitate (circles), oleate (squares), and linoleate (triangles). Solid, dotted, and dash lines are drawn to guide the eye, respectively. Statistical error estimates are less than the size of the symbols for all the simulations (see Table 8.4.1) and are omitted for clarity.

obtain a stable system.

8.4.1   Bilayer Surface Area

The first property analyzed was the size of the bilayer surface area (cross-sectional area of the simulation boxes). This demonstrates the global effect of FAs embedded within the bilayers (see Chapter 7). As shown in Figure 8.4.1, the bilayer surface area increases with increasing FA concentration. This is seen because each FA occupies an additional volume within the bilayer and, due to its alignment with the lipid tails, the bilayer expands in the lateral dimensions. A similar behavior was observed in previous study using POPC embedded with palmitate (see Section 7.4.3). Furthermore, the results indicate that oleate or linoleate induce a larger increase in the bilayer surface area than palmitate. This is seen because the kinked lipid tail of unsaturated FAs occupies a larger lateral surface area when packed within the bilayers compared to a straight-chain lipid tail of saturated FAs. Based on this analysis, the results also indicate that unsaturated FAs induce greater lateral expansion between lipids, possibly decreasing the packing between lipids and increasing membrane fluidity. Further analysis as follows expands on this behavior.

Table 8.4.1: Average bilayer surface area and thickness averaged over the last 60 ns of the simulations. Surface area is estimated from the x- and y-dimensions of the simulation box. Thicknesses are estimated from the DOPC density profiles shown in Figure 8.4.2.

FA (mol%)	palmitate[a]	oleate[a]	linoleate[a]	palmitate[b]	oleate[b]	linoleate[b]
0	69.20±0.03	69.20±0.03	69.20±0.03	2.85±0.04	2.85±0.04	2.85±0.04
5	69.42±0.04	69.46±0.04	69.20±0.03	2.97±0.04	2.91±0.04	2.91±0.04
11	69.84±0.04	70.45±0.04	70.57±0.04	3.04±0.04	3.06±0.04	2.99±0.04
18	70.53±0.04	71.41±0.03	71.16±0.04	3.11±0.04	3.12±0.04	3.08±0.04
25	71.27±0.04	72.24±0.04	72.15±0.04	3.17±0.04	3.16±0.04	3.18±0.04

[a]bilayer surface area (nm^2); [b]bilayer thickness (nm)

8.4.2 Bilayer Thickness

The bilayer thickness was measured to investigate the effect of FAs embedded within the bilayers. Using component density profile analysis, the bilayer thickness was approximated by estimating the distance between the two maximum peaks on the DOPC density profiles, as shown in Figure 8.4.2. Based on the actual values reported in Table 8.4.1, the bilayer thickness increases with increasing FA concentration. This is explained by the fact that DOPC tails are straightened as a result of FA embedded within the bilayers, an indication of reducing membrane fluidity (see Section 7.4.3 for similar results). For the bilayers with the same oleate and linoleate concentrations, the bilayer thickness is essentially the same. These findings are still insufficient to differentiate the properties of saturated and unsaturated FAs on the bilayers and determine how unsaturated FAs reduce membrane fluidity. Analysis of the lipid tail arrangement, as described next, may provide additional insight into these results.

8.4.3 Lipid Tails Order Parameters

As demonstrated in Section 7.4.3, the lipid tail order parameters were used to correlate the MD simulation results to the cellular experiments for the membrane fluidity. Because the FA
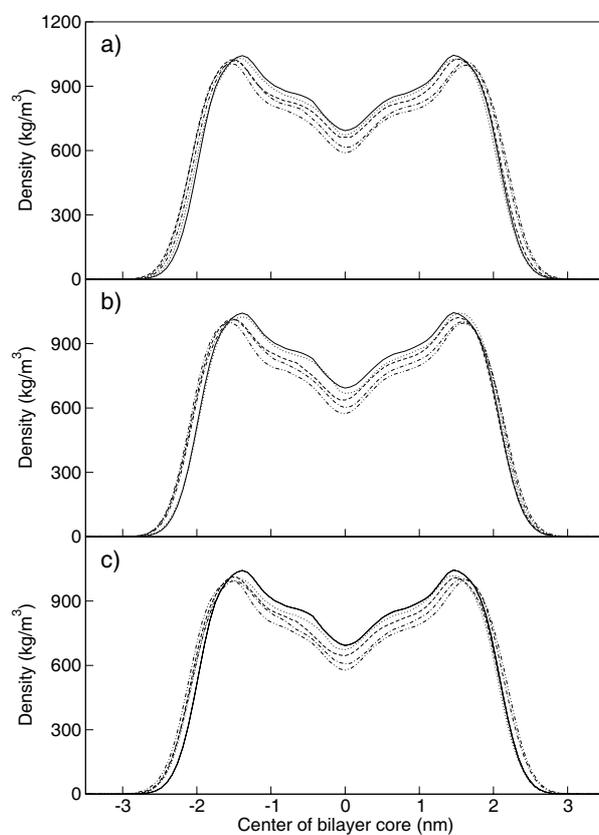
Figure 8.4.2: DOPC density profiles for lipid bilayers containing various concentrations of a) palmitate, b) oleate, and c) linoleate at 310 K. Lines correspond to FA concentrations: 0% (solid), 5% (dot), 11% (dash), 18% (dot-dash), and 25% (dot-dot-dash).

molecules are embedded in the bilayer at random, it was difficult to quantify the local order parameter near each FA molecule, and as such, an average order parameter for the entire leaflet is reported. Following the same approach, the lipid tail order parameters are calculated for all systems considered, as shown in Figure 8.4.3. As seen in the figure, there is a significant increase in the order parameters with increasing FA concentrations. One reason for this behavior is the additional volume occupied by the FA molecules, forcing the surrounding lipid molecules to become highly packed, resulting in a more ordered structure. Consequently, the bilayer thickness increases with the ordered lipid tails, as shown in Figure 8.4.2. Results from this analysis indicate that, despite the double-bonds in the oleate and linoleate chains, FA molecules generally cause an increase in the lipid tail order parameters, a condition resulting in decreasing membrane fluidity. A more discrete method is required to differential the local effect of FAs embedded within the bilayers.

8.4.4   Area per Lipid and FA

To further investigate the effect of FA inside the membrane, a 2-D Voronoi tessellation analysis [324] was conducted on the equilibrium bilayer structure with and without FAs (see Section 7.4.3 for more details). The result of a Voronoi tessellation analysis is a plot representing the spatial distribution of the molecules in the bilayer. Note that a single snapshot at the end of the simulation is used for this analysis. Using this method, the area occupied by the lipid and FA molecules (calculated from the area of the Voronoi polygons) were determined and compared, as shown in Figure 8.4.4. As shown in Figure 8.4.4a, the area per lipid decreases with increasing palmitate, oleate, or linoleate concentrations. For palmitate systems, the area per lipid decreases almost linearly with the concentrations. This behavior was observed in Chapter 7 using mixed 1:1 POPC/POPE bilayers embedded with various palmitate concentrations (see Figure 7.4.7). Unlike palmitate, the area per lipid for oleate and linoleate systems seems to decrease non-linearly and reach values greater than the palmitate system. This indicates that, depending on the type of FA embedded, the packing
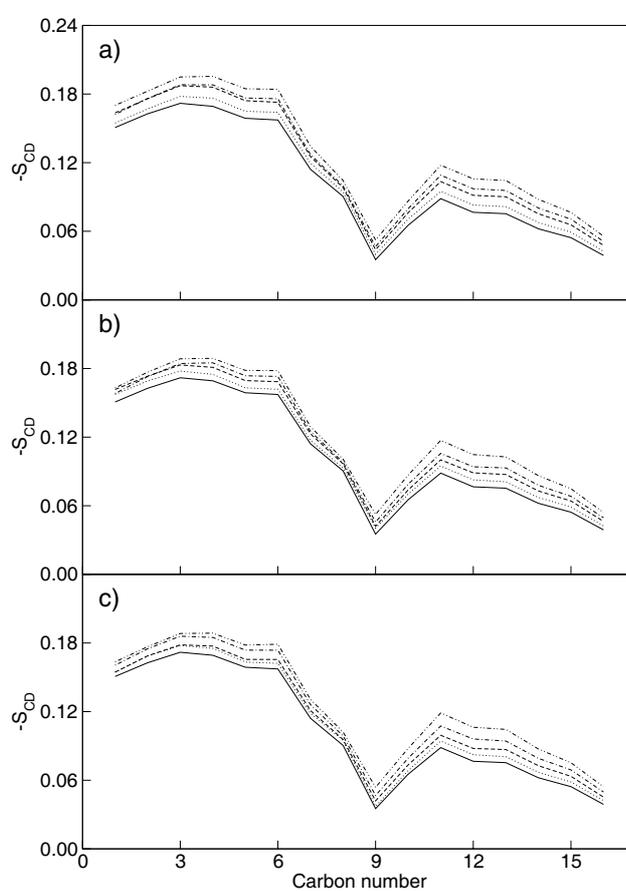
Figure 8.4.3: Deuterium order parameter for bilayer containing various concentrations of a) palmitate, b) oleate, and c) linoleate at 310 K. Lines captions are described in Figure 8.4.2.
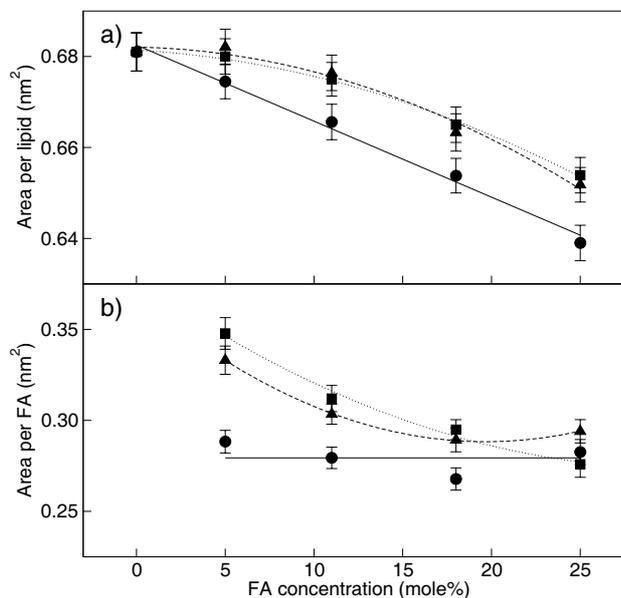
Figure 8.4.4: Average area per a) lipid and b) FA obtained from Voronoi tessellation analysis for the corresponding lipid bilayers with palmitate (circles), oleate (squares), and linoleate (triangles). Solid, dotted, and dash lines are drawn to guide the eye, respectively. Error bars are estimated standard error of the mean area of Voronoi polygons.

between lipids are more complex in the presence of unsaturated FA. Further analysis of the area per FA is required to confirm these findings.

Using the same Voronoi tessellation analysis, the area per FA was calculated, as shown in Figure 8.4.4b. From the figure, the area per palmitate remains constant (within statistical uncertainty), whereas the area per oleate and linoleate, originally starts high at 5 mole% and then decreases significantly until reaching the value obtained for palmitate. As reported in Chapter 7, the same behavior was observed for palmitate systems and concluded that the area per palmitate remains unchanged mainly because palmitate, a fatty acid molecule with a long and straight hydrocarbon tail, is laterally incompressible within the bilayer. In the case of oleate and linoleate systems, the double-bond in the lipid generally produces a large surface area as shown in the bilayer surface analysis in Figure 8.4.1. Therefore, oleate and linoleate have the ability to absorb the lateral compression between lipids by reducing its area per FA. Note that at the highest oleate concentration (25 mole%), the area per FA is

about the same, which means that oleate and linoleate may have reached a maximum lateral compression. From this analysis, the role of saturated and unsaturated FA embedded within the bilayer structure was identified.

8.4.5   Hydrogen Bonding

Additional analysis of the hydrogen bonds was performed to investigate the effect of lipid hydration with increasing FA concentrations. First, radial distribution functions (RDF) between lipid oxygen atoms and water were calculated and the hydration radius for each lipid oxygens (four oxygens in the phosphate group and four oxygens in the ester group) was found by determining the distance to the first minimum in the RDFs. Figure 8.4.5 shows the RDF plots for DOPC bilayers containing 11 mole% FAs (RDFs for the other FA compositions are not shown for the sake of brevity, but they are all similar to those in Figure 8.4.5). The values of the hydration shell for all bilayer systems are reported in Table 8.4.2. Using the hydrogen bond analysis previously described by Brady and Schmidt [285] with the first hydration shell from the RDFs, Figure 8.4.6 shows the average number of hydrogen bonds per lipid between lipid oxygen atoms and water for all systems considered. As seen in the figure, the average number of hydrogen bonds reduces significantly with increasing palmitate concentration. This is caused by the increased packing of the lipids (reduced area per FA – see Figure 8.4.4a), thus resulting in the removal of potential binding sites for water. On the other hand, the number of hydrogen bond for oleate and linoleate systems remains relatively constant regardless of the oleate or linoleate concentrations. This is related to the fact that oleate and linoleate help to maintain the spacing between the lipids, thus resulting in a suitable area per lipid and level of hydration. This analysis confirms that the role of saturated and unsaturated fatty acids are contrasting; even though unsaturated FAs can be as easily incorporated into the lipid bilayer as palmitate, their presence in the bilayer is actually beneficial, as they cause little perturbation to the bilayer structure and help to maintain the level of hydration.
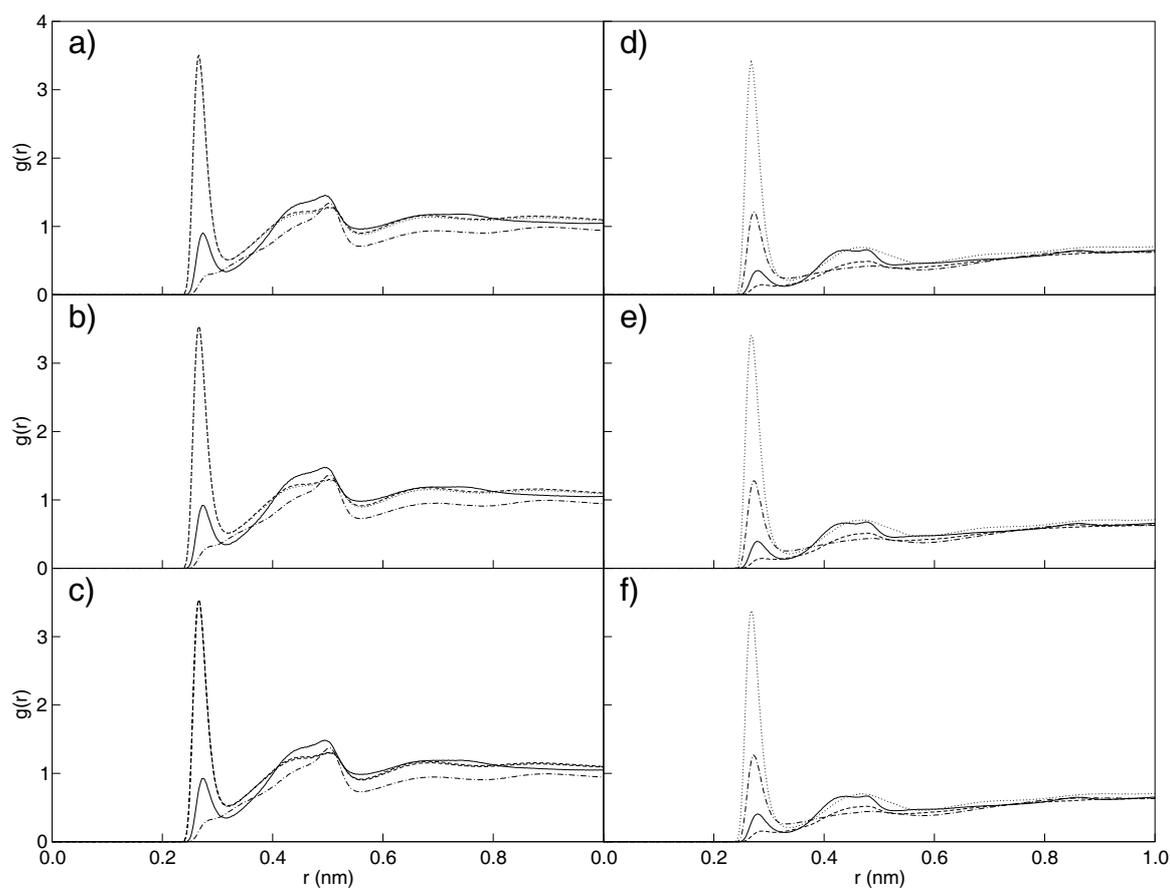
Figure 8.4.5: Radial distribution functions for lipid oxygen atoms and water for bilayers containing FAs. The plots correspond to water interacting with the phosphate group in DOPC bilayers containing 11 mole% a) palmitate, b) oleate, c) linoleate, and with the ester group in DOPC bilayers containing 11 mole% d) palmitate, e) oleate, f) linoleate. Phosphate oxygen atoms are represented as follow: O7 (solid line), O9 (dot line), O10 (dash line), and O11 (dot-dash line). Ester oxygen atoms are represented as follow: O14 (solid line), O16 (dot line), O33 (dash line), and O35 (dot-dash line).

Table 8.4.2: Hydration radius around lipid oxygen atoms. Average values are shown for various DOPC oxygen atoms. All values reported in nm.

FA mol%	O7	O9	O10	O11	O14	O16	O33	O35
0	0.316	0.322	0.322	0.558	0.330	0.338	0.308	0.334
5^a	0.316	0.318	0.318	0.560	0.330	0.340	0.316	0.332
11^a	0.314	0.320	0.320	0.560	0.328	0.336	0.312	0.334
18^a	0.312	0.322	0.318	0.558	0.326	0.336	0.314	0.330
25^a	0.316	0.320	0.320	0.558	0.330	0.338	0.308	0.334
5^b	0.316	0.320	0.320	0.560	0.326	0.339	0.312	0.336
11^b	0.314	0.320	0.318	0.560	0.328	0.338	0.310	0.332
18^b	0.316	0.320	0.320	0.556	0.332	0.338	0.312	0.334
25^b	0.316	0.320	0.320	0.560	0.330	0.336	0.308	0.330
5^c	0.314	0.320	0.318	0.560	0.328	0.336	0.308	0.332
11^c	0.316	0.318	0.320	0.560	0.332	0.338	0.310	0.328
18^c	0.314	0.320	0.318	0.560	0.328	0.338	0.310	0.332
25^c	0.318	0.320	0.320	0.560	0.330	0.338	0.312	0.334
average	0.315	0.320	0.319	0.559	0.329	0.338	0.311	0.332

[a]bilayer containing palmitate
[b]bilayer containing oleate
[c]bilayer containing linoleate
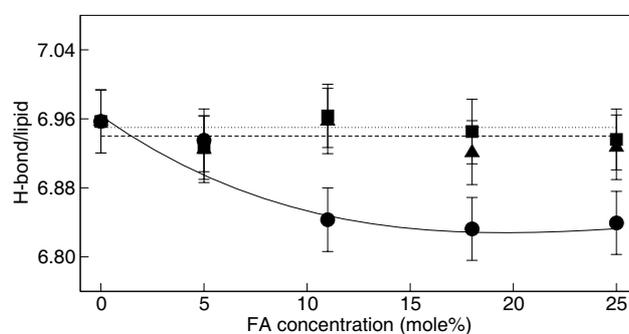
Figure 8.4.6: Average number of hydrogen bonds per lipid for bilayers with palmitate (circles), oleate (square) and linoleate (triangle); water as H-donors. Solid, dotted, and dash lines are drawn to guide the eye, respectively. Error bars represent standard deviations.

8.5   Discussion

Unlike most FFAs, palmitate has been shown to be toxic to HepG2 cells at 0.7 mM. On the other hand, unsaturated FFAs have both positive and negative effects among different types of cells. From the cytotoxicity and peroxide measurements, oleate and linoleate were harmless to HepG2 cells, while palmitate was highly toxic at the same concentration. The EPR measurements indicated that there is a significant change in membrane fluidity in the presence of palmitate, compared to oleate and linoleate systems. This change is mainly associated with the hydrophobic effect of saturated FAs, which resulted in reduced membrane fluidity. To compare the biochemical and biophysical processes associated with the change in membrane fluidity in the presence of palmitate, oleate, or linoleate at a molecular level, the effect of these FFAs on model cell membranes (DOPC lipid bilayers) using MD simulations was studied.

A number of structural properties were analyzed from a series of lipid bilayers simulations containing FAs. From the average size of bilayer surface area, oleate and linoleate significantly expanded the DOPC bilayer surface compared to palmitate. This was expected because the presence of kinked lipid tails (oleate and linoleate) slightly increase the molecular volume for each FA. As a result, the bilayer surface area increases when unsaturated FAs are packed in the bilayer. From the component density profiles, unnoticeable changes were measured for the average bilayer thickness between bilayers containing the same FA concentrations. These results imply that FAs expand the spacing between lipids but have small effect on the packing between each lipid. In confirmation, the lipid tail order parameters show an increase in the order parameters with increasing FA concentrations, however, significant differences among FAs are not observed. These results indicate a packing competition between FA and DOPC, which results in an increase in bilayer surface area and lipid tail order parameters. Based on these findings, a more detailed analysis was necessary to differentiate the properties of various FAs.

The local effect of FAs was calculated using a Voronoi tessellation analysis, which

indicated that unsaturated FAs reduce the packing between lipids. Increasing FA concentrations results in a linear decrease in the area per lipid for palmitate systems and non-linear decrease for either oleate or linoleate systems. This behavior was explained by the average area per FA that showed the area per oleate or linoleate were significantly larger than palmitate at low concentrations but decreased non-linearly to the value for palmitate at high concentration. This reduction indicates straightening of the unsaturated FA chain with increasing FA concentrations. This was not observed for palmitate because the lipid chain is incompressible due to lipid chain saturation. From this analysis, it is evident that unsaturated FAs partially help to maintain membrane fluidity by reducing the packing between lipids, whereas saturated FAs increase the packing between lipids thus reducing membrane fluidity.

Since the packing between lipids was partially unchanged for oleate and linoleate systems, it was speculated that the level of hydration of the bilayer is preserved. Extensive hydrogen bond analysis was performed for each bilayer systems and the results indicated that the number of hydrogen bonds per lipid is unchanged with increasing oleate or linoleate concentrations. Significant reduction in hydrogen bonds was observed for palmitate. These results indicated that the presence of saturated FAs increases the packing between lipids, causing water to be expelled from the vicinity of bilayer surface, an evidence of decreasing membrane fluidity. On the other hand, unsaturated FAs help to maintain the packing between lipids and preserve the level of hydration, thus unaffecting the membrane fluidity.

8.6 Summary

Understanding the effect of saturated and unsaturated fatty acids on biological membranes can provided insight into cures for diseases such as obesity-associated cirrhosis. *In vitro* experiments suggest that unsaturated fatty acids, such as oleate and linoleate, are less toxic and potentially protect hepatocytes from palmitate induced toxicity. Computational results

indicated that the unsaturated fatty acid chain serves as a membrane stabilizer to counteract changes in the membrane fluidity. Unsaturated fatty acids have structural properties that can reduce the lateral compressibility of the lipid component in the membrane. Hydrogen bond analysis indicates a uniform level of membrane hydration in the presence of oleate and linoleate compared to palmitate, which revealed a possible mechanism of how unsaturated fatty acids reduce biophysical changes to the cellular membrane and protect the membrane structure.

Chapter 9

Summary and Future Work

9.1 Summary for Chapter 4

9.1.1 Mixed DPPC/DPPE Bilayers

A systematic simulation study of mixed lipid bilayers containing DPPC and DPPE is presented in this dissertation. For pure DPPC bilayers, the calculated area per lipid and the lipid order parameter agree well with previous experimental and simulation results. Selected experimental results (i.e., area per lipid and lipid order parameter) for pure DPPE are available for comparison, however, no simulations results have been reported. To be consistent with other derivatives of PE bilayer simulations, an appropriate force-field for DPPE molecules was created by modifying the DPPC force-field using the POPE force-field as the basis to replace the choline to the amine headgroup. The results show small discrepancies between the simulation and experimental values in the area per lipid and order parameter for the pure DPPE and mixed 1:1 DPPC/DPPE systems.

DPPE exhibits unique and distinct characteristics, in particular its ability to strongly interact with itself and neighboring lipids through inter and intramolecular hydrogen bonds.

Increasing DPPE content in the bilayer results in a significant decrease in the area per lipid and higher deuterium order parameters (lipid tails become more aligned within the bilayer normal). Detailed analysis of the density profile for the nitrogen and phosphorus atoms in the lipids shows that the amine groups in DPPE prefer to hydrogen bond with lipid oxygens. In this process, the P-N vector of the DPPE headgroup is most often found pointing toward the bilayer core, whereas the P-N vector for DPPC points toward the aqueous phase. The average intramolecular tilt angle, with respect to the bilayer normal, of the P-N vector for both DPPC and DPPE decreases with increasing DPPE concentration. For DPPC, the choline group becomes more aligned with the bilayer normal due to the close packing of the lipids (smaller area per lipid). On the other hand, for DPPE, there are more H-donors from NH_3^+ groups than available H-acceptors from lipid oxygen atoms, thus resulting in a competition between lipid oxygen atoms and water for hydrogen bonds. An increase in the number of hydrogen bonds between the NH_3^+ group and water coupled with a decrease in inter/intramolecular hydrogen bonds between the lipids as the DPPE concentration increases are the main cause for the reduction in the average P-N vector tilt angle.

From the trajectory analysis, the majority of the DPPE molecules rapidly move around the membrane surface, but they become more restricted with increasing DPPE concentrations. The high mobility of DPPE from their original position suggests that there are strong interactions causing the molecules to diffuse laterally through the bilayer. Based on the hydrogen bonding analysis, intermolecular hydrogen bonds between lipids facilitate their diffusion. On the other hand, less movement suggests that the hydrogen bond competition between the amine groups in DPPE and water at the interface reduces the interactions between lipids, resulting in a more localized displacement of DPPE. The random diffusion of DPPE molecules along the membrane leaflet does not indicate any aggregation of lipids within the simulation time considered.

9.1.2   Interactions of Trehalose with Lipid Bilayers

A systematic simulation study of pure and mixed lipid bilayers of DPPC and DPPE with trehalose is also presented in this dissertation. Results indicate that the area per lipid remains relatively constant for the bilayer systems at 350 K. Total density profiles of all bilayers remain relatively unchanged by the presence of trehalose. Preferential binding of trehalose with the lipid systems containing DPPE is observed from the trehalose density profiles where the distributions of trehalose are uneven with a slight concentration of trehalose near one interface of the membrane. From the density profiles, trehalose superficially interacts with the bilayer interface and favorably hydrogen bonds to the phosphate and ester headgroups. Trehalose is unable to penetrate through the interface to the bilayer core, and as a result, the effect of trehalose on the lipid tails is minimal.

With increasing DPPE concentration, the total number of hydrogen bonds from the amine group of DPPE remains unaffected by trehalose as the contribution of hydrogen bonds shifts from lipids (intermolecular and intramolecular hydrogen bond) to water and trehalose. A large increase in the binding of trehalose is observed in the lipid systems with higher DPPE concentration. Trehalose can only bind to the amine groups that are exposed to the aqueous phase. The amine group in DPPE preferentially binds to phosphate and ester oxygen atoms through intra or intermolecular hydrogen bonds. Because there are more H-donors than available H-acceptors as the DPPE concentration increases, the excess H-donors create a competitive hydrogen bonding environment that weaken lipid-lipid interactions and simultaneously allow amine groups to become more hydrated. This provides a more favorable condition for trehalose to bind to the lipids.

A hydrogen bond analysis between the hydroxyl groups of trehalose and lipid oxygen atoms shows that the largest number of hydrogen bond contacts in the pure DPPE bilayer, whereas the pure DPPC bilayer shows the least amount of hydrogen bond contacts. The diffusion coefficient of trehalose calculated from the mean-squared displacement supports this argument, being the highest in the pure DPPE bilayer (the preferential exchange of

hydrogen bonds between lipids and trehalose only occur near the interface). In addition, due to the competitive hydrogen bonding environment of the amine groups in the pure DPPE bilayer, intermolecular and intramolecular hydrogen bonds between lipids are weakened, creating more suitable conditions for trehalose (hydroxyl groups) to bind to lipid oxygen atoms. However, the same conditions are not true in the mixed 1:1 DPPC/DPPE system. From a different standpoint, the strong interaction of DPPE with neighboring lipids also helps to maintain the membrane integrity, creating a self-preserving mechanism under low hydration conditions. This may help to explain the high survival rate of bacteria (contains as much as about 70-80% PE in *E. Coli* [8]) under harsh conditions.

From the trajectory analysis, trehalose is free to diffuse in the aqueous phase and occasionally binds to the bilayer, with multiple lipid-trehalose interaction sites often involved. The binding of trehalose to the bilayer discredits the preferential exclusion model as a major mechanism by which trehalose stabilizes cells. All bilayer systems considered here are fully hydrated which is a condition that may reduce the effectiveness or change the biological properties of trehalose compared to a drier state. The interactions between trehalose and the bilayer are apparent from the hydrogen bond analysis and the dynamic trajectories, and these evidences support the preferential interaction model, even at low trehalose concentrations.

9.2   Summary for Chapter 5

9.2.1   Dehydrated Lipid Bilayers with Sugars

Many saccharide compounds have been successfully identified for their ability to preserve liposomes under dehydrated conditions. By analyzing the phase behavior of liposomes in the presence of these saccharides, experimental studies have shown correlations on their effectiveness based on the number of glucose-rings, phase transition temperature, and membrane fluidity. Although the efficacy of saccharides in stabilization is well-known, a clear

description of the interaction mechanisms remains unsettled, evident from the hypotheses at present. Therefore, this study aimed at providing further insight into the interactions of lipid bilayers with and without glucose and trehalose under dehydrated conditions by ways of MD simulations.

Two bilayer setups were proposed in Chapter 5. The first bilayer setup aimed at verifying the mechanism of preservation proposed by Crowe *et al.* [159], in which saccharide molecules intercalate in between the lipid headgroups, thus preventing lipid aggregation and maintaining the membrane fluidity. In these simulations, the lateral dimensions of the simulation box were constrained and dehydrated conditions were set at water/lipid ratio of 20. Analysis of the simulations showed that the bilayer structures were preserved at 310 K, with and without saccharides. Due to the loosely packing of lipids in this bilayer setup, lipid tail interdigitation was significant at 290 and 300 K, even in the presence of saccharides. One reason for the observed results was the periodic boundary conditions used in the simulations, which allowed self-interactions of the lipids with the periodic images. Analysis of the bilayer structures indicated the distinct formation of ordered domains: long narrow domains in the bilayers without saccharides, multiple small domains in the bilayers with glucose, and single large domains in the bilayers with trehalose. Although these simulations did not demonstrate the stabilizing effect of saccharides on the bilayers, they provided an understanding on distinguishing properties between glucose and trehalose on the bilayers.

In the other bilayer setup at dehydrated conditions, an inert gas layer was introduced so a truly uni-lamellar bilayer was represented. The lateral dimensions of the simulation box were also constrained in these simulations, but a lower water/lipid ratio of 10 was used. For these bilayers without saccharides, the bilayer structures were completely disintegrated at the temperature considered. On the other hand, bilayer structures containing either glucose or trehalose remained stable for the duration of the simulations. Hydrogen bond analysis showed that the saccharide molecules displaced a significant amount of water surrounding the lipid headgroups. However, the additional hydrogen bonds formed between water and

saccharides helped to maintain the hydration layer for the lipid bilayers. Based on these findings, our results support both the "water-replacement" and "water-entrapment" hypotheses. Furthermore, trehalose showed more affinity (more hydrogen bonds) for the lipids in the bilayer than glucose, resulting in part because trehalose has fewer interactions with neighboring saccharide molecules. These results suggested a better preferential binding of trehalose to the lipid bilayer than glucose, thus demonstrating that trehalose is a better stabilizing agent.

9.3 Summary for Chapter 6

9.3.1 Phase Transition for DPPC and DPPE Bilayers

Ordered and disordered lipid domains co-exist within biological membrane for many reasons. These domains are structural components that are associated with several biological processes, such as, signal transduction, protein transport, membrane sorting, and membrane binding site. Recently, the study of phase behavior of lipid bilayers has become more apparent with computational methods, especially through the development of coarse-grained models. Coarse-grained models partially overcome system size and simulation time limitations that are often associated with atomistic simulations, and as such, they are attractive to study phase separation and domain formation. While coarse-grained models are computationally efficient, they lack the detail to describe important features and characteristics of lipid bilayer at the atomistic scale that contribute to the overall properties of lipid bilayers. This preliminary report addresses that missing gap with a comprehensive evaluation of lipid bilayers properties, in particular pertaining to their phase behavior.

MD simulations were performed to investigate the structural properties of DPPC and DPPE bilayers, two of the most abundant lipid components found in living organisms. Lipid bilayers containing 128 lipids (64 per leaflet) were considered. Even though these bilayers are much smaller than coarse-grained model studies, it is demonstrated that they are sufficient

to yield a wealth of structural information on the bilayers and insight into the mechanism of phase transition from a gel ("ordered") to a liquid-crystalline ("disordered") state. Two sets of simulations were carried out: annealing simulations with continuous heating and cooling, and fixed temperature. The annealing simulations provided a first measure of the structural changes of the bilayers by tracing the hysteresis loop from an ordered to a disordered state. The area per lipid and bilayer thickness were used to obtain an estimate of the first-order phase transition temperature, which was identified at about 305 K and 320 K for DPPC and DPPE bilayers, respectively, compared to the experimental values of 315 K for DPPC and 337 K for DPPE.

In the second set of simulations at fixed temperatures, equilibrium properties were calculated for temperatures above and below the estimated T_{m} from the annealing simulations. The area per lipid and bilayer thickness measured from the fixed temperature runs were in consistent agreement to those observed in the annealing simulations, with values within the bounds of the hysteresis loop. The resulting equilibrium structure for DPPC below T_{m} showed "mixed" domains, which consists of lipids that are tilted in the "ordered" domain and partially overlapped in the "disordered" domain. Near T_{m}, a cooperative transformation of the bilayer structure is observed. First, the average area per lipid slightly increases with increasing temperature, followed by a rearrangement of the lipid tails, resulting in a more "ordered" state and a slightly increase in the membrane thickness. The alignment of lipid tails in this state is predominantly tilted with small tilted-angles, in support to the findings by Ruocco *et al.*, in which a tilted lipid arrangement was reported in the gel phase and a more parallel alignment to the bilayer normal near the transition temperature [300]. Above T_{m}, the bilayer structure was characterized by the lipid tails able to freely move in random motion, resulting in an increase in the %*gauche* formed and an increase in the level of interdigitation between lipids in opposite leaflets.

The phase transformation for DPPE was similar to that of DPPC, except that because of its smaller headgroup, bilayers below T_{m} consisted primarily of "ordered" domains. The smaller area per lipid of DPPE is reflected in the tight packing of the lipids, and in turn, with

small tilted-angles. In agreement with the hysteresis loop from the annealing simulations, the DPPE bilayer structure experienced minimal rearrangement of the lipids, as the bilayer thickness gradually decreases near the phase transition. These results support the study by Yao *et al.* in which they were unable to distinguish a stable phase from a gel to a liquid-crystalline phase for DPPE [299]. Near T_m, cooperative structural changes were observed with a decrease in the ordering of the lipid tails and an increase in the %*gauche* formation and level of interdigitation. Because DPPE molecules remain closely packed above T_m, the lipid tails do not overlap, which is confirmed by the density profile of the terminal carbon atoms.

In summary, the mechanism for phase transition from a gel to a liquid-crystalline phase for DPPC and DPPE bilayers involves cooperative changes of the bilayer structure that can be quantified with the area per lipid, bilayer thickness, lipid tail tilt-angle, lipid tail order parameter, hydrocarbon *trans-gauche* isomerization, and level of interdigitation. The implication of all the structural changes observed supports a first-order phase transition for DPPC and DPPE that is in reasonable agreement with experimental observations.

This study demonstrates that one can use atomistic simulations to obtain insightful information on lipid bilayers at and near the main transition state (gel to liquid-crystalline). Moreover, the properties analyzed give valuable structural data to understand the mechanism underlying phase transitions, which may not be readily accessible from experimental measurements.

9.3.2 Phase Transition for POPC and POPE Bilayers

The degree of unsaturation differs among the many types of phospholipids depending on the number of double bonds in the lipid tails. For lipids with the same headgroup, the most pronounced change in the phase transition temperature occurs when comparing saturated to monounsaturated lipids. Using POPC and POPE as modeled lipid bilayers, atomistic simulations have been used to obtain insightful details of the bilayer structures at and near

the main transition state. The properties analyzed here yield valuable structural data to understand the mechanisms underlying the phase transition of monounsaturated lipid bilayers.

Two sets of simulations were considered, annealing simulations on heating and cooling and fixed temperatures simulations from 260-320 K (increments of 10 K). Results from the annealing simulations show a well-defined phase transition point with small hysteresis loops, thus demonstrating a first-order phase transition. The phase transition temperature was identified at about 270 K and 280-300 K for POPC and POPE bilayers, respectively, when measuring the changes in the area per lipid and bilayer thickness. These values are comparable to the experimental ones of 270 K for POPC and 306 K for POPE.

In the second set of simulations at fixed temperatures, equilibrium properties were calculated for temperatures above and below the estimated phase transition temperature, T_{m}, from the annealing simulations. The area per lipid and bilayer thickness measured from the fixed temperature runs were consistent with those observed in the annealing simulations, with values within the bounds of the hysteresis loop. The resulting equilibrium structure for POPC below T_{m} showed a tilted lipid arrangement. Slight interdigitation of the lipids between each leaflet was also observed in parts of the bilayer, which possibly relates to a "mixed" domain formation. Near T_{m}, a cooperative transformation of the bilayer structure is observed, however, general bilayer properties such as area per lipid and bilayer thickness were found less sensitive to the phase transition. On the other hand, other structural properties (lipid order parameters, %*gauche*, tilted lipid arrangement, and level of interdigitation) were sensitive to the phase transition, resulting in a T_{m} at about 270 K. Above T_{m}, the bilayer structures were characterized by lipid tails free to move in random motion.

The phase transformation for POPE was more difficult to identify. Below T_{m}, POPE bilayers consisted primarily of lipids in a tilted arrangement with higher lipid packing compared to POPC, due to the smaller headgroup in POPE molecules. Near T_{m}, a cooperative transformation of the bilayer structure was observed in which pre- and post-transitions states were identified based on structural properties. In this case, the pre-transition state (270 to

280 K) involved a significant change in the number of *gauche* conformations along the Sn-1 tails. Around the main transition point (280 to 290 K), the lowering of the lipid tails order parameter in the Sn-1 tail and the disappearance of the tilted lipid arrangement were observed. In the post-transition state (290 to 300 K), the lowering of the lipid order parameter in the Sn-2 tails and less hindrance in the displacement of the carbon atoms along the lipid tails were observed, as the density profiles evolved from asymmetric to symmetric distributions. Above 300 K, POPE bilayer structures were characterized by lipid tails free to move in random motion. These findings confirm Bryant *et al.* NMR experimental study in which they observed a wide temperature range for the phase transition of POPE bilayers [163].

9.4   Summary for Chapter 7

9.4.1   Trehalose Protection from Palmitate Induced Toxicity

In Chapter 7, series of experimental and computational measurements were performed to gain insight into how trehalose interacts with HepG2 cells in the presence of palmitate. Experimentally, healthy HepG2 cells exposed to palmitate resulted in a significant amount of LDH and H_2O_2 released into the medium, indicating cell death or compromised cellular membrane. Furthermore, it is observed from EPR measurements that the membrane fluidity is significantly decreased in the presence of palmitate, especially in the bilayer core region. The leading hypotheses for the observed results are: i) palmitate dissolves into the membrane, thus reducing the membrane fluidity, ii) palmitate metabolizes into phospholipid components of cell membranes, thus increasing the packing between the lipids, and iii) the remaining fragments of oxidized lipids inside the membrane (oxidized by H_2O_2 and $^*OH$), which are hydrophobic in nature, reduce the membrane fluidity.

       The computational component of this study aimed at interpreting and understanding the experimental results, providing knowledge at the molecular level into the role of

palmitate and trehalose in the toxicity of HepG2 cells. As illustrated by the results, the computation analyses confirmed that palmitate can dissolve into the bilayers within a short time. As the palmitate concentration in the bilayer increased, the order parameter of the lipid tails increased, which was consistent with the experimental results showing reduced membrane fluidity. The ordering of the lipid tails was due to the additional volume occupied by the palmitate molecules, forcing the surrounding lipid molecules to become highly packed, resulting in a more ordered structure. The local effect of palmitate embedded in the bilayer was also considered. The simulation results yielded a highly order bilayer structure with the lipid tails in a tilted arrangement. These results agreed well with DSC measurements for DOPC liposomes containing palmitate and EPR measurements of HepG2 cells exposed to palmitate. Furthermore, the direct interactions of trehalose and palmitate in the medium through hydrogen bonding potentially hindered palmitate from dissolving into the bilayer. The binding of palmitate to trehalose seems beneficial to cell membranes; however, it was discovered that trehalose can potentially modify the bilayer surface by altering the surface hydrogen bond distribution, thus inducing hydrophobic regions for palmitate to penetrate the bilayer.

9.5 Summary for Chapter 8

9.5.1 Effect of Fatty Acids on Biological Membranes

In Chapter 8, additional series of experimental and computational measurements were performed to gain insight into how unsaturated FAs, oleate and linoleate, interact with HepG2 cells in comparison to a saturated FA, palmitate. Experimentally, it was found that healthy HepG2 cells exposed to oleate and linoleate did not induce LDH and H_2O_2 release into the medium compared to palmitate. Furthermore, it is observed from EPR measurements that the membrane fluidity was slightly reduced for HepG2 cells exposed to oleate and linoleate. The leading hypothesis for the observed result is that unsaturated FAs potentially increase

the chain packing between cellular lipids, however, the kinked lipid chains of unsaturated FAs disrupt their normal packing, thus increasing membrane fluidity.

The computational component of this study aimed at interpreting and understanding the experimental results, providing knowledge at the molecular level into the role of unsaturated FAs in reducing the toxicity of HepG2 cells. As illustrated by the results, the average structural properties, such as bilayer surface area, thickness, and order parameters were insufficient to differentiate the effects of saturated and unsaturated FAs on the bilayers. Both saturated and unsaturated FAs increased the bilayer surface area, thickness, and lipid tail order parameters with increasing FA concentrations. As a result, it was necessary to consider the local effect of FAs embedded in the bilayers. Using a Voronoi tessellation analysis, the results demonstrated the ability of unsaturated FAs to absorb the lateral compression between lipids and FAs within the bilayer. Furthermore, water-lipid hydrogen bond analysis indicated that the average number of hydrogen bonds remained relatively the same regardless of oleate or linoleate concentrations, however, significantly reduced for palmitate. From this analysis, it was confirmed that the role of saturated and unsaturated FAs are contrasting: unsaturated FAs induce less changes to the lipid component of the bilayer and help maintain the level of hydration, whereas the converse is true for the saturated FAs.

9.6 Future Work

9.6.1 Membrane Stabilization

In Chapter 4, comprehensive studies of pure and mixed lipid bilayers (DPPC and DPPE) and their interactions with stabilizing agent (trehalose) were considered. Based on the computational analysis, there are two major flaws which require attention for the future studies, specifically lipid force-field parameters and bilayer setup.

For lipid bilayer studies, DPPC molecules are typically used in the simulations. In

order to obtain a better assessment of a more realistic bilayer structure, a second lipid component with a PE headgroup was introduced the current bilayer model. Although a force-field for POPE was available, it was considered that POPE would bring additional complexities to the systematic studies because it has different lipid chain lengths and degree of unsaturation compared to DPPC. For this reason, DPPE was chosen, as it has an identical lipid chain structure as DPPC. As mentioned in Chapter 4, an appropriate force-field for DPPE molecule was created by modifying the DPPC force-field using the POPE force-field. The results demonstrated small discrepancies between the simulation and experimental values in the area per lipid and lipid tail order parameters. This indicated that there are significant errors associated with the mixed bilayer simulations and improvements on the DPPE force-field should be considered in future studies. Since the errors are propagated the same way for bilayers considered in Chapter 4, the comparative study among the lipid systems is justified.

Although the mechanism of membrane stabilization is considered in Chapter 4, it did not address an important issue on how trehalose stabilizes lipid bilayers under dehydrated conditions and low temperatures. Therefore, another set of simulations were performed to specifically investigate the stabilizing effect of saccharide compounds under such conditions. As mentioned in Chapter 5, there were three difficulties arise when performing MD simulations to model uni-lamellar bilayers at dehydrated conditions: 1) existing lipid force-fields (developed for fully-hydrated conditions) may be unsuitable for simulations under dehydrated conditions, 2) periodic boundary conditions (PBC) implemented in typical MD simulations with long-range electrostatic corrections essentially create a multi-lamellar bilayer structure, and 3) due to the low water content at dehydrated conditions, the lipid bilayer lateral compressibility is no longer the same as the typical compressibility derived from a fully-hydrated state.

In terms of lipid force-fields used in MD simulations, recent computational studies indicated that dehydrated structural properties of DPPC bilayers are in good agreement with the experimental results. Based on this fact, the lipid force-field used in Chapter 5 was

used to capture a correct lipid phase behavior under dehydrated conditions.

For the PBC issue, there were no other ways to create a uni-lamellar bilayer structure under dehydrated conditions, unless periodic images of the bilayers are separated in the z-dimension. After careful consideration, a new lipid bilayer setup was engineered to contain an inert gas phase (see Figure 5.1.1). Note that this type of bilayer setup has seldom applied and it should be only considered in especial circumstances. For the simulations presented in Chapter 5, this bilayer setup was used to compare the effectiveness among stabilizing agents. As a comparative study, the ability for saccharide compounds to stabilize the uni-lamellar bilayer structure was sufficient to address the mechanism of stabilization under dehydrated conditions.

By incorporating a gas phase into the bilayer structure, there is a major issue regarding the bilayer compressibility. After careful consideration, NVT simulations were performed by constraining the lateral dimensions of the simulation box (equivalent to the bilayer size at 325 K) to remove artificial lateral compressions. The simulations were then performed at lower temperatures (290, 300, and 310 K). Clearly, there is a discrepancy between the simulating temperatures and bilayer lateral dimensions that should be considered in the future studies.

There is one more issue that was unaddressed for the simulation presented in Chapter 4 and 5. This is related to the realistic environment of cells undergoing a freeze-drying process. According to the hypothesis, the water content in the extracellular region is removed first and, if the stabilizing agents are present, the cellular membranes should remain intact, thus preserving intracellular content and cellular functionalities. The described behavior was not exactly matched by the bilayers constructed in Chapter 5, because both bilayer leaflets were exposed to the dehydrated environment. Figure 9.6.1 shows the proposed bilayer setups that aims to mimic the freeze-drying of cells with and without stabilizing agents. Note that the intracellular regions are always hydrated and, simultaneously, the extracellular regions are exposed to the dehydrated environment. Results from this set of simulation may provide
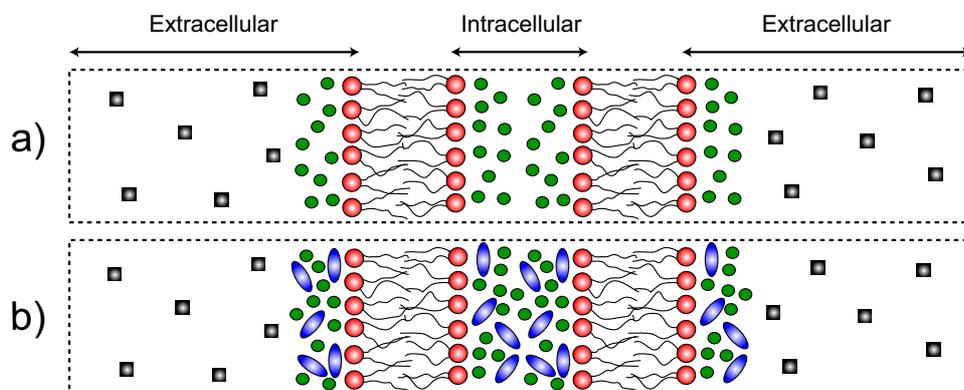
Figure 9.6.1: Proposed lipid bilayer setups a) without and b) with saccharides. Intracellular and extracellular regions are shown in the figure. A lipid molecule is represented with a red circle and two lipid tails. Green circles, blue ovals, and gray squares are water, saccharide, and gas molecules, respectively. Dotted rectangular lines are the bounds of the simulation boxes.

useful information regarding the structural organization of intracellular and extracellular membranes.

9.6.2   Membrane Phase Behavior

One of the major concerns regarding the phase transition study presented in Chapter 6 is the determination of main phase transition temperature of pure DPPC, DPPE, POPC, and POPE lipid bilayers. As mentioned, the major problems reside in the fact that the force-fields for these lipids are optimized for a lipid-crystalline state, not for a gel state. Moreover, the re-parameterization in the double-double region for unsaturated lipids has recently been surfaced to improve the quality of current force-fields and should be considered in the future studies (see Simulation Details in Chapter 8 for more details on the modified lipid tail force-field). Although the results presented in Chapter 6 showed significant structural changes above and below the phase transition temperature, the maximum errors on the estimated temperatures were about 20 K compared to the experimental values. From an experimental standpoint, this is considered inadequate. To have a better estimation of the phase transition
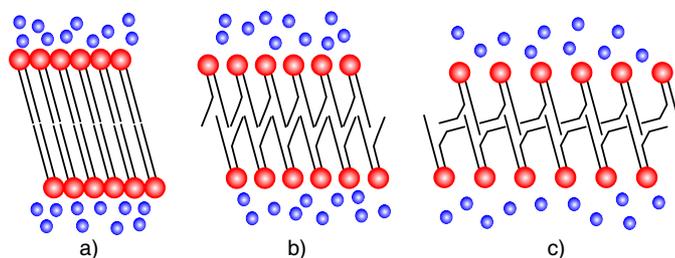
Figure 9.6.2: Proposed starting structures for a) saturated, b) monounsaturated, and c) polyunsaturated lipid bilayers. Red and blue spheres represent the lipid headgroup and water, respectively.

temperature, more simulations at fixed temperatures with narrower temperature range than those reported in Chapter 6 should be considered in the future studies. One suggestion is for smaller lipid bilayers and lower hydration level, which should be sufficient to study the phase transition of pure lipid bilayer systems, however, at extended simulation time into the microsecond range. Results from these sets of simulations may provide a better estimate of the phase transition temperature and the quality of the lipid force-fields.

Another important point that was not considered in the simulation in Chapter 6 is the starting structure of the lipid bilayer simulations. Although these structures were not shown in Chapter 6, they were generated by cooling fully equilibrated bilayers from a liquid-crystalline state to a gel state. With the short equilibrium time considered, these structures may not be optimal starting structures for phase transition studies, especially for POPC and POPE systems. The correct approach would have been to start all the simulations from an equilibrium gel state and then slowly heat up the system to a fixed temperature. Figure 9.6.2 shows the possible starting structures for saturated, monounsaturated, and polyunsaturated lipid bilayers. Low temperature simulations should be considered to equilibrate these structures. This approach should provide well defined structural changes during the phase transition and first-ordered phase transition temperature.
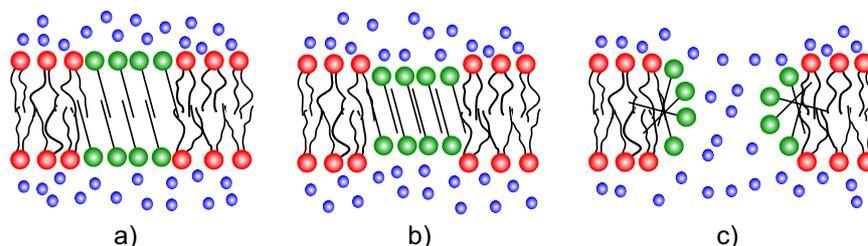
Figure 9.6.3: Schematic representation of lipid bilayer with localized palmitate. Speculated a) starting, b) intermediate, and c) final bilayer structures are shown in the figure. Red, green, and blue spheres represent the lipid headgroup, palmitate, and water, respectively.

9.6.3   Fatty Acid Induced Toxicity

As presented in Chapters 7 and 8, an early stage of research aimed to identify the biophysical interactions of fatty acids with the cellular membranes and the role of trehalose in preventing changes to the membrane structure was studied. Using computational approach, systematic studies were completed by comparing the effect of individual component (fatty acids or trehalose) on model bilayers. Based on these preliminary results, couples of suggestions are available for future studies.

First, the possibility of saturated fatty acids (palmitate) aggregation inside the bilayer was not addressed in Chapter 7. Technically, this is possible because palmitate molecules are more hydrophobic than the phospholipid component of biological membranes. The future study should focus on bilayers with high concentrations of saturated fatty acids (palmitate) localized in a specific area of the bilayer (see Figure 9.6.3a). As shown from a previous study [231], the presence of palmitate (1:2 lipid:pamitate ratio) can induce the formation of non-lamellar bilayer structures. Based on this fact, the localization of palmitate inside the bilayer may disrupt the bilayer lamellar structure. The proposed intermediate and final structures are shown in Figures 9.6.3b and c, respectively, indicating the reduction of bilayer thickness at the localized palmitate region, increasing membrane permeability and potentially pore formation.

Other suggestions are about the fusogenic properties of FFAs and the effect of having

mixed FAs embedded within the bilayers. One of the future studies could focus on evaluating the diffusive properties among FFAs on biological membranes. This comparative study will provide valuable information which relates to the degree of FFA unsaturation to cellular uptakes. To accomplish this, duplicate simulations of bilayers containing one palmitate in the aqueous phase, presented in Chapter 7, should be repeated with oleate and linoleate molecules. In addition to the diffusivity analysis, another study could focus on comparing the effect of saturated FA (palmitate) on biological membranes containing unsaturated FAs (oleate or linoleate). Since the results presented in Chapter 8 indicated that both oleate and linoleate are capable of reducing the packing between the phospholipid components, another set of simulations using mixed FAs should provide a better understanding of how unsaturated FAs reduce cellular toxicity.

9.6.4   Liposomal Drug Delivery System

As demonstrated in Chapters 4-8, molecular dynamics (MD) simulation is a useful tool to study and support experimental studies associated with the biological processes of phospholipid membranes. There are, however, countless number of complex biological processes that need computational support to further our insight into specific mechanisms at the molecular level. This section provides a possible avenue for simulations of liposomal drug delivery systems. The proposed ideas presented here were developed from an internship experience at Merck Research Laboratories, an opportunity that culminated the concluding parts of my doctoral studies by assimilating all elements explored through the studies herein.

In pharmaceutical industries, most of the liposomal delivery systems are made of artificial complex lipids. The formulation and optimization processes are conducted by changing 1) the lipid compositions, 2) the ratio of cholesterol to lipid, and 3) the molecular structure of lead lipid compounds. Even though, liposomal delivery systems have not yet been approved for medical use, the lead lipid compound is well established, dimethylaminopropane (DMA).
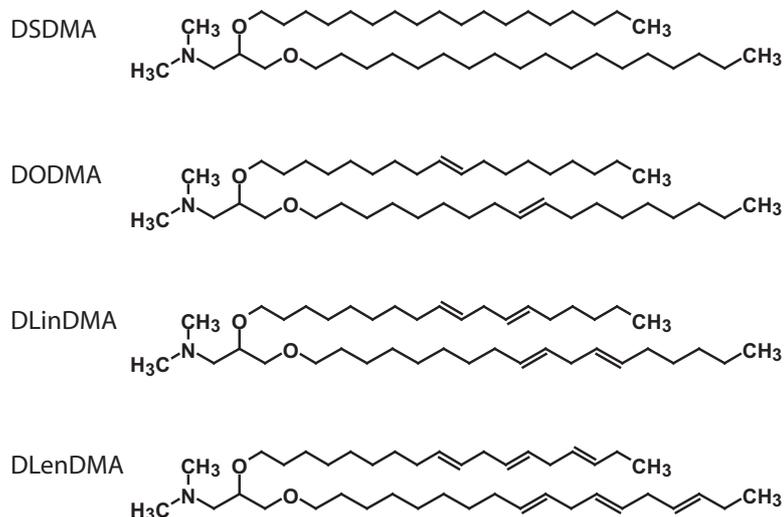
Figure 9.6.4: Molecular structure of DSDMA, DODMA, DLinDMA, and DLenDMA. Note that all the double bonds have the *cis* configuration. Chemical symbols are carbon (C), hydrogen (H), nitrogen (N), oxygen (O), and phosphorus (P).

Suitable test lipids include distearyldimethylammonium (DSDMA), dioctadecyldimethylammonium (DODMA), 1,2-dilinoleyloxy-N,N-dimethylaminopropane (DLinDMA), and l,2-dilinolenyloxy-N,N-dimethylaminopropane (DLenDMA) [340]. Figure 9.6.4 shows the molecular structure of these lipids. Note that these lipids are almost identical with the notable exception of the number of double bonds in the lipid tails. A comparative study by Heyes *et al.* demonstrated an inverse relationship between the number of double bonds and cellular uptake, with DLinDMA liposomes found to be the most potent [340]. The hypothesis for this result was that DLinDMA is more fusogenic to cells and likely to form an inverted hexagonal phase. The ability to understand the difference between these lipids, in particular their phase behavior in liposomes, remains a challenge in the pharmaceutical research. Further studies applying the methods and concepts (e.g., phase behavior and stability) developed in this dissertation will provide insightful and meaningful understanding of the possible interactions between the lipids. This fundamental, molecular level knowledge may eventually serve as significant improvement to current practices in the pharmaceutical field of liposomal drug delivery systems.

Bibliography

[1] van Gunsteren, W. F., P. K. Weiner, and T. Wilkinson. 1997. Computer simulation of biomolecular systems. 3rd edition. Kluwer Academic Publishers, Dordrecht; Boston.

[2] Favre, E., L. Marchal-Heusler, and M. Kind. 2002. Chemical product engineering: Research and educational challenges. *Chemical Engineering Research and Design* 80:65–74.

[3] Gani, R. 2004. Chemical product design: Challenges and opportunities. *Computers and Chemical Engineering* 28:2441–2457.

[4] de Pablo, J. J., and F. A. Escobedo. 2002. Molecular simulations in chemical engineering: Present and future. *AIChE Journal* 48:2716–2721.

[5] Lodish, H. F., D. Baltimore, A. Berk, L. S. Zipursky, P. Matsudaira, and J. E. Darnell. 1995. Molecular cell biology. 3rd edition. Scientific American Books: Distributed by W.H. Freeman and Company, New York.

[6] Fahy, E., S. Subramaniam, H. A. Brown, C. K. Glass, J. Merrill, A. H., R. C. Murphy, C. R. Raetz, D. W. Russell, Y. Seyama, W. Shaw, T. Shimizu, F. Spener, G. van Meer, M. S. VanNieuwenhze, S. H. White, J. L. Witztum, and E. A. Dennis. 2005. A comprehensive classification system for lipids. *Journal of Lipid Research* 46:839–61.

[7] Lipid MAPS. Lipid Metabolites And Pathways Strategy. http://www.lipidmaps.org/.

[8] Dowhan, W. 1997. Molecular basis for membrane phospholipid diversity: Why are there so many lipids? *Annual Reviews of Biochemistry* 66:199–232.

[9] Uran, S., Å. Larsen, P. B. Jacobsen, and T. Skotland. 2001. Analysis of phospholipid species in human blood using normal-phase liquid chromatography coupled with electrospray ionization ion-trap tandem mass spectrometry. *Journal of Chromatography B* 758:265–75.

[10] Emoto, K., T. Kobayashi, A. Yamaji, H. Aizawa, I. Yahara, K. Inoue, and M. Umeda. 1996. Redistribution of phosphatidylethanolamine at the cleavage furrow of dividing cells during cytokinesis. *Proceedings of the National Academy of Sciences of the United States of America* 93:12867–72.

[11] Storey, M. K., K. L. Clay, T. Kutateladze, R. C. Murphy, M. Overduin, and D. R. Voelker. 2001. Phosphatidylethanolamine has an essential role in *Saccharomyces cerevisiae* that is independent of its ability to form hexagonal phase structures. *Journal of Biological Chemistry* 276:48539–48.

[12] Martínez, P., and A. Morros. 1996. Membrane lipid dynamics during human sperm capacitation. *Frontiers in Bioscience* 1:d103–17.

[13] Kearns, D. B., J. Robinson, and L. J. Shimkets. 2001. *Pseudomonas aeruginosa* exhibits directed twitching motility up phosphatidylethanolamine gradients. *Journal of Bacteriology* 183:763–7.

[14] Birner, R., M. Bürgermeister, R. Schneiter, and G. Daum. 2001. Roles of phosphatidylethanolamine and of its several biosynthetic pathways in *Saccharomyces cerevisiae*. *Molecular Biology of the Cell* 12:997–1007.

[15] Jahn, R., and H. Grubmüller. 2002. Membrane fusion. *Current Opinion in Biotechnology* 14:488–95.

[16] Campbell, N. A., and J. B. Reece. 2001. Biology. 6th edition. Benjamin Cummings, San Francisco; London.

[17] Thurmond, R. L., S. W. Dodd, and M. F. Brown. 1991. Molecular areas of phospholipids as determined by ^{2}H NMR spectroscopy. Comparison of phosphatidylethanolamines and phosphatidylcholines. *Biophysical Journal* 59:108–13.

[18] Petrov, A. G., K. Gawrisch, G. Brezesinski, G. Klose, and A. Möps. 1982. Optical detection of phase transitions in simple and mixed lipid-water phases. *Biochimica et Biophysica Acta-Biomembranes* 690:1–7.

[19] Urbina, J. A., B. Moreno, W. Arnold, C. H. Taron, P. Orlean, and E. Oldfield. 1998. A carbon-13 nuclear magnetic resonance spectroscopic study of inter-proton pair order parameters: A new approach to study order and dynamics in phospholipid membrane systems. *Biophysical Journal* 75:1372–83.

[20] Blume, A., R. J. Wittebort, S. K. Das Gupta, and R. G. Griffin. 1982. Phase equilibria, molecular conformation, and dynamics in phosphatidylcholine phosphatidylethanolamine bilayers. *Biochemistry* 21:6243–6253.

[21] Huang, C., and S. Li. 1999. Calorimetric and molecular mechanics studies of the thermotropic phase behavior of membrane phospholipids. *Biochimica et Biophysica Acta-Biomembranes* 1422:273–307.

[22] Lasic, D. D., and D. Papahadjopoulos. 1996. Liposomes and biopolymers in drug and gene delivery. *Current Opinion in Solid State and Materials Science* 1:392–400.

[23] Mattson, F. H., and S. M. Grundy. 1985. Comparison of effects of dietary saturated, monounsaturated, and polyunsaturated fatty acids on plasma lipids and lipoproteins in man. *Journal of Lipid Research* 26:194–202.

[24] Rudel, L. L., J. L. Haines, and J. K. Sawyer. 1990. Effects on plasma lipoproteins of

monounsaturated, saturated, and polyunsaturated fatty acids in the diet of African green monkeys. *Journal of Lipid Research* 31:1873–82.

[25] Nydahl, M. C., I. B. Gustafsson, and B. Vessby. 1994. Lipid-lowering diets enriched with monounsaturated or polyunsaturated fatty acids but low in saturated fatty acids have similar effects on serum lipid concentrations in hyperlipidemic patients. *American Journal of Clinical Nutrition* 59:115–22.

[26] Gardner, C. D., and H. C. Kraemer. 1995. Monounsaturated versus polyunsaturated dietary fat and serum lipids. A meta-analysis. *Arteriosclerosis Thrombosis and Vascular Biology* 15:1917–27.

[27] Kuo, P., M. Weinfeld, M. A. Rudd, P. Amarante, and J. Loscalzo. 1990. Plasma membrane enrichment with cis-unsaturated fatty acids enhances LDL metabolism in U937 monocytes. *Arteriosclerosis* 10:111–8.

[28] Nolan, J. P., and R. H. Hammerstedt. 1997. Regulation of membrane stability and the acrosome reaction in mammalian sperm. *FASEB Journal* 11:670–82.

[29] Russell, N. J. 1997. Psychrophilic bacteria: Molecular adaptations of membrane lipids. *Comparative Biochemistry and Physiology A-Molecular and Integrative Physiology* 118:489–93.

[30] Sajbidor, J. 1997. Effect of some environmental factors on the content and composition of microbial membrane lipids. *Critical Reviews in Biotechnology* 17:87–103.

[31] Tang, G. Q., W. P. Novitzky, H. Carol Griffin, S. C. Huber, and R. E. Dewey. 2005. Oleate desaturase enzymes of soybean: Evidence of regulation through differential stability and phosphorylation. *Plant Journal* 44:433–46.

[32] Ladbrooke, B. D., and D. Chapman. 1969. Thermal analysis of lipids, proteins and biological membranes. A review and summary of some recent studies. *Chemistry and Physics of Lipids* 3:304–56.

[33] Cronan, J., J. E., and E. P. Gelmann. 1975. Physical properties of membrane lipids: Biological relevance and regulation. *Bacteriological Reviews* 39:232–56.

[34] Small, D. M. 1986. The physical chemistry of lipids: From alkanes to phospholipids. Plenum, New York; London.

[35] Tristram-Nagle, S., and J. F. Nagle. 2004. Lipid bilayers: Thermodynamics, structure, fluctuations, and interactions. *Chemistry and Physics of Lipids* 127:3–14.

[36] London, E. 2005. How principles of domain formation in model membranes may explain ambiguities concerning lipid raft formation in cells. *Biochimica et Biophysica Acta-Molecular Cell Research* 1746:203–220.

[37] Brown, D. A., and E. London. 1998. Functions of lipid rafts in biological membranes. *Annual Review of Cell and Developmental Biology* 14:111–36.

[38] Simons, K., and D. Toomre. 2001. Lipid rafts and signal transduction. *Nature Reviews Molecular Cell Biology* 2:216–216.

[39] Simons, K., and E. Ikonen. 1997. Functional rafts in cell membranes. *Nature* 387:569–572.

[40] Ikonen, E. 2001. Roles of lipid rafts in membrane transport. *Current Opinion in Cell Biology* 13:470–7.

[41] Herreros, J., T. Ng, and G. Schiavo. 2001. Lipid rafts act as specialized domains for tetanus toxin binding and internalization into neurons. *Molecular Biology of the Cell* 12:2947–2960.

[42] Fantini, J., N. Garmy, R. Mahfoud, and N. Yahi. 2002. Lipid rafts: structure, function and role in HIV, Alzheimers and prion diseases. *Expert Reviews in Molecular Medicine* 2002:1–22.

[43] Lafont, F., and F. G. van der Goot. 2005. Bacterial invasion via lipid rafts. *Cellular Microbiology* 7:613–20.

[44] Avanti Polar Lipid, Inc. Phase Transition Temperatures for Glycerophospholipids. http://www.avantilipids.com.

[45] Litman, B. J., E. N. Lewis, and I. W. Levin. 1991. Packing characteristics of highly unsaturated bilayer lipids: Raman spectroscopic studies of multilamellar phosphatidyl-choline dispersions. *Biochemistry* 30:313–319.

[46] Keough, K. M., B. Giffin, and P. L. Matthews. 1989. Phosphatidylcholine-cholesterol interactions: Bilayers of heteroacid lipids containing linoleate lose calorimetric transitions at low cholesterol concentration. *Biochimica et Biophysica Acta-Biomembranes* 983:51–5.

[47] Hitchcock, P. B., R. Mason, K. M. Thomas, and G. G. Shipley. 1974. Structural chemistry of 1,2-dilauroyl-DL-phosphatidylethanolamine: Molecular conformation and intermolecular packing of phospholipids. *Proceedings of the National Academy of Sciences of the United States of America* 71:3036–40.

[48] Hitchcock, P. B., R. Mason, and G. G. Shipley. 1975. Phospholipid arrangements in multilayers and artificial membranes: Quantitative analysis of the X-ray diffraction data from a multilayer of 1,2-dimyristoyl-DL-phosphatidylethanolamine. *Journal of Molecular Biology* 94:297–9.

[49] Veatch, S. L., I. V. Polozov, K. Gawrisch, and S. L. Keller. 2004. Liquid domains in vesicles investigated by NMR and fluorescence microscopy. *Biophysical Journal* 86:2910–22.

[50] Schnitzer, E., M. M. Kozlov, and D. Lichtenberg. 2005. The effect of cholesterol on the solubilization of phosphatidylcholine bilayers by the non-ionic surfactant Triton X-100. *Chemistry and Physics of Lipids* 135:69–82.

[51] Karmakar, S., and V. A. Raghunathan. 2005. Structure of phospholipid-cholesterol membranes: An X-ray diffraction study. *Physical Review E* 71:061924.

[52] McQuaw, C. M., A. G. Sostarecz, L. Zheng, A. G. Ewing, and N. Winograd. 2005. Lateral heterogeneity of dipalmitoylphosphatidylethanolamine-cholesterol langmuir-blodgett films investigated with imaging time-of-flight secondary ion mass spectrometry and atomic force microscopy. *Langmuir* 21:807–13.

[53] Elliott, R., K. Katsov, M. Schick, and I. Szleifer. 2005. Phase separation of saturated and mono-unsaturated lipids as determined from a microscopic model. *Journal of Chemical Physics* 122:44904.

[54] Mannock, D. A., R. N. Lewis, and R. N. McElhaney. 2006. Comparative calorimetric and spectroscopic studies of the effects of lanosterol and cholesterol on the thermotropic phase behavior and organization of dipalmitoylphosphatidylcholine bilayer membranes. *Biophysical Journal* 91:3327–40.

[55] Ricker, J. V., N. M. Tsvetkova, W. F. Wolkers, C. Leidy, F. Tablin, M. Longo, and J. H. Crowe. 2003. Trehalose maintains phase separation in an air-dried binary lipid mixture. *Biophysical Journal* 84:3045–51.

[56] Ohtake, S., C. Schebor, S. P. Palecek, and J. J. de Pablo. 2004. Effect of sugar-phosphate mixtures on the stability of DPPC membranes in dehydrated systems. *Cryobiology* 48:81–9.

[57] Ohtake, S., C. Schebor, and J. J. de Pablo. 2006. Effects of trehalose on the phase behavior of DPPC-cholesterol unilamellar vesicles. *Biochimica et Biophysica Acta-Biomembranes* 1758:65–73.

[58] Pedersen, T. B., T. Kaasgaard, M. O. Jensen, S. Frokjaer, O. G. Mouritsen, and K. Jorgensen. 2005. Phase behavior and nanoscale structure of phospholipid membranes incorporated with acylated c_{14}-peptides. *Biophysical Journal* 89:2494–2503.

[59] Nieh, M. P., J. Pencer, J. Katsaras, and X. Y. Qi. 2006. Spontaneously forming ellipsoidal phospholipid unilamellar vesicles and their interactions with helical domains of Saposin C. *Langmuir* 22:11028–11033.

[60] Larios, C., J. Minones, I. Haro, M. A. Alsina, M. A. Busquets, and J. M. Trillo. 2006. Study of adsorption and penetration of E2(279-298) peptide into langmuir phospholipid monolayers. *Journal of Physical Chemistry B* 110:23292–23299.

[61] Zweytick, D., G. Pabst, P. M. Abuja, A. Jilek, S. E. Blondelle, J. Andra, R. Jerala, D. Monreal, G. M. de Tejada, and K. Lohner. 2006. Influence of N-acylation of a peptide derived from human lactoferricin on membrane selectivity. *Biochimica et Biophysica Acta-Biomembranes* 1758:1426–1435.

[62] Nakahara, H., S. Nakamura, T. Hiranita, H. Kawasaki, S. Lee, G. Sugihara, and O. Shibata. 2006. Mode of interaction of amphiphilic alpha-helical peptide with phosphatidylcholines at the air-water interface. *Langmuir* 22:1182–1192.

[63] Lo, Y. L., J. C. Tsai, and J. H. Kuo. 2004. Liposomes and disaccharides as carriers in spray-dried powder formulations of superoxide dismutase. *Journal of Controlled Release* 94:259–72.

[64] Cavalcanti, L. P., and I. L. Torriani. 2006. Thermotropic phase behavior of DPPC liposome systems in the presence of the anti-cancer agent 'Ellipticine'. *European Biophysical Journal* 36:67–71.

[65] Degim, I. T., B. Gumusel, Z. Degim, T. Ozcelikay, A. Tay, and S. Guner. 2006. Oral administration of liposomal insulin. *Journal of Nanoscience and Nanotechnology* 6:2945–9.

[66] Thirumamagal, B. T. S., X. B. Zhao, A. K. Bandyopadhyaya, S. Narayanasamy, J. Johnsamuel, R. Tiwari, D. W. Golightly, V. Patel, B. T. Jehning, M. V. Backer,

R. F. Barth, R. J. Lee, J. M. Backer, and W. Tjarks. 2006. Receptor-targeted liposomal delivery of boron-containing cholesterol mimics for boron neutron capture therapy (BNCT). *Bioconjugate Chemistry* 17:1141–1150.

[67] Matsingou, C., K. Dimas, and C. Demetzos. 2006. Design and development of liposomes incorporating a bioactive labdane-type diterpene. In vitro growth inhibiting and cytotoxic activity against human cancer cell lines. *Biomedicine & Pharmacotherapy* 60:191–199.

[68] Barker, S. A., S. P. Cottrell, S. R. Giblin, and U. A. Jayasooriya. 2006. Preliminary μSR studies on the incorporation of steroidal drug molecules into liposomes. *Physica B* 374:332–335.

[69] Hidalgo, A. A., W. Caetano, M. Tabak, and J. Oliveira, O. N. 2004. Interaction of two phenothiazine derivatives with phospholipid monolayers. *Biophysical Chemistry* 109:85–104.

[70] Ayudhya, C. I. N., V. Prachayasittikul, and H. J. Galla. 2004. Binding of chimeric metal-binding green fluorescent protein to lipid monolayer. *European Biophysics Journal with Biophysics Letters* 33:522–534.

[71] Konczol, F., N. Farkas, T. Dergez, J. Belagyi, and D. Lorinczy. 2005. Effect of tetracaine on model and erythrocyte membranes by DSC and EPR. *Journal of Thermal Analysis and Calorimetry* 82:201–206.

[72] Koukoulitsa, C., I. Kyrikou, C. Demetzos, and T. Mavromoustakos. 2006. The role of the anticancer drug vinorelbine in lipid bilayers using differential scanning calorimetry and molecular modeling. *Chemistry and Physics of Lipids* 144:85–95.

[73] Kontos, M., M. Nikolopoulou, D. T. P. Trafalis, G. D. Geromichalos, C. Koukoulitsa, C. Camoutsis, E. Bastounis, and P. Karamanakos. 2006. The effect of an estrone

D-lactam steroid ester derivative on breast cancer cells and its predicted binding interactions with the ligand binding domain of estrogen receptor-α. *Oncology Research* 16:129–142.

[74] Nagle, J. F., R. Zhang, S. Tristram-Nagle, W. Sun, H. I. Petrache, and R. M. Suter. 1996. X-ray structure determination of fully hydrated L_α phase dipalmitoylphosphatidylcholine bilayers. *Biophysical Journal* 70:1419–31.

[75] Lewis, B. A., and D. M. Engelman. 1983. Lipid bilayer thickness varies linearly with acyl chain length in fluid phosphatidylcholine vesicles. *Journal of Molecular Biology* 166:211–7.

[76] Rand, R. P., and V. A. Parsegian. 1989. Hydration forces between phospholipid-bilayers. *Biochimica et Biophysica Acta-Reviews on Biomembranes* 988:351–376.

[77] Lis, L. J., M. McAlister, N. Fuller, R. P. Rand, and V. A. Parsegian. 1982. Interactions between neutral phospholipid bilayer membranes. *Biophysical Journal* 37:657–65.

[78] Büldt, G., H. U. Gally, J. Seelig, and G. Zaccai. 1979. Neutron diffraction studies on phosphatidylcholine model membranes. I. Head group conformation. *Journal of Molecular Biology* 134:673–91.

[79] Pace, R. J., and S. I. Chan. 1982. Molecular motions in lipid bilayers. I. Statistical mechanical model of acyl chain motion. *Journal of Chemical Physics* 76:4217–4227.

[80] Schindler, H., and J. Seelig. 1975. Deuterium order parameters in relation to thermodynamic properties of a phospholiped bilayer. A statistical mechanical interpretation. *Biochemistry* 14:2283–7.

[81] De Young, L. R., and K. A. Dill. 1988. Solute partitioning into lipid bilayer membranes. *Biochemistry* 27:5281–5289.

[82] Nagle, J. F., and D. A. Wilkinson. 1978. Lecithin bilayers. Density measurement and molecular interactions. *Biophysical Journal* 23:159–75.

[83] Schmidt, G., and W. Knoll. 1985. Densitometric characterization of aqueous lipid dispersions. *Physical Chemistry Chemical Physics* 89:36–43.

[84] Petrache, H. I., S. Tristram-Nagle, and J. F. Nagle. 1998. Fluid phase structure of EPC and DMPC bilayers. *Chemistry and Physics of Lipids* 95:83–94.

[85] Wiener, M. C., and S. H. White. 1992. Structure of a fluid dioleoylphosphatidylcholine bilayer determined by joint refinement of X-ray and neutron-diffraction data. II. Distribution and packing of terminal methyl groups. *Biophysical Journal* 61:428–433.

[86] Tristram-Nagle, S., H. I. Petrache, and J. F. Nagle. 1998. Structure and interactions of fully hydrated dioleoylphosphatidylcholine bilayers. *Biophysical Journal* 75:917–25.

[87] Boggs, J. M., G. Rangaraj, and K. M. Koshy. 1986. Effect of hydrogen-bonding and non-hydrogen-bonding long chain compounds on the phase transition temperatures of phospholipids. *Chemistry and Physics of Lipids* 40:23–34.

[88] Hübner, W., and A. Blume. 1998. Interactions at the lipid-water interface. *Chemistry and Physics of Lipids* 96:99–123.

[89] Dyck, M., P. Krüger, and M. Lösche. 2005. Headgroup organization and hydration of methylated phosphatidylethanolamines in Langmuir monolayers. *Physical Chemistry Chemical Physics* 7:150–156.

[90] Tu, K., D. J. Tobias, J. K. Blasie, and M. L. Klein. 1996. Molecular dynamics investigation of the structure of a fully hydrated gel-phase didipalmitoylphosphatidylcholine bilayer. *Biophysical Journal* 70:595–608.

[91] Tobias, D. J., W. Mar, J. K. Blasie, and M. L. Klein. 1996. Molecular dynamics simulations of a protein on hydrophobic and hydrophilic surfaces. *Biophysical Journal* 71:2933–41.

[92] Tieleman, D. P., S. J. Marrink, and H. J. C. Berendsen. 1997. A computer perspective of membranes: Molecular dynamics studies of lipid bilayer systems. *Biochimica et Biophysica Acta-Biomembranes* 1331:235–270.

[93] Bandyopadhyay, S., M. Tarek, and M. L. Klein. 1998. Computer simulation studies of amphiphilic interfaces. *Current Opinion in Colloid & Interface Science* 3:242–246.

[94] Leekumjorn, S., and A. K. Sum. 2007. Molecular characterization of gel and liquid-crystalline structures of fully hydrated POPC and POPE bilayers. *Journal of Physical Chemistry B* 111:6026–33.

[95] Leekumjorn, S., and A. K. Sum. 2007. Molecular studies of the gel to liquid-crystalline phase transition for fully hydrated DPPC and DPPE bilayers. *Biochimica Et Biophysica Acta-Biomembranes* 1768:354–65.

[96] Chiu, S. W., M. Clark, V. Balaji, S. Subramaniam, H. L. Scott, and E. Jakobsson. 1995. Incorporation of surface tension into molecular dynamics simulation of an interface: A fluid phase lipid bilayer membrane. *Biophysical Journal* 69:1230–1245.

[97] Stouch, T. R. 1993. Lipid membrane structure and dynamics studied by all-atom molecular dynamics simulations of hydrated phospholipid bilayers. *Molecular Simulation* 10:335–362.

[98] Robinson, A. J., W. G. Richards, P. J. Thomas, and M. M. Hann. 1994. Head group and chain behavior in biological membranes: A molecular dynamics computer simulation. *Biophysical Journal* 67:2345–54.

[99] Damodaran, K. V., and K. M. Merz. 1993. Head group-water interactions in lipid bilayers: A comparison between DMPC- and DLPE-based lipid bilayers. *Langmuir* 9:1179–1183.

[100] Pasenkiewicz-Gierula, M., K. Murzyn, T. Róg, and C. Czaplewski. 2000. Molecular

dynamics simulation studies of lipid bilayer systems. *Acta Biochimica Polonica* 47:601–611.

[101] Róg, T., K. Murzyn, R. Gurbiel, Y. Takaoka, A. Kusumi, and M. Pasenkiewicz-Gierula. 2004. Effects of phospholipid unsaturation on the bilayer nonpolar region: A molecular simulation study. *Journal of Lipid Research* 45:326–336.

[102] Venable, R. M., Y. Zhang, B. J. Hardy, and R. W. Pastor. 1993. Molecular dynamics simulations of a lipid bilayer and of hexadecane: An investigation of membrane fluidity. *Science* 262:223–6.

[103] Egberts, E., S. J. Marrink, and H. J. C. Berendsen. 1994. Molecular dynamics simulation of a phospholipid membrane. *European Biophysical Journal* 22:423–436.

[104] Essex, J. W., M. M. Hann, and W. G. Richards. 1994. Molecular dynamics simulation of a hydrated phospholipid bilayer. *Philosophical Transactions of the Royal Society B* 344:239–260.

[105] Feller, S. E., Y. H. Zhang, and R. W. Pastor. 1995. Computer simulation of liquid/liquid interfaces. II. Surface-tension area dependence of a bilayer and monolayer. *Journal of Chemical Physics* 103:10267–10276.

[106] Tu, K. C., D. J. Tobias, and M. L. Klein. 1995. Constant pressure and temperature molecular dynamics simulations of crystals of the lecithin fragments: Glycerylphosphorylcholine and dilauroylglycerol. *Journal of Physical Chemistry* 99:10035–10042.

[107] Shinoda, W., T. Fukada, S. Okazaki, and I. Okada. 1995. Molecular dynamics simulation of the dipalmitoylphosphatidylcholine (DPPC) lipid bilayer in the fluid-phase using the Nose-Parrinello-Rahman NPT ensemble. *Chemical Physics Letters* 232:308–312.

[108] Essman, U., L. Perera, M. L. Berkowitz, T. Darden, H. Lee, and L. G. Pedersen. 1995. A smooth particle mesh Ewald method. *Journal of Chemical Physics* 103:8577–8593.

[109] Tieleman, D. P., and H. J. C. Berendsen. 1996. Molecular dynamics simulations of a fully hydrated dipalmitoylphosphatidylcholine bilayer with different macroscopic boundary conditions and parameters. *Journal of Chemical Physics* 105:4871–4880.

[110] Berger, O., O. Edholm, and F. Jähnig. 1997. Molecular dynamics simulations of a fluid bilayer of dipalmitoylphosphatidylcholine at full hydration, constant pressure, and constant temperature. *Biophysical Journal* 72:2002–2013.

[111] Ceccarelli, M., and M. Marchi. 1998. Molecular dynamics simulation of POPC at low hydration near the liquid crystal phase transition. *Biochimie* 80:415–419.

[112] Feller, S. E., D. X. Yin, R. W. Pastor, and A. D. MacKerell. 1997. Molecular dynamics simulation of unsaturated lipid bilayers at low hydration: Parameterization and comparison with diffraction studies. *Biophysical Journal* 73:2269–2279.

[113] Chiu, S. W., E. Jakobsson, S. Subramaniam, and H. L. Scott. 1999. Combined monte carlo and molecular dynamics simulation of fully hydrated dioleyl and palmitoyl-oleyl phosphatidylcholine lipid bilayers. *Biophysical Journal* 77:2462–2469.

[114] Damodaran, K. V., and K. M. Merz. 1994. A comparison of DMPC- and DLPE-based lipid bilayers. *Biophysical Journal* 66:1076–1087.

[115] de Vries, A. H., A. E. Mark, and S. J. Marrink. 2004. The binary mixing behavior of phospholipids in a bilayer: A molecular dynamics study. *Journal of Physical Chemistry B* 108:2454–2463.

[116] Murzyn, K., T. Róg, and M. Pasenkiewicz-Gierula. 2005. Phosphatidylethanolamine-phosphatidylglycerol bilayer as a model of the inner bacterial membrane. *Biophysical Journal* 88:1091–1103.

[117] Pitman, M. C., A. Grossfield, F. Suits, and S. E. Feller. 2005. Role of cholesterol and polyunsaturated chains in lipid-protein interactions: Molecular dynamics simulation

of rhodopsin in a realistic membrane environment. *Journal of the American Chemical Society* 127:4576–7.

[118] Suits, F., M. C. Pitman, and S. E. Feller. 2005. Molecular dynamics investigation of the structural properties of phosphatidylethanolamine lipid bilayers. *Journal of Chemical Physics* 122:244714.

[119] Pitman, M. C., F. Suits, K. Gawrisch, and S. E. Feller. 2005. Molecular dynamics investigation of dynamical properties of phosphatidylethanolamine lipid bilayers. *Journal of Chemical Physics* 122:244715.

[120] Marrink, S. J., and A. E. Mark. 2004. Molecular view of hexagonal phase formation in phospholipid membranes. *Biophysical Journal* 87:3894–3900.

[121] Shi, Q., and G. A. Voth. 2005. Multi-scale modeling of phase separation in mixed lipid bilayers. *Biophysical Journal* 89:2385–2394.

[122] Crowe, J. H., L. M. Crowe, J. F. Carpenter, and C. A. Wistrom. 1987. Stabilization of dry phospholipid bilayers and proteins by sugars. *Biochemical Journal* 242:1–10.

[123] Crowe, J. H., L. M. Crowe, A. E. Oliver, N. Tsvetkova, W. Wolkers, and F. Tablin. 2001. The trehalose myth revisited: Introduction to a symposium on stabilization of cells in the dry state. *Cryobiology* 43:89–105.

[124] Madden, T. D., M. B. Bally, M. J. Hope, P. R. Cullis, H. P. Schieren, and A. S. Janoff. 1985. Protection of large unilamellar vesicles by trehalose during dehydration: Retention of vesicle contents. *Biochimica et Biophysica Acta-Biomembranes* 817:67–74.

[125] Womersley, C., P. S. Uster, A. S. Rudolph, and J. H. Crowe. 1986. Inhibition of dehydration-induced fusion between liposomal membranes by carbohydrates as measured by fluorescence energy transfer. *Cryobiology* 23:245–255.

[126] Crowe, J. H., L. M. Crowe, and D. Chapman. 1984. Preservation of membranes in anhydrobiotic organisms: The role of trehalose. *Science* 223:701–703.

[127] Hoekstra, F. A., W. F. Wolkers, J. Buitink, E. A. Golovina, J. H. Crowe, and L. M. Crowe. 1997. Membrane stabilization in the dry state. *Comparative Biochemistry and Physiology A: Physiology* 117:335–341.

[128] Arakawa, T., and S. N. Timasheff. 1985. The stabilization of proteins by osmolytes. *Biophysical Journal* 47:411–414.

[129] Schobert, B. 1977. Is there an osmotic regulatory mechanism in algae and higher plants? *Journal of Theoretical Biology* 68:17–26.

[130] Belton, P. S., and A. M. Gil. 1994. IR and Raman spectroscopic studies of the interaction of trehalose with hen egg white lysozyme. *Biopolymers* 34:957–961.

[131] Sun, W. Q., and A. C. Leopold. 1994. Glassy state and seed storage stability: A viability equation analysis. *Annals of Botany* 74:601–604.

[132] Cottone, G., G. Ciccotti, and L. Cordone. 2002. Protein-trehalose-water structures in trehalose coated carboxy-myoglobin. *Journal of Chemical Physics* 117:9862–9866.

[133] Lins, R. D., C. S. Pereira, and P. H. Hünenberger. 2004. Trehalose-protein interaction in aqueous solution. *Proteins* 55:177–186.

[134] Carpenter, J. F., S. J. Prestrelski, T. J. Anchordoguy, and T. Arakawa. 1994. Interactions of stabilizers with proteins during freezing and drying. *ACS Symposium Series* 567:134–147.

[135] Sun, W. Q., and A. C. Leopold. 1997. Cytoplasmic vitrification acid survival of anhydrobiotic organisms. *Comparative Biochemistry and Physiology A: Physiology* 117:327–333.

[136] Sun, W. Q., T. C. Irving, and A. C. Leopold. 1994. The role of sugar, vitrification and membrane phase transition in seed desiccation tolerance. *Physiologia Plantarum* 90:621–628.

[137] Sun, W. Q., A. C. Leopold, L. M. Crowe, and J. H. Crowe. 1996. Stability of dry liposomes in sugar glasses. *Biophysical Journal* 70:1769–1776.

[138] Williams, R. J., and A. C. Leopold. 1989. The glassy state in corn embryos. *Plant Physiology* 89:977–981.

[139] Clegg, J. S. 2001. Cryptobiosis-A peculiar state of biological organization. *Comparative Biochemistry and Physiology A: Biochemistry and Molecular Biology* 128:613–24.

[140] Crowe, L. M. 2002. Lessons from nature: The role of sugars in anhydrobiosis. *Comparative Biochemistry and Physiology A: Physiology* 131:505–13.

[141] Lee, C. W., J. S. Waugh, and R. G. Griffin. 1986. Solid-state NMR study of trehalose/1,2-dipalmitoyl-*sn*-phosphatidylcholine interactions. *Biochemistry* 25:3737–42.

[142] Luzardo, M. C., F. Amalfa, A. M. Nũnez, S. Díaz, A. C. B. de Lopez, and E. A. Disalvo. 2000. Effect of trehalose and sucrose on the hydration and dipole potential of lipid bilayers. *Biophysical Journal* 78:2452–8.

[143] Lambruschini, C., N. Relini, A. Ridi, L. Cordone, and A. Gliozzi. 2000. Trehalose interacts with phospholipid polar heads in Langmuir monolayers. *Langmuir* 16:5467–5470.

[144] Ohtake, S., C. Schebor, S. P. Palecek, and J. J. de Pablo. 2005. Phase behavior of freeze-dried phospholipid-cholesterol mixtures stabilized with trehalose. *Biochimica et Biophysica Acta-Biomembranes* 1713:57–64.

[145] Chandrasekhar, I., and B. P. Gaber. 1988. Stabilization of the bio-membrane by small molecules: Interaction of trehalose with the phospholipid bilayer. *Journal of Biomolecular Structure and Dynamics* 5:1163–1171.

[146] Rudolph, B. R., I. Chandrasekhar, B. P. Gaber, and M. Nagumo. 1990. Molecular modeling of saccharide-lipid interactions. *Chemistry and Physics of Lipids* 53:243–261.

[147] Sum, A. K., and J. J. de Pablo. 2003. Molecular simulation study on the influence of dimethylsulfoxide on the structure of phospholipid bilayers. *Biophysical Journal* 85:3636–3645.

[148] Pereira, C. S., R. D. Lins, I. Chandrasekhar, L. C. G. Freitas, and P. H. Hünenberger. 2004. Interaction of the disaccharide trehalose with a phospholipid bilayer: A molecular dynamics study. *Biophysical Journal* 86:2273–2285.

[149] Villarreal, M. A., S. B. Díaz, E. A. Disalvo, and G. G. Montich. 2004. Molecular dynamics simulation study of the interaction of trehalose with lipid membranes. *Langmuir* 20:7844–51.

[150] Doxastakis, M., A. K. Sum, and J. J. de Pablo. 2005. Modulating membrane properties: The effect of trehalose and cholesterol on a phospholipid bilayer. *Journal of Physical Chemistry B* 109:24173–81.

[151] Pereira, C. S., and P. H. Hunenberger. 2006. Interaction of the sugars trehalose, maltose and glucose with a phospholipid bilayer: A comparative molecular dynamics study. *Journal of Physical Chemistry B* 110:15572–81.

[152] Steponkus, P. L., and M. S. Webb. 1992. Freeze-induced dehydration and membrane destabilization in plants. In: G. N. Somero, C. B. Osmond, C. L. Bolis (eds.) Water and life: Comparative analysis of water relationships at the organismic, cellular, and molecular levels, Springer-Verlag, Berlin; Heidelberg; New York.

[153] Thilo, L., H. Trauble, and P. Overath. 1977. Mechanistic interpretation of influence of lipid phase-transitions on transport functions. *Biochemistry* 16:1283–1290.

[154] Welti, R., D. A. Rintoul, F. Goodsaid-Zalduondo, S. Felder, and D. F. Silbert. 1981. Gel phase phospholipid in the plasma membrane of sterol-depleted mouse LM cells. Analysis by fluorescence polarization and X-ray diffraction. *Journal of Biological Chemistry* 256:7528–35.

[155] Wolfe, J. 1987. Lateral stresses in membranes at low water potential. *Australian Journal of Plant Physiology* 14:311–318.

[156] Wolfe, J., and G. Bryant. 1999. Freezing, drying, and/or vitrification of membrane-solute-water systems. *Cryobiology* 39:103–129.

[157] Crowe, J. H., A. E. Oliver, and F. Tablin. 2002. Is there a single biochemical adaptation to anhydrobiosis? *Integrative and Comparative Biology* 42:497–503.

[158] Crowe, J. H., M. A. Whittam, D. Chapman, and L. M. Crowe. 1984. Interactions of phospholipid monolayers with carbohydrates. *Biochimica Et Biophysica Acta-Biomembranes* 769:151–159.

[159] Crowe, J. H., J. F. Carpenter, and L. M. Crowe. 1998. The role of vitrification in anhydrobiosis. *Annual Review of Physiology* 60:73–103.

[160] Koster, K. L., M. S. Webb, G. Bryant, and D. V. Lynch. 1994. Interactions between soluble sugars and popc (1-palmitoyl-2-oleoylphosphatidylcholine) during dehydration: Vitrification of sugars alters the phase-behavior of the phospholipid. *Biochimica Et Biophysica Acta-Biomembranes* 1193:143–150.

[161] Koster, K. L., Y. P. Lei, M. Anderson, S. Martin, and G. Bryant. 2000. Effects of vitrified and nonvitrified sugars on phosphatidylcholine fluid-to-gel phase transitions. *Biophysical Journal* 78:1932–1946.

[162] Koster, K. L., K. J. Maddocks, and G. Bryant. 2003. Exclusion of maltodextrins from phosphatidylcholine multilayers during dehydration: Effects on membrane phase behaviour. *European Biophysics Journal with Biophysics Letters* 32:96–105.

[163] Bryant, G., J. M. Pope, and J. Wolfe. 1992. Motional narrowing of the ^{2}H NMR spectra near the chain melting transition of phospholipid/D_2O mixtures. *European Biophysical Journal* 21:363–7.

[164] Skibinsky, A., R. M. Venable, and R. W. Pastor. 2005. A molecular dynamics study of the response of lipid bilayers and monolayers to trehalose. *Biophysical Journal* 89:4111–21.

[165] Doxastakis, M., V. G. Sakai, S. Ohtake, J. K. Maranas, and J. J. de Pablo. 2007. A molecular view of melting in anhydrous phospholipidic membranes. *Biophysical Journal* 92:147–161.

[166] Lenné, T., G. Bryant, R. Holcomb, and K. L. Koster. 2007. How much solute is needed to inhibit the fluid to gel membrane phase transition at low hydration? *Biochimica Et Biophysica Acta-Biomembranes* 1768:1019–1022.

[167] Hofsäβ, C., E. Lindahl, and O. Edholm. 2003. Molecular dynamics simulations of phospholipid bilayers with cholesterol. *Biophysical Journal* 84:2192–2206.

[168] Falck, E., M. Patra, M. Karttunen, M. T. Hyvonen, and I. Vattulainen. 2004. Lessons of slicing membranes: interplay of packing, free area, and lateral diffusion in phospholipid/cholesterol bilayers. *Biophysical Journal* 87:1076–91.

[169] Pandit, S. A., E. Jakobsson, and H. L. Scott. 2004. Simulation of the early stages of nano-domain formation in mixed bilayers of sphingomyelin, cholesterol, and dioleylphosphatidylcholine. *Biophysical Journal* 87:3312–3322.

[170] Suurkuusk, J., B. R. Lentz, Y. Barenholz, R. L. Biltonen, and T. E. Thompson. 1976. A calorimetric and fluorescent probe study of the gel-liquid crystalline phase transition in small, single-lamellar dipalmitoylphosphatidylcholine vesicles. *Biochemistry* 15:1393–401.

[171] Davis, J. H. 1979. Deuterium magnetic resonance study of the gel and liquid crystalline phases of dipalmitoyl phosphatidylcholine. *Biophysical Journal* 27:339–58.

[172] Nagle, J. F., and S. Tristram-Nagle. 2000. Structure of lipid bilayers. *Biochimica et Biophysica Acta-Reviews on Biomembranes* 1469:159–95.

[173] Metso, A. J., A. Jutila, J. P. Mattila, J. M. Holopainen, and P. K. J. Kinnunen. 2003. Nature of the main transition of dipahnitoylphosphocholine bilayers inferred from fluorescence spectroscopy. *Journal of Physical Chemistry B* 107:1251–1257.

[174] Barton, P. G., and F. D. Gunstone. 1975. Hydrocarbon chain packing and molecular motion in phospholipid bilayers formed from unsaturated lecithins: Synthesis and properties of sixteen positional isomers of 1,2-dioctadecenoyl-*sn*-glycero-3-phosphorylcholine. *Journal of Biological Chemistry* 250:4470–4476.

[175] Wang, Z. Q., H. N. Lin, S. S. Li, and C. H. Huang. 1994. Calorimetric studies and molecular mechanics simulations of monounsaturated phosphatidylethanolamine bilayers. *Journal of Biological Chemistry* 269:23491–23499.

[176] Huang, C. H., S. Li, H. N. Lin, and G. Q. Wang. 1996. On the bilayer phase transition temperatures for monoenoic phosphatidylcholines and phosphatidylethanolamines and the interconversion between them. *Archives of Biochemistry and Biophysics* 334:135–142.

[177] Shalaev, E. Y., and P. L. Steponkus. 2003. Glass transition of a synthetic phospholipid in the lamellar phase. *Journal of Physical Chemistry B* 107:8734–8737.

[178] Sengupta, K., V. A. Raghunathan, and J. Katsaras. 2003. Structure of the ripple phase of phospholipid multibilayers. *Physical Review E* 68:03171001–03171012.

[179] Mouritsen, O. G., A. Boothroyd, R. Harris, N. Jan, T. Lookman, L. MacDonald, D. A. Pink, and M. J. Zuckermann. 1983. Computer simulation of the main gel-fluid phase transition of lipid bilayers. *Journal of Chemical Physics* 79:2027–2041.

[180] Nielsen, M., L. Miao, J. H. Ipsen, M. J. Zuckermann, and O. G. Mouritsen. 1999. Off-lattice model for the phase behavior of lipid-cholesterol bilayers. *Physical Review E* 59:5790–5803.

[181] Polson, J. M., I. Vattulainen, H. Zhu, and H. Zuckermann. 2001. Simulation study of lateral diffusion in lipid-sterol bilayer mixtures. *European Physical Journal E* 5:485–497.

[182] Brannigan, G., A. C. Tamboli, and F. L. Brown. 2004. The role of molecular shape in bilayer elasticity and phase behavior. *Journal of Chemical Physics* 121:3259–71.

[183] Chen, L. B., M. L. Johnson, and R. L. Biltonen. 2001. A macroscopic description of lipid bilayer phase transitions of mixed-chain phosphatidylcholines: Chain-length and chain-asymmetry dependence. *Biophysical Journal* 80:254–270.

[184] Kranenburg, M., M. Venturoli, and B. Smit. 2003. Phase behavior and induced interdigitation in bilayers studied with dissipative particle dynamics. *Journal of Physical Chemistry B* 107:11491–11501.

[185] Heller, H., M. Schaefer, and K. Schulten. 1993. Molecular-dynamics simulation of a bilayer of 200 lipids in the gel and in the liquid-crystal phases. *Journal of Physical Chemistry* 97:8343–8360.

[186] Venable, R. M., B. R. Brooks, and R. W. Pastor. 2000. Molecular dynamics simulations of gel ($L_{\beta I}$) phase lipid bilayers in constant pressure and constant surface area ensembles. *Journal of Chemical Physics* 112:4822–4832.

[187] de Vries, A. H., S. Yefimov, A. E. Mark, and S. J. Marrink. 2005. Molecular structure of the lecithin ripple phase. *Proceedings of the National Academy of Sciences of the United States of America* 102:5392–6.

[188] Stevens, M. J. 2004. Coarse-grained simulations of lipid bilayers. *Journal of Chemical Physics* 121:11942–11948.

[189] Marrink, S. J., J. Risselada, and A. E. Mark. 2005. Simulation of gel phase formation and melting in lipid bilayers using a coarse grained model. *Chemistry and Physics of Lipids* 135:223–44.

[190] Marsh, D. 1999. Thermodynamic analysis of chain-melting transition temperatures for monounsaturated phospholipid membranes: Dependence on *cis*-monoenoic double bond position. *Biophysical Journal* 77:953–963.

[191] Clandinin, M. T., S. Cheema, C. J. Field, M. L. Garg, J. Venkatraman, and T. R. Clandinin. 1991. Dietary fat: Exogenous determination of membrane structure and cell function. *FASEB Journal* 5:2761–2769.

[192] Galli, C., and F. Marangoni. 1997. Recent advances in the biology of n-6 fatty acids. *Nutrition* 13:978–985.

[193] Yamashita, A., T. Sugiura, and K. Waku. 1997. Acyltransferases and transacylases involved in fatty acid remodeling of phospholipids and metabolism of bioactive lipids in mammalian cells. *Journal of Biochemistry-Tokyo* 122:1–16.

[194] Andrade, L. N., T. M. de Lima, R. Curi, and A. M. Castrucci. 2005. Toxicity of fatty acids on murine and human melanoma cell lines. *Toxicology In Vitro* 19:553–60.

[195] Lima, T. M., C. C. Kanunfre, C. Pompeia, R. Verlengia, and R. Curi. 2002. Ranking the toxicity of fatty acids on jurkat and raji cells by flow cytometric analysis. *Toxicology In Vitro* 16:741–747.

[196] Maedler, K., G. A. Spinas, D. Dyntar, W. Moritz, N. Kaiser, and M. Y. Donath. 2001. Distinct effects of saturated and monounsaturated fatty acids on beta-cell turnover and function. *Diabetes* 50:69–76.

[197] El-Assaad, W., J. Buteau, M. L. Peyot, C. Nolan, R. Roduit, S. Hardy, E. Joly, G. Dbaibo, L. Rosenberg, and M. Prentki. 2003. Saturated fatty acids synergize with elevated glucose to cause pancreatic β-cell death. *Endocrinology* 144:4154–63.

[198] Kong, J. Y., and S. W. Rabkin. 2000. Palmitate-induced apoptosis in cardiomyocytes is mediated through alterations in mitochondria: Prevention by cyclosporin A. *Biochimica et Biophysica Acta-Molecular and Cell Biology of Lipids* 1485:45–55.

[199] Sparagna, G. C., D. L. Hickson-Bick, L. M. Buja, and J. B. McMillin. 2000. A metabolic role for mitochondria in palmitate-induced cardiac myocyte apoptosis. *Am. J.Physiol-Heart C.* 279:H2124–H2132.

[200] Dashti, N., Q. Feng, and F. A. Franklin. 2000. Long-term effects of *cis* and *trans* monounsaturated (18:1) and saturated (16:0) fatty acids on the synthesis and secretion of apolipoprotein A-I- and apolipoprotein B-containing lipoproteins in HepG2 cells. *Journal of Lipid Research* 41:1980–1990.

[201] Ji, J., L. Zhang, P. Wang, Y. M. Mu, X. Y. Zhu, Y. Y. Wu, H. Yu, B. Zhang, S. M. Chen, and X. Z. Sun. 2005. Saturated free fatty acid, palmitic acid, induces apoptosis in fetal hepatocytes in culture. *Experimental and Toxicologic Pathology* 56:369–76.

[202] Srivastava, S., and C. Chan. 2007. Hydrogen peroxide and hydroxyl radicals mediate palmitate-induced cytotoxicity to hepatoma cells: Relation to mitochondrial permeability transition. *Free Radical Research* 41:38–49.

[203] Listenberger, L. L., X. Han, S. E. Lewis, S. Cases, J. Farese, R. V., D. S. Ory, and J. E. Schaffer. 2003. Triglyceride accumulation protects against fatty acid-induced lipotoxicity. *Proceedings of the National Academy of Sciences of the United States of America* 100:3077–82.

[204] Dobrzyn, A., and J. M. Ntambi. 2005. The role of stearoyl-CoA desaturase in the control of metabolism. *Prostaglandins Leukotrienes and Essential Fatty Acids* 73:35–41.

[205] Borradaile, N. M., X. Han, J. D. Harp, S. E. Gale, D. S. Ory, and J. E. Schaffer. 2006. Disruption of endoplasmic reticulum structure and integrity in lipotoxic cell death. *Journal of Lipid Research* 47:2726–37.

[206] Alexander, J. J., A. Snyder, and J. H. Tonsgard. 1998. Omega-oxidation of monocar-boxylic acids in rat brain. *Neurochemical Research* 23:227–33.

[207] Sanders, R. J., R. Ofman, F. Valianpour, S. Kemp, and R. J. Wanders. 2005. Evidence for two enzymatic pathways for omega-oxidation of docosanoic acid in rat liver microsomes. *Journal of Lipid Research* 46:1001–8.

[208] Listenberger, L. L., D. S. Ory, and J. E. Schaffer. 2001. Palmitate-induced apoptosis can occur through a ceramide-independent pathway. *Journal of Biological Chemistry* 276:14890–14895.

[209] Lu, Z.-H., Y.-M. Mu, B.-A. Wang, X.-L. Li, J.-M. Lu, J.-Y. Li, C.-Y. Pan, T. Yanase, and H. Nawata. 2003. Saturated free fatty acids, palmitic acid and stearic acid, induce apoptosis by stimulation of ceramide generation in rat testicular Leydig cell. *Biochemical and Biophysical Research Communications* 303:1002–1007.

[210] Goodman, D. S. 1958. The interaction of human erythrocytes with sodium palmitate. *Journal of Clinical Investigation* 37:1729–35.

[211] Spector, A. A. 1975. Fatty acid binding to plasma albumin. *Journal of Lipid Research* 16:165–79.

[212] Pande, S. V., and J. F. Mead. 1968. Inhibition of enzyme activities by free fatty acids. *Journal of Biological Chemistry* 243:6180–5.

[213] Reaven, P., S. Parthasarathy, B. J. Grasse, E. Miller, F. Almazan, F. H. Mattson, J. C. Khoo, D. Steinberg, and J. L. Witztum. 1991. Feasibility of using an oleate-rich diet to reduce the susceptibility of low-density lipoprotein to oxidative modification in humans. *American Journal of Clinical Nutrition* 54:701–6.

[214] Hart, C. M., M. P. Gupta, and V. Evanoff. 1997. Oleic acid reduces oxidant stress in cultured pulmonary artery endothelial cells. *Experimental Lung Research* 23:405–25.

[215] Toborek, M., Y. W. Lee, R. Garrido, S. Kaiser, and B. Hennig. 2002. Unsaturated fatty acids selectively induce an inflammatory environment in human endothelial cells. *American Journal of Clinical Nutrition* 75:119–25.

[216] Li, Z., S. Srivastava, S. Mittal, X. Yang, L. Sheng, and C. Chan. 2007. A three stage integrative pathway search (TIPS) framework to identify toxicity relevant genes and pathways. *BMC Bioinformatics* 8:202.

[217] Kinter, M., D. R. Spitz, and R. J. Roberts. 1996. Oleic acid incorporation protects cultured hamster fibroblasts from oxygen-induced cytotoxicity. *Journal of Nutrition* 126:2952–9.

[218] Natali, F., L. Siculella, S. Salvati, and G. V. Gnoni. 2007. Oleic acid is a potent inhibitor of fatty acid and cholesterol synthesis in C6 glioma cells. *Journal of Lipid Research* 48:1966–75.

[219] Crowe, J. H., L. M. Crowe, and S. A. Jackson. 1983. Preservation of structural and functional activity in lyophilized sarcoplasmic reticulum. *Archives of Biochemistry and Biophysic* 220:477–84.

[220] Leslie, S. B., E. Israeli, B. Lighthart, J. H. Crowe, and L. M. Crowe. 1995. Trehalose and sucrose protect both membranes and proteins in intact bacteria during drying. *Applied and Environmental Microbiology* 61:3592–7.

[221] Wolkers, W. F., N. J. Walker, F. Tablin, and J. H. Crowe. 2001. Human platelets loaded with trehalose survive freeze-drying. *Cryobiology* 42:79–87.

[222] Elbein, A. D., Y. T. Pan, I. Pastuszak, and D. Carroll. 2003. New insights on trehalose: A multifunctional molecule. *Glycobiology* 13:17r–27r.

[223] Chen, Q., and G. G. Haddad. 2004. Role of trehalose phosphate synthase and trehalose during hypoxia: From flies to mammals. *Journal Experimental Biology* 207:3125–9.

[224] Oku, K., M. Kurose, M. Kubota, S. Fukuda, M. Kurimoto, Y. Tujisaka, A. Okabe, and M. Sakurai. 2005. Combined NMR and quantum chemical studies on the interaction between trehalose and dienes relevant to the antioxidant function of trehalose. *Journal of Physical Chemistry B* 109:3032–40.

[225] Herdeiro, R. S., M. D. Pereira, A. D. Panek, and E. C. A. Eleutherio. 2006. Trehalose protects Saccharomyces cerevisiae from lipid peroxidation during oxidative stress. *Biochim Biophys Acta-General Subjects* 1760:340–346.

[226] Benaroudj, N., D. H. Lee, and A. L. Goldberg. 2001. Trehalose accumulation during cellular stress protects cells and cellular proteins from damage by oxygen radicals. *Journal of Biological Chemistry* 276:24261–7.

[227] Leekumjorn, S., and A. K. Sum. 2006. Molecular investigation of the interactions of trehalose with lipid bilayers of DPPC, DPPE and their mixture. *Molecular Simulation* 32:219–230.

[228] Sum, A. K., R. Faller, and J. J. de Pablo. 2003. Molecular simulation study of phospholipid bilayers and insights of the interactions with disaccharides. *Biophysical Journal* 85:2830–2844.

[229] Choi, Y. H., C. H. Yang, H. W. Kim, and S. H. Jung. 2000. Molecular dynamic simulations of the fatty acid bilayer containing very long chain transmembrane dicarboxylic acids. *Journal of Biochemistry and Molecular Biology* 33:54–58.

[230] Ulander, J., and A. D. J. Haymet. 2003. Permeation across hydrated dppc lipid bilayers: Simulation of the titrable amphiphilic drug valproic acid. *Biophysical Journal* 85:3475–3484.

[231] Knecht, V., A. E. Mark, and S. J. Marrink. 2006. Phase behavior of a phospholipid/fatty acid/water mixture studied in atomic detail. *Journal of the American Chemical Society* 128:2030–4.

[232] Saifer, A., and L. Goldman. 1961. The free fatty acids bound to human serum albumin. *Journal of Lipid Research* 2:268–270.

[233] Awad, A. B., and A. A. Spector. 1976. Modification of the fatty acid composition of Ehrlich ascites tumor cell plasma membranes. *Biochim Biophys Acta-Biomembranes* 426:723–31.

[234] Burns, C. P., D. G. Luttenegger, D. T. Dudley, G. R. Buettner, and A. A. Spector. 1979. Effect of modification of plasma membrane fatty acid composition on fluidity and methotrexate transport in L1210 murine leukemia cells. *Cancer Research* 39:1726–32.

[235] Sunamoto, J., Y. Baba, K. Iwamoto, and H. Kondo. 1985. Liposomal membranes. XX. Autoxidation of unsaturated fatty acids in liposomal membranes. *Biochimica Et Biophysica Acta* 833:144–50.

[236] Lee, C., J. Barnett, and P. D. Reaven. 1998. Liposomes enriched in oleic acid are less susceptible to oxidation and have less proinflammatory activity when exposed to oxidizing conditions. *Journal of Lipid Research* 39:1239–1247.

[237] Samuni, A. M., A. Lipman, and Y. Barenholz. 2000. Damage to liposomal lipids: Protection by antioxidants and cholesterol-mediated dehydration. *Chemistry and physics of lipids* 105:121–34.

[238] Watabe, N., Y. Ishida, A. Ochiai, Y. Tokuoka, and N. Kawashima. 2007. Oxidation decomposition of unsaturated fatty acids by singlet oxygen in phospholipid bilayer membranes. *Journal of Oleo Science* 56:73–80.

[239] Hyvönen, M. T., K. Oorni, P. T. Kovanen, and M. Ala-Korpela. 2001. Changes in a phospholipid bilayer induced by the hydrolysis of a phospholipase A(2) enzyme: A molecular dynamics simulation study. *Biophysical Journal* 80:565–578.

[240] Wong-Ekkabut, J., Z. T. Xu, W. Triampo, I. M. Tang, D. P. Tieleman, and L. Monticelli. 2007. Effect of lipid peroxidation on the properties of lipid bilayers: A molecular dynamics study. *Biophysical Journal* 93:4225–4236.

[241] Pastor, R. W. 1994. Molecular dynamics and monte carlo simulations of lipid bilayers. *Current Opinion in Structure Biology* 4:486–492.

[242] Xiang, T. X., and B. D. Anderson. 1995. Mean molecular potentials in a model lipid bilayer: A molecular dynamics simulation. *Journal of Chemical Physics* 103:8666–8678.

[243] Honig, B., and A. Nicholls. 1995. Classical electrostatics in biology and chemistry. *Science* 268:1144–9.

[244] Biggin, P. C., J. Breed, H. S. Son, and M. S. Sansom. 1997. Simulation studies of alamethicin-bilayer interactions. *Biophysical Journal* 72:627–36.

[245] Mouritsen, O. G., and K. Jorgensen. 1994. Dynamical order and disorder in lipid bilayers. *Chemistry and Physics of Lipids* 73:3–25.

[246] Mouritsen, O. G., B. Dammann, H. C. Fogedby, J. H. Ipsen, C. Jeppesen, K. Jorgensen, J. Risbo, M. C. Sabra, M. M. Sperotto, and M. J. Zuckermann. 1995. The computer as a laboratory for the physical chemistry of membranes. *Biophysical Chemistry* 55:55–68.

[247] van Gunsteren, W. F., and H. J. C. Berendsen. 1990. Computer simulation of molecular dynamics: Methodology, applications, and perspectives in chemistry. *Angewandte Chemie International Edition* 29:992–1023.

[248] Allen, M. P., and D. J. Tildesley. 1987. Computer Simulation of Liquids. Clarendon Press, Oxford.

[249] AMBER. Assisted Model Building with Energy Refinement. http://amber.scripps.edu.

[250] CHARMM. Chemistry at HARvard Macromolecular Mechanics. http://www.cha-rmm.org.

[251] GROMOS. GROningen MOlecular Simulation. http://www.igc.ethz.ch/gromos.

[252] GROMACS. GROningen MAchine for Chemical Simulations. http://www.gro-macs.org.

[253] NAMD. NAnoscale Molecular Dynamics. http://www.ks.uiuc.edu/Research/namd.

[254] Kox, A. J., J. P. J. Michels, and F. W. Wiegel. 1980. Simulation of a lipid monolayer using molecular dynamics. *Nature* 287:317–319.

[255] van der Ploeg, P., and H. J. C. Berendsen. 1982. Molecular dynamics simulation of a bilayer membrane. *Journal of Chemical Physics* 76:3271–3276.

[256] Jönsson, B., O. Edholm, and O. Teleman. 1986. Molecular dynamics simulations of a sodium octanoate micelle in aqueous solution. *Journal of Chemical Physics* 85:2259–2271.

[257] Egberts, E., and H. J. C. Berendsen. 1988. Molecular dynamics simulation of a smectic liquid crystal with atomic detail. *Journal of Chemical Physics* 89:3718–3732.

[258] Berendsen, H. J. C., D. van der Spoel, and R. van Drunen. 1995. GROMACS: A message-passing parallel molecular dynamics implementation. *Computer Physics Communications* 91:43–56.

[259] Lindahl, E., B. Hess, and D. van der Spoel. 2001. GROMACS 3.0: A package for molecular simulation and trajectory analysis. *Journal of Molecular Modeling* 7:306–317.

[260] Frenkel, D., and B. Smit. 2002. Understanding molecular simulation: From algorithms to applications. 2nd edition. Academic Press, San Diego.

[261] Verlet, L. 1967. Computer "experiments" on classical fluids. I. Thermodynamical properties of Lennard-Jones molecules. *Physical Review* 159:98–103.

[262] Allen, M. P., and D. J. Tildesley. 1989. Computer simulation of liquids. Oxford science publications, Clarendon Press; Oxford University Press, Oxford England; New York.

[263] Darden, T., D. York, and L. Pedersen. 1993. Particle mesh Ewald: An $N \cdot \log(N)$ method for Ewald sums in large systems. *Journal of Chemical Physics* 98:10089–10092.

[264] Kittel, C., and H. Kroemer. 2000. Thermal physics. 2nd edition. W.H. Freeman and Co., New York.

[265] Berendsen, H. J. C., J. P. M. Postma, W. F. van Gunsteren, A. DiNola, and J. R. Haak. 1984. Molecular dynamics with coupling to an external heat bath. *Journal of Chemical Physics* 81:3684–3690.

[266] van der Spoel, D., E. Lindahl, B. Hess, A. R. van Buuren, E. Apol, P. J. Meulenhoff, P. D. Tieleman, A. L. T. M. Sijbers, K. A. Feenstra, R. van Drunen, and H. J. C. Berendsen. 2004. GROMACS User Manuel: Version 3.2. 1st edition. Department of Biophysical Chemistry, Groningen, The Netherlands.

[267] Cramer, C. J. 2004. Essentials of computational chemistry: Theories and models. 2nd edition. Wiley, Chichester, West Sussex, England; Hoboken, NJ.

[268] Marrink, S. J., O. Berger, P. Tieleman, and F. Jähnig. 1998. Adhesion forces of lipids in a phospholipid membrane studied by molecular dynamics simulations. *Biophysical Journal* 74:931–943.

[269] Biocomputing at the University Of Calgary. Structures and Topologies of Lipid Molecules. http://moose.bio.ucalgary.ca/index.php?page=Structures_and_Topologies.

[270] van Gunsteren, W. F., S. R. Billeter, A. A. Eising, P. H. Hünenberger, P. Krüger, A. E. Mark, W. R. P. Scott, and I. G. Tironi. 1996. Biomolecular simulation: the

GROMOS96 manual and user guide. vdf Hochschuleverlag AG an der ETH Zürich, Zürich, Switzerland.

[271] Ryckaert, J. P., and A. Bellemans. 1975. Molecular dynamics of liquid *n*-butane near its boiling point. *Chemical Physics Letters* 30:123–125.

[272] Jorgensen, W. L., and J. Tirado-Rives. 1988. The OPLS potential function for proteins. Energy minimizations for crystals of cyclic peptides and crambin. *Journal of the American Chemical Society* 110:1657–1666.

[273] Berendsen, H. J. C., J. P. M. Postma, W. F. van Gunsteren, J. Hermans, and B. Pullman. 1981. Intermolecular Forces. Reidel, Dordrecht, The Netherlands.

[274] Hess, B., H. Bekker, H. J. C. Berendsen, and J. G. E. M. Fraaije. 1997. LINCS: A linear constraint solver for molecular simulations. *Journal of Computational Chemistry* 18:1463–1472.

[275] Miyamoto, S., and P. A. Kollman. 1992. SETTLE - An analytical version of the SHAKE and RATTLE algorithm for rigid water models. *Journal of Computational Chemistry* 13:952–962.

[276] Patra, M., M. Karttunen, M. T. Hyvönen, E. Falck, P. Lindqvist, and I. Vattulainen. 2003. Molecular dynamics simulations of lipid bilayers: Major artifacts due to truncating electrostatic interactions. *Biophysical Journal* 84:3636–3645.

[277] Norberg, J., and L. Nilsson. 2000. On the truncation of long-range electrostatic interactions in DNA. *Biophysical Journal* 79:1537–1553.

[278] Tobias, D. J. 2001. Electrostatics calculations: Recent methodological advances and applications to membranes. *Current Opinion in Structure Biology* 11:253–261.

[279] Faraldo-Gómez, J. D., G. R. Smith, and M. S. P. Sansom. 2002. Setting up and optimization of membrane protein simulations. *European Biophysical Journal* 31:217–227.

[280] Nina, M., and T. Simonson. 2002. Molecular dynamics of the tRNA^{Ala} acceptor stem: Comparison between continuum reaction field and particle-mesh Ewald electrostatic treatments. *Journal of Physical Chemistry B* 106:3696–3705.

[281] Virginia Tech. Terascale Computing Facility. http://www.tcf.vt.edu.

[282] Janiak, M. J., D. M. Small, and G. G. Shipley. 1976. Nature of the thermal pretransition of synthetic phospholipids: Dimyristolyl- and dipalmitoyllecithin. *Biochemistry* 15:4575–80.

[283] Petrache, H. I., S. W. Dodd, and M. F. Brown. 2000. Area per lipid and acyl length distributions in fluid phosphatidylcholines determined by ^{2}H NMR spectroscopy. *Biophysical Journal* 79:3172–3192.

[284] Patra, M., M. Karttunen, M. T. Hyvönen, E. Falck, and I. Vattulainen. 2004. Lipid bilayers driven to a wrong lane in molecular dynamics simulations by subtle changes in long-range electrostatic interactions. *Journal of Physical Chemistry B* 108:4485–4494.

[285] Brady, J. W., and R. K. Schmidt. 1993. The role of hydrogen bonding in carbohydrates: Molecular dynamics simulations of maltose in aqueous solution. *Journal of Physical Chemistry* 97:958–966.

[286] Gurtovenko, A. A., M. Patra, M. Karttunen, and I. Vattulainen. 2004. Cationic DMPC/DMTAP lipid bilayers: Molecular dynamics study. *Biophysical Journal* 86:3461–72.

[287] Ekdawi-Sever, N., J. J. de Pablo, E. Feick, and E. von Meerwall. 2003. Diffusion of sucrose and α,α-trehalose in aqueous solutions. *Journal of Physical Chemistry A* 107:936–943.

[288] Perera, L., U. Essmann, and M. L. Berkowitz. 1996. Role of water in the hydration force acting between lipid bilayers. *Langmuir* 12:2625–2629.

[289] Wennerström, H., and E. Sparr. 2003. Thermodynamics of membrane lipid hydration. *Pure and Applied Chemistry* 75:905–912.

[290] Yoshioka, S., Y. Aso, and S. Kojima. 2003. Prediction of glass transition temperature of freeze-dried formulations by molecular dynamics simulation. *Pharmaceutical Research* 20:873–8.

[291] Simperler, A., A. Kornherr, R. Chopra, P. A. Bonnet, W. Jones, W. D. Motherwell, and G. Zifferer. 2006. Glass transition temperature of glucose, sucrose, and trehalose: An experimental and in silico study. *Journal of Physical Chemistry B* 110:19678–84.

[292] Damm, W., A. Frontera, J. TiradoRives, and W. L. Jorgensen. 1997. OPLS all-atom force field for carbohydrates. *Journal of Computational Chemistry* 18:1955–1970.

[293] van Gunsteren, W. F., and H. J. C. Berendsen. 1987. Gromos-87 manual. Biomos BV, Nijenborgh 4, 9747, AG Groningen, The Netherlands.

[294] Anézo, C., A. H. de Vries, H. D. Höltje, D. P. Tieleman, and S. J. Marrink. 2003. Methodological issues in lipid bilayer simulations. *Journal of Physical Chemistry B* 107:9424–9433.

[295] Van der Spoel, D., E. Lindahl, B. Hess, G. Groenhof, A. E. Mark, and H. J. C. Berendsen. 2005. Gromacs: fast, flexible, and free. *Journal of Computational Chemistry* 26:1701–1718.

[296] Tieleman, D. P., and H. J. C. Berendsen. 1998. A molecular dynamics study of the pores formed by Escherichia coli OmpF porin in a fully hydrated palmitoyloleoylphosphatidylcholine bilayer. *Biophysical Journal* 74:2786–2801.

[297] Tieleman, D. P., L. R. Forrest, M. S. P. Sansom, and H. J. C. Berendsen. 1998. Lipid properties and the orientation of aromatic residues in OmpF, Influenza M2, and alamethicin systems: Molecular dynamics simulations. *Biochemistry* 37:17554–17561.

[298] Chen, T., J. P. Acker, A. Eroglu, S. Cheley, H. Bayley, A. Fowler, and M. L. Toner. 2001. Beneficial effect of intracellular trehalose on the membrane integrity of dried mammalian cells. *Cryobiology* 43:168–181.

[299] Yao, H., I. Hatta, R. Koynova, and B. Tenchov. 1992. Time-resolved X-ray diffraction and calorimetric studies at low scan rates. On the fine structure of the phase transitions in hydrated dipalmitoylphosphatidylethanolamine. *Biophysical Journal* 61:683–693.

[300] Ruocco, M. J., and G. G. Shipley. 1982. Characterization of the sub-transition of hydrated dipalmitoylphosphatidylcholine bilayers. X-ray diffraction study. *Biochimica et Biophysica Acta-Biomembranes* 684:59–66.

[301] Perly, B., I. C. P. Smith, and H. C. Jarrell. 1985. Acyl chain dynamics of phosphatidylethanolamines containing oleic acid and dihydrosterculic acid ^{2}H NMR relaxation studies. *Biochemistry* 24:4659–4665.

[302] Yellin, N., and I. W. Levin. 1977. Hydrocarbon chain *trans-gauche* isomerization in phospholipid bilayer gel assemblies. *Biochemistry* 16:642–647.

[303] Mason, J. T., C. Huang, and R. L. Biltonen. 1981. Calorimetric investigations of saturated mixed-chain phosphatidylcholine bilayer dispersions. *Biochemistry* 20:6086–92.

[304] Huang, C., J. T. Mason, and I. W. Levin. 1983. Raman spectroscopic study of saturated mixed-chain phosphatidylcholine multilamellar dispersions. *Biochemistry* 22:2775–80.

[305] Cirelli, N., P. Lebrun, C. Gueuning, J. Delogne-Desnoeck, A.-M. Vanbellinghen, G. Graff, and S. Meuris. 2001. Physiological concentrations of albumin stimulate chorionic gonadotrophin and placental lactogen release from human term placental explants. *Human Reproduction* :441–448.

[306] Boden, G., X. Chen, E. Capulong, and M. Mozzoli. 2001. Effects of free fatty acids on

gluconeogenesis and autoregulation of glucose production in type 2 diabetes. *Diabetes* 50:810–816.

[307] Mensink, M., E. E. Blaak, M. A. van Baak, A. J. Wagenmakers, and W. H. Saris. 2001. Plasma free fatty acid uptake and oxidation are already diminished in subjects at high risk for developing type 2 diabetes. *Diabetes* 50:2548–2554.

[308] Skowronski, R., C. B. Hollenbeck, B. B. Varasteh, Y. D. Chen, and G. M. Reaven. 1991. Regulation of non-esterified fatty acid and glycerol concentration by insulin in normal individuals and patients with type 2 diabetes. *Diabetic Medicine* 8:330–333.

[309] Woerle, H. J., E. Popa, J. Dostou, S. Welle, J. Gerich, and C. Meyer. 2002. Exogenous insulin replacement in type 2 diabetes reverses excessive hepatic glucose release, but not excessive renal glucose release and impaired free fatty acid clearance. *Metabolism* 51:1494–1500.

[310] Haak, R. A., L. M. Ingraham, R. L. Baehner, and L. A. Boxer. 1979. Membrane fluidity in human and mouse Chediak-Higashi leukocytes. *Journal of Clinical Investment* 64:138–44.

[311] Squier, T. C., D. J. Bigelow, and D. D. Thomas. 1988. Lipid fluidity directly modulates the overall protein rotational mobility of the Ca-ATPase in sarcoplasmic reticulum. *Journal of Biological Chemistry* 263:9178–86.

[312] Tsuda, K., Y. Kinoshita, K. Kimura, I. Nishio, and Y. Masuyama. 2001. Electron paramagnetic resonance investigation on modulatory effect of 17β-estradiol on membrane fluidity of erythrocytes in postmenopausal women. *Arteriosclerosis Thrombosis and Vascular Biology* 21:1306–12.

[313] Richieri, G. V., A. Anel, and A. M. Kleinfeld. 1993. Interactions of long-chain fatty acids and albumin: Determination of free fatty acid levels using the fluorescent probe ADIFAB. *Biochemistry* 32:7574–7580.

[314] Raz, A., and A. Livne. 1973. Differential effects of lipids on the osmotic fragility of erythrocytes. *Biochimica et Biophysica Acta-Biomembranes* 311:222–9.

[315] Massenburg, D., and B. R. Lentz. 1993. Poly(ethylene glycol)-induced fusion and rupture of dipalmitoylphosphatidylcholine large, unilamellar extruded vesicles. *Biochemistry* 32:9172–80.

[316] Burgess, S. W., D. Massenburg, J. Yates, and B. R. Lentz. 1991. Poly(ethylene glycol)-induced lipid mixing but not fusion between synthetic phosphatidylcholine large unilamellar vesicles. *Biochemistry* 30:4193–4200.

[317] Crowe, J. H., B. D. McKersie, and L. M. Crowe. 1989. Effects of free fatty acids and transition temperature on the stability of dry liposomes. *Biochimica et Biophysica Acta-Biomembranes* 979:7–10.

[318] Rudolph, A. S., and J. H. Crowe. 1985. Membrane stabilization during freezing: The role of two natural cryoprotectants, trehalose and proline. *Cryobiology* 22:367–77.

[319] Eliasz, A. W., D. Chapman, and D. F. Ewing. 1976. Phospholipid phase transitions. effects of n-alcohols, n-monocarboxylic acids, phenylalkyl alcohols and quaternary ammonium compounds. *Biochimica et Biophysica Acta-Biomembranes* 448:220–30.

[320] Mabrey, S., and J. M. Sturtevant. 1977. Incorporation of saturated fatty acids into phosphatidylcholine bilayers. *Biochimica et Biophysica Acta-Lipids and Lipid Metabolism* 486:444–50.

[321] Venable, R. M., A. Skibinsky, and R. W. Pastor. 2006. Constant surface tension molecular dynamics simulations of lipid bilayers with trehalose. *Molecular Simulation* 32:849–855.

[322] Edholm, O., and J. F. Nagle. 2005. Areas of molecules in membranes consisting of mixtures. *Biophysical Journal* 89:1827–1832.

[323] König, B., U. Dietrich, and G. Klose. 1997. Hydration and structural properties of mixed lipid/surfactant model membranes. *Langmuir* 13:525–532.

[324] Shinoda, W., and S. Okazaki. 1998. A Voronoi analysis of lipid area fluctuation in a bilayer. *Journal of Chemical Physics* 109:1517–1521.

[325] Smondyrev, A. M., and M. L. Berkowitz. 1999. Molecular dynamics simulation of DPPC bilayer in DMSO. *Biophysical Journal* 76:2472–2478.

[326] Chiu, S. W., E. Jakobsson, and H. L. Scott. 2001. Combined monte carlo and molecular dynamics simulation of hydrated lipid-cholesterol lipid bilayers at low cholesterol concentration. *Biophysical Journal* 80:1104–1114.

[327] Róg, T., and M. Pasenkiewicz-Gierula. 2006. Cholesterol effects on a mixed-chain phosphatidylcholine bilayer: A molecular dynamics simulation study. *Biochimie* 88:449–460.

[328] Cournia, Z., G. M. Ullman, and J. C. Smith. 2007. Differential effects of cholesterol, ergosterol and lanosterol on a dipalmitoyl phosphatidylcholine membrane: A molecular dynamics simulation study. *Journal of Physical Chemistry B* 111:1786–1801.

[329] Unger, R. H., and Y. T. Zhou. 2001. Lipotoxicity of β-cells in obesity and in other causes of fatty acid spillover. *Diabetes* 50 Suppl 1:S118–21.

[330] Girotti, A. W. 1998. Lipid hydroperoxide generation, turnover, and effector action in biological systems. *Journal of Lipid Research* 39:1529–1542.

[331] Aldini, G., P. Granata, M. Orioli, E. Santaniello, and M. Carini. 2003. Detoxification of 4-hydroxynonenal (HNE) in keratinocytes: Characterization of conjugated metabolites by liquid chromatography/electrospray ionization tandem mass spectrometry. *Journal of Mass Spectrometry* 38:1160–1168.

[332] Hoff, H. F., J. O'Neil, Z. P. Wu, G. Hoppe, and R. L. Salomon. 2003. Phospholipid hydroxyalkenals - biological and chemical properties of specific oxidized lipids present

in atherosclerotic lesions. *Arteriosclerosis, thrombosis, and vascular biology* 23:275–282.

[333] Reis, A., M. R. Domingues, F. M. Amado, A. J. Ferrer-Correia, and P. Domingues. 2005. Separation of peroxidation products of diacyl-phosphatidylcholines by reversed-phase liquid chromatography-mass spectrometry. *Biomedical Chromatography* 19:129–37.

[334] Chatterjee, S. N., and S. Agarwal. 1988. Liposomes as membrane model for study of lipid peroxidation. *Free radical biology & medicine* 4:51–72.

[335] Goldstein, R. M., and G. Weissmann. 1977. Effects of the generation of superoxide anion on permeability of liposomes. *Biochemical and Biophysical Research Communications* 75:604–9.

[336] Mandal, T. K., and S. N. Chatterjee. 1980. Ultraviolet- and sunlight-induced lipid peroxidation in liposomal membrane. *Radiation research* 83:290–302.

[337] Kunimoto, M., K. Inoue, and S. Nojima. 1981. Effect of ferrous ion and ascorbate-induced lipid peroxidation on liposomal membranes. *Biochimica Et Biophysica Acta* 646:169–78.

[338] Bachar, M., P. Brunelle, D. P. Tieleman, and A. Rauk. 2004. Molecular dynamics simulation of a polyunsaturated lipid bilayer susceptible to lipid peroxidation. *Journal of Physical Chemistry B* 108:7170–7179.

[339] Martinez-Seara, H., T. Róg, M. Pasenkiewicz-Gierula, I. Vattulainen, M. Karttunen, and R. Reigada. 2007. Effect of double bond position on lipid bilayer properties: Insight through atomistic simulations. *Journal of Physical Chemistry B* 111:11162–11168.

[340] Heyes, J., L. Palmer, K. Bremner, and I. MacLachlan. 2005. Cationic lipid saturation influences intracellular delivery of encapsulated nucleic acids. *Journal of Controlled Release* 107:276–287.

List of Appendices

A. **Force-Field**

B. **Analysis Codes**

C. **Additional Publications**

Appendix A

Force-Field

A.1 Force-Field File Formats

The GROMACS force-field format is explained in this section. A full list of force-field parameters are given in Section A.2.

A.1.1 Bonded Force-Field Formats

```
[ moleculetype ]
; Name    nrexcl
  DPPC        3
```

This section contains the name of the molecule "`Name`" and the number of exclusion "`nrexcl`". The name "`DPPC`" must be consistent with the parameter listed in the .mdp file (see Section A.3 for more details). The number of exclusions indicates the number of bonded atoms to be excluded in the non-bonded interaction calculations. By specifying "`3`", the atoms within the same molecule that are separated by four or more bonds will have non-bonded interactions (excluding those interactions that are accounted by the bond, angle, and dihedral).

```
[atoms]
;nr  type  resnr  residu  atom  cgnr  charge
  1  LC3N      1   DPPC    C1     1     0.40
```

This section lists the atom number "`nr`", atom type "`type`", residue number "`resnr`", residue identification "`residu`", atom type "`atom`", charge group "`cgnr`", and partial atomic charge "`charge`". The atom number "1" indicates the atom number of a molecule. The atom type "`LC3N`" is a variable that link the bonded and non-bonded parameters to this particular atom. The residue number "1" refers to the residue number, usually "1" is used for each molecule. The residue identification "`DPPC`" and atom type "`C1`" identify the molecule and molecule type during calculation. The charge group "1" indicate the first set of atoms within a molecule with the combine net charge that is integer (e.g. -1, 0, 1). "0.40" indicate the partial atomic charge of this particular atom within this charge group.

```
[ bonds ]
;ai  aj  fun     l0      kl
  1   2   1   0.1529  224420
```

Bonds between atoms are defined by specifying the bonded atom numbers ("`ai`" and "`aj`"), the bond function "`fu`", the bond length "`l0`", and the bond force constant "`kl`". For this entry, atoms "1" and "2" are bonded by a harmonic bond potential ("`fu`" = 1) with a bond length of "0.1529" nm and a force constant of "224420" kJ/mol. For consistency, the bond length "`l0`" and the bond force constant "`kl`" are usually listed in a separate section if a similar pair interaction is used multiple times (see Appendix A.1.2).

```
[ pairs ]
;ai  aj  fun           c6             c12
  1   6   1   1.0324742e-03  3.5181067e-06
```

Extra Lennard-Jones and electrostatic interactions between pairs of atoms in a molecule is required in selected molecule. In this case, pair interactions are explicitly listed with the specified function. Here, the atoms "1" and "6" are separated by three bonds and are considered for 1,4 pair interactions. A function of "1" indicates that these interactions are scaled according to the fudge factors defined in the head force-field file (see later section).

```
[ angles ]
;ai  aj  ak  fun     a0       ka
  1   2   3    1   112.7   488.60
```

Like bonds, angles are defined by listing the three atoms ("`ai`", "`aj`", and "`ak`") involved in the angle (`1 2 3`), the angle function "`fu`", the angle "`a0`", and the force constant "`ka`". For this entry a harmonic potential is used ("`fu`" = 1) with an angle of "112.7" degrees and a force constant of "488.60" kJ/mol. For consistency, the angle "`a0`" and the force constant "`ka`" are usually listed in a separate section if a similar pair interaction is used multiple times (see Appendix A.1.2).

```
[ dihedrals ]
; torsion
;ai  aj  ak  al  fu     phi0      cp      mult
  1   4   5   6   1        0   3.766         3
; improper dihedral
;ai  aj  ak  al  fu     phi0      cp      mult
 13  14  32  12   2   35.264   34.72
; Ryckaert-Bellemans
;ai  aj  ak  al  fu      c0       c1       c2       c3       c4       c5
 17  18  19  20   3   9.2789   12.156  -13.120  -3.0597   26.240  -31.495
```

Dihedrals are categorized as torsion, improper dihedral, and Ryckaert-Bellemans (see Chapter 3 for more details), where four atoms are listed ("`ai`", "`aj`", "`ak`", and "`al`") and the type

of dihedral is specified by the functions number "`fu`". Function "`1`" is a torsion potential, "`2`" is an improper dihedral, and "`3`" is a Ryckaert-Bellemans potential. Three parameters are required for torsion potential "`phi0`", "`cp`", "`mult`' (periodic potential); two parameters are required for improper dihedral potential "`phi0`", "`cp`" (harmonic potential); and six parameters are required for Ryckaert-Bellemans potential "`c0`"-"`c5`" (6 parameters periodic potential).

A.1.2   Non-bonded Force-Field Formats

```
[ atomtypes ]
;name      mass  charge  ptype          c6          c12
   OW  15.99940  0.000       A  0.26171E-02  0.26331E-05
```

Non-bonded parameters are included in a separate file, where parameters for all atoms in a simulation are listed. The "`name`" corresponds to the "`atomtype`" listed in the [`atoms`] section of the bonded force-field parameters. The "`mass`" of the atom is listed here and the "`charge`" is redundant and not required in this section (see previous section). The "`ptype`" indicates that the listing parameters is an atom "`A`". The "`c6`" and "`c12`" entries are the values for the Lennard-Jones potential in kJ/mol. "`c6`" and "`c12`" can be calculated from σ and ϵ using the relationship "`c6`" $= 4\epsilon_{i,j}(\sigma_{i,j})^6$ and "`c12`" $= 4\epsilon_{i,j}(\sigma_{i,j})^{12}$.

Although this section is dedicated for non-bonded parameters, [`bondtypes`] and [`angletypes`] for different atoms in a molecule (also with molecules that have identical atom types) are listed here for to reduce redundancy.

```
[ bondtypes ]
;  ai    aj    fun     l0        kl
  LNL   LC3N     1   0.147    376560

[ angletypes ]
```

```
;  ai    aj    ak  fun    a0      ka
 LC3N   LNL  LC3N    1  109.5  334.72
```

The details are given in the previous sections for [bond] and [angle] . The only different is that the atom number is replaced by atom type which was previously defined in [moleculetype] section.

A.2 Force-Field Parameters

The following sections are listed of force-field parameters for DPPC, DPPE, POPC, POPE, water, and trehalose. The last section is the combined non-bonded parameters.

A.2.1 DPPC

```
[ moleculetype ]
;Name      nrexcl
DPPC        3

[atoms]
;nr  type  resnr  residu  atom  cgnr  charge
  1  LC3N    1    DPPC    C1     1    0.40
  2  LC3N    1    DPPC    C2     1    0.40
  3  LC3N    1    DPPC    C3     1    0.40
  4   LNL    1    DPPC    N4     1   -0.50
  5   LC2    1    DPPC    C5     1    0.30
  6  LC2O    1    DPPC    C6     2    0.40
  7   LOS    1    DPPC    O7     2   -0.80
  8    LP    1    DPPC    P8     2    1.70
  9   LOM    1    DPPC    O9     2   -0.80
 10   LOM    1    DPPC    O10    2   -0.80
 11   LOS    1    DPPC    O11    2   -0.70
 12  LC2O    1    DPPC    C12    3    0.40
 13  LCH1    1    DPPC    C13    3    0.30
 14   LOS    1    DPPC    O14    3   -0.70
 15    LC    1    DPPC    C15    3    0.70
 16   LO2    1    DPPC    O16    3   -0.70
 17  LCH2    1    DPPC    C17    4    0.0
 18  LCH2    1    DPPC    C18    5    0.0
 19  LCH2    1    DPPC    C19    6    0.0
 20  LCH2    1    DPPC    C20    7    0.0
 21  LCH2    1    DPPC    C21    8    0.0
 22  LCH2    1    DPPC    C22    9    0.0
 23  LCH2    1    DPPC    C23   10    0.0
 24  LCH2    1    DPPC    C24   11    0.0
 25  LCH2    1    DPPC    C25   12    0.0
 26  LCH2    1    DPPC    C26   13    0.0
 27  LCH2    1    DPPC    C27   14    0.0
 28  LCH2    1    DPPC    C28   15    0.0
 29  LCH2    1    DPPC    C29   16    0.0
 30  LCH2    1    DPPC    C30   17    0.0
 31  LCH3    1    DPPC    C31   18    0.0
 32  LC2O    1    DPPC    C32   19    0.50
 33   LOS    1    DPPC    O33   19   -0.70
 34    LC    1    DPPC    C34   19    0.80
 35   LO2    1    DPPC    O35   19   -0.60
 36  LCH2    1    DPPC    C36   20    0.0
 37  LCH2    1    DPPC    C37   21    0.0
 38  LCH2    1    DPPC    C38   22    0.0
 39  LCH2    1    DPPC    C39   23    0.0
 40  LCH2    1    DPPC    C40   24    0.0
 41  LCH2    1    DPPC    C41   25    0.0
 42  LCH2    1    DPPC    C42   26    0.0
 43  LCH2    1    DPPC    C43   27    0.0
 44  LCH2    1    DPPC    C44   28    0.0
 45  LCH2    1    DPPC    C45   29    0.0
 46  LCH2    1    DPPC    C46   30    0.0
 47  LCH2    1    DPPC    C47   31    0.0
 48  LCH2    1    DPPC    C48   32    0.0
 49  LCH2    1    DPPC    C49   33    0.0
 50  LCH3    1    DPPC    C50   34    0.0

[bonds]
```

```
;ai  aj  fun    l0      kl
  1   4   1
  2   4   1
  3   4   1
  4   5   1
  5   6   1
  6   7   1
  7   8   1
  8   9   1
  8  10   1
  8  11   1
 11  12   1
 12  13   1
 13  14   1
 13  32   1
 14  15   1
 15  16   1
 15  17   1
 17  18   1
 18  19   1
 19  20   1
 20  21   1
 21  22   1
 22  23   1
 23  24   1
 24  25   1
 25  26   1
 26  27   1
 27  28   1
 28  29   1
 29  30   1
 30  31   1
 32  33   1
 33  34   1
 34  35   1
 34  36   1
 36  37   1
 37  38   1
 38  39   1
 39  40   1
 40  41   1
 41  42   1
 42  43   1
 43  44   1
 44  45   1
 45  46   1
 46  47   1
 47  48   1
 48  49   1
 49  50   1

[ pairs ]
;ai  aj  fun          c6              c12
  1   6   1  1.0324742e-03  3.5181067e-06
  2   6   1  1.0324742e-03  3.5181067e-06
  3   6   1  1.0324742e-03  3.5181067e-06
  4   7   1  3.2949910e-04  3.0539735e-07
  5   8   1  1.1086361e-03  3.4535341e-06
```

```
  6   9   1  5.1901029e-04  7.3857637e-07
  6  10   1  5.1901029e-04  7.3857637e-07
  6  11   1  4.8624808e-04  7.2038415e-07
  7  12   1  4.8624808e-04  7.2038415e-07
  8  13   1  7.5842381e-04  2.1771004e-06
  9  12   1  5.1901029e-04  7.3857637e-07
 10  12   1  5.1901029e-04  7.3857637e-07
 11  14   1  2.5916250e-04  1.8892500e-07
 11  32   1  4.8624808e-04  7.2038415e-07
 12  15   1  7.4539997e-04  2.1568903e-06
 12  33   1  4.8624808e-04  7.2038415e-07
 13  16   1  3.2011832e-04  1.4405955e-06
 13  17   1  6.0697598e-04  2.0682859e-06
 13  34   1  5.5338320e-04  1.6012958e-06
 14  18   1  4.3576181e-04  7.3062136e-07
 14  33   1  2.5916250e-04  1.8892500e-07
 15  19   1  6.6800642e-04  2.1875414e-06
 15  32   1  7.4539997e-04  2.1568903e-06
 16  18   1  3.8642497e-04  1.9680076e-06
 32  35   1  4.3119519e-04  1.9404326e-06
 32  36   1  8.1758876e-04  2.7859100e-06
 33  37   1  4.3576181e-04  7.3062136e-07
 34  38   1  6.6800642e-04  2.1875414e-06
 35  37   1  3.8642497e-04  1.9680076e-06

[ angles ]
;ai  aj  ak  fun    a0      ka
  1   4   2   1
  1   4   3   1
  1   4   5   1
  2   4   3   1
  2   4   5   1
  3   4   5   1
  4   5   6   1
  5   6   7   1
  6   7   8   1
  7   8   9   1
  7   8  10   1
  7   8  11   1
  8  11  12   1
  9   8  10   1
  9   8  11   1
 10   8  11   1
 11  12  13   1
 12  13  14   1
 12  13  32   1
 13  14  15   1
 13  32  33   1
 14  13  32   1
 14  15  16   1
 14  15  17   1
 15  17  18   1
 16  15  17   1
 17  18  19   1
 18  19  20   1
 19  20  21   1
 20  21  22   1
 21  22  23   1
```

```
22  23  24   1
23  24  25   1
24  25  26   1
25  26  27   1
26  27  28   1
27  28  29   1
28  29  30   1
29  30  31   1
32  33  34   1
33  34  35   1
33  34  36   1
34  36  37   1
35  34  36   1
36  37  38   1
37  38  39   1
38  39  40   1
39  40  41   1
40  41  42   1
41  42  43   1
42  43  44   1
43  44  45   1
44  45  46   1
45  46  47   1
46  47  48   1
47  48  49   1
48  49  50   1

[ dihedrals ]

;ai aj  ak  al  fu    phi0    cp    mult
 1   4   5   6   1       0   3.766      3
 4   5   6   7   1       0   5.858      3
 5   6   7   8   1       0   3.766      3
 6   7   8  11   1       0   1.046      3
 6   7   8  11   1       0   3.138      2
 7   8  11  12   1       0   1.046      3
 7   8  11  12   1       0   3.138      2
 8  11  12  13   1       0   3.766      3
11  12  13  14   1       0   2.092      2
11  12  13  32   1       0   5.858      3
11  12  13  32   1       0   0.418      2
12  13  32  33   1       0   5.858      3
12  13  32  33   1       0   0.418      2
```

```
12  13  14  15   1       0   3.766      3
13  32  33  34   1       0   3.766      3
13  14  15  17   1     180  16.736      2
14  13  32  33   1       0   2.092      2
14  15  17  18   1       0   0.418      6
15  17  18  19   1       0   5.858      3
17  18  19  20   3  9.2789 12.156 -13.120 -3.0597 26.240 -31.495
18  19  20  21   3  9.2789 12.156 -13.120 -3.0597 26.240 -31.495
19  20  21  22   3  9.2789 12.156 -13.120 -3.0597 26.240 -31.495
20  21  22  23   3  9.2789 12.156 -13.120 -3.0597 26.240 -31.495
21  22  23  24   3  9.2789 12.156 -13.120 -3.0597 26.240 -31.495
22  23  24  25   3  9.2789 12.156 -13.120 -3.0597 26.240 -31.495
23  24  25  26   3  9.2789 12.156 -13.120 -3.0597 26.240 -31.495
24  25  26  27   3  9.2789 12.156 -13.120 -3.0597 26.240 -31.495
25  26  27  28   3  9.2789 12.156 -13.120 -3.0597 26.240 -31.495
26  27  28  29   3  9.2789 12.156 -13.120 -3.0597 26.240 -31.495
27  28  29  30   3  9.2789 12.156 -13.120 -3.0597 26.240 -31.495
28  29  30  31   3  9.2789 12.156 -13.120 -3.0597 26.240 -31.495
13  32  33  34   1       0   3.766      3
32  33  34  36   1     180  16.736      2
33  34  36  37   1       0   0.418      6
34  36  37  38   1       0   5.858      3
36  37  38  39   3  9.2789 12.156 -13.120 -3.0597 26.240 -31.495
37  38  39  40   3  9.2789 12.156 -13.120 -3.0597 26.240 -31.495
38  39  40  41   3  9.2789 12.156 -13.120 -3.0597 26.240 -31.495
39  40  41  42   3  9.2789 12.156 -13.120 -3.0597 26.240 -31.495
40  41  42  43   3  9.2789 12.156 -13.120 -3.0597 26.240 -31.495
41  42  43  44   3  9.2789 12.156 -13.120 -3.0597 26.240 -31.495
42  43  44  45   3  9.2789 12.156 -13.120 -3.0597 26.240 -31.495
43  44  45  46   3  9.2789 12.156 -13.120 -3.0597 26.240 -31.495
44  45  46  47   3  9.2789 12.156 -13.120 -3.0597 26.240 -31.495
45  46  47  48   3  9.2789 12.156 -13.120 -3.0597 26.240 -31.495
46  47  48  49   3  9.2789 12.156 -13.120 -3.0597 26.240 -31.495
47  48  49  50   3  9.2789 12.156 -13.120 -3.0597 26.240 -31.495

[ dihedrals ]
;ai aj  ak  al  fu    phi0    cp    mult
13  14  32  12   2  35.264  34.72
15  14  17  16   2       0 167.36
34  33  36  35   2       0 167.36
```

A.2.2   DPPE

```
[ moleculetype ]
;Name        nrexcl
DPPE          3

[atoms]
;nr  type resnr residu atom cgnr charge
 1  LH3N    1   DPPE   H1    1    0.40
 2  LH3N    1   DPPE   H2    1    0.40
 3  LH3N    1   DPPE   H3    1    0.40
 4  LNL     1   DPPE   N4E   1   -0.50
```

```
 5  LC2     1   DPPE   C5E   1    0.30
 6  LC2O    1   DPPE   C6E   2    0.40
 7  LOS     1   DPPE   O7E   2   -0.80
 8  LP      1   DPPE   P8E   2    1.70
 9  LOM     1   DPPE   O9E   2   -0.80
10  LOM     1   DPPE   O10E  2   -0.80
11  LOS     1   DPPE   O11E  2   -0.70
12  LC2O    1   DPPE   C12E  3    0.40
13  LCH1    1   DPPE   C13E  3    0.30
14  LOS     1   DPPE   O14E  3   -0.70
```

```
15   LC    1   DPPE  C15E   3    0.70
16   LO2   1   DPPE  O16E   3   -0.70
17   LCH2  1   DPPE  C17E   4    0.0
18   LCH2  1   DPPE  C18E   5    0.0
19   LCH2  1   DPPE  C19E   6    0.0
20   LCH2  1   DPPE  C20E   7    0.0
21   LCH2  1   DPPE  C21E   8    0.0
22   LCH2  1   DPPE  C22E   9    0.0
23   LCH2  1   DPPE  C23E  10    0.0
24   LCH2  1   DPPE  C24E  11    0.0
25   LCH2  1   DPPE  C25E  12    0.0
26   LCH2  1   DPPE  C26E  13    0.0
27   LCH2  1   DPPE  C27E  14    0.0
28   LCH2  1   DPPE  C28E  15    0.0
29   LCH2  1   DPPE  C29E  16    0.0
30   LCH2  1   DPPE  C30E  17    0.0
31   LCH3  1   DPPE  C31E  18    0.0
32   LC2O  1   DPPE  C32E  19    0.50
33   LOS   1   DPPE  O33E  19   -0.70
34   LC    1   DPPE  C34E  19    0.80
35   LO2   1   DPPE  O35E  19   -0.60
36   LCH2  1   DPPE  C36E  20    0.0
37   LCH2  1   DPPE  C37E  21    0.0
38   LCH2  1   DPPE  C38E  22    0.0
39   LCH2  1   DPPE  C39E  23    0.0
40   LCH2  1   DPPE  C40E  24    0.0
41   LCH2  1   DPPE  C41E  25    0.0
42   LCH2  1   DPPE  C42E  26    0.0
43   LCH2  1   DPPE  C43E  27    0.0
44   LCH2  1   DPPE  C44E  28    0.0
45   LCH2  1   DPPE  C45E  29    0.0
46   LCH2  1   DPPE  C46E  30    0.0
47   LCH2  1   DPPE  C47E  31    0.0
48   LCH2  1   DPPE  C48E  32    0.0
49   LCH2  1   DPPE  C49E  33    0.0
50   LCH3  1   DPPE  C50E  34    0.0

[bonds]
;ai  aj  fun    l0    kl
  1   4   1
  2   4   1
  3   4   1
  4   5   1
  5   6   1
  6   7   1
  7   8   1
  8   9   1
  8  10   1
  8  11   1
 11  12   1
 12  13   1
 13  14   1
 13  32   1
 14  15   1
 15  16   1
 15  17   1
 17  18   1
 18  19   1
```

```
19  20   1
20  21   1
21  22   1
22  23   1
23  24   1
24  25   1
25  26   1
26  27   1
27  28   1
28  29   1
29  30   1
30  31   1
32  33   1
33  34   1
34  35   1
34  36   1
36  37   1
37  38   1
38  39   1
39  40   1
40  41   1
41  42   1
42  43   1
43  44   1
44  45   1
45  46   1
46  47   1
47  48   1
48  49   1
49  50   1


[ pairs ]
;ai  aj  fun         c6           c12
  4   7   1  3.2949910e-04  3.0539735e-07
  5   8   1  1.1086361e-03  3.4535341e-06
  6   9   1  5.1901029e-04  7.3857637e-07
  6  10   1  5.1901029e-04  7.3857637e-07
  6  11   1  4.8624808e-04  7.2038415e-07
  7  12   1  4.8624808e-04  7.2038415e-07
  8  13   1  7.5842381e-04  2.1771004e-06
  9  12   1  5.1901029e-04  7.3857637e-07
 10  12   1  5.1901029e-04  7.3857637e-07
 11  14   1  2.5916250e-04  1.8892500e-07
 11  32   1  4.8624808e-04  7.2038415e-07
 12  15   1  7.4539997e-04  2.1568903e-06
 12  33   1  4.8624808e-04  7.2038415e-07
 13  16   1  3.2011832e-04  1.4405955e-06
 13  17   1  6.0697598e-04  2.0682859e-06
 13  34   1  5.5338320e-04  1.6012958e-06
 14  18   1  4.3576181e-04  7.3062136e-07
 14  33   1  2.5916250e-04  1.8892500e-07
 15  19   1  6.6800642e-04  2.1875414e-06
 15  32   1  7.4539997e-04  2.1568903e-06
 16  18   1  3.8642497e-04  1.9680076e-06
 32  35   1  4.3119519e-04  1.9404326e-06
 32  36   1  8.1758876e-04  2.7859100e-06
 33  37   1  4.3576181e-04  7.3062136e-07
 34  38   1  6.6800642e-04  2.1875414e-06
```

```
 35  37    1 3.8642497e-04  1.9680076e-06

[ angles ]
;ai aj ak fun    a0     ka
  1  4  2   1
  1  4  3   1
  1  4  5   1
  2  4  3   1
  2  4  5   1
  3  4  5   1
  4  5  6   1
  5  6  7   1
  6  7  8   1
  7  8  9   1
  7  8 10   1
  7  8 11   1
  8 11 12   1
  9  8 10   1
  9  8 11   1
 10  8 11   1
 11 12 13   1
 12 13 14   1
 12 13 32   1
 13 14 15   1
 13 32 33   1
 14 13 32   1
 14 15 16   1
 14 15 17   1
 15 17 18   1
 16 15 17   1
 17 18 19   1
 18 19 20   1
 19 20 21   1
 20 21 22   1
 21 22 23   1
 22 23 24   1
 23 24 25   1
 24 25 26   1
 25 26 27   1
 26 27 28   1
 27 28 29   1
 28 29 30   1
 29 30 31   1
 32 33 34   1
 33 34 35   1
 33 34 36   1
 34 36 37   1
 35 34 36   1
 36 37 38   1
 37 38 39   1
 38 39 40   1
 39 40 41   1
 40 41 42   1
 41 42 43   1
 42 43 44   1
 43 44 45   1
 44 45 46   1
 45 46 47   1
 46 47 48   1
```

```
 47  48  49    1
 48  49  50    1

[ dihedrals ]
;ai aj ak al fu   phi0    cp    mult
  1  4  5  6  1     0  3.766      3
  4  5  6  7  1     0  5.858      3
  5  6  7  8  1     0  3.766      3
  6  7  8 11  1     0  1.046      3
  6  7  8 11  1     0  3.138      2
  7  8 11 12  1     0  1.046      3
  7  8 11 12  1     0  3.138      2
  8 11 12 13  1     0  3.766      3
 11 12 13 14  1     0  2.092      2
 11 12 13 32  1     0  5.858      3
 11 12 13 32  1     0  0.418      2
 12 13 32 33  1     0  5.858      3
 12 13 32 33  1     0  0.418      2
 12 13 14 15  1     0  3.766      3
 13 32 33 34  1     0  3.766      3
 13 14 15 17  1   180 16.736      2
 14 13 32 33  1     0  2.092      2
 14 15 17 18  1     0  0.418      6
 15 17 18 19  1     0  5.858      3
 17 18 19 20  3 9.2789 12.156 -13.120 -3.0597 26.240 -31.495
 18 19 20 21  3 9.2789 12.156 -13.120 -3.0597 26.240 -31.495
 19 20 21 22  3 9.2789 12.156 -13.120 -3.0597 26.240 -31.495
 20 21 22 23  3 9.2789 12.156 -13.120 -3.0597 26.240 -31.495
 21 22 23 24  3 9.2789 12.156 -13.120 -3.0597 26.240 -31.495
 22 23 24 25  3 9.2789 12.156 -13.120 -3.0597 26.240 -31.495
 23 24 25 26  3 9.2789 12.156 -13.120 -3.0597 26.240 -31.495
 24 25 26 27  3 9.2789 12.156 -13.120 -3.0597 26.240 -31.495
 25 26 27 28  3 9.2789 12.156 -13.120 -3.0597 26.240 -31.495
 26 27 28 29  3 9.2789 12.156 -13.120 -3.0597 26.240 -31.495
 27 28 29 30  3 9.2789 12.156 -13.120 -3.0597 26.240 -31.495
 28 29 30 31  3 9.2789 12.156 -13.120 -3.0597 26.240 -31.495
 13 32 33 34  1     0  3.766      3
 32 33 34 36  1   180 16.736      2
 33 34 36 37  1     0  0.418      6
 34 36 37 38  1     0  5.858      3
 36 37 38 39  3 9.2789 12.156 -13.120 -3.0597 26.240 -31.495
 37 38 39 40  3 9.2789 12.156 -13.120 -3.0597 26.240 -31.495
 38 39 40 41  3 9.2789 12.156 -13.120 -3.0597 26.240 -31.495
 39 40 41 42  3 9.2789 12.156 -13.120 -3.0597 26.240 -31.495
 40 41 42 43  3 9.2789 12.156 -13.120 -3.0597 26.240 -31.495
 41 42 43 44  3 9.2789 12.156 -13.120 -3.0597 26.240 -31.495
 42 43 44 45  3 9.2789 12.156 -13.120 -3.0597 26.240 -31.495
 43 44 45 46  3 9.2789 12.156 -13.120 -3.0597 26.240 -31.495
 44 45 46 47  3 9.2789 12.156 -13.120 -3.0597 26.240 -31.495
 45 46 47 48  3 9.2789 12.156 -13.120 -3.0597 26.240 -31.495
 46 47 48 49  3 9.2789 12.156 -13.120 -3.0597 26.240 -31.495
 47 48 49 50  3 9.2789 12.156 -13.120 -3.0597 26.240 -31.495


[ dihedrals ]
;ai aj ak al fu   phi0    cp    mult
 13 14 32 12  2 35.264 334.72
 15 14 17 16  2     0 167.36
 34 33 36 35  2     0 167.36
```

A.2.3   POPC

[moleculetype]
; Name   nrexcl
POPC   3

[atoms]

;nr	type	resnr	residu	atom	cgnr	charge
1	LC3N	1	POPC	C1a	0	0.400
2	LC3N	1	POPC	C2a	0	0.400
3	LC3N	1	POPC	C3a	0	0.400
4	LNL	1	POPC	N4a	0	-0.500
5	LC2	1	POPC	C5a	0	0.300
6	LC2O	1	POPC	C6a	1	0.400
7	LOS	1	POPC	O7a	1	-0.800
8	LP	1	POPC	P8a	1	1.700
9	LOM	1	POPC	O9a	1	-0.800
10	LOM	1	POPC	O10a	1	-0.800
11	LOS	1	POPC	O11a	1	-0.700
12	LC2O	1	POPC	C12a	2	0.400
13	LCH1	1	POPC	C13a	2	0.300
14	LOS	1	POPC	O14a	2	-0.700
15	LC	1	POPC	C15a	2	0.700
16	LO2	1	POPC	O16a	2	-0.700
17	LCH2	1	POPC	C17a	3	0
18	LCH2	1	POPC	C18a	4	0
19	LCH2	1	POPC	C19a	5	0
20	LCH2	1	POPC	C20a	6	0
21	LCH2	1	POPC	C21a	7	0
22	LCH2	1	POPC	C22a	8	0
23	LCH2	1	POPC	C23a	9	0
24	LCH1	1	POPC	C24a	10	0
25	LCH1	1	POPC	C25a	11	0
26	LCH2	1	POPC	C26a	12	0
27	LCH2	1	POPC	C27a	13	0
28	LCH2	1	POPC	C28a	14	0
29	LCH2	1	POPC	C29a	15	0
30	LCH2	1	POPC	C30a	16	0
31	LCH2	1	POPC	C31a	17	0
32	LC2O	1	POPC	C32a	18	0.50
33	LOS	1	POPC	O33a	18	-0.70
34	LC	1	POPC	C34a	18	0.80
35	LO2	1	POPC	O35a	18	-0.60
36	LCH2	1	POPC	C36a	19	0
37	LCH2	1	POPC	C37a	20	0
38	LCH2	1	POPC	C38a	21	0
39	LCH2	1	POPC	C39a	22	0
40	LCH2	1	POPC	C40a	23	0
41	LCH2	1	POPC	C41a	24	0
42	LCH2	1	POPC	C42a	25	0
43	LCH2	1	POPC	C43a	26	0
44	LCH2	1	POPC	C44a	27	0
45	LCH2	1	POPC	C45a	28	0
46	LCH2	1	POPC	C46a	29	0
47	LCH2	1	POPC	C47a	30	0
48	LCH2	1	POPC	C48a	31	0
49	LCH2	1	POPC	C49a	32	0
50	LCH3	1	POPC	C50a	33	0
51	LCH2	1	POPC	CA1a	34	0
52	LCH3	1	POPC	CA2a	35	0

[bonds]

;ai	aj	fun	l0	kl
4	5	1		
5	6	1		
6	7	1		
7	8	1		
8	9	1		
8	10	1		
8	11	1		
11	12	1		
12	13	1		
13	14	1		
13	32	1		
14	15	1		
15	16	1		
15	17	1		
17	18	1		
18	19	1		
19	20	1		
20	21	1		
21	22	1		
22	23	1		
23	24	1		
24	25	1		
25	26	1		
26	27	1		
27	28	1		
28	29	1		
29	30	1		
30	31	1		
31	51	1		
51	52	1		
32	33	1		
33	34	1		
34	35	1		
34	36	1		
36	37	1		
37	38	1		
38	39	1		
39	40	1		
40	41	1		
41	42	1		
42	43	1		
43	44	1		
44	45	1		
45	46	1		
46	47	1		
47	48	1		
48	49	1		
49	50	1		
1	4	1		
2	4	1		

```
  3    4    1
```

[pairs]

;ai	aj	fun	c6	c12
1	6	1	1.03247422e-03	3.51810672e-06
2	6	1	1.03247422e-03	3.51810672e-06
3	6	1	1.03247422e-03	3.51810672e-06
4	7	1	3.29499090e-04	3.05397363e-07
5	8	1	1.10863618e-03	3.45353422e-06
6	9	1	5.19010279e-04	7.38576360e-07
6	10	1	5.19010279e-04	7.38576360e-07
6	11	1	4.86248073e-04	7.20384175e-07
7	12	1	4.86248073e-04	7.20384175e-07
8	13	1	7.58423799e-04	2.17710042e-06
9	12	1	5.19010279e-04	7.38576360e-07
10	12	1	5.19010279e-04	7.38576360e-07
11	14	1	2.59162500e-04	1.88925000e-07
11	32	1	4.86248073e-04	7.20384175e-07
12	15	1	7.45399973e-04	2.15689039e-06
12	33	1	4.86248073e-04	7.20384175e-07
13	16	1	3.20118314e-04	1.44059554e-06
13	17	1	6.06976011e-04	2.06828601e-06
13	34	1	5.53383227e-04	1.60129580e-06
14	18	1	4.35761820e-04	7.30621371e-07
14	33	1	2.59162500e-04	1.88925000e-07
15	19	1	6.68006450e-04	2.18754141e-06
15	32	1	7.45399973e-04	2.15689039e-06
16	18	1	3.86424973e-04	1.96800765e-06
22	25	1	6.06976011e-04	2.06828601e-06
24	27	1	6.06976011e-04	2.06828601e-06
32	35	1	4.31195185e-04	1.94043266e-06
32	36	1	8.17588753e-04	2.78591014e-06
33	37	1	4.35761820e-04	7.30621371e-07
34	38	1	6.68006450e-04	2.18754141e-06
35	37	1	3.86424973e-04	1.96800765e-06

[angles]

;ai	aj	ak	fun	a0	ka
4	5	6	1		
5	6	7	1		
6	7	8	1		
7	8	9	1		
7	8	10	1		
7	8	11	1		
8	11	12	1		
9	8	10	1		
9	8	11	1		
10	8	11	1		
11	12	13	1		
12	13	14	1		
12	13	32	1		
13	14	15	1		
13	32	33	1		
14	13	32	1		
14	15	16	1		
14	15	17	1		
15	17	18	1		
16	15	17	1		

```
17  18  19    1
18  19  20    1
19  20  21    1
20  21  22    1
21  22  23    1
22  23  24    1
23  24  25    1
24  25  26    1
25  26  27    1
26  27  28    1
27  28  29    1
28  29  30    1
29  30  31    1
30  31  51    1
31  51  52    1
32  33  34    1
33  34  35    1
33  34  36    1
34  36  37    1
35  34  36    1
36  37  38    1
37  38  39    1
38  39  40    1
39  40  41    1
40  41  42    1
41  42  43    1
42  43  44    1
43  44  45    1
44  45  46    1
45  46  47    1
46  47  48    1
47  48  49    1
48  49  50    1
 1   4   2    1
 2   4   3    1
 3   4   1    1
 1   4   5    1
 2   4   5    1
 3   4   5    1
```

[dihedrals]

;ai	aj	ak	al	fu	phi0	cp	mult
1	4	5	6	1	0	3.766	3
4	5	6	7	1	0	5.858	3
5	6	7	8	1	0	3.766	3
6	7	8	11	1	0	1.046	3
6	7	8	11	1	0	3.138	2
7	8	11	12	1	0	1.046	3
7	8	11	12	1	0	3.138	2
8	11	12	13	1	0	3.766	3
11	12	13	14	1	0	2.092	2
11	12	13	32	1	0	5.858	3
11	12	13	32	1	0	0.418	2
12	13	32	33	1	0	5.858	3
12	13	32	33	1	0	0.418	2
12	13	14	15	1	0	3.766	3
13	32	33	34	1	0	3.766	3
13	14	15	17	1	180	16.736	2

```
14  13  32  33   1      0   2.092        2        36  37  38  39   3   9.2789 12.156 -13.120 -3.0597 26.240 -31.495
14  15  17  18   1      0   0.418        6        37  38  39  40   3   9.2789 12.156 -13.120 -3.0597 26.240 -31.495
15  17  18  19   1      0   5.858        3        38  39  40  41   3   9.2789 12.156 -13.120 -3.0597 26.240 -31.495
17  18  19  20   3   9.2789 12.156 -13.120 -3.0597 26.240 -31.495   39  40  41  42   3   9.2789 12.156 -13.120 -3.0597 26.240 -31.495
18  19  20  21   3   9.2789 12.156 -13.120 -3.0597 26.240 -31.495   40  41  42  43   3   9.2789 12.156 -13.120 -3.0597 26.240 -31.495
19  20  21  22   3   9.2789 12.156 -13.120 -3.0597 26.240 -31.495   41  42  43  44   3   9.2789 12.156 -13.120 -3.0597 26.240 -31.495
20  21  22  23   3   9.2789 12.156 -13.120 -3.0597 26.240 -31.495   42  43  44  45   3   9.2789 12.156 -13.120 -3.0597 26.240 -31.495
21  22  23  24   3   9.2789 12.156 -13.120 -3.0597 26.240 -31.495   43  44  45  46   3   9.2789 12.156 -13.120 -3.0597 26.240 -31.495
22  23  24  25   1      0   5.858        3        44  45  46  47   3   9.2789 12.156 -13.120 -3.0597 26.240 -31.495
24  25  26  27   1      0   5.858        3        45  46  47  48   3   9.2789 12.156 -13.120 -3.0597 26.240 -31.495
25  26  27  28   3   9.2789 12.156 -13.120 -3.0597 26.240 -31.495   46  47  48  49   3   9.2789 12.156 -13.120 -3.0597 26.240 -31.495
26  27  28  29   3   9.2789 12.156 -13.120 -3.0597 26.240 -31.495   47  48  49  50   3   9.2789 12.156 -13.120 -3.0597 26.240 -31.495
27  28  29  30   3   9.2789 12.156 -13.120 -3.0597 26.240 -31.495
28  29  30  31   3   9.2789 12.156 -13.120 -3.0597 26.240 -31.495
29  30  31  51   3   9.2789 12.156 -13.120 -3.0597 26.240 -31.495   [ dihedrals ]
30  31  51  52   3   9.2789 12.156 -13.120 -3.0597 26.240 -31.495   ;ai aj ak al fu   phi0     cp    mult
13  32  33  34   1      0   3.766        3        13  14  32  12   2  35.264 334.72
32  33  34  36   1    180  16.736        2        15  14  17  16   2     0  167.36
33  34  36  37   1      0   0.418        6        34  33  36  35   2     0  167.36
34  36  37  38   1      0   5.858        3        23  24  25  26   2     0  167.36
```

A.2.4   POPE

```
[ moleculetype ]                                 27  LCH2    1   POPE  C27b   13    0
; Name   nrexcl                                  28  LCH2    1   POPE  C28b   14    0
POPE    3                                        29  LCH2    1   POPE  C29b   15    0
                                                 30  LCH2    1   POPE  C30b   16    0
[ atoms ]                                        31  LCH2    1   POPE  C31b   17    0
;nr  type resnr residu atom cgnr charge          32  LC2O    1   POPE  C32b   18   0.50
 1  LH3N    1   POPE  H1b    0   0.400           33  LOS     1   POPE  O33b   18  -0.70
 2  LH3N    1   POPE  H2b    0   0.400           34  LC      1   POPE  C34b   18   0.80
 3  LH3N    1   POPE  H3b    0   0.400           35  LO2     1   POPE  O35b   18  -0.60
 4  LNL     1   POPE  N4b    0  -0.500           36  LCH2    1   POPE  C36b   19    0
 5  LC2     1   POPE  C5b    0   0.300           37  LCH2    1   POPE  C37b   20    0
 6  LC2O    1   POPE  C6b    1   0.400           38  LCH2    1   POPE  C38b   21    0
 7  LOS     1   POPE  O7b    1  -0.800           39  LCH2    1   POPE  C39b   22    0
 8  LP      1   POPE  P8b    1   1.700           40  LCH2    1   POPE  C40b   23    0
 9  LOM     1   POPE  O9b    1  -0.800           41  LCH2    1   POPE  C41b   24    0
10  LOM     1   POPE  O10b   1  -0.800           42  LCH2    1   POPE  C42b   25    0
11  LOS     1   POPE  O11b   1  -0.700           43  LCH2    1   POPE  C43b   26    0
12  LC2O    1   POPE  C12b   2   0.400           44  LCH2    1   POPE  C44b   27    0
13  LCH1    1   POPE  C13b   2   0.300           45  LCH2    1   POPE  C45b   28    0
14  LOS     1   POPE  O14b   2  -0.700           46  LCH2    1   POPE  C46b   29    0
15  LC      1   POPE  C15b   2   0.700           47  LCH2    1   POPE  C47b   30    0
16  LO2     1   POPE  O16b   2  -0.700           48  LCH2    1   POPE  C48b   31    0
17  LCH2    1   POPE  C17b   3    0              49  LCH2    1   POPE  C49b   32    0
18  LCH2    1   POPE  C18b   4    0              50  LCH3    1   POPE  C50b   33    0
19  LCH2    1   POPE  C19b   5    0              51  LCH2    1   POPE  CA1b   34    0
20  LCH2    1   POPE  C20b   6    0              52  LCH3    1   POPE  CA2b   35    0
21  LCH2    1   POPE  C21b   7    0
22  LCH2    1   POPE  C22b   8    0              [ bonds ]
23  LCH2    1   POPE  C23b   9    0              ;ai aj fun    l0     kl
24  LCH1    1   POPE  C24b  10    0               4   5   1
25  LCH1    1   POPE  C25b  11    0               5   6   1
26  LCH2    1   POPE  C26b  12    0               6   7   1
```

```
   7    8    1
   8    9    1
   8   10    1
   8   11    1
  11   12    1
  12   13    1
  13   14    1
  13   32    1
  14   15    1
  15   16    1
  15   17    1
  17   18    1
  18   19    1
  19   20    1
  20   21    1
  21   22    1
  22   23    1
  23   24    1
  24   25    1
  25   26    1
  26   27    1
  27   28    1
  28   29    1
  29   30    1
  30   31    1
  31   51    1
  51   52    1
  32   33    1
  33   34    1
  34   35    1
  34   36    1
  36   37    1
  37   38    1
  38   39    1
  39   40    1
  40   41    1
  41   42    1
  42   43    1
  43   44    1
  44   45    1
  45   46    1
  46   47    1
  47   48    1
  48   49    1
  49   50    1
   1    4    1
   2    4    1
   3    4    1

[ pairs ]
;ai  aj  fun          c6             c12
   4    7    1  3.29499090e-04  3.05397363e-07
   5    8    1  1.10863618e-03  3.45353422e-06
   6    9    1  5.19010279e-04  7.38576360e-07
   6   10    1  5.19010279e-04  7.38576360e-07
   6   11    1  4.86248073e-04  7.20384175e-07
   7   12    1  4.86248073e-04  7.20384175e-07
   8   13    1  7.58423799e-04  2.17710042e-06
```

```
   9   12    1  5.19010279e-04  7.38576360e-07
  10   12    1  5.19010279e-04  7.38576360e-07
  11   14    1  2.59162500e-04  1.88925000e-07
  11   32    1  4.86248073e-04  7.20384175e-07
  12   15    1  7.45399973e-04  2.15689039e-06
  12   33    1  4.86248073e-04  7.20384175e-07
  13   16    1  3.20118314e-04  1.44059554e-06
  13   17    1  6.06976011e-04  2.06828601e-06
  13   34    1  5.53383227e-04  1.60129580e-06
  14   18    1  4.35761820e-04  7.30621371e-07
  14   33    1  2.59162500e-04  1.88925000e-07
  15   19    1  6.68006450e-04  2.18754141e-06
  15   32    1  7.45399973e-04  2.15689039e-06
  16   18    1  3.86424973e-04  1.96800765e-06
  22   25    1  6.06976011e-04  2.06828601e-06
  24   27    1  6.06976011e-04  2.06828601e-06
  32   35    1  4.31195185e-04  1.94043266e-06
  32   36    1  8.17588753e-04  2.78591014e-06
  33   37    1  4.35761820e-04  7.30621371e-07
  34   38    1  6.68006450e-04  2.18754141e-06
  35   37    1  3.86424973e-04  1.96800765e-06

[ angles ]
;ai  aj  ak  fun    a0      ka
   4    5    6    1
   5    6    7    1
   6    7    8    1
   7    8    9    1
   7    8   10    1
   7    8   11    1
   8   11   12    1
   9    8   10    1
   9    8   11    1
  10    8   11    1
  11   12   13    1
  12   13   14    1
  12   13   32    1
  13   14   15    1
  13   32   33    1
  14   13   32    1
  14   15   16    1
  14   15   17    1
  15   17   18    1
  16   15   17    1
  17   18   19    1
  18   19   20    1
  19   20   21    1
  20   21   22    1
  21   22   23    1
  22   23   24    1
  23   24   25    1
  24   25   26    1
  25   26   27    1
  26   27   28    1
  27   28   29    1
  28   29   30    1
  29   30   31    1
  30   31   51    1
```

31	51	52	1							
32	33	34	1							
33	34	35	1							
33	34	36	1							
34	36	37	1							
35	34	36	1							
36	37	38	1							
37	38	39	1							
38	39	40	1							
39	40	41	1							
40	41	42	1							
41	42	43	1							
42	43	44	1							
43	44	45	1							
44	45	46	1							
45	46	47	1							
46	47	48	1							
47	48	49	1							
48	49	50	1							
1	4	2	1							
2	4	3	1							
3	4	1	1							
1	4	5	1							
2	4	5	1							
3	4	5	1							

[dihedrals]

;ai	aj	ak	al	fu	phi0	cp	mult
1	4	5	6	1	0	3.766	3
4	5	6	7	1	0	5.858	3
5	6	7	8	1	0	3.766	3
6	7	8	11	1	0	1.046	3
6	7	8	11	1	0	3.138	2
7	8	11	12	1	0	1.046	3
7	8	11	12	1	0	3.138	2
8	11	12	13	1	0	3.766	3
11	12	13	14	1	0	2.092	2
11	12	13	32	1	0	5.858	3
11	12	13	32	1	0	0.418	2
12	13	32	33	1	0	5.858	3
12	13	32	33	1	0	0.418	2
12	13	14	15	1	0	3.766	3

;ai	aj	ak	al	fu	phi0	cp	mult			
13	32	33	34	1	0	3.766	3			
13	14	15	17	1	180	16.736	2			
14	13	32	33	1	0	2.092	2			
14	15	17	18	1	0	0.418	6			
15	17	18	19	1	0	5.858	3			
17	18	19	20	3	9.2789	12.156	-13.120	-3.0597	26.240	-31.495
18	19	20	21	3	9.2789	12.156	-13.120	-3.0597	26.240	-31.495
19	20	21	22	3	9.2789	12.156	-13.120	-3.0597	26.240	-31.495
20	21	22	23	3	9.2789	12.156	-13.120	-3.0597	26.240	-31.495
21	22	23	24	3	9.2789	12.156	-13.120	-3.0597	26.240	-31.495
22	23	24	25	1	0	5.858	3			
24	25	26	27	1	0	5.858	3			
25	26	27	28	3	9.2789	12.156	-13.120	-3.0597	26.240	-31.495
26	27	28	29	3	9.2789	12.156	-13.120	-3.0597	26.240	-31.495
27	28	29	30	3	9.2789	12.156	-13.120	-3.0597	26.240	-31.495
28	29	30	31	3	9.2789	12.156	-13.120	-3.0597	26.240	-31.495
29	30	31	51	3	9.2789	12.156	-13.120	-3.0597	26.240	-31.495
30	31	51	52	3	9.2789	12.156	-13.120	-3.0597	26.240	-31.495
13	32	33	34	1	0	3.766	3			
32	33	34	36	1	180	16.736	2			
33	34	36	37	1	0	0.418	6			
34	36	37	38	1	0	5.858	3			
36	37	38	39	3	9.2789	12.156	-13.120	-3.0597	26.240	-31.495
37	38	39	40	3	9.2789	12.156	-13.120	-3.0597	26.240	-31.495
38	39	40	41	3	9.2789	12.156	-13.120	-3.0597	26.240	-31.495
39	40	41	42	3	9.2789	12.156	-13.120	-3.0597	26.240	-31.495
40	41	42	43	3	9.2789	12.156	-13.120	-3.0597	26.240	-31.495
41	42	43	44	3	9.2789	12.156	-13.120	-3.0597	26.240	-31.495
42	43	44	45	3	9.2789	12.156	-13.120	-3.0597	26.240	-31.495
43	44	45	46	3	9.2789	12.156	-13.120	-3.0597	26.240	-31.495
44	45	46	47	3	9.2789	12.156	-13.120	-3.0597	26.240	-31.495
45	46	47	48	3	9.2789	12.156	-13.120	-3.0597	26.240	-31.495
46	47	48	49	3	9.2789	12.156	-13.120	-3.0597	26.240	-31.495
47	48	49	50	3	9.2789	12.156	-13.120	-3.0597	26.240	-31.495

[dihedrals]

;ai	aj	ak	al	fu	phi0	cp	mult
13	14	32	12	2	35.264	334.72	
15	14	17	16	2	0	167.36	
34	33	36	35	2	0	167.36	
23	24	25	26	2	0	167.36	

A.2.5 DOPC

[moleculetype]

; Name   nrexcl

DOPC   3

[atoms]

;nr	type	resnr	residu	atom	cgnr	charge	mass
1	LC3	1	DOPC	C1d	0	0.4000	15.0350
2	LC3	1	DOPC	C2d	0	0.4000	15.0350
3	LC3	1	DOPC	C3d	0	0.4000	15.0350
4	LNL	1	DOPC	N4d	0	-0.5000	14.0067
5	LH2	1	DOPC	C5d	0	0.3000	14.0270
6	LC2	1	DOPC	C6d	1	0.4000	14.0270
7	LOS	1	DOPC	O7d	1	-0.800	15.9994
8	LP	1	DOPC	P8d	1	1.700	30.9738
9	LOM	1	DOPC	O9d	1	-0.800	15.9994
10	LOM	1	DOPC	O10d	1	-0.800	15.9994
11	LOS	1	DOPC	O11d	1	-0.700	15.9994
12	LC2	1	DOPC	C12d	2	0.400	14.0270
13	LH1	1	DOPC	C13d	2	0.300	13.0190

14	LOS	1	DOPC	O14d	2	-0.700	15.9994
15	LC	1	DOPC	C15d	2	0.700	12.0110
16	LO	1	DOPC	O16d	2	-0.700	15.9994
17	LP2	1	DOPC	C17d	3	0	14.0270
18	LP2	1	DOPC	C18d	4	0	14.0270
19	LP2	1	DOPC	C19d	5	0	14.0270
20	LP2	1	DOPC	C20d	6	0	14.0270
21	LP2	1	DOPC	C21d	7	0	14.0270
22	LP2	1	DOPC	C22d	8	0	14.0270
23	LP2	1	DOPC	C23d	9	0	14.0270
24	LH1	1	DOPC	C24d	10	0	13.0190
25	LH1	1	DOPC	C25d	11	0	13.0190
26	LP2	1	DOPC	C26d	12	0	14.0270
27	LP2	1	DOPC	C27d	13	0	14.0270
28	LP2	1	DOPC	C28d	14	0	14.0270
29	LP2	1	DOPC	C29d	15	0	14.0270
30	LP2	1	DOPC	C30d	16	0	14.0270
31	LP2	1	DOPC	C31d	17	0	14.0270
32	LC2	1	DOPC	C32d	18	0.500	14.0270
33	LOS	1	DOPC	O33d	18	-0.700	15.9994
34	LC	1	DOPC	C34d	18	0.800	12.0110
35	LO	1	DOPC	O35d	18	-0.600	15.9994
36	LP2	1	DOPC	C36d	19	0	14.0270
37	LP2	1	DOPC	C37d	20	0	14.0270
38	LP2	1	DOPC	C38d	21	0	14.0270
39	LP2	1	DOPC	C39d	22	0	14.0270
40	LP2	1	DOPC	C40d	23	0	14.0270
41	LP2	1	DOPC	C41d	24	0	14.0270
42	LP2	1	DOPC	C42d	25	0	14.0270
43	LH1	1	DOPC	C43d	26	0	13.0190
44	LH1	1	DOPC	C44d	27	0	13.0190
45	LP2	1	DOPC	C45d	28	0	14.0270
46	LP2	1	DOPC	C46d	29	0	14.0270
47	LP2	1	DOPC	C47d	30	0	14.0270
48	LP2	1	DOPC	C48d	31	0	14.0270
49	LP2	1	DOPC	C49d	32	0	14.0270
50	LP2	1	DOPC	C50d	33	0	14.0270
51	LP2	1	DOPC	CA1d	34	0	14.0270
52	LP3	1	DOPC	CA2d	35	0	15.0350
53	LP2	1	DOPC	CA3d	36	0	14.0270
54	LP3	1	DOPC	CA4d	37	0	15.0350

[bonds]

;ai	aj	fun	l0	kl
4	5	1	0.14700E+00	0.37660E+06
5	6	1	0.15300E+00	0.33470E+06
6	7	1	0.14300E+00	0.25100E+06
7	8	1	0.16100E+00	0.25100E+06
8	9	1	0.14800E+00	0.37660E+06
8	10	1	0.14800E+00	0.37660E+06
8	11	1	0.16100E+00	0.25100E+06
11	12	1	0.14300E+00	0.25100E+06
12	13	1	0.15300E+00	0.33470E+06
13	14	1	0.14350E+00	0.25100E+06
13	32	1	0.15300E+00	0.33470E+06
14	15	1	0.13600E+00	0.37660E+06
15	16	1	0.12300E+00	0.50210E+06
15	17	1	0.15300E+00	0.33470E+06

17	18	1	0.15300E+00	0.33470E+06
18	19	1	0.15300E+00	0.33470E+06
19	20	1	0.15300E+00	0.33470E+06
20	21	1	0.15300E+00	0.33470E+06
21	22	1	0.15300E+00	0.33470E+06
22	23	1	0.15300E+00	0.33470E+06
23	24	1	0.15300E+00	0.33470E+06
24	25	1	0.13900E+00	0.41840E+06 ;double bond
25	26	1	0.15300E+00	0.33470E+06
26	27	1	0.15300E+00	0.33470E+06
27	28	1	0.15300E+00	0.33470E+06
28	29	1	0.15300E+00	0.33470E+06
29	30	1	0.15300E+00	0.33470E+06
30	31	1	0.15300E+00	0.33470E+06
31	53	1	0.15300E+00	0.33470E+06
53	54	1	0.15300E+00	0.33470E+06
32	33	1	0.14300E+00	0.25100E+06
33	34	1	0.13600E+00	0.37660E+06
34	35	1	0.12300E+00	0.50210E+06
34	36	1	0.15300E+00	0.33470E+06
36	37	1	0.15300E+00	0.33470E+06
37	38	1	0.15300E+00	0.33470E+06
38	39	1	0.15300E+00	0.33470E+06
39	40	1	0.15300E+00	0.33470E+06
40	41	1	0.15300E+00	0.33470E+06
41	42	1	0.15300E+00	0.33470E+06
42	43	1	0.15300E+00	0.33470E+06
43	44	1	0.13900E+00	0.41840E+06 ;double bond
44	45	1	0.15300E+00	0.33470E+06
45	46	1	0.15300E+00	0.33470E+06
46	47	1	0.15300E+00	0.33470E+06
47	48	1	0.15300E+00	0.33470E+06
48	49	1	0.15300E+00	0.33470E+06
49	50	1	0.15300E+00	0.33470E+06
50	51	1	0.15300E+00	0.33470E+06
51	52	1	0.15300E+00	0.33470E+06
1	4	1	0.14700E+00	0.37450E+06
2	4	1	0.14700E+00	0.37450E+06
3	4	1	0.14700E+00	0.37450E+06

[pairs]

;ai	aj	fun	c6	c12
1	6	1	9.32500e-04	3.17700e-06
2	6	1	9.32500e-04	3.17700e-06
3	6	1	9.32500e-04	3.17700e-06
4	7	1	3.66500e-04	3.39600e-07
5	8	1	1.00100e-03	3.11900e-06
6	9	1	4.68500e-04	6.66800e-07
6	10	1	4.68500e-04	6.66800e-07
6	11	1	4.88000e-04	7.22800e-07
7	12	1	4.88000e-04	7.22800e-07
8	13	1	7.59200e-04	2.18000e-06
9	12	1	4.68500e-04	6.66800e-07
10	12	1	4.68500e-04	6.66800e-07
11	14	1	3.20300e-04	2.33400e-07
11	32	1	4.88000e-04	7.22800e-07
12	15	1	6.73700e-04	1.95000e-06
12	33	1	4.88000e-04	7.22800e-07

```
13  16   1    3.85500e-04    5.49000e-07
13  17   1    6.08200e-04    2.07300e-06
13  34   1    5.54500e-04    1.60500e-06
14  18   1    4.85100e-04    8.12900e-07
14  33   1    3.20300e-04    2.33400e-07
15  19   1    6.69700e-04    2.19300e-06
15  32   1    6.73700e-04    1.95000e-06
16  18   1    4.65700e-04    7.50000e-07
23  26   1    7.34600e-04    2.83100e-06
42  45   1    7.34600e-04    2.83100e-06
32  35   1    4.68500e-04    6.66800e-07
32  36   1    9.26900e-04    3.57400e-06
33  37   1    4.85100e-04    8.12900e-07
34  38   1    6.69700e-04    2.19300e-06
35  37   1    4.65700e-04    7.50000e-07


[ angles ]
;ai  aj  ak  fun    a0       ka
  4   5   6   1 0.10950E+03 0.46020E+03
  5   6   7   1 0.10950E+03 0.46020E+03
  6   7   8   1 0.12000E+03 0.39750E+03
  7   8   9   1 0.10960E+03 0.39750E+03
  7   8  10   1 0.10960E+03 0.39750E+03
  7   8  11   1 0.10300E+03 0.39750E+03
  8  11  12   1 0.12000E+03 0.39750E+03
  9   8  10   1 0.12000E+03 0.58580E+03
  9   8  11   1 0.10960E+03 0.39750E+03
 10   8  11   1 0.10960E+03 0.39750E+03
 11  12  13   1 0.11100E+03 0.46020E+03
 12  13  14   1 0.10950E+03 0.46020E+03
 12  13  32   1 0.10950E+03 0.46020E+03
 13  14  15   1 0.12000E+03 0.41840E+03
 13  32  33   1 0.11100E+03 0.46020E+03
 14  13  32   1 0.10950E+03 0.46020E+03
 14  15  16   1 0.12400E+03 0.50210E+03
 14  15  17   1 0.11500E+03 0.50210E+03
 15  17  18   1 0.11100E+03 0.46020E+03
 16  15  17   1 0.12100E+03 0.50210E+03
 17  18  19   1 0.11100E+03 0.46020E+03
 18  19  20   1 0.11100E+03 0.46020E+03
 19  20  21   1 0.11100E+03 0.46020E+03
 20  21  22   1 0.11100E+03 0.46020E+03
 21  22  23   1 0.11100E+03 0.46020E+03
 22  23  24   1 0.11100E+03 0.46020E+03
 23  24  25   1   120.000     502.080  ; cis
 24  25  26   1   120.000     502.080  ; cis
 25  26  27   1 0.11100E+03 0.46020E+03
 26  27  28   1 0.11100E+03 0.46020E+03
 27  28  29   1 0.11100E+03 0.46020E+03
 28  29  30   1 0.11100E+03 0.46020E+03
 29  30  31   1 0.11100E+03 0.46020E+03
 30  31  53   1 0.11100E+03 0.46020E+03
 31  53  54   1 0.11100E+03 0.46020E+03
 32  33  34   1 0.12000E+03 0.41840E+03
 33  34  35   1 0.12400E+03 0.50210E+03
 33  34  36   1 0.11500E+03 0.50210E+03
 34  36  37   1 0.11100E+03 0.46020E+03
 35  34  36   1 0.12100E+03 0.50210E+03
```

```
36  37  38   1 0.11100E+03 0.46020E+03
37  38  39   1 0.11100E+03 0.46020E+03
38  39  40   1 0.11100E+03 0.46020E+03
39  40  41   1 0.11100E+03 0.46020E+03
40  41  42   1 0.11100E+03 0.46020E+03
41  42  43   1 0.11100E+03 0.46020E+03
42  43  44   1   120.000     502.080  ; cis
43  44  45   1   120.000     502.080  ; cis
44  45  46   1 0.11100E+03 0.46020E+03
45  46  47   1 0.11100E+03 0.46020E+03
46  47  48   1 0.11100E+03 0.46020E+03
47  48  49   1 0.11100E+03 0.46020E+03
48  49  50   1 0.11100E+03 0.46020E+03
49  50  51   1 0.11100E+03 0.46020E+03
50  51  52   1 0.11100E+03 0.46020E+03
 1   4   2   1 0.10950E+03 0.33470E+03
 2   4   3   1 0.10950E+03 0.33470E+03
 3   4   1   1 0.10950E+03 0.33470E+03
 1   4   5   1 0.10950E+03 0.37660E+03
 2   4   5   1 0.10950E+03 0.37660E+03
 3   4   5   1 0.10950E+03 0.37660E+03


[ dihedrals ]
;ai  aj  ak  al  fu    phi0      cp     mult
  1   4   5   6   1    0.0      3.76    3
  4   5   6   7   1    0.0      5.85    3
  5   6   7   8   1    0.0      3.76    3
  6   7   8  11   1    0.0      1.05    3
  6   7   8  11   1    0.0      3.14    2
  7   8  11  12   1    0.0      1.05    3
  7   8  11  12   1    0.0      3.14    2
  8  11  12  13   1    0.0      3.76    3
 11  12  13  14   1    0.0      2.09    2
 11  12  13  32   1    0.0      5.85    3
 11  12  13  32   1    0.0      0.42    2
 12  13  32  33   1    0.0      5.85    3
 12  13  32  33   1    0.0      0.42    2
 12  13  14  15   1    0.0      3.77    3
 13  32  33  34   1    0.0      3.76    3
 13  14  15  17   1  180.0     16.74    2
 14  13  32  33   1    0.0      2.09    2
 14  15  17  18   1    0.0      0.42    6
 15  17  18  19   1    0.0      5.86    3
 17  18  19  20   3 9.2789 12.156 -13.120 -3.0597 26.240 -31.495
 18  19  20  21   3 9.2789 12.156 -13.120 -3.0597 26.240 -31.495
 19  20  21  22   3 9.2789 12.156 -13.120 -3.0597 26.240 -31.495
 20  21  22  23   3 9.2789 12.156 -13.120 -3.0597 26.240 -31.495
 24  23  22  21   1    0.0    3.34957   1
 24  23  22  21   1  180.0   -1.66004   2
 24  23  22  21   1    0.0    7.33265   3
 25  24  23  22   1    0.0      7.47    1
 25  24  23  22   1    0.0      3.90    2
 25  24  23  22   1  180.0      1.10    3
 25  24  23  22   1    0.0     -2.8425  0
 27  26  25  24   1    0.0      7.47    1
 27  26  25  24   1    0.0      3.90    2
 27  26  25  24   1  180.0      1.10    3
 27  26  25  24   1    0.0     -2.8425  0
```

```
25  26  27  28   1     0.0  3.34957   1
25  26  27  28   1   180.0 -1.66004   2
25  26  27  28   1     0.0  7.33265   3
26  27  28  29   3   9.2789 12.156 -13.120 -3.0597 26.240 -31.495
27  28  29  30   3   9.2789 12.156 -13.120 -3.0597 26.240 -31.495
28  29  30  31   3   9.2789 12.156 -13.120 -3.0597 26.240 -31.495
29  30  31  53   3   9.2789 12.156 -13.120 -3.0597 26.240 -31.495
30  31  53  54   3   9.2789 12.156 -13.120 -3.0597 26.240 -31.495
13  32  33  34   1     0.0     3.76   3
32  33  34  36   1   180.0    16.74   2
33  34  36  37   1     0.0     0.42   6
34  36  37  38   1     0.0     5.86   3
36  37  38  39   3   9.2789 12.156 -13.120 -3.0597 26.240 -31.495
37  38  39  40   3   9.2789 12.156 -13.120 -3.0597 26.240 -31.495
38  39  40  41   3   9.2789 12.156 -13.120 -3.0597 26.240 -31.495
39  40  41  42   3   9.2789 12.156 -13.120 -3.0597 26.240 -31.495
43  42  41  40   1     0.0  3.34957   1
43  42  41  40   1   180.0 -1.66004   2
43  42  41  40   1     0.0  7.33265   3
44  43  42  41   1     0.0     7.47   1
44  43  42  41   1     0.0     3.90   2
44  43  42  41   1   180.0     1.10   3
44  43  42  41   1     0.0  -2.8425   0
```

```
46  45  44  43   1     0.0     7.47   1
46  45  44  43   1     0.0     3.90   2
46  45  44  43   1   180.0     1.10   3
46  45  44  43   1     0.0  -2.8425   0
44  45  46  47   1     0.0  3.34957   1
44  45  46  47   1   180.0 -1.66004   2
44  45  46  47   1     0.0  7.33265   3
45  46  47  48   3   9.2789 12.156 -13.120 -3.0597 26.240 -31.495
46  47  48  49   3   9.2789 12.156 -13.120 -3.0597 26.240 -31.495
47  48  49  50   3   9.2789 12.156 -13.120 -3.0597 26.240 -31.495
48  49  50  51   3   9.2789 12.156 -13.120 -3.0597 26.240 -31.495
49  50  51  52   3   9.2789 12.156 -13.120 -3.0597 26.240 -31.495

[ dihedrals ]
;ai aj ak al fu   phi0      cp
13  14  32  12   2  35.264  0.33470E+03
15  14  17  16   2    0.0   0.16740E+03
34  33  36  35   2    0.0   0.16740E+03
23  24  25  26   2    0.0   167.360
42  43  44  45   2    0.0   167.360
```

A.2.6 Palmitate

```
[ moleculetype ]
;Name      nrexcl
PALM         3

[atoms]
;nr  type resnr residu  atom cgnr  charge
  1  HOP    1   PALM    H1P   1    0.398
  2  LOS    1   PALM    O2P   1   -0.548
  3   LC    1   PALM    C3P   1    0.530
  4   LO    1   PALM    O4P   1   -0.380
  5  LP2    1   PALM    C5P   2    0.0
  6  LP2    1   PALM    C6P   3    0.0
  7  LP2    1   PALM    C7P   4    0.0
  8  LP2    1   PALM    C8P   5    0.0
  9  LP2    1   PALM    C9P   6    0.0
 10  LP2    1   PALM   C10P   7    0.0
 11  LP2    1   PALM   C11P   8    0.0
 12  LP2    1   PALM   C12P   9    0.0
 13  LP2    1   PALM   C13P  10    0.0
 14  LP2    1   PALM   C14P  11    0.0
 15  LP2    1   PALM   C15P  12    0.0
 16  LP2    1   PALM   C16P  13    0.0
 17  LP2    1   PALM   C17P  14    0.0
 18  LP2    1   PALM   C18P  15    0.0
 19  LP3    1   PALM   C19P  16    0.0

[bonds]
;ai  aj  fun    l0     kl
```

```
 1   2   1  0.100      313800
 2   3   1  0.136      376560
 3   4   1  0.123      502080
 3   5   1  0.153      334720
 5   6   1  0.15300E+00 0.33470E+06
 6   7   1  0.15300E+00 0.33470E+06
 7   8   1  0.15300E+00 0.33470E+06
 8   9   1  0.15300E+00 0.33470E+06
 9  10   1  0.15300E+00 0.33470E+06
10  11   1  0.15300E+00 0.33470E+06
11  12   1  0.15300E+00 0.33470E+06
12  13   1  0.15300E+00 0.33470E+06
13  14   1  0.15300E+00 0.33470E+06
14  15   1  0.15300E+00 0.33470E+06
15  16   1  0.15300E+00 0.33470E+06
16  17   1  0.15300E+00 0.33470E+06
17  18   1  0.15300E+00 0.33470E+06
18  19   1  0.15300E+00 0.33470E+06

[ pairs ]
;ai aj fun         c6           c12
  2   6  1   4.85100e-04   8.12900e-07
  3   7  1   6.69700e-04   2.19300e-06
  4   6  1   4.65700e-04   7.50000e-07

[ angles ]
;ai aj ak fun   a0      ka
  1  2  3   1  109.5    397.48
  2  3  4   1  124.0    502.08
```

```
 2   3   5   1  115.0      502.08
 3   5   6   1  111.0      460.24
 4   3   5   1  121.0      502.08
 5   6   7   1  0.11100E+03 0.46020E+03
 6   7   8   1  0.11100E+03 0.46020E+03
 7   8   9   1  0.11100E+03 0.46020E+03
 8   9  10   1  0.11100E+03 0.46020E+03
 9  10  11   1  0.11100E+03 0.46020E+03
10  11  12   1  0.11100E+03 0.46020E+03
11  12  13   1  0.11100E+03 0.46020E+03
12  13  14   1  0.11100E+03 0.46020E+03
13  14  15   1  0.11100E+03 0.46020E+03
14  15  16   1  0.11100E+03 0.46020E+03
15  16  17   1  0.11100E+03 0.46020E+03
16  17  18   1  0.11100E+03 0.46020E+03
17  18  19   1  0.11100E+03 0.46020E+03

[ dihedrals ]
;ai  aj  ak  al  fu    phi0     cp
 3   2   5   4   2    0.0      167.36
```

```
[ dihedrals ]
;ai aj ak al fu    phi0    cp    mult
 1   2   3   5   1   180    16.736  2  ; OA-C ffgmxbon.itp
 2   3   5   6   1     0     0.418  6  ; C-CH2 ffgmxbon.itp
 3   5   6   7   1     0     5.858  3  ; CH2-CH2 ffgmxbon.itp
 5   6   7   8   3   9.2789 12.156 -13.120 -3.0597 26.240 -31.495
 6   7   8   9   3   9.2789 12.156 -13.120 -3.0597 26.240 -31.495
 7   8   9  10   3   9.2789 12.156 -13.120 -3.0597 26.240 -31.495
 8   9  10  11   3   9.2789 12.156 -13.120 -3.0597 26.240 -31.495
 9  10  11  12   3   9.2789 12.156 -13.120 -3.0597 26.240 -31.495
10  11  12  13   3   9.2789 12.156 -13.120 -3.0597 26.240 -31.495
11  12  13  14   3   9.2789 12.156 -13.120 -3.0597 26.240 -31.495
12  13  14  15   3   9.2789 12.156 -13.120 -3.0597 26.240 -31.495
13  14  15  16   3   9.2789 12.156 -13.120 -3.0597 26.240 -31.495
14  15  16  17   3   9.2789 12.156 -13.120 -3.0597 26.240 -31.495
15  16  17  18   3   9.2789 12.156 -13.120 -3.0597 26.240 -31.495
16  17  18  19   3   9.2789 12.156 -13.120 -3.0597 26.240 -31.495
```

A.2.7   Oleate

```
[ moleculetype ]
; Name   nrexcl
OLEA     3


[ atoms ]
;nr  type resnr residu atom cgnr  charge
 1   HOP   1   OLEA  H10   1   0.398
 2   LOS   1   OLEA  O20   1  -0.548
 3   LC    1   OLEA  C30   1   0.530
 4   LO    1   OLEA  O40   1  -0.380
 5   LP2   1   OLEA  C50   2   0
 6   LP2   1   OLEA  C60   3   0
 7   LP2   1   OLEA  C70   4   0
 8   LP2   1   OLEA  C80   5   0
 9   LP2   1   OLEA  C90   6   0
10   LP2   1   OLEA  C100  7   0
11   LP2   1   OLEA  C110  8   0
12   LH1   1   OLEA  C120  9   0
13   LH1   1   OLEA  C130 10   0
14   LP2   1   OLEA  C140 11   0
15   LP2   1   OLEA  C150 12   0
16   LP2   1   OLEA  C160 13   0
17   LP2   1   OLEA  C170 14   0
18   LP2   1   OLEA  C180 15   0
19   LP2   1   OLEA  C190 16   0
20   LP2   1   OLEA  C200 17   0
21   LP3   1   OLEA  C210 18   0


[ bonds ]
;ai  aj  fun    l0     kl
```

```
 1   2   1  0.100      313800
 2   3   1  0.136      376560
 3   4   1  0.123      502080
 3   5   1  0.153      334720
 5   6   1  0.15300E+00 0.33470E+06
 6   7   1  0.15300E+00 0.33470E+06
 7   8   1  0.15300E+00 0.33470E+06
 8   9   1  0.15300E+00 0.33470E+06
 9  10   1  0.15300E+00 0.33470E+06
10  11   1  0.15300E+00 0.33470E+06
11  12   1  0.15300E+00 0.33470E+06
12  13   1  0.13900E+00 0.41840E+06
13  14   1  0.15300E+00 0.33470E+06
14  15   1  0.15300E+00 0.33470E+06
15  16   1  0.15300E+00 0.33470E+06
16  17   1  0.15300E+00 0.33470E+06
17  18   1  0.15300E+00 0.33470E+06
18  19   1  0.15300E+00 0.33470E+06
19  20   1  0.15300E+00 0.33470E+06
20  21   1  0.15300E+00 0.33470E+06


[ pairs ]
;ai  aj  fun         c6          c12
 2   6   1   4.85100e-04  8.12900e-07
 3   7   1   6.69700e-04  2.19300e-06
 4   6   1   4.65700e-04  7.50000e-07
11  14   1   7.34600e-04  2.83100e-06


[ angles ]
;ai  aj  ak  fun   a0     ka
 1   2   3   1  109.5   397.48
```

```
 2   3   4   1 124.0      502.08
 2   3   5   1 115.0      502.08
 3   5   6   1 111.0      460.24
 4   3   5   1 121.0      502.08
 5   6   7   1 0.111E+03  0.4602E+03
 6   7   8   1 0.111E+03  0.4602E+03
 7   8   9   1 0.111E+03  0.4602E+03
 8   9  10   1 0.111E+03  0.4602E+03
 9  10  11   1 0.111E+03  0.4602E+03
10  11  12   1 0.111E+03  0.4602E+03
11  12  13   1 120.0      502.080  ; cis thingies
12  13  14   1 120.0      502.080  ; cis thingies
13  14  15   1 0.111E+03  0.4602E+03
14  15  16   1 0.111E+03  0.4602E+03
15  16  17   1 0.111E+03  0.4602E+03
16  17  18   1 0.111E+03  0.4602E+03
17  18  19   1 0.111E+03  0.4602E+03
18  19  20   1 0.111E+03  0.4602E+03
19  20  21   1 0.111E+03  0.4602E+03

[ dihedrals ]
;ai aj ak al fu   phi0    cp    mult
 1   2   3   5  1  180.0  16.736  2 ; OA-C ffgmxbon.itp
 2   3   5   6  1    0.0   0.418  6 ; C-CH2 ffgmxbon.itp
 3   5   6   7  1    0.0   5.858  3 ; CH2-CH2 ffgmxbon.itp
 5   6   7   8  3  9.2789 12.156 -13.120 -3.0597 26.240 -31.495
 6   7   8   9  3  9.2789 12.156 -13.120 -3.0597 26.240 -31.495
```

```
 7   8   9  10  3  9.2789 12.156 -13.120 -3.0597 26.240 -31.495
 8   9  10  11  3  9.2789 12.156 -13.120 -3.0597 26.240 -31.495
12  11  10   9  1    0.0  3.34957 1
12  11  10   9  1  180.0 -1.66004 2
12  11  10   9  1    0.0  7.33265 3
13  12  11  10  1    0.0  7.47   1
13  12  11  10  1    0.0  3.9    2
13  12  11  10  1  180.0  1.1    3
13  12  11  10  1    0.0 -2.8425 0
15  14  13  12  1    0.0  7.47   1
15  14  13  12  1    0.0  3.9    2
15  14  13  12  1  180.0  1.1    3
15  14  13  12  1    0.0 -2.8425 0
13  14  15  16  1    0.0  3.34957 1
13  14  15  16  1  180.0 -1.66004 2
13  14  15  16  1    0.0  7.33265 3
14  15  16  17  3  9.2789 12.156 -13.120 -3.0597 26.240 -31.495
15  16  17  18  3  9.2789 12.156 -13.120 -3.0597 26.240 -31.495
16  17  18  19  3  9.2789 12.156 -13.120 -3.0597 26.240 -31.495
17  18  19  20  3  9.2789 12.156 -13.120 -3.0597 26.240 -31.495
18  19  20  21  3  9.2789 12.156 -13.120 -3.0597 26.240 -31.495

[ dihedrals ]
;ai aj ak al fu   phi0    cp
 3   2   5   4  2   0.0  167.36
11  12  13  14  2   0.0  167.36
```

A.2.8   Linoleate

```
[ moleculetype ]
; Name   nrexcl
LINO    3

[ atoms ]
;nr  type resnr residu atom cgnr charge
 1   HOP    1   LINO   H1L   1   0.398
 2   LOS    1   LINO   O2L   1  -0.548
 3   LC     1   LINO   C3L   1   0.530
 4   LO     1   LINO   O4L   1  -0.380
 5   LP2    1   LINO   C5L   2    0
 6   LP2    1   LINO   C6L   3    0
 7   LP2    1   LINO   C7L   4    0
 8   LP2    1   LINO   C8L   5    0
 9   LP2    1   LINO   C9L   6    0
10   LP2    1   LINO  C10L   7    0
11   LP2    1   LINO  C11L   8    0
12   LH1    1   LINO  C12L   9    0
13   LH1    1   LINO  C13L  10    0
14   LP2    1   LINO  C14L  11    0
15   LH1    1   LINO  C15L  12    0
16   LH1    1   LINO  C16L  13    0
17   LP2    1   LINO  C17L  14    0
18   LP2    1   LINO  C18L  15    0
```

```
19   LP2    1   LINO  C19L  16    0
20   LP2    1   LINO  C20L  17    0
21   LP3    1   LINO  C21L  18    0

[ bonds ]
;ai aj fun    l0       kl
 1   2  1  0.100      313800
 2   3  1  0.136      376560
 3   4  1  0.123      502080
 3   5  1  0.153      334720
 5   6  1  0.153E+00  0.3347E+06
 6   7  1  0.153E+00  0.3347E+06
 7   8  1  0.153E+00  0.3347E+06
 8   9  1  0.153E+00  0.3347E+06
 9  10  1  0.153E+00  0.3347E+06
10  11  1  0.153E+00  0.3347E+06
11  12  1  0.153E+00  0.3347E+06
12  13  1  0.139E+00  0.4184E+06
13  14  1  0.153E+00  0.3347E+06
14  15  1  0.153E+00  0.3347E+06
15  16  1  0.139E+00  0.4184E+06
16  17  1  0.153E+00  0.3347E+06
17  18  1  0.153E+00  0.3347E+06
18  19  1  0.153E+00  0.3347E+06
19  20  1  0.153E+00  0.3347E+06
```

```
 20  21   1  0.153E+00  0.3347E+06


[ pairs ]
;ai  aj  fun         c6              c12
  2   6   1    4.85100e-04    8.12900e-07
  3   7   1    6.69700e-04    2.19300e-06
  4   6   1    4.65700e-04    7.50000e-07
 11  14   1    7.34600e-04    2.83100e-06
 14  17   1    7.34600e-04    2.83100e-06


[ angles ]
;ai  aj  ak  fun   a0       ka
  1   2   3   1  109.5      397.48
  2   3   4   1  124.0      502.08
  2   3   5   1  115.0      502.08
  3   5   6   1  111.0      460.24
  4   3   5   1  121.0      502.08
  5   6   7   1  0.111E+03  0.4602E+03
  6   7   8   1  0.111E+03  0.4602E+03
  7   8   9   1  0.111E+03  0.4602E+03
  8   9  10   1  0.111E+03  0.4602E+03
  9  10  11   1  0.111E+03  0.4602E+03
 10  11  12   1  0.111E+03  0.4602E+03
 11  12  13   1  120.0      502.080 ; cis
 12  13  14   1  120.0      502.080 ; cis
 13  14  15   1  0.111E+03  0.4602E+03
 14  15  16   1  120.0      502.080 ; cis
 15  16  17   1  120.0      502.080 ; cis
 16  17  18   1  0.111E+03  0.4602E+03
 17  18  19   1  0.111E+03  0.4602E+03
 18  19  20   1  0.111E+03  0.4602E+03
 19  20  21   1  0.111E+03  0.4602E+03


[ dihedrals ]
;ai  aj  ak  al  fu    phi0    cp     mult
  1   2   3   5   1   180.0   16.736  2  ; OA-C ffgmxbon.itp
  2   3   5   6   1     0.0    0.418  6  ; C-CH2 ffgmxbon.itp
```

```
  3   5   6   7   1     0.0    5.858   3  ; CH2-CH2 ffgmxbon.itp
  5   6   7   8   3  9.2789 12.156 -13.120 -3.0597 26.240 -31.495
  6   7   8   9   3  9.2789 12.156 -13.120 -3.0597 26.240 -31.495
  7   8   9  10   3  9.2789 12.156 -13.120 -3.0597 26.240 -31.495
  8   9  10  11   3  9.2789 12.156 -13.120 -3.0597 26.240 -31.495
 12  11  10   9   1     0.0    3.34957 1
 12  11  10   9   1   180.0   -1.66004 2
 12  11  10   9   1     0.0    7.33265 3
 13  12  11  10   1     0.0    7.47    1
 13  12  11  10   1     0.0    3.9     2
 13  12  11  10   1   180.0    1.1     3
 13  12  11  10   1     0.0   -2.8425  0
 15  14  13  12   1   180.0    4.533   1
 15  14  13  12   1     0.0    3       2
 15  14  13  12   1   180.0    1.550   3
 15  14  13  12   1     0.0   -2.65    0
 15  14  13  12   1     0.0    1.3     1
 13  14  15  16   1   180.0    4.533   1
 13  14  15  16   1     0.0    3       2
 13  14  15  16   1   180.0    1.550   3
 13  14  15  16   1     0.0   -2.65    0
 13  14  15  16   1     0.0    1.3     1
 18  17  16  15   1     0.0    7.47    1
 18  17  16  15   1     0.0    3.9     2
 18  17  16  15   1   180.0    1.1     3
 18  17  16  15   1     0.0   -2.8425  0
 19  18  17  16   1     0.0    3.34957 1
 19  18  17  16   1   180.0   -1.66004 2
 19  18  17  16   1     0.0    7.33265 3
 17  18  19  20   3  9.2789 12.156 -13.120 -3.0597 26.240 -31.495
 18  19  20  21   3  9.2789 12.156 -13.120 -3.0597 26.240 -31.495


[ dihedrals ]
;ai  aj  ak  al  fu    phi0    cp
  3   2   5   4   2    0.0  167.36
 11  12  13  14   2    0.0  167.36
 14  15  16  17   2    0.0  167.36
```

A.2.9   Water

```
[ moleculetype ]
; molname nrexcl
WAT 2


[ atoms ]
;nr  type  resnr  residu  atom  cgnr  charge
  1   OW     1     WAT     OW     1    -0.82
  2   HW     1     WAT     HW1    1     0.41
  3   HW     1     WAT     HW2    1     0.41


#ifdef FLEXIBLE
[ bonds ]
;ai  aj  fun    l0      kl
  1   2   1    0.1   345000
  1   3   1    0.1   345000
```

```
[ angles ]
;ai  aj  ak  fun   a0       ka
  2   1   3   1  109.47     383
#else
[ settles ]
; OW fun  doh      dhh
  1    1  0.1   0.16333


[ exclusions ]
  1  2  3
  2  1  3
  3  1  2
#endif
```

A.2.10 Glucose

```
[ moleculetype ]
; name nrexcl
GLC    3


[ atoms ]
;nr  type  resnr  residu  atom  cgnr  charge
  1   gC1    1     GLC     C1    1   0.3650
  2   gC2    1     GLC     C2    2   0.2050
  3   gC2    1     GLC     C3    3   0.2050
  4   gC2    1     GLC     C4    4   0.2050
  5   gC3    1     GLC     C5    5   0.1700
  6   gC4    1     GLC     C6    6   0.1450
  7   gO1    1     GLC     O1    7  -0.4000
  8   gO2    1     GLC     O2    1  -0.7000
  9   gO2    1     GLC     O3    2  -0.7000
 10   gO2    1     GLC     O4    3  -0.7000
 11   gO2    1     GLC     O5    4  -0.7000
 12   gO3    1     GLC     O6    6  -0.6830
 13   gH1    1     GLC     H1C   1   0.1000
 14   gH2    1     GLC     H2C   2   0.0600
 15   gH2    1     GLC     H3C   3   0.0600
 16   gH2    1     GLC     H4C   4   0.0600
 17   gH3    1     GLC     H5C   5   0.0300
 18   gH2    1     GLC     H6C   6   0.0600
 19   gH2    1     GLC     H6C   6   0.0600
 20   gH4    1     GLC     H1O   1   0.4350
 21   gH4    1     GLC     H2O   2   0.4350
 22   gH4    1     GLC     H3O   3   0.4350
 23   gH4    1     GLC     H4O   4   0.4350
 24   gH5    1     GLC     H5O   6   0.4180


[ bonds ]
;ai  aj  fun    l0      kl
  1   2   1  0.1529  224262
  1   7   1  0.1410  267776
  1   8   1  0.1410  267776
  1  13   1  0.1090  284512
  2   3   1  0.1529  224262
  2   9   1  0.1410  267776
  2  14   1  0.1090  284512
  3   4   1  0.1529  224262
  3  10   1  0.1410  267776
  3  15   1  0.1090  284512
  4   5   1  0.1529  224262
  4  11   1  0.1410  267776
  4  16   1  0.1090  284512
  5   6   1  0.1529  224262
  5   7   1  0.1410  267776
  5  17   1  0.1090  284512
  6  12   1  0.1410  267776
  6  18   1  0.1090  284512
  6  19   1  0.1090  284512
  8  20   1  0.0945  462750
  9  21   1  0.0945  462750
 10  22   1  0.0945  462750
```

```
 11  23   1  0.0945  462750
 12  24   1  0.0945  462750


[ angles ]
;ai  aj  ak  fun    a0      ka
  1   2   3   1  112.7  488.60
  1   2   9   1  109.5  418.60
  1   2  14   1  110.7  314.00
  1   8  20   1  108.5  460.30
  2   3   4   1  112.7  488.60
  2   3  10   1  109.5  418.60
  2   3  15   1  110.7  314.00
  2   9  21   1  108.5  460.30
  3   4   5   1  112.7  488.60
  3   4  11   1  109.5  418.60
  3   4  16   1  110.7  314.00
  3  10  22   1  108.5  460.30
  4   5   6   1  112.7  488.60
  4   5   7   1  109.5  418.60
  4   5  17   1  110.7  314.00
  4  11  23   1  108.5  460.30
  5   6  12   1  109.5  418.60
  5   6  18   1  110.7  314.00
  5   6  19   1  110.7  314.00
  5   7   1   1  109.5  502.40
  6  12  24   1  108.5  460.30
  7   1   2   1  109.5  418.60
  7   1   8   1  111.5  775.40
  7   1  13   1  109.5  293.00
  8   1   2   1  109.5  418.60
  8   1  13   1  109.5  293.00
  9   2   3   1  109.5  418.60
  9   2  14   1  109.5  293.00
 10   3   4   1  109.5  418.60
 10   3  15   1  109.5  293.00
 11   4   5   1  109.5  418.60
 11   4  16   1  109.5  293.00
 12   6  18   1  109.5  293.00
 12   6  19   1  109.5  293.00
 13   1   2   1  110.7  314.00
 14   2   3   1  110.7  314.00
 15   3   4   1  110.7  314.00
 16   4   5   1  110.7  314.00
 17   5   6   1  110.7  314.00
 17   5   7   1  109.5  293.00
 18   6  19   1  107.8  276.40


[ dihedrals ]
;ai  aj  ak  al  fu    phi0      cp   mult
  1   2   3   4   1      0  3.640080   1
  1   2   3   4   1    180 -0.328444   2
  1   2   3   4   1      0  0.583668   3
  1   2   3  10   1      0 -2.794912   1
  1   2   3  15   1      0  0.765672   3
  1   2   9  21   1      0  5.594008   1
  1   2   9  21   1    180 -6.031236   2
```

```
1   2   9   21   1     0   2.146392   3        7   1   2   9    1     0   9.035348    1
1   7   5   4    1     0   1.359800   1        7   1   2   14   1     0   0.979056    3
1   7   5   4    1   180  -0.523000   2        7   1   8   20   1     0  -2.629644    1
1   7   5   4    1     0   1.401640   3        7   1   8   20   1   180  -3.778152    2
1   7   5   6    1     0   1.359800   1        7   1   8   20   1     0   0.006276    3
1   7   5   6    1   180  -0.523000   2        7   5   4   11   1     0   9.035348    1
1   7   5   6    1     0   1.401640   3        7   5   4   16   1     0   0.979056    3
1   7   5   17   1     0   1.589920   3        7   5   6   12   1     0   9.035348    1
2   3   4   5    1     0   3.640080   1        7   5   6   18   1     0   0.979056    3
2   3   4   5    1   180  -0.328444   2        7   5   6   19   1     0   0.979056    3
2   3   4   5    1     0   0.583668   3        8   1   2   9    1     0  18.96607     1
2   3   4   11   1     0  -2.794912   1        8   1   2   14   1     0   0.979056    3
2   3   4   16   1     0   0.765672   3        9   2   1   13   1     0   0.979056    3
2   3  10   22   1     0   5.594008   1        9   2   3   10   1     0  18.96607     1
2   3  10   22   1   180  -6.031236   2        9   2   3   15   1     0   0.979056    3
2   3  10   22   1     0   2.146392   3       10   3   2   14   1     0   0.979056    3
2   1   7   5    1     0   1.359800   1       10   3   4   11   1     0  18.96607     1
2   1   7   5    1   180  -0.523000   2       10   3   4   16   1     0   0.979056    3
2   1   7   5    1     0   1.401640   3       11   4   3   15   1     0   0.979056    3
2   1   8   20   1     0   5.594008   1       11   4   5   17   1     0   0.979056    3
2   1   8   20   1   180  -6.031236   2       12   6   5   17   1     0   0.979056    3
2   1   8   20   1     0   2.146392   3       13   1   2   14   1     0   0.665256    3
3   4   5   6    1     0   3.640080   1       13   1   8   20   1     0   0.941400    3
3   4   5   6    1   180  -0.328444   2       14   2   3   15   1     0   0.665256    3
3   4   5   6    1     0   0.583668   3       14   2   9   21   1     0   0.941400    3
3   4   5   7    1     0  -2.794912   1       15   3   4   16   1     0   0.665256    3
3   4   5   17   1     0   0.765672   3       15   3  10   22   1     0   0.941400    3
3   4  11   23   1     0   5.594008   1       16   4   5   17   1     0   0.665256    3
3   4  11   23   1   180  -6.031236   2       16   4  11   23   1     0   0.941400    3
3   4  11   23   1     0   2.146392   3       17   5   6   18   1     0   0.665256    3
3   2   1   7    1     0  -2.794912   1       17   5   6   19   1     0   0.665256    3
3   2   1   8    1     0  -2.794912   1       18   6  12   24   1     0   0.941400    3
3   2   1   13   1     0   0.765672   3       19   6  12   24   1     0   0.941400    3
3   2   9   21   1     0   5.594008   1
3   2   9   21   1   180  -6.031236   2    [ pairs ]
3   2   9   21   1     0   2.146392   3    ;ai  aj  fun          c6            c12
4   5   6   12   1     0  -2.794912   1    1    4
4   5   6   18   1     0   0.765672   3    1    6
4   5   6   19   1     0   0.765672   3    1   10
4   3   2   14   1     0   0.765672   3    1   15
4   3   2   9    1     0  -2.794912   1    1   17
4   3  10   22   1     0   5.594008   1    1   21
4   3  10   22   1   180  -6.031236   2    2    5
4   3  10   22   1     0   2.146392   3    2   11
5   6  12   24   1     0   5.594008   1    2   16
5   6  12   24   1   180  -6.031236   2    2   20
5   6  12   24   1     0   2.146392   3    2   22
5   7   1   8    1     0  -0.784500   1    3    6
5   7   1   8    1   180  -2.840936   2    3    7
5   7   1   8    1     0   0.008368   3    3    8
5   7   1   13   1     0   1.589920   3    3   13
5   4   3   10   1     0  -2.794912   1    3   17
5   4   3   15   1     0   0.765672   3    3   21
5   4  11   23   1     0   5.594008   1    3   23
5   4  11   23   1     0  -6.031236   2    4    9
5   4  11   23   1     0   2.146392   3    4   12
6   5   4   11   1     0  -2.794912   1    4   14
6   5   4   16   1     0   0.765672   3    4   18
```

```
4  19                                          9  13
4  22                                          9  15
5   8                                         10  11
5  10                                         10  14
5  13                                         10  16
5  15                                         11  15
5  23                                         11  17
5  24                                         12  17
6  11                                         13  14
6  16                                         13  20
7   9                                         14  15
7  11                                         14  21
7  12                                         15  16
7  14                                         15  22
7  16                                         16  17
7  18                                         16  23
7  19                                         17  18
7  20                                         17  19
8   9                                         18  24
8  14                                         19  24
9  10
```

A.2.11   Trehalose

```
[ moleculetype ]                              26   TH2   1   TRE   H3C   3   0.060
; name nrexcl                                 27   TH2   1   TRE   H4C   4   0.060
TRE    3                                      28   TH3   1   TRE   H5C   5   0.030
                                              29   TH2   1   TRE   H6C   6   0.060
                                              30   TH2   1   TRE   H6C   6   0.060
[ atoms ]                                     31   TH4   1   TRE   H2O   2   0.435
;nr  type  resnr  residu  atom  cgnr  charge  32   TH4   1   TRE   H3O   3   0.435
  1   TC1    1     TRE     C1    1   0.300     33   TH4   1   TRE   H4O   4   0.435
  2   TC2    1     TRE     C2    2   0.205     34   TH5   1   TRE   H6O   6   0.418
  3   TC2    1     TRE     C3    3   0.205     35   TH1   1   TRE   H1C   9   0.100
  4   TC2    1     TRE     C4    4   0.205     36   TH2   1   TRE   H2C  10   0.060
  5   TC3    1     TRE     C5    5   0.170     37   TH2   1   TRE   H3C  11   0.060
  6   TC4    1     TRE     C6    6   0.145     38   TH2   1   TRE   H4C  12   0.060
  7   TO1    1     TRE     O1    8  -0.400     39   TH3   1   TRE   H5C  13   0.030
  8   TO2    1     TRE     O2    2  -0.700     40   TH2   1   TRE   H6C  14   0.060
  9   TO2    1     TRE     O3    3  -0.700     41   TH2   1   TRE   H6C  14   0.060
 10   TO2    1     TRE     O4    4  -0.700     42   TH4   1   TRE   H2O  10   0.435
 11   TO1    1     TRE     O5    7  -0.400     43   TH4   1   TRE   H3O  11   0.435
 12   TO3    1     TRE     O6    6  -0.683     44   TH4   1   TRE   H4O  12   0.435
 13   TC1    1     TRE     C1    9   0.300     45   TH5   1   TRE   H6O  14   0.418
 14   TC2    1     TRE     C2   10   0.205
 15   TC2    1     TRE     C3   11   0.205
 16   TC2    1     TRE     C4   12   0.205     [ bonds ]
 17   TC3    1     TRE     C5   13   0.170     ;ai  aj  fun    l0      kl
 18   TC4    1     TRE     C6   14   0.145      1    2   1  0.1529  224420
 19   TO2    1     TRE     O2   10  -0.700      1    7   1  0.1380  267960
 20   TO2    1     TRE     O3   11  -0.700      1   11   1  0.1380  267960
 21   TO2    1     TRE     O4   12  -0.700      1   24   1  0.1090  284700
 22   TO1    1     TRE     O5   15  -0.400      2    3   1  0.1529  224420
 23   TO3    1     TRE     O6   14  -0.683      2    8   1  0.1410  267960
 24   TH1    1     TRE     H1C   1   0.100      2   25   1  0.1090  284700
 25   TH2    1     TRE     H2C   2   0.060      3    4   1  0.1529  224420
```

```
 3    9   1  0.1410  267960                              3   24
 3   26   1  0.1090  284700                              3   28
 4    5   1  0.1529  224420                              3   31
 4   10   1  0.1410  267960                              3   33
 4   27   1  0.1090  284700                              4    8
 5    6   1  0.1529  224420                              4   12
 5   11   1  0.1410  267960                              4   25
 5   28   1  0.1090  284700                              4   29
 6   12   1  0.1410  267960                              4   30
 6   29   1  0.1090  284700                              4   32
 6   30   1  0.1090  284700                              5    7
 7   13   1  0.1380  267960                              5    9
13   14   1  0.1529  224420                              5   24
13   22   1  0.1380  267960                              5   26
13   35   1  0.1090  284700                              5   33
14   15   1  0.1529  224420                              5   34
14   19   1  0.1410  267960                              6   10
14   36   1  0.1090  284700                              6   27
15   16   1  0.1529  224420                              7    8
15   20   1  0.1410  267960                              7   15
15   37   1  0.1090  284700                              7   17
16   17   1  0.1529  224420                              7   19
16   21   1  0.1410  267960                              7   25
16   38   1  0.1090  284700                              7   36
17   18   1  0.1529  224420                              8    9
17   22   1  0.1410  267960                              8   11
17   39   1  0.1090  284700                              8   24
18   23   1  0.1410  267960                              8   26
18   40   1  0.1090  284700                              9   10
18   41   1  0.1090  284700                              9   25
19   42   1  0.0945  462772                              9   27
20   43   1  0.0945  462772                             10   11
21   44   1  0.0945  462772                             10   26
23   45   1  0.0945  462772                             10   28
 8   31   1  0.0945  462772                             11   12
 9   32   1  0.0945  462772                             11   13
10   33   1  0.0945  462772                             11   25
12   34   1  0.0945  462772                             11   27
                                                        11   29
                                                        11   30
[ pairs ]                                               12   28
;ai  aj  fun           c6          c12                  13   16
 1    4                                                 13   18
 1    6                                                 13   20
 1    9                                                 13   24
 1   14                                                 13   37
 1   22                                                 13   39
 1   26                                                 13   42
 1   28                                                 14   17
 1   31                                                 14   21
 1   35                                                 14   38
 2    5                                                 14   43
 2   10                                                 15   18
 2   13                                                 15   22
 2   27                                                 15   35
 2   32                                                 15   39
 3    6                                                 15   42
 3    7                                                 15   44
 3   11
```

16	19
16	23
16	36
16	40
16	41
16	43
17	20
17	35
17	37
17	44
17	45
18	21
18	38
19	20
19	22
19	35
19	37
20	21
20	36
20	38
21	22
21	37
21	39
22	23
22	36
22	38
22	40
22	41
23	39
24	25
25	26
25	31
26	27
26	32
27	28
27	33
28	29
28	30
29	34
30	34
35	36
36	37
36	42
37	38
37	43
38	39
38	44
39	40
39	41
40	45
41	45

[angles]

;ai	aj	ak	fun	a0	ka
1	2	3	1	112.7	488.60
1	2	8	1	109.5	418.60
1	2	25	1	110.7	314.00
1	7	13	1	109.5	502.20
2	1	7	1	109.5	418.60
2	1	11	1	109.5	418.60
2	1	24	1	110.7	314.00
2	3	4	1	112.7	488.60
2	3	9	1	109.5	418.60
2	3	26	1	110.7	314.00
2	8	31	1	108.5	460.30
3	2	25	1	110.7	314.00
3	4	5	1	112.7	488.60
3	4	10	1	109.5	418.60
3	4	27	1	110.7	418.60
3	9	32	1	108.5	460.60
4	3	26	1	110.7	418.00
4	5	6	1	112.7	488.60
4	5	11	1	109.5	418.60
4	5	28	1	110.7	314.00
4	10	33	1	108.5	460.30
5	4	27	1	110.7	314.00
5	6	12	1	109.5	408.30
5	6	29	1	110.7	314.00
5	6	30	1	110.7	314.00
5	11	1	1	109.5	502.20
6	5	28	1	110.7	314.00
6	12	34	1	108.5	460.30
7	1	11	1	111.6	775.40
7	1	24	1	109.5	293.00
7	13	14	1	109.5	418.60
7	13	22	1	111.6	775.40
7	13	35	1	109.5	293.00
8	2	3	1	109.5	418.60
9	3	4	1	109.5	418.60
10	4	5	1	109.5	418.60
11	5	6	1	109.5	418.60
11	5	28	1	109.5	293.00
11	1	24	1	109.5	293.00
12	6	29	1	109.5	418.60
12	6	30	1	109.5	418.60
13	14	15	1	112.7	488.60
13	14	19	1	109.5	418.60
13	14	36	1	110.7	314.00
13	22	17	1	109.5	502.40
14	13	22	1	109.5	418.60
14	13	35	1	110.7	314.00
14	15	16	1	112.7	488.60
14	15	20	1	109.5	418.60
14	15	37	1	110.7	314.00
14	19	42	1	108.5	460.30
15	14	36	1	110.7	314.00
15	16	17	1	112.7	488.60
15	16	21	1	109.5	418.60
15	16	38	1	110.7	314.00
15	20	43	1	108.5	460.60
16	15	37	1	110.7	314.00
16	17	18	1	112.7	488.30
16	17	22	1	109.5	418.60
16	17	39	1	110.7	314.00
16	21	44	1	108.5	460.30
17	16	38	1	110.7	314.00

```
17  18  23   1  109.5  418.60          2   3   9  32  1   180 -6.031235    2
17  18  40   1  110.7  314.00          2   3   9  32  1     0  2.146390    3
17  18  41   1  110.7  314.00          3   4   5   6  1     0  3.640080    1
18  17  39   1  110.7  314.00          3   4   5   6  1   180 -0.328445    2
18  23  45   1  108.5  460.30          3   4   5   6  1     0  0.583670    3
19  14  36   1  109.5  293.00          3   2   1   7  1     0 -2.794910    1
19  14  15   1  109.5  418.60          3   4   5  11  1     0 -2.794910    1
20  15  37   1  109.5  293.00          3   2   1  11  1     0 -2.794910    1
20  15  16   1  109.5  418.60          3   2   1  24  1     0  0.765670    3
21  16  17   1  109.5  418.60          3   4   5  28  1     0  0.765670    3
21  16  38   1  109.5  293.00          3   2   8  31  1     0  5.594010    1
22  17  18   1  109.5  418.60          3   2   8  31  1   180 -6.031235    2
23  18  40   1  109.5  293.00          3   2   8  31  1     0  2.146390    3
23  18  41   1  109.5  293.00          3   4  10  33  1     0  5.594010    1
25   2   8   1  109.5  293.00          3   4  10  33  1   180 -6.031235    2
26   3   9   1  109.5  293.00          3   4  10  33  1     0  2.146390    3
27   4  10   1  109.5  293.00          4   3   2   8  1     0 -2.794910    1
29   6  30   1  107.8  276.40          4   5   6  12  1     0 -2.794910    1
35  13  22   1  109.5  293.00          4   3   2  25  1     0  0.765670    3
39  17  22   1  109.5  293.00          4   5   6  29  1     0  0.765670    3
40  18  41   1  107.8  276.40          4   5   6  30  1     0  0.765670    3
                                       4   3   9  32  1     0  5.594010    1
[ dihedrals ]                          4   3   9  32  1   180 -6.031235    2
;ai aj ak al fu    phi0     cp mult     4   3   9  32  1     0  2.146390    3
 1   2   3   4  1     0  3.640080    1  5  11   1   7  1     0 -0.784500    1
 1   2   3   4  1   180 -0.328445    2  5  11   1   7  1   180 -2.840935    2
 1   2   3   4  1     0  0.583670    3  5  11   1   7  1     0  0.008370    3
 1  11   5   4  1     0  1.359800    1  5   4   3   9  1     0 -2.794910    1
 1  11   5   4  1   180 -0.523000    2  5  11   1  24  1     0  1.589920    3
 1  11   5   4  1     0  1.401640    3  5   4   3  26  1     0  0.765670    3
 1  11   5   6  1     0  1.359800    1  5   4  10  33  1     0  5.594010    1
 1  11   5   6  1   180 -0.523000    2  5   4  10  33  1   180 -6.031235    2
 1  11   5   6  1     0  1.401640    3  5   4  10  33  1     0  2.146390    3
 1   2   3   9  1     0 -2.794910    0  5   6  12  34  1     0  5.594010    1
 1   7  13  14  1     0  1.359800    1  5   6  12  34  1   180 -6.031235    2
 1   7  13  14  1   180 -0.523000    2  5   6  12  34  1     0  2.146390    3
 1   7  13  14  1     0  1.401640    3  6   5   4  10  1     0 -2.794910    1
 1   7  13  22  1     0 -0.784500    1  6   5   4  27  1     0  0.765670    3
 1   7  13  22  1   180 -2.840935    2  7   1   2   8  1     0  9.035350    1
 1   7  13  22  1     0  0.008370    3  7  13  14  15  1     0 -2.794910    1
 1   2   3  26  1     0  0.765670    3  7  13  22  17  1     0 -0.784500    1
 1  11   5  28  1     0  1.589920    3  7  13  22  17  1   180 -2.840935    2
 1   2   8  31  1     0  5.594010    1  7  13  22  17  1     0  0.008370    3
 1   2   8  31  1   180 -6.031235    2  7  13  14  19  1     0  9.035350    1
 1   2   8  31  1     0  2.146390    3  7   1   2  25  1     0  0.979055    3
 1   7  13  35  1     0  1.589920    3  7  13  14  36  1     0  0.979055    3
 2   3   4   5  1     0  3.640080    1  8   2   3   9  1     0 18.966070    1
 2   3   4   5  1   180 -0.328445    2  8   2   1  11  1     0  9.035350    1
 2   3   4   5  1     0  0.583670    3  8   2   1  24  1     0  0.979055    3
 2   1  11   5  1     0  1.359800    1  8   2   3  26  1     0  0.979055    3
 2   1  11   5  1   180 -0.523000    2  9   3   4  10  1     0 18.966070    1
 2   1  11   5  1     0  1.401640    3  9   3   2  25  1     0  0.979055    3
 2   3   4  10  1     0 -2.794910    1  9   3   4  27  1     0  0.979055    3
 2   1   7  13  1     0  1.359800    1 10   4   5  11  1     0  9.035350    1
 2   1   7  13  1   180 -0.523000    2 10   4   3  26  1     0  0.979055    3
 2   1   7  13  1     0  1.401640    3 10   4   5  28  1     0  0.979055    3
 2   3   4  27  1     0  0.765670    3 11   5   6  12  1     0  9.035350    1
 2   3   9  32  1     0  5.594010    1 11   1   7  13  1     0 -0.784500    1
```

11	1	7	13	1	180	-2.840935	2
11	1	7	13	1	0	0.008370	3
11	1	2	25	1	0	0.979055	1
11	5	4	27	1	0	0.979055	1
11	5	6	29	1	0	0.979055	1
11	5	6	30	1	0	0.979055	1
12	6	5	28	1	0	0.979055	1
13	14	15	16	1	0	3.640080	1
13	14	15	16	1	180	-0.328445	2
13	14	15	16	1	0	0.583670	3
13	22	17	18	1	0	1.359800	1
13	22	17	18	1	180	-0.523000	2
13	22	17	18	1	0	1.401640	3
13	14	15	20	1	0	-2.794910	1
13	7	1	24	1	0	1.589920	3
13	14	15	37	1	0	0.765670	3
13	22	17	39	1	0	1.589920	3
13	14	19	42	1	0	5.594010	1
13	14	19	42	1	180	-6.031235	2
13	14	19	42	1	0	2.146390	3
14	15	16	17	1	0	3.640080	1
14	15	16	17	1	180	-0.328445	2
14	15	16	17	1	0	0.583670	3
14	13	22	17	1	0	1.359800	1
14	13	22	17	1	180	-0.523000	2
14	13	22	17	1	0	1.401640	3
14	15	16	21	1	0	-2.794910	1
14	15	16	38	1	0	0.765670	3
14	15	20	43	1	0	5.594010	1
14	15	20	43	1	180	-6.031235	2
14	15	20	43	1	0	2.146390	3
15	16	17	18	1	0	3.640080	1
15	16	17	18	1	180	-0.328445	2
15	16	17	18	1	0	0.583670	3
15	16	17	22	1	0	-2.794910	1
15	14	13	22	1	0	2.794910	1
15	14	13	35	1	0	0.765670	3
15	16	17	39	1	0	0.765670	3
15	14	19	42	1	0	5.594010	1
15	14	19	42	1	180	-6.031235	2
15	14	19	42	1	0	2.146390	3
15	16	21	44	1	0	5.594010	1
15	16	21	44	1	180	-6.031235	2
15	16	21	44	1	0	2.146390	3
16	15	14	19	1	0	-2.794910	1
16	17	18	23	1	0	-2.794910	1
16	15	14	36	1	0	0.765670	3
16	17	18	40	1	0	0.765670	3
16	17	18	41	1	0	0.765670	3
16	15	20	43	1	0	5.594010	1
16	15	20	43	1	180	-6.031235	2

16	15	20	43	1	0	2.146390	3
17	16	15	20	1	0	-2.794910	1
17	22	13	35	1	0	1.589920	3
17	16	15	37	1	0	0.765670	3
17	16	21	44	1	0	5.594010	1
17	16	21	44	1	180	-6.031235	2
17	16	21	44	1	0	2.146390	3
17	18	23	45	1	0	5.594010	1
17	18	23	45	1	180	-6.031235	2
17	18	23	45	1	0	2.146390	3
18	17	16	21	1	0	-2.794910	1
18	17	16	38	1	0	0.765670	3
19	14	15	20	1	0	18.966070	1
19	14	13	22	1	0	9.035350	1
19	14	13	35	1	0	0.979055	3
19	14	15	37	1	0	0.979055	3
20	15	16	21	1	0	18.966070	1
20	15	14	36	1	0	0.979055	3
20	15	16	38	1	0	0.979055	3
21	16	17	22	1	0	9.035350	1
21	16	15	37	1	0	0.979055	3
21	16	17	39	1	0	0.979055	3
22	17	18	23	1	0	9.035350	1
22	13	14	36	1	0	0.979055	3
22	17	16	38	1	0	0.979055	3
22	17	18	40	1	0	0.979055	3
22	17	18	41	1	0	0.979055	3
23	18	17	39	1	0	0.979055	3
24	1	2	25	1	0	0.665255	3
25	2	3	26	1	0	0.665255	3
25	2	8	31	1	0	0.941400	3
26	3	4	27	1	0	0.665255	3
26	3	9	32	1	0	0.941400	3
27	4	5	28	1	0	0.665255	3
27	4	10	33	1	0	0.941400	3
28	5	6	29	1	0	0.665255	3
28	5	6	30	1	0	0.665255	3
29	6	12	34	1	0	0.941400	3
30	6	12	34	1	0	0.941400	3
35	13	14	36	1	0	0.665255	3
36	14	15	37	1	0	0.665255	3
36	14	19	42	1	0	0.941400	3
37	15	16	38	1	0	0.665255	3
37	15	20	43	1	0	0.941400	3
38	16	17	39	1	0	0.665255	3
38	16	21	44	1	0	0.941400	3
39	17	18	40	1	0	0.665255	3
39	17	18	41	1	0	0.665255	3
40	18	23	45	1	0	0.941400	3
41	18	23	45	1	0	0.941400	3

A.2.12   Non-Bonded Parameters

[atomtypes]

;name	mass	charge	ptype	c6	c12
OW	15.99940	0.000	A	0.26171E-02	0.26331E-05
HW	1.00800	0.000	A	0.00000E+00	0.00000E+00
LC3N	15.03500	0.000	A	0.93477E-02	0.36047E-04
LNL	14.00670	0.000	A	0.33514E-02	0.39494E-05
LC2	14.02700	0.000	A	0.85953E-02	0.30478E-04
LC2O	14.02700	0.000	A	0.72985E-02	0.21975E-04
LOS	15.99940	0.000	A	0.20733E-02	0.15114E-05
LP	30.97380	0.000	A	0.91516E-02	0.25045E-04
LOM	15.99940	0.000	A	0.23621E-02	0.15887E-05
LCH1	13.01900	0.000	A	0.40226E-02	0.12112E-04
LC	12.01100	0.000	A	0.48722E-02	0.13549E-04
LO2	15.99940	0.000	A	0.16304E-02	0.10966E-04
LCH2	14.02700	0.000	A	0.58616E-02	0.22604E-04
LCH3	15.03500	0.000	A	0.87924E-02	0.33906E-04
LH3N	1.00800	0.000	A	0.00000E+00	0.00000E+00
dO1	15.99940	0.000	A	1.55079E-03	5.13199E-07
dS1	32.06600	0.000	A	1.05609E-02	2.14981E-05
dC1	15.03450	0.000	A	1.02889E-02	2.81125E-05
TC1	12.01100	0.000	A	2.03186E-03	3.73510E-06
TC2	12.01100	0.000	A	2.03186E-03	3.73510E-06
TC3	12.01100	0.000	A	2.03186E-03	3.73510E-06
TC4	12.01100	0.000	A	2.03186E-03	3.73510E-06
TO1	15.99940	0.000	A	1.39463E-03	8.29557E-07
TO2	15.99940	0.000	A	2.38353E-03	1.99550E-06
TO3	15.99940	0.000	A	2.62614E-03	2.42240E-06
TH1	1.00800	0.000	A	1.22660E-04	2.99463E-08
TH2	1.00800	0.000	A	1.22660E-04	2.99463E-08
TH3	1.00800	0.000	A	1.22660E-04	2.99463E-08
TH4	1.00800	0.000	A	0.00000E+00	0.00000E+00
TH5	1.00800	0.000	A	0.00000E+00	0.00000E+00

[bondtypes]

; ai	aj	fun	l0	kl
LNL	LC3N	1	0.147	376560
LNL	LC2	1	0.147	376560
LC2	LC2O	1	0.153	334720
LOS	LC2O	1	0.143	251040
LOS	LP	1	0.161	251040
LOM	LP	1	0.148	376560
LO2	LC	1	0.123	502080
LCH1	LC2O	1	0.153	334720
LOS	LCH1	1	0.143	251040
LOS	LC	1	0.136	376560
LC	LCH2	1	0.153	334720
LCH2	LCH3	1	0.153	334720
LCH2	LCH2	1	0.153	334720
LNL	LH3N	1	0.100	374468
LCH1	LCH2	1	0.153	334720
LCH1	LCH1	1	0.139	418400

[angletypes]

; ai	aj	ak	fun	a0	ka
LC3N	LNL	LC3N	1	109.5	334.72
LC3N	LNL	LC2	1	109.5	376.56
LNL	LC2	LC2O	1	109.5	460.24
LC2	LC2O	LOS	1	109.5	460.24
LC2O	LOS	LP	1	120.0	397.48
LOS	LP	LOM	1	109.6	397.48
LOS	LP	LOS	1	103.0	397.48
LOM	LP	LOM	1	120.0	585.76
LOS	LC2O	LCH1	1	111.0	460.24
LC2O	LCH1	LOS	1	109.5	460.24
LC2O	LCH1	LC2O	1	109.5	460.24
LCH1	LOS	LC	1	120.0	418.40
LC2O	LOS	LC	1	120.0	418.40
LOS	LC	LO2	1	124.0	502.08
LOS	LC	LCH2	1	115.0	502.08
LO2	LC	LCH2	1	121.0	502.08
LC	LCH2	LCH2	1	111.0	460.24
LCH2	LCH2	LCH2	1	111.0	460.24
LCH2	LCH2	LCH3	1	111.0	460.24
LH3N	LNL	LH3N	1	109.5	334.72
LH3N	LNL	LC2	1	109.5	376.56
LCH1	LCH1	LCH2	1	120.0	502.08
LCH1	LCH2	LCH2	1	111.0	460.24

Appendix B

Analysis Codes

This chapter contains a list of analysis codes that are not part of the GROMACS distribution. All codes are developed from a GROMACS template, given for all GROMACS distributions, to read the simulation output trajectory files (xtc, trr, and edr format).

B.1 Index Selection

B.1.1 Lipid Phosphorus

```
/*
 * $Id: template.c,v 1.4 2001/07/23 15:28:29 lindahl Exp $
 *
 *              This source code is part of
 *
 *              G   R   O   M   A   C   S
 *
 *      GROningen MAchine for Chemical Simulations
 *
 *                     VERSION 3.0
 *
 * Copyright (c) 1991-2001
 * BIOSON Research Institute, Dept. of Biophysical Chemistry
 * University of Groningen, The Netherlands
 *
 * This program is free software; you can redistribute it and/or
 * modify it under the terms of the GNU General Public License
 * as published by the Free Software Foundation; either version 2
```

```
 * of the License, or (at your option) any later version.
 *
 * If you want to redistribute modifications, please consider that
 * scientific software is very special. Version control is crucial -
 * bugs must be traceable. We will be happy to consider code for
 * inclusion in the official distribution, but derived work must not
 * be called official GROMACS. Details are found in the README & COPYING
 * files - if they are missing, get the official version at www.gromacs.org.
 *
 * To help us fund GROMACS development, we humbly ask that you cite
 * the papers on the package - you can find them in the top README file.
 *
 * Do check out http://www.gromacs.org , or mail us at gromacs@gromacs.org .
 *
 * And Hey:
 * Gyas ROwers Mature At Cryogenic Speed
 */

/* This line is only for CVS version info */

static char *SRCID_template_c = "$Id: template.c,v 1.4 2001/07/23 15:28:29 lindahl Exp $";

#include "statutil.h"
#include "typedefs.h"
#include "smalloc.h"
#include "vec.h"
#include "copyrite.h"
#include "statutil.h"
#include "tpxio.h"
#include "index.h"
#include "xvgr.h"

#define ANINT(A) (double) (long) (((A)<0.0) ? ((A)-0.5) : ((A)+0.5))
#define PI 3.14159265358979323846264338


// structure for output file

  struct hydanalys {
    double t, x, y, z, a, b, c;
  } *hydallx;

  struct hydanaly {
    int a, b, c, d, aa, bb, cc, dd;
  } *hydall;

// start main here

  int main(int argc,char *argv[])
  {
  static char *desc[] = {
    "this is a small test program meant to serve as a template ",
    "when writing your own analysis tools. The advantage of ",
    "using gromacs for this is that you have access to all ",
    "information in the topology, and your program will be ",
    "able to handle all types of coordinates and trajectory ",
    "files supported by gromacs. Go ahead and try it! ",
    "This test version just writes the coordinates of an ",
```

```
    "arbitrary atom to standard out for each frame. You can ",
    "select which atom you want to examine with the -n argument."
  };

// allocate memory for output here

   hydallx = (struct hydanalys*) calloc(999999,sizeof(struct hydanalys));
   hydall = (struct hydanaly*) calloc(999999,sizeof(struct hydanaly));

// default value for rcut (hydration radius)

   static real n=8.12;

   /* Extra arguments - but note how you always get the begin/end
   * options when running the program, without mentioning them here!
   */

// passing a value through -rcut and save as "n"

   t_pargs pa[] = {
   { "-int", FALSE, etREAL, {&n},
     "no input is required here, just pick P8 or P8E index"
   }
   };

// define variables

   t_topology top;
   char       title[STRLEN];
   t_trxframe fr;
   rvec       *xtop;
   matrix     box;
   int        status;
   int        flags = TRX_READ_X;
   int        *isize;             // size of index
   char       **grpnames;         // group name of index
   atom_id    **index;            // index values
   int        i,j;
   int        number=0;           // counter
   FILE       *fp;                // output file
   int        lasttime;           // last timestep

   t_filenm fnm[] = {
   { efTPS,  NULL,  NULL, ffREAD },      /* this is for the topology */
   { efTRX, "-f", NULL, ffREAD },        /* this is for the trajectory */
   { efNDX, NULL , NULL, ffOPTRD },      /* this is for index */
   { efXVG, "-o", "N_P_vector", ffOPTWR }   /* this is for output in xvg */
   };

   #define NFILE asize(fnm)

   CopyRight(stderr,argv[0]);

   /* This is the routine responsible for adding default options,
   * calling the X/motif interface, etc. */

   parse_common_args(&argc,argv,PCA_CAN_TIME | PCA_CAN_VIEW,
    NFILE,fnm,asize(pa),pa,asize(desc),desc,0,NULL);
```

```
/* We don't need any topology information to write the coordinates,
 * but to show how it works we start by writing the name and
 * charge of the selected atom. It returns a boolean telling us
 * whether the topology was found and could be read
 */

read_tps_conf(ftp2fn(efTPS,NFILE,fnm),title,&top,&xtop,NULL,box,TRUE);
sfree(xtop);

// allocate memory for read variable using snew

int grNR=999999;
snew(grpnames,grNR);
snew(index,grNR);
snew(isize,grNR);
snew(fp,grNR);

get_index(&(top.atoms),ftp2fn_null(efNDX,NFILE,fnm),1,isize,index,grpnames);

/* The first time we read data is a little special */

read_first_frame(&status,ftp2fn(efTRX,NFILE,fnm),&fr,flags);

/* This is the main loop over frames */

do {
int atom1=0;
int atom2=0;
int atom3=0;
int atom4=0;
double phiangle1=0;
double phiangle2=0;
double phiangle3=0;
double phiangle4=0;
double phiangle5=0;
double phiangle6=0;
double phiangle7=0;
double phiangle8=0;


// calcute atom number for N after pick P

for(i = 0; (i < isize[0]); i++) {
  int aa = index[0][i];

  if (fr.x[aa][ZZ]<fr.box[ZZ][ZZ]/2){

    hydall[atom1].a = aa + 1;
    atom1++;
    //phiangle1=phiangle1+fr.x[aa][ZZ];
    //phiangle2=phiangle2+fr.x[bb][ZZ];
    // printf("%g\n",phi*180/PI);
  }

  else{
   hydall[atom4].d = aa + 1;
    atom4++;
```

```
    //phiangle4=phiangle4+fr.x[aa][ZZ];
    //phiangle4=phiangle4+fr.x[bb][ZZ];
    //printf("%g\n",180-phi*180/PI);
  }
}

hydall[number].aa=atom1;
hydall[number].bb=atom2;
hydall[number].cc=atom3;
hydall[number].dd=atom4;

number++;

lasttime=fr.time;

} while(read_next_frame(status,&fr));

printf("%d %d %d %d\n",hydall[0].aa, hydall[0].bb, hydall[0].cc, hydall[0].dd);
 fp = xvgropen(opt2fn("-o",NFILE,fnm),
"","Time(ps)","Angle (degree)");

    fprintf(fp,"[ Pup ]\n");
    for (j=0; j<hydall[0].aa; j++) {
    fprintf(fp,"%6d",  hydall[j].a);
    }
    fprintf(fp,"\n");

    fprintf(fp,"[ Pdown ]\n");
    for (j=0; j<hydall[0].dd; j++) {
    fprintf(fp,"%6d",  hydall[j].d);
    }

  fclose(fp);
  thanx(stderr);
  return 0;
}
```

B.1.2 Lipid Oxygens

```
/*
 * $Id: template.c,v 1.4 2001/07/23 15:28:29 lindahl Exp $
 *
 *                This source code is part of
 *
 *                 G   R   O   M   A   C   S
 *
 *          GROningen MAchine for Chemical Simulations
 *
 *                        VERSION 3.0
 *
 * Copyright (c) 1991-2001
 * BIOSON Research Institute, Dept. of Biophysical Chemistry
 * University of Groningen, The Netherlands
 *
 * This program is free software; you can redistribute it and/or
 * modify it under the terms of the GNU General Public License
```

```
/* This line is only for CVS version info */

static char *SRCID_template_c = "$Id: template.c,v 1.4 2001/07/23 15:28:29 lindahl Exp $";

#include "statutil.h"
#include "typedefs.h"
#include "smalloc.h"
#include "vec.h"
#include "copyrite.h"
#include "statutil.h"
#include "tpxio.h"
#include "index.h"
#include "xvgr.h"

#define ANINT(A) (double) (long) (((A)<0.0) ? ((A)-0.5) : ((A)+0.5))
#define PI 3.14159265358979323846264338


// structure for output file

  struct hydanalys {
    double t, x, y, z, a, b, c;
  } *hydallx;

  struct hydanaly {
    int a, b, c, d, e, f, g, h, i, j, k, l, m, n, o, p, aa, bb, cc, dd;
  } *hydall;

// start main here

  int main(int argc,char *argv[])
  {
  static char *desc[] = {
    "this is a small test program meant to serve as a template ",
    "when writing your own analysis tools. The advantage of ",
    "using gromacs for this is that you have access to all ",
    "information in the topology, and your program will be ",
    "able to handle all types of coordinates and trajectory ",
    "files supported by gromacs. Go ahead and try it! ",
```

```
   "This test version just writes the coordinates of an ",
   "arbitrary atom to standard out for each frame. You can ",
   "select which atom you want to examine with the -n argument."
 };


// allocate memory for output here

   hydallx = (struct hydanalys*) calloc(999999,sizeof(struct hydanalys));
   hydall = (struct hydanaly*) calloc(999999,sizeof(struct hydanaly));


// default value for rcut (hydration radius)

   static real n=8.12;

   /* Extra arguments - but note how you always get the begin/end
   * options when running the program, without mentioning them here!
   */


// passing a value through -rcut and save as "n"

   t_pargs pa[] = {
   { "-int", FALSE, etREAL, {&n},
     "no input is required here, just pick P8 or P8E index"
   }
   };


// define variables

   t_topology top;
   char        title[STRLEN];
   t_trxframe fr;
   rvec        *xtop;
   matrix      box;
   int         status;
   int         flags = TRX_READ_X;
   int         *isize;            // size of index
   char        **grpnames;       // group name of index
   atom_id     **index;          // index values
   int         i,j;
   int         number=0;         // counter
   FILE        *fp;              // output file
   int         lasttime;         // last timestep

   t_filenm fnm[] = {
   { efTPS,  NULL,  NULL, ffREAD },       /* this is for the topology */
   { efTRX, "-f", NULL, ffREAD },         /* this is for the trajectory */
   { efNDX, NULL , NULL, ffOPTRD },       /* this is for index */
   { efXVG, "-o", "N_P_vector", ffOPTWR }   /* this is for output in xvg */
   };


   #define NFILE asize(fnm)


   CopyRight(stderr,argv[0]);


   /* This is the routine responsible for adding default options,
    * calling the X/motif interface, etc. */


   parse_common_args(&argc,argv,PCA_CAN_TIME | PCA_CAN_VIEW,
```

```
   NFILE,fnm,asize(pa),pa,asize(desc),desc,0,NULL);

/* We don't need any topology information to write the coordinates,
 * but to show how it works we start by writing the name and
 * charge of the selected atom. It returns a boolean telling us
 * whether the topology was found and could be read
 */

read_tps_conf(ftp2fn(efTPS,NFILE,fnm),title,&top,&xtop,NULL,box,TRUE);
sfree(xtop);

// allocate memory for read variable using snew

int grNR=999999;
snew(grpnames,grNR);
snew(index,grNR);
snew(isize,grNR);
snew(fp,grNR);

// getting index from -n

get_index(&(top.atoms),ftp2fn_null(efNDX,NFILE,fnm),1,isize,index,grpnames);

/* The first time we read data is a little special */

read_first_frame(&status,ftp2fn(efTRX,NFILE,fnm),&fr,flags);

/* This is the main loop over frames */

do {
  j=0;
int atom1=0;
int atom2=0;
int atom3=0;
int atom4=0;
double phiangle1=0;
double phiangle2=0;
double phiangle3=0;
double phiangle4=0;
double phiangle5=0;
double phiangle6=0;
double phiangle7=0;
double phiangle8=0;

// calcute atom number for N after pick P

for(i = 0; (i < isize[0]); i++) {
  int aa = index[0][i];
  hydall[atom1].a = aa - 1 + 1;
  hydall[atom1].b = aa + 1 + 1;
  hydall[atom1].c = aa + 2 + 1;
  hydall[atom1].d = aa + 3 + 1;
  hydall[atom1].e = aa + 6 + 1;
  hydall[atom1].f = aa + 8 + 1;
  hydall[atom1].g = aa + 25 + 1;
  hydall[atom1].h = aa + 27 + 1;
  atom1++;
}
```

```
   number++;

   lasttime=fr.time;

 } while(read_next_frame(status,&fr));

printf("%d %d %d %d\n",hydall[0].aa, hydall[0].bb, hydall[0].cc, hydall[0].dd);
 fp = xvgropen(opt2fn("-o",NFILE,fnm),
"","Time(ps)","Angle (degree)");


 fprintf(fp,"[ o7 ]\n");
 for (i=0; i<isize[0]; i++) {
   fprintf(fp,"%6d",  hydall[i].a);
 }
 fprintf(fp,"\n");

 fprintf(fp,"[ o9 ]\n");
 for (i=0; i<isize[0]; i++) {
   fprintf(fp,"%6d",  hydall[i].b);
 }
 fprintf(fp,"\n");

 fprintf(fp,"[ o10 ]\n");
 for (i=0; i<isize[0]; i++) {
   fprintf(fp,"%6d",  hydall[i].c);
 }
 fprintf(fp,"\n");

 fprintf(fp,"[ o11 ]\n");
 for (i=0; i<isize[0]; i++) {
   fprintf(fp,"%6d",  hydall[i].d);
 }
 fprintf(fp,"\n");

 fprintf(fp,"[ o14 ]\n");
 for (i=0; i<isize[0]; i++) {
   fprintf(fp,"%6d",  hydall[i].e);
 }
 fprintf(fp,"\n");

 fprintf(fp,"[ o16 ]\n");
 for (i=0; i<isize[0]; i++) {
   fprintf(fp,"%6d",  hydall[i].f);
 }
 fprintf(fp,"\n");

 fprintf(fp,"[ o33 ]\n");
 for (i=0; i<isize[0]; i++) {
   fprintf(fp,"%6d",  hydall[i].g);
 }
 fprintf(fp,"\n");

 fprintf(fp,"[ o35 ]\n");
 for (i=0; i<isize[0]; i++) {
   fprintf(fp,"%6d",  hydall[i].h);
 }
```

```
  fprintf(fp,"\n");
  fclose(fp);
  thanx(stderr);
  return 0;
}
```

B.1.3   *Sn*-1 Hydrocarbon Chain

```
/*
 * $Id: template.c,v 1.4 2001/07/23 15:28:29 lindahl Exp $
 *
 *                This source code is part of
 *
 *                 G   R   O   M   A   C   S
 *
 *          GROningen MAchine for Chemical Simulations
 *
 *                       VERSION 3.0
 *
 * Copyright (c) 1991-2001
 * BIOSON Research Institute, Dept. of Biophysical Chemistry
 * University of Groningen, The Netherlands
 *
 * This program is free software; you can redistribute it and/or
 * modify it under the terms of the GNU General Public License
 * as published by the Free Software Foundation; either version 2
 * of the License, or (at your option) any later version.
 *
 * If you want to redistribute modifications, please consider that
 * scientific software is very special. Version control is crucial -
 * bugs must be traceable. We will be happy to consider code for
 * inclusion in the official distribution, but derived work must not
 * be called official GROMACS. Details are found in the README & COPYING
 * files - if they are missing, get the official version at www.gromacs.org.
 *
 * To help us fund GROMACS development, we humbly ask that you cite
 * the papers on the package - you can find them in the top README file.
 *
 * Do check out http://www.gromacs.org , or mail us at gromacs@gromacs.org .
 *
 * And Hey:
 * Gyas ROwers Mature At Cryogenic Speed
 */

/* This line is only for CVS version info */

static char *SRCID_template_c = "$Id: template.c,v 1.4 2001/07/23 15:28:29 lindahl Exp $";

#include "statutil.h"
#include "typedefs.h"
#include "smalloc.h"
#include "vec.h"
#include "copyrite.h"
#include "statutil.h"
#include "tpxio.h"
#include "index.h"
```

```
#include "xvgr.h"

#define ANINT(A) (double) (long) (((A)<0.0) ? ((A)-0.5) : ((A)+0.5))
#define PI 3.14159265358979323846264338


// structure for output file

  struct hydanalys {
    double t, x, y, z, a, b, c;
  } *hydallx;

  struct hydanaly {
    int a, b, c, d, e, f, g, h, i, j, k, l, m, n, o, p, q, r, aa, bb, cc, dd;
  } *hydall;

// start main here

  int main(int argc,char *argv[])
   {
   static char *desc[] = {
     "this is a small test program meant to serve as a template ",
     "when writing your own analysis tools. The advantage of ",
     "using gromacs for this is that you have access to all ",
     "information in the topology, and your program will be ",
     "able to handle all types of coordinates and trajectory ",
     "files supported by gromacs. Go ahead and try it! ",
     "This test version just writes the coordinates of an ",
     "arbitrary atom to standard out for each frame. You can ",
     "select which atom you want to examine with the -n argument."
   };

// allocate memory for output here

   hydallx = (struct hydanalys*) calloc(999999,sizeof(struct hydanalys));
   hydall = (struct hydanaly*) calloc(999999,sizeof(struct hydanaly));

// default value for rcut (hydration radius)

   static real n=8.12;

   /* Extra arguments - but note how you always get the begin/end
    * options when running the program, without mentioning them here!
    */

// passing a value through -rcut and save as "n"

   t_pargs pa[] = {
    { "-int", FALSE, etREAL, {&n},
      "no input is required here, just pick P8 or P8E index"
    }
   };

// define variables

   t_topology top;
   char       title[STRLEN];
   t_trxframe fr;
```

```
rvec       *xtop;
matrix     box;
int        status;
int        flags = TRX_READ_X;
int        *isize;            // size of index
char       **grpnames;       // group name of index
atom_id    **index;          // index values
int        i,j;
int        number=0;         // counter
FILE       *fp;              // output file
int        lasttime;         // last timestep

t_filenm fnm[] = {
 { efTPS,  NULL,  NULL, ffREAD },      /* this is for the topology */
 { efTRX, "-f", NULL, ffREAD },        /* this is for the trajectory */
 { efNDX, NULL , NULL, ffOPTRD },      /* this is for index */
 { efXVG, "-o", "N_P_vector", ffOPTWR }  /* this is for output in xvg */
};

#define NFILE asize(fnm)

CopyRight(stderr,argv[0]);

/* This is the routine responsible for adding default options,
 * calling the X/motif interface, etc. */

parse_common_args(&argc,argv,PCA_CAN_TIME | PCA_CAN_VIEW,
 NFILE,fnm,asize(pa),pa,asize(desc),desc,0,NULL);

/* We don't need any topology information to write the coordinates,
 * but to show how it works we start by writing the name and
 * charge of the selected atom. It returns a boolean telling us
 * whether the topology was found and could be read
 */

read_tps_conf(ftp2fn(efTPS,NFILE,fnm),title,&top,&xtop,NULL,box,TRUE);
sfree(xtop);

// allocate memory for read variable using snew

int grNR=999999;
snew(grpnames,grNR);
snew(index,grNR);
snew(isize,grNR);
snew(fp,grNR);

// getting index from -n

get_index(&(top.atoms),ftp2fn_null(efNDX,NFILE,fnm),1,isize,index,grpnames);

/* The first time we read data is a little special */

read_first_frame(&status,ftp2fn(efTRX,NFILE,fnm),&fr,flags);

/* This is the main loop over frames */

do {
  j=0;
```

```
  int atom1=0;
  int atom2=0;
  int atom3=0;
  int atom4=0;
  double phiangle1=0;
  double phiangle2=0;
  double phiangle3=0;
  double phiangle4=0;
  double phiangle5=0;
  double phiangle6=0;
  double phiangle7=0;
  double phiangle8=0;

  // calcute atom number for N after pick P

  for(i = 0; (i < isize[0]); i++) {
    int aa = index[0][i];
    hydall[atom1].a = aa + 7 + 1;
    hydall[atom1].b = aa + 9 + 1;
    hydall[atom1].c = aa + 10 + 1;
    hydall[atom1].d = aa + 11 + 1;
    hydall[atom1].e = aa + 12 + 1;
    hydall[atom1].f = aa + 13 + 1;
    hydall[atom1].g = aa + 14 + 1;
    hydall[atom1].h = aa + 15 + 1;
    hydall[atom1].i = aa + 16 + 1;
    hydall[atom1].j = aa + 17 + 1;
    hydall[atom1].k = aa + 18 + 1;
    hydall[atom1].l = aa + 19 + 1;
    hydall[atom1].m = aa + 20 + 1;
    hydall[atom1].n = aa + 21 + 1;
    hydall[atom1].o = aa + 22 + 1;
    hydall[atom1].p = aa + 23 + 1;
    hydall[atom1].q = aa + 45 + 1;
    hydall[atom1].r = aa + 46 + 1;
    atom1++;
  }

  number++;

  lasttime=fr.time;

  } while(read_next_frame(status,&fr));
  printf("%d %d %d %d\n",hydall[0].aa, hydall[0].bb, hydall[0].cc, hydall[0].dd);
   fp = xvgropen(opt2fn("-o",NFILE,fnm),
  "","Time(ps)","Angle (degree)");


  fprintf(fp,"[ c15 ]\n");
  for (i=0; i<isize[0]; i++) {
    fprintf(fp,"%6d",  hydall[i].a);
  }
  fprintf(fp,"\n");

//   fprintf(fp,"[ o36 ]\n");
  for (i=0; i<isize[0]; i++) {
    fprintf(fp,"%6d",  hydall[i].b);
```

```
     }
     fprintf(fp,"\n");

//    fprintf(fp,"[ o37 ]\n");
     for (i=0; i<isize[0]; i++) {
       fprintf(fp,"%6d",  hydall[i].c);
     }
     fprintf(fp,"\n");

//    fprintf(fp,"[ o38 ]\n");
     for (i=0; i<isize[0]; i++) {
       fprintf(fp,"%6d",  hydall[i].d);
     }
     fprintf(fp,"\n");

//    fprintf(fp,"[ o39 ]\n");
     for (i=0; i<isize[0]; i++) {
       fprintf(fp,"%6d",  hydall[i].e);
     }
     fprintf(fp,"\n");

//    fprintf(fp,"[ o40 ]\n");
     for (i=0; i<isize[0]; i++) {
       fprintf(fp,"%6d",  hydall[i].f);
     }
     fprintf(fp,"\n");

//    fprintf(fp,"[ o41 ]\n");
     for (i=0; i<isize[0]; i++) {
       fprintf(fp,"%6d",  hydall[i].g);
     }
     fprintf(fp,"\n");

//    fprintf(fp,"[ o42 ]\n");
     for (i=0; i<isize[0]; i++) {
       fprintf(fp,"%6d",  hydall[i].h);
     }
     fprintf(fp,"\n");

     fclose(fp);
     thanx(stderr);
     return 0;
  }
```

B.1.4 Sn-2 Hydrocarbon Chain

```
/*
 * $Id: template.c,v 1.4 2001/07/23 15:28:29 lindahl Exp $
 *
 *                This source code is part of
 *
 *                 G   R   O   M   A   C   S
 *
 *          GROningen MAchine for Chemical Simulations
 *
 *                        VERSION 3.0
```

```
 *
 * Copyright (c) 1991-2001
 * BIOSON Research Institute, Dept. of Biophysical Chemistry
 * University of Groningen, The Netherlands
 *
 * This program is free software; you can redistribute it and/or
 * modify it under the terms of the GNU General Public License
 * as published by the Free Software Foundation; either version 2
 * of the License, or (at your option) any later version.
 *
 * If you want to redistribute modifications, please consider that
 * scientific software is very special. Version control is crucial -
 * bugs must be traceable. We will be happy to consider code for
 * inclusion in the official distribution, but derived work must not
 * be called official GROMACS. Details are found in the README & COPYING
 * files - if they are missing, get the official version at www.gromacs.org.
 *
 * To help us fund GROMACS development, we humbly ask that you cite
 * the papers on the package - you can find them in the top README file.
 *
 * Do check out http://www.gromacs.org , or mail us at gromacs@gromacs.org .
 *
 * And Hey:
 * Gyas ROwers Mature At Cryogenic Speed
 */

/* This line is only for CVS version info */

static char *SRCID_template_c = "$Id: template.c,v 1.4 2001/07/23 15:28:29 lindahl Exp $";

#include "statutil.h"
#include "typedefs.h"
#include "smalloc.h"
#include "vec.h"
#include "copyrite.h"
#include "statutil.h"
#include "tpxio.h"
#include "index.h"
#include "xvgr.h"

#define ANINT(A) (double) (long) (((A)<0.0) ? ((A)-0.5) : ((A)+0.5))
#define PI 3.14159265358979323846264338


// structure for output file

  struct hydanalys {
    double t, x, y, z, a, b, c;
  } *hydallx;

  struct hydanaly {
    int a, b, c, d, e, f, g, h, i, j, k, l, m, n, o, p, q, r, aa, bb, cc, dd;
  } *hydall;

// start main here

  int main(int argc,char *argv[])
  {
```

```
  static char *desc[] = {
    "this is a small test program meant to serve as a template ",
    "when writing your own analysis tools. The advantage of ",
    "using gromacs for this is that you have access to all ",
    "information in the topology, and your program will be ",
    "able to handle all types of coordinates and trajectory ",
    "files supported by gromacs. Go ahead and try it! ",
    "This test version just writes the coordinates of an ",
    "arbitrary atom to standard out for each frame. You can ",
    "select which atom you want to examine with the -n argument."
  };

// allocate memory for output here

  hydallx = (struct hydanalys*) calloc(999999,sizeof(struct hydanalys));
  hydall = (struct hydanaly*) calloc(999999,sizeof(struct hydanaly));

// default value for rcut (hydration radius)

  static real n=8.12;

  /* Extra arguments - but note how you always get the begin/end
   * options when running the program, without mentioning them here!
   */

// passing a value through -rcut and save as "n"

  t_pargs pa[] = {
   { "-int", FALSE, etREAL, {&n},
     "no input is required here, just pick P8 or P8E index"
   }
  };

// define variables

  t_topology top;
  char       title[STRLEN];
  t_trxframe fr;
  rvec       *xtop;
  matrix     box;
  int        status;
  int        flags = TRX_READ_X;
  int        *isize;            // size of index
  char       **grpnames;       // group name of index
  atom_id    **index;          // index values
  int        i,j;
  int        number=0;         // counter
  FILE       *fp;              // output file
  int        lasttime;         // last timestep

  t_filenm fnm[] = {
   { efTPS, NULL,  NULL, ffREAD },      /* this is for the topology */
   { efTRX, "-f", NULL, ffREAD },       /* this is for the trajectory */
   { efNDX, NULL , NULL, ffOPTRD },     /* this is for index */
   { efXVG, "-o", "N_P_vector", ffOPTWR }  /* this is for output in xvg */
  };

  #define NFILE asize(fnm)
```

```
CopyRight(stderr,argv[0]);

/* This is the routine responsible for adding default options,
 * calling the X/motif interface, etc. */

parse_common_args(&argc,argv,PCA_CAN_TIME | PCA_CAN_VIEW,
 NFILE,fnm,asize(pa),pa,asize(desc),desc,0,NULL);

/* We don't need any topology information to write the coordinates,
 * but to show how it works we start by writing the name and
 * charge of the selected atom. It returns a boolean telling us
 * whether the topology was found and could be read
 */

read_tps_conf(ftp2fn(efTPS,NFILE,fnm),title,&top,&xtop,NULL,box,TRUE);
sfree(xtop);

// allocate memory for read variable using snew

int grNR=999999;
snew(grpnames,grNR);
snew(index,grNR);
snew(isize,grNR);
snew(fp,grNR);

// getting index from -n

get_index(&(top.atoms),ftp2fn_null(efNDX,NFILE,fnm),1,isize,index,grpnames);

/* The first time we read data is a little special */

read_first_frame(&status,ftp2fn(efTRX,NFILE,fnm),&fr,flags);

/* This is the main loop over frames */

do {
  j=0;

int atom1=0;
int atom2=0;
int atom3=0;
int atom4=0;
double phiangle1=0;
double phiangle2=0;
double phiangle3=0;
double phiangle4=0;
double phiangle5=0;
double phiangle6=0;
double phiangle7=0;
double phiangle8=0;


// calcute atom number for N after pick P

for(i = 0; (i < isize[0]); i++) {
  int aa = index[0][i];
  hydall[atom1].a = aa + 7 + 1;
```

```
   hydall[atom1].b = aa + 9 + 1;
   hydall[atom1].c = aa + 10 + 1;
   hydall[atom1].d = aa + 11 + 1;
   hydall[atom1].e = aa + 12 + 1;
   hydall[atom1].f = aa + 13 + 1;
   hydall[atom1].g = aa + 14 + 1;
   hydall[atom1].h = aa + 15 + 1;
   hydall[atom1].i = aa + 16 + 1;
   hydall[atom1].j = aa + 17 + 1;
   hydall[atom1].k = aa + 18 + 1;
   hydall[atom1].l = aa + 19 + 1;
   hydall[atom1].m = aa + 20 + 1;
   hydall[atom1].n = aa + 21 + 1;
   hydall[atom1].o = aa + 22 + 1;
   hydall[atom1].p = aa + 23 + 1;
   hydall[atom1].q = aa + 45 + 1;
   hydall[atom1].r = aa + 46 + 1;
   atom1++;
  }


  number++;

  lasttime=fr.time;

 } while(read_next_frame(status,&fr));

 // open output "fp"
 printf("%d %d %d %d\n",hydall[0].aa, hydall[0].bb, hydall[0].cc, hydall[0].dd);
  fp = xvgropen(opt2fn("-o",NFILE,fnm),
 "","Time(ps)","Angle (degree)");


  fprintf(fp,"[ c15 ]\n");
  for (i=0; i<isize[0]; i++) {
    fprintf(fp,"%6d",  hydall[i].a);
  }
  fprintf(fp,"\n");

  fprintf(fp,"[ c17 ]\n");
  for (i=0; i<isize[0]; i++) {
    fprintf(fp,"%6d",  hydall[i].b);
  }
  fprintf(fp,"\n");

  fprintf(fp,"[ c18 ]\n");
  for (i=0; i<isize[0]; i++) {
    fprintf(fp,"%6d",  hydall[i].c);
  }
  fprintf(fp,"\n");

  fprintf(fp,"[ c19 ]\n");
  for (i=0; i<isize[0]; i++) {
    fprintf(fp,"%6d",  hydall[i].d);
  }
  fprintf(fp,"\n");

  fprintf(fp,"[ c20 ]\n");
  for (i=0; i<isize[0]; i++) {
```

```
    fprintf(fp,"%6d", hydall[i].e);
  }
  fprintf(fp,"\n");

  fprintf(fp,"[ c21 ]\n");
  for (i=0; i<isize[0]; i++) {
    fprintf(fp,"%6d", hydall[i].f);
  }
  fprintf(fp,"\n");

  fprintf(fp,"[ c22 ]\n");
  for (i=0; i<isize[0]; i++) {
    fprintf(fp,"%6d", hydall[i].g);
  }
  fprintf(fp,"\n");

  fprintf(fp,"[ c23 ]\n");
  for (i=0; i<isize[0]; i++) {
    fprintf(fp,"%6d", hydall[i].h);
  }
  fprintf(fp,"\n");

  fprintf(fp,"[ c24 ]\n");
  for (i=0; i<isize[0]; i++) {
    fprintf(fp,"%6d", hydall[i].i);
  }
  fprintf(fp,"\n");

  fprintf(fp,"[ c25 ]\n");
  for (i=0; i<isize[0]; i++) {
    fprintf(fp,"%6d", hydall[i].j);
  }
  fprintf(fp,"\n");

  fprintf(fp,"[ c26 ]\n");
  for (i=0; i<isize[0]; i++) {
    fprintf(fp,"%6d", hydall[i].k);
  }
  fprintf(fp,"\n");

  fprintf(fp,"[ c27 ]\n");
  for (i=0; i<isize[0]; i++) {
    fprintf(fp,"%6d", hydall[i].l);
  }
  fprintf(fp,"\n");

  fprintf(fp,"[ c28 ]\n");
  for (i=0; i<isize[0]; i++) {
    fprintf(fp,"%6d", hydall[i].m);
  }
  fprintf(fp,"\n");

  fprintf(fp,"[ c29 ]\n");
  for (i=0; i<isize[0]; i++) {
    fprintf(fp,"%6d", hydall[i].n);
  }
  fprintf(fp,"\n");
```

```
  fprintf(fp,"[ c30 ]\n");
  for (i=0; i<isize[0]; i++) {
    fprintf(fp,"%6d",  hydall[i].o);
  }
  fprintf(fp,"\n");

  fprintf(fp,"[ c31 ]\n");
  for (i=0; i<isize[0]; i++) {
   fprintf(fp,"%6d",  hydall[i].p);
  }
  fprintf(fp,"\n");

  fprintf(fp,"[ c53 ]\n");
  for (i=0; i<isize[0]; i++) {
   fprintf(fp,"%6d",  hydall[i].q);
  }
  fprintf(fp,"\n");

  fprintf(fp,"[ c54 ]\n");
  for (i=0; i<isize[0]; i++) {
   fprintf(fp,"%6d",  hydall[i].r);
  }
  fprintf(fp,"\n");

  fclose(fp);
  thanx(stderr);
  return 0;
 }
```

B.2   Lipid Tail Order Parameters

B.2.1   DPPC and DPPE

```
/*
 * $Id: template.c,v 1.4 2001/07/23 15:28:29 lindahl Exp $
 *
 *                This source code is part of
 *
 *                 G   R   O   M   A   C   S
 *
 *         GROningen MAchine for Chemical Simulations
 *
 *                        VERSION 3.0
 *
 * Copyright (c) 1991-2001
 * BIOSON Research Institute, Dept. of Biophysical Chemistry
 * University of Groningen, The Netherlands
 *
 * This program is free software; you can redistribute it and/or
 * modify it under the terms of the GNU General Public License
 * as published by the Free Software Foundation; either version 2
 * of the License, or (at your option) any later version.
 *
```

```
 * If you want to redistribute modifications, please consider that
 * scientific software is very special. Version control is crucial -
 * bugs must be traceable. We will be happy to consider code for
 * inclusion in the official distribution, but derived work must not
 * be called official GROMACS. Details are found in the README & COPYING
 * files - if they are missing, get the official version at www.gromacs.org.
 *
 * To help us fund GROMACS development, we humbly ask that you cite
 * the papers on the package - you can find them in the top README file.
 *
 * Do check out http://www.gromacs.org , or mail us at gromacs@gromacs.org .
 *
 * And Hey:
 * Gyas ROwers Mature At Cryogenic Speed
 */

/* This line is only for CVS version info */

static char *SRCID_template_c = "$Id: template.c,v 1.4 2001/07/23 15:28:29 lindahl Exp $";

#include "statutil.h"
#include "typedefs.h"
#include "smalloc.h"
#include "vec.h"
#include "copyrite.h"
#include "statutil.h"
#include "tpxio.h"
#include "index.h"
#include "xvgr.h"

#define ANINT(A) (double) (long) (((A)<0.0) ? ((A)-0.5) : ((A)+0.5))
#define PI 3.14159265358979323846264338

  struct hydanaly {
    int t, x, z, xx, zz, xy, zy, xxy, zzy;
    double  a, b, c, d, e, f, g, h, aa, bb, cc, dd, ee, ff, gg, hh;
  } *hydall;

struct propb {
  double a, b, c, d, e, f, g, h, aa, bb, cc, dd, ee, ff, gg, hh;
} **traj;

// start main here

  int main(int argc,char *argv[])
  {
  static char *desc[] = {
    "this is a small test program meant to serve as a template ",
    "when writing your own analysis tools. The advantage of ",
    "using gromacs for this is that you have access to all ",
    "information in the topology, and your program will be ",
    "able to handle all types of coordinates and trajectory ",
    "files supported by gromacs. Go ahead and try it! ",
    "This test version just writes the coordinates of an ",
    "arbitrary atom to standard out for each frame. You can ",
    "select which atom you want to examine with the -n argument."
  };
```

```
   hydall = (struct hydanaly*) calloc(999999,sizeof(struct hydanaly));

// default value for rcut (hydration radius)

   static real n=8.12;

   /* Extra arguments - but note how you always get the begin/end
    * options when running the program, without mentioning them here!
    */

// passing a value through -rcut and save as "n"

   t_pargs pa[] = {
    { "-int", FALSE, etREAL, {&n},
      "no input is required here, just pick P8 or P8E index"
    }
   };

// define variables

   t_topology top;
   char        title[STRLEN];
   t_trxframe fr;
   rvec        *xtop;
   matrix      box;
   int         status;
   int         flags = TRX_READ_X;
   int         *isize;             // size of index
   char        **grpnames;         // group name of index
   atom_id     **index;            // index values
   int         i,j,k;
   int         number=0;           // counter
   int         sn1=16;
   int         sn2=16;
   double      rsquare = 0.5795015625;
   FILE        *fp;                // output file
   int         lasttime;           // last timestep

   t_filenm fnm[] = {
    { efTPS, NULL,  NULL, ffREAD },      /* this is for the topology */
    { efTRX, "-f", NULL, ffREAD },       /* this is for the trajectory */
    { efNDX, NULL , NULL, ffOPTRD },     /* this is for index */
    { efXVG, "-o", "N_P_vector", ffOPTWR }  /* this is for output in xvg */
   };

   #define NFILE asize(fnm)

   CopyRight(stderr,argv[0]);

   /* This is the routine responsible for adding default options,
    * calling the X/motif interface, etc. */

   parse_common_args(&argc,argv,PCA_CAN_TIME | PCA_CAN_VIEW,
    NFILE,fnm,asize(pa),pa,asize(desc),desc,0,NULL);

   /* We don't need any topology information to write the coordinates,
    * but to show how it works we start by writing the name and
    * charge of the selected atom. It returns a boolean telling us
```

```
 * whether the topology was found and could be read
 */

read_tps_conf(ftp2fn(efTPS,NFILE,fnm),title,&top,&xtop,NULL,box,TRUE);
sfree(xtop);

// allocate memory for read variable using snew

int grNR=999999;
snew(grpnames,grNR);
snew(index,grNR);
snew(isize,grNR);
snew(fp,grNR);

// getting index from -n
 printf("*********Please select phosphorus atom P of both top and bottom leaflet**********\n");
get_index(&(top.atoms),ftp2fn_null(efNDX,NFILE,fnm),2,isize,index,grpnames);

/* The first time we read data is a little special */

read_first_frame(&status,ftp2fn(efTRX,NFILE,fnm),&fr,flags);

/* This is the main loop over frames */

traj = (struct propb**) calloc(999999,sizeof(struct propb*));
if(traj == NULL) { fprintf(stderr,"ERROR: cannot allocate memory for traj\n");
  exit(1); }
for(i=0; i<100; i++) {
traj[i] = (struct propb*) calloc(999999,sizeof(struct propb));
if(traj[i] == NULL) { fprintf(stderr,"ERROR: cannot allocate memory for traj*\n");
exit(1); }
 }

do {

  int aa ;
  int bb ;
  int cc ;
  int aaa ;
  int bbb ;
  int ccc ;
  int ddd ;

  // long tail index
  int newindex[isize[0]];
  for(j = 0; (j < isize[0]); j++) {
    newindex[j] = 0;
  }

  // short tail index
  int newindex2[isize[0]];
  for(j = 0; (j < isize[0]); j++) {
    newindex2[j] = 0;
  }

  // long tail close to palmitate //
  int countlip = 0;
```

```
    for(j = 0; (j < isize[0]); j++) {
      //int aaa = newindex[j];
      int aaa = index[0][j];

      if (aaa > 0){
for(i = 0; (i < sn1-2); i++) {
  if (i==0){
    bbb = aaa + 7 + i;
    ccc = bbb + 3;
    ddd = ccc - 1;
  }
  else if (i>0 && i<14){
    bbb = aaa + 8 + i;
    ccc = bbb + 2;
    ddd = ccc - 1;
  }
  else if (i==14) {
    bbb = aaa + 8 + i;
    ccc = bbb + 23;
    ddd = bbb + 1;
  }
  else{
    bbb = aaa + 8 + i;
    ccc = bbb + 23;
    ddd = ccc - 1;
  }

  // vector between 1 and 3
  double zzx = fr.x[bbb][XX] - fr.x[ccc][XX];
  double zzy = fr.x[bbb][YY] - fr.x[ccc][YY];
  double zzz = fr.x[bbb][ZZ] - fr.x[ccc][ZZ];

  zzx -= fr.box[XX][XX] * ANINT(1 / fr.box[XX][XX] * zzx);
  zzy -= fr.box[YY][YY] * ANINT(1 / fr.box[YY][YY] * zzy);
  zzz -= fr.box[ZZ][ZZ] * ANINT(1 / fr.box[ZZ][ZZ] * zzz);

  double zrr = zzx * zzx + zzy * zzy + zzz * zzz;

  double hzrr = 1.0 / sqrt(zrr);
  double zux = zzx * hzrr;
  double zuy = zzy * hzrr;
  double zuz = zzz * hzrr;
  //printf("%g %g %g\n",zux, zuy, zuz);

  // vector between 1 and 2
  double xxx = fr.x[bbb][XX] - fr.x[ddd][XX];
  double xxy = fr.x[bbb][YY] - fr.x[ddd][YY];
  double xxz = fr.x[bbb][ZZ] - fr.x[ddd][ZZ];

  xxx -= fr.box[XX][XX] * ANINT(1 / fr.box[XX][XX] * xxx);
  xxy -= fr.box[YY][YY] * ANINT(1 / fr.box[YY][YY] * xxy);
  xxz -= fr.box[ZZ][ZZ] * ANINT(1 / fr.box[ZZ][ZZ] * xxz);

  double xrr = xxx * xxx + xxy * xxy + xxz * xxz;

  double hxrr = 1.0 / sqrt(xrr);
  double xux = xxx * hxrr;
  double xuy = xxy * hxrr;
```

```
    double xuz = xxz * hxrr;
    //printf("%g %g %g\n",xux, xuy, xuz);

    // dot product
    double dott = zux * xux + zuy * xuy + zuz * xuz;

    // scale vector
    double szx = dott * zux;
    double szy = dott * zuy;
    double szz = dott * zuz;

    // subtract vector
    double mxx = xux - szx;
    double mxy = xuy - szy;
    double mxz = xuz - szz;

    // unit vector
    double mrr = mxx * mxx + mxy * mxy + mxz * mxz;
    double mxrr = 1.0 / sqrt(mrr);
    double mux = mxx * mxrr;
    double muy = mxy * mxrr;
    double muz = mxz * mxrr;

    // cross vector
    double crx = muy * zuz - zuy * muz;
    double cry = zux * muz - mux * zuz;
    double crz = mux * zuy - zux * muy;

    double crr = crx * crx + cry * cry + crz * crz;
    double ccrr = 1.0 / sqrt(crr);
    double cux = crx * ccrr;
    double cuy = cry * ccrr;
    double cuz = crz * ccrr;
    //printf("%g %g %g\n",crx, cry, crz);

    double scxx = 0.5 * (3 * cuz * cuz -1);
    double scyy = 0.5 * (3 * muz * muz -1);
    double sczz = 0.5 * (3 * zuz * zuz -1);
    double scd = (2 * scyy +  scxx) / 3;
    //printf("%g %g %g %g\n",scxx,scyy,sczz,scd);
    hydall[i].a += scd;
    //printf("%g %g %g\n",sxx,syy,hydall[i].y);
}
countlip++;

hydall[0].t = countlip;
//printf("%d \n",hydall[0].t);
        }
      }
      for(i = 0; (i < sn1-2); i++) {

        double dump = hydall[i].a / hydall[0].t;
        traj[i][number].a = dump;
        //printf("%g \n",traj[i][number].z);
      }

      //short tail close to palmitate//
```

```c
    int countlip2 = 0;

    for(j = 0; (j < isize[0]); j++) {
      //int aaa = newindex2[j];
      int aaa = index[1][j];
      if (aaa > 0){
for(i = 0; (i < sn2-2); i++) {
  if (i==0){
    bbb = aaa + 26 + i;
    ccc = bbb + 3;
    ddd = ccc - 1;
  }
  else {
    bbb = aaa + 27 + i;
    ccc = bbb + 2;
    ddd = ccc - 1;
  }

  // vector between 1 and 3
  double zzx = fr.x[bbb][XX] - fr.x[ccc][XX];
  double zzy = fr.x[bbb][YY] - fr.x[ccc][YY];
  double zzz = fr.x[bbb][ZZ] - fr.x[ccc][ZZ];

  zzx -= fr.box[XX][XX] * ANINT(1 / fr.box[XX][XX] * zzx);
  zzy -= fr.box[YY][YY] * ANINT(1 / fr.box[YY][YY] * zzy);
  zzz -= fr.box[ZZ][ZZ] * ANINT(1 / fr.box[ZZ][ZZ] * zzz);

  double zrr = zzx * zzx + zzy * zzy + zzz * zzz;

  double hzrr = 1.0 / sqrt(zrr);
  double zux = zzx * hzrr;
  double zuy = zzy * hzrr;
  double zuz = zzz * hzrr;
  //printf("%g %g %g\n",zux, zuy, zuz);

  // vector between 1 and 2
  double xxx = fr.x[bbb][XX] - fr.x[ddd][XX];
  double xxy = fr.x[bbb][YY] - fr.x[ddd][YY];
  double xxz = fr.x[bbb][ZZ] - fr.x[ddd][ZZ];

  xxx -= fr.box[XX][XX] * ANINT(1 / fr.box[XX][XX] * xxx);
  xxy -= fr.box[YY][YY] * ANINT(1 / fr.box[YY][YY] * xxy);
  xxz -= fr.box[ZZ][ZZ] * ANINT(1 / fr.box[ZZ][ZZ] * xxz);

  double xrr = xxx * xxx + xxy * xxy + xxz * xxz;

  double hxrr = 1.0 / sqrt(xrr);
  double xux = xxx * hxrr;
  double xuy = xxy * hxrr;
  double xuz = xxz * hxrr;
  //printf("%g %g %g\n",xux, xuy, xuz);

  // dot product
  double dott = zux * xux + zuy * xuy + zuz * xuz;

  // scale vector
  double szx = dott * zux;
  double szy = dott * zuy;
```

```
    double szz = dott * zuz;

    // subtract vector
    double mxx = xux - szx;
    double mxy = xuy - szy;
    double mxz = xuz - szz;

    // unit vector
    double mrr = mxx * mxx + mxy * mxy + mxz * mxz;
    double mxrr = 1.0 / sqrt(mrr);
    double mux = mxx * mxrr;
    double muy = mxy * mxrr;
    double muz = mxz * mxrr;

    // cross vector
    double crx = muy * zuz - zuy * muz;
    double cry = zux * muz - mux * zuz;
    double crz = mux * zuy - zux * muy;

    double crr = crx * crx + cry * cry + crz * crz;
    double ccrr = 1.0 / sqrt(crr);
    double cux = crx * ccrr;
    double cuy = cry * ccrr;
    double cuz = crz * ccrr;
    //printf("%g %g %g\n",crx, cry, crz);

    double scxx = 0.5 * (3 * cuz * cuz -1);
    double scyy = 0.5 * (3 * muz * muz -1);
    double sczz = 0.5 * (3 * zuz * zuz -1);
    double scd = (2 * scyy +  scxx) / 3;
    hydall[i].c += scd;

}
countlip2++;

hydall[2].t = countlip2;
//printf("%d \n",hydall[0].t);
    }
  }
  for(i = 0; (i < sn2-2); i++) {

    double dump = hydall[i].c / hydall[2].t;
    traj[i][number].c = dump;
    //printf("%g \n",traj[i][number].z);
  }

  int newindex3[isize[0]];
  for(j = 0; (j < isize[0]); j++) {
    newindex3[j] = index[0][j]-newindex2[j];
  }

number++;

// printf("%g %g\n",phiangle1/atomtop*180/PI, phiangle2/atombot*180/PI;
lasttime=fr.time;
/*   hydall[0].t=fr.time; */
hydall[5].t=number;
// printf("%d\n",hydall[0].t);
```

```
///////////////////////clear save data////////////////////////////////////////
  for(j = 0; (j < sn1-2); j++) {
    hydall[j].a = 0;
    //hydall[j].b = 0;
  }

  for(j = 0; (j < sn2-2); j++) {
    hydall[j].c = 0;
    //hydall[j].d = 0;
  }

  } while(read_next_frame(status,&fr));

    for(i = 0; (i < sn1-2); i++) {
for(j = 0; (j < hydall[5].t); j++) {
  hydall[i].aa  += traj[i][j].a;
  //hydall[i].bb  += traj[i][j].b;
}
    }

    for(i = 0; (i < sn2-2); i++) {
for(j = 0; (j < hydall[5].t); j++) {
  hydall[i].cc  += traj[i][j].c;
  //hydall[i].dd  += traj[i][j].d;
}
    }
  fp = xvgropen(opt2fn("-o",NFILE,fnm),
 "","Angle (degree)","Normalized angle distribution");

  fprintf(fp, "long tail order parameters near and far from palmitate\n");
  for(i = 0; (i < sn1-2); i++) {
    hydall[i].aa = hydall[i].aa / hydall[5].t;
    fprintf(fp, "%d %g \n",i+1, -hydall[i].aa);
  }
  fprintf(fp, "short tail order parameters near and far from palmitate\n");
  for(i = 0; (i < sn2-2); i++) {
    hydall[i].cc = hydall[i].cc / hydall[5].t;
    fprintf(fp, "%d %g \n",i+1, -hydall[i].cc);

  }

  fclose(fp);
  thanx(stderr);
  return 0;
}
```

B.2.2   POPC, POPE, and DOPC

```
/*
 * $Id: template.c,v 1.4 2001/07/23 15:28:29 lindahl Exp $
 *
 *                This source code is part of
 *
 *                 G   R   O   M   A   C   S
 *
```

```
*            GROningen MAchine for Chemical Simulations
*
*                         VERSION 3.0
*
* Copyright (c) 1991-2001
* BIOSON Research Institute, Dept. of Biophysical Chemistry
* University of Groningen, The Netherlands
*
* This program is free software; you can redistribute it and/or
* modify it under the terms of the GNU General Public License
* as published by the Free Software Foundation; either version 2
* of the License, or (at your option) any later version.
*
* If you want to redistribute modifications, please consider that
* scientific software is very special. Version control is crucial -
* bugs must be traceable. We will be happy to consider code for
* inclusion in the official distribution, but derived work must not
* be called official GROMACS. Details are found in the README & COPYING
* files - if they are missing, get the official version at www.gromacs.org.
*
* To help us fund GROMACS development, we humbly ask that you cite
* the papers on the package - you can find them in the top README file.
*
* Do check out http://www.gromacs.org , or mail us at gromacs@gromacs.org .
*
* And Hey:
* Gyas ROwers Mature At Cryogenic Speed
*/

/* This line is only for CVS version info */

static char *SRCID_template_c = "$Id: template.c,v 1.4 2001/07/23 15:28:29 lindahl Exp $";

#include "statutil.h"
#include "typedefs.h"
#include "smalloc.h"
#include "vec.h"
#include "copyrite.h"
#include "statutil.h"
#include "tpxio.h"
#include "index.h"
#include "xvgr.h"

#define ANINT(A) (double) (long) (((A)<0.0) ? ((A)-0.5) : ((A)+0.5))
#define PI 3.14159265358979323846264338


// structure for output file

//struct hydanalys {
//  int t, x, y, a, b, c, d, e, f, g, h, i, j, k, l, m, n, o, p, q, r;
//} *hydallx;

  struct hydanaly {
    int t, x, z, xx, zz, xy, zy, xxy, zzy;
    double  a, b, c, d, e, f, g, h, aa, bb, cc, dd, ee, ff, gg, hh;
  } *hydall;
```

```
struct propb {
  double a, b, c, d, e, f, g, h, aa, bb, cc, dd, ee, ff, gg, hh;
} **traj;


// start main here

  int main(int argc,char *argv[])
  {
  static char *desc[] = {
    "this is a small test program meant to serve as a template ",
    "when writing your own analysis tools. The advantage of ",
    "using gromacs for this is that you have access to all ",
    "information in the topology, and your program will be ",
    "able to handle all types of coordinates and trajectory ",
    "files supported by gromacs. Go ahead and try it! ",
    "This test version just writes the coordinates of an ",
    "arbitrary atom to standard out for each frame. You can ",
    "select which atom you want to examine with the -n argument."
  };

// allocate memory for output here

  // hydallx = (struct hydanalys*) calloc(999999,sizeof(struct hydanalys));

   hydall = (struct hydanaly*) calloc(999999,sizeof(struct hydanaly));




// default value for rcut (hydration radius)

   static real n=8.12;

   /* Extra arguments - but note how you always get the begin/end
   * options when running the program, without mentioning them here!
   */

// passing a value through -rcut and save as "n"

   t_pargs pa[] = {
   { "-int", FALSE, etREAL, {&n},
     "no input is required here, just pick P8 or P8E index"
    }
   };

// define variables

   t_topology top;
   char        title[STRLEN];
   t_trxframe fr;
   rvec        *xtop;
   matrix      box;
   int         status;
   int         flags = TRX_READ_X;
   int         *isize;              // size of index
   char        **grpnames;         // group name of index
```

```
atom_id   **index;              // index values
int       i,j,k;
int       number=0;            // counter
int       sn1=18;
int       sn2=18;
double    rsquare = 0.5795015625;
FILE      *fp;                  // output file
int       lasttime;            // last timestep

t_filenm fnm[] = {
 { efTPS,  NULL,  NULL, ffREAD },      /* this is for the topology */
 { efTRX, "-f", NULL, ffREAD },        /* this is for the trajectory */
 { efNDX, NULL , NULL, ffOPTRD },      /* this is for index */
 { efXVG, "-o", "N_P_vector", ffOPTWR }  /* this is for output in xvg */
};

#define NFILE asize(fnm)

CopyRight(stderr,argv[0]);

/* This is the routine responsible for adding default options,
 * calling the X/motif interface, etc. */

parse_common_args(&argc,argv,PCA_CAN_TIME | PCA_CAN_VIEW,
 NFILE,fnm,asize(pa),pa,asize(desc),desc,0,NULL);

/* We don't need any topology information to write the coordinates,
 * but to show how it works we start by writing the name and
 * charge of the selected atom. It returns a boolean telling us
 * whether the topology was found and could be read
 */

read_tps_conf(ftp2fn(efTPS,NFILE,fnm),title,&top,&xtop,NULL,box,TRUE);
sfree(xtop);

// allocate memory for read variable using snew

int grNR=999999;
snew(grpnames,grNR);
snew(index,grNR);
snew(isize,grNR);
snew(fp,grNR);

//for(i = 0; (i < 181); i++){
//  hydall[i].x = 0;
//}

// getting index from -n
 printf("********Please select phosphorus atom P of both top and bottom leaflet*********\n");
get_index(&(top.atoms),ftp2fn_null(efNDX,NFILE,fnm),2,isize,index,grpnames);

/* The first time we read data is a little special */

read_first_frame(&status,ftp2fn(efTRX,NFILE,fnm),&fr,flags);

/* This is the main loop over frames */

traj = (struct propb**) calloc(999999,sizeof(struct propb*));
```

```
   if(traj == NULL) { fprintf(stderr,"ERROR: cannot allocate memory for traj\n");
     exit(1); }
   for(i=0; i<100; i++) {
   traj[i] = (struct propb*) calloc(999999,sizeof(struct propb));
   if(traj[i] == NULL) { fprintf(stderr,"ERROR: cannot allocate memory for traj*\n");
exit(1); }
 }

   do {
     int aa ;
     int bb ;
     int cc ;
     int aaa ;
     int bbb ;
     int ccc ;
     int ddd ;

     // first tail up //
     int countlip = 0;

     for(j = 0; (j < isize[0]); j++) {
       //int aaa = newindex[j];
       int aaa = index[0][j];

       if (aaa > 0){
 for(i = 0; (i < sn1-2); i++) {
   if (i==0){
     bbb = aaa + 7 + i;
     ccc = bbb + 3;
     ddd = ccc - 1;
   }
   else if (i>0 && i<14){
     bbb = aaa + 8 + i;
     ccc = bbb + 2;
     ddd = ccc - 1;
   }
   else if (i==14) {
     bbb = aaa + 8 + i;
     ccc = bbb + 23;
     ddd = bbb + 1;
   }
   else{
     bbb = aaa + 8 + i;
     ccc = bbb + 23;
     ddd = ccc - 1;
   }

   // vector between 1 and 3
   double zzx = fr.x[bbb][XX] - fr.x[ccc][XX];
   double zzy = fr.x[bbb][YY] - fr.x[ccc][YY];
   double zzz = fr.x[bbb][ZZ] - fr.x[ccc][ZZ];

   zzx -= fr.box[XX][XX] * ANINT(1 / fr.box[XX][XX] * zzx);
   zzy -= fr.box[YY][YY] * ANINT(1 / fr.box[YY][YY] * zzy);
   zzz -= fr.box[ZZ][ZZ] * ANINT(1 / fr.box[ZZ][ZZ] * zzz);

   double zrr = zzx * zzx + zzy * zzy + zzz * zzz;
```

```
double hzrr = 1.0 / sqrt(zrr);
double zux = zzx * hzrr;
double zuy = zzy * hzrr;
double zuz = zzz * hzrr;
//printf("%g %g %g\n",zux, zuy, zuz);

// vector between 1 and 2
double xxx = fr.x[bbb][XX] - fr.x[ddd][XX];
double xxy = fr.x[bbb][YY] - fr.x[ddd][YY];
double xxz = fr.x[bbb][ZZ] - fr.x[ddd][ZZ];

xxx -= fr.box[XX][XX] * ANINT(1 / fr.box[XX][XX] * xxx);
xxy -= fr.box[YY][YY] * ANINT(1 / fr.box[YY][YY] * xxy);
xxz -= fr.box[ZZ][ZZ] * ANINT(1 / fr.box[ZZ][ZZ] * xxz);

double xrr = xxx * xxx + xxy * xxy + xxz * xxz;

double hxrr = 1.0 / sqrt(xrr);
double xux = xxx * hxrr;
double xuy = xxy * hxrr;
double xuz = xxz * hxrr;
//printf("%g %g %g\n",xux, xuy, xuz);

// dot product
double dott = zux * xux + zuy * xuy + zuz * xuz;

// scale vector
double szx = dott * zux;
double szy = dott * zuy;
double szz = dott * zuz;

// subtract vector
double mxx = xux - szx;
double mxy = xuy - szy;
double mxz = xuz - szz;

// unit vector
double mrr = mxx * mxx + mxy * mxy + mxz * mxz;
double mxrr = 1.0 / sqrt(mrr);
double mux = mxx * mxrr;
double muy = mxy * mxrr;
double muz = mxz * mxrr;

// cross vector
double crx = muy * zuz - zuy * muz;
double cry = zux * muz - mux * zuz;
double crz = mux * zuy - zux * muy;

double crr = crx * crx + cry * cry + crz * crz;
double ccrr = 1.0 / sqrt(crr);
double cux = crx * ccrr;
double cuy = cry * ccrr;
double cuz = crz * ccrr;
//printf("%g %g %g\n",crx, cry, crz);

double scxx = 0.5 * (3 * cuz * cuz -1);
double scyy = 0.5 * (3 * muz * muz -1);
double sczz = 0.5 * (3 * zuz * zuz -1);
```

```
  double scd = (2 * scyy +  scxx) / 3;
 //printf("%g %g %g %g\n",scxx,scyy,sczz,scd);
 hydall[i].a += scd;
 //printf("%g %g %g\n",sxx,syy,hydall[i].y);
}
countlip++;

hydall[0].t = countlip;
//printf("%d \n",hydall[0].t);
    }
   }
   for(i = 0; (i < sn1-2); i++) {

     double dump = hydall[i].a / hydall[0].t;
     traj[i][number].a = dump;
     //printf("%g \n",traj[i][number].a);
   }

   //second tail up//

   int countlip2 = 0;

   for(j = 0; (j < isize[0]); j++) {
     //int aaa = newindex2[j];
     int aaa = index[0][j];

     if (aaa > 0){
for(i = 0; (i < sn2-2); i++) {
 if (i==0){
   bbb = aaa + 26 + i;
   ccc = bbb + 3;
   ddd = ccc - 1;
 }
 else {
   bbb = aaa + 27 + i;
   ccc = bbb + 2;
   ddd = ccc - 1;
 }

   // vector between 1 and 3
 double zzx = fr.x[bbb][XX] - fr.x[ccc][XX];
 double zzy = fr.x[bbb][YY] - fr.x[ccc][YY];
 double zzz = fr.x[bbb][ZZ] - fr.x[ccc][ZZ];

 zzx -= fr.box[XX][XX] * ANINT(1 / fr.box[XX][XX] * zzx);
 zzy -= fr.box[YY][YY] * ANINT(1 / fr.box[YY][YY] * zzy);
 zzz -= fr.box[ZZ][ZZ] * ANINT(1 / fr.box[ZZ][ZZ] * zzz);

 double zrr = zzx * zzx + zzy * zzy + zzz * zzz;

 double hzrr = 1.0 / sqrt(zrr);
 double zux = zzx * hzrr;
 double zuy = zzy * hzrr;
 double zuz = zzz * hzrr;
 //printf("%g %g %g\n",zux, zuy, zuz);

 // vector between 1 and 2
 double xxx = fr.x[bbb][XX] - fr.x[ddd][XX];
```

```
  double xxy = fr.x[bbb][YY] - fr.x[ddd][YY];
  double xxz = fr.x[bbb][ZZ] - fr.x[ddd][ZZ];

  xxx -= fr.box[XX][XX] * ANINT(1 / fr.box[XX][XX] * xxx);
  xxy -= fr.box[YY][YY] * ANINT(1 / fr.box[YY][YY] * xxy);
  xxz -= fr.box[ZZ][ZZ] * ANINT(1 / fr.box[ZZ][ZZ] * xxz);

  double xrr = xxx * xxx + xxy * xxy + xxz * xxz;

  double hxrr = 1.0 / sqrt(xrr);
  double xux = xxx * hxrr;
  double xuy = xxy * hxrr;
  double xuz = xxz * hxrr;
  //printf("%g %g %g\n",xux, xuy, xuz);

  // dot product
  double dott = zux * xux + zuy * xuy + zuz * xuz;

  // scale vector
  double szx = dott * zux;
  double szy = dott * zuy;
  double szz = dott * zuz;

  // subtract vector
  double mxx = xux - szx;
  double mxy = xuy - szy;
  double mxz = xuz - szz;

  // unit vector
  double mrr = mxx * mxx + mxy * mxy + mxz * mxz;
  double mxrr = 1.0 / sqrt(mrr);
  double mux = mxx * mxrr;
  double muy = mxy * mxrr;
  double muz = mxz * mxrr;

  // cross vector
  double crx = muy * zuz - zuy * muz;
  double cry = zux * muz - mux * zuz;
  double crz = mux * zuy - zux * muy;

  double crr = crx * crx + cry * cry + crz * crz;
  double ccrr = 1.0 / sqrt(crr);
  double cux = crx * ccrr;
  double cuy = cry * ccrr;
  double cuz = crz * ccrr;


  double scxx = 0.5 * (3 * cuz * cuz -1);
  double scyy = 0.5 * (3 * muz * muz -1);
  double sczz = 0.5 * (3 * zuz * zuz -1);
  double scd = (2 * scyy +  scxx) / 3;

  hydall[i].c += scd;
}
countlip2++;

hydall[2].t = countlip2;
//printf("%d \n",hydall[0].t);
```

```
      }
    }
    for(i = 0; (i < sn2-2); i++) {

        double dump = hydall[i].c / hydall[2].t;
        traj[i][number].c = dump;
        //printf("%g \n",traj[i][number].c);
    }


    // first tail down //
    int countlip1 = 0;

    for(j = 0; (j < isize[1]); j++) {
      //int aaa = newindex[j];
        int aaa = index[1][j];

        if (aaa > 0){
for(i = 0; (i < sn1-2); i++) {
  if (i==0){
    bbb = aaa + 7 + i;
    ccc = bbb + 3;
    ddd = ccc - 1;
  }
  else if (i>0 && i<14){
    bbb = aaa + 8 + i;
    ccc = bbb + 2;
    ddd = ccc - 1;
  }
  else if (i==14) {
    bbb = aaa + 8 + i;
    ccc = bbb + 23;
    ddd = bbb + 1;
  }
  else{
    bbb = aaa + 8 + i;
    ccc = bbb + 23;
    ddd = ccc - 1;
  }

  // vector between 1 and 3
  double zzx = fr.x[bbb][XX] - fr.x[ccc][XX];
  double zzy = fr.x[bbb][YY] - fr.x[ccc][YY];
  double zzz = fr.x[bbb][ZZ] - fr.x[ccc][ZZ];

  zzx -= fr.box[XX][XX] * ANINT(1 / fr.box[XX][XX] * zzx);
  zzy -= fr.box[YY][YY] * ANINT(1 / fr.box[YY][YY] * zzy);
  zzz -= fr.box[ZZ][ZZ] * ANINT(1 / fr.box[ZZ][ZZ] * zzz);

  double zrr = zzx * zzx + zzy * zzy + zzz * zzz;

  double hzrr = 1.0 / sqrt(zrr);
  double zux = zzx * hzrr;
  double zuy = zzy * hzrr;
  double zuz = zzz * hzrr;
  //printf("%g %g %g\n",zux, zuy, zuz);

  // vector between 1 and 2
```

```
    double xxx = fr.x[bbb][XX] - fr.x[ddd][XX];
    double xxy = fr.x[bbb][YY] - fr.x[ddd][YY];
    double xxz = fr.x[bbb][ZZ] - fr.x[ddd][ZZ];

    xxx -= fr.box[XX][XX] * ANINT(1 / fr.box[XX][XX] * xxx);
    xxy -= fr.box[YY][YY] * ANINT(1 / fr.box[YY][YY] * xxy);
    xxz -= fr.box[ZZ][ZZ] * ANINT(1 / fr.box[ZZ][ZZ] * xxz);

    double xrr = xxx * xxx + xxy * xxy + xxz * xxz;

    double hxrr = 1.0 / sqrt(xrr);
    double xux = xxx * hxrr;
    double xuy = xxy * hxrr;
    double xuz = xxz * hxrr;
    //printf("%g %g %g\n",xux, xuy, xuz);

    // dot product
    double dott = zux * xux + zuy * xuy + zuz * xuz;

    // scale vector
    double szx = dott * zux;
    double szy = dott * zuy;
    double szz = dott * zuz;

    // subtract vector
    double mxx = xux - szx;
    double mxy = xuy - szy;
    double mxz = xuz - szz;

    // unit vector
    double mrr = mxx * mxx + mxy * mxy + mxz * mxz;
    double mxrr = 1.0 / sqrt(mrr);
    double mux = mxx * mxrr;
    double muy = mxy * mxrr;
    double muz = mxz * mxrr;

    // cross vector
    double crx = muy * zuz - zuy * muz;
    double cry = zux * muz - mux * zuz;
    double crz = mux * zuy - zux * muy;

    double crr = crx * crx + cry * cry + crz * crz;
    double ccrr = 1.0 / sqrt(crr);
    double cux = crx * ccrr;
    double cuy = cry * ccrr;
    double cuz = crz * ccrr;
    //printf("%g %g %g\n",crx, cry, crz);

    double scxx = 0.5 * (3 * cuz * cuz -1);
    double scyy = 0.5 * (3 * muz * muz -1);
    double sczz = 0.5 * (3 * zuz * zuz -1);
    double scd = (2 * scyy +  scxx) / 3;
    //printf("%g %g %g %g\n",scxx,scyy,sczz,scd);
    hydall[i].b += scd;
    //printf("%g %g %g\n",sxx,syy,hydall[i].y);
  }
  countlip1++;
```

```
hydall[1].t = countlip1;
//printf("%d \n",hydall[0].t);
      }
    }
    for(i = 0; (i < sn1-2); i++) {

      double dump = hydall[i].b / hydall[1].t;
      traj[i][number].b = dump;
      //printf("%g \n",traj[i][number].b);
    }


    //second tail down//

    int countlip4 = 0;

    for(j = 0; (j < isize[1]); j++) {
      //int aaa = newindex2[j];
      int aaa = index[1][j];

      if (aaa > 0){
for(i = 0; (i < sn2-2); i++) {
  if (i==0){
    bbb = aaa + 26 + i;
    ccc = bbb + 3;
    ddd = ccc - 1;
  }
  else {
    bbb = aaa + 27 + i;
    ccc = bbb + 2;
    ddd = ccc - 1;
  }
    // vector between 1 and 3
  double zzx = fr.x[bbb][XX] - fr.x[ccc][XX];
  double zzy = fr.x[bbb][YY] - fr.x[ccc][YY];
  double zzz = fr.x[bbb][ZZ] - fr.x[ccc][ZZ];

  zzx -= fr.box[XX][XX] * ANINT(1 / fr.box[XX][XX] * zzx);
  zzy -= fr.box[YY][YY] * ANINT(1 / fr.box[YY][YY] * zzy);
  zzz -= fr.box[ZZ][ZZ] * ANINT(1 / fr.box[ZZ][ZZ] * zzz);

  double zrr = zzx * zzx + zzy * zzy + zzz * zzz;

  double hzrr = 1.0 / sqrt(zrr);
  double zux = zzx * hzrr;
  double zuy = zzy * hzrr;
  double zuz = zzz * hzrr;
  //printf("%g %g %g\n",zux, zuy, zuz);

  // vector between 1 and 2
  double xxx = fr.x[bbb][XX] - fr.x[ddd][XX];
  double xxy = fr.x[bbb][YY] - fr.x[ddd][YY];
  double xxz = fr.x[bbb][ZZ] - fr.x[ddd][ZZ];

  xxx -= fr.box[XX][XX] * ANINT(1 / fr.box[XX][XX] * xxx);
  xxy -= fr.box[YY][YY] * ANINT(1 / fr.box[YY][YY] * xxy);
  xxz -= fr.box[ZZ][ZZ] * ANINT(1 / fr.box[ZZ][ZZ] * xxz);

  double xrr = xxx * xxx + xxy * xxy + xxz * xxz;
```

```
    double hxrr = 1.0 / sqrt(xrr);
    double xux = xxx * hxrr;
    double xuy = xxy * hxrr;
    double xuz = xxz * hxrr;
    //printf("%g %g %g\n",xux, xuy, xuz);

    // dot product
    double dott = zux * xux + zuy * xuy + zuz * xuz;

    // scale vector
    double szx = dott * zux;
    double szy = dott * zuy;
    double szz = dott * zuz;

    // subtract vector
    double mxx = xux - szx;
    double mxy = xuy - szy;
    double mxz = xuz - szz;

    // unit vector
    double mrr = mxx * mxx + mxy * mxy + mxz * mxz;
    double mxrr = 1.0 / sqrt(mrr);
    double mux = mxx * mxrr;
    double muy = mxy * mxrr;
    double muz = mxz * mxrr;

    // cross vector
    double crx = muy * zuz - zuy * muz;
    double cry = zux * muz - mux * zuz;
    double crz = mux * zuy - zux * muy;

    double crr = crx * crx + cry * cry + crz * crz;
    double ccrr = 1.0 / sqrt(crr);
    double cux = crx * ccrr;
    double cuy = cry * ccrr;
    double cuz = crz * ccrr;
    //printf("%g %g %g\n",crx, cry, crz);

    double scxx = 0.5 * (3 * cuz * cuz -1);
    double scyy = 0.5 * (3 * muz * muz -1);
    double sczz = 0.5 * (3 * zuz * zuz -1);
    double scd = (2 * scyy +  scxx) / 3;
    //printf("%g %g %g %g\n",scxx,scyy,sczz,scd);
    hydall[i].d += scd;
    //printf("%g %g %g\n",sxx,syy,hydall[i].y);
}
countlip4++;

hydall[3].t = countlip4;
//printf("%d \n",hydall[0].t);
        }
      }
    for(i = 0; (i < sn2-2); i++) {

        double dump = hydall[i].d / hydall[3].t;
        traj[i][number].d = dump;
        //printf("%g \n",traj[i][number].d);
```

```
    }
```

```
  number++;

  // printf("%g %g\n",phiangle1/atomtop*180/PI, phiangle2/atombot*180/PI;
  lasttime=fr.time;
  /*   hydall[0].t=fr.time; */
  hydall[5].t=number;
  // printf("%d\n",hydall[0].t);


  /////////////////////////clear save data///////////////////////////////////////////
    for(j = 0; (j < sn1-2); j++) {
      hydall[j].a = 0;
      hydall[j].b = 0;
    }

    for(j = 0; (j < sn2-2); j++) {
      hydall[j].c = 0;
      hydall[j].d = 0;
    }

  } while(read_next_frame(status,&fr));

  // open output "fp"



      for(i = 0; (i < sn1-2); i++) {
for(j = 0; (j < hydall[5].t); j++) {
  hydall[i].aa  += traj[i][j].a;
  hydall[i].bb  += traj[i][j].b;
}
      }

      for(i = 0; (i < sn2-2); i++) {
for(j = 0; (j < hydall[5].t); j++) {
  hydall[i].cc  += traj[i][j].c;
  hydall[i].dd  += traj[i][j].d;
}
      }
```

```
      for(i = 0; (i < sn1-2); i++) {
//printf("%g %g %g %g \n",hydall[i].aa, hydall[i].bb, hydall[i].cc, hydall[i].dd);
      }


  fp = xvgropen(opt2fn("-o",NFILE,fnm),
  "","Angle (degree)","Normalized angle distribution");

  fprintf(fp, "first tail up\n");
  for(i = 0; (i < sn1-2); i++) {
    hydall[i].aa = hydall[i].aa / hydall[5].t;
    //hydall[i].bb = hydall[i].bb / hydall[5].t;
    fprintf(fp, "%d %g \n",i+1, -hydall[i].aa);
  }
  fprintf(fp, "socond teil up\n");
  for(i = 0; (i < sn2-2); i++) {
    hydall[i].cc = hydall[i].cc / hydall[5].t;
    //hydall[i].dd = hydall[i].dd / hydall[5].t;
    fprintf(fp, "%d %g \n",i+1, -hydall[i].cc);
  }
  fprintf(fp, "first tail down\n");
  for(i = 0; (i < sn1-2); i++) {
    //hydall[i].aa = hydall[i].aa / hydall[5].t;
    hydall[i].bb = hydall[i].bb / hydall[5].t;
    fprintf(fp, "%d %g \n",i+1, -hydall[i].bb);
  }
  fprintf(fp, "socond teil down\n");
  for(i = 0; (i < sn2-2); i++) {
    //hydall[i].cc = hydall[i].cc / hydall[5].t;
    hydall[i].dd = hydall[i].dd / hydall[5].t;
    fprintf(fp, "%d %g \n",i+1, -hydall[i].dd);

  }



  fclose(fp);

  thanx(stderr);

  return 0;
 }
```

B.3   Hydrogen Bond Analysis

B.3.1   Water as H-donor

```
/*
 * $Id: template.c,v 1.4 2001/07/23 15:28:29 lindahl Exp $
 *
 *                This source code is part of
```

```
*
*                 G   R   O   M   A   C   S
*
*         GROningen MAchine for Chemical Simulations
*
*                     VERSION 3.0
*
* Copyright (c) 1991-2001
* BIOSON Research Institute, Dept. of Biophysical Chemistry
* University of Groningen, The Netherlands
*
* This program is free software; you can redistribute it and/or
* modify it under the terms of the GNU General Public License
* as published by the Free Software Foundation; either version 2
* of the License, or (at your option) any later version.
*
* If you want to redistribute modifications, please consider that
* scientific software is very special. Version control is crucial -
* bugs must be traceable. We will be happy to consider code for
* inclusion in the official distribution, but derived work must not
* be called official GROMACS. Details are found in the README & COPYING
* files - if they are missing, get the official version at www.gromacs.org.
*
* To help us fund GROMACS development, we humbly ask that you cite
* the papers on the package - you can find them in the top README file.
*
* Do check out http://www.gromacs.org , or mail us at gromacs@gromacs.org .
*
* And Hey:
* Gyas ROwers Mature At Cryogenic Speed
*/

/* This line is only for CVS version info */

static char *SRCID_template_c = "$Id: template.c,v 1.4 2001/07/23 15:28:29 lindahl Exp $";


#include "statutil.h"
#include "typedefs.h"
#include "smalloc.h"
#include "vec.h"
#include "copyrite.h"
#include "statutil.h"
#include "tpxio.h"
#include "index.h"
#include "xvgr.h"


#define ANINT(A) (double) (long) (((A)<0.0) ? ((A)-0.5) : ((A)+0.5))
#define HBANGLE 120.0*3.14159265358979323846264643383/180.0
#define HBOND 0.35
#define HBOND2 HBOND*HBOND


// structure for output file

  struct hydanalys {
    int t, x, y, zzz;
  } *hydallx;


// start main here
```

```
  int main(int argc,char *argv[])
  {
  static char *desc[] = {
    "this is a small test program meant to serve as a template ",
    "when writing your own analysis tools. The advantage of ",
    "using gromacs for this is that you have access to all ",
    "information in the topology, and your program will be ",
    "able to handle all types of coordinates and trajectory ",
    "files supported by gromacs. Go ahead and try it! ",
    "This test version just writes the coordinates of an ",
    "arbitrary atom to standard out for each frame. You can ",
    "select which atom you want to examine with the -n argument."
  };

// allocate memory for output here

  hydallx = (struct hydanalys*) calloc(999999,sizeof(struct hydanalys));

// default value for rcut (hydration radius)

  static real n=0.35;

  /* Extra arguments - but note how you always get the begin/end
  * options when running the program, without mentioning them here!
  */

// passing a value through -rcut and save as "n"

  t_pargs pa[] = {
   { "-rcut", FALSE, etREAL, {&n},
     "hydration radius (nm) obtained first minimum of rdf"
   }
  };

// define variables

  t_topology top;
  char       title[STRLEN];
  t_trxframe fr;
  rvec       *xtop;
  matrix     box;
  int        status;
  int        flags = TRX_READ_X;
  int        *isize;           // size of index
  char       **grpnames;       // group name of index
  atom_id    **index;          // index values
  int        i,j;
  int        *hydall;
  int        number=0;         // counter
  FILE       *fp;              // output file
  int        lasttime;         // last timestep

  t_filenm fnm[] = {
   { efTPS,  NULL,  NULL, ffREAD },      /* this is for the topology */
   { efTRX, "-f", NULL, ffREAD },        /* this is for the trajectory */
   { efNDX, NULL , NULL, ffOPTRD },      /* this is for index */
   { efXVG, "-hbn", "hbond", ffOPTWR }   /* this is for output in xvg */
```

```
};

#define NFILE asize(fnm)

CopyRight(stderr,argv[0]);

/* This is the routine responsible for adding default options,
 * calling the X/motif interface, etc. */

parse_common_args(&argc,argv,PCA_CAN_TIME | PCA_CAN_VIEW,
 NFILE,fnm,asize(pa),pa,asize(desc),desc,0,NULL);

/* We don't need any topology information to write the coordinates,
 * but to show how it works we start by writing the name and
 * charge of the selected atom. It returns a boolean telling us
 * whether the topology was found and could be read
 */

read_tps_conf(ftp2fn(efTPS,NFILE,fnm),title,&top,&xtop,NULL,box,TRUE);
sfree(xtop);

// allocate memory for read variable using snew

int grNR=999999;
snew(grpnames,grNR);
snew(index,grNR);
snew(isize,grNR);
snew(fp,grNR);

get_index(&(top.atoms),ftp2fn_null(efNDX,NFILE,fnm),2,isize,index,grpnames);

/* The first time we read data is a little special */

read_first_frame(&status,ftp2fn(efTRX,NFILE,fnm),&fr,flags);

/* This is the main loop over frames */

do {

// start counting atoms in the first hydration and hbond

real rhydration=n*n;
int hydstat=0;
int hbondstat=0;

// check hydration aa=acceptor bb=donor

for(i = 0; (i < isize[0]); i++) {
  int aa = index[0][i];
for(j = 0; (j < isize[1]); j++) {
  int bb = index[1][j];
  double bx = fr.x[aa][XX]-fr.x[bb][XX];
  bx -= fr.box[XX][XX] * ANINT(1 / fr.box[XX][XX] * bx);
  double by = fr.x[aa][YY]-fr.x[bb][YY];
  by -= fr.box[YY][YY] * ANINT(1 / fr.box[YY][YY] * by);
  double bz = fr.x[aa][ZZ] - fr.x[bb][ZZ];
  bz -= fr.box[ZZ][ZZ] * ANINT(1 / fr.box[ZZ][ZZ] * bz);
  double rr = bx * bx + by * by + bz * bz;
```

```
        if(rr > rhydration) continue;
        hydstat++;

        // check hydrogen bond distance (hbond <= 0.35nm)

        if(rr > HBOND2) continue;

        // check closest water hydrogen to acceptor

        // hyda hydb are the indexs for water hydrogens

        int hyda = index[1][j] + 1;
        int hydb = index[1][j] + 2;

        double hax = fr.x[aa][XX] - fr.x[hyda][XX];
        hax -= fr.box[XX][XX] * ANINT(1 / fr.box[XX][XX] * hax);
        double hay = fr.x[aa][YY] - fr.x[hyda][YY];
        hay -= fr.box[YY][YY] * ANINT(1 / fr.box[YY][YY] * hay);
        double haz = fr.x[aa][ZZ] - fr.x[hyda][ZZ];
        haz -= fr.box[ZZ][ZZ] * ANINT(1 / fr.box[ZZ][ZZ] * haz);
        double har = hax * hax+hay * hay + haz * haz;

        double hbx = fr.x[aa][XX] - fr.x[hydb][XX];
        hbx -= fr.box[XX][XX] * ANINT(1 / fr.box[XX][XX] * hbx);
        double hby = fr.x[aa][YY] - fr.x[hydb][YY];
        hby -= fr.box[YY][YY] * ANINT(1 / fr.box[YY][YY] * hby);
        double hbz = fr.x[aa][ZZ] - fr.x[hydb][ZZ];
        hbz -= fr.box[ZZ][ZZ] * ANINT(1 / fr.box[ZZ][ZZ] * hbz);
        double hbr = hbx * hbx + hby * hby + hbz * hbz;

        int hn = 1;
        if(hbr < har) hn = 2;

        // calculate the angle D--H--A (greater than 120)
        // Ref: Brady and Schmidt (1993)

        // distance between acceptor and closest hydrogen
        // hydf is the closest hydorgen index

        int hydf = bb + hn;
        double aax = fr.x[aa][XX] - fr.x[hydf][XX];
        aax -= fr.box[XX][XX] * ANINT(1 / fr.box[YY][YY] * aax);
        double aay = fr.x[aa][YY] - fr.x[hydf][YY];
        aay -= fr.box[YY][YY] * ANINT(1 / fr.box[YY][YY] * aay);
        double aaz = fr.x[aa][ZZ] - fr.x[hydf][ZZ];
        aaz -= fr.box[ZZ][ZZ] * ANINT(1 / fr.box[ZZ][ZZ] * aaz);
        double aar = aax * aax + aay * aay + aaz * aaz;

        // distance between donor and cloest hydrogen

        double abx = fr.x[bb][XX] - fr.x[hydf][XX];
        abx -= fr.box[XX][XX] * ANINT(1 / fr.box[XX][XX] * abx);
        double aby = fr.x[bb][YY] - fr.x[hydf][YY];
        aby -= fr.box[YY][YY] * ANINT(1 / fr.box[YY][YY] * aby);
        double abz = fr.x[bb][ZZ] - fr.x[hydf][ZZ];
        abz -= fr.box[ZZ][ZZ] * ANINT(1 / fr.box[ZZ][ZZ] * abz);
        double abr = abx * abx + aby * aby + abz * abz;
```

```
    // convert to unit vector

    double harr = 1.0 / sqrt(aar);
    double erax = aax * harr;
    double eray = aay * harr;
    double eraz = aaz * harr;
    double hcrr = 1.0 / sqrt(abr);
    double ercx = abx * hcrr;
    double ercy = aby * hcrr;
    double ercz = abz * hcrr;

    // dot product

    double cosphi = erax * ercx + eray * ercy + eraz * ercz;
    double phi = acos(cosphi);

    // record number of hydrogen bonding

    if(phi > HBANGLE) hbondstat++;

  }
  }

  hydallx[number].t=fr.time;
  hydallx[number].x=hydstat;
  hydallx[number].y=hbondstat;


  number++;
  hydallx[0].zzz = number;

  // saving the last time frame

  lasttime=fr.time;

  } while(read_next_frame(status,&fr));

  // open output "fp"

  fp = xvgropen(opt2fn("-hbn",NFILE,fnm),
"","Time(ns)","Count");

  for (i=0; i<hydallx[0].zzz; i++) {
    fprintf(fp,"%8.6i %8.6i %8.6i \n", hydallx[i].t/1000,hydallx[i].x, hydallx[i].y);
  }

  fclose(fp);
  thanx(stderr);
  return 0;
}
```

B.3.2   Glucose as H-donor

```
/*
 * $Id: template.c,v 1.4 2001/07/23 15:28:29 lindahl Exp $
```

```
*
*             This source code is part of
*
*              G   R   O   M   A   C   S
*
*        GROningen MAchine for Chemical Simulations
*
*                     VERSION 3.0
*
* Copyright (c) 1991-2001
* BIOSON Research Institute, Dept. of Biophysical Chemistry
* University of Groningen, The Netherlands
*
* This program is free software; you can redistribute it and/or
* modify it under the terms of the GNU General Public License
* as published by the Free Software Foundation; either version 2
* of the License, or (at your option) any later version.
*
* If you want to redistribute modifications, please consider that
* scientific software is very special. Version control is crucial -
* bugs must be traceable. We will be happy to consider code for
* inclusion in the official distribution, but derived work must not
* be called official GROMACS. Details are found in the README & COPYING
* files - if they are missing, get the official version at www.gromacs.org.
*
* To help us fund GROMACS development, we humbly ask that you cite
* the papers on the package - you can find them in the top README file.
*
* Do check out http://www.gromacs.org , or mail us at gromacs@gromacs.org .
*
* And Hey:
* Gyas ROwers Mature At Cryogenic Speed
*/

/* This line is only for CVS version info */

static char *SRCID_template_c = "$Id: template.c,v 1.4 2001/07/23 15:28:29 lindahl Exp $";


#include "statutil.h"
#include "typedefs.h"
#include "smalloc.h"
#include "vec.h"
#include "copyrite.h"
#include "statutil.h"
#include "tpxio.h"
#include "index.h"
#include "xvgr.h"


#define ANINT(A) (double) (long) (((A)<0.0) ? ((A)-0.5) : ((A)+0.5))
#define HBANGLE 120.0*3.141592653589793238462643383/180.0
#define HBOND 0.35
#define HBOND2 HBOND*HBOND


// structure for output file

  struct hydanalys {
    int t, a, e, i, m, q, u, y, cc, zzz;
    double b, c, d, f, g, h, j, k, l, n, o, p, r, s, tt, v, w, x, z, aa, bb, dd, ee, ff;
```

```c
  } *hydallx;

// start main here

  int main(int argc,char *argv[])
  {
  static char *desc[] = {
    "this is a small test program meant to serve as a template ",
    "when writing your own analysis tools. The advantage of ",
    "using gromacs for this is that you have access to all ",
    "information in the topology, and your program will be ",
    "able to handle all types of coordinates and trajectory ",
    "files supported by gromacs. Go ahead and try it! ",
    "This test version just writes the coordinates of an ",
    "arbitrary atom to standard out for each frame. You can ",
    "select which atom you want to examine with the -n argument."
  };

// allocate memory for output here

  hydallx = (struct hydanalys*) calloc(999999,sizeof(struct hydanalys));

// default value for rcut (hydration radius)

  static real n=0.35;

  /* Extra arguments - but note how you always get the begin/end
   * options when running the program, without mentioning them here!
   */

// passing a value through -rcut and save as "n"

  t_pargs pa[] = {
  { "-rcut", FALSE, etREAL, {&n},
    "hydration radius (nm) obtained first minimum of rdf"
  }
  };

// define variables

  t_topology top;
  char       title[STRLEN];
  t_trxframe fr;
  rvec       *xtop;
  matrix     box;
  int        status;
  int        flags = TRX_READ_X;
  int        *isize;              // size of index
  char       **grpnames;         // group name of index
  atom_id    **index;            // index values
  int        i, j;
  int        *hydall;
  int        number=0;           // counter
  FILE       *fp;                // output file
  int        lasttime;           // last timestep
  //   int        ccnumber;
```

```
t_filenm fnm[] = {
 { efTPS,  NULL,  NULL, ffREAD },      /* this is for the topology */
 { efTRX, "-f", NULL, ffREAD },        /* this is for the trajectory */
 { efNDX, NULL , NULL, ffOPTRD },      /* this is for index */
 { efXVG, "-hbn", "hbond", ffOPTWR }   /* this is for output in xvg */
};

#define NFILE asize(fnm)

CopyRight(stderr,argv[0]);

/* This is the routine responsible for adding default options,
 * calling the X/motif interface, etc. */

parse_common_args(&argc,argv,PCA_CAN_TIME | PCA_CAN_VIEW,
 NFILE,fnm,asize(pa),pa,asize(desc),desc,0,NULL);

/* We don't need any topology information to write the coordinates,
 * but to show how it works we start by writing the name and
 * charge of the selected atom. It returns a boolean telling us
 * whether the topology was found and could be read
 */

read_tps_conf(ftp2fn(efTPS,NFILE,fnm),title,&top,&xtop,NULL,box,TRUE);
sfree(xtop);

// allocate memory for read variable using snew

int grNR=999999;
snew(grpnames,grNR);
snew(index,grNR);
snew(isize,grNR);
snew(fp,grNR);

get_index(&(top.atoms),ftp2fn_null(efNDX,NFILE,fnm),2,isize,index,grpnames);

/* The first time we read data is a little special */

read_first_frame(&status,ftp2fn(efTRX,NFILE,fnm),&fr,flags);


/* This is the main loop over frames */

do {

// start counting atoms in the first hydration and hbond

real rhydration=n*n;
int hydstat=0;
int ccc=0;
int ddd=0;
int eee=0;
int fff=0;
int ggg=0;
int hhhh=0;
int iii=0;
int jjj=0;
```

```
///////////////////////////////////////// check hydration aa=acceptor bb=donor

// double accc[3]={0,0,0};
for(i = 0; (i < isize[0]); i++) {
  int aa = index[0][i];
  for(j = 0; (j < isize[1]); j++) {
    int bb = index[1][j];
    // O donor
    int cc = bb + 1;
    // H donor
    int hcc = bb + 13;

    double cx = fr.x[aa][XX]-fr.x[cc][XX];
    cx -= fr.box[XX][XX] * ANINT(1 / fr.box[XX][XX] * cx);
    double cy = fr.x[aa][YY]-fr.x[cc][YY];
    cy -= fr.box[YY][YY] * ANINT(1 / fr.box[YY][YY] * cy);
    double cz = fr.x[aa][ZZ] - fr.x[cc][ZZ];
    cz -= fr.box[ZZ][ZZ] * ANINT(1 / fr.box[ZZ][ZZ] * cz);
    double rcc = cx * cx + cy * cy + cz * cz;
    if(rcc > rhydration) continue;
    hydstat++;

    if(rcc > HBOND2) continue;
    double accx = fr.x[aa][XX] - fr.x[hcc][XX];
    accx -= fr.box[XX][XX] * ANINT(1 / fr.box[XX][XX] * accx);
    double accy = fr.x[aa][YY] - fr.x[hcc][YY];
    accy -= fr.box[YY][YY] * ANINT(1 / fr.box[YY][YY] * accy);
    double accz = fr.x[aa][ZZ] - fr.x[hcc][ZZ];
    accz -= fr.box[ZZ][ZZ] * ANINT(1 / fr.box[ZZ][ZZ] * accz);
    double accr = accx * accx + accy * accy + accz * accz;

    // distance between donor and cloest hydrogen

    double bccx = fr.x[cc][XX] - fr.x[hcc][XX];
    bccx -= fr.box[XX][XX] * ANINT(1 / fr.box[XX][XX] * bccx);
    double bccy = fr.x[cc][YY] - fr.x[hcc][YY];
    bccy -= fr.box[YY][YY] * ANINT(1 / fr.box[YY][YY] * bccy);
    double bccz = fr.x[cc][ZZ] - fr.x[hcc][ZZ];
    bccz -= fr.box[ZZ][ZZ] * ANINT(1 / fr.box[ZZ][ZZ] * bccz);
    double bccr = bccx * bccx + bccy * bccy + bccz * bccz;

    // convert to unit vector
    double xxcc = 1.0 / sqrt(accr);
    double eccx = accx * xxcc;
    double eccy = accy * xxcc;
    double eccz = accz * xxcc;
    double yycc = 1.0 / sqrt(bccr);
    double fccx = bccx * yycc;
    double fccy = bccy * yycc;
    double fccz = bccz * yycc;

    // dot product
    double cosphicc = eccx * fccx + eccy * fccy + eccz * fccz;
    double phicc = acos(cosphicc);

    // record number of hydrogen bonding
    if(phicc > HBANGLE) {
```

```
//accc[ccc]=aa+1;
ccc++;
      }
    }
  }

  hydallx[number].t=fr.time;
  hydallx[number].a=ccc;
  ///////////////////////////////////////// check hydration aa=acceptor bb=donor

  //double addd[3]={0,0,0};
  for(i = 0; (i < isize[0]); i++) {
    int aa = index[0][i];
    for(j = 0; (j < isize[1]); j++) {
      int bb = index[1][j];
      // O donor
      int dd = bb + 2;
      // H donor
      int hdd = bb + 14;

      double dx = fr.x[aa][XX]-fr.x[dd][XX];
      dx -= fr.box[XX][XX] * ANINT(1 / fr.box[XX][XX] * dx);
      double dy = fr.x[aa][YY]-fr.x[dd][YY];
      dy -= fr.box[YY][YY] * ANINT(1 / fr.box[YY][YY] * dy);
      double dz = fr.x[aa][ZZ] - fr.x[dd][ZZ];
      dz -= fr.box[ZZ][ZZ] * ANINT(1 / fr.box[ZZ][ZZ] * dz);
      double rdd = dx * dx + dy * dy + dz * dz;
      if(rdd > rhydration) continue;
      hydstat++;

      if(rdd > HBOND2) continue;
      double addx = fr.x[aa][XX] - fr.x[hdd][XX];
      addx -= fr.box[XX][XX] * ANINT(1 / fr.box[XX][XX] * addx);
      double addy = fr.x[aa][YY] - fr.x[hdd][YY];
      addy -= fr.box[YY][YY] * ANINT(1 / fr.box[YY][YY] * addy);
      double addz = fr.x[aa][ZZ] - fr.x[hdd][ZZ];
      addz -= fr.box[ZZ][ZZ] * ANINT(1 / fr.box[ZZ][ZZ] * addz);
      double addr = addx * addx + addy * addy + addz * addz;

      // distance between donor and cloest hydrogen

      double bddx = fr.x[dd][XX] - fr.x[hdd][XX];
      bddx -= fr.box[XX][XX] * ANINT(1 / fr.box[XX][XX] * bddx);
      double bddy = fr.x[dd][YY] - fr.x[hdd][YY];
      bddy -= fr.box[YY][YY] * ANINT(1 / fr.box[YY][YY] * bddy);
      double bddz = fr.x[dd][ZZ] - fr.x[hdd][ZZ];
      bddz -= fr.box[ZZ][ZZ] * ANINT(1 / fr.box[ZZ][ZZ] * bddz);
      double bddr = bddx * bddx + bddy * bddy + bddz * bddz;

      // convert to unit vector
      double xxdd = 1.0 / sqrt(addr);
      double eddx = addx * xxdd;
      double eddy = addy * xxdd;
      double eddz = addz * xxdd;
      double yydd = 1.0 / sqrt(bddr);
      double fddx = bddx * yydd;
      double fddy = bddy * yydd;
      double fddz = bddz * yydd;
```

```
      // dot product
      double cosphidd = eddx * fddx + eddy * fddy + eddz * fddz;
      double phidd = acos(cosphidd);

      // record number of hydrogen bonding
      if(phidd > HBANGLE) {
//addd[ddd]=aa+1;
ddd++;
      }
    }
  }

  hydallx[number].e=ddd;
  //////////////////////////////////////////// check hydration aa=acceptor bb=donor

  //double aeee[3]={0,0,0};
  for(i = 0; (i < isize[0]); i++) {
    int aa = index[0][i];
    for(j = 0; (j < isize[1]); j++) {
      int bb = index[1][j];
      // O donor
      int ee = bb + 3;
      // H donor
      int hee = bb + 15;

      double ex = fr.x[aa][XX]-fr.x[ee][XX];
      ex -= fr.box[XX][XX] * ANINT(1 / fr.box[XX][XX] * ex);
      double ey = fr.x[aa][YY]-fr.x[ee][YY];
      ey -= fr.box[YY][YY] * ANINT(1 / fr.box[YY][YY] * ey);
      double ez = fr.x[aa][ZZ] - fr.x[ee][ZZ];
      ez -= fr.box[ZZ][ZZ] * ANINT(1 / fr.box[ZZ][ZZ] * ez);
      double ree = ex * ex + ey * ey + ez * ez;
      if(ree > rhydration) continue;
      hydstat++;

      if(ree > HBOND2) continue;
      double aeex = fr.x[aa][XX] - fr.x[hee][XX];
      aeex -= fr.box[XX][XX] * ANINT(1 / fr.box[XX][XX] * aeex);
      double aeey = fr.x[aa][YY] - fr.x[hee][YY];
      aeey -= fr.box[YY][YY] * ANINT(1 / fr.box[YY][YY] * aeey);
      double aeez = fr.x[aa][ZZ] - fr.x[hee][ZZ];
      aeez -= fr.box[ZZ][ZZ] * ANINT(1 / fr.box[ZZ][ZZ] * aeez);
      double aer = aeex * aeex + aeey * aeey + aeez * aeez;

      // distance between donor and cloest hydrogen

      double beex = fr.x[ee][XX] - fr.x[hee][XX];
      beex -= fr.box[XX][XX] * ANINT(1 / fr.box[XX][XX] * beex);
      double beey = fr.x[ee][YY] - fr.x[hee][YY];
      beey -= fr.box[YY][YY] * ANINT(1 / fr.box[YY][YY] * beey);
      double beez = fr.x[ee][ZZ] - fr.x[hee][ZZ];
      beez -= fr.box[ZZ][ZZ] * ANINT(1 / fr.box[ZZ][ZZ] * beez);
      double beer = beex * beex + beey * beey + beez * beez;

      // convert to unit vector
      double xxee = 1.0 / sqrt(aer);
      double eeex = aeex * xxee;
```

```
        double eeey = aeey * xxee;
        double eeez = aeez * xxee;
        double yyee = 1.0 / sqrt(beer);
        double feex = beex * yyee;
        double feey = beey * yyee;
        double feez = beez * yyee;

        // dot product
        double cosphiee = eeex * feex + eeey * feey + eeez * feez;
        double phiee = acos(cosphiee);

        // record number of hydrogen bonding
        if(phiee > HBANGLE) {
//aeee[eee]=aa+1;
eee++;
        }
    }
  }

  hydallx[number].i=eee;
  ///////////////////////////////////////////// check hydration aa=acceptor bb=donor

  //double afff[3]={0,0,0};
  for(i = 0; (i < isize[0]); i++) {
    int aa = index[0][i];
    for(j = 0; (j < isize[1]); j++) {
      int bb = index[1][j];
      // O donor
      int ff = bb + 4;
      // H donor
      int hff = bb + 16;

      double fx = fr.x[aa][XX]-fr.x[ff][XX];
      fx -= fr.box[XX][XX] * ANINT(1 / fr.box[XX][XX] * fx);
      double fy = fr.x[aa][YY]-fr.x[ff][YY];
      fy -= fr.box[YY][YY] * ANINT(1 / fr.box[YY][YY] * fy);
      double fz = fr.x[aa][ZZ] - fr.x[ff][ZZ];
      fz -= fr.box[ZZ][ZZ] * ANINT(1 / fr.box[ZZ][ZZ] * fz);
      double rff = fx * fx + fy * fy + fz * fz;
      if(rff > rhydration) continue;
      hydstat++;

      if(rff > HBOND2) continue;
      double affx = fr.x[aa][XX] - fr.x[hff][XX];
      affx -= fr.box[XX][XX] * ANINT(1 / fr.box[XX][XX] * affx);
      double affy = fr.x[aa][YY] - fr.x[hff][YY];
      affy -= fr.box[YY][YY] * ANINT(1 / fr.box[YY][YY] * affy);
      double affz = fr.x[aa][ZZ] - fr.x[hff][ZZ];
      affz -= fr.box[ZZ][ZZ] * ANINT(1 / fr.box[ZZ][ZZ] * affz);
      double affr = affx * affx + affy * affy + affz * affz;

      // distance between donor and cloest hydrogen

      double bffx = fr.x[ff][XX] - fr.x[hff][XX];
      bffx -= fr.box[XX][XX] * ANINT(1 / fr.box[XX][XX] * bffx);
      double bffy = fr.x[ff][YY] - fr.x[hff][YY];
      bffy -= fr.box[YY][YY] * ANINT(1 / fr.box[YY][YY] * bffy);
      double bffz = fr.x[ff][ZZ] - fr.x[hff][ZZ];
```

```
        bffz -= fr.box[ZZ][ZZ] * ANINT(1 / fr.box[ZZ][ZZ] * bffz);
        double bffr = bffx * bffx + bffy * bffy + bffz * bffz;

        // convert to unit vector
        double xxff = 1.0 / sqrt(affr);
        double effx = affx * xxff;
        double effy = affy * xxff;
        double effz = affz * xxff;
        double yyff = 1.0 / sqrt(bffr);
        double fffx = bffx * yyff;
        double fffy = bffy * yyff;
        double fffz = bffz * yyff;

        // dot product
        double cosphiff = effx * fffx + effy * fffy + effz * fffz;
        double phiff = acos(cosphiff);

        // record number of hydrogen bonding
        if(phiff > HBANGLE) {
//afff[fff]=aa+1;
fff++;
        }
      }
    }
  }

  hydallx[number].m=fff;
  ///////////////////////////////////////////// check hydration aa=acceptor bb=donor

  //double aggg[3]={0,0,0};
  for(i = 0; (i < isize[0]); i++) {
    int aa = index[0][i];
    for(j = 0; (j < isize[1]); j++) {
      int bb = index[1][j];
      // O donor
      int gg = bb + 5;
      // H donor
      int hgg = bb + 17;

      double gx = fr.x[aa][XX]-fr.x[gg][XX];
      gx -= fr.box[XX][XX] * ANINT(1 / fr.box[XX][XX] * gx);
      double gy = fr.x[aa][YY]-fr.x[gg][YY];
      gy -= fr.box[YY][YY] * ANINT(1 / fr.box[YY][YY] * gy);
      double gz = fr.x[aa][ZZ] - fr.x[gg][ZZ];
      gz -= fr.box[ZZ][ZZ] * ANINT(1 / fr.box[ZZ][ZZ] * gz);
      double rgg = gx * gx + gy * gy + gz * gz;
      if(rgg > rhydration) continue;
      hydstat++;

      if(rgg > HBOND2) continue;
      double aggx = fr.x[aa][XX] - fr.x[hgg][XX];
      aggx -= fr.box[XX][XX] * ANINT(1 / fr.box[XX][XX] * aggx);
      double aggy = fr.x[aa][YY] - fr.x[hgg][YY];
      aggy -= fr.box[YY][YY] * ANINT(1 / fr.box[YY][YY] * aggy);
      double aggz = fr.x[aa][ZZ] - fr.x[hgg][ZZ];
      aggz -= fr.box[ZZ][ZZ] * ANINT(1 / fr.box[ZZ][ZZ] * aggz);
      double aggr = aggx * aggx + aggy * aggy + aggz * aggz;

      // distance between donor and cloest hydrogen
```

```
        double bggx = fr.x[gg][XX] - fr.x[hgg][XX];
        bggx -= fr.box[XX][XX] * ANINT(1 / fr.box[XX][XX] * bggx);
        double bggy = fr.x[gg][YY] - fr.x[hgg][YY];
        bggy -= fr.box[YY][YY] * ANINT(1 / fr.box[YY][YY] * bggy);
        double bggz = fr.x[gg][ZZ] - fr.x[hgg][ZZ];
        bggz -= fr.box[ZZ][ZZ] * ANINT(1 / fr.box[ZZ][ZZ] * bggz);
        double bggr = bggx * bggx + bggy * bggy + bggz * bggz;

        // convert to unit vector
        double xxgg = 1.0 / sqrt(aggr);
        double eggx = aggx * xxgg;
        double eggy = aggy * xxgg;
        double eggz = aggz * xxgg;
        double yygg = 1.0 / sqrt(bggr);
        double fggx = bggx * yygg;
        double fggy = bggy * yygg;
        double fggz = bggz * yygg;

        // dot product
        double cosphigg = eggx * fggx + eggy * fggy + eggz * fggz;
        double phigg = acos(cosphigg);

        // record number of hydrogen bonding
        if(phigg > HBANGLE) {
//aggg[ggg]=aa+1;
ggg++;
        }
      }
    }

    hydallx[number].q=ggg;

    number++;
    hydallx[0].zzz = number;
    // saving the last time frame

    lasttime=fr.time;

    } while(read_next_frame(status,&fr));

    // open output "fp"

    fp = xvgropen(opt2fn("-hbn",NFILE,fnm),
"","Time(ps)","Count");

    for (i=0; i<hydallx[0].zzz; i++) {

fprintf(fp,"%5i %5i %5i %5i %5i %5i\n", hydallx[i].t, hydallx[i].a, hydallx[i].e, hydallx[i].i, hydallx[i].m, hydallx[i].q);

    }

    fclose(fp);
    thanx(stderr);
    return 0;
}
```

B.3.3   Trehalose as H-donor

```
/*
 * $Id: template.c,v 1.4 2001/07/23 15:28:29 lindahl Exp $
 *
 *                This source code is part of
 *
 *                 G   R   O   M   A   C   S
 *
 *          GROningen MAchine for Chemical Simulations
 *
 *                        VERSION 3.0
 *
 * Copyright (c) 1991-2001
 * BIOSON Research Institute, Dept. of Biophysical Chemistry
 * University of Groningen, The Netherlands
 *
 * This program is free software; you can redistribute it and/or
 * modify it under the terms of the GNU General Public License
 * as published by the Free Software Foundation; either version 2
 * of the License, or (at your option) any later version.
 *
 * If you want to redistribute modifications, please consider that
 * scientific software is very special. Version control is crucial -
 * bugs must be traceable. We will be happy to consider code for
 * inclusion in the official distribution, but derived work must not
 * be called official GROMACS. Details are found in the README & COPYING
 * files - if they are missing, get the official version at www.gromacs.org.
 *
 * To help us fund GROMACS development, we humbly ask that you cite
 * the papers on the package - you can find them in the top README file.
 *
 * Do check out http://www.gromacs.org , or mail us at gromacs@gromacs.org .
 *
 * And Hey:
 * Gyas ROwers Mature At Cryogenic Speed
 */


/* This line is only for CVS version info */

static char *SRCID_template_c = "$Id: template.c,v 1.4 2001/07/23 15:28:29 lindahl Exp $";


#include "statutil.h"
#include "typedefs.h"
#include "smalloc.h"
#include "vec.h"
#include "copyrite.h"
#include "statutil.h"
#include "tpxio.h"
#include "index.h"
#include "xvgr.h"


#define ANINT(A) (double) (long) (((A)<0.0) ? ((A)-0.5) : ((A)+0.5))
#define HBANGLE 120.0*3.1415926535897932384626433383/180.0
#define HBOND 0.35
#define HBOND2 HBOND*HBOND


// structure for output file
```

```
  struct hydanalys {
    int t, a, e, i, m, q, u, y, cc, zzz;
    double b, c, d, f, g, h, j, k, l, n, o, p, r, s, tt, v, w, x, z, aa, bb, dd, ee, ff;
  } *hydallx;

// start main here

  int main(int argc,char *argv[])
  {
  static char *desc[] = {
    "this is a small test program meant to serve as a template ",
    "when writing your own analysis tools. The advantage of ",
    "using gromacs for this is that you have access to all ",
    "information in the topology, and your program will be ",
    "able to handle all types of coordinates and trajectory ",
    "files supported by gromacs. Go ahead and try it! ",
    "This test version just writes the coordinates of an ",
    "arbitrary atom to standard out for each frame. You can ",
    "select which atom you want to examine with the -n argument."
  };

// allocate memory for output here

  hydallx = (struct hydanalys*) calloc(999999,sizeof(struct hydanalys));

// default value for rcut (hydration radius)

  static real n=0.35;

  /* Extra arguments - but note how you always get the begin/end
   * options when running the program, without mentioning them here!
   */

// passing a value through -rcut and save as "n"

  t_pargs pa[] = {
  { "-rcut", FALSE, etREAL, {&n},
    "hydration radius (nm) obtained first minimum of rdf"
  }
  };

// define variables

  t_topology top;
  char       title[STRLEN];
  t_trxframe fr;
  rvec       *xtop;
  matrix     box;
  int        status;
  int        flags = TRX_READ_X;
  int        *isize;            // size of index
  char       **grpnames;        // group name of index
  atom_id    **index;           // index values
  int        i, j;
  int        *hydall;
  int        number=0;          // counter
  FILE       *fp;               // output file
```

```
int       lasttime;            // last timestep
//   int       ccnumber;

t_filenm fnm[] = {
 { efTPS,  NULL,  NULL, ffREAD },      /* this is for the topology */
 { efTRX, "-f", NULL, ffREAD },        /* this is for the trajectory */
 { efNDX, NULL , NULL, ffOPTRD },      /* this is for index */
 { efXVG, "-hbn", "hbond", ffOPTWR }   /* this is for output in xvg */
};

#define NFILE asize(fnm)

CopyRight(stderr,argv[0]);

/* This is the routine responsible for adding default options,
 * calling the X/motif interface, etc. */

parse_common_args(&argc,argv,PCA_CAN_TIME | PCA_CAN_VIEW,
 NFILE,fnm,asize(pa),pa,asize(desc),desc,0,NULL);

/* We don't need any topology information to write the coordinates,
 * but to show how it works we start by writing the name and
 * charge of the selected atom. It returns a boolean telling us
 * whether the topology was found and could be read
 */

read_tps_conf(ftp2fn(efTPS,NFILE,fnm),title,&top,&xtop,NULL,box,TRUE);
sfree(xtop);

// allocate memory for read variable using snew

int grNR=999999;
snew(grpnames,grNR);
snew(index,grNR);
snew(isize,grNR);
snew(fp,grNR);

get_index(&(top.atoms),ftp2fn_null(efNDX,NFILE,fnm),2,isize,index,grpnames);

/* The first time we read data is a little special */

read_first_frame(&status,ftp2fn(efTRX,NFILE,fnm),&fr,flags);


/* This is the main loop over frames */

do {

// start counting atoms in the first hydration and hbond

real rhydration=n*n;
int hydstat=0;
int ccc=0;
int ddd=0;
int eee=0;
int fff=0;
int ggg=0;
int hhhh=0;
```

```
    int iii=0;
    int jjj=0;


    ///////////////////////////////////////// check hydration aa=acceptor bb=donor

    // double accc[3]={0,0,0};
    for(i = 0; (i < isize[0]); i++) {
      int aa = index[0][i];
      for(j = 0; (j < isize[1]); j++) {
        int bb = index[1][j];
        // O donor
        int cc = bb + 1;
        // H donor
        int hcc = bb + 24;

        double cx = fr.x[aa][XX]-fr.x[cc][XX];
        cx -= fr.box[XX][XX] * ANINT(1 / fr.box[XX][XX] * cx);
        double cy = fr.x[aa][YY]-fr.x[cc][YY];
        cy -= fr.box[YY][YY] * ANINT(1 / fr.box[YY][YY] * cy);
        double cz = fr.x[aa][ZZ] - fr.x[cc][ZZ];
        cz -= fr.box[ZZ][ZZ] * ANINT(1 / fr.box[ZZ][ZZ] * cz);
        double rcc = cx * cx + cy * cy + cz * cz;
        if(rcc > rhydration) continue;
        hydstat++;

        if(rcc > HBOND2) continue;
        double accx = fr.x[aa][XX] - fr.x[hcc][XX];
        accx -= fr.box[XX][XX] * ANINT(1 / fr.box[XX][XX] * accx);
        double accy = fr.x[aa][YY] - fr.x[hcc][YY];
        accy -= fr.box[YY][YY] * ANINT(1 / fr.box[YY][YY] * accy);
        double accz = fr.x[aa][ZZ] - fr.x[hcc][ZZ];
        accz -= fr.box[ZZ][ZZ] * ANINT(1 / fr.box[ZZ][ZZ] * accz);
        double accr = accx * accx + accy * accy + accz * accz;

        // distance between donor and cloest hydrogen

        double bccx = fr.x[cc][XX] - fr.x[hcc][XX];
        bccx -= fr.box[XX][XX] * ANINT(1 / fr.box[XX][XX] * bccx);
        double bccy = fr.x[cc][YY] - fr.x[hcc][YY];
        bccy -= fr.box[YY][YY] * ANINT(1 / fr.box[YY][YY] * bccy);
        double bccz = fr.x[cc][ZZ] - fr.x[hcc][ZZ];
        bccz -= fr.box[ZZ][ZZ] * ANINT(1 / fr.box[ZZ][ZZ] * bccz);
        double bccr = bccx * bccx + bccy * bccy + bccz * bccz;

        // convert to unit vector
        double xxcc = 1.0 / sqrt(accr);
        double eccx = accx * xxcc;
        double eccy = accy * xxcc;
        double eccz = accz * xxcc;
        double yycc = 1.0 / sqrt(bccr);
        double fccx = bccx * yycc;
        double fccy = bccy * yycc;
        double fccz = bccz * yycc;

        // dot product
        double cosphicc = eccx * fccx + eccy * fccy + eccz * fccz;
        double phicc = acos(cosphicc);
```

```
      // record number of hydrogen bonding
      if(phicc > HBANGLE) {
//accc[ccc]=aa+1;
ccc++;
      }
    }
  }

  hydallx[number].t=fr.time;
  hydallx[number].a=ccc;
  ///////////////////////////////////////// check hydration aa=acceptor bb=donor

  //double addd[3]={0,0,0};
  for(i = 0; (i < isize[0]); i++) {
    int aa = index[0][i];
    for(j = 0; (j < isize[1]); j++) {
      int bb = index[1][j];
      // O donor
      int dd = bb + 2;
      // H donor
      int hdd = bb + 25;

      double dx = fr.x[aa][XX]-fr.x[dd][XX];
      dx -= fr.box[XX][XX] * ANINT(1 / fr.box[XX][XX] * dx);
      double dy = fr.x[aa][YY]-fr.x[dd][YY];
      dy -= fr.box[YY][YY] * ANINT(1 / fr.box[YY][YY] * dy);
      double dz = fr.x[aa][ZZ] - fr.x[dd][ZZ];
      dz -= fr.box[ZZ][ZZ] * ANINT(1 / fr.box[ZZ][ZZ] * dz);
      double rdd = dx * dx + dy * dy + dz * dz;
      if(rdd > rhydration) continue;
      hydstat++;

      if(rdd > HBOND2) continue;
      double addx = fr.x[aa][XX] - fr.x[hdd][XX];
      addx -= fr.box[XX][XX] * ANINT(1 / fr.box[XX][XX] * addx);
      double addy = fr.x[aa][YY] - fr.x[hdd][YY];
      addy -= fr.box[YY][YY] * ANINT(1 / fr.box[YY][YY] * addy);
      double addz = fr.x[aa][ZZ] - fr.x[hdd][ZZ];
      addz -= fr.box[ZZ][ZZ] * ANINT(1 / fr.box[ZZ][ZZ] * addz);
      double addr = addx * addx + addy * addy + addz * addz;

      // distance between donor and cloest hydrogen

      double bddx = fr.x[dd][XX] - fr.x[hdd][XX];
      bddx -= fr.box[XX][XX] * ANINT(1 / fr.box[XX][XX] * bddx);
      double bddy = fr.x[dd][YY] - fr.x[hdd][YY];
      bddy -= fr.box[YY][YY] * ANINT(1 / fr.box[YY][YY] * bddy);
      double bddz = fr.x[dd][ZZ] - fr.x[hdd][ZZ];
      bddz -= fr.box[ZZ][ZZ] * ANINT(1 / fr.box[ZZ][ZZ] * bddz);
      double bddr = bddx * bddx + bddy * bddy + bddz * bddz;

      // convert to unit vector
      double xxdd = 1.0 / sqrt(addr);
      double eddx = addx * xxdd;
      double eddy = addy * xxdd;
      double eddz = addz * xxdd;
      double yydd = 1.0 / sqrt(bddr);
      double fddx = bddx * yydd;
```

```
      double fddy = bddy * yydd;
      double fddz = bddz * yydd;

      // dot product
      double cosphidd = eddx * fddx + eddy * fddy + eddz * fddz;
      double phidd = acos(cosphidd);

      // record number of hydrogen bonding
      if(phidd > HBANGLE) {
//addd[ddd]=aa+1;
ddd++;
      }
    }
  }

  hydallx[number].e=ddd;
  /////////////////////////////////////////// check hydration aa=acceptor bb=donor

  //double aeee[3]={0,0,0};
  for(i = 0; (i < isize[0]); i++) {
    int aa = index[0][i];
    for(j = 0; (j < isize[1]); j++) {
      int bb = index[1][j];
      // O donor
      int ee = bb + 3;
      // H donor
      int hee = bb + 26;

      double ex = fr.x[aa][XX]-fr.x[ee][XX];
      ex -= fr.box[XX][XX] * ANINT(1 / fr.box[XX][XX] * ex);
      double ey = fr.x[aa][YY]-fr.x[ee][YY];
      ey -= fr.box[YY][YY] * ANINT(1 / fr.box[YY][YY] * ey);
      double ez = fr.x[aa][ZZ] - fr.x[ee][ZZ];
      ez -= fr.box[ZZ][ZZ] * ANINT(1 / fr.box[ZZ][ZZ] * ez);
      double ree = ex * ex + ey * ey + ez * ez;
      if(ree > rhydration) continue;
      hydstat++;

      if(ree > HBOND2) continue;
      double aeex = fr.x[aa][XX] - fr.x[hee][XX];
      aeex -= fr.box[XX][XX] * ANINT(1 / fr.box[XX][XX] * aeex);
      double aeey = fr.x[aa][YY] - fr.x[hee][YY];
      aeey -= fr.box[YY][YY] * ANINT(1 / fr.box[YY][YY] * aeey);
      double aeez = fr.x[aa][ZZ] - fr.x[hee][ZZ];
      aeez -= fr.box[ZZ][ZZ] * ANINT(1 / fr.box[ZZ][ZZ] * aeez);
      double aeer = aeex * aeex + aeey * aeey + aeez * aeez;

      // distance between donor and cloest hydrogen

      double beex = fr.x[ee][XX] - fr.x[hee][XX];
      beex -= fr.box[XX][XX] * ANINT(1 / fr.box[XX][XX] * beex);
      double beey = fr.x[ee][YY] - fr.x[hee][YY];
      beey -= fr.box[YY][YY] * ANINT(1 / fr.box[YY][YY] * beey);
      double beez = fr.x[ee][ZZ] - fr.x[hee][ZZ];
      beez -= fr.box[ZZ][ZZ] * ANINT(1 / fr.box[ZZ][ZZ] * beez);
      double beer = beex * beex + beey * beey + beez * beez;

      // convert to unit vector
```

```
    double xxee = 1.0 / sqrt(aeer);
    double eeex = aeex * xxee;
    double eeey = aeey * xxee;
    double eeez = aeez * xxee;
    double yyee = 1.0 / sqrt(beer);
    double feex = beex * yyee;
    double feey = beey * yyee;
    double feez = beez * yyee;

    // dot product
    double cosphiee = eeex * feex + eeey * feey + eeez * feez;
    double phiee = acos(cosphiee);

    // record number of hydrogen bonding
    if(phiee > HBANGLE) {
//aeee[eee]=aa+1;
eee++;
    }
  }
}

hydallx[number].i=eee;
///////////////////////////////////////////// check hydration aa=acceptor bb=donor

//double afff[3]={0,0,0};
for(i = 0; (i < isize[0]); i++) {
  int aa = index[0][i];
  for(j = 0; (j < isize[1]); j++) {
    int bb = index[1][j];
    // O donor
    int ff = bb + 5;
    // H donor
    int hff = bb + 27;

    double fx = fr.x[aa][XX]-fr.x[ff][XX];
    fx -= fr.box[XX][XX] * ANINT(1 / fr.box[XX][XX] * fx);
    double fy = fr.x[aa][YY]-fr.x[ff][YY];
    fy -= fr.box[YY][YY] * ANINT(1 / fr.box[YY][YY] * fy);
    double fz = fr.x[aa][ZZ] - fr.x[ff][ZZ];
    fz -= fr.box[ZZ][ZZ] * ANINT(1 / fr.box[ZZ][ZZ] * fz);
    double rff = fx * fx + fy * fy + fz * fz;
    if(rff > rhydration) continue;
    hydstat++;

    if(rff > HBOND2) continue;
    double affx = fr.x[aa][XX] - fr.x[hff][XX];
    affx -= fr.box[XX][XX] * ANINT(1 / fr.box[XX][XX] * affx);
    double affy = fr.x[aa][YY] - fr.x[hff][YY];
    affy -= fr.box[YY][YY] * ANINT(1 / fr.box[YY][YY] * affy);
    double affz = fr.x[aa][ZZ] - fr.x[hff][ZZ];
    affz -= fr.box[ZZ][ZZ] * ANINT(1 / fr.box[ZZ][ZZ] * affz);
    double affr = affx * affx + affy * affy + affz * affz;

    // distance between donor and cloest hydrogen

    double bffx = fr.x[ff][XX] - fr.x[hff][XX];
    bffx -= fr.box[XX][XX] * ANINT(1 / fr.box[XX][XX] * bffx);
    double bffy = fr.x[ff][YY] - fr.x[hff][YY];
```

```
        bffy -= fr.box[YY][YY] * ANINT(1 / fr.box[YY][YY] * bffy);
        double bffz = fr.x[ff][ZZ] - fr.x[hff][ZZ];
        bffz -= fr.box[ZZ][ZZ] * ANINT(1 / fr.box[ZZ][ZZ] * bffz);
        double bffr = bffx * bffx + bffy * bffy + bffz * bffz;

        // convert to unit vector
        double xxff = 1.0 / sqrt(affr);
        double effx = affx * xxff;
        double effy = affy * xxff;
        double effz = affz * xxff;
        double yyff = 1.0 / sqrt(bffr);
        double fffx = bffx * yyff;
        double fffy = bffy * yyff;
        double fffz = bffz * yyff;

        // dot product
        double cosphiff = effx * fffx + effy * fffy + effz * fffz;
        double phiff = acos(cosphiff);

        // record number of hydrogen bonding
        if(phiff > HBANGLE) {
//afff[fff]=aa+1;
fff++;
      }
    }
  }

  hydallx[number].m=fff;
  ///////////////////////////////////////////// check hydration aa=acceptor bb=donor

  //double aggg[3]={0,0,0};
  for(i = 0; (i < isize[0]); i++) {
    int aa = index[0][i];
    for(j = 0; (j < isize[1]); j++) {
      int bb = index[1][j];
      // O donor
      int gg = bb + 12;
      // H donor
      int hgg = bb + 35;

      double gx = fr.x[aa][XX]-fr.x[gg][XX];
      gx -= fr.box[XX][XX] * ANINT(1 / fr.box[XX][XX] * gx);
      double gy = fr.x[aa][YY]-fr.x[gg][YY];
      gy -= fr.box[YY][YY] * ANINT(1 / fr.box[YY][YY] * gy);
      double gz = fr.x[aa][ZZ] - fr.x[gg][ZZ];
      gz -= fr.box[ZZ][ZZ] * ANINT(1 / fr.box[ZZ][ZZ] * gz);
      double rgg = gx * gx + gy * gy + gz * gz;
      if(rgg > rhydration) continue;
      hydstat++;

      if(rgg > HBOND2) continue;
      double aggx = fr.x[aa][XX] - fr.x[hgg][XX];
      aggx -= fr.box[XX][XX] * ANINT(1 / fr.box[XX][XX] * aggx);
      double aggy = fr.x[aa][YY] - fr.x[hgg][YY];
      aggy -= fr.box[YY][YY] * ANINT(1 / fr.box[YY][YY] * aggy);
      double aggz = fr.x[aa][ZZ] - fr.x[hgg][ZZ];
      aggz -= fr.box[ZZ][ZZ] * ANINT(1 / fr.box[ZZ][ZZ] * aggz);
      double aggr = aggx * aggx + aggy * aggy + aggz * aggz;
```

```
        // distance between donor and cloest hydrogen

        double bggx = fr.x[gg][XX] - fr.x[hgg][XX];
        bggx -= fr.box[XX][XX] * ANINT(1 / fr.box[XX][XX] * bggx);
        double bggy = fr.x[gg][YY] - fr.x[hgg][YY];
        bggy -= fr.box[YY][YY] * ANINT(1 / fr.box[YY][YY] * bggy);
        double bggz = fr.x[gg][ZZ] - fr.x[hgg][ZZ];
        bggz -= fr.box[ZZ][ZZ] * ANINT(1 / fr.box[ZZ][ZZ] * bggz);
        double bggr = bggx * bggx + bggy * bggy + bggz * bggz;

        // convert to unit vector
        double xxgg = 1.0 / sqrt(aggr);
        double eggx = aggx * xxgg;
        double eggy = aggy * xxgg;
        double eggz = aggz * xxgg;
        double yygg = 1.0 / sqrt(bggr);
        double fggx = bggx * yygg;
        double fggy = bggy * yygg;
        double fggz = bggz * yygg;

        // dot product
        double cosphigg = eggx * fggx + eggy * fggy + eggz * fggz;
        double phigg = acos(cosphigg);

        // record number of hydrogen bonding
        if(phigg > HBANGLE) {
//aggg[ggg]=aa+1;
ggg++;
        }
    }
  }

  hydallx[number].q=ggg;
  ///////////////////////////////////////////// check hydration aa=acceptor bb=donor

  //double ahhh[3]={0,0,0};
  for(i = 0; (i < isize[0]); i++) {
    int aa = index[0][i];
    for(j = 0; (j < isize[1]); j++) {
      int bb = index[1][j];
      // O donor
      int hh = bb + 13;
      // H donor
      int hhh = bb + 36;

      double hx = fr.x[aa][XX]-fr.x[hh][XX];
      hx -= fr.box[XX][XX] * ANINT(1 / fr.box[XX][XX] * hx);
      double hy = fr.x[aa][YY]-fr.x[hh][YY];
      hy -= fr.box[YY][YY] * ANINT(1 / fr.box[YY][YY] * hy);
      double hz = fr.x[aa][ZZ] - fr.x[hh][ZZ];
      hz -= fr.box[ZZ][ZZ] * ANINT(1 / fr.box[ZZ][ZZ] * hz);
      double rhh = hx * hx + hy * hy + hz * hz;
      if(rhh > rhydration) continue;
      hydstat++;

      if(rhh > HBOND2) continue;
      double ahhx = fr.x[aa][XX] - fr.x[hhh][XX];
```

```
        ahhx -= fr.box[XX][XX] * ANINT(1 / fr.box[XX][XX] * ahhx);
        double ahhy = fr.x[aa][YY] - fr.x[hhh][YY];
        ahhy -= fr.box[YY][YY] * ANINT(1 / fr.box[YY][YY] * ahhy);
        double ahhz = fr.x[aa][ZZ] - fr.x[hhh][ZZ];
        ahhz -= fr.box[ZZ][ZZ] * ANINT(1 / fr.box[ZZ][ZZ] * ahhz);
        double ahhr = ahhx * ahhx + ahhy * ahhy + ahhz * ahhz;


        // distance between donor and cloest hydrogen

        double bhhx = fr.x[hh][XX] - fr.x[hhh][XX];
        bhhx -= fr.box[XX][XX] * ANINT(1 / fr.box[XX][XX] * bhhx);
        double bhhy = fr.x[hh][YY] - fr.x[hhh][YY];
        bhhy -= fr.box[YY][YY] * ANINT(1 / fr.box[YY][YY] * bhhy);
        double bhhz = fr.x[hh][ZZ] - fr.x[hhh][ZZ];
        bhhz -= fr.box[ZZ][ZZ] * ANINT(1 / fr.box[ZZ][ZZ] * bhhz);
        double bhhr = bhhx * bhhx + bhhy * bhhy + bhhz * bhhz;


        // convert to unit vector
        double xxhh = 1.0 / sqrt(ahhr);
        double ehhx = ahhx * xxhh;
        double ehhy = ahhy * xxhh;
        double ehhz = ahhz * xxhh;
        double yyhh = 1.0 / sqrt(bhhr);
        double fhhx = bhhx * yyhh;
        double fhhy = bhhy * yyhh;
        double fhhz = bhhz * yyhh;


        // dot product
        double cosphihh = ehhx * fhhx + ehhy * fhhy + ehhz * fhhz;
        double phihh = acos(cosphihh);

        // record number of hydrogen bonding
        if(phihh > HBANGLE) {
//ahhh[hhh]=aa+1;
hhhh++;
        }
    }
  }

  hydallx[number].u=hhhh;
  ////////////////////////////////////////// check hydration aa=acceptor bb=donor

  //double aiii[3]={0,0,0};
  for(i = 0; (i < isize[0]); i++) {
    int aa = index[0][i];
    for(j = 0; (j < isize[1]); j++) {
      int bb = index[1][j];
      // O donor
      int ii = bb + 14;
      // H donor
      int hii = bb + 37;

      double ix = fr.x[aa][XX]-fr.x[ii][XX];
      ix -= fr.box[XX][XX] * ANINT(1 / fr.box[XX][XX] * ix);
      double iy = fr.x[aa][YY]-fr.x[ii][YY];
      iy -= fr.box[YY][YY] * ANINT(1 / fr.box[YY][YY] * iy);
      double iz = fr.x[aa][ZZ] - fr.x[ii][ZZ];
      iz -= fr.box[ZZ][ZZ] * ANINT(1 / fr.box[ZZ][ZZ] * iz);
```

```
    double rii = ix * ix + iy * iy + iz * iz;
    if(rii > rhydration) continue;
    hydstat++;

    if(rii > HBOND2) continue;
    double aiix = fr.x[aa][XX] - fr.x[hii][XX];
    aiix -= fr.box[XX][XX] * ANINT(1 / fr.box[XX][XX] * aiix);
    double aiiy = fr.x[aa][YY] - fr.x[hii][YY];
    aiiy -= fr.box[YY][YY] * ANINT(1 / fr.box[YY][YY] * aiiy);
    double aiiz = fr.x[aa][ZZ] - fr.x[hii][ZZ];
    aiiz -= fr.box[ZZ][ZZ] * ANINT(1 / fr.box[ZZ][ZZ] * aiiz);
    double aiir = aiix * aiix + aiiy * aiiy + aiiz * aiiz;

    // distance between donor and cloest hydrogen

    double biix = fr.x[ii][XX] - fr.x[hii][XX];
    biix -= fr.box[XX][XX] * ANINT(1 / fr.box[XX][XX] * biix);
    double biiy = fr.x[ii][YY] - fr.x[hii][YY];
    biiy -= fr.box[YY][YY] * ANINT(1 / fr.box[YY][YY] * biiy);
    double biiz = fr.x[ii][ZZ] - fr.x[hii][ZZ];
    biiz -= fr.box[ZZ][ZZ] * ANINT(1 / fr.box[ZZ][ZZ] * biiz);
    double biir = biix * biix + biiy * biiy + biiz * biiz;

    // convert to unit vector
    double xxii = 1.0 / sqrt(aiir);
    double eiix = aiix * xxii;
    double eiiy = aiiy * xxii;
    double eiiz = aiiz * xxii;
    double yyii = 1.0 / sqrt(biir);
    double fiix = biix * yyii;
    double fiiy = biiy * yyii;
    double fiiz = biiz * yyii;

    // dot product
    double cosphiii = eiix * fiix + eiiy * fiiy + eiiz * fiiz;
    double phiii = acos(cosphiii);

    // record number of hydrogen bonding
    if(phiii > HBANGLE) {
//aiii[iii]=aa+1;
iii++;
    }
   }
  }

  hydallx[number].y=iii;
  ///////////////////////////////////////////// check hydration aa=acceptor bb=donor

  //double ajjj[3]={0,0,0};
  for(i = 0; (i < isize[0]); i++) {
    int aa = index[0][i];
    for(j = 0; (j < isize[1]); j++) {
      int bb = index[1][j];
      // O donor
      int jj = bb + 16;
      // H donor
      int hjj = bb + 38;
```

```
    double jx = fr.x[aa][XX]-fr.x[jj][XX];
    jx -= fr.box[XX][XX] * ANINT(1 / fr.box[XX][XX] * jx);
    double jy = fr.x[aa][YY]-fr.x[jj][YY];
    jy -= fr.box[YY][YY] * ANINT(1 / fr.box[YY][YY] * jy);
    double jz = fr.x[aa][ZZ] - fr.x[jj][ZZ];
    jz -= fr.box[ZZ][ZZ] * ANINT(1 / fr.box[ZZ][ZZ] * jz);
    double rjj = jx * jx + jy * jy + jz * jz;
    if(rjj > rhydration) continue;
    hydstat++;

    if(rjj > HBOND2) continue;
    double ajjx = fr.x[aa][XX] - fr.x[hjj][XX];
    ajjx -= fr.box[XX][XX] * ANINT(1 / fr.box[XX][XX] * ajjx);
    double ajjy = fr.x[aa][YY] - fr.x[hjj][YY];
    ajjy -= fr.box[YY][YY] * ANINT(1 / fr.box[YY][YY] * ajjy);
    double ajjz = fr.x[aa][ZZ] - fr.x[hjj][ZZ];
    ajjz -= fr.box[ZZ][ZZ] * ANINT(1 / fr.box[ZZ][ZZ] * ajjz);
    double ajjr = ajjx * ajjx + ajjy * ajjy + ajjz * ajjz;

    // distance between donor and cloest hydrogen

    double bjjx = fr.x[jj][XX] - fr.x[hjj][XX];
    bjjx -= fr.box[XX][XX] * ANINT(1 / fr.box[XX][XX] * bjjx);
    double bjjy = fr.x[jj][YY] - fr.x[hjj][YY];
    bjjy -= fr.box[YY][YY] * ANINT(1 / fr.box[YY][YY] * bjjy);
    double bjjz = fr.x[jj][ZZ] - fr.x[hjj][ZZ];
    bjjz -= fr.box[ZZ][ZZ] * ANINT(1 / fr.box[ZZ][ZZ] * bjjz);
    double bjjr = bjjx * bjjx + bjjy * bjjy + bjjz * bjjz;

    // convert to unit vector
    double xxjj = 1.0 / sqrt(ajjr);
    double ejjx = ajjx * xxjj;
    double ejjy = ajjy * xxjj;
    double ejjz = ajjz * xxjj;
    double yyjj = 1.0 / sqrt(bjjr);
    double fjjx = bjjx * yyjj;
    double fjjy = bjjy * yyjj;
    double fjjz = bjjz * yyjj;

    // dot product
    double cosphijj = ejjx * fjjx + ejjy * fjjy + ejjz * fjjz;
    double phijj = acos(cosphijj);

    // record number of hydrogen bonding
    if(phijj > HBANGLE) {
//ajjj[jjj]=aa+1;
jjj++;
    }
  }
  }

  hydallx[number].cc=jjj;

  number++;
  hydallx[0].zzz = number;
  // saving the last time frame

  lasttime=fr.time;
```

```
  } while(read_next_frame(status,&fr));

  // open output "fp"

  fp = xvgropen(opt2fn("-hbn",NFILE,fnm),
 "","Time(ps)","Count");

  for (i=0; i<hydallx[0].zzz; i++) {

fprintf(fp,"%5i %5i %5i %5i %5i %5i %5i %5i %5i\n", hydallx[i].t, hydallx[i].a, hydallx[i].e,
hydallx[i].i, hydallx[i].m, hydallx[i].q, hydallx[i].u, hydallx[i].y, hydallx[i].cc);

  }
  fclose(fp);
  thanx(stderr);
  return 0;
}
```

B.3.4   Amine as H-donor

```
/*
 * $Id: template.c,v 1.4 2001/07/23 15:28:29 lindahl Exp $
 *
 *                This source code is part of
 *
 *                 G   R   O   M   A   C   S
 *
 *          GROningen MAchine for Chemical Simulations
 *
 *                        VERSION 3.0
 *
 * Copyright (c) 1991-2001
 * BIOSON Research Institute, Dept. of Biophysical Chemistry
 * University of Groningen, The Netherlands
 *
 * This program is free software; you can redistribute it and/or
 * modify it under the terms of the GNU General Public License
 * as published by the Free Software Foundation; either version 2
 * of the License, or (at your option) any later version.
 *
 * If you want to redistribute modifications, please consider that
 * scientific software is very special. Version control is crucial -
 * bugs must be traceable. We will be happy to consider code for
 * inclusion in the official distribution, but derived work must not
 * be called official GROMACS. Details are found in the README & COPYING
 * files - if they are missing, get the official version at www.gromacs.org.
 *
 * To help us fund GROMACS development, we humbly ask that you cite
 * the papers on the package - you can find them in the top README file.
 *
 * Do check out http://www.gromacs.org , or mail us at gromacs@gromacs.org .
 *
 * And Hey:
 * Gyas ROwers Mature At Cryogenic Speed
 */
```

```c
/* This line is only for CVS version info */

static char *SRCID_template_c = "$Id: template.c,v 1.4 2001/07/23 15:28:29 lindahl Exp $";

#include "statutil.h"
#include "typedefs.h"
#include "smalloc.h"
#include "vec.h"
#include "copyrite.h"
#include "statutil.h"
#include "tpxio.h"
#include "index.h"
#include "xvgr.h"

#define ANINT(A) (double) (long) (((A)<0.0) ? ((A)-0.5) : ((A)+0.5))
#define HBANGLE 120.0*3.1415926535897932384462643383/180.0
#define HBOND 0.35
#define HBOND2 HBOND*HBOND

// structure for output file

  struct hydanalys {
    int t, x, y, z;
  } *hydallx;

// start main here

  int main(int argc,char *argv[])
  {
  static char *desc[] = {
    "this is a small test program meant to serve as a template ",
    "when writing your own analysis tools. The advantage of ",
    "using gromacs for this is that you have access to all ",
    "information in the topology, and your program will be ",
    "able to handle all types of coordinates and trajectory ",
    "files supported by gromacs. Go ahead and try it! ",
    "This test version just writes the coordinates of an ",
    "arbitrary atom to standard out for each frame. You can ",
    "select which atom you want to examine with the -n argument."
  };

// allocate memory for output here

  hydallx = (struct hydanalys*) calloc(999999,sizeof(struct hydanalys));

// default value for rcut (hydration radius)

  static real n=0.35;

  /* Extra arguments - but note how you always get the begin/end
  * options when running the program, without mentioning them here!
  */

// passing a value through -rcut and save as "n"

  t_pargs pa[] = {
    { "-rcut", FALSE, etREAL, {&n},
```

```
    "hydration radius (nm) obtained first minimum of rdf"
 }
};

// define variables

  t_topology top;
  char       title[STRLEN];
  t_trxframe fr;
  rvec       *xtop;
  matrix     box;
  int        status;
  int        flags = TRX_READ_X;
  int        *isize;              // size of index
  char       **grpnames;         // group name of index
  atom_id    **index;            // index values
  int        i,j;
  int        *hydall;
  int        number=0;           // counter
  FILE       *fp;                // output file
  int        lasttime;           // last timestep

  t_filenm fnm[] = {
   { efTPS, NULL,  NULL, ffREAD },      /* this is for the topology */
   { efTRX, "-f", NULL, ffREAD },        /* this is for the trajectory */
   { efNDX, NULL , NULL, ffOPTRD },      /* this is for index */
   { efXVG, "-hbn", "hbond", ffOPTWR }   /* this is for output in xvg */
  };

  #define NFILE asize(fnm)

  CopyRight(stderr,argv[0]);

  /* This is the routine responsible for adding default options,
   * calling the X/motif interface, etc. */

  parse_common_args(&argc,argv,PCA_CAN_TIME | PCA_CAN_VIEW,
   NFILE,fnm,asize(pa),pa,asize(desc),desc,0,NULL);

  /* We don't need any topology information to write the coordinates,
   * but to show how it works we start by writing the name and
   * charge of the selected atom. It returns a boolean telling us
   * whether the topology was found and could be read
   */

  read_tps_conf(ftp2fn(efTPS,NFILE,fnm),title,&top,&xtop,NULL,box,TRUE);
  sfree(xtop);

  // allocate memory for read variable using snew

  int grNR=999999;
  snew(grpnames,grNR);
  snew(index,grNR);
  snew(isize,grNR);
  snew(fp,grNR);

  // getting index from -n
```

```
get_index(&(top.atoms),ftp2fn_null(efNDX,NFILE,fnm),2,isize,index,grpnames);

/* The first time we read data is a little special */

read_first_frame(&status,ftp2fn(efTRX,NFILE,fnm),&fr,flags);


/* This is the main loop over frames */

do {

// start counting atoms in the first hydration and hbond

real rhydration=n*n;
int hydstat=0;
int hbondstat=0;

// check hydration aa=acceptor bb=donor

for(i = 0; (i < isize[0]); i++) {
  int aa = index[0][i];
for(j = 0; (j < isize[1]); j++) {
  int bb = index[1][j] - 4;
  double bx = fr.x[aa][XX]-fr.x[bb][XX];
  bx -= fr.box[XX][XX] * ANINT(1 / fr.box[XX][XX] * bx);
  double by = fr.x[aa][YY]-fr.x[bb][YY];
  by -= fr.box[YY][YY] * ANINT(1 / fr.box[YY][YY] * by);
  double bz = fr.x[aa][ZZ] - fr.x[bb][ZZ];
  bz -= fr.box[ZZ][ZZ] * ANINT(1 / fr.box[ZZ][ZZ] * bz);
  double rr = bx * bx + by * by + bz * bz;
  if(rr > rhydration) continue;
  hydstat++;

  // check hydrogen bond distance (hbond <= 0.35nm)

  if(rr > HBOND2) continue;

  // check closest water hydrogen to acceptor

  // hyda hydb are the indexs for water hydrogens

  int hyda = index[1][j] - 3 - 4 ;
  int hydb = index[1][j] - 2 - 4 ;
  int hydc = index[1][j] - 1 - 4 ;

  double hax = fr.x[aa][XX] - fr.x[hyda][XX];
  hax -= fr.box[XX][XX] * ANINT(1 / fr.box[XX][XX] * hax);
  double hay = fr.x[aa][YY] - fr.x[hyda][YY];
  hay -= fr.box[YY][YY] * ANINT(1 / fr.box[YY][YY] * hay);
  double haz = fr.x[aa][ZZ] - fr.x[hyda][ZZ];
  haz -= fr.box[ZZ][ZZ] * ANINT(1 / fr.box[ZZ][ZZ] * haz);
  double har = hax * hax+hay * hay + haz * haz;

  double hbx = fr.x[aa][XX] - fr.x[hydb][XX];
  hbx -= fr.box[XX][XX] * ANINT(1 / fr.box[XX][XX] * hbx);
  double hby = fr.x[aa][YY] - fr.x[hydb][YY];
  hby -= fr.box[YY][YY] * ANINT(1 / fr.box[YY][YY] * hby);
  double hbz = fr.x[aa][ZZ] - fr.x[hydb][ZZ];
```

```
hbz -= fr.box[ZZ][ZZ] * ANINT(1 / fr.box[ZZ][ZZ] * hbz);
double hbr = hbx * hbx + hby * hby + hbz * hbz;


double hcx = fr.x[aa][XX] - fr.x[hydc][XX];
hcx -= fr.box[XX][XX] * ANINT(1 / fr.box[XX][XX] * hcx);
double hcy = fr.x[aa][YY] - fr.x[hydc][YY];
hcy -= fr.box[YY][YY] * ANINT(1 / fr.box[YY][YY] * hcy);
double hcz = fr.x[aa][ZZ] - fr.x[hydc][ZZ];
hcz -= fr.box[ZZ][ZZ] * ANINT(1 / fr.box[ZZ][ZZ] * hcz);
double hcr = hcx * hcx + hcy * hcy + hcz * hcz;



int hn = 3;
if(hbr < har) hn = 2;
if(hcr < hbr) hn = 1;

// calculate the angle D--H--A (greater than 120)
// Ref: Brady and Schmidt (1993)

// distance between acceptor and closest hydrogen
// hydf is the closest hydorgen index

int hydf = bb - hn;
double aax = fr.x[aa][XX] - fr.x[hydf][XX];
aax -= fr.box[XX][XX] * ANINT(1 / fr.box[YY][YY] * aax);
double aay = fr.x[aa][YY] - fr.x[hydf][YY];
aay -= fr.box[YY][YY] * ANINT(1 / fr.box[YY][YY] * aay);
double aaz = fr.x[aa][ZZ] - fr.x[hydf][ZZ];
aaz -= fr.box[ZZ][ZZ] * ANINT(1 / fr.box[ZZ][ZZ] * aaz);
double aar = aax * aax + aay * aay + aaz * aaz;


// distance between donor and cloest hydrogen

double abx = fr.x[bb][XX] - fr.x[hydf][XX];
abx -= fr.box[XX][XX] * ANINT(1 / fr.box[XX][XX] * abx);
double aby = fr.x[bb][YY] - fr.x[hydf][YY];
aby -= fr.box[YY][YY] * ANINT(1 / fr.box[YY][YY] * aby);
double abz = fr.x[bb][ZZ] - fr.x[hydf][ZZ];
abz -= fr.box[ZZ][ZZ] * ANINT(1 / fr.box[ZZ][ZZ] * abz);
double abr = abx * abx + aby * aby + abz * abz;


// convert to unit vector

double harr = 1.0 / sqrt(aar);
double erax = aax * harr;
double eray = aay * harr;
double eraz = aaz * harr;
double hcrr = 1.0 / sqrt(abr);
double ercx = abx * hcrr;
double ercy = aby * hcrr;
double ercz = abz * hcrr;


// dot product

double cosphi = erax * ercx + eray * ercy + eraz * ercz;
double phi = acos(cosphi);


// record number of hydrogen bonding
```

```
    if(phi > HBANGLE) hbondstat++;
if (aa-bb>50){
 printf("%g %g \n", fr.x[aa][XX], fr.x[aa][YY]);
}
  }
  }

  // saving data in the output memory

  hydallx[number].t=fr.time;
  hydallx[number].x=hydstat;
  hydallx[number].y=hbondstat;

  number++;
  hydallx[0].z=number;

  // saving the last time frame

  lasttime=fr.time;

  } while(read_next_frame(status,&fr));

  // open output "fp"

  fp = xvgropen(opt2fn("-hbn",NFILE,fnm),
 "","Time(ps)","Count");

  for (i=0; i<hydallx[0].z; i++) {
    fprintf(fp,"%5i %5i %5i \n", hydallx[i].t,hydallx[i].x, hydallx[i].y);
  }

  fclose(fp);
  thanx(stderr);
  return 0;
}
```

B.3.5 Hydroxyl as H-donor

```
/*
 * $Id: template.c,v 1.4 2001/07/23 15:28:29 lindahl Exp $
 *
 *               This source code is part of
 *
 *                G   R   O   M   A   C   S
 *
 *         GROningen MAchine for Chemical Simulations
 *
 *                        VERSION 3.0
 *
 * Copyright (c) 1991-2001
 * BIOSON Research Institute, Dept. of Biophysical Chemistry
 * University of Groningen, The Netherlands
 *
 * This program is free software; you can redistribute it and/or
 * modify it under the terms of the GNU General Public License
```

```
 * as published by the Free Software Foundation; either version 2
 * of the License, or (at your option) any later version.
 *
 * If you want to redistribute modifications, please consider that
 * scientific software is very special. Version control is crucial -
 * bugs must be traceable. We will be happy to consider code for
 * inclusion in the official distribution, but derived work must not
 * be called official GROMACS. Details are found in the README & COPYING
 * files - if they are missing, get the official version at www.gromacs.org.
 *
 * To help us fund GROMACS development, we humbly ask that you cite
 * the papers on the package - you can find them in the top README file.
 *
 * Do check out http://www.gromacs.org , or mail us at gromacs@gromacs.org .
 *
 * And Hey:
 * Gyas ROwers Mature At Cryogenic Speed
 */

/* This line is only for CVS version info */

static char *SRCID_template_c = "$Id: template.c,v 1.4 2001/07/23 15:28:29 lindahl Exp $";


#include "statutil.h"
#include "typedefs.h"
#include "smalloc.h"
#include "vec.h"
#include "copyrite.h"
#include "statutil.h"
#include "tpxio.h"
#include "index.h"
#include "xvgr.h"

#define ANINT(A) (double) (long) (((A)<0.0) ? ((A)-0.5) : ((A)+0.5))
#define HBANGLE 120.0*3.1415926535897932384626643383/180.0
#define HBOND 0.35
#define HBOND2 HBOND*HBOND

// structure for output file

  struct hydanalys {
    int t, x, y;
  } *hydallx;

// start main here

  int main(int argc,char *argv[])
  {
  static char *desc[] = {
    "this is a small test program meant to serve as a template ",
    "when writing your own analysis tools. The advantage of ",
    "using gromacs for this is that you have access to all ",
    "information in the topology, and your program will be ",
    "able to handle all types of coordinates and trajectory ",
    "files supported by gromacs. Go ahead and try it! ",
    "This test version just writes the coordinates of an ",
    "arbitrary atom to standard out for each frame. You can ",
    "select which atom you want to examine with the -n argument."
```

```c
  };

// allocate memory for output here

   hydallx = (struct hydanalys*) calloc(999999,sizeof(struct hydanalys));

// default value for rcut (hydration radius)

   static real n=0.35;

   /* Extra arguments - but note how you always get the begin/end
    * options when running the program, without mentioning them here!
    */

// passing a value through -rcut and save as "n"

   t_pargs pa[] = {
    { "-rcut", FALSE, etREAL, {&n},
      "hydration radius (nm) obtained first minimum of rdf"
    }
   };

// define variables

   t_topology top;
   char       title[STRLEN];
   t_trxframe fr;
   rvec       *xtop;
   matrix     box;
   int        status;
   int        flags = TRX_READ_X;
   int        *isize;            // size of index
   char       **grpnames;        // group name of index
   atom_id    **index;           // index values
   int        i,j;
   int        *hydall;
   int        number=0;          // counter
   FILE       *fp;               // output file
   int        lasttime;          // last timestep

   t_filenm fnm[] = {
    { efTPS,  NULL,  NULL,  ffREAD },      /* this is for the topology */
    { efTRX, "-f", NULL, ffREAD },         /* this is for the trajectory */
    { efNDX, NULL , NULL, ffOPTRD },       /* this is for index */
    { efXVG, "-hbn", "hbond", ffOPTWR }    /* this is for output in xvg */
   };

   #define NFILE asize(fnm)

   CopyRight(stderr,argv[0]);

   /* This is the routine responsible for adding default options,
    * calling the X/motif interface, etc. */

   parse_common_args(&argc,argv,PCA_CAN_TIME | PCA_CAN_VIEW,
    NFILE,fnm,asize(pa),pa,asize(desc),desc,0,NULL);

   /* We don't need any topology information to write the coordinates,
```

```
 * but to show how it works we start by writing the name and
 * charge of the selected atom. It returns a boolean telling us
 * whether the topology was found and could be read
 */

read_tps_conf(ftp2fn(efTPS,NFILE,fnm),title,&top,&xtop,NULL,box,TRUE);
sfree(xtop);

// allocate memory for read variable using snew

int grNR=999999;
snew(grpnames,grNR);
snew(index,grNR);
snew(isize,grNR);
snew(fp,grNR);

// getting index from -n

get_index(&(top.atoms),ftp2fn_null(efNDX,NFILE,fnm),2,isize,index,grpnames);

/* The first time we read data is a little special */

read_first_frame(&status,ftp2fn(efTRX,NFILE,fnm),&fr,flags);

/* This is the main loop over frames */

do {

// start counting atoms in the first hydration and hbond

real rhydration=n*n;
int hydstat=0;
int hbondstat=0;

// check hydration aa=acceptor bb=donor

for(i = 0; (i < isize[0]); i++) {
  int aa = index[0][i];
for(j = 0; (j < isize[1]); j++) {
  int bb = index[1][j];
  double bx = fr.x[aa][XX]-fr.x[bb][XX];
  bx -= fr.box[XX][XX] * ANINT(1 / fr.box[XX][XX] * bx);
  double by = fr.x[aa][YY]-fr.x[bb][YY];
  by -= fr.box[YY][YY] * ANINT(1 / fr.box[YY][YY] * by);
  double bz = fr.x[aa][ZZ] - fr.x[bb][ZZ];
  bz -= fr.box[ZZ][ZZ] * ANINT(1 / fr.box[ZZ][ZZ] * bz);
  double rr = bx * bx + by * by + bz * bz;
  if(rr > rhydration) continue;
  hydstat++;

  // check hydrogen bond distance (hbond <= 0.35nm)

  if(rr > HBOND2) continue;
  // calculate the angle D--H--A (greater than 120)
  // Ref: Brady and Schmidt (1993)

  // distance between acceptor and closest hydrogen
  // hydf is the closest hydorgen index
```

```
        // for OH of hydroxyl group 1 H-2 O

        int hydf = bb -1;
        double aax = fr.x[aa][XX] - fr.x[hydf][XX];
        aax -= fr.box[XX][XX] * ANINT(1 / fr.box[YY][YY] * aax);
        double aay = fr.x[aa][YY] - fr.x[hydf][YY];
        aay -= fr.box[YY][YY] * ANINT(1 / fr.box[YY][YY] * aay);
        double aaz = fr.x[aa][ZZ] - fr.x[hydf][ZZ];
        aaz -= fr.box[ZZ][ZZ] * ANINT(1 / fr.box[ZZ][ZZ] * aaz);
        double aar = aax * aax + aay * aay + aaz * aaz;

        // distance between donor and cloest hydrogen

        double abx = fr.x[bb][XX] - fr.x[hydf][XX];
        abx -= fr.box[XX][XX] * ANINT(1 / fr.box[XX][XX] * abx);
        double aby = fr.x[bb][YY] - fr.x[hydf][YY];
        aby -= fr.box[YY][YY] * ANINT(1 / fr.box[YY][YY] * aby);
        double abz = fr.x[bb][ZZ] - fr.x[hydf][ZZ];
        abz -= fr.box[ZZ][ZZ] * ANINT(1 / fr.box[ZZ][ZZ] * abz);
        double abr = abx * abx + aby * aby + abz * abz;

        // convert to unit vector

        double harr = 1.0 / sqrt(aar);
        double erax = aax * harr;
        double eray = aay * harr;
        double eraz = aaz * harr;
        double hcrr = 1.0 / sqrt(abr);
        double ercx = abx * hcrr;
        double ercy = aby * hcrr;
        double ercz = abz * hcrr;

        // dot product

        double cosphi = erax * ercx + eray * ercy + eraz * ercz;
        double phi = acos(cosphi);

        // record number of hydrogen bonding

        if(phi > HBANGLE) hbondstat++;
    }
    }

    // saving data in the output memory

    hydallx[number].t=fr.time;
    hydallx[number].x=hydstat;
    hydallx[number].y=hbondstat;

    number++;

    // saving the last time frame

    lasttime=fr.time;

    } while(read_next_frame(status,&fr));
```

```
  // open output "fp"

  fp = xvgropen(opt2fn("-hbn",NFILE,fnm),
"","Time(ps)","Count");

  for (i=0; i<(lasttime/2)+1; i++) {
    fprintf(fp,"%5i %5i %5i \n", hydallx[i].t,hydallx[i].x, hydallx[i].y);
  }

  fclose(fp);

  thanx(stderr);

  return 0;
}
```

Appendix C

Additional Publications

This chapter contains a re-print of a publication for the results not discussed in the main body of the dissertation.

Molecular study of the diffusional process of DMSO in double lipid bilayers

Sukit Leekumjorn, Amadeu K. Sum *

Virginia Polytechnic Institute and State University, Department of Chemical Engineering, Blacksburg, 24061 VA, USA

Abstract

As a way to quantify the diffusion process of molecular compounds through biological membranes, we investigated in this study the dynamics of DMSO through an 1,2-Dipalmitoyl-*sn*-Glycero-3-Phosphocholine (DPPC) bilayer system. To properly account for the diffusion of DMSO due to a concentration gradient, a double DPPC bilayer was setup for our simulations. In such configuration, the aqueous phases can be explicitly associated with the extra and intracellular domains of the membrane, which is seldom the case in studies of single lipid bilayer due to the periodicity imposed by the simulations. DMSO molecules were initially contained in one of the aqueous phases (extracellular region) at a concentration of 5 wt.%. Molecular dynamics simulation was performed in this system for 95 ns at 350 K and 1 bar. The simulations showed that although many DMSO molecules penetrated the lipid bilayer, only about 10% of them crossed the bilayer to reach the other aqueous phase corresponding to the intracellular region of the membrane. The simulation time considered was insufficient to reach equilibrium of the DMSO concentration between the aqueous phases. However, the simulations provided sufficient information to estimate parameters to apply Fick's Law to model the diffusion process of the system. Using this model, we predicted that for the time considered in our simulation, the concentration of DMSO in the intracellular domain should have been about half of the actual value obtained. The model also predicted that equilibrium of the DMSO concentration in the system would be reached after about 2000 ns, approximately 20 times longer than the performed simulation.
© 2006 Elsevier B.V. All rights reserved.

Keywords: Molecular dynamic; Double bilayer; Diffusion; Concentration gradient; DMSO; DPPC

1. Introduction

There have been numerous studies and hypotheses on the effectiveness of cryoprotectant agents based on their chemical properties and their interactions with biological organisms. Dimethylsulfoxide (DMSO) is the most common agent currently used for enzyme and cell preservation at low temperature along with naturally occurring stabilizing agents such as disaccharides (e.g., trehalose and sucrose) [1–4]. In the absence of disaccharides, DMSO alone exhibits many biological functions such as inducing cell fusion [5], promoting cell differentiation [6], and increasing cell permeability [7]. Although the usage of DMSO in therapeutic applications remains controversial due to its toxicity at high concentration, there have also been reports on the beneficial aspects of DMSO, such as reduced anti-inflammatory response, analgesic effects

[8], and anti-viral/bacterial activities [9]. For a better understanding of the cell preservation process, several investigations of modeled cell membranes (phospholipid bilayers) in the presence of DMSO have been studied experimentally [10–17] and computationally [18–20]. A summary of these studies have been discussed elsewhere [20].

In terms of the cell membrane complexity, there are several theories and hypotheses that describe the mechanism by which solute is transported across membranes. Overton et al. were the first to correlate the permeability of membranes to the octanol/water partition coefficient of the solute [21], which was later found to deviate for small molecules, such as electrolytes [22]. Walter and Gutknecht showed that the permeation of electrolytes through membranes is inversely proportional to the membrane permeability and molecular size [23]. This was explained by the "soft polymer hypothesis" or "hopping mechanism," in which small molecules are able to diffuse faster through the void regions of the lipid acyl chains [24]. As a result, it was concluded that the diffusion process is heavily

* Corresponding author.
  E-mail address: asum@vt.edu (A.K. Sum).

dependent on the properties of the solute and the packing of the membrane.

Several investigations of model membranes in the presence of a solute have been reported experimentally [25,26] and computationally [27–29]. Dix et al. used NMR ^{13}C relaxation experiments to probe nitroxide derivatives in di-palmitoylle-cithin liposomes and found that the permeation of small molecules through the bilayer is the rate determining step in the diffusion process [25]. DeYoung and Dill showed from NMR experiments that the partitioning of benzene in DMPC and DPPC bilayers is dependent upon the packing density of the lipid tails, and that the transport properties significantly change as molecules transverse through the bilayer [26]. McKinnon et al. used MD simulations to investigate the diffusion of oxygen in a hexadecane/cholesterol monolayer, and concluded that the rate of diffusion increases with increasing cholesterol content [27]. Kilimas et al. were the first to use MD simulations to investigate the diffusion of benzene through DMPC and DPPC bilayers [29]. Upon penetration of benzene into the bilayer, they observed a slight change in the order parameter of the lipid tails and obtained a reasonable estimate of the diffusion coefficient for benzene through the bilayer, which compared favorably to experimental results. Their results also supported the "hopping mechanism" suggested by Lieb et al. [24].

Although the structural changes caused by DMSO on phospholipid bilayers have been carefully investigated from a molecular scale, the diffusive properties of DMSO in biological membranes is less understood. In general, the diffusion process for various types of molecular compounds usually occurs in time-scales ranging from micro-seconds to days. Atomistic simulations of this time-scale are a daunting task at present, as they would require massive computational resources for extensive periods of time. As a result, it remains a major challenge to obtain accurate diffusional properties of molecular compounds through model biological membranes by simulation methods. Experimental studies coupled with macroscopic diffusion models (Fick's Law of diffusion) remain as the main approach for elucidating and quantifying diffusional processes. Despite the advantages of using macroscopic modeling equations, these are insufficient to provide detailed information about the diffusion process due to the complex interactions of molecular compounds with the membrane environment. The molecular properties of DMSO, such as its hydrophobic and hydrophilic properties and the localized active diffusion process (breaking of the hydrogen-bond between DMSO and water to cross the interfacial region), are not readily accessible, except from molecular descriptions [30]. Therefore, molecular simulations are needed to investigate how molecular compounds interact with the bilayer structure in the diffusion process, which in turn sheds greater insight into diffusional properties.

There has been only a selected number of simulations of model biological membranes in the presence of DMSO [18–20], and these have only addressed selected characteristics of the bilayer structure. Paci and Marchi examined the transport of a single DMSO molecule through a glycerolipid bilayer with MD simulations [18]; their study showed DMSO diffusing through the bilayer, locally modifying the membrane surface,

and rapidly being expelled from the bilayer core. That study investigated structural changes to the bilayer in the presence of DMSO and excluded its diffusive properties. Smondyrev and Berkowitz considered the properties of a DPPC bilayer in the presence of pure DMSO [19]. Their results, in agreement to Paci and Marchi [18], showed that DMSO did not extensively diffuse through bilayers nor significantly modified the bilayer surface in term of the area per headgroup. They also reported that DMSO molecules remained underneath the DPPC head-groups and some actually remained in the bilayer core region during the 2 ns simulation. There was no concentration gradient across the membrane in their study because the DPPC bilayer was solvated by pure DMSO. In a recent study, Sum and de Pablo were the first to consider the properties of lipid bilayers with various DMSO concentrations using MD simulations [20]. Their findings showed that DMSO penetrated and diffused through the bilayer and significantly increased the area per headgroup of the bilayer over a wide range of concentrations. Their results concluded that changes in the structure and properties of the bilayer are mainly due to the indirect interaction (induced dehydration) of DMSO with the interface and to the direct interaction of DMSO with the inner bilayer region.

Most simulations to date, equilibrium and transport proper-ties have been studied considering a single lipid bilayer in which, due to periodic boundary conditions, the aqueous phase is usually connected in the direction normal to the bilayer plane. In such case, a solute molecule in the aqueous phase may leave the simulation box on one side and re-enter in the opposite side, thus nullifying the diffusive effect using bilayer as a barrier. In such configuration, one is unable to distinguish what would realistically be the extra and intracellular environments and to observe changes to the system caused by concentration gradients. The latter is an important aspect in drug-design since most drugs need to reach the intracellular domain to be active. One approach to correct this shortcoming is to explicitly consider a membrane with distinct regions that correspond to the extra and intracellular environments, which can be obtained with a double bilayer configuration. Double bilayers have been employed sparingly in simulations mainly because they are computationally expensive (system size is doubled). There are two well-documented MD simulations of double bilayer systems. Sachs et al. used a double lipid bilayer configuration to investigate the penetration of ions through a bilayer, thus creating a transmembrane potential gradient without having to consider a continuum approximation [31]. In another study, Gertovenko et al. used a double bilayer configuration to study the interaction of salt ions with lipid species [32]; they imposed various electrolyte compositions across the membrane, resulting in asymmetric bilayer structure. Here, we present our MD simulations of a double DPPC bilayer in the presence of DMSO initially contained in one of the aqueous phases. This setup is used to obtain a better understanding of the transmembrane diffusive properties for a given concentration gradient in the system. The simulations are complemented with an analysis of a diffusive model describing the concentration profile in the bilayer over time.

2. Simulation details

Molecular dynamics simulations were performed on a system containing a total of 512 DPPC and 15,360 water molecules (30 waters/lipid) arranged in a double bilayer configuration in the presence of DMSO. The initial configuration for the system consisted of fully hydrated double bilayer containing 128 DPPC molecules on each leaflet (a total of four leaflets constructed by stacking an equilibrated single bilayer on top of itself). This configuration aims to represent an actual cell membrane with the water layers corresponding to the extra and intracellular domains of a cell. A short equilibration of 5 ns was performed on the system prior to the insertion of DMSO. For the purpose of this study, the composition of DMSO in one of the two water layers was initially 5 wt.% (92 DMSO in 7584 H_2O) (cryopreservation experiments often employ a concentration of 10 wt.% [33]). DMSO molecules were randomly inserted into the aqueous phase; water molecules overlapping with DMSO were removed as well as any additional ones to obtain the desired DMSO concentration. Fig. 1 shows a snapshot of the initial double lipid bilayer configuration in the presence of DMSO.

The force field for DPPC and water are the same as those employed in a previous study [34]. For DPPC, intramolecular parameters for bonds, angles, proper dihedral, and improper dihedral were consistent with previous studies [35,36]. The Ryckaert–Bellemans potential was used for the torsion potential of the hydrocarbon chains [37]. Non-bonded interactions were described by the parameters from Berger et al. [38–40] and partial atomic charges were obtained from Chiu et al. [41]. The united-atom representation was used for the methyl/methylene groups in the alkyl chains of DPPC. For water, the single point charge (SPC) model was adopted [42]. The force field from
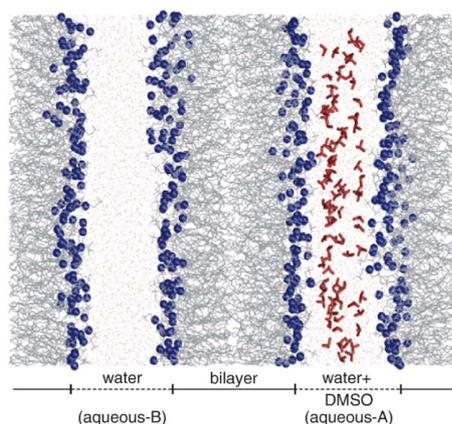
Fig. 1. Initial configuration of the double DPPC bilayer. The system contains a total of 512 DPPC (128 per leaflet), 15,360 water, and 92 DMSO molecules. All DMSO molecules were initially inserted into one of the aqueous phases. The colored groups correspond to the DPPC headgroups (blue), lipid tails (gray), DMSO (red), and water (pink). (For interpretation of the references to colour in this figure legend, the reader is referred to the web version of this article.)

Bordat et al. was used for DMSO [43]. Fig. S1 in the Supporting Information shows the chemical structures and atomic charges for DPPC, water, and DMSO.

Steepest-decent energy minimizations were performed on the lipid systems before starting the simulations. All simulations were performed in the *NPT* ensemble, at a temperature and pressure of 350 K and 1 bar, respectively (see Ref. [34] for more details on the parameters used in the simulations). Long-range electrostatic interactions were corrected with the particle-mesh Ewald method (PME) [44,45]. Periodic boundary conditions were applied in all directions. Simulations for the double bilayer systems lasted 95 ns and trajectories were collected every 2 ps. All simulations were performed with the GROMACS 3.3-beta software package [46,47] (single-precision mode) in parallel using Virginia Tech's System X (dual 2.3 GHz Apple Xserve G5) [48].

3. Results and discussion

The main focus of this study was to obtain a better understanding of the diffusion process of DMSO through the bilayer. Simulations of molecular compounds in a single bilayer are deficient in describing the diffusion process due to concentration gradients in actual cell membranes because of the periodic boundaries employed in the simulation, which treat the systems as being "infinite." Such approach, although computationally efficient, makes impossible to differentiate between the extra and intracellular domains of the membrane. To overcome this inherent problem, we have used a double bilayer configuration setup with a transmembrane concentration gradient (see Fig. 1), mimicking the initial exposure of cell to a DMSO solution. Simulations for the double bilayer with DMSO were conducted for 95 ns, which was sufficiently long to observe several DMSO molecules diffusing through the bilayer and reaching the intracellular domain.

Although equilibrium of the DMSO concentration across the transmembrane was not reached for the simulation time considered, structural properties were analyzed for the double bilayer to ensure consistency with previous single bilayer simulations. The initial area per headgroup prior to the insertion of DMSO was about 0.67 nm^2 and converged to 0.69±0.01 nm^2 for the major portion of the 95 ns while DMSO diffused through the bilayer (see Fig. S2 in the Supporting Information). This value is consistent with previous simulation reporting an area per headgroup for single bilayers of 0.68±0.01 nm^2 for pure DPPC at 350 K [34] and 0.712±0.007 nm^2 for DPPC containing 8.1 wt.% DMSO at 350 K [20]. Fig. 2 shows the density profile for the system, including the regions that correspond to the two bilayers and the two aqueous phases. The location of the peaks for the nitrogen and phosphorus atoms indicates the interfacial regions. In the configuration considered, the aqueous phase with a high DMSO concentration represents the extracellular region of the cell membrane (aqueous-A), and the one with low concentration is the intracellular region (aqueous-B). For the bilayer surfaces next to aqueous-A, there is an accumulation of DMSO immediately underneath the interfacial region, which indicates the repulsion of DMSO with the lipid polar groups and
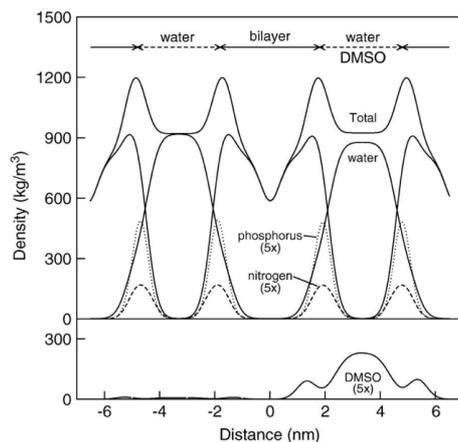
Fig. 2. Density profiles for the various groups in the double bilayer system with DMSO at 350 K. The density profiles represent the averaging of only the last 10 ns of the simulation. Dot and dash lines are density profiles for phosphorus and nitrogen atoms, respectively. The density profile for DMSO is plotted separately in the bottom portion of the graph for clarity. Number in parenthesis is magnification of profiles. The different regions of the system correspond to those shown in Fig. 1.

favorable interaction with the lipid hydrophobic segments. This behavior is consistent with previous observations by Sum and de Pablo [20]. The order parameter (measure of the bilayer fluidity) was calculated for each leaflet separately, since one side of each bilayer was exposed to a high DMSO concentration causing an anisotropic environment (see Fig. 3). The side with high DMSO

concentration refers to the two leaflets that are adjacent to aqueous-A (see Fig. 1). For the two leaflets with high DMSO concentration, DMSO affects the structure and ordering of the interfacial region. In the region where DMSO concentrates underneath the headgroup, the order parameter is slightly higher than the system without DMSO, caused by the packing of DMSO with the first few carbon atoms in the lipid tails. On the other hand, the order parameter for the carbon atoms closer to the middle of the bilayer is slightly lower, which is a consequence of the larger area per headgroup in the presence of DMSO and leads to greater mobility of the lipid tails end region.

Trajectories for all species were collected over the course of the simulation. In particular, we monitored the dynamics of all 92 DMSO molecules in order to observe their diffusive path through the transmembrane and into intracellular region (aqueous-B). As shown by the density profile in Fig. 2, several DMSO molecules actually penetrate into the bilayer, mostly concentrating near the interfacial region underneath the head-groups. Unlike previous single lipid bilayer simulations [19,20], the double bilayer is setup with a concentration gradient across the transmembrane. As the system evolves to equilibrium, the distribution of DMSO should eventually become uniform throughout. Although our simulation was insufficiently long to observe the complete equilibration of DMSO between the different phases, we obtained significant information about the diffusion process. After 95 ns, a total of nine DMSO molecules (about 10%) had completely diffused through the bilayer and reached aqueous-B. Fig. 4 shows the trajectory for each of the nine DMSO molecules along the coordinate normal to the

Fig. 3. Deuterium order parameter for the lipid tails of DPPC in the double bilayer. The order parameter has been separated for the different leaflets: lipid tails in the leaflet exposed to the aqueous phase with high (solid line) and low (dash line) DMSO concentration. The calculation for the order parameter considers only the last 10 ns of the simulation. Open circles are previous simulation results for a single DPPC bilayer without DMSO at 350 K [34].
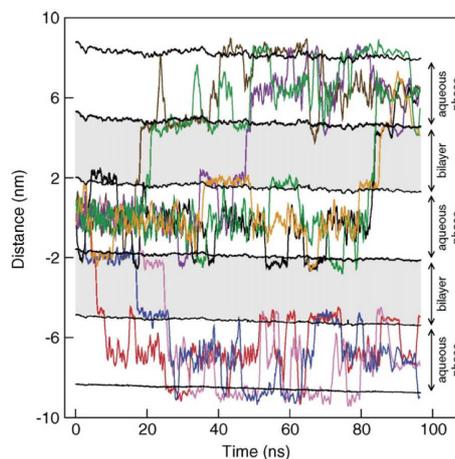

Fig. 4. Dynamics of the nine DMSO molecules that penetrated and crossed the bilayer to reach the other aqueous phase (interior of the membrane). The trajectories represent the position of the sulfur atom of DMSO. Periodic boundary conditions along the *z*-coordinate have been removed. The jigged horizontal lines correspond to the average position of phosphorus atoms along the interface and are used to identify the boundaries of each phase. Gray areas denote the bilayer regions (see Fig. 1 for more information). Note that an additional periodic image of an aqueous phase was added to help to visualize the trajectory of the DMSO molecules.

bilayer surfaces as they diffuse through the system (periodic boundary was removed from the trajectories for clarity). DMSO molecules were initially inserted into aqueous-A (aqueous phase centered at about zero in Fig. 4). For the purposes of discussion, this aqueous phase will be considered as the extracellular region of the membrane. The layers adjacent to the central aqueous phase (shaded gray area) correspond to the lipid bilayers, which are then followed by aqueous-B (intracellular region of the membrane). There are a number of interesting observations from the DMSO trajectories. DMSO diffuses freely in the aqueous phase prior to entering the bilayer. The crossing of DMSO through the interfacial region, either entering or exiting the bilayer, is a fast process (few picoseconds). Once inside, the dynamics of DMSO near the interface underneath the headgroups is very localized. The diffusion of DMSO in the bilayer from one leaflet to another is a fast but infrequent process. Much of the behavior of DMSO can be attributed to its dual character of possessing both hydrophobic and hydrophilic properties (see Sum and de Pablo for more details [30]).

For the nine DMSO molecules shown in Fig. 4 that diffused through the transmembrane, they either remained in aqueous-B or entered the bilayer staying in the vicinity of the headgroups. None of these molecules diffused back across the transmembrane (against the concentration gradient) and returned to aqueous-A. From a macroscopic perspective, the diffusion of DMSO across the transmembrane is a passive process [49], however, from a molecular perspective, the observed process is an active process because it requires a substantial amount of energy (both kinetic and potential) to overcome the energy barrier of crossing the interfacial region and the bilayer core region [20]. This can be understood from the trajectories for DMSO (Fig. 4). As discussed in the previous paragraph, the crossing of DMSO through the interfacial region and from one leaflet to another is a fast process. This process happens because DMSO has acquired enough energy to overcome unfavorably interactions with the polar headgroups and to penetrate the bilayer. This energy is gained from the detachment of water hydrogen bonded to DMSO as it passes through the interfacial region (there are no water molecules in the interior of the bilayer). Even though the oxygen in DMSO is the hydrophilic group, it is a hydrogen bond acceptor, and so are all the polar lipid headgroups. Therefore, there is no opportunity for DMSO to "bind" to any other groups. On the other hand, the methyl groups in DMSO, which are hydrophobic, will interact favorably with the lipid tails. Because DMSO is both hydrophobic and hydrophilic, it prefers the region underneath the lipid headgroups, which transitions from the polar groups to the hydrocarbon segments. A similar explanation can account for the fast crossing of DMSO inside the bilayer, from one leaflet to another is a fast process. In the bilayer core, only the lipid tails, which are hydrophobic, are present. This is an unfavorable environment for the polar part of DMSO, thus causing DMSO to quickly move from one side to another. It is in part for these reasons that we only observe nine DMSO molecules diffusing through the entire length of the transmembrane from one aqueous phase to another. One should note that we disregard the path the nine DMSO molecules take to reach aqueous-B. In the trajectories

shown in Fig. 4, DMSO diffuses through both bilayers exposed to the aqueous phase with a high DMSO concentration.

The double bilayer system was setup with a concentration gradient across the transmembrane. If we had carried out the simulations sufficiently long, the distribution of DMSO along the system would eventually reach equilibrium, that is, the amount of DMSO in both aqueous phases would be about the same (equality of chemical potential). However, if after 95 ns only nine molecules had diffused through, a simulation time of five to ten times longer would be required until equilibrium. Although computational resources are currently available for such task, the simulation would last several months. A more sensible approach is to use the available information to obtain an estimate of the behavior of the system as it progresses to equilibrium.

The rate of penetration of a molecule across a membrane is proportional to the concentration gradient, which can be described by Fick's Law of Diffusion, and for the presented purpose has the following form,

$$\frac{dn}{dt} = \frac{K_p D}{z_b} A \left(C_B - C_A \right) = \frac{K_p D}{z_b} \left(\frac{n_0 - n}{z_B} - \frac{n}{z_A} \right) \qquad (1)$$

where n is the amount of DMSO in the aqueous phase, t is the time, K_p is the partition coefficient of DMSO between the lipid and aqueous phases, D is the diffusion coefficient of DMSO through the bilayer, z_b is the thickness of the bilayer, A is the membrane cross-sectional area, C is the concentration of DMSO in aqueous-A and aqueous-B, n_0 is the initial amount of DMSO, and z is the thickness of aqueous-A and aqueous-B. Note that the general form of the Fick's Law given above is based on the assumption that the cross-sectional area of the bilayer is constant (the average area per headgroup is relatively constant—see Fig. S2 in the Supporting Information).

The parameters required in Eq. (1) can all be obtained from our double bilayer simulation, with the exception of the partition coefficient. Here, the partition coefficient is the ratio of the concentration of DMSO in the lipid and aqueous phases at equilibrium. Since the double bilayer system is not at equilibrium, we estimated the partition coefficient from simulations of DMSO in a single bilayer system, as the equilibration is much faster. The details of the single bilayer system are included as Supporting Information (see Table S1, Figs. S3–S6). Note that in the single bilayer, the periodicity is irrelevant in determining the partition coefficient because the interfaces made by both leaflets are used to determine the equilibrium properties.

As a way to quantify the permeation of DMSO into the bilayer, we calculated its partition coefficient between the aqueous and lipid phases using DPPC-DMSO single bilayer system (see the Supporting Information). For this analysis, we defined regions in the system and determined the location of DMSO molecules relative to those regions throughout the simulations. These regions, shown in Fig. 5, consist of the aqueous phase, the interfacial region, and the bilayer core. The reason for choosing these regions is because the lipid head-group span over a relatively large volume and it is unclear where one should define the limits for the boundary between the
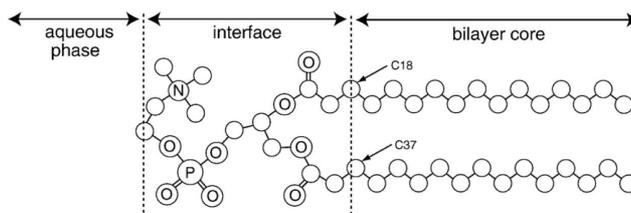
Fig. 5. Schematic of the regions in the bilayer system projected onto a lipid molecule. Dash line indicates the boundary between the different regions.

lipid and aqueous phases. As a result, we adopted the following criteria. The aqueous phase/interfacial region boundary was defined as the distance to the first minimum of the radial distribution curve between the lipid phosphorus and DMSO sulfur atom, which is approximately 0.72 nm (see Fig. S6 in the Supporting Information). Therefore, a DMSO molecule centered in the aqueous phase and located 0.72 nm or further from the lipid phosphorus atom is counted toward the aqueous phase concentration. At the other end, the interfacial region/bilayer core boundary is defined as the average position of the C18 and C37 atoms (see Fig. 5). In this case, a DMSO molecule with z-coordinate below the average position of C18 or C37 is counted toward the concentration in the bilayer core. DMSO molecules found in interfacial region are excluded from this part of the calculation, since it is ambiguous to which phase they belong. Using these criteria, the ensemble average number of DMSO in the aqueous phase and the bilayer core was determined from a separate single DPPC bilayer containing DMSO. Characterization of the bilayer system for this simulation is summarized in Table S1 in the Supporting Information.

With the results obtained from the single bilayer simulations, the partition coefficient (K_p) was calculated from the ratio of the amount of DMSO in the bilayer core and in aqueous phase based on the following relation,

$$K_p = \frac{C_{bc}}{C_{aq}} = \frac{N_{bc}/z_{bc}}{N_{aq}/z_{aq}} \qquad (2)$$

where C is the concentration of DMSO in the bilayer core (bc) and aqueous phase (aq). Since the cross-sectional area along the bilayer interface is uniform along all regions, the ratio of concentrations in Eq. (2) reduces to the number of DMSO molecules (N) in the bilayer core and aqueous phase divided by their corresponding thickness (z). Using this information from the single DPPC bilayer (see Table S1 in the Supporting Information), we obtained a value of $K_p = 0.088$ for the DMSO/DPPC bilayer system.

The diffusion coefficient of DMSO was calculated from the mean-squared displacement of only the nine DMSO molecules that diffused through the entire length of the bilayer (see Fig. 4). Only those molecules were considered because their trajectories represent the actual path in the diffusion process, whereas the molecules that remained in aqueous-A are excluded from interactions with the bilayer and aqueous-B. The estimated diffusion coefficient for each of those nine

DMSO molecules was calculated from the time each initially crossed the exterior membrane surface (aqueous-A) until the time each reached aqueous-B. This procedure yielded an average diffusion coefficient for the nine DMSO molecules of $3.74 \pm 1.00 \times 10^{-6}$ cm^2/s (large error is mainly due to the wide range of values). This value is slightly lower than previously reported diffusion coefficients: 6.1×10^{-6} cm^2/s from NMR measurements for 1:3 DMSO/water mixtures at 303 K [50], $9.5 \pm 0.2 \times 10^{-6}$ cm^2/s from MD simulations of liquid DMSO at 298 K [51], and $8.9 \pm .2 \times 10^{-6}$ cm^2/s from simulation of DMSO in a DPPC bilayer system at 350 K [30]. It is interesting to note that the diffusion coefficient obtained for DMSO is comparable and consistent with other molecules of similar size and molecular weight, such as that of benzene in bilayers ($1.3–4.6 \times 10^{-6}$ cm^2/s) [29].

The thicknesses for Eq. (1) were estimated under the assumption that the average area per headgroup is relatively constant throughout the simulation (see Fig. S2 in the Supporting Information). The thicknesses of aqueous-A, aqueous-B, and bilayer were obtained from the average position of the phosphorus atoms, which as seen from Fig. 4, can be easily calculated. The respective values for z_b, z_B, and z_A are 3.29, 3.59, and 3.48 nm.

Having estimated all the required parameters for Eq. (1), we solved it to predict the diffusion process of DMSO through the bilayer. Fig. 6 shows the solution of Eq. (1) for the number of DMSO molecules in the aqueous phase as a function of time. As expected, at equilibrium there is no concentration gradient (i.e., the flux of molecules between the aqueous phase across the bilayer is the same) and the number of DMSO molecules in each of the aqueous phase will be equal ($\sim$46 for this particular case). According to the prediction in Fig. 6, the system would reach equilibrium after about 2000 ns, which is about 20 times longer than our simulation. We compared these results with those obtained from our simulation of DMSO in the double bilayer, in which case, we explicitly know the number of DMSO molecules at each instant during the simulation. The inset in Fig. 6 shows the comparison of the results for the duration of our simulation. At the conclusion of the simulation after 95 ns, 84 DMSO molecules remained in aqueous-A, whereas the model predicts that 72 molecules should be left. This difference of about 13%, even though significant, gives a reasonable description of the diffusion process for DMSO. There are, however, several points that should be noted about the use of Eq. (1) that may be a source
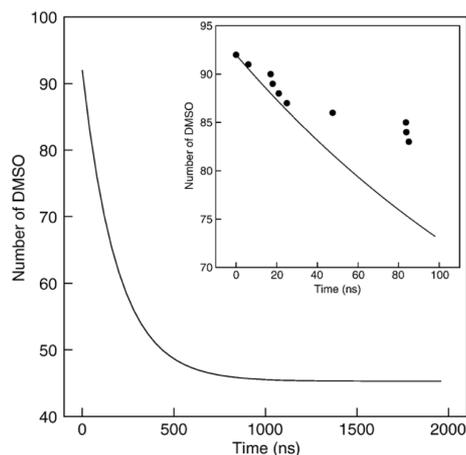
Fig. 6. Predicted DMSO concentration profile in the aqueous phase corresponding to the exterior of the membrane as calculated from the model equation and parameters estimated from the simulation results. The inset shows a comparison between the prediction and actual simulation results (circles) for the DMSO concentration for the considered simulation time.

of uncertainty. First, the partition coefficient was obtained from single bilayer simulations, which may deviate significantly from experimental measurements. Second, the diffusion coefficient for DMSO was calculated from the mean-squared displacement of the DMSO molecules from the time each initially entered and exited the transmembrane (from aqueous-A to aqueous-B). This value may deviate from actual experimental measurements, however, it is comparable and consistent with the diffusion coefficient of other molecular compounds, which is in the order of $\sim 10^{-6}$ cm^2/s [29,49]. And finally, the thickness of the various regions of the bilayer was assumed constant, but fluctuations in the thickness may affect the permeability of DMSO in the bilayers.

4. Conclusions

In order to properly study the diffusion process of molecular compounds through a transmembrane in the presence of a concentration gradient, we have performed a simulation of a double DPPC bilayer in the presence of DMSO. DMSO was initially contained in one of the aqueous phases, which represented the extracellular region of the membrane. After 95 ns of simulation time, several DMSO molecules diffused through the lipid bilayer, reaching the intracellular region of the membrane. A large number of DMSO molecules penetrated the lipid bilayer, most concentrating in the region that transitions from the polar to the hydrophobic parts of the bilayer. Of those molecules in the bilayer, only a few actually crossed the lipid domain from one leaflet to another and eventually out of the bilayer into the intracellular aqueous phase.

Using the results from the simulation, we estimated the required parameters to apply Fick's Law in modeling the

DMSO profile in the system as a function of time. The parameters included the partition coefficient of DMSO between the aqueous and lipid phases, the diffusion coefficient of DMSO, and the thickness of the bilayer and aqueous phases. Application of these quantities in the modeling equation resulted in a reasonable estimate of the DMSO concentration profile compared with the actual values obtained in the simulation. The aqueous phase corresponding to the exterior of the membrane contained initially 92 DMSO molecules, and after 95 ns, 84 remained in our simulations, whereas the model predicted that 72 should be left. Part of the deviation between these values may be attributed to the estimated parameters, including the partition coefficient, the diffusion coefficient, and the thickness of the different phases. According to the model, the system would reach equilibrium in terms of the DMSO concentration between the two aqueous phases after about 2,000 ns, approximately 20 times longer than the performed simulation.

The purpose of this study is to demonstrate that one can use simulations to obtain important information on the diffusional properties of molecular compounds, and these can be applied toward drug design for determining partition coefficient, rate of diffusion/permeation, and understanding the mechanism of diffusion through biological membranes. Moreover, the careful analysis of simulation data can yield the necessary parameters required for modeling of diffusion processes which may not be readily accessible from other means, such as experimental measurements.

Appendix A. Supplementary data

Supplementary data associated with this article can be found, in the online version, at doi:10.1016/j.bbamem.2006.06.010.

References

[1] S.L. Passani, G.D. Angelini, I.M. Breckenridge, A.C. Newby, Endothelial function can be preserved during cryo-storage of human saphenous vein, Eur. J. Cardio-Thorac. Surg. 2 (1988) 233–236.
[2] M. Bock, M. Schleuning, M.U. Heim, W. Mempel, Cryopreservation of human platelets with dimethyl sulfoxide: changes in biochemistry and cell function, Transfusion 35 (11) (1995) 921–924.
[3] M.J. Dijkstra-Tiekstra, D. de Korte, R.N.I. Pietersz, H.W. Reesink, P.F. van der Meer, A.J. Verhoeven, Comparison of various dimethylsulphoxide-containing solutions for cryopreservation of leucoreduced platelet concentrates, Vox Sang. 85 (4) (2003) 276–282.
[4] R.J. Egli, A. Sckell, C.R. Fraitzl, R. Felix, R. Ganz, W. Hofstetter, M. Leunig, Cryopreservation with dimethyl sulfoxide sustains partially the biological function of osteochondral tissue, Bone 33 (3) (2003) 352–361.
[5] Q.F. Ahkong, D. Fisher, W. Tampion, J.A. Lucy, Mechanisms of cell fusion, Nature 253 (5488) (1975) 194–195.
[6] G.H. Lyman, H.D. Preisler, D. Papahadjopoulos, Membrane action of dmso and other chemical inducers of friend Leukemic cell differentiation, Nature 262 (5567) (1976) 360–363.

[7] T.J. Anchordoguy, J.F. Carpenter, J.H. Crowe, L.M. Crowe, Temperature-dependent perturbation of phospholipid-bilayers by dimethylsulfoxide, Biochim. Biophys. Acta, Biomembr. 1104 (1) (1992) 117–122.

[8] S.W. Jacob, R. Herschler, Pharmacology of DMSO, Cryobiology 23 (1986) 14–27.

[9] J.R. Milligan, J.F. Ward, Yield of single-strand breaks due to attack on DNA by scavenger-derived radicals, Radiat. Res. 137 (3) (1994) 295–299.

[10] V.I. Gordeliy, M.A. Kiselev, P. Lesieur, J. Teixeira, Lipid membranes structure and interactions in dimethyl sulfoxide/water mixtures, Biophys. J. 75 (1998) 2343–2351.

[11] S. Tristram-Nagle, T. Moore, H.I. Petrache, J.F. Nagle, DMSO produces a new subgel phase in DPPC: DSC and X-ray diffraction study, Biochim. Biophys. Acta-Biomembr. 1369 (1998) 19–33.

[12] M.A. Kiselev, P. Lesieur, A.M. Kisselev, C. Grabielle-Madelmond, M. Ollivon, DMSO-induced dehydration of DPPC membranes studied by X-ray diffraction, small-angle neutron scattering, and calorimetry, J. Alloys Compd. 286 (1999) 195–202.

[13] S.N. Shashkov, M.A. Kiselev, S.N. Tioutiounnikov, A.M. Kiselev, P. Lesieur, The study of DMSO/water and DPPC/DMSO/water system by means of the X-ray, neutron small-angle scattering, calorimetry and IR spectroscopy, Physica, B 271 (1999) 184–191.

[14] Y. Yamashita, K. Kinoshita, M. Yamazaki, Low concentration of DMSO stabilizes the bilayer gel phase rather than the interdigitated gel phase in dihexdecylphosphatidylcholine membrane, Biochim. Biophys. Acta, Biomembr. 1467 (2000) 395–405.

[15] H.H. Chang, P.K. Dea, Insights into de dynamics of DMSO in phosphatidylcholine bilayers, Biophys. Chem. 94 (2001) 33–40.

[16] Z. Yu, P.J. Quinn, Solvation effects of dimethyl sulphoxide on the structure of phospholipid bilayers, Biophys. Chem. 70 (1998) 35–39.

[17] Z. Yu, P.J. Quinn, The effect of dimethyl sulphoxide on the structure and phase behaviour of palmitoleoylphosphatidylethanolamine, Biochim. Biophys. Acta, Biomembr. 1509 (2000) 440–450.

[18] E. Paci, M. Marchi, Membrane crossing by a polar molecule: a molecular dynamics simulation, Mol. Simul. 14 (1994) 1–10.

[19] A.M. Smondyrev, M.L. Berkowitz, Molecular dynamics simulation of DPPC bilayer in DMSO, Biophys. J. 76 (5) (1999) 2472–2478.

[20] A.K. Sum, J.J. de Pablo, Molecular simulation study on the influence of dimethylsulfoxide on the structure of phospholipid bilayers, Biophys. J. 85 (6) (2003) 3636–3645.

[21] E. Overton, On the general osmotic properties of the cell, their probable origin, and their significance for physiology, Vierteljahrsschr. Nat. Forsch. Ges. Zür. 44 (1899) 88–135.

[22] A. Walter, J. Gutknecht, Monocarboxylic acid permeation through lipid bilayer membranes, J. Membr. Biol. 77 (3) (1984) 255–264.

[23] A. Walter, J. Gutknecht, Permeability of small nonelectrolytes through lipid bilayer membranes, J. Membr. Biol. 90 (3) (1986) 207–217.

[24] W.R. Lieb, W.D. Stein, Biological membranes behave as non-porous polymeric sheets with respect to the diffusion of non-electrolytes, Nature 224 (216) (1969) 240–243.

[25] J.A. Dix, D. Kivelson, J.M. Diamond, Molecular motion of small nonelectrolyte molecules in lecithin bilayers, J. Membr. Biol. 40 (4) (1978) 315–342.

[26] L.R. DeYoung, K.A. Dill, Solute partitioning into lipid bilayer membranes, Biochemistry 27 (14) (1988) 5281–5289.

[27] S.J. McKinnon, S.L. Whittenburg, B. Brooks, Nonequilibrium molecular dynamics simulation of oxygen diffusion through hexadecane monolayers with varying concentrations of cholesterol, J. Phys. Chem. 96 (25) (1992) 10497–10506.

[28] F. Müller-Plathe, Diffusion of penetrants in amorphous polymers: a molecular dynamics study, J. Chem. Phys. 94 (4) (1990) 3192–3199.

[29] D. Bassolino-Klimas, H.E. Alper, T.R. Stouch, Solute diffusion in lipid bilayer membranes: an atomic level study by molecular dynamics simulation, Biochemistry 32 (47) (1993) 12624–12637.

[30] A.K. Sum, R. Faller, J.J. de Pablo, Molecular simulation study of phospholipid bilayers and insights of the interactions with disaccharides, Biophys. J. 85 (5) (2003) 2830–2844.

[31] J.N. Sachs, P.S. Crozier, T.B. Woolf, Atomistic simulations of biologically realistic transmembrane potential gradients, J. Chem. Phys. 121 (22) (2004) 10847–10851.

[32] A.A. Gurtovenko, Asymmetry of lipid bilayers induced by monovalent salt: atomistic molecular-dynamics study, J. Chem. Phys. 122 (24) (2005) 244902.

[33] R. Freshney, Culture of Animal Cells: A Manual of Basic Technique, Alan R. Liss, Inc., New York, 1987.

[34] S. Leekumjorn, A.K. Sum, Molecular simulation study of structural and dynamic properties of mixed DPPC/DPPE bilayers, Biophys. J. 90 (11) (2006) 3951–3965.

[35] E. Egberts, S.J. Marrink, H.J.C. Berendsen, Molecular dynamics simulation of a phospholipid membrane, Eur. Biophys. J. 22 (6) (1994) 423–436.

[36] W.F. van Gunsteren, S.R. Billeter, A.A. Eising, P.H. Hünenberger, P. Krüger, A.E. Mark, W.R.P. Scott, I.G. Tironi, Biomolecular simulation: the GROMOS96 manual and user guide, vdf Hochschuleverlag AG an der ETH Zürich, Zürich, Switzerland, 1996.

[37] J.P. Ryckaert, A. Bellemans, Molecular dynamics of liquid n-butane near its boiling point, Chem. Phys. Lett. 30 (1) (1975) 123–125.

[38] O. Berger, O. Edholm, F. Jähnig, Molecular dynamics simulations of a fluid bilayer of dipalmitoylphosphatidylcholine at full hydration, constant pressure, and constant temperature, Biophys. J. 72 (5) (1997) 2002–2013.

[39] W.L. Jorgensen, J. Tirado-Rives, The OPLS potential function for proteins. Energy minimizations for crystals of cyclic peptides and crambin, J. Am. Chem. Soc. 110 (1988) 1657–1666.

[40] J.W. Essex, M.M. Hann, W.G. Richards, Molecular dynamics simulation of a hydrated phospholipid bilayer, Philos. Trans. R. Soc., B 344 (1309) (1994) 239–260.

[41] S.W. Chiu, M. Clark, V. Balaji, S. Subramaniam, H.L. Scott, E. Jakobsson, Incorporation of surface tension into molecular dynamics simulation of an interface: a fluid phase lipid bilayer membrane, Biophys. J. 69 (4) (1995) 1230–1245.

[42] H.J.C. Berendsen, J.P.M. Postma, W. van Gunsteren, J. Hermans, Intermolecular Forces, Reidel, Dordrecht, The Netherlands, 1981.

[43] P. Bordat, J. Sacristan, D. Reith, S. Girard, A. Glättli, F. Müller-Plathe, An improved dimethyl sulfoxide force field for molecular dynamics simulations, Chem. Phys. Lett. 374 (2003) 201–205.

[44] T. Darden, D. York, L. Pedersen, Particle mesh Ewald: an Nlog(N) method for Ewald sums in large systems, J. Chem. Phys. 98 (1993) 10089–10092.

[45] U. Essman, L. Perera, M.L. Berkowitz, T. Darden, H. Lee, L.G. Pedersen, A smooth particle mesh Ewald method, J. Chem. Phys. 103 (1995) 8577–8593.

[46] H.J.C. Berendsen, D. van der Spoel, R. van Drunen, GROMACS: a message-passing parallel molecular dynamics implementation, Comput. Phys. Commun. 91 (1–3) (1995) 43–56.

[47] E. Lindahl, B. Hess, D. van der Spoel, GROMACS 3.0: a package for molecular simulation and trajectory analysis, J. Mol. Model. 7 (8) (2001) 306–317.

[48] Virginia Tech, http://www.tcf.vt.edu (Terascale Computing Facility).

[49] H.F. Lodish, D. Baltimore, A. Berk, L.S. Zipursky, P. Matsudaira, J.E. Darnell, Molecular cell biology, Scientific American Books 3rd ed., 1995 Distributed by W.H. Freeman and Company, New York.

[50] K.J. Packer, D.J. Tomlinson, Nuclear spin relaxation and self-diffusion in the binary system, dimethyl sulfoxide (dmso)+water, Trans. Faraday Soc. 67 (1971) 1302–1314.

[51] A. Vishnyakov, A.P. Lyubartsev, A. Laaksonen, Molecular dynamics simulations of dimethyl sulfoxide and dimethyl sulfoxide–water mixture, J. Phys. Chem., A 105 (10) (2001) 1702–1710.